Doctoral Thesis

On Generalized Signal Waveforms for Satellite Navigation

by

José Ángel Ávila Rodríguez

Munich, June 2008

Vorsitzender (Chairman)	Univ.-Prof. Dr.sc.math.habil. J. Gwinner
1. Berichterstatter (1st Reviewer)	Univ.-Prof. Dr.-Ing. G. W. Hein
2. Berichterstatter (2nd Reviewer)	Univ.-Prof. Dr.-Ing. B. Eissfeller
3. Berichterstatter (3rd Reviewer)	Prof. Dr.-Ing. A.R. Pratt

Vollständiger Abdruck der bei der Fakultät für Luft- und Raumfahrttechnik der Universität der Bundeswehr München zur Erlangung des akademischen Grades eines Doktor-Ingenieurs (Dr.-Ing.) eingereichten Dissertation. (2008)

UNIVERSITY FAF MUNICH

On Generalized Signal Waveforms for Satellite Navigation

by

José Ángel Ávila Rodríguez

A THESIS
SUBMITTED TO THE FACULTY OF
AEROSPACE ENGINEERING
IN FULFILMENT OF THE REQUIREMENTS FOR THE
DEGREE OF DOCTOR OF ENGINEERING

MUNICH, GERMANY

JUNE, 2008

Abstract

This thesis provides a comprehensive overview of all current and planned satellite navigation systems, either global or regional, putting special emphasis on their signal structure. Particular attention is paid to the European Global Navigation Satellite System Galileo, under development at the moment. The results of this work can be considered as a significant contribution to the design and development of the Galileo's Open Service (OS) in the E1 frequency band.

The present work provides as main contribution a generally valid theoretical framework with which all current and future navigation signals can be described. Generalized signal waveforms and their corresponding time and spectral characteristics are derived and investigated. Complete families of signals are presented and analyzed regarding their spectral and performance characteristics, underlining their potential for future generations of satellite navigation systems. This thesis proves that the generalized signal waveforms proposed in this work cover any current and other optimized signals that could be proposed in the future. In this sense, it is shown that all current navigation signals can be mathematically described as Multilevel Coded spreading Symbols or, in particular, as Binary Coded Symbols.

Using the analytical expressions of the generalized signal model, the corresponding generalized signal waveforms are further studied regarding their Spectral Separation Coefficients (SSCs). This parameter is of great interest in satellite navigation to understand the compatibility between different signals. Generalized formulas for smooth spectra are also derived to calculate the SSCs between any two arbitrary signals. Particular cases of interest are computed following the obtained analytical expressions and by means of simulations with real Pseudo Random Noise (PRN) codes. Results from this comparison show a perfect matching between the predicted analytical results and the numerical computations. Realistic scenarios are carried out to assess the impact of non-ideal PRN codes and navigation data onto the spectral properties that have been derived analytically.

Finally, current and new multiplexing schemes are studied in detail together with the feasibility to introduce optimized signal waveforms. Special attention is paid to understand the required changes that are necessary to multiplex non-binary signals. Pros and Cons of the different solutions are discussed and investigated with regard to the application of future signal waveforms. Among these last ones, the Composite Binary Offset Carrier (CBOC) implementation of the Multiplexed Binary Offset Carrier (MBOC) modulation for the Galileo's Open Service signal in the E1 frequency band deserves an important chapter. In addition, some chapters are dedicated to analyze receiver structures optimized to work with MBOC for both GPS and Galileo.

Acknowledgements

A doctoral thesis is very much like climbing a mountain. You start the trip a sunny day in the hope that the weather will remain favourable for the rest of the adventure. You walk fast at the beginning and the first steps are always full of confidence. The summit is most of the time in sight. But then come the moments of frustration, bitterness and not always things come out as planned. Many times it looks like you are wandering in circles and instead of moving ahead, the goal seems to be every day further. Other times you concentrate so much on reaching the goal that you trip over the little stones in the way.

It is however in those moments and especially when you are about to cross the goal line that you feel thankful to those people who have backed you all along the hard route, all those who have given you all the their trust and support. Indeed, without the help and encouragement from several persons, this thesis would have never been written. Let me therefore try to express my gratitude to all of them.

I would like to express my deepest and most sincere gratitude to my supervisor, Professor Guenter W. Hein. His profound knowledge and logical way of thinking have been the most valuable and important guide to me in this work. His brilliant understanding, encouraging and personal guidance have provided the fundamental basis of this thesis. In spite of his busy agenda, there was always time to discuss on technical problems. I am really thankful for all the time he has spent helping me and all what I have learnt from him in the past years.

I would also like to thank Professor Bernd Eissfeller, with whom I have also had the pleasure and luck to work with. I am in great debt also to him for all the opportunities he has offered to me as well as all the trust he has put in my work over the past years. I am very thankful for the many technical discussions from which I have so much profited.

To my third supervisor, Professor Anthony R. Pratt, I would like to equally express my deepest gratitude for the careful reading of this thesis and for all the time that he has invested in helping me improve it. During the past years I have had many times the opportunity to discuss with him on many different theoretical problems. His broad and accurate technical picture on GNSS have been guidance to me in so many occasions.

Warm thanks also to my colleagues and friends Stefan Wallner, Daniel Sanroma and Thomas Pany for all the time and patience that they have dedicated in reading several times the thesis. Their contributions were of enormous value to me and I owe many interesting comments of the thesis to them. In particular I would like to express my deep gratitude to Stefan with whom I have shared the office room since I started my work at the Institute. He has been

intellectual inspiration to me in many times and had the patience to read this thesis a couple times, contributing clearly to improving the quality of this thesis.

I would never have attempted or finished the doctoral thesis without the support of my wife, Anastasia. Her love and support without any complaint or regret has enabled me to complete my doctoral studies. She is the origin and backbone of my happiness. I am especially grateful to her for her love and patience during all the past years of hard work. She has been my spiritual inspiration and the star that has guided me when I weakened. I owe my every achievement in this thesis to her.

I feel a deep sense of gratitude for my mother, Sara, and my father, Ángel, who have taught me the things that really matter in life. I am deeply thankful for the time they dedicated to me when I was a child satisfying my thirst for knowledge always I wanted to understand something. All what I am now is thanks to them and I am forever indebted.

Finally, my special gratitude is to my brother, Javier, who has taught me the importance of perseverance in achieving one´s personal goal. I am thankful for all his support, love and understanding.

Table of Contents

List of Figures

List of Tables

List of Acronyms

AltBOC	Alternative Binary Offset Carrier
AS	Anti-Spoofing
AWGN	Additive White Gaussian Noise
BCS	Binary Coded Symbols
BOC	Binary Offset Carrier
BPSK	Binary Phase Shift Keying
CASM	Coherent Adaptive Sub-carrier Modulation
CASTC	China Aerospace Science and Technology Corporation
CBCS	Composite BCS
CBOC	Composite Binary Offset Carrier
CCIR	Comité Consultatif International des Radio Communications
CDMA	Code Division Multiple Access
CNES	Centre National d'Études Spaciales
COSPAS	COsmicheskaya Systyema Poiska Avariynich Sudov
CPSD	Cross Power Spectral Density
CRLB	Cramér Rao Lower Bound
CS	Commercial Service
DAC	Digital to Analog Converters
DDMA	Doppler Division Multiple Access
DLL	Delay Lock Loop
DME	Distance Measuring Equipment
DP	Dot Product
DSSS	Direct Sequence Spread Spectrum
EGNOS	European Geostationary Navigation Overlay Service
EMLP	Early Minus Late Power
ENSS	European global Navigation Satellite System
EU	European Union
FDMA	Frequency Division Multiple Access

FFT	Fast Fourier Transform
FHSS	Frequency Hopping Spread Spectrum
FIR	Finite Impulse Response Filter
FLL	Frequency Lock Loop
FOC	Full Operational Capability
FSK	Frequency Shift Keying
GAGAN	GPS Aided GEO Augmented Navigation
GATE	German Galileo Test and Development Environment
GBAS	Ground Based Augmentation System
GEO	Geostationary Earth Orbit
GJU	Galileo Joint Undertaking
GLONASS	GLObal NAvigation Satellite System
GMV	Generalized Majority Voting
GNSS	Global Navigation Satellite System
GPS	Global Positioning System
GRAS	Ground-Based Regional Augmentation System
GRR	Galileo Ground Reference Receiver
GSA	European GNSS Supervisory Authority
GSS	Galileo Sensor Station
GSLV	Geostationary Satellite Launch Vehicle
GSO	GeoSynchronous Orbit
GSTB	Galileo System Test Bed
GSVF	Galileo Signal Validation Facility
GT	Ground Transmitters
HP	High Precision
HPA	High Power Amplifier
ICAO	International Civil Aviation Organization
ICD	Interface Control Document
ICG	International Committee on GNSS

I&D	Integrate and Dump
IGSO	Inclined Geosynchronous Orbit
IOC	Initial Operational Capability
IOV	In-Orbit Validation
IRNSS	Indian Radio-Navigation Satellite System
ISI	Inter Symbol Interference
ISRO	Indian Space and Research Organization
ITU	International Telecommunications Union
JTIDS	Joint Tactical Information Distribution System
KMF	Key Management Facility
L1C	L1 Civil Signal
L2 CL	L2 Civil Long Signal
L2 CM	L2 Civil Moderate Signal
LOC	Linear Offset Carrier
MA	Military Acquisition
MBOC	Multiplexed Binary Offset Carrier
MCS	Multilevel Coded Symbols
MEO	Medium Earth Orbit
MIDS	Multifunctional Information Distribution System
MLS	Microwave Landing System
MMSSS	Multi-Mode Spread-Spectrum Sub-carrier Modulation
MSAS	MTSAT Spacebased Augmentation System
MT	Military Tracking
MTSAT	Multifunctional Transport SATellite
MV	Majority Vote
NAS	National Airspace System
NRSCC	National Remote Sensing Center of China
NRZ	Non Return to Zero
NSCC	National Security Compatibility Compliance

OC	Offset Carrier
OS	Open Service
PDF	Probability Density Function
PL	PseudoLite
PLL	Phase Lock Loop
PPS	Precise Positioning Service
PRN	Pseudo Random Noise
PRNG	Pseudo Random Noise Generator
PRS	Public Regulated Service
PSD	Power Spectral Density
PSK	Phase Shift Keying
PSWF	Prolate Spheroidal Wave Functions
QPSM	Quadrature Product sub-carrier Modulation
QZSS	Quasi-Zenith Satellite System
RCF	Raised Cosine Filter
RISDE	Russian Institute of Space Device Engineering
RF	Radio Frequency
RFSA	Russian Federal Space Agency
RNSS	Regional Navigation Satellite Systems
RTCA	Radio Technical Commission for Aeronautics
RX	Receiver
SA	Select Availability
SAR	Search and Rescue
SARP	Standards and Recommended Practices
SARSAT	Search and Rescue Satellite Aided Tracking
SBAS	Satellite-Based Augmentation Systems
SCPL	Single Chip PseudoLites
SGLS	Space Ground Link Subsystem
SIS	Signal In Space

SMCS	Sinosoidal Multilevel Coded Symbols
SNIR	Signal to Noise plus Interference Ratio
SNR	Signal to Noise Ratio
SOC	Sinusoidal Offset Carrier
SPS	Standard Positioning Service
SRRC	Squared Root Raised Cosine
SS	Spread Spectrum
SSC	Spectral Separation Coefficients
STF	Signal Task Force
SV	Space Vehicle
SVN	Space Vehicle Number
TACAN	Tactical Air Navigation System
TBD	To Be Determined
TCS	Tertiary Coded Symbols
TDMA	Time-Division Multiple Access
TMBOC	Time Multiplexed Binary Offset Carrier
TMR	Triple Modular Redundancy
TX	Transmitter
UERE	User Equivalent Range Error
URE	User Range Errors
US	United States
UTCS	Unilateral Tertiary Coded Symbols symbols
WAAS	Wide Area Augmentation System
WG A	Working Group A
WG 1	Working Group 1

1. Introduction

Seven years ago, the U.S. Global Positioning System was the only operative Global Satellite System (GNSS) worldwide. The GLONASS constellation had dwindled down to seven satellites. Final approval and funding of Europe's Galileo program was yet to be achieved. Since then, Russia has gone a long way towards rebuilding and modernizing GLONASS. Galileo has put its two first experimental GNSS satellites, GIOVE-A and GIOVE-B, into space and China has announced plans to build a full-fledged GNSS of its own, Compass.

Today there is not any more a sole global positioning system and the coexistence between different GNSSes particularly challenges engineers to understand how the coexistence of current and future signals can be guaranteed. As the evolution of the different navigation systems mentioned above has shown, all modernized GNSSes provide more complex signal waveforms compared to the past and signal design has become a topic of great interest and subject to intensive research. This thesis will analyze the problems and challenges that this new world poses from the point of view of the signal structure, describing how future generalized GNSS signal waveforms could look like.

1.1 Objectives of this Thesis

The first main objective of this thesis is the derivation of a generally valid theoretical model under which all current and future navigation signals can be described. This thesis proves that the generalized signal waveforms can cover all current signals and other optimized signals that could potentially be proposed in the future. Chapters 2 and 3 give a general overview of today's satellite navigation, paying special attention to those aspects related to signal and frequency design. Chapter 4 presents the theoretical framework this thesis relies on.

A second objective of this work is to assess the spectral performance of these generalized signal waveforms by analyzing the Spectral Separation Coefficient (SSC). This figure is of great interest in satellite navigation to understand the interaction of any two signals. Building on the generic signal formulas defining the spectrum, generalized expressions are derived for the SSCs. Particular cases of interest are investigated in detail, using on the one hand side the obtained analytical expression and on the other hand real simulations under ideal conditions. Results show a perfect matching between the predicted analytical results and those obtained from numerical computations, under multiple assumptions. Furthermore, the SSC theory is extended to account also for imperfections and non-ideal effects induced by the codes.

Finally, the third main objective of this thesis is to provide a full understanding on current and future multiplexing techniques. This work proposes different solutions to integrate any

generalized signal waveform into an unique multiplexed signal to be transmitted by the satellite. Pros and Cons of the different solutions are discussed and investigated with regards to the application for future signal waveforms.

To accomplish all these objectives, several tasks have been identified:

- **To provide an actual description of the signal and frequency plan of all the Global Navigation Systems that have played or will play an important role in the coming decades.** The American GPS and the Russian GLONASS are today in a process of modernization that will transform both in dual-use systems. In parallel, the European Galileo project will soon start to work and the Chinese Compass is under current development. This thesis presents their main constellation figures together with other relevant signal and frequency characteristics.
- **To present a general description of all the Regional Satellite Navigation Systems that exist or are under design.** In order to provide improved positioning performance, Japan (QZSS), India (IRNSS) and China (Beidou) are currently developing their own regional satellite navigation systems. A detailed description of their main parameters will be provided together with a discussion on the future and utility of these regional approaches.
- **To provide an actual and detailed description of all the current and planned GNSS Augmentation Systems.** As the number of countries with a global navigation system increases, also the requirement to give an answer to particular needs in certain regions gains in interest. To cover this demand, the USA (WAAS), Europe (EGNOS), Japan (MSAS), Russia (SDCM), India (GAGAN), Nigeria (NIGCOMSAT), Canada (CWAAS), China (SNAS) and South America (CSTB), have planned or are currently developing satellite based augmentation systems to enhance the capabilities of the global navigation systems, providing in most cases common operations between different systems. In addition, other means to augment the navigation signals on a terrestrial basis (GRAS, LAAS, Pseudolites) are also shortly discussed in this work.
- **To present a clear picture of the evolution of the Galileo Signal and Frequency Plan over the past years**, covering all the gaps in the signal design history that have not been covered sufficiently in the literature. An important objective in this regard is indeed to present the evolution of the Galileo Signal Baseline in a comprehensive way, underlining the drivers that have led Galileo to the final plan it presents today.
- **To provide a complete description of all the services and signal characteristics of Galileo.** This work pursues to present a correct and complete overview of all the aspects of the Galileo's Signal and Frequency plan, emphasizing on those signals that due to their still short life are less known in the literature. Given the importance that Galileo has played in past years, special attention is dedicated to it.

- **To provide a theoretical framework that describes all current and future navigation signals.** After a complete overview of the signal structure of current GNSSes and future modernizations, all the potential modulations of interest for satellite navigation are presented. These are shown to belong to a generalized family of signals, known as Multilevel Coded Symbols (MCS). A theoretical framework will be set up and used to derive analytical expressions of generic signal waveforms.
- **To prove that the theoretical framework that describes any generalized navigation signals covers all current and all new modulations.** This thesis further proves that all current signal waveforms are in fact particular cases of the generalized modulations that are proposed in this work.
- **To provide the reader with a list of appropriate tools to evaluate the goodness of a signal waveform against other potential alternatives.** Designing the signal and frequency plan of any navigation system requires the deep understanding of the effect of any signal characteristic aspect onto the final positioning accuracy. This work provides answers to this.
- **To understand the meaning and importance of the Spectral Separation Coefficient (SSC), stressing the value of this parameter in the design of the Signal and Frequency plan of any navigation system.** The SSCs have been widely used over the past years to assess compatibility of the candidate signals of all the navigation systems that exist or are under development. Furthermore, a good understanding of them provides a very rich insight into the global compatibility and interoperability performance of a modulation.
- **Based on the theoretical framework that describes analytically any generic signal, analytical expressions are also derived for the Spectral Separation Coefficient (SSC) between any two signals.** The analytical SSCs are further cross-checked with results coming from numerical computation showing the validity of the derived expressions.
- **To assess how non-idealities of the real signal implementations are reflected in the final performance of a signal.** This work will assess the SSCs under ideal and more realistic conditions, evaluating the potential effects that the drift from the ideal case can cause onto the final performance of a navigation signal.
- **To investigate the effects of the SSCs on the mutual interference and compatibility among different navigation systems.** Using a generally accepted interference model, the influence of the signal waveform on the final compatibility and interference will be assessed.
- **One final but ambitious task of this work will be to provide a complete overview of all the current and potential multiplexing schemes of future and modernized navigation systems.** Signal Multiplexing has gained in importance over the past years as an increasing number of signals and services are planned to be shared in the very

scarce Radio-Navigation bands that satellite navigation has assigned today. This thesis will try to give a comprehensive and complete overview of all the multiplexing schemes that are relevant for satellite navigation, paying special attention to those approaches that GPS and Galileo presently use and will potentially implement in the future.

The organization of the thesis is determined by these objectives and will be further outlined in chapter 1.3.

1.2 Contributions of this Thesis

The major achievements of this thesis are enumerated next:

- Review of current satellite navigation systems and signal waveforms:
    - A detailed description of the signal and frequency plans, including the main constellation parameters, of all the global, regional and augmentation navigation systems that exist today or are planned for the coming years.
    - A detailed overview of how the Galileo Signal and Frequency Plan has evolved over the past years, providing insight into the technical drivers that have led to the baseline that Galileo presents today.
    - A complete overview of all the signal waveforms that have been relevant in the past decades and of those that could potentially become alternative for modernized Satellite Navigation Systems.
    - A complete description of the Galileo baseline signals and services as well as of other candidates that were relevant in the past years together with an assessment of their potential positioning performance.

- Development of new theory on signal design for satellite navigation:
    - A mathematical framework capable of describing any generic signal waveform is developed and analytical expressions derived. This is further used to obtain general expressions for the Spectral Separation Coefficients.
    - Derivation of analytical expressions and theory of generic Multi-Coded Symbol (MCS) Signals and their particular cases. By using this theoretical framework it is shown that any signal can be in principle expressed following the generalized theory on MCS signals.
    - Derivation of analytical generalized expressions for the Power Spectral Densities that can describe all signals, modulations and multiplexing schemes that are used today or could be used some day in the future to enhance navigation.

- Analysis of the MBOC modulation and its different implementations by GPS and Galileo as well as possible receiver architectures for GPS and Galileo E1/L1 common receivers.
- Derivation of analytical expressions for the Spectral Separation Coefficients (SSC) of generic Multi-Coded Symbol signals with infinite and limited bandwidth and generalization to more complex waveforms. Original formulas are proposed to calculate the SSC between any two arbitrary signals.
- Assessment of the effect of non-random codes and data on the Spectral Separation Coefficients. Particular examples for Galileo and GPS signals are provided and the consequences are discussed.
- Overview of the most representative multiplexing schemes in satellite navigation with special emphasis on those modulations that GPS, Galileo and potentially other navigation systems will use in the future. Furthermore, the possibility to use the above described multiplexing schemes to accommodate the generalized signal waveforms is also discussed in this thesis.

1.3 Thesis Outline

This thesis focuses on the derivation of general analytical expressions that can describe all the current signal waveforms, modulations and multiplexing schemes today or that could be implemented in the future. Furthermore, given the importance that the Spectral Separation Coefficient plays in the design of any Satellite Navigation System's signal plan, special attention is paid to this figure. The thesis concludes discussing existing and new theory on multiplexing. In order to provide a comprehensive overview, this thesis has been divided in the following chapters:

- **Chapter 1** gives and introduction to the semantics and to the scope of this thesis, giving a brief overview of the current situation and expectations on the future development of satellite navigation in the next decades.
- **Chapter 2** concentrates on giving a detailed overview of all the current and planned Satellite Navigation Systems, summarizing the main constellation parameters and envisioned signal and frequency plans. The chapter begins with a brief discussion on the direction in which GNSS could evolve in the coming years. Then, the American Global Positioning System (GPS) is presented, followed by the European Galileo, the Russian GLONASS and the Chinese Compass system. After summarizing the main characteristics of these four systems, additional regional and augmentation satellite systems are introduced and their main figures are briefly outlined. To conclude the chapter, actual information on other augmentation systems that are not based on satellite technology is also provided.

- **Chapter 3** makes a review of the evolution of the Galileo's Signal and Frequency Plan since it was officially announced that Europe would also pursue to have its own Global Navigation Satellite System. The chapter begins with the description of the first signal plan back in the late 1990´s and concludes with the newly adopted MBOC modulation. In recognition of the difficulty that the signal design represents, this chapter tries to provide the technical arguments that were used to justify each of the signal waveform that form today's signal plan. Furthermore a brief description of the navigation services that Galileo will offer is equally provided.
- **Chapter 4** presents the theory on generalized signal waveforms, setting up a complete theory framework with which all of the signals used today for satellite navigation can be described mathematically. The chapter begins defining the main spectral and time characteristics of any signal waveform, introducing then the generic Multi-Coded Symbol (MCS) modulation. After that, general and particular analytical expressions are derived and compared with the well known expressions that can be found in the literature. Generalized waveforms are further introduced concluding the chapter with the recently adopted MBOC modulation and an assessment of its performance for different receiver configurations.
- **Chapter 5** is dedicated to the derivation of analytical expressions for the Spectral Separation Coefficients (SSC) using the theory presented in chapter 4. The chapter begins deriving generic expression for the SSCs between any two generic BCS signals with infinite bandwidth. It concludes giving general expressions for the power in the band and for different efficiency parameters of interest. Analytical results and numerical computations are compared to show the validity of the model.
- **Chapter 6** concentrates on assessing the validity of the expressions derived in chapter 5 under more realistic scenarios. The effect of non-random codes and data is further examined and different signal waveforms are further investigated regarding their spectral properties as seen in the receiver.
- **Chapter 7** deals with signal multiplex techniques for GNSS. After giving a quick review of all the techniques that are relevant for satellite navigation, the most relevant ones are investigated in detailed. The chapter begins with a brief discussion on the need of multiplexing and the requirement on constant envelope to justify the different solutions that will be later studied. Beginning with non-constant envelope, the chapter goes through more flexible techniques such as Interplex and its generalization to any number of sub-carriers, to finally conclude with new multiplexing schemes. To conclude, this chapter presents a brief discussion on CDMA and FDMA stressing its importance on the modernization of GLONASS.
- **Annexes A to N** derive the analytical expressions for the Power Spectral Densities, Spectral Separation Coefficients, Multiplexing schemes and interference models that are presented in the previous chapters.

2. Global Navigation Satellite Systems (GNSS)

2.1 GNSS – Thinking global

The USA entered the global navigation satellite system (GNSS) era with the Global Positioning System as the result of efforts that began in the late 1960s. The Russians followed soon afterwards with GLONASS. Both systems are now undergoing extensive modernization. Moreover, the European Galileo system is joining the GNSS club, and China is now planning its own version called Compass.

In the meantime lots of augmentation and regional systems have been developed or are currently under consideration. From military to civil signals, from Medium Earth Orbit (MEO) to Geostationary Earth Orbit (GEO) and Inclined GeoSynchronous Orbits (IGSO), the palette of systems and offered services is considerably wide.

It is time to pause and think for a moment about where we want GNSS to move. It is already time to really think *global* and to coordinate and harmonize all the existing and projected navigation satellite systems. Indeed the question naturally arises: what should the *Global Navigation Satellite System of Systems* look like?

This chapter describes the world of GNSS in which we will live around the year 2020 if all the currently modernizing and planned new systems come into reality. The word *coordination* will be the key since, if things are well done, it will give the users the possibility to profit from all the navigation systems as if they were only one. After all, GNSS users should not care about whether one of the signals comes from GPS, the other from Galileo, the third from GLONASS and the fourth from Compass as long as the GNSS receiver works well.

2.2 Scenes from the Present

Today only GPS is fully operational. Nevertheless, Russia hopes to return GLONASS to full operation capability (FOC) with a completed constellation by 2009, and Galileo's FOC is now expected end of 2013. Compass has also ambitious plans and in spite of the fact that China has still a long way to go and lengthy negotiations will be needed, a scenario of four global coverage satellite systems seems to be very likely in a future not so far away from today.

From the experience with Galileo, we know how important the roles of interoperability and compatibility with GPS were from the very beginning. Unfortunately, major differences between those two systems using the Code Division Multiple Access (CDMA) and GLONASS using the Frequency Division Multiple Access (FDMA) approach still exist today. However, GLONASS seems to have made first movement into adopting CDMA as will be shown in chapter 2.5. It seems that Compass will use CDMA too.

On the GPS/GLONASS side, work for reaching real interoperability continues. During the GPS/GLONASS Working Group 1 meeting in December 2006 both sides emphasized the benefit to the user community that a common approach concerning FDMA/CDMA will bring in terms of interoperability. The Russian side announced that they would come to a decision by the end of 2007 [US-Russia Statement, 2006] but it was not until April 2008 that the final decision was taken. GLONASS seems to plan now CDMA signals in L1 and L5 as we will show in chapter 2.5.

In fact, if the need of standardization was always there, it seems that the concept is gaining in interest the more systems come into play. But before dreaming with our ideal GNSS, let us first look more closely into what the current reality is and the plans for new GNSS systems.

If we take a look at the signal structure, we can recognize that all the present GNSS systems are based on the *Direct Sequence Spread Spectrum* (DSSS) technique which is a particular case of the more general Spread Spectrum (SS) method. Moreover, Code Division Multiple Access (CDMA), Frequency Division Multiple Access (FDMA) and Time Division Multiple Access (TDMA) are particular cases of DSSS. The overall constellation parameters of the four global GNSSes are shown in Table 2.1 next.

Table 2.1. Space Constellation Parameters

Parameter	Galileo	GPS	GLONASS	Compass
Constellation	Walker MEO (27/3/1) plus 3 non-active spares	MEO (24/6) including 3 active spares	MEO (24/3)	GEO (5), MEO (27), IGSO (3)
GEO Longitudes	-	-	-	58.75°, 80°, 110.5°, 140° and 160° E
GSO Equatorial Crossing	-	-	-	118°
Eccentricity	0	0	0	0
GSO Inclination	-	-	-	55°
MEO Inclination	56°	55°	64.8°	55°
Semi-major axis	29,601.297 km	26,559.7 km	25,440 km	MEO 27,878 km IGSO 42,146 km

As we know, in spread spectrum communications a higher-frequency signal is injected into a baseband signal bandwidth. This results in the energy used in transmitting the information of the baseband signal being spread over a wider bandwidth. Typically, the SS power level drops below the RF noise floor, which makes the SS signal invisible for unauthorized users. The ratio (in dB) between the spread baseband and the original signal is called processing gain and typical SS processing gains range from 10 dB to 60 dB [G.W. Hein et al., 2006c].

For the particular case of the DSSS technique, the Pseudo Random Noise Code (PRN) is inserted at the data level. How this is realized makes the difference between CDMA, FDMA and TDMA. In the case of GPS and Galileo, the pseudo-random sequence is mixed or multiplied with the information signal (CDMA) while GLONASS employs different frequencies for each signal (FDMA).

To facilitate the reading in the next chapters and given that the different existing and planned GNSSes refer sometimes to different bands with the same notation and other times to the same band with different names, the following table of correspondences is presented for clarification. Furthermore, it is interesting to note that Galileo used for a long time L1 to refer to the actual E1 band. In fact, only after [Galileo SIS ICD, 2008] the notation has changed from L1 to E1 to make it consistent with the rest of the bands.

Table 2.2. Correspondence between frequency bands of different GNSSes

System	GPS	GLONASS	Galileo	Compass
Frequency Band	L1	L1	E1	B1
Centre Frequency	1575.42 MHz	1602 MHz	1575.42 MHz	1561.098 MHz (B1) 1589.742 MHz (B1-2)

System	GPS	GLONASS	Galileo	Compass
Frequency Band	L2	L2	-	-
Centre Frequency	1227.60 MHz	1246 MHz	-	-

System	GPS	GLONASS	Galileo	Compass
Frequency Band	L5	-	E5a	-
Centre Frequency	1176.45 MHz	-	1176.45 MHz	-

System	GPS	GLONASS	Galileo	Compass
Frequency Band	-	-	E6	B3
Centre Frequency	-	-	1278.75 MHz	1268.52 MHz

System	GPS	GLONASS	Galileo	Compass
Frequency Band	-	L3	E5b	B2
Centre Frequency	-	1201 MHz	1207.14 MHz	1207.14 MHz

Finally, Figure 2.1 next shows the signal structure of all the existing and planned GNSSes. Negotiations among the involved countries are still needed to ensure compatibility (and to fulfil ITU regulations) and interoperability of the signals. It is important to note that the GPS L1C pilot and data signals are shown in quadrature in the figure although according to [GPS ICD-800, 2006] the final phasing is still open.

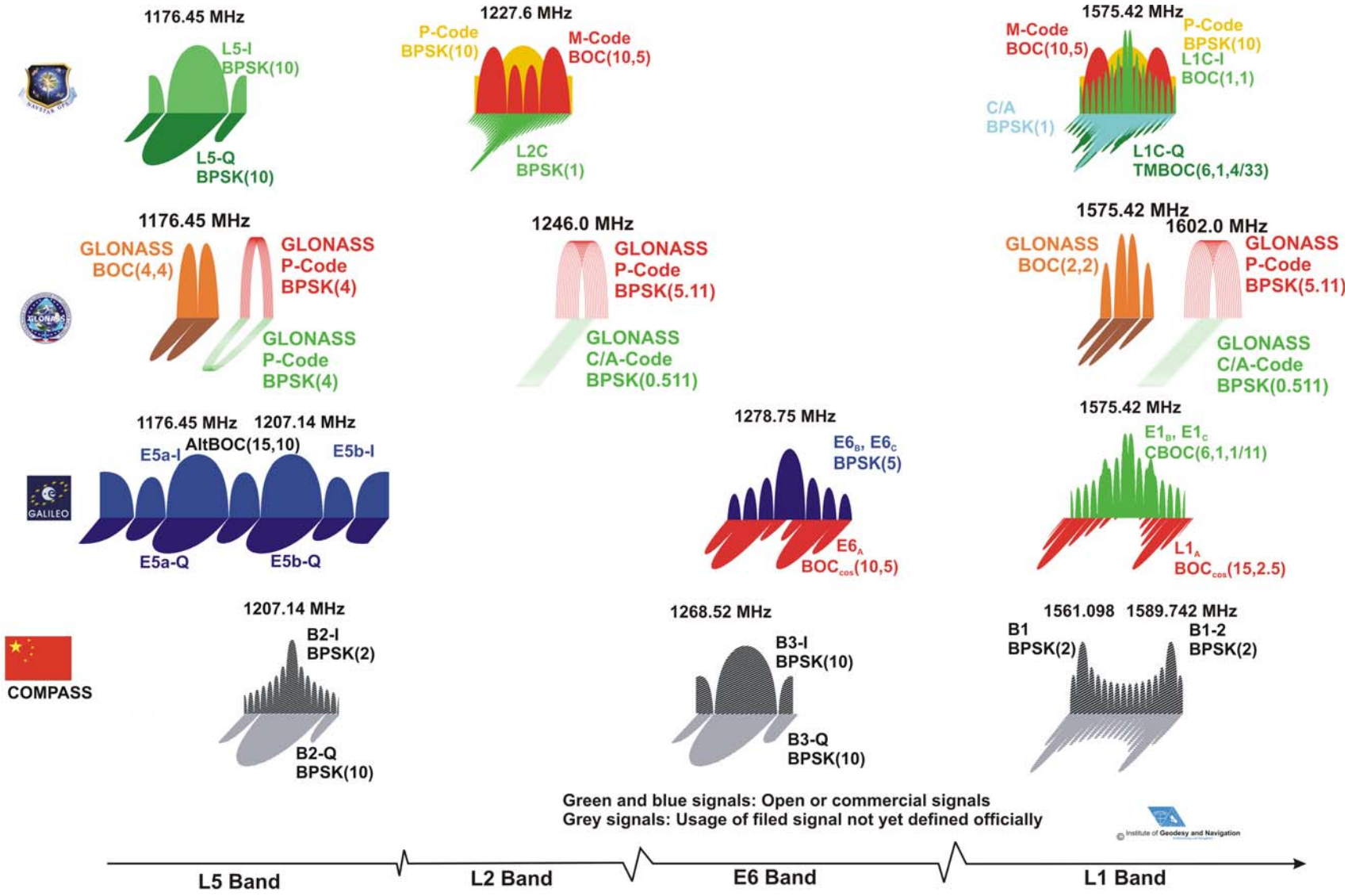

Figure 2.1. GPS, GLONASS, Galileo, and planned Compass signals (Courtesy of Stefan Wallner)

2.3 The Global Positioning System (GPS)

2.3.1 GPS System Overview

GPS is made up of a network of initially 24 active satellites placed into orbit by the U.S. Department of Defense. Although originally developed for military applications, the U.S. government made GPS available to civilians, transforming it into the dual-use system it is today. Accordingly, certain signal capabilities are reserved for U.S. and allied military applications while the civilian signals are open and free for worldwide use.

The GPS baseline constellation consists of 24 satellites (21 + 3 active spares) in six orbital positioned circular MEO planes at a nominal average orbit semi-major axis of 26559.7 km, and at an inclination of the orbital planes of 55 degrees with reference to the equatorial plane.

The first developmental satellites were launched beginning in 1978, and the first operational satellites went on orbit in 1989. The system reached initial operational capability (IOC) in 1993 and FOC, in 1995. The present GPS constellation exceeds the baseline constellation with 32 orbiting satellites after the last successful launch was on March 15th, 2008. The history of all GPS launches can be seen in Figure 2.2.

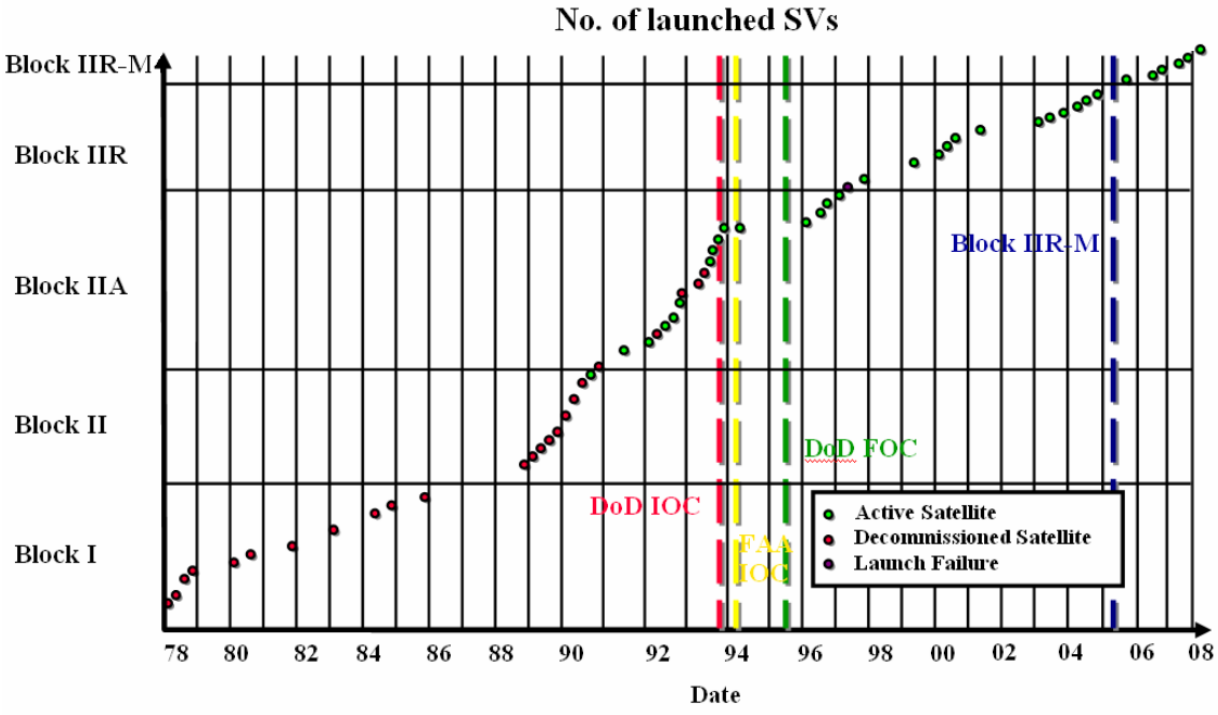

Figure 2.2. Launch History of GPS

2.3.2 GPS Signal Plan

2.3.2.1 GPS L1 Band

The GPS L1 band (1575.42 MHz) has turned to be the most important band for navigation purposes. Indeed most of the applications in the world nowadays are based on the signals transmitted at this frequency. As stated in [GPS ICD 200], three signals are transmitted at the moment by GPS in L1: C/A Code, P(Y) Code and M-Code. In the future, an additional new civil signal, known as L1C, will also be transmitted. We describe all of them in the next lines:

- The Coarse/Acquisition (C/A) code signal was primarily thought for acquisition of the P (or Y) code and has become nowadays the most important signal for mass market applications. The PRN C/A Code for SV ID number i is a Gold code, $G_i(t)$, of 1 millisecond in length at a chipping rate of 1.023 Mbps. The $G_i(t)$ sequence is a linear pattern generated by the Modulo-2 addition of two subsequences, G_1 and G_{2i}, each of them being a 1023 chip long linear pattern. The epochs of the Gold code are synchronized with the X_1 epochs of the P-code.
- The P Code is the precision signal and is coded by the precision code. Moreover the Y-Code is used in place of the P-code whenever the Anti-Spoofing (AS) mode of operation is activated as described in the ICDs 203, 224 and 225. The PRN P-code for SV number i is a ranging code, $P_i(t)$, 7 days long at a chipping rate of 10.23 Mbps. The 7 day sequence is the Modulo-2 sum of two sub-sequences referred to as X_1 and X_{2i} with 15,345,000 chips and 15,345,037 chips, respectively. The X_{2i} sequence is an X_2 sequence selectively delayed by 1 to 37 chips allowing the basic code generation technique to produce a set of 37 mutually exclusive P-code sequences 7 days long.
- The modernized military signal (M-Code) is designed exclusively for military use and is intended to eventually replace the P(Y) code [E. D. Kaplan and C. Hegarty, 2006]. The M-Code provides better jamming resistance than the P(Y) signal, primarily through enabling transmission at much higher power without interference with C/A code or P(Y) code receivers [B.C. Barker et al., 2000]. Moreover, the M-Code provides more robust signal acquisition than is achieved today, while offering better security in terms of exclusivity, authentication, and confidentiality, along with streamlined key distribution. In other aspects, the M-Code signal provides much better performance than the P(Y) Code and more flexibility.
- The L1 Civil signal (L1C), defined in the [GPS ICD-800, 2006], consists of two main components; one denoted L1C_P to represent the pilot signal, consisting of a time-multiplexing of BOC(1,1) and BOC(6,1), thus without any data message, and L1C_D, with a pure BOC(1,1), for the data channel. This is spread by a ranging code and modulated by a data message. The pilot channel L1C_P is also modulated by an SV unique overlay secondary code, L1C_O.

For more details on the code generation refer to the [GPS ICD 200] and [GPS ICD-800, 2006]. Finally, the technical characteristics of the existing and planned GPS signals in the L1 band are summarized in the following table.

Table 2.3. GPS L1 signal technical characteristics

GNSS System	GPS	GPS		GPS	GPS
Service Name	C/A	L1C		P(Y) Code	M-Code
Centre Frequency	1575.42 MHz	1575.42 MHz		1575.42 MHz	1575.42 MHz
Frequency Band	L1	L1		L1	L1
Access Technique	CDMA	CDMA		CDMA	CDMA
Signal Component	Data	Data	Pilot	Data	N.A.
Modulation	BPSK(1)	TMBOC(6,1,1/11)		BPSK(10)	$BOC_{sin}(10,5)$
Sub-carrier frequency [MHz]	-	1.023	1.023 & 6.138	-	10.23
Code frequency	1.023 MHz	1.023 MHz		10.23 MHz	5.115 MHz
Primary PRN Code length	1023	10230		$6.19 \cdot 10^{12}$	N.A.
Code Family	Gold Codes	Weil Codes		Combination and short-cycling of M-sequences	N.A.
Secondary PRN Code length	-	-	1800	-	N.A.
Data rate	50 bps / 50 sps	50 bps / 100 sps	-	50 bps / 50 sps	N.A.
Minimum Received Power [dBW]	-158.5	-157		-161.5	N.A.
Elevation	5°	5°		5°	5°

Of all the signals above, the C/A Code is the best known as most of the receivers that have been built until today are based on it. The C/A Code was open from the very beginning to all users, although until May 1st, 2000 an artificial degradation was introduced by means of the Select Availability (SA) mechanism which added an intentional distortion to degrade the positioning quality of the signal to non-desired users. As we have already mentioned, the C/A Code was thought to be an aid for the P(Y) Code (to realize a Coarse Acquisition). The M-Code is the last military signal that has been introduced in GPS.

For a long time different signal structures for the M-Code were under consideration [J.W. Betz, 2001] being the Manchester code signals (BPSK) and the binary offset carrier

(BOC) signals the two favoured candidates. Both solutions result from the modulation of a non-return to zero (NRZ) pseudo random noise spreading code by a square-wave sub-carrier. While the Manchester code has a spreading code of rate equal to that of the square-wave, the BOC signal does not necessarily have to be so, being the only constraint that the rate of the spreading code must be less than the sub-carrier frequency.

The interesting aspect about these signals is that, like the conventional sub-carrier modulation, the waveform presents a zero at the carrier frequency due to the square-wave sub-carrier. In fact, their split-power spectra clearly facilitate the compatibility of the GPS military M-Code signal with the existing C/A Code and P(Y) Code.

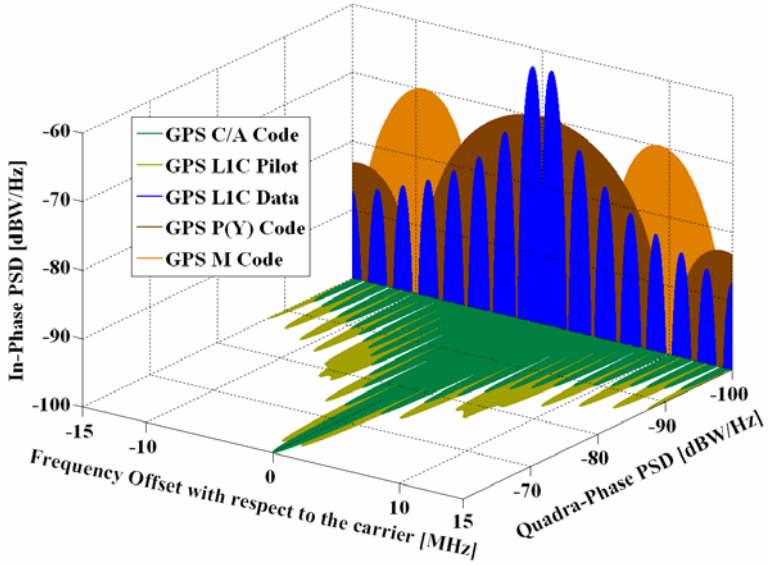

Figure 2.3. Spectra of GPS Signals in L1

It is important to note that although the GPS L1C pilot and data signals are shown in quadrature in the figure above, according to [GPS ICD-800, 2006] the final phasing is still to be decided. Furthermore, we can clearly recognize that GPS L1C concentrates more power at higher frequencies – due to BOC(6,1) – in the pilot channel than in the data channel. This will be described in detail in chapter 4.7.4

Finally, it is important to note that for all the figures next the commonly used expressions for bandwidths in MHz must be understood as multiplied by the factor 1.023. Thus BPSK(10) refers in reality to a BPSK signal with a chip rate of 10.23 MHz. This remains valid for all the bandwidths in this thesis, unless different stated.

2.3.2.2 GPS L2 Band

GPS is transmitting in the L2 band (1227.60 MHz) a modernized civil signal known as L2C together with the P(Y) Code and the M-Code. The P(Y) Code and M-Code were already described shortly in the previous chapter and the properties and parameters are thus similar to

those in the L1 band. In addition, for Block IIR-M, IIF, and subsequent blocks of SVs, two additional PRN ranging codes will be transmitted. They are the L2 Civil Moderate (L2 CM) code and the L2 Civil Long (L2 CL) code. These two signals are time multiplexed so that the resulting chipping rate is double as high as that of each individual signal. We further describe them in the next lines more in detail:

- L2 CM Code is transmitted in the IIR-M, IIF, and subsequent blocks. The PRN L2 CM Code for SV number *i* is a ranging code, $CM_i(t)$, which is 20 milliseconds in length at a chipping rate of 511.5 Kbps. The epochs of the L2 CM Code are synchronized with the X_1 epochs of the P-code. The $CM_i(t)$ sequence is a linear pattern which is short cycled every count period of 10,230 chips by resetting with a particular initial state. Furthermore, for Block IIR-M, the navigation data is also Modulo-2 added to the L2 CM Code. It is interesting to note that the navigation data can be used in one of two different data rates selectable by ground command:
  - $D(t)$ with a data rate of 50 bps
  - $D(t)$ with a symbol rate of 50 symbols per second (sps) which is obtained by encoding $D(t)$ with a data rate of 25 bps coded in a rate 1/2 convolutional code. Finally, the resultant bit-train is combined with the L2 CL Code using time-division multiplexing.
- L2 CL Code is transmitted in the IIR-M, IIF, and subsequent blocks. The PRN L2 CL Code for SV number *i* is a ranging code, $CL_i(t)$, which is 1.5 seconds in length at a chipping rate of 511.5 Kbps. The epochs of the L2 CL Code are synchronized with the X_1 epochs of the P Code. The $CL_i(t)$ sequence is a linear pattern which is generated using the same code generator polynomial as of $CM_i(t)$. However, the $CL_i(t)$ sequence is short cycled by resetting with an initial state every count period of 767,250 chips.

Finally, it is important to note that the GPS L2 band will have a transition period from the C/A Code to L2C and mixed configurations could occur. Next figure shows the baseband L2 signal generation scheme. As we can recognize, although the chipping rate of the L2 CM and L2 CL signals is of 511.5 Kbps individually, after the time multiplexing the composite signal results in a stream of 1.023 MHz.

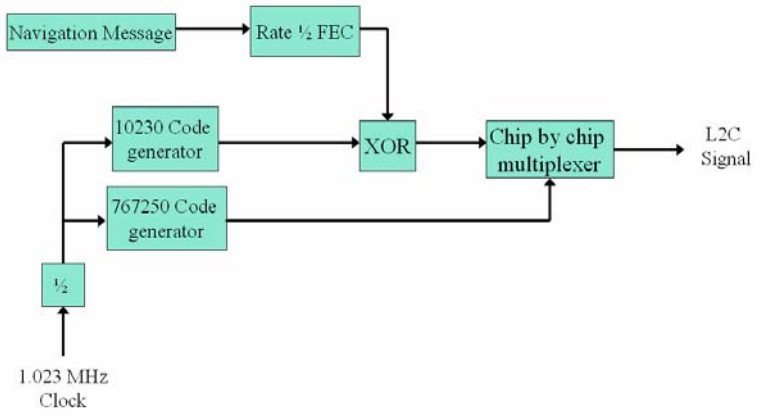

Figure 2.4. Modulation scheme for the GPS L2 Signals

The technical characteristics of the GPS L2 signals are summarized next:

Table 2.4. GPS L2 signal technical characteristics

GNSS System	GPS	GPS	GPS	GPS
Service Name	L2 CM	L2 CL	P(Y) Code	M-Code
Centre Frequency	1227.60 MHz	1227.60 MHz	1227.60 MHz	1227.60 MHz
Frequency Band	L2	L2	L2	L2
Access Technique	CDMA	CDMA	CDMA	CDMA
Spreading modulation	BPSK(1) result of multiplexing 2 streams at 511.5 kHz		BPSK(10)	$BOC_{sin}(10,5)$
Sub-carrier frequency	-	-	-	10.23 MHz
Code frequency	511.5 kHz	511.5 kHz	10.23 MHz	5.115 MHz
Signal Component	Data	Pilot	Data	N.A.
Primary PRN Code length	10,230 (20 ms)	767,250 (1.5 seconds)	6.19×10^{12}	N.A.
Code Family	M-sequence from a maximal polynomial of degree 27		Combination and short-cycling of M-sequences	N.A.
Secondary PRN Code length	-	-	-	N.A.
Data rate	IIF 50 bps / 50 sps IIR-M Also 25 bps 50 sps with FEC	-	50 bps / 50 sps	N.A.
Minimum Received Power [dBW]	II/IIA/IIR -164.5 dBW IIR-M -161.5 dBW IIF -161.5 dBW		II/IIA/IIR -164.5 dBW IIR-M -161.4 dBW IIF -160.0 dBW	N.A.
Elevation	5°		5°	5°

The spectra of the different signals described in the preceding lines are shown in the next figure:

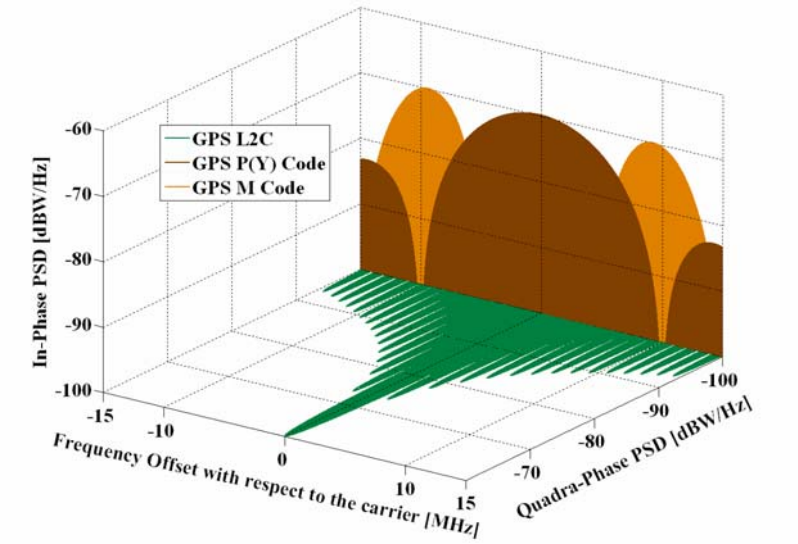

Figure 2.5. Spectra of the GPS Signals in L2

2.3.2.3 GPS L5 Band

The GPS L5 (1176.45 MHz) signal will be transmitted for the first time on board IIF satellites. The GPS carriers of the L5 band are modulated by two bit trains in phase quadrature: the L5 data channel and the L5 pilot channel. Moreover, two PRN ranging codes are transmitted on L5: the in-phase code (denoted as the I_5-code) and the quadraphase code (denoted as the Q_5-code). The PRN L5-codes for SV number i are independent, but time synchronized ranging codes $X_I^i(t)$ and $X_Q^i(t)$, of 1 millisecond in length at a chipping rate of 10.23 Mbps [GPS ICD-705, 2005]. For each code, the 1-millisecond sequences are the modulo-2 sum of two sub-sequences referred to as X_A and X_{Bi} with lengths of 8,190 chips and 8,191 chips respectively, which restart to generate the 10,230 chip code. The X_{Bi} sequence is selectively delayed, thereby allowing the basic code generation technique to produce the different satellite codes.

The generation scheme can be shown graphically as follows:

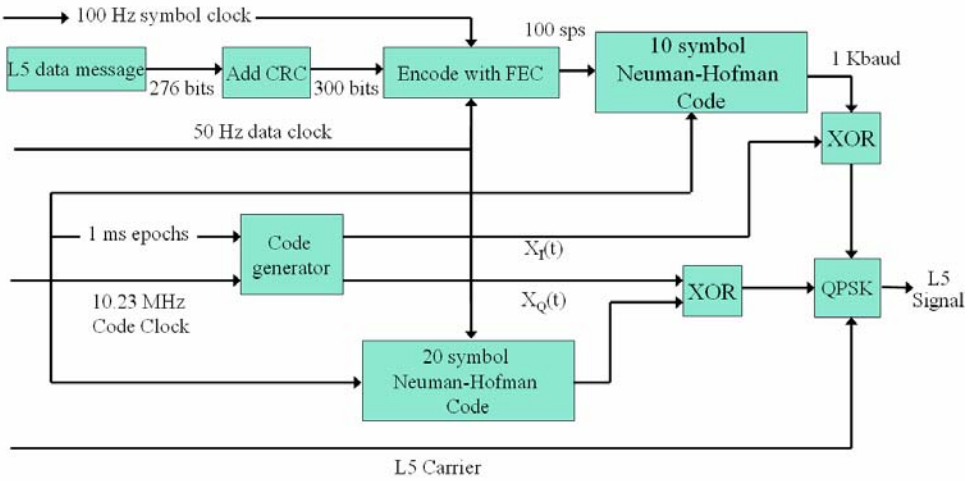

Figure 2.6. Modulation scheme for the GPS L5 signals

For more details on L5, refer to [E. D. Kaplan and C. Hegarty, 2006]. The different signals present the following spectrum:

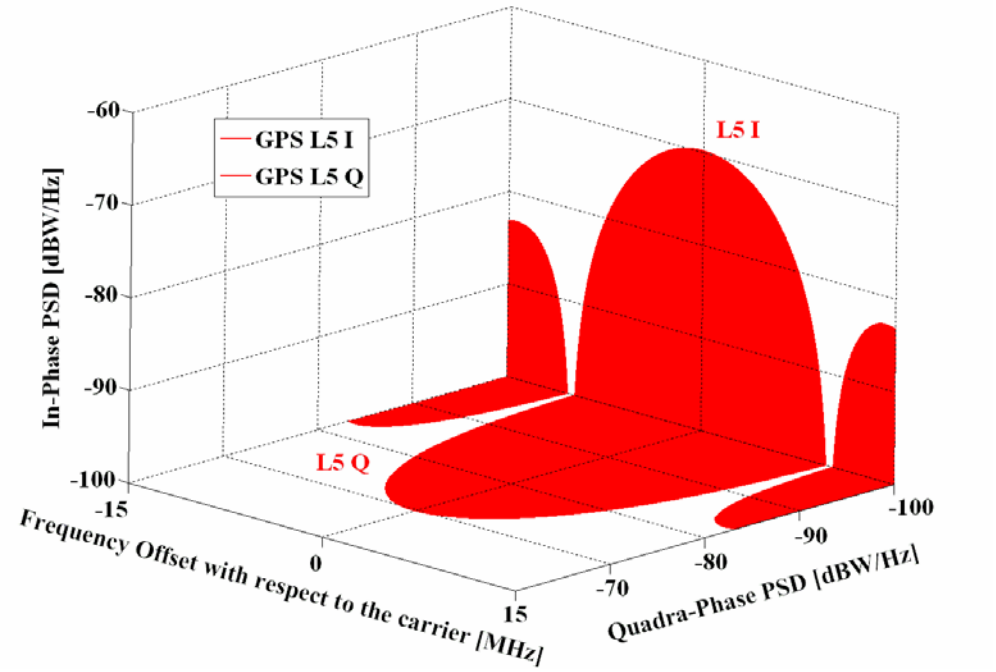

Figure 2.7. Spectra of GPS Signals in L5

To conclude, the technical characteristics of the GPS signals in L5 can be summarized as follows:

Table 2.5. GPS L5 signal technical characteristics

GNSS System	GPS	GPS
Service Name	L5 I	L5 Q
Centre Frequency	1176.45 MHz	1176.45 MHz
Frequency Band	L5	L5
Access Technique	CDMA	CDMA
Spreading modulation	BPSK(10)	BPSK(10)
Sub-carrier frequency	-	-
Code frequency	10.23 MHz	10.23 MHz
Signal Component	Data	Pilot
Primary PRN Code length	10230	10230
Code Family	Combination and short-cycling of M-sequences	
Secondary PRN Code length	10	20
Data rate	50 bps / 100 sps	-
Minimum Received Power [dBW]	-157.9 dBW	-157.9 dBW
Elevation	5°	5°

2.3.3 GPS Modernization

Before December 2005 the basic GPS capability consisted of the Standard Positioning Service (SPS) provided by the C/A Code on the L1 frequency and the Precise Positioning Service (PPS) provided by the P(Y) Code on L1 and L2. Although those services are of relatively good quality, the United States envisaged modernizing the signals in order to improve the quality and protection of both civil and military users. To that objective, the following GPS Modernization plan was proposed. This can be timely divided in the following three blocks:

- **Block IIR-M (Replenishment-Modernized) satellites.** This generation of spacecraft has introduced a second civil signal with improved services (L2C) and is planning to reach the 24-satellite FOC around 2012. Additionally, for military purposes the modernized M-Code — BOC(10,5) — will be placed on L1 and L2 signals. Block IIR-M satellites also have antijam flex power capabilities for military needs. More details on the planned signal plan can be found in Figure 2.1. The first operational IIR-M satellite was launched on December 16th, 2005 and the last on March 15th, 2008.

- **Block IIF (Follow-on) satellites.** With the design of GPS Block IIF, the American navigation system has undergone an important transformation that has finally redefined GPS from a military service with the guarantee of civil use to a true dual service [P.A. Dafesh et al., 1999a]. Indeed, what started as a modest upgrade to introduce a new civil frequency quickly evolved into a complement of new signals for enhanced military and civil use. The culmination of this transformation will be GPS Block III. The third civil signal (L5), namely BPSK(10), will begin with the IIF satellites and the FOC with 24 satellites is expected to be reached around 2015.

- **Block III** is still in the design phase. GPS Block III includes prospective improvements to both the ground and space segments. These will most likely include increased anti-jam power, increased security, increased accuracy, navigation surety, backward compatibility, assured availability, system survivability, and controlled integrity among other improvements. The fourth civil signal (L1C) will also be introduced with this block. In the 2004 GNSS cooperation Agreement between the United States and the European Union, the two parties agreed to have BOC(1,1) as the baseline waveform on both the GPS L1C and Galileo E1 Open Service (OS) signals. Nevertheless, a group of experts from Working Group A set up under the 2004 Agreement proposed to optimize this signal using MBOC(6,1,1/11) as shown in [G.W. Hein et al., 2006a] and [G.W. Hein et al., 2006b]. Although an earlier schedule is under consideration, the first Block III satellite launch will probably occur somewhere around 2014 with FOC being reached by about 2020.

2.4 Galileo

2.4.1 Galileo System Overview

Galileo is the European global navigation satellite system (ENSS) and provides a highly accurate, guaranteed global positioning service under civilian control. According to [Galileo SIS ICD, 2008], the system will be interoperable with GPS and — at least to some extent, excluding the real-time high-precision part — with GLONASS, the two global satellite navigation systems available today.

The fully deployed Galileo system will consist of 30 satellites (27 operational + 3 non-active spares), positioned in three circular MEO planes at a nominal average orbit semi-major axis of 29,601.297 kilometres, and at an inclination of the orbital planes of 56 degrees with reference to the equatorial plane. Once FOC is achieved, the Galileo navigation signals will provide good coverage even at latitudes up to 75 degrees north and 75 degrees south. Galileo provides enhanced distress localization and call features for the provision of a Search And Rescue (SAR) service interoperable with the COSPAS-SARSAT system.

Figure 2.8. Galileo Space Segment [Figure from ESA Website]

The Galileo orbit altitude results in a repeat cycle of ten sidereal days during which each satellite completes seventeen revolutions. Indeed this repetition period of seventeen revolutions was chosen because simulation analyses showed that with seventeen terms to represent the series of the gravitational field satisfactory results were obtained. In order to avoid the gravitational resonance associated with a 12 hour orbital period as it is the case of GPS, the Galileo satellites will have an altitude approximately 3000 km higher than that of GPS. The relatively short repeat period is convenient for mission planning purposes. The constellation lifetime is of 20 years, while the Galileo satellites have a design lifetime of 12 years [R. Zandbergen et al., 2004] and [R. Piriz et al., 2005].

The European GNSS approach began with the European Geostationary Navigation Overlay Service (EGNOS), which provides civil complements to GPS since mid-2005 in its initial operation. From the very beginning, EGNOS was meant to be the bridge to Europe's own full-fledged GNSS. Galileo's first developmental satellites, GIOVE-A and GIOVE-B, were launched in December 2005 and April 2008 respectively. The Galileo In-Orbit Validation (IOV) phase is planned to start at the end of 2008 with four satellites and FOC should be achieved end of 2013. Furthermore, diverse options are being considered to launch the Galileo satellites including Ariane 5, Proton, Soyuz or Zenit rockets.

2.4.2 Galileo Signal Plan

2.4.2.1 Galileo E1 Band

The E1 Open Service (OS) modulation receives the name of CBOC (Composite Binary Offset Carrier) and is a particular implementation of MBOC (Multiplexed BOC) [J.-A. Avila-Rodriguez et al., 2007]. This signal will be explained in detail in chapter 4.7. MBOC(6,1,1/11) is the result of multiplexing a wideband signal – BOC(6,1) – with a narrowband signal – BOC(1,1) – in such a way that 1/11 of the power is allocated, in average, to the high frequency component. This signal was the last one to be defined.

The normalized (unit power) power spectral density, specified without the effect of band-limiting filters and payload imperfections, is given by

$$G_{\mathrm{MBOC}(6,1,1/11)}(f) = \frac{10}{11} G_{\mathrm{BOC}(1,1)}(f) + \frac{1}{11} G_{\mathrm{BOC}(6,1)}(f) \tag{2.1}$$

As shown in [Galileo SIS ICD, 2008], the generic view of the E1 Open Service signal generation can be depicted as follows [J.-A. Avila-Rodriguez et al., 2007]:

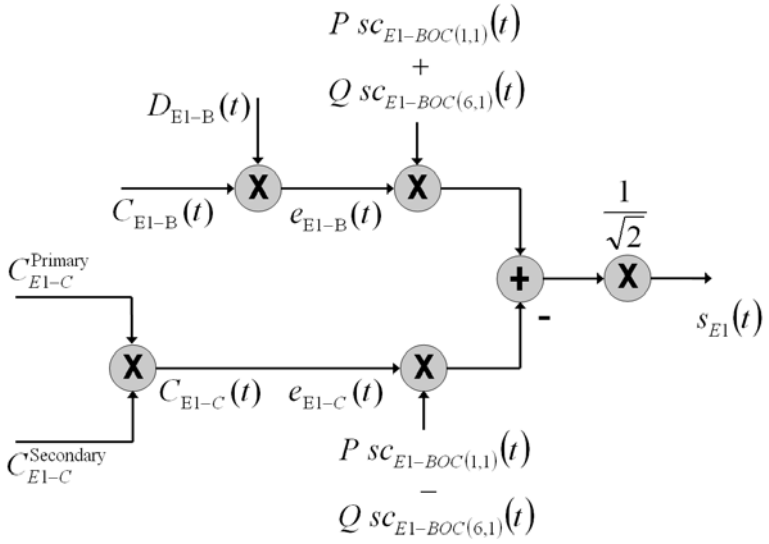

Figure 2.9. Modulation Scheme for the Galileo E1 OS Signals

The whole transmitted Galileo E1 signal consists of the multiplexing of the three following components:

- The E1 Open Service Data channel $e_{\text{E1-B}}(t)$ is generated from the I/NAV navigation data stream $D_{\text{E1-B}}(t)$ and the ranging code $C_{\text{E1-B}}(t)$, which are then modulated with the sub-carriers $sc_{\text{E1-BOC(1,1)}}(t)$ and $sc_{\text{E1-BOC(6,1)}}(t)$ of BOC(1,1) and BOC(6,1) respectively.
- The E1 Open Service Pilot channel $e_{\text{E1-C}}(t)$ is generated from the ranging code $C_{\text{E1-C}}(t)$, including its secondary code, which is then modulated with the sub-carriers $sc_{\text{E1-BOC(1,1)}}(t)$ and $sc_{\text{E1-BOC(6,1)}}(t)$ in anti-phase.
- The E1 PRS channel, also denoted as E1-A, which results from the modulo-two addition (respectively product if we consider the physical bipolar representation of the signal) of the PRS data stream $D_{\text{PRS}}(t)$, the PRS code sequence $C_{\text{PRS}}(t)$ and the sub-carrier $sc_{\text{PRS}}(t)$. This sub-carrier consists of a BOC(15,2.5) in cosine phasing.

For more details on the mathematical definition of the signal refer to chapter 7.7.8 where it is described more in detail.

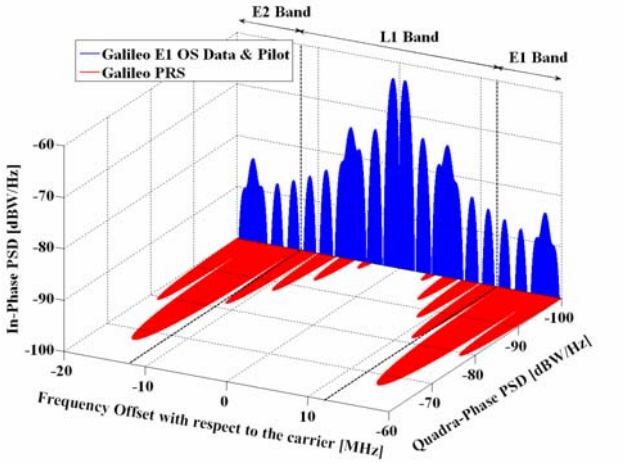

Figure 2.10. Spectra of Galileo Signals in E1

It is interesting to see how the spectra of the two systems described so far in E1/L1 overlap:

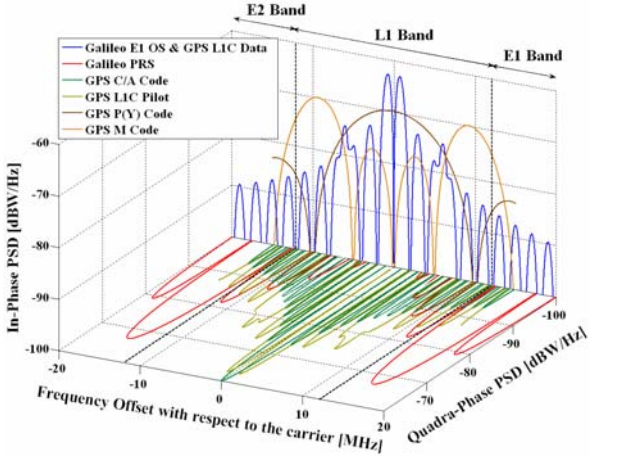

Figure 2.11. Spectra of GPS and Galileo Signals in L1

It is important to note that the GPS L1C pilot and data signals are shown in quadrature in the figure although according to [GPS ICD-800, 2006] the final phasing is still open. Furthermore it is important to recall that for a long time the actual E1 band received the name of L1 band in analogy with GPS and it was not until the publication of the [Galileo SIS ICD, 2008] that L1 changed to the current E1.

The E1 Open Service (OS) codes are, as well as the E6 CS codes that we will see later, also random memory codes. The plain number of choices to set the 0's and 1's for the whole code family is enormous and thus special algorithms have to be applied to generate random codes efficiently [J.-A. Avila-Rodriguez et al., 2007].

Finally, the technical characteristics of all the Galileo signals in E1 can be summarized in the following table:

Table 2.6. Galileo E1 signal technical characteristics

GNSS System	Galileo	Galileo	Galileo
Service Name	E1 OS		PRS
Centre Frequency	1575.42 MHz		
Frequency Band	E1		
Access Technique	CDMA		
Spreading modulation	CBOC(6,1,1/11)		$BOC_{cos}(15,2.5)$
Sub-carrier frequency	1.023 MHz and 6.138 (Two sub-carriers)		15.345 MHz
Code frequency	1.023 MHz		2.5575 MHz
Signal Component	Data	Pilot	Data
Primary PRN Code length	4092		N/A
Code Family	Random Codes		N/A
Secondary PRN Code length	-	25	N/A
Data rate	250 sps	-	N/A
Minimum Received Power [dBW]	-157		N/A
Elevation	10°		N/A

2.4.2.2 Galileo E6 Band

As shown in [Galileo SIS ICD, 2008], the transmitted Galileo E6 signal consists of the following three components:

- The E6 Commercial Service (CS) *data* channel: this modulating signal is the modulo-two addition of the E6 CS navigation data stream $D_{\mathrm{CS}}(t)$ with the CS data channel code sequence $C_{\mathrm{CS}}^{D}(t)$. This last one is already modulated by a BPSK(5) at 5.115 MHz.
- The E6 Commercial Service (CS) *pilot* channel: this modulating signal is the modulo-two addition of the E6 CS pilot channel code $C_{\mathrm{CS}}^{P}(t)$ with a BPSK(5) at 5.115 MHz.
- Finally, the E6 PRS channel is the modulo-two addition of the E6 PRS navigation data stream $D_{\mathrm{PRS}}(t)$ with the PRS channel code sequence $C_{\mathrm{PRS}}(t)$ at 5.115 MHz. This signal is further modulated by a sub-carrier of 10.23 MHz in cosine phasing.

This is graphically shown as follows:

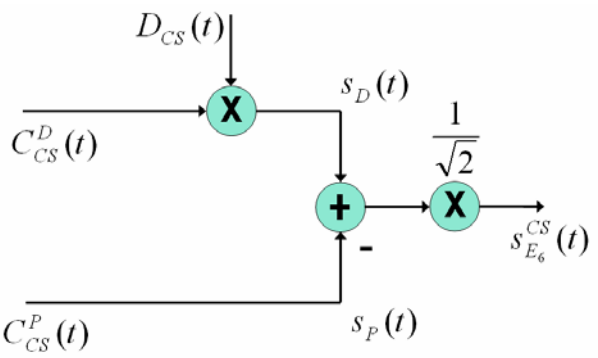

Figure 2.12. Modulation Scheme for the Galileo E6 Signals

Moreover, the spectrum of the different E6 signals is shown to be as follows:

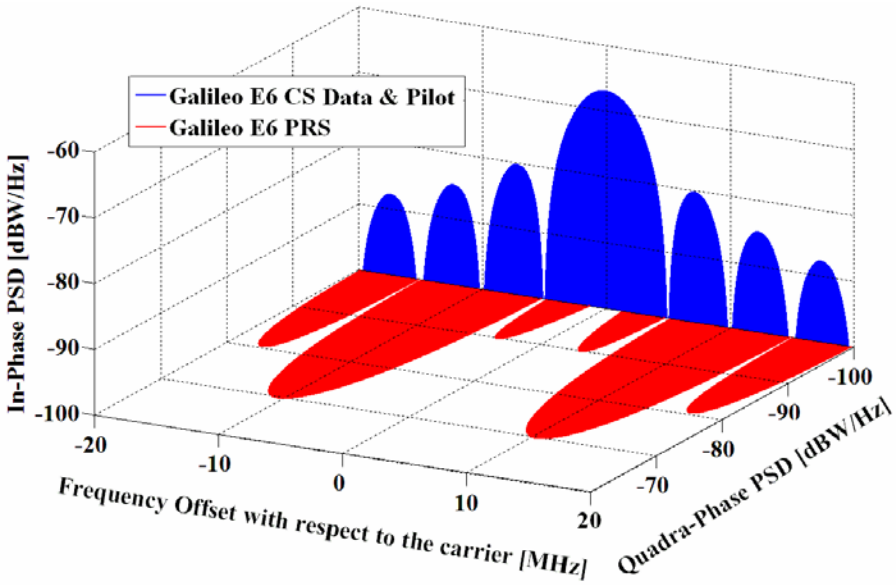

Figure 2.13. Spectra of Galileo Signals in E6

The E6 Commercial Service (CS) codes are *random* codes [J. Winkel, 2006]. The main idea behind is to generate a family of codes that fulfils the properties of randomness as well as possible [J.-A. Avila-Rodriguez et al., 2007]. The codes can be driven to fulfil special properties such as balance and weakened balance, where the probability of 0's and 1's must not be identical but within a well-defined range, or to realize the autocorrelation side-lobe zero (ASZ) property. This latter property guarantees that the autocorrelation values of every code correlate to zero with a delayed version of itself, shifted by one chip.

Table 2.7. Galileo E6 signal technical characteristics

GNSS System	Galileo	Galileo	Galileo
Service Name	E6 CS data	E6 CS pilot	E6 PRS
Centre Frequency	1278.75 MHz		
Frequency Band	E6		
Access Technique	CDMA		
Spreading modulation	BPSK(5)	BPSK(5)	$BOC_{cos}(10,5)$
Sub-carrier frequency	-	-	10.23 MHz
Code frequency	5.115 MHz		
Signal Component	Data	Pilot	Data
Primary PRN Code length	5115	5115	N/A
Code Family	Memory codes		N/A
Secondary PRN Code length	-	100	N/A
Data rate	1000 sps	-	N/A
Minimum Received Power [dBW]	-155		N/A
Elevation	10°		N/A

2.4.2.3 Galileo E5 Band

The different Galileo E5 signal components are generated according to the following [Galileo SIS ICD, 2008]:

- The E5a *data* channel: This channel is the modulo-two addition of the E5a navigation data stream $D_{E5a}(t)$ with the E5a data channel PRN code sequence $C^{D}_{E5a}(t)$ of chipping rate 10.23 MHz.
- The E5a *pilot* channel: This channel is the E5a pilot channel PRN code sequence $C^{P}_{E5a}(t)$ of chipping rate 10.23 MHz.
- The E5b *data* channel: This channel is the modulo-two addition of the E5b navigation data stream $D_{E5b}(t)$ with the E5b data channel PRN code sequence $C^{D}_{E5b}(t)$ of chipping rate 10.23 MHz.
- The E5b *pilot* channel: This channel is the E5b pilot channel PRN code sequence $C^{P}_{E5b}(t)$ of chipping rate 10.23 MHz.

The E5 modulation receives the name of AltBOC and is a modified version of a Binary Offset Carrier (BOC) with code rate of 10.23 MHz and a sub-carrier frequency of 15.345 MHz. AltBOC(15,10) is a wideband signal that is transmitted at 1191.795 MHz. More details on the mathematical definition will be given in chapter 4.8.1. Next figure shows the Galileo E5 signal modulation diagram:

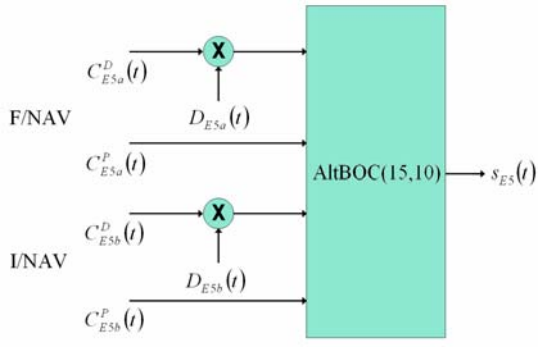

Figure 2.14. Modulation Scheme for the Galileo E5 Signals

The power spectral density for the modified AltBOC(15,10) modulation with constant envelope is shown to adopt the form:

$$G_{\text{AltBOC}}(f) = \frac{4f_c}{\pi^2 f^2} \frac{\cos^2\left(\frac{\pi f}{f_c}\right)}{\cos^2\left(\frac{\pi f}{2f_s}\right)} \left[\cos^2\left(\frac{\pi f}{2f_s}\right) - \cos\left(\frac{\pi f}{2f_s}\right) - 2\cos\left(\frac{\pi f}{2f_s}\right)\cos\left(\frac{\pi f}{4f_s}\right) + 2\right] \tag{2.2}$$

adopting the spectrum of the E5 signal modulation the following form:

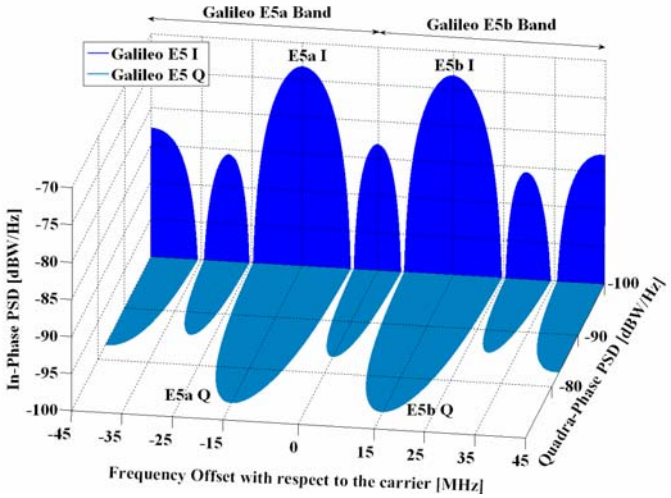

Figure 2.15. Spectra of Galileo Signals in E5

which was generated following the theory of chapter 4.8.1 and Appendix I. As we can recognize from the figure above, the AltBOC(15,10) modulation is very similar to two BPSK(10) signals shifted by 15 MHz to the left and right of the carrier frequency. Indeed, since to acquire all the main lobes of the modulation a very wide bandwidth is necessary, many receivers will operate correlating the AltBOC signal with a BPSK(10) replica.

To have a better feeling about the overlapping between GPS and Galileo in E5, the next figure shows all the signals described so far for this band.

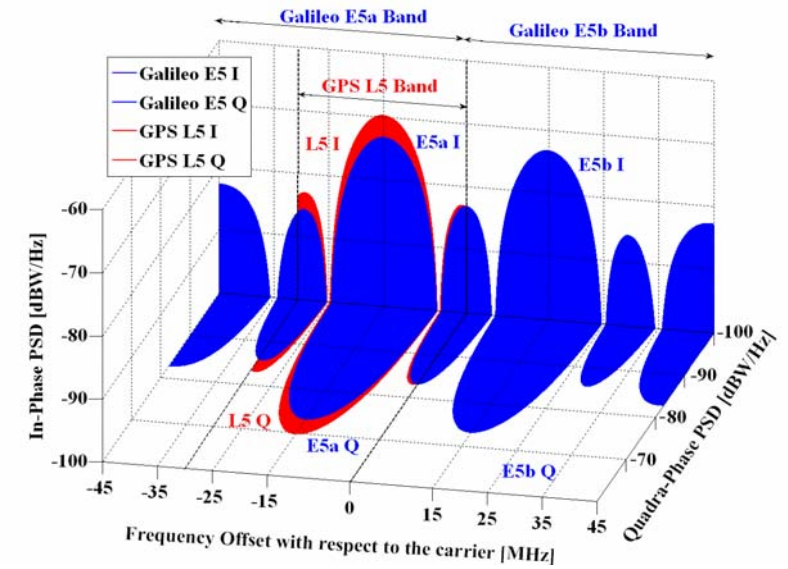

Figure 2.16. Spectra of GPS and Galileo Signals in E5

The E5 primary codes can be generated with shift registers. Indeed, the outputs of two parallel registers are modulo-two added to generate the primary codes. For more details on the start values of the primary codes and the corresponding secondary codes of each satellite, refer to [Galileo SIS ICD, 2008]. Finally, some details on the technical characteristics of the E5 signal are presented.

Table 2.8. Galileo E5 signal technical characteristics

GNSS System	Galileo	Galileo	Galileo	Galileo
Service Name	E5a data	E5a pilot	E5b data	E5b pilot
Centre Frequency	1191.795 MHz			
Frequency Band	E5			
Access Technique	CDMA			
Spreading modulation	AltBOC(15,10)			
Sub-carrier frequency	15.345 MHz			
Code frequency	10.23 MHz			
Signal Component	Data	Pilot	Data	Pilot
Primary PRN Code length	10230			
Code Family	Combination and short-cycling of M-sequences			
Secondary PRN Code length	20	100	4	100
Data rate	50 sps	-	250 sps	-
Minimum Received Power [dBW]	-155 dBW		-155 dBW	
Elevation	10°		10°	

2.4.2.4 Galileo Services

The Galileo signals will be assigned to provide the service categories which are summarized in the following Table [J.-A. Avila-Rodriguez et al., 2008].

Table 2.9. Galileo Services mapped to signals

Id	OS	SoL	CS	PRS	SAR
E5a					
E5b					
$E6_A$					
$E6_{B,C}$					
L6					
$E1_A$					
$E1_{B,C}$					

2.4.2.4.1 Open Service (OS)

The single-frequency (SF) OS will be provided by each of the three signals: E1, E5a and E5b. The dual-frequency (DF) OS will be provided by the dual-frequency signal combinations E1(B&C) - E5a and E1(B&C) - E5b

2.4.2.4.2 Commercial Service (CS)

The CS will be provided by the E6 (B&C) signal plus the OS signals – E1 (B&C), E5a and E5b. The E6 (B&C) signal contains the value-added data and it is combined with OS signals for improved performance.

2.4.2.4.3 Safety of Life (SoL)

The mono-frequency SoL will be provided by each of the two signals: E1(B&C) and E5b. The dual-frequency SoL will be provided by the following dual-frequency signal combination: E1(B&C) - E5b. It has to be noted that the Galileo Safety of Life frequencies are in Aeronautical Radio-Navigation Service (ARNS) bands allocated for GNSS. The integrity broadcast and the protection provided in the ARNS bands are two important features of the Galileo SoL. A third important added value provided by Galileo to safety critical operations is the frequency diversity offered by E1, E5a and E5b ARNS Galileo bands. Assuming combined E1, E5a and E5b receivers and using a probabilistic theory related to involuntary jamming of GNSS receivers, it has been shown that the probability of losing the dual frequency navigation function has been assessed and computed to be approximately 15,000 times lower in the case where a tri-frequency single system receiver is used instead of a dual-frequency single system receiver, making this event an improbable case. This result is particularly important for safety of life applications, such as civil aviation. Therefore, frequency diversity has an enormous potential as a simple interference mitigation means [J.-A. Avila-Rodriguez et al., 2007].

2.4.2.4.4 Public Regulated Service (PRS)

The PRS service will be provided by the E1-A and E6-A signals. These will use encrypted ranging codes, navigation data and sub-carriers improving signal processing performances.

2.4.2.4.5 Search And Rescue Service (SAR)

The SAR distress messages will be detected by the Galileo satellites in the 406-406.1 MHz band and then broadcasted to the dedicated receiving ground stations in the 1544-1545 MHz band, called L6 (below the E2 navigation band and reserved for the emergency services). The SAR data transmitted from SAR operators to distress emitting beacons will be used for alert acknowledgement of distress alerts and coordination of rescue teams. The data will be embedded in the OS data of the signal transmitted in the E1 carrier frequency

2.4.2.5 Galileo C-band

The Radio-Navigation Satellite Service (RNSS) portion of the RF spectrum is overcrowded. This is especially true on the E1/L1 band. Nevertheless even those bands that have not been used yet will certainly be shared by many systems in the near future. Thus, the search of other free frequency resources is something that will occur with a high probability in the next years.

During the World Radio Conference 2000 (WRC-2000), the Galileo program obtained authorization to use C-band frequencies between 5010 and 5030 MHz. At the time, a dedicated portion of the C-band was assigned for Radio-Navigation, but technical complexities made it impossible for the first generation of Galileo.

Indeed, phase noise problems, the higher free space attenuation (related to the use of omni directional antennae) and the strong signal attenuation due to rain made all the proposed solutions not adequate for the first Galileo constellation. However, in some decades things could have changed and C-band could be a real alternative. As suggested in [G.W. Hein et al., 2007b] and [G.W. Hein et al., 2007c], the C-band could be reserved for military/governmental applications leaving the L-band alone for civil users. This would have interesting benefits to both types of user and consequences as depicted in that article.

2.4.3 Galileo Modernization

Galileo is not yet in operation but already the so-called evolution program for the second generation has started end of 2007. Galileo II could arrive somewhere around 2020 and is expected to introduce new modernization elements analogous to the steps made by its counterparts GPS and GLONASS. Inter-Satellite Links (ISL) could be introduced at that time and aeronautical certification could be of relevance. In fact, under current plans only the first phase of Galileo – EGNOS – will be certified for aeronautical users.

2.5 GLONASS

2.5.1 GLONASS System Overview

The GLObal NAvigation Satellite System (GLONASS – ГЛОНАСС: ГЛОбальная НАвигационная Спутниковая Система) is the Russian navigation satellite system and, like GPS, it defines itself as a dual-use system. It is operated for the Russian Federation government by the Russian Space Forces. The system is governed by the Coordination Scientific Information Centre of the Ministry of Defense of the Russian Federation. Since some years the responsibility for GLONASS has been nominally delegated to Roscosmos, with funding coming from both Ministry of Defense and space agency budgets. When GLONASS was at peak efficiency it offered a standard – Coarse-Acquisition or "C/A" – positioning and timing service for civil users and a more accurate signal – Precision or "P Code" – available for Russian military use. The first three test satellites were placed in orbit in October 1982 with the first operational satellite entering service in December 1983. First plans aimed at making the system operational in 1991 but it was not until September 24th, 1993 that the system was finally announced to enter operation.

The GLONASS ground segment is entirely located within the former Soviet Union territory, thus regionally, unlike for GPS and Galileo where it is spread all over the world. As a consequence, GLONASS presents an inferior performance in the stability and predictability of the satellite orbits. The Ground Control Centre and Time Standards are located in Moscow and the telemetry and tracking stations are in Saint Petersburg, Ternopol, Eniseisk and Komsomolsk-na-Amure.

The GLONASS nominal constellation is composed of 24 satellites in three orbital planes with ascending nodes 120 degrees apart. Of the 24 satellites, 21 are active while the other three, one in each plane, are spare satellites. In each plane, the eight satellites are equally spaced with argument of latitude displacement of 45 degrees. Each of the satellites is identified by a slot number, which defines the corresponding orbital plane and the location within the plane: 1-8 for the first plane, 9-16 for the second place and 17-24 for the third plane. The orbital planes have 15-degree argument of latitude displacement relative to each other.

The satellites operate in circular orbits of 19,100 kilometres (25,440 km semi-major axis) at an inclination of 64.8 degrees, and each satellite completes the orbit in approximately 11 hours 15 minutes. The satellite orbit repeats thus after approximately 8 days and since each plane contains 8 satellites there is a non-identical repeat after one sidereal day (not to confuse with the GPS sidereal day, which is different). The spacing of the satellites allows for continuous and global coverage of the terrestrial surface and the near-earth space, so that a minimum of 5 satellites are in view at any given time.

As shown in Figure 2.17, the current GLONASS status is far away from its nominal numbers and as of May 9th, 2008, only 14 active GLONASS satellites are transmitting from space (these are green in the figure). Two additional spacecraft are on orbit but have been temporarily switched off and are currently in maintenance (in yellow in the figure). However, in September and November 2008, Russia plans to conduct triple launches of modernized GLONASS satellites (GLONASS-M). If successful, that could ensure the envisaged completion of an 18-spacecraft constellation comprising all GLONASS-M satellites by the end of 2008.

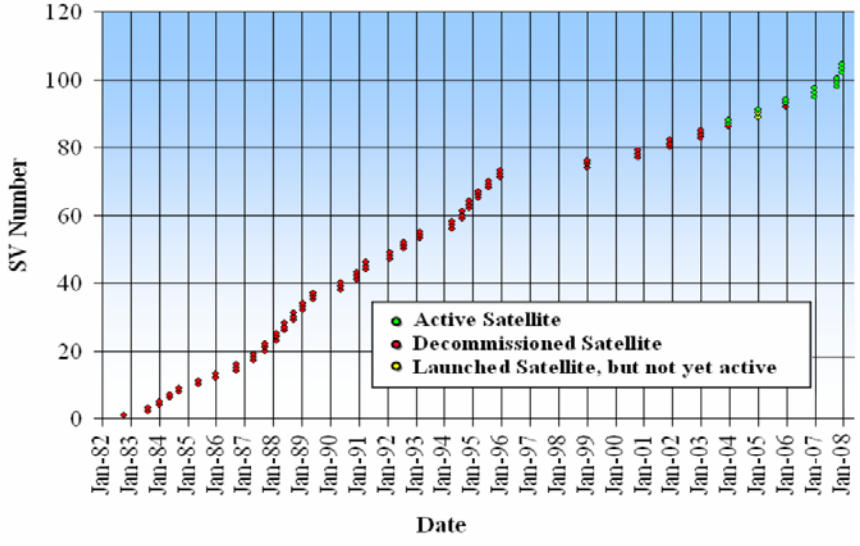

Figure 2.17. Launch History of GLONASS

The initial GLONASS Program Budget of 2001 was arranged for reaching FOC in 2011. However the GLONASS program is speeding up on its course in accordance with a presidential directive issued January 18th, 2006. The new ambitious modernization plans of GLONASS envisioned the achievement of minimal operational capability (18 satellites) again by end of 2007 and FOC by end of 2009. While this ambitious schedule has failed as of May 2008, the program still pursues to reach the objectives by the end of 2008 with the extra budget that has been set up for the years 2007 to 2011. See Figure 2.18 for more details. Besides reaching FOC, Russia also wants to achieve a comparable performance of GLONASS to that of GPS and Galileo until 2010 [G.W. Hein et al., 2007a].

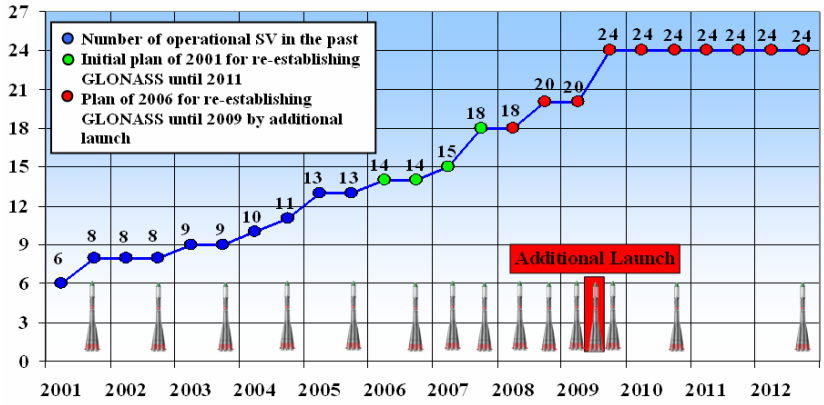

Figure 2.18. Plans to re-establish Full Operation Capability of GLONASS

These plans to re-establish FOC for GLONASS are supported by cooperation works between the governments of India and Russia. According to them, Russia will launch two GLONASS-M satellites on Indian Geostationary Satellite Launch Vehicle (GSLV) rockets. Additionally, during the December 2005 summit between the Indian Prime Minister and the Russian President, it was agreed that India would share the development costs of the GLONASS-K series and launch them from India.

As mentioned above, as of May 9th, 2008, the real number of satellites in operation (14) is lower than the planned 18, making the real fulfilment of the GLONASS program objectives very difficult. Indeed, although Russia added six GLONASS-M satellites to the constellation during 2007 as planned, it was forced to decommission other five satellites since the beginning of 2008 due to the short design life of the first generation spacecraft. The next figure shows the availability of GLONASS over the earth on May 9th, 2008 as provided by [GLONASS Centre].

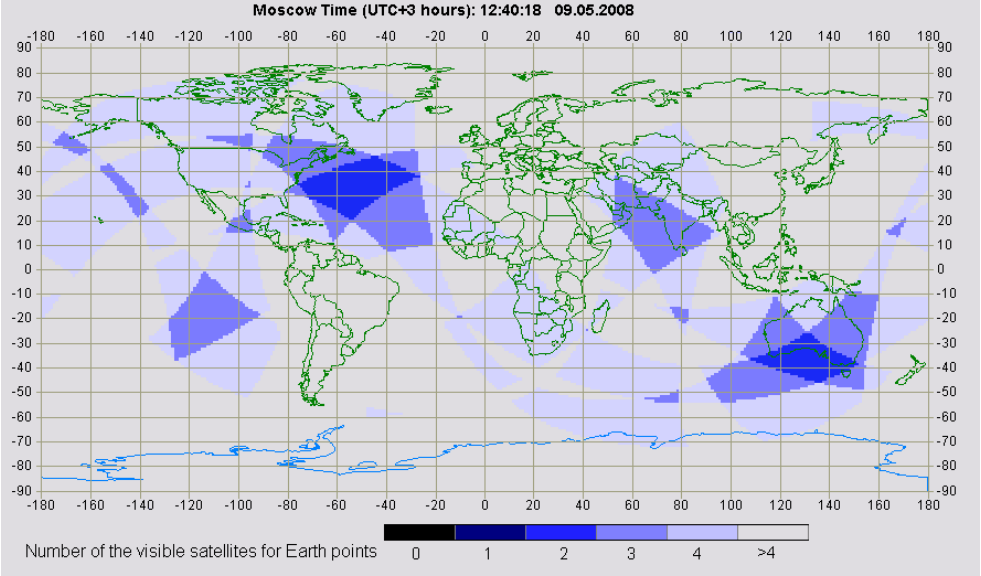

Figure 2.19. Availability of GLONASS May 9th, 2008 (Minimum Elevation Angle 5°)

For more information on the current status of all the GLONASS satellites, we refer to [GLONASS Centre] and [GLONASS Constellation Status]. Equally important as the number of satellites in sight is the power level of the received RF signals from GLONASS satellites. When measured at the output of a 3 dBi linearly polarized antenna the value is assured to be not lower than -161 dBW for the L1 band at an elevation of 5° or more. For the modernized GLONASS-M satellites transmitting also in the L2 band, the power level under the same conditions can not be lower than -167 dBW for this band.

In the same manner as with the minimum received power, similar figures can be derived for the maximum received power of GLONASS. According to this, the maximum received power level will not be more than –155.2 dBW in the specific configuration, as described in [GLONASS ICD, 2002].

2.5.2 GLONASS Signal Plan

As it was mentioned at the beginning of this chapter, GLONASS, unlike the other GNSS systems, makes use of a different DSSS technique [G.W. Hein et al., 2006c] based on Frequency Division Multiple Access (FDMA) to transmit its ranging signals.

GLONASS uses FDMA in both the L1 and L2 sub-bands. According to this scheme, each satellite transmits navigation signals on its own carrier frequency, so that two GLONASS satellites may transmit navigation signals on the same carrier frequency if they are located in antipodal slots of a single orbital plane [GLONASS ICD, 2002]. Indeed the actual constellation is taking advantage of this property since 2005 when the higher frequency channels had to be turned off to fulfil the CCIR Recommendation 769. We can clearly see this if we have a look at the satellites assigned to each of the GLONASS planes as shown in the following figure with status as of May 2008. As is clear to see, antipodal satellites are transmitting at the same frequency.

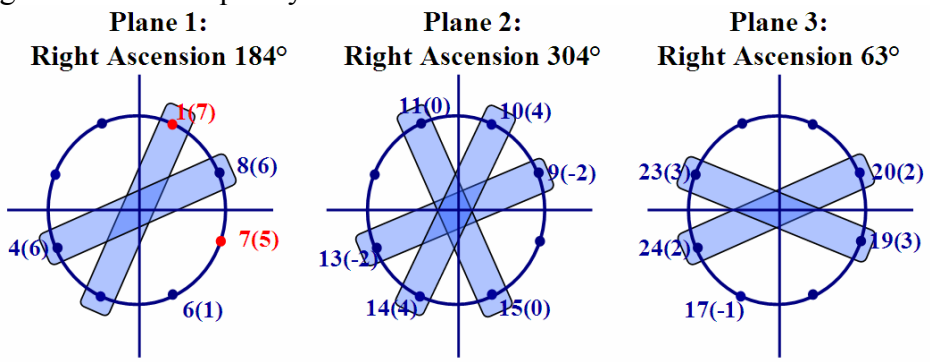

Figure 2.20. Antipodal Assignment of GLONASS Satellites. The parameter *i*(*k*) indicates that the satellite in almanac slot *i* transmits on frequency number *k*

The red slots indicate that the satellite is in maintenance. Blue means correct operation. Moreover, two different types of signals [GLONASS ICD, 2002] are transmitted by GLONASS satellites: Standard Precision (SP) and High Precision (HP) in both the L1 and L2 bands. The GLONASS standard accuracy signal, also known as C/A Code, has a clock rate of 0.511 MHz and is designed for use by civil users worldwide while the high accuracy signal (P Code) has a clock rate of 5.11 MHz and is modulated by a special code which is only available to users authorized by the Ministry of Defence. Since GLONASS-M, both L1 and L2 provide users with the standard accuracy code C/A. Moreover, the modernized GLONASS will also transmit FDMA signals on the L3 band and CDMA signals in L1 and L5 as we will see in chapter 2.5.3.

The nominal values of the FDMA L1, L2 and L3 carrier frequencies are defined as:

$$\begin{aligned} f_{k_{L1}} &= f_{0_{L1}} + k\,\Delta f_{L1} \\ f_{k_{L2}} &= f_{0_{L2}} + k\,\Delta f_{L2} \\ f_{k_{L3}} &= f_{0_{L3}} + k\,\Delta f_{L3} \end{aligned} \qquad (2.3)$$

where:

- k represents the frequency channel,
- $f_{0_{L1}}$ = 1602 MHz for the GLONASS L1 band,
- Δf_{L1} = 562.5 kHz frequency separation between GLONASS carriers in the L1 band,
- $f_{0_{L2}}$ = 1246 MHz for the GLONASS L2 band,
- Δf_{L1} = 437.5 kHz frequency separation between GLONASS carriers in the L2 band,
- $f_{0_{L3}}$ = 1201 MHz for the GLONASS L3 band, and
- Δf_{L3} = 437.5 kHz frequency separation between GLONASS carriers in the L3 band.

As we can see, the GLONASS L2 carrier reference signal is 7/9 of the L1 carrier reference and the GLONASS L3 carrier reference is 3/4 of the L1 carrier reference. Moreover, it must be noted that until 2005 the GLONASS satellites used the frequency channels k = 0,...,12 without any restrictions and the channel numbers k = 0 and 13 for technical purposes.

Since then GLONASS is only using the frequency channels k = -7,...,+6 and all the satellites launched beyond that year will use filters, limiting out-of-band emissions to the harmful interference limit contained in CCIR-ITU Recommendation 769 for the 1610.6 – 1613.8 MHz and 1660 – 1670 MHz Radio-Astronomy bands. It is interesting to note that although the limitation to use the higher frequency channels does only affect the L1 band, since the parameter k determines the channel in both the L1 and L2 bands, the upper frequencies of L2 corresponding to channels +7 to +13 were automatically sacrificed.

To have a clearer insight into how the spectra of the GLONASS signals look like, we study next all the bands in detail.

GLONASS L1 Band

The transmitted navigation signal is in both services of L1 a bipolar phase-shift key (BPSK) waveform with clock rates of 0.511 and 5.11 MHz for the standard and accuracy signals respectively. The L1 signal is modulated by the Modulo-2 addition of the pseudo random (PR) ranging code, the digital data of the navigation message and an auxiliary meander sequence. All above-mentioned frequencies are generated coherently using a single onboard time/frequency oscillator standard [GLONASS ICD, 2002]. For the case of the standard accuracy signals (C/A), the PR ranging code is a sequence with length the maximum of a shift register (m-sequence) and a period of 1 millisecond with bit rate of 511 kbps. The navigation message is sent at 50 bps and the auxiliary meander sequence at 100 Hz.

Moreover, it is important to note that the GLONASS FDMA L1 band does not exactly coincide with the GPS and Galileo L1 band. In fact, the GLONASS L1 band ranges from 1592.9525 MHz to 1610.485 MHz when only the 14 channels k = -7...+6 are employed. In the

next figures, each of the channels was filtered to only transmit the main lobe of the BPSK signal and the PSD was normalized to have unit power within the corresponding transmission bandwidth.

The PSDs of the GLONASS signals are shown in the following figure:

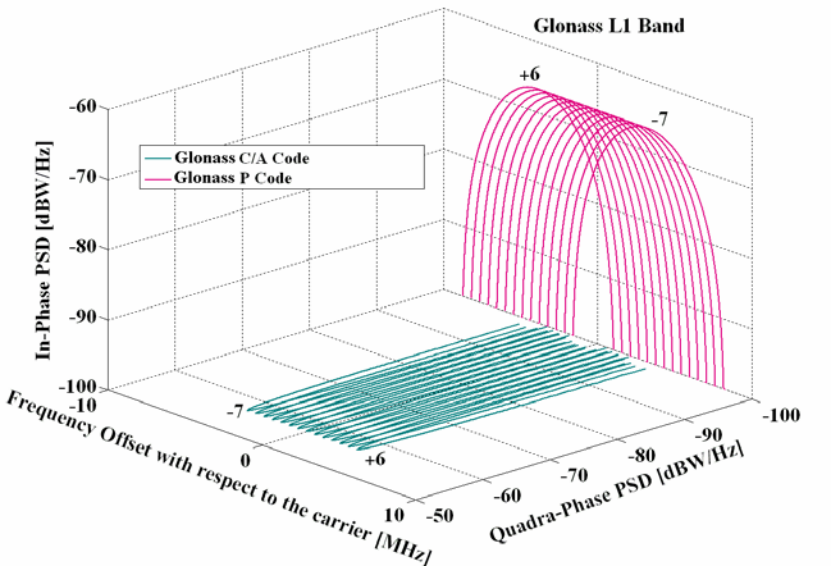

Figure 2.21. Spectra of GLONASS signals in L1

Once again, in order to have a clearer picture of how overcrowded the RNSS bands are becoming as more and more countries claim their rights to have their own GNSS, Figure 2.22 shows all the systems described so far in the E1/L1 band.

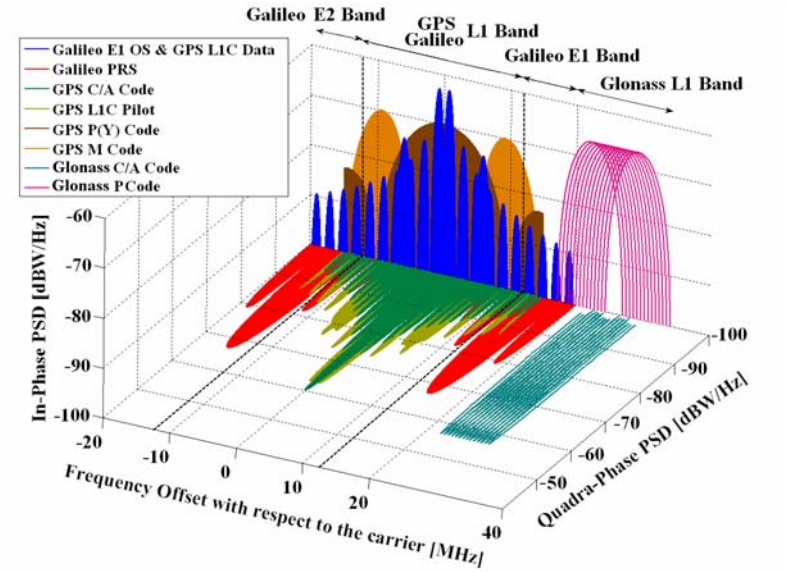

Figure 2.22. Spectra of GPS, Galileo and GLONASS Signals in E1/L1

It is important to note that the GPS L1C pilot and data signals are shown in quadrature in the figure although according to [GPS ICD-800, 2006] the final phasing is still open. To finalize some details on the technical characteristics of the GLONASS L1 signals are presented next:

Table 2.10. GLONASS L1 signal technical characteristics

GNSS System	GLONASS	GLONASS
Service Name	C/A Code	P Code
Centre Frequency	(1598.0625-1605.375) MHz ± 0.511 MHz	
Frequency Band	L1	L1
Access Technique	FDMA	FDMA
Spreading modulation	BPSK(0.511)	BPSK(5.11)
Sub-carrier frequency	-	-
Code frequency	0.511 MHz	5.11 MHz
Signal Component	Data	Data
Primary PRN Code length	511	N/A
Code Family	M-sequences	N/A
Meander sequence	100 Hz	N/A
Data rate	50 bps	N/A
Minimum Received Power [dBW]	-161 dBW	N/A
Elevation	5°	N/A

It is important to note that unlike for the case of GPS and Galileo in the previous chapters, the frequencies do not have to be multiplied by the factor 1.023.

2.5.2.1 GLONASS L2 Band

The transmitted navigation signal is, as also in L1, a bipolar phase-shift key (BPSK) waveform with similar clock rates as in the L1 band. The L2 signal is modulated by the Modulo-2 addition of the PR ranging code and the auxiliary meander sequence. For the case of the standard accuracy signals (C/A), the PR ranging code is a sequence of the maximum length of a shift register (M-sequence) with a period of 1 millisecond and a bit rate of 511 kbps. The navigation message is sent at 50 bps and the auxiliary meander at 100 Hz.

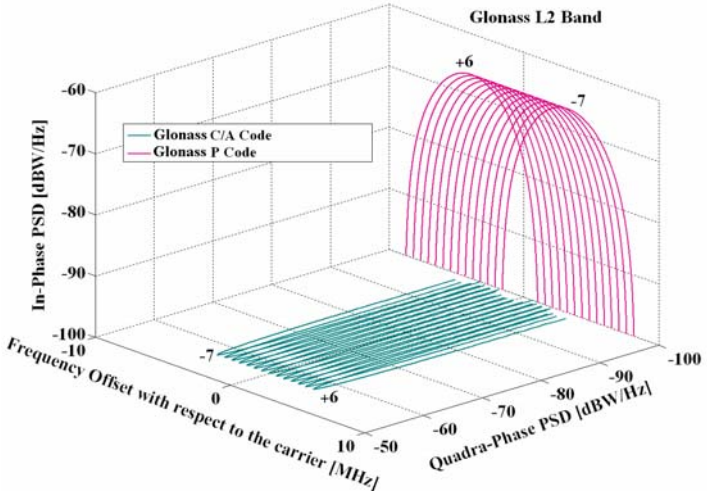

Figure 2.23. Spectra of GLONASS Signals in L2

We show in the figure next all the signals of GPS and GLONASS in the L2 band together

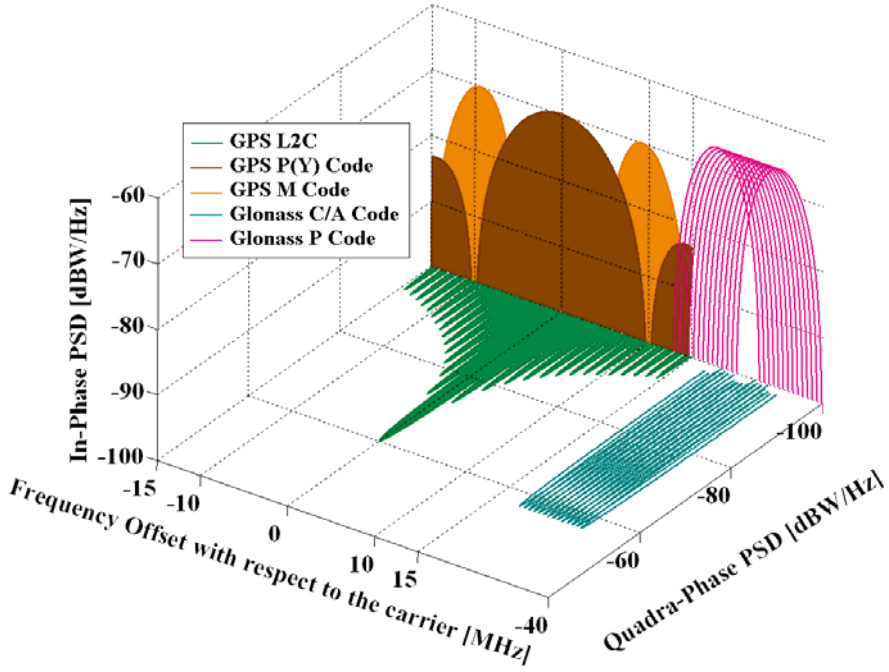

Figure 2.24. Spectra of GPS and GLONASS Signals in L2

To finalize some details on the technical characteristics of the GLONASS L2 signals are presented in the next table:

Table 2.11. GLONASS L2 signal technical characteristics

GNSS System	GLONASS	GLONASS
Service Name	C/A Code	P Code
Centre Frequency	(1242.9375…1248.625) MHz ± 0.511 MHz	
Frequency Band	L2	L2
Access Technique	FDMA	FDMA
Spreading modulation	BPSK(0.511)	BPSK(5.11)
Sub-carrier frequency	-	-
Code frequency	0.511 MHz	5.11 MHz
Signal Component	Data	Data
Primary PRN Code length	511	N/A
Code Family	M-sequences	N/A.
Meander sequence	100 Hz	N/A
Data rate	50 bps	N/A
Minimum Received Power [dBW]	-167 dBW	N/A
Elevation	5°	N/A

It is important to note again that unlike for the case of GPS and Galileo in the previous chapters, the frequencies do not have to be multiplied by the factor 1.023.

2.5.2.2 GLONASS L3 Band

As shown during the Munich Satellite Navigation Summit of 2008, GLONASS is planning to transmit navigation signals also on the L3 band, although the definite signal plan has not been decided yet. Indeed, four possible scenarios are being studied at the moment:

- Option 1: GLONASS K satellites would use a bandwidth of approximately 15 MHz with 16 channels. Both the in-phase and quadrature signals would be BPSK(4) with a chip rate of 4.092 MHz. It is interesting to note that as GPS and Galileo, the factor 4 must be understood as multiplied by 1.023 although we talk about FDMA signals.
- Option 2: GLONASS-L3 would have a 24 MHz bandwidth and would transmit BPSK(8) for the in-phase channel and BPSK(2) for the quadrature signals.
- Option 3: This option is identical to option 1 but shifted by 3 MHz to higher frequencies to achieve better isolation with Galileo E6.
- Option 4: This option is identical to option 2 but shifted by 3 MHz to higher frequencies, also to improve the spectral isolation with other signals in the band.

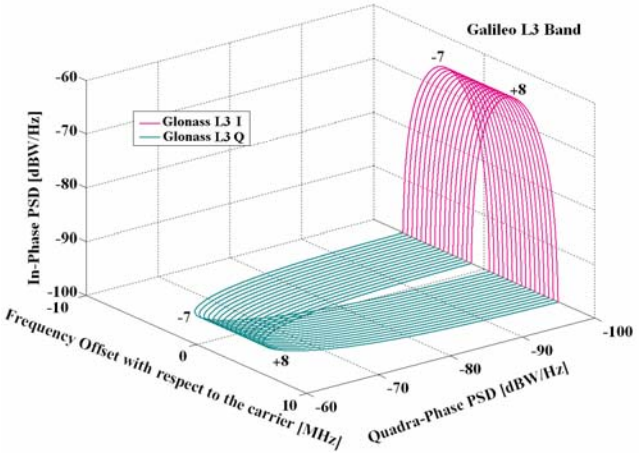

Figure 2.25. Spectra of GLONASS Signals in L3 (Option 1)

And now with GPS and Galileo together:

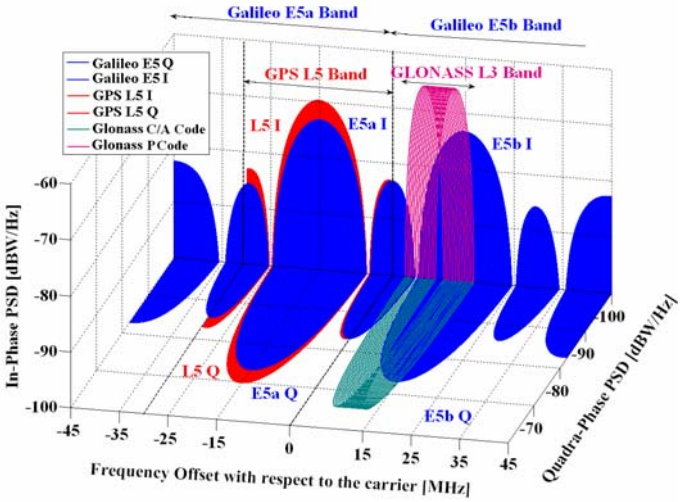

Figure 2.26. Spectra of GPS, Galileo and GLONASS Signals in L3 (Option 1)

We analyze now the second option for the GLONASS signals in L3. The following figure shows the different spectra.

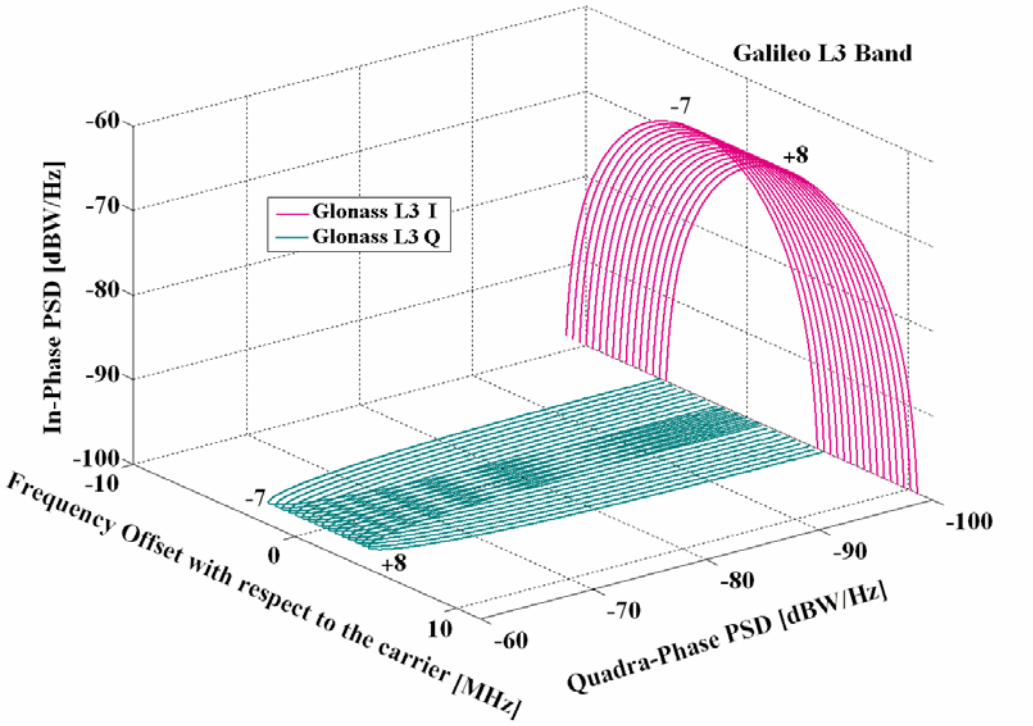

Figure 2.27. Spectra of GLONASS Signals in L3 (Option 2)

and again, with GPS and Galileo together:

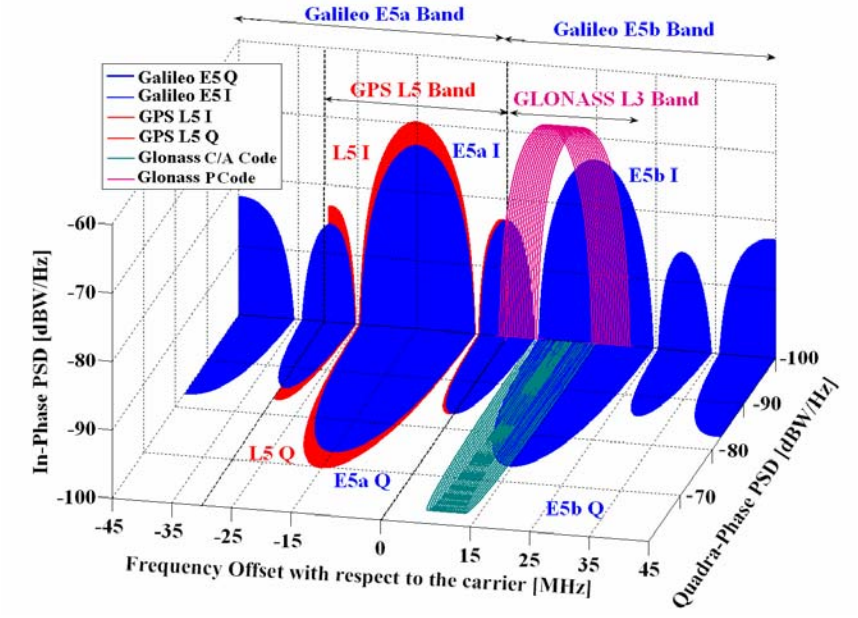

Figure 2.28. Spectra of GPS, Galileo and GLONASS Signals in L3 (Option 2)

To finalize, the technical characteristics of the GLONASS L3 signals are summarized in the next table:

Table 2.12. GLONASS L3 signal technical characteristics

GNSS System	GLONASS	GLONASS
Service Name	L3 I	L3 Q
Centre Frequency	1201 MHz	
Frequency Band	L3	L3
Access Technique	FDMA	FDMA
Spreading modulation	Option 1 BPSK(4) Option 2 BPSK(8)	Option 1 BPSK(4) Option 2 BPSK(2)
Sub-carrier frequency	-	-
Code frequency	Option 1 4.092 MHz Option 2 8.184 MHz	Option 1 4.092 MHz Option 2 2.046 MHz
Data Rate	100 or 125 bps	N.A.

2.5.3 GLONASS Modernization

Similar to GPS, GLONASS is on the way to modernizing its infrastructure. Apart from the signals in the L1 band, the Russian system has already established a second civil signal at L2 upon launch of the first GLONASS-M satellite in 2003. The new GLONASS-M satellites have better signal characteristics as well as a longer design life (7-8 years instead of the current 3 years) and a third civil signal at the L3 band is planned to start in 2010 aboard GLONASS-K satellites. The different options have been discussed some lines above. In addition, GLONASS also intends to transmit CDMA signals in L1 and L5.

This last generation of satellites is planned to be based on low mass satellites with a guaranteed lifespan of 10 to 12 years. The new GLONASS satellites are planned to reduce their weight by 50 %. This will allow to significantly lower launch costs by using the Soyuz-U launch vehicles. Regarding the number of satellites, it seems that GLONASS envisions updating its constellation up to 36 satellites.

GLONASS is not yet fully compatible and interoperable with the rest of GNSS systems. Indeed, major differences between GPS and Galileo using the Code Division Multiple Access (CDMA) and GLONASS using the Frequency Division Multiple Access (FDMA) approach still exist. A deeper insight into this topic will be provided in the next chapters. However, it is important to note at this point that in spite of the fundamental differences that the FDMA and CDMA approaches represent, solutions for common receivers can be found today. Nonetheless, common receiver architectures are considerably more complex and expensive.

The experience of Galileo has shown how important the roles of interoperability and compatibility with GPS were from the very beginning. Fortunately, it seems that GLONASS is taking important steps towards increasing compatibility and interoperability in the future as the common GPS/GLONASS statements in the framework of Working Group 1 (WG 1) seem to show. Indeed, during the GPS/GLONASS meeting in December 2006 in Yaroslavl (Russia), both sides emphasized the benefit to the user community that a common approach concerning the use of FDMA and CDMA would bring in terms of interoperability. The memorandum textually states *"Both sides noted that concerning the question of the use of FDMA and CDMA, significant progress was made in understanding the benefit to the user community of using a common approach*." [US-Russia Statement, 2006].

Russia announced then that they would come to a decision on the change from FDMA to CDMA by the end of 2007 [US-Russia Statement, 2006]. Finally, on February 15th, 2008, a government decree on new GLONASS requirements announced that GLONASS will also transmit open CDMA BOC(2,2) signals at 1575.42 MHz (GPS and Galileo E1/L1 band) and a BOC(4,4) signal centred at 1176.45 MHz (GPS L5 or Galileo E5a bands). It is however also possible that GLONASS could offer MBOC in E1 and BPSK(10) in L5 instead in its final CDMA Signal baseline plan in order to enhance interoperability with the rest of navigation systems in the band, namely with GPS and Galileo. As we have seen, these frequencies essentially correspond to the centre points of GPS and Galileo. According to this, GLONASS will be able to implement CDMA signals on L1 and L5 already in the GLONASS-K satellites planned for Phase 3 of the GLONASS modernization. This will imply a tremendous effort in the design of the satellite's payload regarding the power consumption, because if GLONASS moves to CDMA, this does not mean that FDMA will be completely abandoned. Indeed, for legacy and security reasons, FDMA and CDMA payloads will fly together increasing considerably their weight and required power. If all the modernization plans are thus realized, GLONASS will transmit FDMA signals in the current L1 and L2 GLONASS FDMA bands, together with the new FDMA signals in L3. In addition, CDMA open signals will also be provided in E1/L1 and L5. It is important to note that as shown in Table 2.2, the current GLONASS FDMA L1 band and the GPS and Galileo L1 band do not coincide. However, the new GLONASS CDMA signals will be allocated in the same E1/L1 band and the same E5a/L5 band as Galileo and GPS. This implies that GLONASS will transmit 5 bands in total, what is a considerable effort.

2.6 Compass

2.6.1 Compass System Overview

Compass is the GNSS system planned by China [G.W. Hein et al., 2007a] and will consist of a constellation of 30 Non-GEOstationary (3 IGSOs and 27 MEOs) satellites and 5 GEOstationary satellites with positions at 58.75º E, 80º E, 110.5º E, 140º E and 160º E. Each satellite transmits the same four carrier frequencies for navigational signals, where B1 and B1-2 are counted as separate bands. These navigational signals are modulated with a predetermined bit stream, containing coded ephemeris data and time.

China has sent three Compass navigation test satellites into orbit between 2000 and 2003. The launch of the two *Beidou* (Compass first version) satellites early 2007 is expected to cover China and parts of neighbouring countries by 2008, before expanding into a global system. The Compass satellites will be developed, manufactured, and launched by the China Aerospace Science and Technology Corporation (CASTC).

The will of China to develop its own global navigation system is clearly reflected in the policy document released by the State Council Information Office of October 12th, 2006. Here it was stated that China will *independently develop application technologies and products in applying satellite navigation, positioning and timing services*. Compass could begin operation in 2012 if the political statements are brought into reality.

Although the intentions and services that Compass will provide are still unclear, it seems that Compass will offer two levels of services: free open and commercial services for users in China, and licensed service for the military. As in GPS, Galileo and GLONASS, the licensed service will be more accurate than the free service and might be used for communication too.

In October 2003 the Galileo Joint Undertaking (GJU) signed a cooperation agreement with China. The National Remote Sensing Centre of China (NRSCC) was designated as the European Union's Chinese partner on the Galileo Project.

2.6.2 Compass Signal Plan

The current frequency filings [Compass ITU Filing] for radio bands made by China to the International Telecommunications Union (ITU) indicate that it would overlay both the Galileo Public Regulated Service (PRS) and the military GPS M-code at E1/L1, as well as in the L2 band. Given the importance of these protected signals and bands, we describe next in detail the intended signal plan of Compass. Since the use that China plans to do with Compass is still unclear, the spectra will be plotted in the next figures in grey to underline this fact.

2.6.2.1 Compass B1 Band

Although not all the technical aspects of the Compass signals in B1 are defined yet, an envisaged signal waveform has already been submitted to the ITU [Compass ITU Filing]. Next figure shows the spectral details of the studied option in the B1 and B1-2 bands.

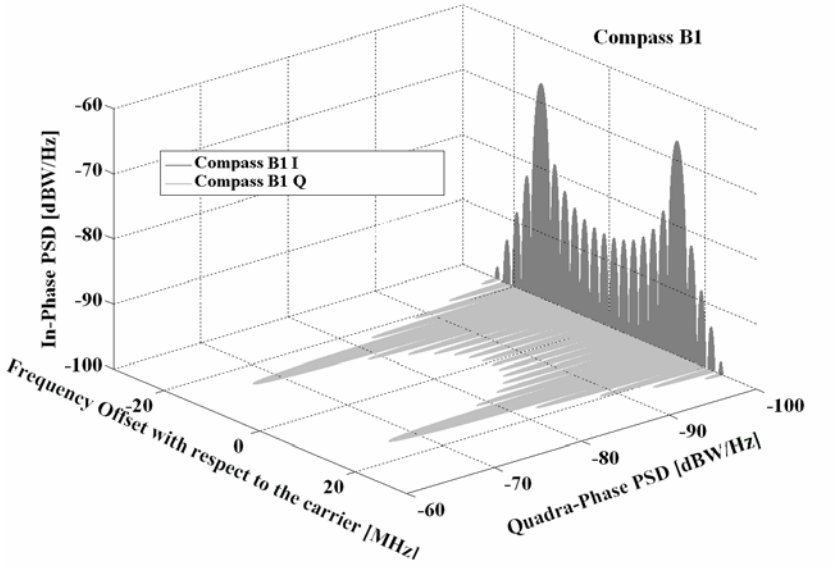

Figure 2.29. Spectra of Compass Signals in B1 and B1-2 bands

As also done in previous chapters, in order to have a better overview of all the GNSS signals around the Compass B1 and B1-2 bands, next figure depicts the spectral environment:

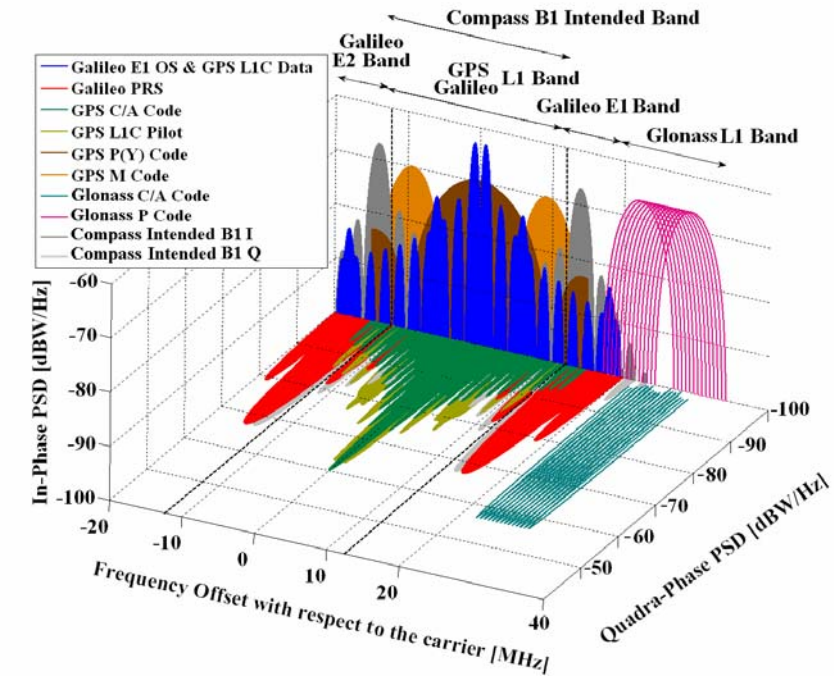

Figure 2.30. Spectra of GPS, Galileo, GLONASS (Option 2) and Compass Signals in L1

It is important to note that the GPS L1C pilot and data signals are shown in quadrature in the figure although according to [GPS ICD-800, 2006] the final phasing is still to be decided. To conclude some technical characteristics of the Compass B1 signals are given next:

Table 2.13. Compass B1 signal characteristics [Compass ITU Filing]

GNSS System	Compass	Compass	Compass
Service Name	B1 GSO	B1 N-GSO	B1 GSO and N-GSO
Phase	I		Q
Centre Frequency	Carriers at 1561.098 MHz (B1) and 1589.742 MHz (B1-2)		
Frequency Band	B1		
Access Technique	CDMA		
Spreading modulation	QPSK(2)		
Sub-carrier frequency	-		
Code frequency	2.046 MHz		2.046 MHz
Signal Component	Data	Data	Data
Primary PRN Code length	-	-	-
Code Family	-	-	-
Secondary PRN Code length	-	-	-
Data rate	500 bps	50 bps	500 bps
Minimum Received Power [dBW]	-163 dBW		
Elevation	-	-	-

2.6.2.2 Compass B2 Band

Similar to the B1 and B1-2 bands, not all the technical aspects of the Compass signals in B2 have been defined yet. Nonetheless a proposed signal waveform has already been submitted to the ITU [Compass ITU Filing]. Next figure shows the spectral details of the studied option.

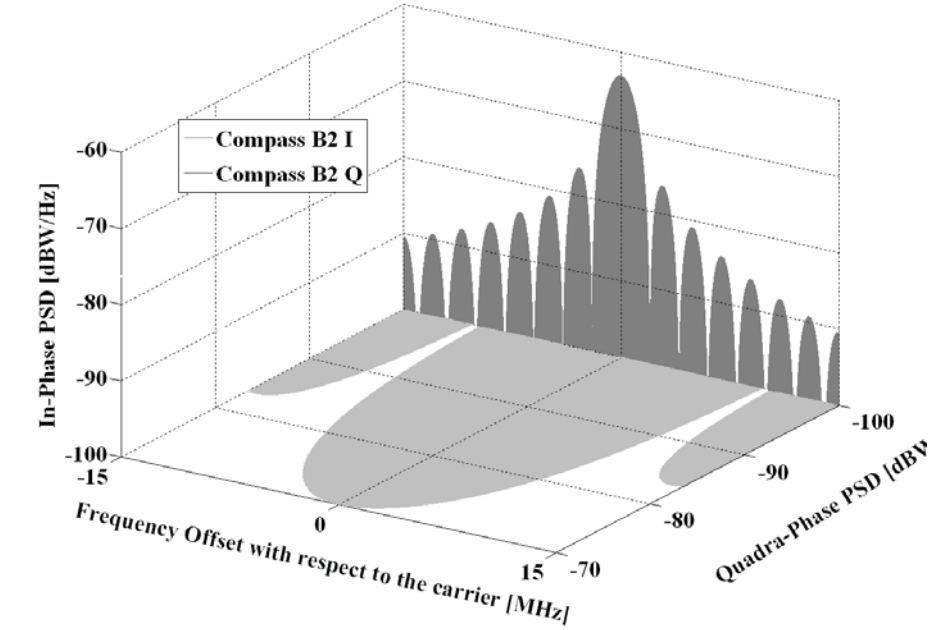

Figure 2.31. Spectra of Compass Signals in the B2 band

As also done for the rest of GNSS bands, we show in the next figure all the systems together.

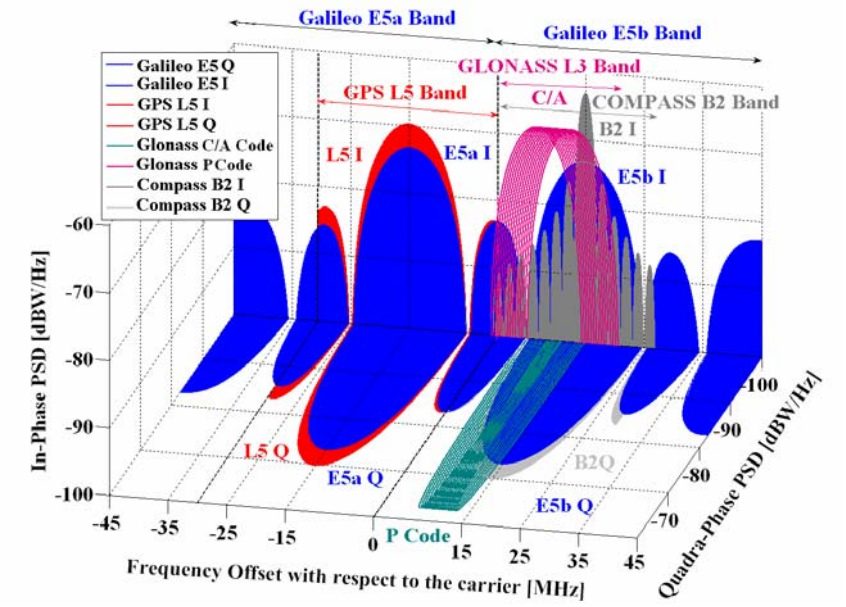

Figure 2.32. Spectra of Galileo and Compass signals in the E5 - B2 bands

To conclude, some technical characteristics on the Compass B2 signals are presented more in detail in the next table:

Table 2.14. Compass B2 signal technical characteristics [Compass ITU Filing]

GNSS System	Compass	Compass	Compass
Service Name	B2 GSO	B2 N-GSO	B2 GSO and N-GSO
Phase	I		Q
Centre Frequency	1207.14 MHz		
Frequency Band	B2		
Access Technique	CDMA		
Spreading modulation	QPSK		
Sub-carrier frequency	-		
Code frequency	2.046 MHz		10.23 MHz
Signal Component	Data	Data	Data
Primary PRN Code length	-	-	-
Code Family	-	-	-
Secondary PRN Code length	-	-	-
Data rate	500 bps	50 bps	500 bps
Minimum Received Power [dBW]	-163 dBW		
Elevation	-	-	-

2.6.2.3 Compass B3 Band

Finally, the spectral characteristics of the Compass B3 signals are also shown here. Similar to the B1, B1-2 and B2 bands, not all the technical aspects of the Compass signals are defined yet. Next figure shows the Power Spectral densities of the proposed Compass signals in B3:

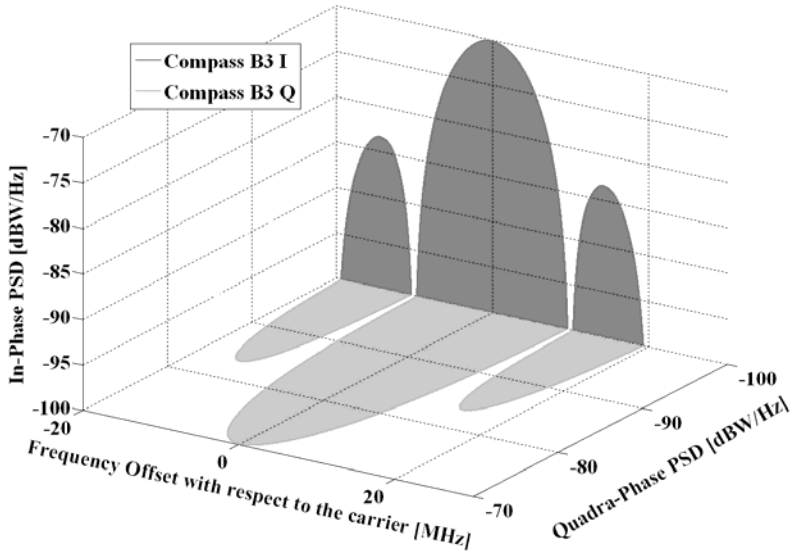

Figure 2.33. Spectra of Compass Signals in the E6 - B3 band

In order to have a better insight on how the Galileo E6 – Compass B3 band looks like, the following figure presents all the planned signals together.

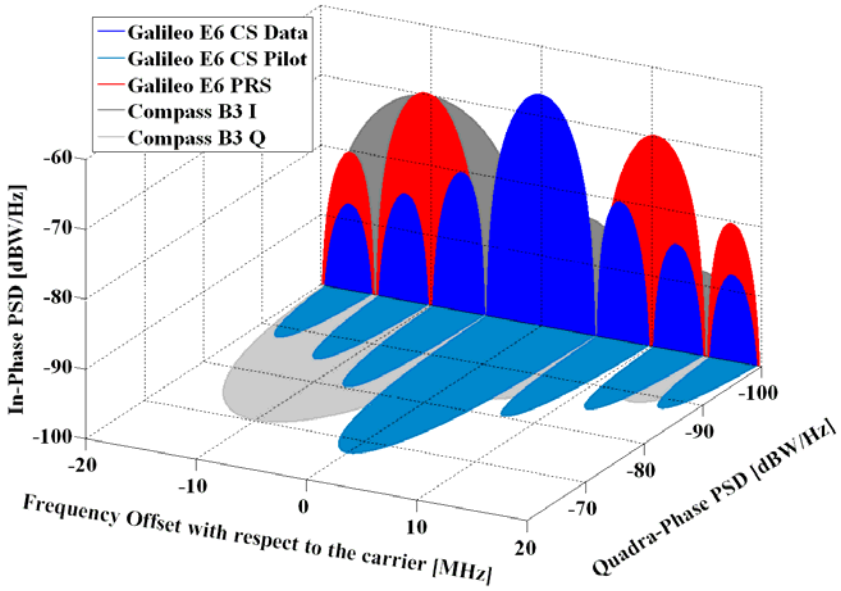

Figure 2.34. Spectra of Galileo and Compass Signals in the E6 - B3 band

To conclude, some technical characteristics on the Compass B3 signals are provided next [Compass ITU Filing].

Table 2.15. Compass B3 signal technical characteristics [Compass ITU Filing]

GNSS System	Compass	Compass	Compass
Service Name	B3 GSO	B3 N-GSO	B3 GSO and N-GSO
Phase	I		Q
Centre Frequency	1268.52 MHz		
Frequency Band	B3		
Access Technique	CDMA		
Spreading modulation	QPSK(10)		
Sub-carrier frequency	-		
Code frequency	10.23 MHz		10.23 MHz
Signal Component	Data	Data	Data
Primary PRN Code length	-	-	-
Code Family	-	-	-
Secondary PRN Code length	-	-	-
Data rate	500 bps	50 bps	500 bps
Minimum Received Power [dBW]	-163 dBW		
Elevation	-	-	-

2.7 Summary on Global Navigation Satellite Systems

Satellite navigation has become a technology of great acceptance. Every superpower wants to have a satellite navigation system and preferably a global one. As suggested in [G.W. Hein et al., 2007a], the real need of having multiple systems is questionable at some point from an economic perspective.

A very different issue, but one of great importance, is whether we can have so many systems coexisting together without degrading the performance of one another. The interference caused on one system by the rest is technically difficult to measure, and especially if each system would develop its own compatibility and interoperability concept without taking the rest into account. As shown in Appendix M, there are methodologies to assess interference but to what extent they accurately describe the real interference environment is a different issue.

In the 2004 *Agreement on the Promotion, Provision, and Use of Galileo and GPS Satellite-Based Navigation Systems and Related Applications* an interference and compatibility methodology was developed following ITU standards. The bilateral Agreement, however, is only between Americans and Europeans.

A natural solution would be to develop general methodologies valid for all GNSS systems on a multilateral basis but then it would be difficult to find out who should or could be responsible for coordinating these actions. It seems that the United Nations Office of Outer Space Affairs or the ITU could play such a role, extending its efforts in sponsoring formation of the International Committee on GNSS (ICG). But transforming existing bilateral agreements into compatible multilateral fora is not an easy task.

GPS and Galileo are compatible, and interoperable to a high degree, but they are not equal. Although important common actions have occurred in recent years, there is still a long way to go. And the difficulties are compounded when we compare the evolution of both systems with that of GLONASS or the planned Compass.

No matter what the system designers do, the fact is that the user market will explode in the next years. GNSS receivers will work better and almost everywhere, and the fusion with other communication devices is already on the threshold. International standards and certification are urgently needed and although it is true that ICAO, ITU, RTCA and other for a already provide models for certification and regulation, the market forces are stronger and demand faster reactions.

2.8 Regional Satellite Navigation Systems

In addition to the global satellite-based navigation systems already under way, three regional satellite navigation systems are also being developed by Japan, India and China: namely QZSS, IRNSS and Beidou respectively. But before we describe them in detail together with all the augmentation systems that already exist or are planned to be set up in the coming years, it is the right moment to make some reflexions on the need of regional and augmentation systems if, as we saw in the lines above, in a not so far future four global systems might already be reality.

As we have seen above, four global navigation systems might be operational in two decades providing thus an excellent coverage of most of the locations on earth. Today with GPS alone as the only real operational system, an average of approximately 10 satellites can be seen at any point of the earth. When GPS, GLONASS, Galileo, and Compass are in operation and assuming they would be fully interoperable, four times more satellites could be available for navigation, positioning, and timing [G.W. Hein et al., 2007b].

Locations with poor coverage today might not need any more a regional augmentation. As a result, the added value of using regional systems when all the planned global systems would already deliver good accuracy is questionable.

In the framework of Galileo, different studies have been carried out in the past years to assess the effect of increasing the number of satellites of an existing constellation as shown in [G.W. Hein et al., 2006a]. Here the effect of doubling the number of satellites was studied. In terms of positioning accuracy, the improvement resulting from the better geometry is clear to see in [G.W. Hein et al., 2006a]. Indeed, the step from GPS alone to Galileo + GPS represents with no doubt a clear gain for the final user. Nevertheless, once a pretty dense constellation of satellites is achieved, other measures such as the increase of power in the satellite would be of more profit to the final user. Let us think of a hypothetical scenario of 110 satellites as described in [G.W. Hein et al., 2007b].

Indeed, one might expect that the relative gain brought by 30 satellites when there already exist 30 is higher than that of 30 additional satellites when there are already 60. This is equivalent to saying that the marginal gain diminishes as the size of the constellation grows. Such a conclusion should not come as a surprise, because it reflects a well known economic law that applies to most goods and services in the world.

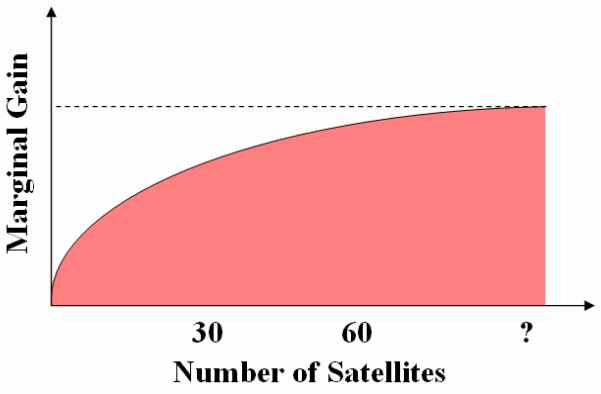

Figure 2.35. Qualitative analysis of the expected marginal gain as a function of the number of GNSS satellites

The four global satellite systems now in existence or under development will have around 110 satellites altogether. As shown by [G.W. Hein et al., 2007b], it seems that the saturation level in terms of geometry lies around this number.

The problem gains even more multidimensionality if we recall the development of the semiconductor industry in recent years. It is not so unrealistic to think that not too far in the future pseudolites could be a cheap product that anyone could place in locations with poor GNSS coverage. These single-chip pseudolites (SCPL) could thus meet users' positioning requirements in areas where the satellites signals could not be received.

Only time will tell if there will be a real need of regional and augmentation systems in the future. Nevertheless, since they are still an important component of today's GNSS, we will pay them the attention they deserve in the next lines.

2.8.1 Quasi Zenith Satellite System(QZSS)

2.8.1.1 QZSS System Overview

QZSS is the Japanese regional system that will serve as enhancement for GPS in Japan. The constellation consists of three satellites inclined in elliptic orbits with different orbital planes in order to pass over the same ground track. QZSS was designed so as to guarantee that at any time at least one of its three satellites is close to the zenith over Japan.

Initially, QZSS was conceived as a government – private sector program aiming for new satellite business, in which the private sector would be responsible for mobile communications and mobile broadcasting while the government would be responsible for the navigation part. However, due to the lack of participation by the Japanese communication industry, the QZSS satellites will not carry any communication payloads but rather will concentrate on the navigation element funded by the government alone.

QZSS and GPS will be fully interoperable and the first satellite launch date is planned for the year 2008. Figure 2.36 below shows in detail the ground track of the three QZSS satellites. The ground tracks of the Indian Regional Navigation Satellite System (IRNSS) satellites, the modernization of GAGAN, are also shown. Next chapter will be dedicated to this regional navigation satellite system.

The overall constellation parameters of both systems together are shown next in Table 2.16.

Table 2.16. Space Constellation Parameters of QZSS and IRNSS

Parameter	QZSS	IRNSS
Constellation	GSO(3)	GEO(3)+GSO(4)
GEO Longitudes	-	34°, 83°, 132° E
GSO Equatorial Crossing	-	55°(2), 112°(2)
Eccentricity	0.099	0
Inclination	45°	29°
Semi-major axis	42,164.0 km	42,164.0 km

The ground tracks of the two systems are graphically shown as follows:

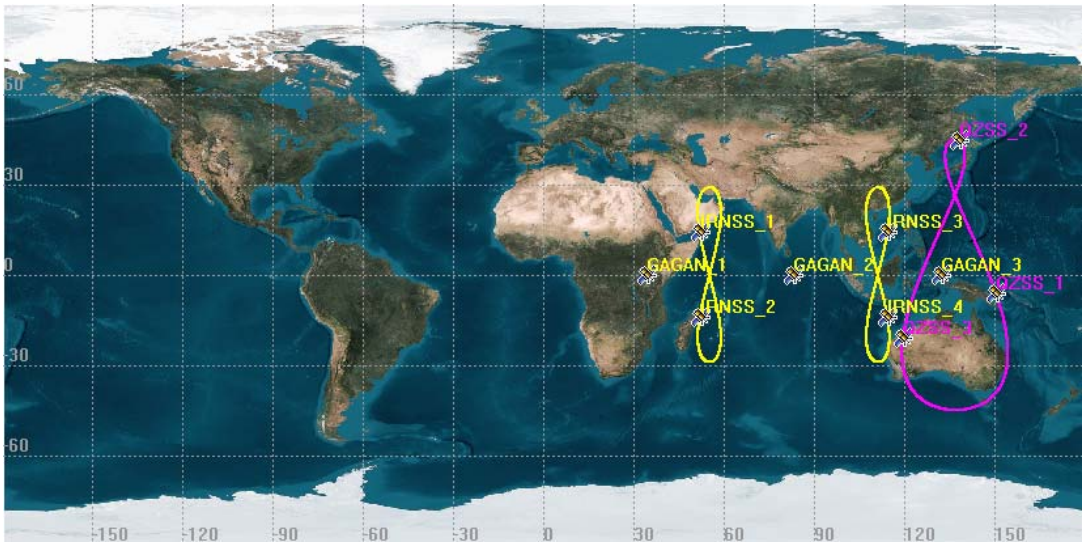

Figure 2.36. Ground Tracks of QZSS and IRNSS. This figure was generated using the Satellite Tool Kit (STK) [Satellite Tool Kit STK, 2006]

Moreover, the Maximal Number of QZSS Satellites visible at a Minimum Elevation Angle of 10° is shown in the next figure.

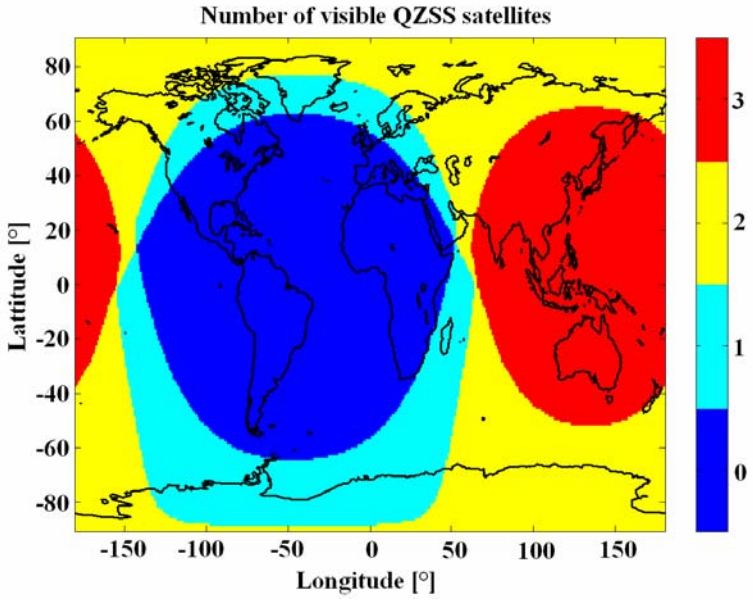

Figure 2.37. Number of visible QZSS Satellites at Minimum Elevation Angle of 10°

2.8.1.2 QZSS Signal Plan

QZSS and GPS have the highest level of interoperability among all the Satellite Navigation Systems as we will see in the following tables. In fact, the spectral properties are equivalent to those that we saw in chapter 2.3.2 and therefore will not be shown here. The characteristics of the different signals in particular are summarized in detail in the following tables. For the case of the L1 band the technical characteristics of the QZSS signals are presented next:

Table 2.17. QZSS L1 signal technical characteristics

GNSS System	QZSS	QZSS		QZSS
Service Name	C/A	L1C		SAIF
Centre Frequency	1575.42 MHz	1575.42 MHz		1575.42 MHz
Frequency Band	L1	L1		L1
Access Technique	CDMA	CDMA		CDMA
Spreading modulation	BPSK(1)	BOC(1,1)		BPSK(1)
Sub-carrier frequency	-	1.023 MHz		-
Code frequency	1.023 MHz	1.023 MHz		1.023 MHz
Signal Component	Data	Data	Pilot	Data
Primary PRN Code length	1023	10230		1023
Code Family	Gold Codes	Weil Codes		Gold Codes
Secondary PRN Code length	-	-	1800	-
Data rate	50 bps	50 bps	-	250 bps
Symbol rate	50 sps	100 sps	-	500 sps
Minimum Received Power [dBW]	-158.5	-157		-161
Elevation	5°	5°		5°

Equally, for L2, L5 and E6, the technical characteristics of the QZSS signals are summarized in the following table. As we can clearly recognize, except for the LEX signal in E6, QZSS and GPS are practically identical. It is interesting to note that this signal makes use of a very interesting multiplexing scheme for its experimental LEX signal, based on Code Shift Keying (CSK) [QZSS SIS ICD].

Table 2.18. QZSS L2, L5 and E6 signal technical characteristics

GNSS System	QZSS	QZSS	QZSS	QZSS	QZSS	QZSS
Service Name	L2CM	L2CL	L5 I	L5 Q	LEX	LEX
Centre Frequency	1227.60 MHz	1227.60 MHz	1176.45 MHz	1176.45 MHz	1278.75 MHz	1278.75 MHz
Frequency Band	L2	L2	L5	L5	E6	
Access Technique	CDMA	CDMA	CDMA	CDMA	CDMA	
Spreading modulation	BPSK(1) result of multiplexing 2 streams at 511.5 kHz		BPSK(10)	BPSK(10)	BPSK(5)	
Sub-carrier frequency	-	-	-	-	-	
Code frequency	511.5 kHz	511.5 kHz	10.23 MHz	10.23 MHz	5.115 MHz	
Signal Component	Data	Pilot	Data	Pilot	Data	Pilot
Primary PRN Code length	10230 (20 ms)	767250 (1.5 s)	10230	10230	10230	1048575
Code Family	M-sequence from a maximal polynomial of degree 27		Combination and short-cycling of M-sequences		Small Kasami Set. Chip by chip multiplex	
Secondary PRN Code length	-	-	10	20	-	
Data rate	IIF 50 bps IIR-M Also 25 bps	-	50 bps	-	2 kbps	-
		-	100 sps	-	250 sps	-
Minimum Received Power [dBW]	-160.0 dBW		-157.9 dBW		-155.7 dBW	
Elevation	5°		5°	5°	5°	

2.8.2 Indian Regional Navigation Satellite System (IRNSS)

2.8.2.1 IRNSS System Overview

The IRNSS is an independent seven-satellite constellation that will be built and operated by India. IRNSS will seek to maintain compatibility with other GNSS and augmentation systems of the region and is planned to provide services for critical national applications.

Of the seven satellites that comprise the constellation, three are geostationary and are known as GAGAN. GAGAN will be further explained in the following chapter. The other four, geosynchronous. The geostationary satellites have designated positions at 34º E, 83º E and 132º E, while the geosynchronous (GSO) have equatorial crossings at 55° E (two satellites) and 111° E (two satellites), with an inclination of 29° and a relative phasing of 56°.

The first IRNSS payload is expected to reach FOC in 2012. The constellation parameters of IRNSS as well as the ground tracks were shown in the previous chapter together with QZSS.

2.8.2.2 IRNSS Signal Plan

The final definition of all the IRNSS signals has not been concluded yet and investigations are still on course. We summarize in the next table the first proposal for the Signal and Frequency Plan presented in November 2006 during the First ICG Meeting in Vienna.

Table 2.19. IRNSS L5 Band technical characteristics

GNSS System	IRNSS	IRNSS	IRNSS	IRNSS
Service Name	L-band	L-band	L-band	S-band
Centre Frequency [MHz]	1191.795	1191.795	1191.795	2491.75
Frequency Band	L5 A	L5 B	L5 C	S
Access Technique	CDMA	CDMA	CDMA	CDMA
Spreading modulation	BOC(10,2)	BPSK(10)	BPSK(10)	N/A
Sub-carrier frequency	10.23 MHz	-	-	N/A
Code frequency	2.046 MHz	10.23 MHz	10.23 MHz	N/A
Signal Component	Data	Data	Pilot	N/A
Primary PRN Code length	N/A	N/A	N/A	N/A
Code Family	N/A	N/A	N/A	N/A
Secondary PRN Code length	N/A	N/A	N/A	N/A
Data rate	N/A	50 bps /100 sps	N/A	50 bps /100 sps
Minimum Received Power	N/A	N/A	N/A	N/A
Elevation	N/A	N/A	N/A	N/A

Given the similarity with the Galileo signals in terms of services that IRNSS might be providing, the same convention as for Galileo was employed. That is A for the PRS and B and C for the Open Service data and pilot signals respectively. Furthermore, the spectral properties of the IRNSS signal would be as follows:

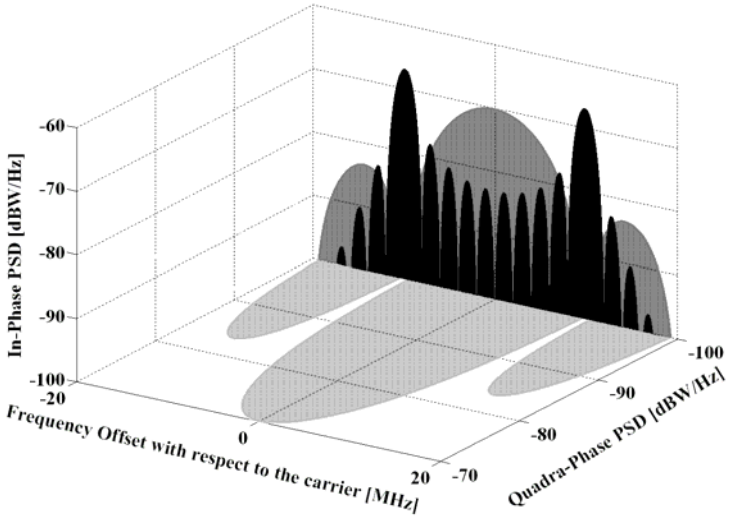

Figure 2.38. Spectra of IRNSS Signals in the E5b band

To conclude, it is interesting to mention that the Indian Satellite Navigation Programme has been doing much work in the past years on ionospheric and tropospheric modelling in the Region of India what could mean that IRNSS does not plan to use dual frequency at least in the first generation.

Moreover, India also plans to transmit similar signals for the S-band to those we have just described for the L5 band. The carrier frequency of S-band is at 2491.75 MHz. The modulation schemes and data rates would be the same as for L5 but no final decision on the other parameters has been made yet. In addition, it seems that India also plans to transmit signals in L1 as announced during the second Meeting of the ICG in India, in 2007.

As a summary of the studied regional satellite systems so far, the signal plan of QZSS and IRNSS is shown in the next figure

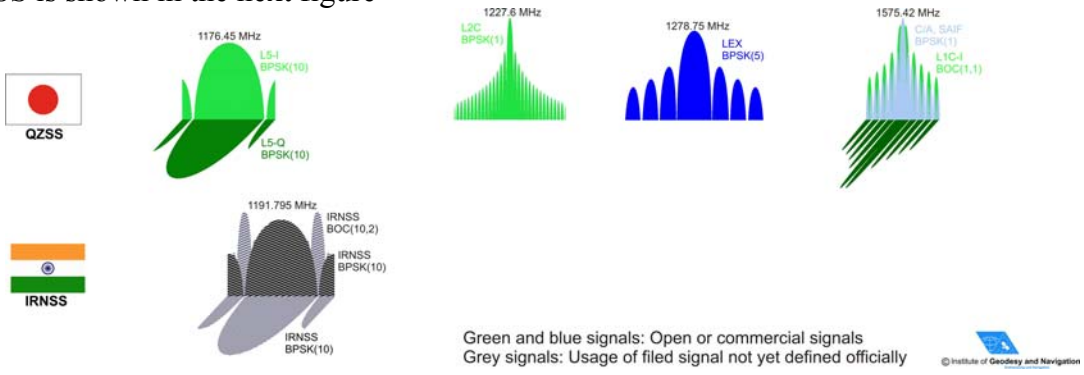

Figure 2.39. QZSS and IRNSS planned signals. It must be noted that IRNSS is also expected to send augmentation signals on L1

2.8.3 Beidou

Beidou (in Chinese 北斗卫星导航定位系统 where 北斗 means *North Dipper*) is the first stone to build up Compass, an independent Global Navigation System under control of the People's Republic of China. Beidou is the name of a Chinese constellation, which is equivalent in the Chinese astronomony to the Big Dipper of Western culture.

In September 2003, China joined the Galileo project after signing an Agreement with the Galileo Joint Undertaking (GJU). It was agreed that China would invest 230 € million in Galileo over the following years. On November 2nd, 2006 however, China announced its intention of building its own navigation system, Beidou, offering equivalent open services to those of Galileo. The Chinese Council Information Office on October 12th, 2006 publicly announced that China will *independently develop application technologies and products in applying satellite navigation, positioning and timing services.*

China is planning to build Beidou and its modernized version Compass on the basis of pure Chinese technology. Both the satellite and carrier rocket are being developed by the Chinese Research Institute of Space Technology and China Academy of Launch Vehicle Technology, which are under the China Space Science and Technology Group.

2.8.3.1 Beidou System Overview

Beidou is the experimental version of the Global Navigation System Compass that we saw in the previous chapter. Beidou will be composed of 5 geostationary satellites, covering an area on earth from 70°E to 140°E and from 5°N to 55°N.

The first Beidou Navigation Test Satellite, Beidou 1A, was launched by a Chinese Long March 3M booster on October 31st, 2000, into a geostationary orbit slot at 140° E, to the east of China. It was followed by Beidou 1B on December 21st, 2000, which was placed in a geostationary slot at 80 degrees East longitude. Beidou 1C was launched into an orbit at 110.5°E on May 25th, 2003 from the Xichang Satellite Launch Centre on a CZ-3A booster and the last Beidou satellite of the 1X generation, namely Beidou 1D, has been successfully put in orbit on February 2nd, 2007, on another CZ-3A booster. Some weeks later, on April 13th, 2007 China made the first clear step to the Global Navigation System Compass after launching its first MEO, known as Beidou 2A. The spacecraft began transmitting signals on three of four frequencies within a few days.

2.8.3.2 Beidou Signal Plan

The Beidou signal plan was already described in chapter 2.6.2. Indeed, Beidou is the first stone to Compass and the five GEO satellites we talked about in this chapter constitute what we call here the Beidou system. For more details on the technical characteristics of the signals, refer thus to this chapter.

2.8.3.3 Beidou Modernization (Compass)

The four GEO satellites (1A, 1B, 1C, 1D) mentioned above were designed as experimental satellites. Nevertheless, the plans for the modernized system, also known as Compass (see chapter 2.6 for more details) are to have 35 satellites in orbit, offering then a complete coverage of the globe. Of the 35 satellites, 30 will be MEO satellites (Beidou 2) and the rest five will be the geostationary satellites of Beidou 1.

The first MEO Beidou 2 satellite is already in the space and as we show in the next figures, the emitted signals correspond to those we have described in chapter 2.6.1. The measurements were made by the French Space Agency CNES on April 24th, 2007. In addition, it must be noted that the following figures include partial RF equalization.

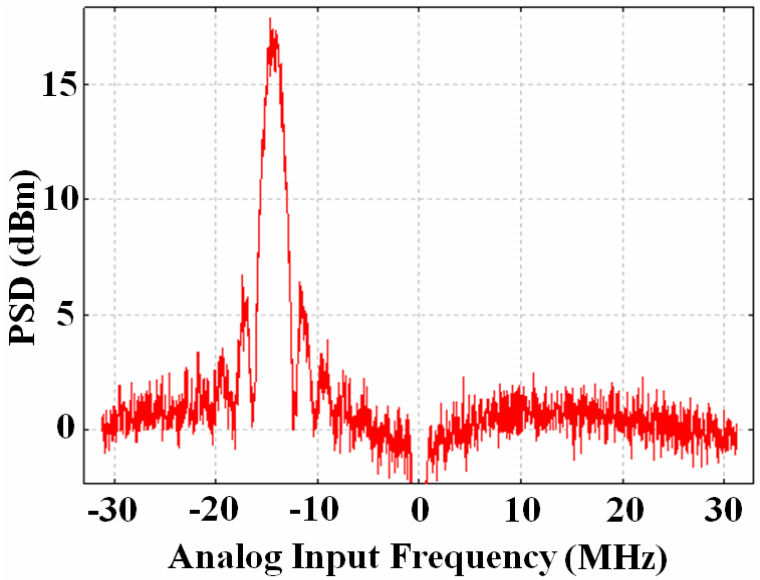

Figure 2.40. Compass Spectra centered on E1 carrier, observed on April 24th, 2007 (Courtesy of CNES)

Compass Spectra centered on L1 carrier, observed on

As we can clearly recognize from the figure above, of the two planned QPSK(2) signals at -14 and +14 MHz with respect to the L1 carrier, only the left side was being transmitted as of May 10th, 2007.

In the case of E6, we can clearly recognize the BPSK(10) signal. If we recall the parameters and description given in chapter 2.6.1, we can clearly see that this signal will be sitting directly on top of the Galileo PRS of E6.

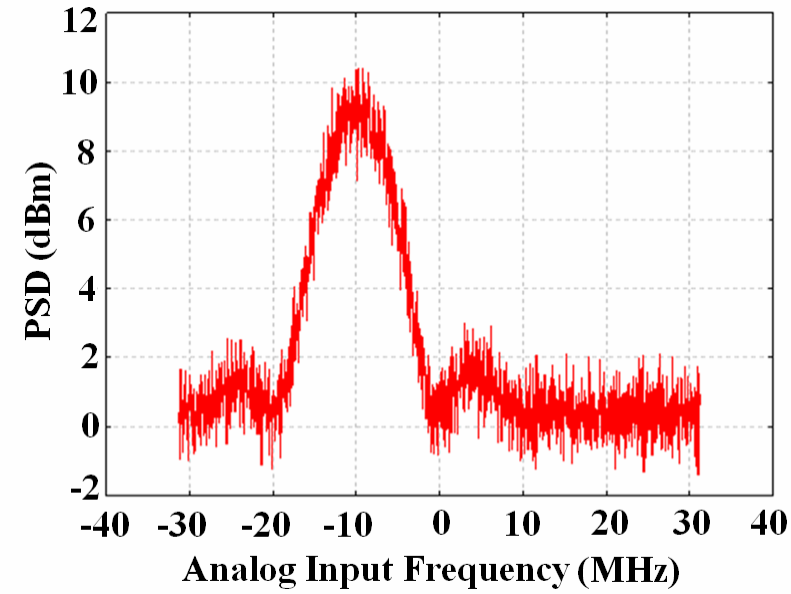

Figure 2.41. Compass Spectra observed on E6 carrier, observed on April 24th, 2007 (Courtesy of CNES)

Finally, the results for E5 show the superposition of a BPSK(2) and a BPSK(10) at 1207.14 MHz in consonance with the description of Compass given in chapter 2.6.2 of this chapter.

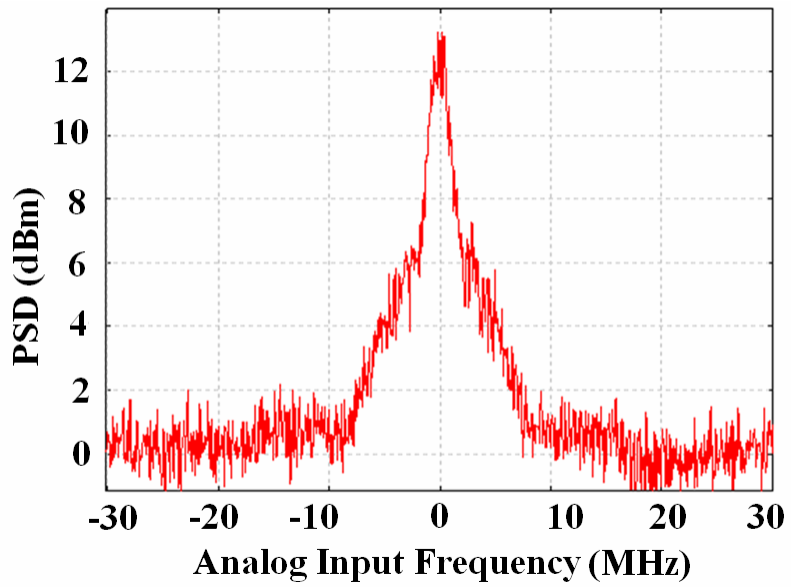

Figure 2.42. Compass Spectra observed on E5 carrier, observed on April 24th, 2007 (Courtesy of CNES)

2.9 GNSS Augmentation Systems

2.9.1 Satellite Based Augmentation Systems

A Satellite Based Augmentation System (SBAS) is a system that supports wide-area or regional augmentation of any GNSS in general through the use of at least one dedicated satellite. If we recall the thoughts on regional augmentation systems of previous chapters, we can see that the same reflexions on the future need of such systems are also valid here.

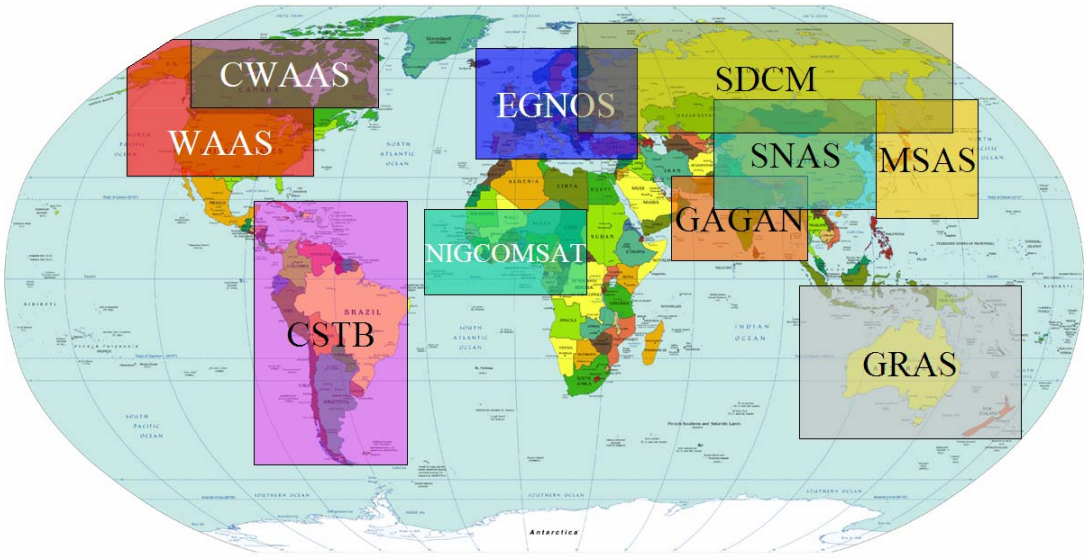

Figure 2.43. Existing and planned GNSS Augmentation Systems

From the figure above it is important to note that the GRAS system is Australia was included for completeness although it is not a satellite based augmentation system (SBAS) but a Ground Based Augmentation System (GBAS).

We describe next all the different Augmentation Systems that already exist or are planned.

2.9.1.1 Wide Area Augmentation System (WAAS)

The Wide Area Augmentation System (WAAS) augments GPS over the North American territory to provide the additional accuracy, integrity, and availability needed to enable users to rely on GPS for safety-critical applications, particularly in the field of aviation. Before WAAS, the U.S. National Airspace System (NAS) did not have the capability of providing horizontal and vertical navigation for aviation precision approach operations for all users at all locations. WAAS is constituted by four geostationary satellites.

2.9.1.2 European Geostationary Navigation Overlay Service (EGNOS)

The European Geostationary Navigation Overlay Service (EGNOS) is a satellite-based augmentation system (SBAS) under development by the European Space Agency (ESA), the European Commission (EC), and EUROCONTROL. EGNOS supplements GPS by reporting on the reliability and accuracy of the signals. It consists of three geostationary satellites (AOR-E, IOR-W and ARTEMIS) and a network of ground stations. The system started its initial operations in July 2005, and is intended to be certified for use in safety of life applications in 2008.

2.9.1.3 MTSAT Space-based Augmentation System (MSAS)

The Japanese equivalent to WAAS and EGNOS incorporates the Multifunctional Transport Satellite (MTSAT) into MSAS (MTSAT Space-based Augmentation System). In addition to transmitting correction and integrity data for GPS, the MTSAT satellites are used for meteorological observations and communication services following a multi-mission concept. After failing with the initial launch of the first MTSAT satellite in 1999 the substitute satellite MTSAT-1R was set into orbit in February 2005. An additional satellite, MTSAT-2, was put into mission in February 2006.

2.9.1.4 Russian Differential Correction and Monitoring (SDCM) System

The Russian System for Differential Correction and Monitoring (SDCM) is the Russian version of SBAS. It is being developed under the leading role of the Russian Institute of Space Device Engineering (RISDE) and will augment GLONASS, GPS and Galileo signals in E1/L1, providing real-time corrections for all the systems over the Russian territory from two geostationary satellites. SDCM will use eight tracking stations within Russia, plus others on foreign ground yet to be decided, and will provide WAAS- and EGNOS-like capabilities over the Russian airspace, monitoring the integrity and quality of the GLONASS, GPS and Galileo navigation services. The design of the system started in 2002 in accordance with the contract signed with the Federal Space Agency of Russia. As announced during the Second Meeting of the International Committee on GNSS (ICG) celebrated in Bangalore, India, in 2007, the system is planned to be validated in 2010 and operational by 2011.

2.9.1.5 GPS and GEO Augmented Navigation system (GAGAN)

The GPS and GEO Augmented Navigation system (GAGAN) is India's SBAS for the South Asian region. Established by the Indian Space and Research Organization (ISRO) and the Airports Authority of India to aid civil aviation in the country, GAGAN will expand into IRNSS.

The first geostationary navigation payload in the C-band and the L1 and L5 frequencies (L-band) will be carried on an Indian geostationary satellite, GSAT-4, placed at 82°E. Two more satellites, GSAT8 and GSAT9 will follow it to complete the augmentation system, with FOC expected by 2009.

2.9.1.6 Nigerian Communications Satellite System (NIGCOMSAT)

With its Communications Satellite (NIGCOMSAT-1), Nigeria is the first African country in planning to enter the stage of GNSS Augmentation Systems by transmitting two L-band augmentation signals in L1 and L5. The manufacturing of the satellite was assigned to China's state-owned space hardware manufacturer and is thus China's first satellite export sale [GAGAN, 2006d]. The satellite was launched by a Long March 3B carrier rocket at the Xichang Satellite Launch Centre on May 14th, 2007. Two ground stations are going to be built in Nigeria and in China. NIGCOMSAT-1 will be placed in a geostationary orbit at 42°E, although it is a suboptimal location for covering Nigeria.

2.9.1.7 Other Satellite Augmentation Navigation Systems

2.9.1.7.1 Canadian Wide Area Augmentation System (CWAAS)

The United States Wide Area Augmentation System (WAAS) that was described in chapter 2.9.1.1 can only be partially used in southern Canada. In order the full territory of Canada to have too augmentation of the GNSS signals, the Canadian WAAS (CWAAS) is under development. First studies started as soon as mid 1990s.

2.9.1.7.2 South American Satellite Augmentation System (CSTB)

The Caribbean and South American Region have taken initial steps to establish a GNSS Augmentation Test Bed (CSTB) throughout the region to support and facilitate research, development, acquisition, and implementation efforts associated with an operational transition to satellite navigation.

2.9.1.7.3 Chinese Satellite Navigation Augmentation System (SNAS)

Finally, also China plans its own satellite augmentation system. The Chinese version receives the name of Satellite Navigation System (SNAS) and is under current development.

The overall constellation parameters of those GNSS Augmentation Systems whose specifications are well defined are shown next in Table 2.20.

Table 2.20. GNSS Augmentation Systems Constellation Parameters

Parameter	WAAS	EGNOS	SDCM	MSAS	GAGAN	NIGCOMSAT
Constellation	GEO(4)	GEO(3)	GEO(2)	GEO(2)	GEO(3)	GEO(1)
GEO Longitudes	53° W 98° W 120° W 178° W	15.5° W 25.0° E 21.5° E	TBD	140° E 145° E	34° E 83° E 132° E	42° E
Semi-major axis (km)	42,164.0	42,164.0	42,164.0	42,164.0	42,164.0	42,164.0

Figure 2.44 next shows the coverage region of the satellite-based augmentation systems visible to users at elevations higher than 10 degrees.

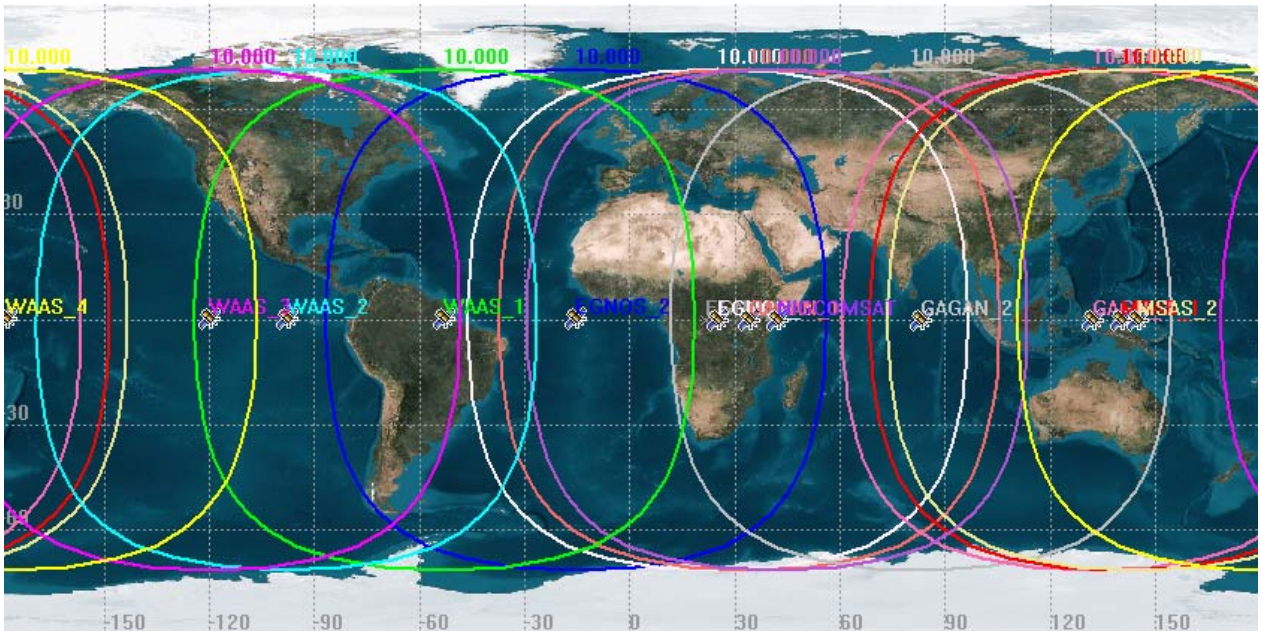

Figure 2.44. Ground tracks of EGNOS, WAAS, MSAS, GAGAN and NIGCOMSAT [Satellite Tool Kit STK, 2006]

2.9.2 Other Augmentation systems (GBAS, LAAS)

The previous chapters dealt with the different regional and augmentation systems on a satellite basis. In this chapter we will shortly describe other approaches to generate ranging signals from the ground, being the Ground Based Augmentation (GBAS) and the Local Area Augmentation System (LAAS) the two most important exponents.

2.9.2.1 Ground Based Regional Augmentation System (GRAS)

The Ground-based Regional Augmentation System (GRAS) is the Australian system to provide GNSS augmentation from the ground. The system is complementary to any of the Satellite Based Augmentation Systems (SBAS) that we saw above and also complements the Ground Based Augmentation Systems (GBAS) in general.

The user receives information directly from ground based transmitters allowing thus continuous reception of the service over a large geographical area of approximately 200 nautical miles. GRAS supports GNSS operations in all the phases of flight including en-route, terminal and instrument approach. GRAS is made up of multiple ground stations with overlapping coverage.

Regarding the operational requirements, The GRAS SARPs (Standards and Recommended Practices) have been submitted to ICAO for acceptance and amendment in the ICAO Annexure-10 volume I.

2.9.2.2 Local Area Augmentation System (LAAS)

The Local Area Augmentation System (LAAS) is a ground-based augmentation to GPS that focuses its service on the airport area (approximately a 20-30 mile radius) for precision approach, departure procedures and terminal area operations.

LAAS broadcasts its correction message via a very high frequency (VHF) radio data link from a ground-based transmitter. LAAS is expected to yield the extremely high accuracy, availability, and integrity necessary for Category I, II, and III precision approaches, and will provide the ability for flexible, curved approach paths. LAAS demonstrated accuracy is less than 1 meter in both the horizontal and vertical axis.

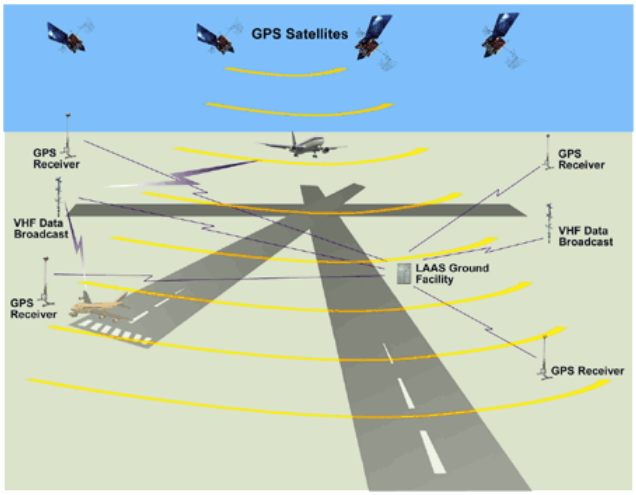

Figure 2.45. Typical Architecture of LAAS [Federal Aviation Administration FAA]

2.10 Pseudolites

A pseudolite (or pseudo-satellite) is a ground-based transmitter that broadcasts GNSS like signals [T.G. Morley, 1997]. The concept of a terrestrial GNSS transmitter is actually quite mature. In fact, as early as 1977, the Inverted Range, a GPS user equipment test facility located at the Yuma Proving Ground, used four ground transmitters (GTs) to augment the limited number of space-borne GPS satellites during initial GPS trials. Since then, interest in augmenting GPS with pseudolites (PLs) has grown steadily. One of the first papers to suggest the use of PLs for civilian aviation and maritime users was presented by [D. Klein and B.W. Parkinson, 1984].

We can also find some modifications to this concept in what is known as synchrolites or synchronized pseudolites, which derive their timing from individual GNSS satellites. Synchrolites are especially interesting for differential applications [H. S. Cobb, 1997].

One of the clearest examples of the pseudolite concept even for experimentation is the European GATE project. As we could see some lines above, the European satellite navigation system Galileo is under development, with a planned operational availability around 2011. The development of Galileo based applications and products becomes thus a matter of major importance. In the region of Bavaria, Germany, the GATE project has been set up. GATE is the German Galileo Test and Development Environment, a ground based, realistic test bed that was developed to cover the needs of receiver manufacturers and application developers [GATE Testbed]. It must be noted that the GATE transmissions are continuous and not pulsed.

Figure 2.46. German Galileo Test and Development Environment [GATE Testbed]

3. Galileo Baseline Evolution

3.1 Introduction

Once we have taken a close look at the different existing and planned navigation systems, it is time to start analyzing one of the main elements of any navigation system: its signals. Our objective in the coming chapters and indeed in the whole thesis is to underline the problematic of developing optimum signal waveforms for navigation. With that in mind, the Galileo signal design and GPS modernization will be special focus of this work. Nonetheless, given the importance that the Galileo programme has played in the last years, we dedicate this chapter to talk a little bit on the historical process that has lead to the Galileo Signal and Frequency Plan that we have today.

Galileo is an impressive technological achievement and one of the most important projects that are meant to unite the different countries of Europe. Given the enormous interest that Galileo is arising in the GNSS community, we will dedicate a whole chapter to describe how the Galileo Baseline has evolved in the last years and shortly describe what ideas were in the mind of those engineers that made it possible. This chapter aims thus at giving a historical overview of how the Galileo Signal and Frequency Plan has evolved over the time.

3.2 Square-Root Raised Cosine (SRRC) Signal waveforms for Galileo?

The Square-Root Raised Cosine (SRRC) was the first option for the Galileo Signal and Frequency Plan. It is already long time ago since the proposal was made but these first works deeply influenced the evolution of the coming years. At the time when the first analyses on the future Galileo signals were made [R. De Gaudenzi et al., 2000], the current frequency band assignments had not taken place yet. Thus, to limit the number of signal and frequency combinations, a set of seven candidate signal structures was identified, such that each of them could be independently assigned to a particular frequency. These are shown in Table 3.1.

As we can recognize, all the signals from Table 3.1, with the exception of S3, consist of an in-phase BPSK modulated spread-spectrum signal and an unmodulated quadrature spread-spectrum pilot that uses a different spreading sequence. It is also interesting to note the presence of an unmodulated pilot to achieve robust carrier phase tracking. This idea would remain until the final baseline of Galileo as we will see. Indeed, in spite of the fact that the SRRC was quickly abandoned due to its limitations, some original ideas present in Table 3.1 were kept until the end.

Table 3.1. Galileo Signal Plan proposed in [R. De Gaudenzi et al., 2000]. N/A* indicates that the pilot channel is not modulated by data

Signal Identifier	Spreading code Length	Chipping Rate (Mcps)	Modulation Arm	Information Rate	Coding Rate	Data Rate
S1	10230	3.069	I	750	1/2	1500
			Q	N/A*		
S2	10230	3.069	I	250	1/2	500
			Q	N/A*		
S3	1023	3.069	I	250	1/2	500
			Q	250	1/2	500
S4	10230	15.345	I	1500	1/2	3000
			Q	N/A*		
S5	10230	15.345	I	250	1/2	500
			Q	N/A*		
S6	10230	15.345	I	750	1/2	1500
			Q	N/A*		
S7	10230	15.345	I	2000	2/3	3000
			Q	N/A*		

In addition, the S3 signal used a short spreading code of 1023 chips as the GPS C/A to support fast acquisition of the S3 signal. The driver behind was to use this signal to assist acquisition of the longer codes on other frequencies and thus the implicit assumption was also that the S3 signal would always be present regardless of the combination of other signals. On the other hand, all other signals were planned to use longer spreading codes of length 10230 to provide increased robustness against inter- and intra-system interference. The proposed signals allowed a strict occupancy for the narrowband and wideband cases respectively.

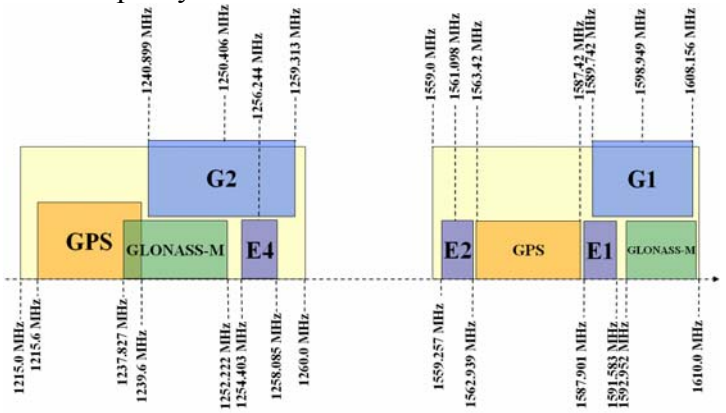

Figure 3.1. Galileo first Frequency plan for L-band [R. De Gaudenzi et al., 2000]

For the purposes of the Galileo Signal Validation Facility (GSVF) project, the frequency bands of interest were assumed to be El, E2, E4 as well as GPS-L1 and GLONASS-G1 as shown in the previous figure.

The centre frequency and available bandwidth for the different frequency designators are also shown in Table 3.2. It is important to note that all the signals are band-limited with a square root raised cosine filter. The basic signals used a roll-off factor, $\alpha = 0.22$ although other roll-off factors such as $\alpha = 0.28$ and $\alpha = 0.35$ were also under consideration. In chapter 4.8.2 a more detailed description of the Square-Root Raised Cosine (SRRC) modulation is given.

Table 3.2. First studied Galileo Frequency bands [R. De Gaudenzi et al., 2000]

Frequency Designator	Available Bandwidth [MHz]	Centre Frequency [MHz]
E1	4.0	1598.742
E2	4.0	1561.098
E4	4.0	1256.244
E5	20.0	1202.025
E6	20.0	1278.750
C1	20.0	5014.746

The Signal Plan presented above was not the only proposed solution from [R. De Gaudenzi et al., 2000]. In fact additional solutions were proposed as shown in the following table:

Table 3.3. Galileo Signal parameters for different options [R. De Gaudenzi et al., 2000]

Freq. Band	Target C/N_0 (dB-Hz)	EIRP (dBW)	Carrier Frequency (MHz)	Chip Rate (Mcps)	Data Stream	Info. Bit Rate (bps)	FEC, Coded data rate (bps)	Code length, Gold seq. (chips)	Code duration (μs)
Baseline									
E1	45	31.0	1589.742	3.069	E-NAV'	1500	½, 3000	1023	333,3
E2	45	30.8	1561.098	3.069	E-NAV'	1500	½, 3000	1023	333,3
E4	45	28.4	1256.244	3.069	E-NAV'	750	½, 1500	1023	333,3
Option 1									
G1	45	31.0	1598.949	15.345	E-NAV'	1500	½, 3000	1023	66,7
E2	45	30.3	1561.098	3.069	E-NAV'	750	½, 1500	1023	333,3
G2	45	28.9	1589.106	15.345	E-NAV'	1500	½, 3000	1023	66,7
Option 2									
E1	45	31.0	1589.742	3.069	E-NAV'	1500	½, 3000	1023	333,3
E4	45	28.4	1256.244	3.069	E-NAV'	750	½, 1500	1023	333,3
C	38	34.0	5014.746	15.345	E-NAV'	1500	½, 3000	1023	66,7

Finally, in regards to the Galileo orbit parameters, the following values were suggested.

Table 3.4. Galileo MEO Orbit Parameters [R. De Gaudenzi et al., 2000]

Orbital height	20,230 km
Orbital plane inclination	55°
Maximum Doppler Shift	4.4-5.2 kHz (L-band) 14.7-17.3 kHz (C-band)
Maximum Number of satellites in view	7-12
Elevation angle	5°-90°

As we can recognize, changes were also made here with respect to the final configuration of Galileo that we saw in chapter 2.4.1.

The Square-Root Raised Cosine (SRRC) modulation comes from the communications world and was proposed at that time due to its optimum spectral efficiency in the sense that for a limited bandwidth it is capable of transmitting more power than any other signal waveforms, such as the rectangular one. But as we know, the needs of navigation and communication do not always go hand by hand and what is good for the one is not necessarily also good for the other. The SRRC signal is band-limited as we will thoroughly describe in chapter 4.8.2 and even though it performs very well for narrow bandwidths the signal would have been handicapped from the beginning regarding its navigation performance since no matter how much we would broaden the receiver bandwidth, the performance would never be able to get any better. Indeed, this was its major drawback.

The intersymbol interference is better with the SRRC waveform than with a rectangular solution being this a very important aspect to take into account in environments with extremely low SNR as in the case of deep space transmissions. Nonetheless, the limited bandwidth of the signal to a very narrow value as shown above, condemned the signal to never being able to perform any better further away than 3 MHz. Of course the signal would be very good in terms of power transmission for that very narrow bandwidth, but no matter what we would do, we would never be able to improve its limited natural performance of 3 MHz. The ACF would present a very rounded peak and for navigation purposes this would imply a low intrinsic quality in terms of tracking.

Other consequences from the band-limited property of the SRRC pulse would be that compared to the GPS signals, for example, no improvement due to narrow correlation would be possible. In terms of receiver complexity in comparison with the rectangular waveform solution an additional degradation was observed.

Last but not the least, such a signal would have a degraded antijamming protection. We will see more in detail this in the coming chapters but we can already mention here that the antijamming protection against narrowband and wideband interference, may it be due to an intentional or unintentional source, increases as the spectrum of the signal widens. For the case of a limited-band signal thus, an important degradation in this regard would be observed. This would be especially critical for the Public Regulated Service (PRS) of Galileo. To finalize, it is important to mention that at the time as the studies were made [R. De Gaudenzi et al., 2000], the PRS signal was not even planned yet.

3.3 Galileo Baseline of 2002

The first tentative Galileo frequency and signal plan alternative to the one that we saw in the previous chapter was presented in [G.W. Hein et al., 2001] and it slowly became the baseline for the development of Europe's satellite navigation system. The Galileo carrier frequency, modulation scheme and data rate of all the 10 Galileo navigation signals as of September 2002 had experienced very important changes with respect to the first proposals. Moreover, the band frequency assignment was not an unknown any more and Galileo was developing similar concepts with regards to signal modulation as GPS. This means in other words, that the SRRC concept was abandoned and similar signal structures as those of GPS were now proposed for Galileo too. As we will point out later again, the status was already in a very mature phase and until the final signal plan not many substantial changes were required.

The main changes and add-ons with respect to the initial Signal Plan of chapter 3.2 are summarized in the following lines [G.W. Hein et al., 2001]:

- In the lower L-band (i.e. E5a and E5b) the central frequency for E5b was moved to 1207.14 MHz in order to minimize possible interference from the Joint Tactical Information Distribution System (JTIDS) and the Multifunctional Information Distribution System (MIDS). All signals on E5a and E5b would be using chip rates of 10 Mcps but the modulation scheme for that band was not decided yet. The idea in mind was to have a modulation that allowed processing of very wideband signals by jointly using the E5a and E5b bands. This joint use of the bands has the potential to offer enormous accuracy for precise positioning with a low multipath as we will see in the next chapters. This final wideband signal would be the AltBOC modulation. Furthermore, data rates had also been fixed in the baseline of 2002.
- In the middle (i.e. E6) and upper (i.e. E2-L1-E1) L-band, data and chip rates were also defined as well as the Search and Rescue (SAR) up- and downlink frequencies. Furthermore, extensive interference considerations took place in E5a/E5b concerning Distance Measuring Equipment (DME), the Tactical Air Navigation System (TACAN) and the Galileo overlay on GPS L5; in E6 concerning the mutual interference to/from radars and in E2-L1-E1 frequencies with regard to the Galileo overlay on GPS L1.

In addition, by 2002 the EC Signal Task Force and ESA had refined criteria for the code selection and had also formulated the requirements on each frequency. Nonetheless, different code structures were still under investigation.

It is also important to note that the Transport Council of the European Union in its meeting of $25^{th}/26^{th}$, March 2002, where the development phase of Galileo was finally decided,

underlined that compatibility and interoperability to GPS should be one of the key drivers for Galileo. With this signal plan, Galileo presented a good interoperability to GPS but still slight changes would be required. Next figure summarizes the characteristics of the resulting baseline signal plan of 2002.

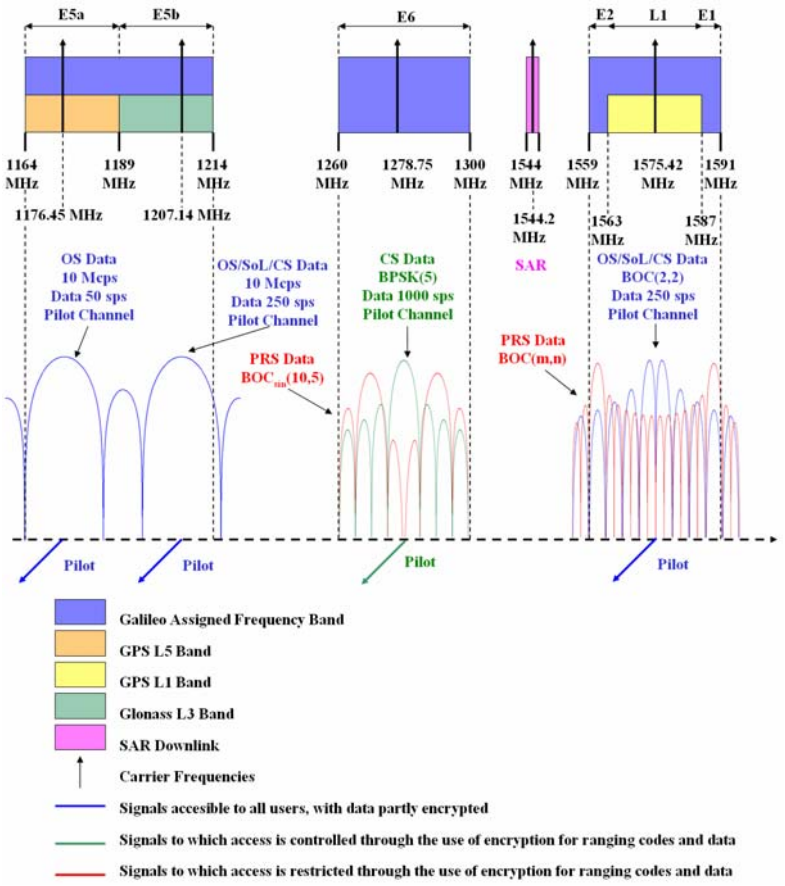

Figure 3.2. Galileo Frequency plan of September 2002

3.4 The Long Way to the Agreement

As we saw in the figure above, the signal plan of 2002 was already very mature in its design and with respect to today's baseline only little changes can be observed, especially in the E1 band, where a slight modification was needed to ensure compatibility between GPS and Galileo. The main changes are summarized next:

- E6: the PRS changed the phasing of the BOC(10,5) signal from sine to cosine.
- E1: The OS signals changed from BOC(2,2) to BOC(1,1) and the PRS moved from $BOC_{sin}(14,2)$ to $BOC_{cos}(15,2.5)$ in order to fulfil the Agreement of 2004 as we will mention in the next lines.
- E5: AltBOC remains until the end as the wideband signal of E5.

Let us analyze the changes that took place in a shorter time frame and with special attention to the most troublesome band: the E1 band.

3.4.1 Public Regulated Service in E1

Following the guidelines set up by the Transport Council of the European Union, beginning of 2004 the negotiations between the European Commission and the United States had clearly intensified with the objective of reaching compatibility and interoperability. At that moment, it was clear that Galileo would have to change its PRS signal from $BOC_{sin}(14,2)$ to another solution. In the preceding months different solution for the PRS had been thoroughly assessed:

- BPSK(5) at 1593.834 MHz as Public Regulated Service instead of $BOC_{sin}(14,2)$. As we can see in the following figure, such a signal would concentrate its PSD asymmetrically, allocating most on the power on the upper part of the E1 band.

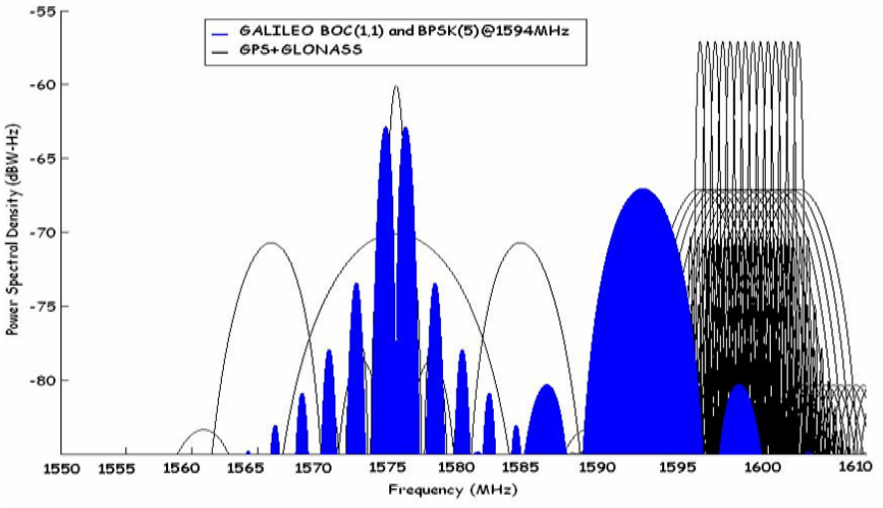

Figure 3.3. Signal Plan for E1 studied in 2004: PRS with BPSK(5)@1594 MHz

- BOC(2.5,2.5) at 1593.834 MHz was another alternative that was object of analysis. Similar to the solution described above, the signal would concentrate all its power on the upper part of the spectrum.

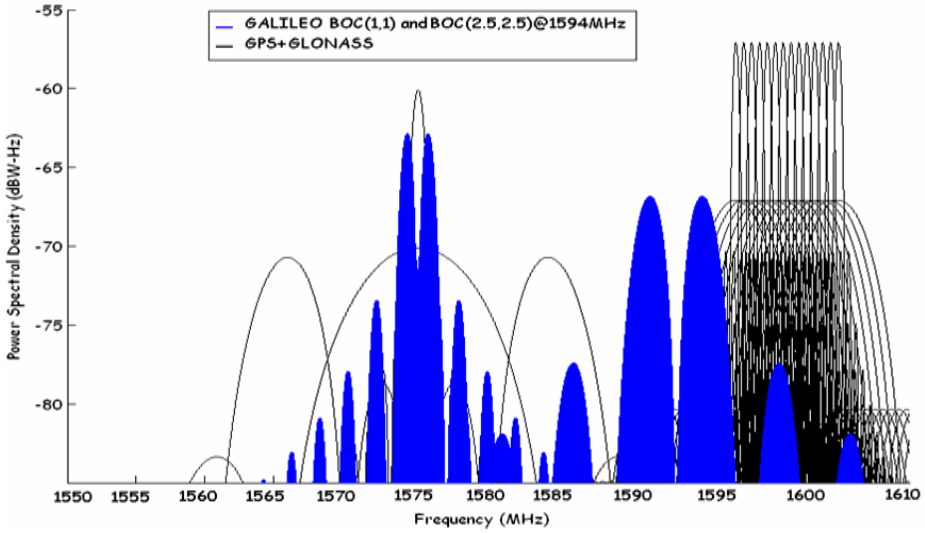

Figure 3.4. Signal Plan for E1 studied in 2004: PRS with BOC(2.5,2.5)@1594 MHz

- $BOC_{cos}(15,2.5)$. This was indeed the solution that was found to be the optimum one. Its Power Spectral Density is shown in the next figure.

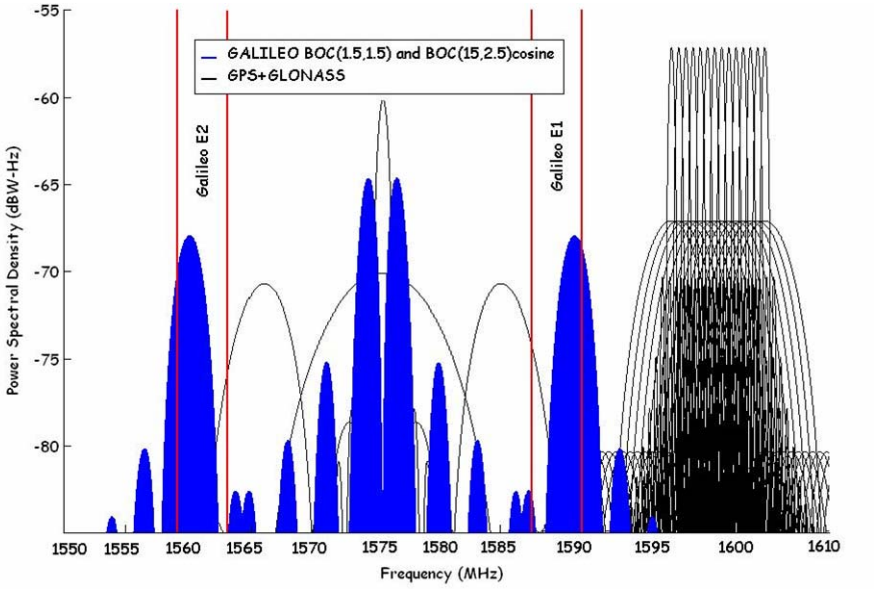

Figure 3.5. Signal Plan for E1 studied in 2004: PRS with $BOC_{cos}(15,2.5)$

3.4.2 Open Service: BOC(2,2) - BOC(1.5, 1.5) - $BOC_8(2,2)$ - BOC(1,1)

While there was common agreement on both the American and European side that the PRS signal had to change from $BOC_{sin}(14,2)$ to $BOC_{cos}(15,2.5)$ to preserve compatibility between GPS and Galileo, the Open Service signal and Civil signal of Galileo and GPS were still object of long discussions. Indeed, in Figure 3.5 above we can clearly recognize that although the PRS corresponds to the actual signal waveform, other signals such as BOC(1.5,1.5) were also being studied for the OS service. Some results on the performance of such solutions were also presented by [M. Irsigler et al., 2005]. Additionally, other interesting solutions were being explored such as $BOC_8(2,2)$, also known as the 8-PSK BOC(2,2), to which we will dedicate more time in chapter 4.5.5.1.

3.5 Agreement of 2004: BOC(1,1)+$BOC_{cos}(15, 2.5)$

Finally, after many years of fruitful cooperation, the member states of the European Union and the United States signed on June 26th, 2004, the *Agreement on the Promotion, Provision, and Use of Galileo and GPS Satellite-Based Navigation Systems and Related Applications*. With it, a new world of possibilities in satellite navigation opened. The agreement fixed BOC(1,1) as the baseline for both Galileo and GPS future OS signals, but at the same time opened the door to future possible implementations under the condition that they should have the current baseline as the core of potential optimizations and that they would be compatible with both the GPS M-Code and Galileo PRS. The PRS was raised to the same category as the M-Code. Next figure shows the resulting baseline of 2004:

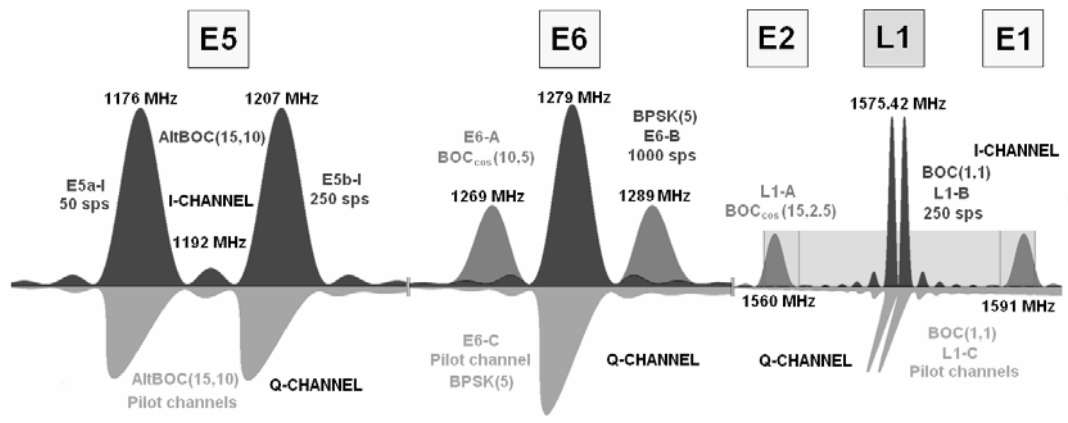

Figure 3.6. Galileo baseline after the Agreement of 2004

We can also take a closer look at the L1 band to see more in detail the spectral environment of the band. It must be noted that RAS refers to the Radio-Astronomy Service.

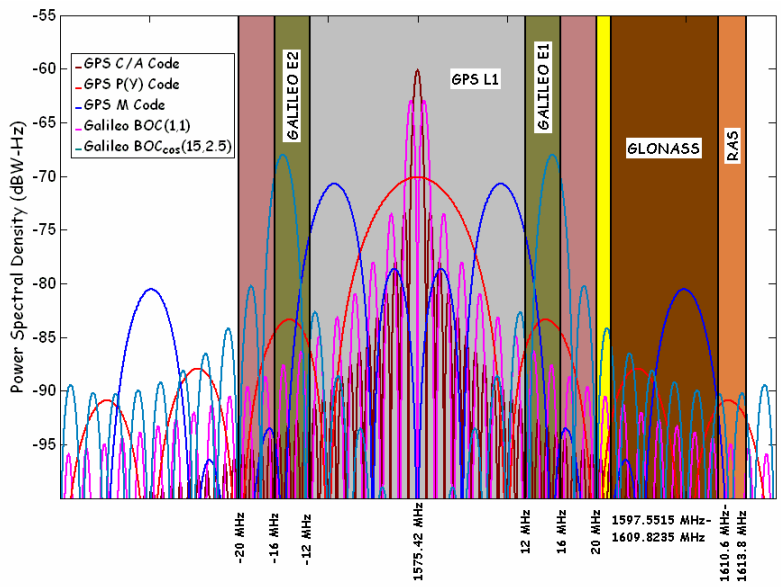

Figure 3.7. Galileo and GPS baseline in E1/L1 after the Agreement of 2004

3.6 The Way to Today's Baseline

3.6.1 *Crazy* BPSK, CBOC(5) and Others

Shortly after the Agreement of 2004 was signed, experts from both sides of the Atlantic started to work together to find possible alternatives to the common BOC(1,1) modulation that would clearly outperform the Open Service and Civil signals of the baseline and fulfil at the same time the requirements of the Agreement. Among the many solutions that were investigated at that time, we underline the following:

- MBOC(5) as the result of multiplexing BOC(1,1) and BOC(5,1)
- *Crazy* BPSK. This signal is a particular BCS sequence with 1.5 MHz chip rate and can

be described as BCS([15x0,1,4x0],1.5). The notation [15x0,1,4x0] denotes that the code chip is divided in 20 parts of equal length being the first 15 subchips logical zeros (or physically -1), then comes a +1 and finally 4 zeros (-1) are placed at the end. For more details on the mathematical properties of these signals refer to chapter 4.3. Given its great similarity with a BPSK signal, but with an additional quick flip, the signal was baptized as *crazy* BPSK.

- BCS signals with chip rates of 1.023 MHz or multiplexed versions with BOC(1,1).

3.6.2 Composite BCS (CBCS)

As we underlined in the chapter above, although the Agreement fixed BOC(1,1) as the baseline for both Galileo E1 Open Service and GPS future L1C signals, it also stated that the Parties would work together toward achieving optimization of that modulation for their respective systems, within the constraints of the Agreement. In September 2005 [G.W. Hein et al., 2005], a sophisticated signal known as CBCS was presented by members of the Signal Task Force of the EC. This signal promised improvement of more than 40 % in multipath performance with respect to BOC(1,1) under certain conditions. We will talk about it more in detail in chapter 4.6.

CBCS was highly compatible with BOC(1,1) receivers and fulfilled to a high degree the requirements of the Agreement of 2004. Moreover, it offered an important improvement in terms of performance.

3.6.3 Alternating Composite BCS (CBCS*)

CBCS had some inconvenient properties that we will analyze more in detail in chapter 4.6. Among them, the existence of a tracking bias that could potentially appear due to the cross-correlation between the CBCS signal and BOC(1,1) legacy receivers. This problem could be solved in different manners being the most interesting that of alternating the BCS sequence. The resulting signal thus received the name CBCS* where the * refers to the phase-alternation of the BCS component.

3.6.4 MBOC(4,1)

Shortly before MBOC(6,1) was selected, one more signal was intensely studied as potential alternative to BOC(1,1). This signal was MBOC(4,1). MBOC(4,1) was the result of multiplexing BOC(1,1) and BOC(4,1) but due to its spectral properties it showed a lower degree of growth potential than MBOC(6,1) and was thus abandoned.

3.7 MBOC(6,1)

Finally, a joint design activity involving experts from the United States and Europe produced a recommended optimized spreading modulation for the L1C signal and the Galileo E1 OS signal [MBOC Recommendation, 2006] and [GPS ICD-800, 2006]. The spreading modulation design places a small amount of additional power at higher frequencies in order to improve signal tracking performance. The signal was found to be satisfactory to both parties and significantly improved BOC(1,1). More details on MBOC will be provided in chapter 4.7. Next picture shows the working group members that participated in the informal meeting of Munich on March 9th, 2005 where MBOC was selected as candidate for the E1 Open Service and the L1 Civil Signal in L1.

Figure 3.8. Members of the US/EU working group celebrate their agreement on a recommended common MBOC structure for GPS and Galileo L1 civil signals: from left to right: Chris Hegarty, Tony Pratt, Jean-Luc Issler, John Owen, José-Ángel Ávila-Rodríguez, John W. Betz, Sean Lenahan, Stefan Wallner, and Günter W. Hein

The final frequency plan of Galileo is shown in the next figure in detail:

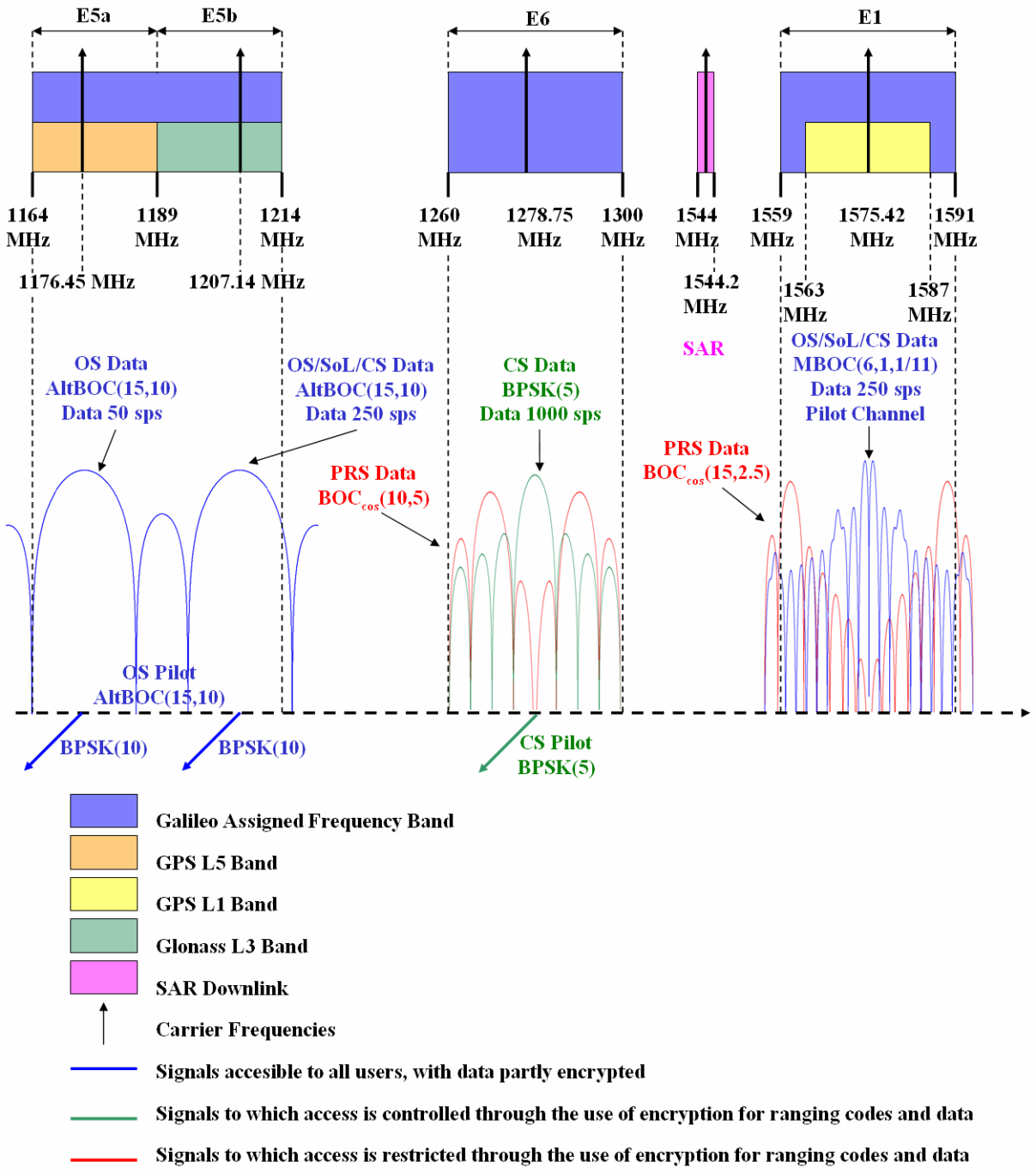

Figure 3.9. Final Galileo Frequency Plan

4. GNSS Signal Structure

Once a general overview on all the current and planned navigation systems has been provided, we will deal in the next chapters with the task of finding general expressions to define any navigation signal.

4.1 GNSS Modulation Schemes

Galileo and GPS signals are generated using the well known Direct Sequence Spread Spectrum (DSSS) technique. DSSS is a particular case of Spread Spectrum (SS) technique.

The SS principle seems simple and evident, but its implementation is indeed complex. In order to accomplish this objective, different SS techniques are available, but they all have one thing in common: they perform the spreading and dispreading operation by means of a pseudo random noise (PRN) code attached to the communication channel. The manner of inserting this code into the transmitting chain before the antenna is actually what defines the particular SS technique, as next figure shows:

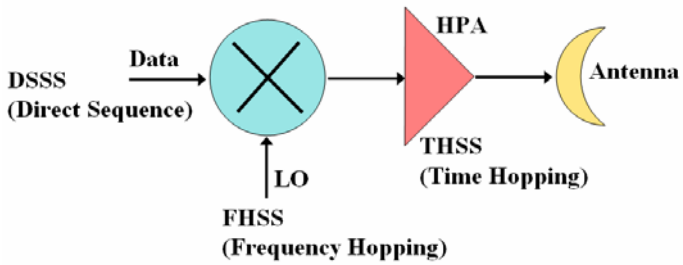

Figure 4.1. SS techniques classification depending on the point in the system at which the PRN code is inserted in the communication channel

According to this, a DSSS signal, $s(t)$ can be represented as follows [C.J. Hegarty, 2003] and [C.J. Hegarty et al., 2005]:

$$s(t) = \sum_{k=-\infty}^{+\infty} c_k(t) p\left(t - k\frac{T_c}{N}\right) \tag{4.1}$$

where $\{c_k\}$ represents the pseudorandom code symbols (which may be periodic), $p(t)$ is the *chip* waveform which is non-zero only over the interval support $[0, T_c)$ refers to the chip period and N is the number of equal length divisions of one chip period. In the next chapters of this chapter we will study different waveforms and analyze them in terms of their spectral efficiency and characteristics.

Of all the possible chip waveforms, the binary solutions belong to the most interesting for satellite navigation. Nevertheless, technology progresses so fast that it is possible to imagine more complex non-binary alternative spreading waveforms in a near future. In this chapter we will discuss the possibilities and potential they could bring to the navigation world.

4.1.1 Autocorrelation and Power Spectral Density

When dealing with DSSS signals, two very important characteristics are the autocorrelation function and the power spectrum, since they determine the navigation performance of a signal.

Let us assume that our signal is stationary in wide sense and can be expressed as follows:

$$s(t) = \sum_k c_k(t)\, p(t - kT_c - \theta) \tag{4.2}$$

where θ is a uniformly distributed variable within $[0, T_c)$. As we know, we say that a signal is stationary in wide sense when the first and second moments do not change with the time. This means in other words:

$$E\{s(t)\} = E\{s(t+\tau)\} \quad \forall\, \tau \in R \tag{4.3}$$

and

$$E\{s(t_1)s^*(t_2)\} = \Re_s(t_1, t_2) = \Re_s(t_1 + \tau, t_2 + \tau) = \Re_s(t_1 - t_2, 0) \quad \forall\, \tau \in R \tag{4.4}$$

what is equivalent to saying that the mean is constant and the correlation function does only depend on the difference of time between t_1 and t_2. It must be noted that θ does not vary with time representing thus an initial random shift in the signal that remains constant over time.

Assuming that our signal fulfils the above described properties, we can show that the autocorrelation function is defined thus as:

$$\begin{aligned}
\Re_s(\tau) &= E\left[s(t)s^*(t-\tau)\right] = \sum_k \sum_n E\left[c_k c_n^*\right] E\left[p(t - kT_c - \theta)\, p^*(t - nT_c - \theta - \tau)\right] \\
\Re_s(\tau) &= \sum_m \sum_k E\left[c_k c_{k-m}^*\right] \frac{1}{T_c} \int_0^{T_c} p(t - kT_c - \theta)\, p^*(t - \tau - kT_c + mT_c - \theta)\, \mathrm{d}t \Big|_{m=k-n} \\
\Re_s(\tau) &= \sum_m \sum_k \Re_c(m) \frac{1}{T_c} \int_0^{T_c} p(t - kT_c)\, p^*(t - \tau - kT_c + mT_c)\, \mathrm{d}t \Big|_{m=k-n}
\end{aligned} \tag{4.5}$$

since the signal is assumed to be stationary. We can further simplify this expression as:

$$\Re_s(\tau) = \frac{1}{T_c} \sum_m \Re_c(m)\, \Re_p(\tau - mT_c) \tag{4.6}$$

According to this, the power spectral density of $s(t)$ can be obtained from the Fourier Transform of the autocorrelation of $s(t)$, $\Re_s(\tau)$ derived above, according to:

$$\begin{aligned}
G_s(f) &= FT\left[\Re_s(\tau)\right] = FT\left[\frac{1}{T_c} \sum_m \Re_c(m)\, \Re_p(\tau - mT_c)\right] \\
G_s(f) &= \frac{1}{T_c} \sum_m \Re_c(m) \left|P(f)\right|^2 \mathrm{e}^{-j2\pi f m T_c}
\end{aligned} \tag{4.7}$$

where $P(f)$ is the Fourier Transform of the waveform $p(t)$. Moreover, the signal was assumed to be real. Assuming now that the PRN codes show ideal properties – that is random, non periodic, identically distributed, equiprobable and independent – then the crosscorrelation can be approximated as $E\{c_k c_n^*\} \approx \delta_{kn}$ or what is equivalent $\Re_c(m) \approx \delta(m)$, and the power spectrum density simplifies to:

$$G_s(f) = \frac{|P(f)|^2}{T_c} = f_c |P(f)|^2 \tag{4.8}$$

For further justification on the use of the Dirac delta in the previous lines, refer to [M. J. Lighthill, 1958] where additional arguments are provided. This expression is of great value since it will allow us to calculate the power spectral density of the different signals we will analyze in our work. Indeed, if we can express all the different signal waveforms by means of their chip waveform we will be able to use this expression to obtain the power spectral density. As we will mention later, this is not possible in a general case but fortunately it is a good approximation for most of the cases.

Moreover, real DSSS signals are not stationary in wide sense. Thus, it is better to work with the average autocorrelation function in general. According to this, the average autocorrelation function can be expressed as follows:

$$\overline{\Re}_s(\tau) = \frac{1}{T_c}\int_{t=0}^{T_c} \Re_s(t+\tau,\tau)\mathrm{d}t = \frac{1}{T_c}\sum_{k=-\infty}^{+\infty}\sum_{n=-\infty}^{+\infty} E[c_k c_n]\int_{t=0}^{T_c} p(t-nT_c)\,p(t-\tau-kT_c)\,\mathrm{d}t \tag{4.9}$$

where $p(t)$ was assumed to be real. This expression can be further developed as follows:

$$\overline{\Re}_s(\tau) = \frac{1}{T_c}\sum_{k=-\infty}^{+\infty}\sum_{n=-\infty}^{+\infty} E[c_k c_n]\int_{t=-nT_c}^{T_c(1-n)} p(t)\,p[t-\tau-(k-n)T_c]\mathrm{d}t \tag{4.10}$$

where $\Re_s(\tau)$ was derived some lines above in (4.6). Again, assuming the codes show ideal properties, the crosscorrelation will be $E[c_k c_n] \approx \delta_{kn}$.

Observing the equation above we can clearly recognize that the average autocorrelation function for a DSSS signal is equal to the aperiodic autocorrelation function of the chip waveform under the assumption that the codes are ideally random. This is a very important result since we will base most of the derivations of this chapter on it. Later we will relax this strong assumption on the ideality of the codes and see how the results differ when actual non-ideal codes are employed to modulate the chip waveform.

Once we have derived the expression for the average autocorrelation function (ACF) of a generic DSSS signal, the first question that arises is how the ACF of an ideal waveform should look like in order to be able to accomplish the best possible precise ranging in satellite navigation. As shown in the following figure, the sharper the peak of the autocorrelation function, the more precise the ranging will be with this waveform. Similar works with band-limited signals have been carried out by [F. Antreich and J. A. Nossek, 2007]. An

E-L discriminator with 0.1 chips of spacing was employed in this example.

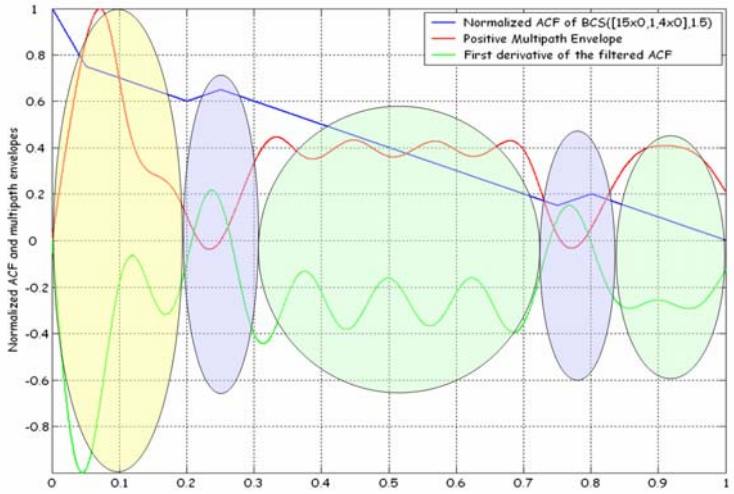

Figure 4.2. Example of the relationship between ACF and multipath performance

The following conclusions can be obtained from the figure above:

- If an E-L tracker is used, there is a high correlation between the multipath performance of a signal and the first derivative of the autocorrelation function.
- The first plateau (in yellow in the figure) or peak of the multipath envelopes is determined by the spacing of the correlator, by the location of the first secondary peak of the ACF and by the slope of the ACF around the main peak.
- The steeper the slope, the better as it reduces the plateau of the multipath envelopes.
- The nearer to the main peak the inversion of the sign of the secondary peak takes place, the better the multipath since the envelope is obligated to fall to 0 (blue).
- An inversion in the slope of the ACF forces the multipath envelopes to pass through zero. Therefore the closer this inversion is to the main peak, the lower the multipath envelopes will be for short multipath (blue).
- No inversion in the slope makes the multipath envelope to move/keep the height of the plateau (green).
- A change in the slope (not in the sign) makes the multipath envelope tend to a new plateau (yellow).
- The sensitivity of a signal to multipath is lower the higher the chipping rate is since the effect of multipath is invisible to the receiver once the multipath signal comes from a given distance that depends on the particular discriminator.

As a conclusion, the steeper the main peak of the autocorrelation and the more ripples this has, the better the potential performance of the signal will be. The counterpart is that the higher the number of elements in one chip, the higher will be the number of ripples of the autocorrelation so that the receiver might have problems to track or acquire the correct peak.

From (4.10) we can deduce that a signal with a *sharp* autocorrelation function can be generated by selecting $p(t)$ with good aperiodic correlation properties. In the ideal case, *p(t)*

should be a Dirac delta.
The expression for the chip waveform $p(t)$ is given by

$$p(t) = \sum_{i=0}^{n-1} p_i \, p_{T_c/n}\left(t - i\frac{T_c}{n}\right) \tag{4.11}$$

According to this, each chip waveform is broken up into n rectangular pulses of duration T_c/n with amplitudes defined by the sequence $\{p_i\}$. Furthermore, $p_{T_c/n}(t)$ represents the shape of each of the rectangular pulses the chip waveform is broken up into. In principle $\{p_i\}$, defined as MCS (Multilevel Coded Symbols) sequence in this thesis, could adopt any real value, although for satellite navigation a bi-phase signal with $\{p_i\} \in \{+1,-1\}$ is typical.

Finally, the power spectral density of the DSSS signal can be obtained as the Fourier Transform of the autocorrelation function derived above, according to

$$G_s(f) = \int_{\tau=-\infty}^{\infty} \overline{\Re}_s(\tau) \mathrm{e}^{-j2\pi f\tau} \, \mathrm{d}\tau \tag{4.12}$$

The interesting thing about the derivations above is that since the autocorrelation function was expressed in a *tailored* way using the general formulation of (4.11), the power spectrum can also be *tailored* shaping thus the attributes of the desired signal as we wish. This is of great interest for navigation applications, since on the one hand, as we mentioned above, we are interested in having autocorrelation functions as sharp as possible around the main peak, while at the same time a broad spectrum with minimum overlapping with other signals would minimize mutual interference with other existing signals in the band.

One final but important comment is that normally it is assumed that the transmitted GNSS interfering signals are band limited at the satellite transmitter. Thus, if we assume an ideal transmit filter of rectangular form (also referred to as brick-wall filter in this thesis) with bandwidth β_T, the normalized power spectral density of unit power within the satellite transmission bandwidth should be expressed as follows:

$$\overline{G}(f) = \begin{cases} \dfrac{G(f)}{\int_{-\beta_T/2}^{\beta_T/2} G(f)\mathrm{d}f} & |f| \le \beta_T/2 \\ 0 & |f| > \beta_T/2 \end{cases} \tag{4.13}$$

4.2 Multilevel Coded Spreading Symbols (MCS)

Generalizing the definition of [J.W. Betz, 2003], [C.J. Hegarty, 2003] and [A.R. Pratt and J.I.R. Owen, 2003b] to non-binary signals, Multilevel Coded Spreading Symbols can be seen as generalizations of BPSK and BOC. Each spreading symbol (which is phase modulated by a spreading code value) is divided into a number of equal-length segments, each of which is assigned a deterministic value. As we can infere from this definition, each of the segments, also called *subchips* in this thesis, can in principle adopt any value. The shape of the subchip could be thus rectangular, sinusoidal or something different.

The notation we will follow in this work to define an MCS signal as MCS([s], f_c) where [s] represents the MCS sequence in one chip and f_c is the chip rate. For the particular case that we work with binary signals we will have a BCS (Binary Coded Symbols) signal instead.

As shown in [C.J. Hegarty et al., 2005] and [C.J. Hegarty et al., 2004], Binary Coded Symbols are already present in the literature since long time ago but it has not been until recent times that they have been considered as a serious alternative to the current BPSK and BOC modulations. In fact, the BPSK modulation can also be denoted as BCS([1], f_c) having each segment unit value all over the chip. In a similar way, BOC(1,1) has f_s=1 and f_c=1 and thus a BCS sequence with values [+1,-1] spread with a 1.023 MHz code would uniquely define it. According to our definition, BOC(1,1) can also be denoted as BCS([1,-1],1). The following figure shows how a particular BCS signal could look like.

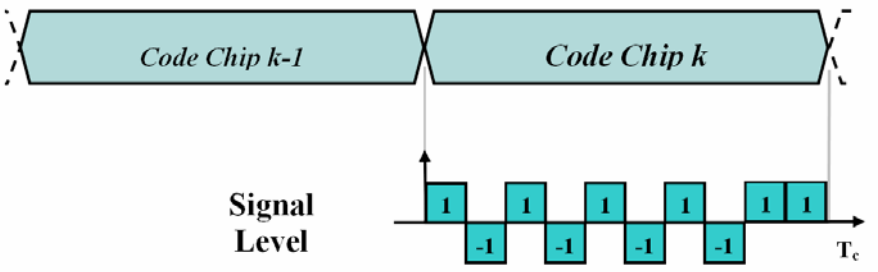

Figure 4.3. BCS([1,-1,1,-1,1,-1,1,-1,1,1], f_c) chip waveform in signal levels. This corresponds to the BCS component proposed for Galileo E1 OS (CBCS proposal)

We can go one step further in our definition of Binary Coded Symbols in line with [J.W. Betz, 2003] and define BCS([s_1],[s_2],…,[s_n], f_c) as the result of blending n different binary coded symbols at a chip rate f_c. This can be achieved for example by time multiplexing the different spreading symbols or by using different BCS sequences on In-phase and quadrature phase channels with independent spreading channels. As we will see in the following chapters, the MBOC signal relies on this blending concept. In the same manner MCS([s_1],[s_2],…,[s_n], f_c) would be the result of blending n different Multilevel coded symbols at a chip rate f_c.

Binary Coded Symbols have gained in interest for the enormous flexibility that they could offer for future GNSS optimizations.

In this chapter we will derive general expressions to calculate the power spectral density of BCS and MCS sequences in general. Additionally, analytical expressions for calculating the Spectral Separation Coefficient (SSC) between two BCS signals will be derived in chapter 5. Finally, more complex signal waveforms that result from applying the theory on MCS and BCS sequences will be obtained and analyzed in terms of their potential use for navigation.

MCS sequences are a promising field since well selected configurations offer clear performance advantages as well as the possibility to control spectral properties in a more efficient way. This aspect has been of crucial importance during the design of Galileo in order to be compatible and interoperable with GPS, and could show us the way to proceed in the future when new signals are planned to be placed in the already crowded RNSS bands.

4.2.1 MCS Power Spectral Density

The power spectrum of any DSSS signal can be obtained by means of its corresponding autocorrelation function as we saw in (4.12):

$$G_s(f) = \int_{\tau=-\infty}^{\infty} \overline{\Re}_s(\tau) \mathrm{e}^{-j2\pi f\tau} \mathrm{d}\tau \tag{4.14}$$

or by means of the Fourier Transform of the signal, as defined in (4.8).

$$G_s(f) = \frac{\left|P(f)\right|^2}{T_c} = f_c \left|P(f)\right|^2 = f_c \left|S(f)\right|^2 \tag{4.15}$$

For the sake of convenience we will use the notation $S(f)$ to refer to the chip waveform spectrum. In the following lines, we will make use of this latter expression to derive the PSD of a generic MCS signal. Indeed, the Fourier transform of a generic signal MCS([s], f_c) is shown to be:

$$S_{\mathrm{MCS}}(j\omega) = \sum_{k=1}^{n} \int_{\frac{(k-1)T_c}{n}}^{\frac{kT_c}{n}} s_k \mathrm{e}^{-j\omega t} \mathrm{d}t = \frac{2}{\omega} \sin\left(\frac{\omega T_c}{2n}\right) \mathrm{e}^{\frac{j\omega T_c}{2n}} \sum_{k=1}^{n} s_k \mathrm{e}^{-\frac{jk\omega T_c}{n}} \tag{4.16}$$

where n refers to the number of symbols in one chip and f_c is the chip rate of the MCS signal. This can be further expressed in the frequency domain as follows:

$$S_{\mathrm{MCS}}(f) = \mathrm{e}^{-\frac{j\pi f}{nf_c}} \frac{\sin\left(\frac{\pi f}{nf_c}\right)}{(\pi f)} \sum_{k=1}^{n} s_k \mathrm{e}^{-j2\pi fk/nf_c} \tag{4.17}$$

Once we have a general expression for the Fourier transform of an MCS signal, the power spectral density can be derived according to (4.8) as follows:

$$G_{\mathrm{MCS}([s],f_c)}(f)=G_{\mathrm{MCS}([\bar{s}],f_c)}(f)=f_c\frac{\sin^2\left(\frac{\pi f}{nf_c}\right)}{(\pi f)^2}\left\|\sum_{k=1}^{n}s_k\mathrm{e}^{-j\frac{2\pi fk}{nf_c}}\right\|^2 \tag{4.18}$$

We can go one step further in our derivation if we assume that the sequence consists of real coefficients (not necessarily binary) such that $s_k=s_k^*$. In this case,

$$\left\|\sum_{k=1}^{n}s_k\mathrm{e}^{-\frac{j2k\pi f}{nf_c}}\right\|^2=\left(\sum_{k=1}^{n}s_k\mathrm{e}^{-\frac{j2k\pi f}{nf_c}}\right)\left(\sum_{k=1}^{n}s_k\mathrm{e}^{-\frac{j2k\pi f}{nf_c}}\right)^*=\left(\sum_{k=1}^{n}s_k\mathrm{e}^{-\frac{j2k\pi f}{nf_c}}\right)\left(\sum_{k=1}^{n}s_k^*\mathrm{e}^{\frac{j2k\pi f}{nf_c}}\right)= \tag{4.19}$$
$$\left(s_1\mathrm{e}^{-j\frac{2\pi f}{nf_c}}+s_2\mathrm{e}^{-2j\frac{2\pi f}{nf_c}}+\ldots+s_n\mathrm{e}^{-nj\frac{2\pi f}{nf_c}}\right)\left(s_1\mathrm{e}^{j\frac{2\pi f}{nf_c}}+s_2\mathrm{e}^{2j\frac{2\pi f}{nf_c}}+\ldots+s_n\mathrm{e}^{nj\frac{2\pi f}{nf_c}}\right)$$

For simplicity in the notation we call $\mathrm{e}^{jk\frac{2\pi f}{nf_c}}=\{k\}$ and we will express the product of sums of (4.19) by means of the following *matrix* representation:

$$\Rightarrow m$$

$$l\Downarrow\quad M^n([\bar{s}])=\begin{pmatrix} s_1s_1\{0\} & s_1s_2\{1\} & s_1s_3\{2\} & \ldots & s_1s_n\{n-1\}\\ s_2s_1\{-1\} & s_2s_2\{0\} & s_2s_3\{1\} & \ldots & s_2s_n\{n-2\}\\ s_3s_1\{-2\} & s_3s_2\{-1\} & s_3s_3\{0\} & \ldots & s_3s_n\{n-3\}\\ \ldots & \ldots & \ldots & \ldots & \ldots\\ s_ns_1\{1-n\} & s_ns_2\{2-n\} & s_ns_3\{3-n\} & \ldots & s_ns_n\{0\}\end{pmatrix} \tag{4.20}$$

where *l* denotes the row index and *m* the column index. Since the coefficients are assumed to be real, $s_ls_m^*=s_l^*s_m=s_ls_m$ and the sum of all the terms in the matrix above can be expressed as follows:

$$\left\|\sum_{k=1}^{n}s_k\mathrm{e}^{-\frac{j2k\pi f}{nf_c}}\right\|^2=\begin{cases}\sum_{l=1}^{n}s_l^2+2\sum_{l=1}^{n-1}s_ls_{l+1}\cos\left(\frac{\omega T_c}{n}\right)+\\ +2\sum_{l=1}^{n-2}s_ls_{l+2}\cos\left(2\frac{\omega T_c}{n}\right)+\ldots\end{cases}=\left\{2\sum_{l=1}^{n}\sum_{m=1}^{n-l+1}s_ls_{l+m-1}\cos\left[(l-1)\frac{\omega T_c}{n}\right]-\sum_{l=1}^{n}s_l^2\right. \tag{4.21}$$

Furthermore, we can express the term is parentheses in a more simplified form if we apply the variable change *l*+*m*-1=*k'*, yielding thus:

$$\left\|\sum_{k=1}^{n}s_k\mathrm{e}^{-\frac{j2k\pi f}{nf_c}}\right\|^2=2\sum_{l=1}^{n}\sum_{k'=l}^{n}s_ls_{k'}\cos\left[(k'-l)\frac{\omega T_c}{n}\right]-\sum_{l=1}^{n}s_l^2 \tag{4.22}$$

Observing the matrix of (4.20) above, we can clearly see that we only need to look at the terms of the right superior triangular part of the matrix to compute the PSD of the MCS signal for any given real sequence. Moreover, it must be noted again that this sequence has not to be necessarily binary, being BCS a particular case of MCS as defined in the lines above. Combining now (4.18) and (4.22) we have the general expression for the power spectral density of a generic MCS signal:

$$G_{\mathrm{MCS}([\bar{s}],f_c)}(f)=f_c\frac{\sin^2\left(\frac{\pi f}{nf_c}\right)}{(\pi f)^2}\left\{\sum_{l=1}^{n}s_l^2+2\sum_{l=1}^{n-1}\sum_{k'=l+1}^{n}s_l s_{k'}\cos\left[(k'-l)\frac{\omega T_c}{n}\right]\right\} \tag{4.23}$$

or equivalently,

$$G_{\mathrm{MCS}([\bar{s}],f_c)}(f)=f_c\frac{\sin^2\left(\frac{\pi f}{nf_c}\right)}{(\pi f)^2}\left\{2\sum_{l=1}^{n}\sum_{k'=l}^{n}s_l s_{k'}\cos\left[(k'-l)\frac{\omega T_c}{n}\right]-\sum_{l=1}^{n}s_l^2\right\} \tag{4.24}$$

4.3 Binary Coded Symbols (BCS)

Binary coded symbols are a particular case of MCS signal with a binary chip sequence $s_l\in\{+1,-1\}$. The power spectral density of a generic $\mathrm{BCS}\left([s_1,s_2,s_3,...,s_n],f_c\right)$ can thus be derived from (4.23) or (4.24) and is shown to adopt the following simplified form:

$$G_{\mathrm{BCS}([\bar{s}],1)}(f)=f_c\frac{\sin^2\left(\frac{\pi f}{nf_c}\right)}{(\pi f)^2}\left\{\sum_{l=1}^{n}\sum_{k'=l}^{n}2s_l s_{k'}\cos\left[(k'-l)\frac{2\pi f}{nf_c}\right]-n\right\} \tag{4.25}$$

Or equivalently:

$$G_{\mathrm{BCS}([\bar{s}],1)}(f)=nf_c\frac{\sin^2\left(\frac{\pi f}{nf_c}\right)}{(\pi f)^2}\left\{1+\frac{1}{n}\sum_{l=1}^{n-1}\sum_{k'=l+1}^{n}2s_l s_{k'}\cos\left[(k'-l)\frac{2\pi f}{nf_c}\right]\right\} \tag{4.26}$$

where the first term of the product corresponds to the PSD of a BPSK with nf_c MHz of chip rate and the second term can be represented by the matrix defined in (4.20) and is shown to have a power of 1 in an infinite bandwidth. We can thus represent the PSD as follows:

$$G_{\mathrm{BCS}([\bar{s}],1)}(f)=G_{\mathrm{BPSK}(nf_c)}(f)G_{\mathrm{Mod}}(f) \tag{4.27}$$

According to this, the function that seems to bring more information about the BCS sequence is the sum of the second factor. This term, namely $G_{\mathrm{Mod}}(f)$, can be easily computed with the matrix we defined in (4.20) and we will call it *modulation* term for short. Furthermore, it is important to realize that the *modulation* term and the spreading symbol are used indistinctly in the literature to indicate the same.

Furthermore, it is important to note that (4.27) can be further generalized to

$$G_{\mathrm{BCS}([s],1)}(f)=G_{\mathrm{Subchip\ pulse}}(f)G_{\mathrm{Mod}}(f) \tag{4.28}$$

for the case that the sub-chip is modulated by a generic non-rectangular pulse. This will be used in further chapters when we derive more general expressions and is also shown in the Appendixes of this thesis.

The main conclusion that can be drawn from observing this definition matrix is that a subchip alone, or in other words an element of the sequence alone, does not directly affect the PSD of the whole signal. It must be understood in relationship with all the other elements of the sequence. This adds an important complexity. In fact, it is not trivial to derive qualitatively the shape of any generic BCS signal by only having a look at its generation sequence $[\bar{s}] = \bar{s}$.

We can clearly see this in the following example. Let us imagine different BCS signals of length 21 consisting only of ones expect for one logical zero (or -1 at signal level) where the zero subchip is placed at different locations within the BCS vector.

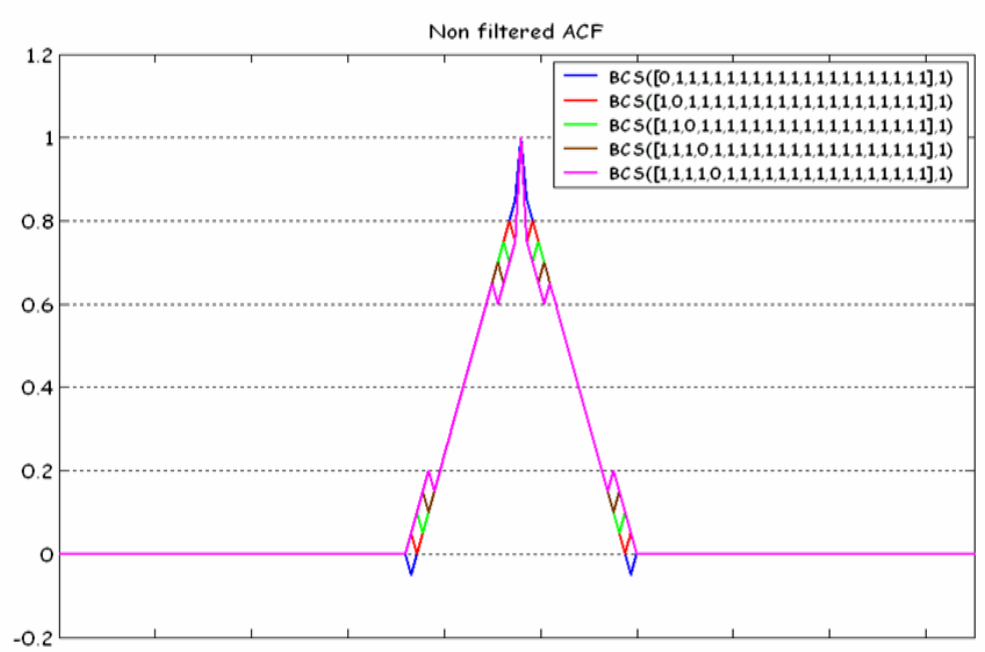

Figure 4.4. Autocorrelation Function of different BCS sequences

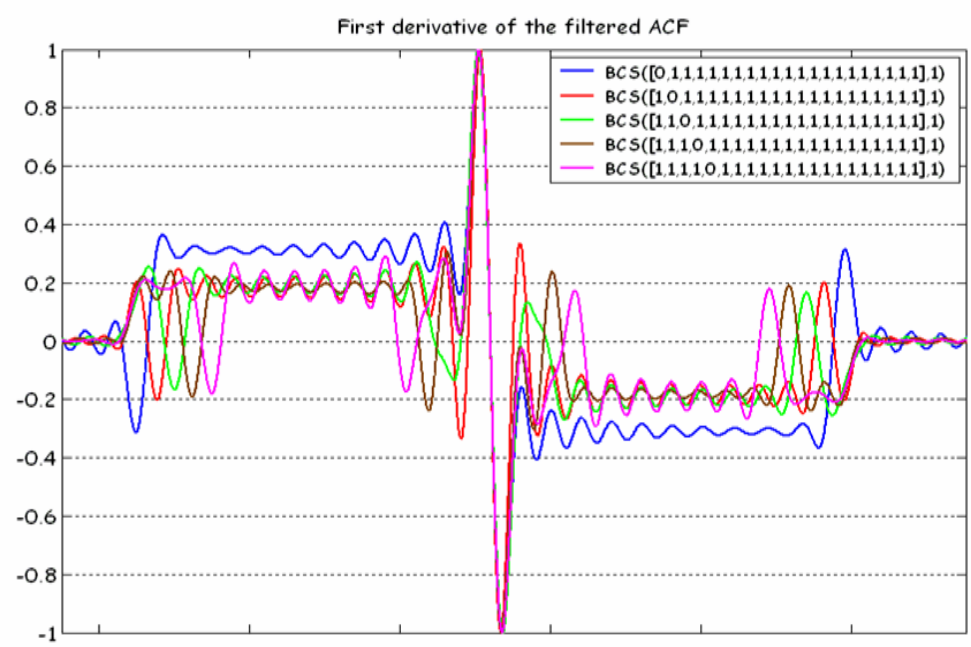

Figure 4.5. First Derivative of the Autocorrelation of different BCS sequences

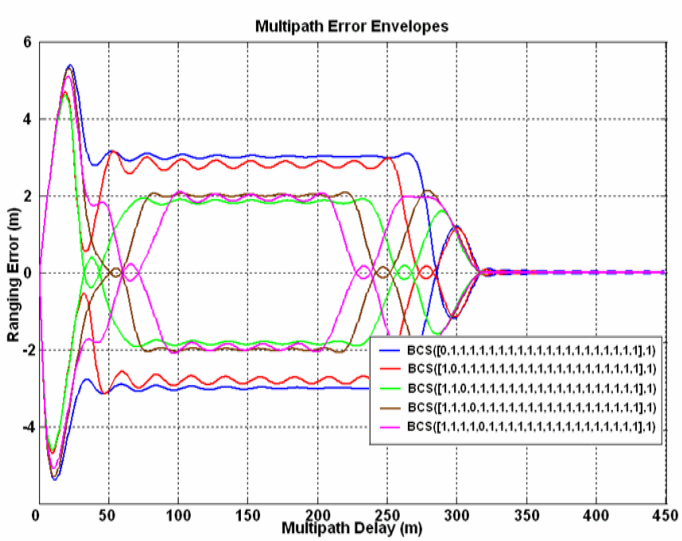

Figure 4.6. Multipath Envelopes of different BCS

For the previous figures, an E-L discriminator with 0.1 chips of spacing was employed. As we can recognize, a single shift to the right in the BCS sequence alters the final multipath performance significantly. This leads us thus to the conclusion that evaluating the multipath performance of a signal with a quick look is not an easy task as it was with BPSK and BOC signals, for example. Even though we knew how the BCS sequence looks like, a simple shift would significantly modify the multipath properties of the signal. Indeed, the mathematical ideas and conclusions gathered above have driven many of the works that were carried out in the past years to find the MBOC signal.

4.3.1 Binary Phase Shift Keying Modulation (BPSK)

A very important and useful signal in satellite navigation is the BPSK modulation which was in fact the first one to be used for Satellite Navigation. In spite of its simplicity, it is still used nowadays but could eventually be substituted by the BCS modulation or combinations with this one in the medium-long term.

We will derive now the power spectral density of a BPSK(f_c) using the general definition of BCS that we saw in chapter 4.3. According to this, any BPSK(f_c) signal can be described as a BCS sequence with vector $\bar{s} = [1\ 1\ 1\ \ldots 1]$ whatever the length of the vector. We will derive the expression of the PSD generalizing over n.

First we build the $M^n([\bar{s}])$ matrix for any n, which is shown to be:

$$M^n([1,1,\ldots,1]) = \begin{pmatrix} 1\{0\} & 1\{1\} & 1\{2\} & \ldots & 1\{n-1\} \\ & 1\{0\} & 1\{1\} & \ldots & 1\{n-2\} \\ & & 1\{0\} & \ldots & 1\{n-3\} \\ & & & \ldots & \ldots \\ & & & & 1\{0\} \end{pmatrix} \tag{4.29}$$

According to this, the modulating function will be:

$$G_{\text{Mod}}(f) = n + 2\left\{\sum_{i=1}^{n-1}(n-i)\cos\left[i\frac{2\pi f}{nf_c}\right]\right\} \tag{4.30}$$

Similar to how we will do with the BOC modulation, once the modulating term has been calculated, the power spectral density can be expressed as follows:

$$G_{\text{BPSK}}(f_c) = G_{subchip\ pulse}^{\text{BPSK}(nf_c)}(f)\,G_{\text{Mod}}^{\text{BPSK}(f_c)}(f) = f_c\frac{\sin^2\left(\frac{\pi f}{nf_c}\right)}{(\pi f)^2}\left\{n + 2\left[\sum_{i=1}^{n-1}(n-i)\cos\left[i\frac{2\pi f}{nf_c}\right]\right]\right\} \tag{4.31}$$

After some math, it has been shown in Appendix M that (4.31) can be simplified to the well known expression that we can find everywhere in the literature:

$$G_{\text{BPSK}}(f_c) = f_c\frac{\sin^2\left(\frac{\pi f}{f_c}\right)}{(\pi f)^2} \tag{4.32}$$

4.3.2 Binary Offset Carrier (BOC)

Binary Offset Carrier Signals are a particular case of BCS signals with a representation vector formed by +1's and -1's alternating in a particular defined way. Two notations [E. Rebeyrol et al., 2005] can be found in the literature to define the BOC signals. We describe them shortly in the following lines.

The first model defines the BOC modulation as the result of multiplying the PRN code with a sub-carrier which is equal to the sign of a sine or a cosine waveform, yielding so-called sine-phased or cosine-phased BOC signals respectively as shown in [J.W. Betz, 2001], [L.R.Weill, 2003], [J. Godet, 2001] and [E. Rebeyrol et al., 2005]. According to this definition, the expression of the sine-phased BOC signal would be:

$$s(t) = c(t)\,\text{sign}\left[\sin(2\pi f_S t)\right] \tag{4.33}$$

with

$$c(t) = \sum_k c_k\, h(t - kT_c) \tag{4.34}$$

where

- c_k is the code sequence waveform,
- f_s is the sub-carrier frequency,
- and $h(t)$ is the Non Return to Zero (NRZ) code materialization with value 1 over the support $[0, T_c)$.

The second model defines the BOC modulation as follows:

$$s(t) = \sum_k c_k\, p_{T_c}(t - kT_c) \tag{4.35}$$

where $p_{T_c}(t)$ describes the chip waveform and is broken up into n rectangular pulses of duration T_c/n with amplitude ±1. It is important to note that in this case the sine-phasing or cosine-phasing is considered as part of the chip waveform definition. This convention has been introduced in [A.R. Pratt and J.I.R. Owen, 2003a] and [J.W. Betz, 2001].

No matter what definition we choose to describe the BOC modulation in the time domain, the BOC signal is commonly referred to as BOC(f_s, f_c) where $f_s = m \cdot 1.023$ and $f_c = n \cdot 1.023$ so that generally one only says BOC(m, n) for simplicity. Moreover, unless it is indicated in a different way, when we talk about BOC signals we will always mean the sine-phased variant.

The parameter Φ is of great interest when analyzing BOC signals. It is defined as two times the ratio between the sub-carrier and the chip frequency as follows:

$$\Phi = 2\frac{f_s}{f_c} = 2\frac{m}{n} \tag{4.36}$$

As we can see, Φ represents the number of half periods of the sub-carrier that fit in a code chip so that this ratio can be even or odd. When Φ is even, the two definitions presented above for the BOC modulation coincide since we can consider the sub-carrier as included in the chip waveform. However, when Φ is odd the second definition is not valid any more. The following example shows this. Indeed, depending on the convention that we adopt to define the BOC signal we can see that different time series result.

Consider the code sequence {1,-1,1, -1,1,1} and a sine-phased waveform with $2f_s/f_c = 3$. If we employ the first convention, the rectangular sub-carrier that results from taking the sign of the sine waveform will be as follows:

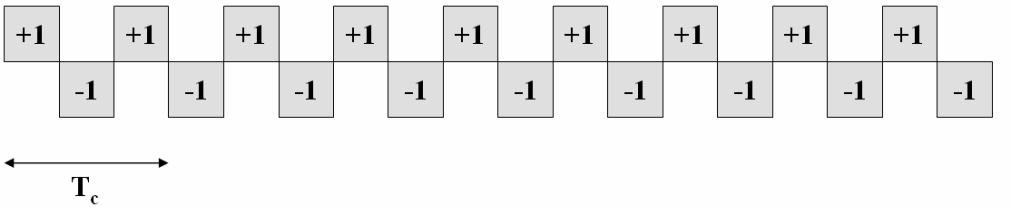

Figure 4.7. Sine-phased sub-carrier for the BOC modulation

Accordingly, the product of the binary sub-carrier (4.33) with the code sequence results in the following time series:

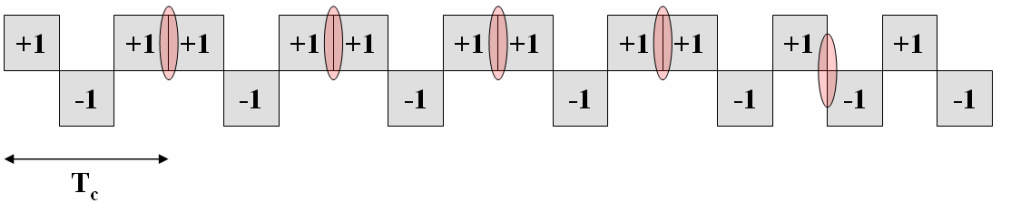

Figure 4.8. Product of the sine-phased sub-carrier and the code sequence {1,-1,1,-1,1,1}

where all the transitions have been underlined in red. If we follow now the approach of defining the sub-carrier as part of the chip waveform as it is done in the second definition, the

chip waveform to use will be:

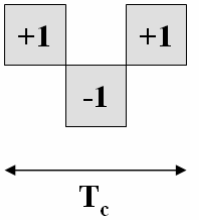

Figure 4.9. Chip waveform to represent the sine-phasing according to the second definition of BOC

and the resulting time series will be as follows:

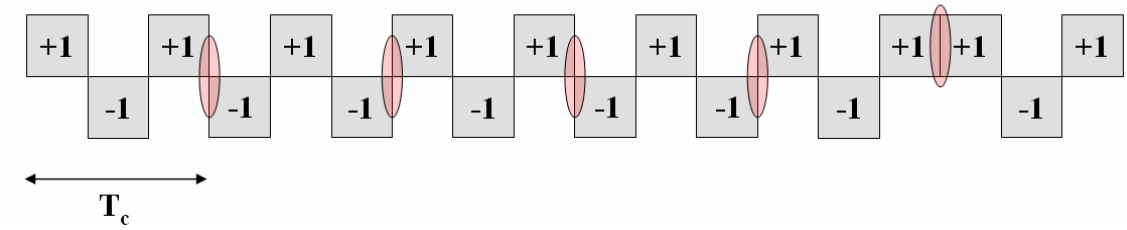

Figure 4.10. Product of the sine-phased chip waveform and the sequence {1,-1,1,-1,1,1}

If we compare now Figure 4.8 and Figure 4.10 we can clearly recognize that the two definitions of BOC do not lead to an unique time series representation. Indeed the difference is a polarity inversion every two bits as identified in [E. Rebeyrol et al., 2005].

We conclude thus that if Φ is odd, a slight modification must be made in the second definition to account for the effect of the sub-carrier onto the code as shown in [J.W. Betz, 2001]. Indeed, the new definition should be for the case of Φ odd as follows:

$$s(t) = \sum_k (-1)^k c_k \; p_{T_c}(t - k T_c) \tag{4.37}$$

resulting then both conventions in the same time series.

If we look at the equations above in detail, we can recognize the term $(-1)^k$ introduced in the expression, what can be interpreted as a modification of the PRN sequence so that all the even code positions would alternate. Indeed, the new code would be then $(-1)^k c_k$ instead of the original c_k. As a conclusion, in the case of Φ odd a modification must be made on the code sequence if we want the sub-carrier to be included in the chip waveform. This does not represent a real problem from a theoretical point of view but it is important to note that depending on which convention is used, the receiver must be adapted consequently because otherwise it would suffer from non desired losses [E. Rebeyrol et al., 2005].

Once the two definitions of BOC have been presented, it seems that the first one represents better the original definition of the BOC signal since no exception in the definition must be

made depending on whether the figure $\Phi = 2\frac{f_s}{f_c}$ is even or odd. Nonetheless, the second convention allows for easier and more tractable derivations in some cases and thus both conventions will be indistinctively used in this thesis.

Moreover, we have shown that the second convention is also correct as long as the PRN code is correspondingly modified. Since in this chapter we will derive expressions for smooth spectra and assume consequently that the PRN code shows ideal properties, also the modified code version should present similar ideal properties and we can directly consider the sub-carrier as included in the code materialization. This will considerably simplify the derivations as we will see. Consequently we can use (4.8) to calculate the power spectral density of BOC as shown in the different Appendixes. This is actually not only valid for the BOC modulation, but for all the signals that can be expressed as shown in (4.2).

Last but not the least, it must be noted that for non-ideal codes or very short codes this is not true any more. We will analyze these effects in chapter 6.2.2.

It is important to note that the conclusions derived above for the sine-phased BOC modulation can easily be extended to the cosine case and to any BCS signal in general. In fact, also for a BCS signal we can distinguish between even and odd BCS signals in a similar manner as we did above. However, the examples might not be so easy to analyze in this case.

4.3.2.1 Binary Offset Carrier with sine phasing: $BOC_{sin}(f_s, f_c)$

As we saw in chapter 4.3.2 the Binary Offset Carrier Modulation can be expressed as a BCS sequence with a vector that is formed by alternating +1 and -1 a number of times f_s/f_c. In the next lines we will derive the general expression of the power spectral density. To do so, we recall (4.26) and we build up the corresponding matrix to calculate $G_{\text{Mod}}(f)$ as defined in the previous chapter. As we will see next, the matrix shows symmetry properties that will allow to simplify the problem considerably.

To start, let us analyze the particular case of BOC(f_c, f_c). As we saw in the preceding lines, BOC(f_c, f_c), also known as $BOC_{sin}(f_c, f_c)$, can be expressed as BCS([1,-1], f_c) and presents thus the following matrix:

$$M^2\left([1,-1]\right) = \begin{pmatrix} s_1 s_1\{0\} & s_1 s_2\{1\} \\ & s_2 s_2\{0\} \end{pmatrix} = \begin{pmatrix} 1\{0\} & -1\{1\} \\ & 1\{0\} \end{pmatrix} \tag{4.38}$$

According to this

$$G_{\text{Mod}}^{\text{BOC}(f_c,f_c)}(f) = 2 - 2\cos\left(\frac{2\pi f}{2f_c}\right) = 4\sin^2\left(\frac{\pi f}{2f_c}\right) \tag{4.39}$$

adopting the pulse term of the PSD the following form:

$$G_{\text{pulse}}^{\text{BPSK}(2f_c)}(f) = f_c \frac{\sin^2\left(\frac{\pi f}{2f_c}\right)}{(\pi f)^2} \tag{4.40}$$

Finally, according to (4.26), the power spectral density of this particular case would be:

$$G_{\text{BOC}(f_c,f_c)}(f) = G_{\text{pulse}}^{\text{BPSK}(2f_c)}(f) G_{\text{Mod}}^{\text{BOC}(f_c,f_c)}(f) = f_c \left[\frac{\sin\left(\frac{\pi f}{f_c}\right)\sin\left(\frac{\pi f}{2f_c}\right)}{\pi f \cos\left(\frac{\pi f}{2f_c}\right)} \right]^2 \tag{4.41}$$

Let us now extend this expression to any $\text{BOC}_{\text{sin}}(f_s, f_c)$ generalizing on f_s/f_c with f_s/f_c being an integer, namely the number of times that the pair {1,-1} repeats. Indeed, once we have found the expression $G_{\text{Mod}}(f)$ with $f_s/f_c = 1$, we calculate for $f_s/f_c = 2$ in the same manner:

$$\text{BOC}_{\text{sin}}(f_s, f_c) = \text{BOC}_{\text{sin}}(2f_c, f_c) \text{ or } \text{BCS}([1,-1,1,-1], f_c) \tag{4.42}$$

where the definition matrix is shown to be:

$$M^4([1,-1,1,-1]) = \begin{pmatrix} s_1s_1\{0\} & s_1s_2\{1\} & s_1s_3\{2\} & s_1s_4\{3\} \\ & s_2s_2\{0\} & s_2s_3\{1\} & s_2s_4\{2\} \\ & & s_3s_3\{0\} & s_3s_4\{1\} \\ & & & s_4s_4\{0\} \end{pmatrix} = \begin{pmatrix} 1\{0\} & -1\{1\} & 1\{2\} & -1\{3\} \\ & 1\{0\} & -1\{1\} & 1\{2\} \\ & & 1\{0\} & -1\{1\} \\ & & & 1\{0\} \end{pmatrix} \tag{4.43}$$

and thus

$$G_{\text{Mod}}^{\text{BOC}(2f_c,f_c)}(f) = 4 + 2\left[-3\cos\left(\frac{2\pi f}{4f_c}\right) + 2\cos\left(2\frac{2\pi f}{4f_c}\right) - \cos\left(3\frac{2\pi f}{4f_c}\right) \right] \tag{4.44}$$

It is interesting to note that the term in the brackets resembles a Fourier series until term *n*-1. If we continue now by induction we can see that the expression for any *n* adopts the following form:

$$G_{\text{Mod}}^{\text{BOC}(nf_c/2,f_c)}(f) = n + 2\sum_{i=1}^{n-1}(-1)^i(n-i)\cos\left(i\frac{2\pi f}{nf_c}\right) \tag{4.45}$$

where $n \in \{2,4,6,8...\}$. It must be noted that the variable *n* refers to the number of subchips and not to the number of times that the sub-carrier contains the code rate as usually done in the literature. Once we have obtained the modulating term of the power spectral density, the general form of the PSD for any sine-phased BOC modulation can be expressed as:

$$G_{\text{BOC}_{\text{sin}}\left(f_s=\frac{nf_c}{2},f_c\right)} = G_{\text{pulse}}^{\text{BPSK}(nf_c)}(f) G_{\text{Mod}}^{\text{BOC}(nf_c/2,f_c)}(f) = f_c \frac{\sin^2\left(\frac{\pi f}{nf_c}\right)}{(\pi f)^2} \left\{ n + 2\sum_{i=1}^{n-1}(-1)^i(n-i)\cos\left(i\frac{2\pi f}{nf_c}\right) \right\} \tag{4.46}$$

which can be explicitly simplified as shown in Appendix B:

$$G_{\mathrm{BOC}_{\sin}\left(f_s=\frac{nf_c}{2},f_c\right)}=f_c\frac{\sin^2\left(\frac{\pi f}{f_c}\right)}{(\pi f)^2}\tan^2\left(\frac{\pi f}{nf_c}\right) \tag{4.47}$$

As a conclusion, the BOC signal in sine phase can be considered as a BCS signal whose sequence is formed by concatenating [+1,-1] a number of times f_s/f_c. Thus the length *n* will be $2f_s/f_c$ and (4.47) can also be expressed as:

$$G_{\mathrm{BOC}_{\sin}(f_s,f_c)}=f_c\frac{\sin^2\left(\frac{\pi f}{f_c}\right)}{(\pi f)^2}\tan^2\left(\frac{\pi f}{2f_s}\right)=f_c\left[\frac{\sin\left(\frac{\pi f}{f_c}\right)\sin\left(\frac{\pi f}{2f_s}\right)}{\pi f\cos\left(\frac{\pi f}{2f_s}\right)}\right]^2 \tag{4.48}$$

which is the well known form we find in the literature [J.W. Betz, 2001].

4.3.2.2 Binary Offset Carrier with cosine phasing: $\mathrm{BOC}_{\cos}(f_s, f_c)$

Following the same approach of the previous chapter, we will derive next the well known expression for the power spectral density of the BOC modulation with sub-carrier in cosine phasing. Taking as an example the sine-phased BOC signal of the lines above, we will derive now also a general expression by induction over *n*. Let us begin with $\mathrm{BOC}_{\cos}(f_c, f_c)$:

$$\mathrm{BOC}_{\cos}(f_s, f_c)=\mathrm{BOC}_{\cos}(f_c, f_c) \text{ or } \mathrm{BCS}([1,-1,-1,1], f_c) \text{ with } f_c=1.023 \text{ MHz} \tag{4.49}$$

The corresponding definition matrix under these assumptions is shown to be:

$$M^4\left([1,-1,-1,1]\right)=\begin{pmatrix} s_1s_1\{0\} & s_1s_2\{1\} & s_1s_3\{2\} & s_1s_4\{3\} \\ & s_2s_2\{0\} & s_2s_3\{1\} & s_2s_4\{2\} \\ & & s_3s_3\{0\} & s_3s_4\{1\} \\ & & & s_4s_4\{0\} \end{pmatrix}=\begin{pmatrix} 1\{0\} & -1\{1\} & -1\{2\} & 1\{3\} \\ & 1\{0\} & 1\{1\} & -1\{2\} \\ & & 1\{0\} & -1\{1\} \\ & & & 1\{0\} \end{pmatrix} \tag{4.50}$$

Thus, the modulating function adopts the following form:

$$G_{\mathrm{Mod}}^{\mathrm{BOC}_{\cos}(f_c,f_c)}(f)=4+2\left[-\cos\left(\frac{2\pi f}{4f_c}\right)-2\cos\left(2\frac{2\pi f}{4f_c}\right)+\cos\left(3\frac{2\pi f}{4f_c}\right)\right] \tag{4.51}$$

If we repeat now the calculation for $\mathrm{BOC}_{\cos}(2f_c, f_c)$ in order to derive the generalized expression by induction over *n*, we have $\mathrm{BOC}_{\cos}(f_s, f_c) = \mathrm{BOC}_{\cos}(2f_c, f_c)$ or $\mathrm{BCS}([1,-1,-1,1,1,-1,-1,1], f_c)$, so that

$$G_{\mathrm{Mod}}^{\mathrm{BOC}_{\cos}(2f_c,f_c)}(f)=8+2\left[\begin{aligned}&-\cos\left(\frac{2\pi f}{8f_c}\right)-6\cos\left(2\frac{2\pi f}{8f_c}\right)+\cos\left(3\frac{2\pi f}{8f_c}\right)+\\&+4\cos\left(4\frac{2\pi f}{8f_c}\right)-\cos\left(5\frac{2\pi f}{8f_c}\right)-2\cos\left(6\frac{2\pi f}{8f_c}\right)+\cos\left(7\frac{2\pi f}{8f_c}\right)\end{aligned}\right] \tag{4.52}$$

If we generalize now, we can see that the expression for any *n* will adopt the following form:

$$G_{\text{Mod}}^{\text{BOC}_{\cos}(nf_c/4,f_c)}(f)=n+2\left\{\sum_{i=1}^{n/2}(-1)^i\cos\left[(2i-1)\frac{2\pi f}{nf_c}\right]+\sum_{i=1}^{n/2-1}2(-1)^i(n/2-i)\cos\left(2i\frac{2\pi f}{nf_c}\right)\right\} \tag{4.53}$$

where $n\in\{4,8,12,16...\}$. Finally, once we have obtained the modulating term of the power spectral density for any *n*, we can express the power spectral density of any cosine-phase BOC signal as follows:

$$G_{\text{BOC}_{\cos}\left(f_s=\frac{nf_c}{4},f_c\right)}=f_c\frac{\sin^2\left(\frac{\pi f}{nf_c}\right)}{(\pi f)^2}\left\{n+2\left[\begin{array}{l}\sum_{i=1}^{n/2}(-1)^i\cos\left[(2i-1)\frac{2\pi f}{nf_c}\right]+\\+\sum_{i=1}^{n/2-1}2(-1)^i(n/2-i)\cos\left(2i\frac{2\pi f}{nf_c}\right)\end{array}\right]\right\} \tag{4.54}$$

As derived in Appendix C, after some math (4.54) can still be explicitly expressed for the even case as follows:

$$G_{\text{BOC}_{\cos}\left(f_s=\frac{nf_c}{4},f_c\right)}=4f_c\frac{\sin^2\left(\frac{\pi f}{f_c}\right)\sin^4\left(\frac{\pi f}{nf_c}\right)}{(\pi f)^2\cos^2\left(\frac{2\pi f}{nf_c}\right)} \tag{4.55}$$

The BOC signal in cosine phase can be considered as a BCS signal whose sequence is formed by concatenating [1,-1,-1,1] a number of times f_s/f_c. Thus the length *n* will be $4f_s/f_c$ and (4.55) simplifies to:

$$G_{\text{BOC}_{\cos}(f_s,f_c)}=4f_c\frac{\sin^2\left(\frac{\pi f}{f_c}\right)\sin^4\left(\frac{\pi f}{4f_s}\right)}{(\pi f)^2\cos^2\left(\frac{\pi f}{2f_s}\right)}=f_c\left[\frac{2\sin\left(\frac{\pi f}{f_c}\right)\sin^2\left(\frac{\pi f}{4f_s}\right)}{\pi f\cos\left(\frac{\pi f}{2f_s}\right)}\right]^2 \tag{4.56}$$

In the same manner, for the odd case cosine-phase we have according to Appendix C:

$$G_{\text{BOC}_{\cos}(f_s,f_c)}=4f_c\frac{\cos^2\left(\frac{\pi f}{f_c}\right)\sin^4\left(\frac{\pi f}{4f_s}\right)}{(\pi f)^2\cos^2\left(\frac{\pi f}{2f_s}\right)}=f_c\left[\frac{2\cos\left(\frac{\pi f}{f_c}\right)\sin^2\left(\frac{\pi f}{4f_s}\right)}{\pi f\cos\left(\frac{\pi f}{2f_s}\right)}\right]^2 \tag{4.57}$$

4.3.2.3 Autocorrelation function of a generic BOC signal

One of the most interesting figures in the analysis of the signal structure is the autocorrelation function of the chip waveform as we saw at the beginning of this chapter. In this chapter we will derive general expressions to define the analytical shape of the autocorrelation function a generic BOC signal with infinite bandwidth. This will help us understand the importance of having a good autocorrelation function in order to have good ranging potential for positioning. Additionally, analytical expressions will permit us establishing comparisons between sine- and cosine-phased BOC modulations and investigate the effect that extra terms in the definition of the ACF can bring.

Before that, we derive first the inverse Fourier Transform of some functions of interest. The importance of these functions lies in the fact that since the Power Spectral Density of any MCS signal can be developed as a series with them, the derivation of analytical expressions for the ACF will be then possible no matter how complex the shape of the signal is.

As we know, the inverse Fourier transform of $T_k(\omega)=\cos(k\omega/f_c)/\omega^2$ can be defined as follows:

$$T_k(\tau)=\begin{cases}\dfrac{\tau}{2} & \tau<-k\\ -\dfrac{k}{2} & -k\le\tau\le k\\ -\dfrac{\tau}{2} & \tau>k\end{cases} \tag{4.58}$$

where k fixes the height of the function at $\tau=0$. Moreover, the function $T_k(\tau)$ is expressed as a function of τ [chips]. Next the trapezoid function is shown graphically:

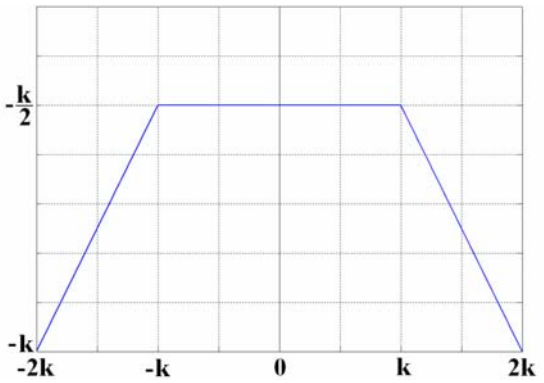

Figure 4.11. Definition of the trapezoid function $T_k(\tau)$

Also, the Fourier inverse Transform of $S_k(\omega)=\dfrac{1}{(k\omega)^2}$ can be expressed by means of a function that we will call $S_k(\tau)$ as follows:

$$S_k(\tau)=\begin{cases}\dfrac{\tau}{2k^2} & \tau<0\\ -\dfrac{\tau}{2k^2} & \tau>0\end{cases} \tag{4.59}$$

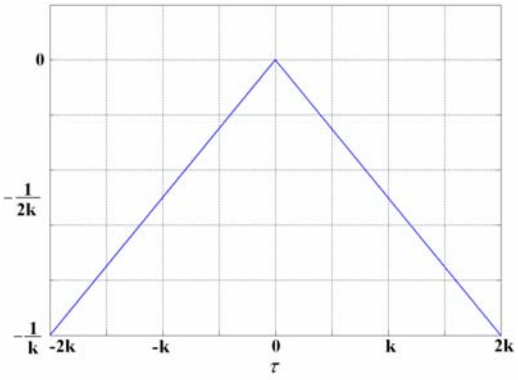

Figure 4.12. Definition of the $S_k(\tau)$ function

For the more general case, we will define the inverse Fourier Transform of

$$M_{k_1,k_2}(\omega)=\frac{\cos\left(k_1\frac{\omega}{f_c}\right)\cos\left(k_2\frac{\omega}{f_c}\right)}{\omega^2} \tag{4.60}$$

as:

$$M_{k_1,k_2}(\tau)=\begin{cases}-\frac{k_2}{2} & |\tau|\le(k_2-k_1)\\ -\frac{(\tau+k_1+k_2)}{4} & (k_2-k_1)\le|\tau|\le(k_2+k_1)\\ -\frac{\tau}{2} & |\tau|\ge(k_2+k_1)\end{cases} \tag{4.61}$$

where we assume that $k_2 \ge k_1$ without loss of generality. In addition, we can clearly see that $T_k(\tau)$ is a particular case of $M_{k_1,k_2}(\tau)$ since $M_{(0,k_2)}(\tau)=T_{k_2}(\tau)$.

Next we compare the BOC signal in sine and cosine phasing for different chip rates. For exemplification we will take a sub-carrier rate of 10.23 MHz and a code rate of 5.115 MHz. We recall that these modulations correspond to the GPS M-Code and the Galileo PRS (E6).

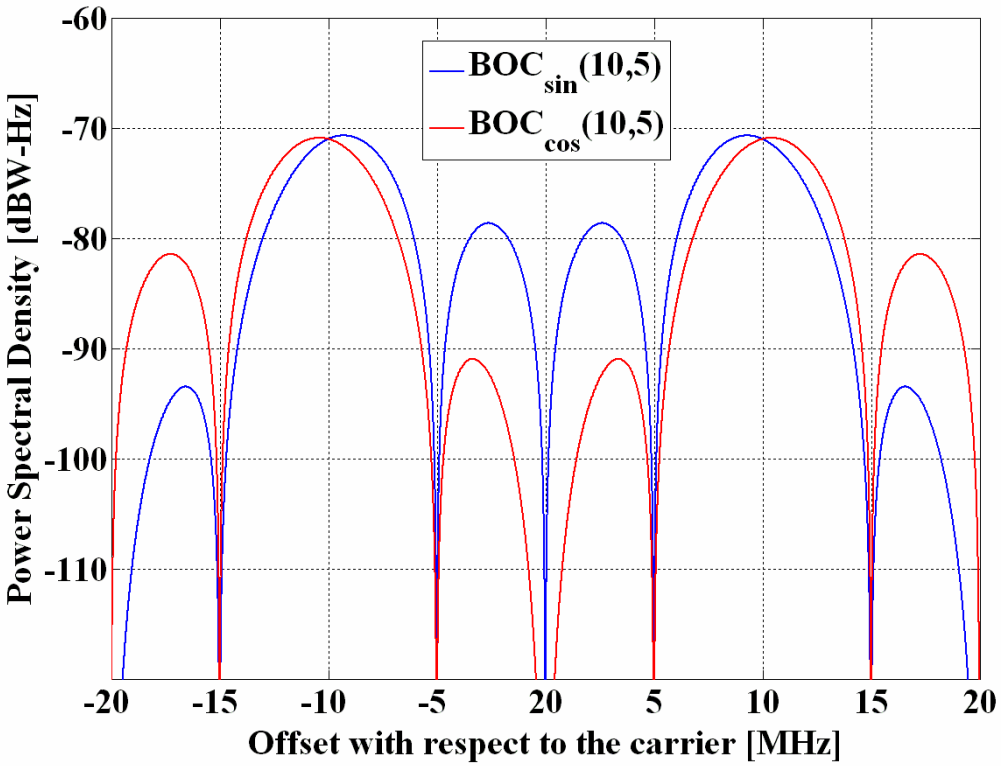

Figure 4.13. Power Spectral Densities of $BOC_{sin}(10,5)$ and $BOC_{cos}(10,5)$

The difference between the sine-phased and cosine-phased BOC modulation is even more obvious when we look at the $BOC_{sin}(15,2.5)$ and $BOC_{cos}(15,2.5)$ signals. As we can see, while the sine-phased concentrates more power at inner frequencies, so does the cosine version at outer frequencies.

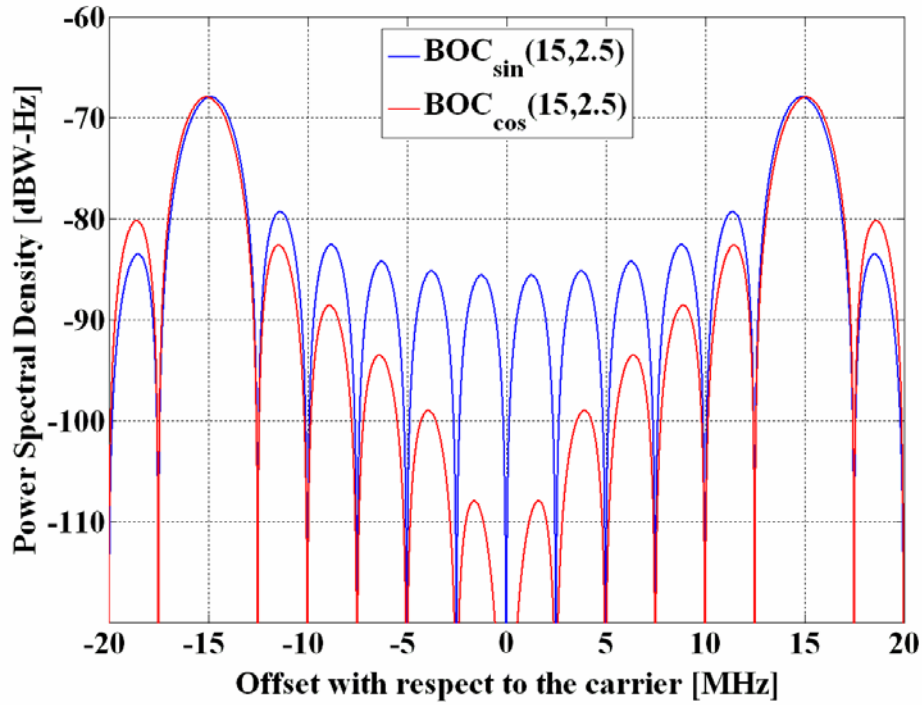

Figure 4.14. Power Spectral Densities of $BOC_{sin}(15,2.5)$ and $BOC_{cos}(15,2.5)$

Now that we have the tools to derive the generic form of the ACF of any MCS signal, we develop the power spectral density of $BOC_{sin}(15,2.5)$ as follows:

$$G_{\mathrm{BOC}_{\sin}(f_s=15,f_c=2.5)} = f_c\left[\frac{2\sin\left(\frac{\pi f}{f_c}\right)\sin^2\left(\frac{\pi f}{4f_s}\right)}{\pi f\cos\left(\frac{\pi f}{2f_s}\right)}\right]^2 \overset{f=\omega/2\pi}{=} f_c\left[\frac{4\sin\left(\frac{\omega}{2f_c}\right)\sin^2\left(\frac{\omega\pi}{8f_s}\right)}{\omega\cos\left(\frac{\omega}{4f_s}\right)}\right]^2 =$$

$$= \frac{f_c}{\omega^2}\left[\begin{array}{l} -88\cos\left(\frac{1}{12}\frac{\omega}{f_c}\right)+16\cos\left(\frac{5}{6}\frac{\omega}{f_c}\right)-24\cos\left(\frac{3}{4}\frac{\omega}{f_c}\right)+32\cos\left(\frac{2}{3}\frac{\omega}{f_c}\right)-72\cos\left(\frac{1}{4}\frac{\omega}{f_c}\right)+ \\ +80\cos\left(\frac{1}{6}\frac{\omega}{f_c}\right)+64\cos\left(\frac{1}{3}\frac{\omega}{f_c}\right)+48\cos\left(\frac{1}{2}\frac{\omega}{f_c}\right)-40\cos\left(\frac{7}{12}\frac{\omega}{f_c}\right)-56\cos\left(\frac{5}{12}\frac{\omega}{f_c}\right)- \\ -8\cos\left(\frac{11}{12}\frac{\omega}{f_c}\right)+2\cos\left(\frac{\omega}{f_c}\right)+46 \end{array}\right] \tag{4.62}$$

And using the formulations derived in previous pages, we can express the ACF as follows:

$$ACF_{\mathrm{BOC}_{\sin}(15,2.5)}(\tau) = \left[\begin{array}{l} -88T_{\frac{1}{12}}(\tau)+16T_{\frac{5}{6}}(\tau)-24T_{\frac{3}{4}}(\tau)+32T_{\frac{2}{3}}(\tau)-72T_{\frac{1}{4}}(\tau)+ \\ +80T_{\frac{1}{6}}(\tau)+64T_{\frac{1}{3}}(\tau)+48T_{\frac{1}{2}}(\tau)-40T_{\frac{7}{12}}(\tau)-56T_{\frac{5}{12}}(\tau)- \\ -8T_{\frac{11}{12}}(\tau)+2T_1(\tau)+46S_1(\tau) \end{array}\right] \tag{4.63}$$

which adopts graphically the following form:

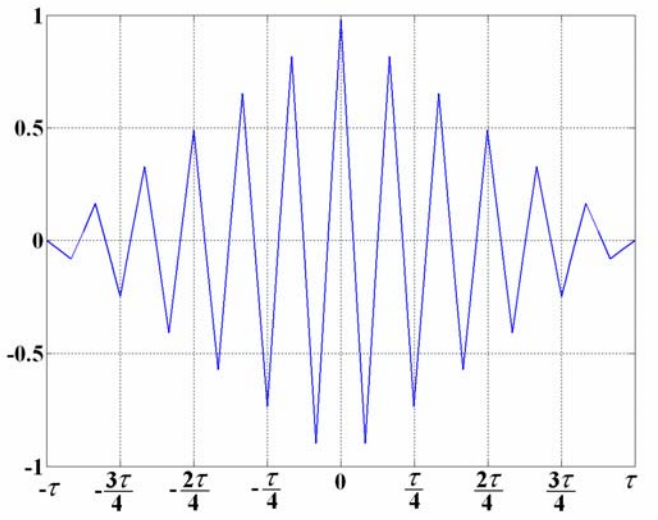

Figure 4.15. Autocorrelation Function of $BOC_{sin}(15,2.5)$

In the same manner, the power spectral density of $BOC_{cos}(15,2.5)$ can be equally expressed in terms of the functions defined above such that the ACF is shown to adopt the following form:

$$ACF_{BOC_{cos}(15,2.5)}(\tau)=\left[\begin{array}{l}-88T_{\frac{1}{12}}(\tau)+16T_{\frac{5}{6}}(\tau)-24T_{\frac{3}{4}}(\tau)+32T_{\frac{2}{3}}(\tau)-72T_{\frac{1}{4}}(\tau)+\\+80T_{\frac{1}{6}}(\tau)+64T_{\frac{1}{3}}(\tau)+48T_{\frac{1}{2}}(\tau)-40T_{\frac{7}{12}}(\tau)-56T_{\frac{5}{12}}(\tau)-\\-8T_{\frac{11}{12}}(\tau)-2T_{1}(\tau)+50S_{1}(\tau)-8T_{\frac{1}{24}}(\tau)+8T_{\frac{23}{24}}(\tau)+80T_{\frac{1}{6}}(\tau)+\\+8T_{\frac{1}{8}}(\tau)-8T_{\frac{5}{24}}(\tau)-8T_{\frac{13}{24}}(\tau)+8T_{\frac{5}{8}}(\tau)+8T_{\frac{11}{24}}(\tau)+8T_{\frac{7}{24}}(\tau)-\\-8T_{\frac{17}{24}}(\tau)+8T_{\frac{19}{24}}(\tau)-8T_{\frac{3}{8}}(\tau)-8T_{\frac{7}{8}}(\tau)\end{array}\right] \quad (4.64)$$

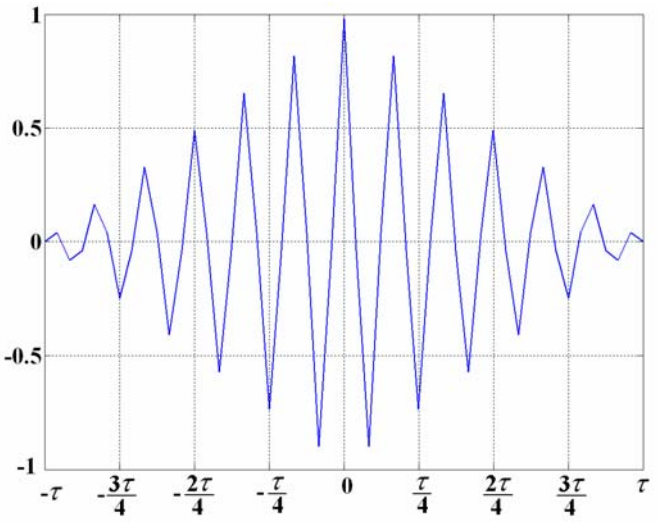

Figure 4.16. Autocorrelation Function of $BOC_{cos}(15,2.5)$

If we compare now (4.63) and (4.64) we see that we can express the ACF of the cosine-phase BOC as a function of the ACF of the sine-phased BOC in the following way:

$$ACF_{\mathrm{BOC}_{\cos}(15,2.5)}(\tau) = ACF_{\mathrm{BOC}_{\sin}(15,2.5)}(\tau) + D_{\mathrm{BOC}(15,2.5)}(\tau) \tag{4.65}$$

where

$$D_{\mathrm{BOC}(15,2.5)}(\tau) = \left[\begin{array}{l} -4T_1(\tau) + 4S_1(\tau) - 8T_{\frac{1}{24}}(\tau) + 8T_{\frac{23}{24}}(\tau) + 80T_{\frac{1}{6}}(\tau) + 8T_{\frac{1}{8}}(\tau) - 8T_{\frac{5}{24}}(\tau) - 8T_{\frac{13}{24}}(\tau) + \\ +8T_{\frac{5}{8}}(\tau) + 8T_{\frac{11}{24}}(\tau) + 8T_{\frac{7}{24}}(\tau) - 8T_{\frac{17}{24}}(\tau) + 8T_{\frac{19}{24}}(\tau) - 8T_{\frac{3}{8}}(\tau) - 8T_{\frac{7}{8}}(\tau) \end{array} \right] \tag{4.66}$$

what can be graphically shown as follows:

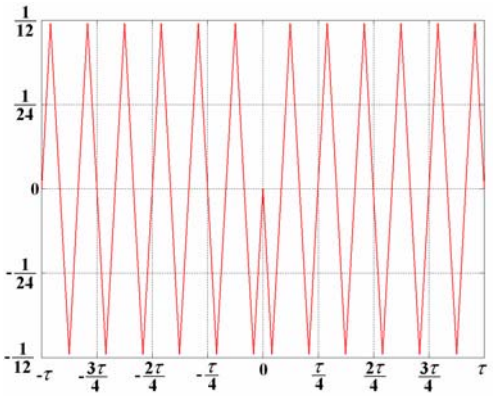

Figure 4.17. Difference $D_{\mathrm{BOC}(15,2.5)}(\tau)$ of ACF of $\mathrm{BOC}_{\cos}(15,2.5)$ and $\mathrm{BOC}_{\sin}(15,2.5)$

By looking at Figure 4.17 the following interesting properties can be observed:

- We can distinguish 6 peaks on every side with an amplitude of $1/(2\cdot 6)$. In fact, for the general case we will have n peaks on every side with an amplitude $1/(2\cdot n)$ where $n = f_s / f_c$.
- This function shows the interesting property that we can easily convert the sine-phased autocorrelation function of any BOC signal into its cosine-phased counterpart by adding the corresponding difference function shown above.

Moreover, if we calculate now the Fourier transform of (4.66), we obtain the following spectrum:

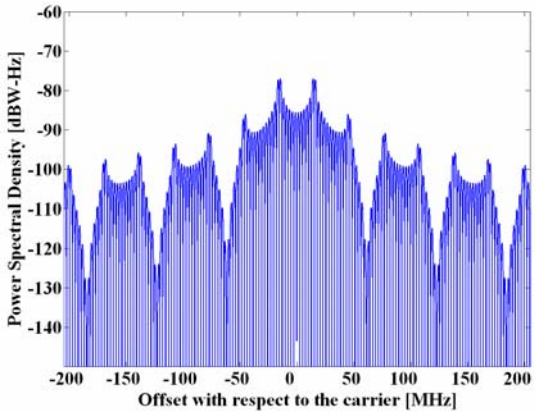

Figure 4.18. Power Spectral Density of the Difference Function $D_{\mathrm{BOC}(15,2.5)}(\tau)$

As we can recognize, this spectrum is the difference between the power spectral densities of the sine-phased and cosine-phased BOC(15,2.5) modulations.

4.3.2.4 BOC signals vs. BPSK signals

The BOC modulation was the first attempt to modernize the GNSS signals and has indeed opened a new field of research in navigation that has recently lead to the AltBOC and MBOC solutions. These will be described in the following pages. As commented by [J.-A. Avila-Rodriguez et al., 2006d] and [G.W. Hein et al., 2006a], *while very good performance can be obtained with the C/A code signal, it has been recognized that better performance can be obtained using spreading modulations that provide more power at high frequencies away from the centre frequency*. In fact, this is the main idea behind the BOC modulation where a sub-carrier signal shifts spectral components to outer parts of the. The old BPSK modulation that is currently still used for GPS C/A code *has limited capability* for ranging and requires *high performance receivers* to use very wide front-end bandwidths as shown in [J. W. Betz and D. B. Goldstein, 2002]. Moreover, *Intra-system interference is exacerbated by the short C/A codes. The relatively slow* 1.023 *MHz spreading code rate of the BPSK-R modulation offers limited channel capacity, restricting the number of simultaneous signals as well as the tolerable power differential between signals. Additionally, the data message modulated on the C/A code signal is inefficient and inflexible*.

An interesting aspect of the BOC signal regarding its complexity is that it can be considered as two BPSKs shifted to $-f_s$ and $+f_s$ by the sub-carrier signal. Indeed many receiver implementations will make use of this principle to receive the future BOC signals. Side-lobe processing is thus a promising solution to treat BOC signals using the old BPSK architecture if we realize that a BOC signal is qualitatively similar to two BPSK signals with each half the power [J.W. Betz et al., 2005]. This idea is also of interest to process AltBOC.

4.3.3 Generic BCS Signals

In the previous lines we have studied two particular cases of the BCS modulation, namely the BPSK and BOC modulations. Nonetheless, the general expression derived at the beginning of the chapter is valid for any BCS vector. For exemplification, we show in the next lines how the PSD of a generic BCS could be derived.

Let us assume a BCS signal with vector s = [+1, +1, -1]. We have thus $s_1 = +1$, $s_2 = +1$, $s_3 = -1$. The modulating term of the PSD can be easily calculated as:

$$G_{\text{Mod}}^{\text{BCS}([+1,+1,-1],f_c)}(f) = 3 + 2s_1s_2\cos\left(\frac{2\pi f}{3f_c}\right) + 2s_1s_3\cos\left(2\frac{2\pi f}{3f_c}\right) + 2s_2s_3\cos\left(\frac{2\pi f}{3f_c}\right) \quad (4.67)$$

which can be further simplified to:

$$G_{\text{Mod}}^{\text{BCS}([+1,+1,-1],f_c)}(f) = 3 + 2\cos\left(\frac{2\pi f}{3f_c}\right) - 2\cos\left(2\frac{2\pi f}{3f_c}\right) - 2\cos\left(\frac{2\pi f}{3f_c}\right) = 3 - 2\cos\left(2\frac{2\pi f}{3f_c}\right) \quad (4.68)$$

while

$$G_{\text{pulse}}^{\text{BPSK}(3f_c)}(f) = f_c \frac{\sin^2\left(\frac{\pi f}{3f_c}\right)}{(\pi f)^2} \tag{4.69}$$

Thus the spectrum of this BCS sequence would adopt the following form:

$$G_{\text{BCS}([+1,+1,-1],f_c)}(f) = f_c \frac{\sin^2\left(\frac{\pi f}{3f_c}\right)}{(\pi f)^2}\left[3 - 2\cos\left(2\frac{2\pi f}{3f_c}\right)\right] \tag{4.70}$$

In general, in order to understand how the spectrum will look like for a given sequence, we have to be able to understand how every term of the sum above contributes to the total PSD.

4.4 Sinusoidal Multilevel Coded Symbol (SMCS) Signals

In the previous chapter we have examined signal waveforms with rectangular pulse shape. This is indeed the most typical case in most of the applications. Now we will go one step further and we will discuss a family of signals that results from modulating each subchip of the generation vector $\bar{s}$ with a sinusoidal function. Such signals receive the name of Sinusoidal Offset Carrier signals or SOC for short if the sinusoidal function is modulated by a binary code. The alternative use of Linear Offset Carrier or LOC is also offen observed in the literature. As we can recognize, SMCS can be interpreted as a particular MCS that uses subchip pulses with sinusoidal shape. Accordingly, (4.28) could be applied. The original idea to use this signal for satellite navigation was presented in [J. W. Betz, 1999] and has been further developed in [J. Winkel, 2002]. The SOC signal can be defined as follows:

$$s_{\text{SOC}}(t) = \sqrt{2}\, c_k \sin(2\pi n f_c t) \tag{4.71}$$

where *n* corresponds to the number of periods of the sine wave that are contained in each code bit and the factor $\sqrt{2}$ was introduced to normalize the power to 1. Furthermore, c_k refers to the subchips modulating the chip waveform. It is important to note that the chip waveform is defined by the sequence of subchips that forms it according to the generation vector $\bar{s}$ as defined in chapter 4.2.

While this definition applies only to the case of Offset Carrier Chips ([1, -1, 1, -1, …]), one can imagine a generalized version for Binary Coded Symbols. We will define these signals thus in general as Sinusoidal Binary Coded Symbols or SBCS for short. Next figure shows an example of SBCS with vector [1,-1,1].

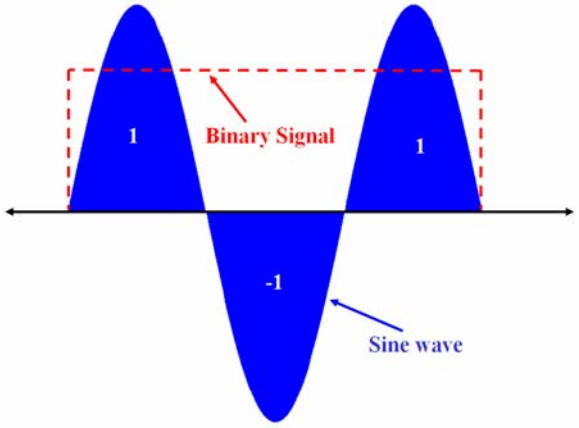

Figure 4.19. Sinusoidal Binary Coded Symbol signal with generation vector [+1,-1,+1]

As we can clearly recognize, there exists the same relationship between SBCS signals and SOCs as there was between BCS and BOC. In fact, the SOC signal that we defined above is a particular case of the SBCS modulation that we have just described. According to this, if we talk about SBCS([1,-1],1) and SOC(1,1) we are indeed referring to the same signal.

In addition, it is important to mention that since, as we know from theory, the square-wave contains tones at odd frequencies multiple of the elemental frequency, the SOC signal can be interpreted qualitatively as a BOC signal that is filtered to have only the first tone.

To summarize, we can conclude that this idea can be understood as a particular case of Multilevel Coded Symbols (MCS) modulation with a pulse waveform of sinusoidal form. Next figure shows another example.

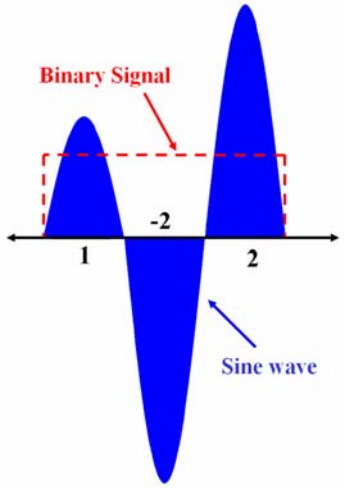

Figure 4.20. Sinusoidal Multilevel Coded Symbol signal with generation vector [1,-2,2]. In this example the amplitude was not normalized to have 1 W of power

Furthermore, it is important to note that unlike in the most straightforward definition of the SOC modulation, the factor accompanying the sine signal will not be in general $\sqrt{2}$ and will depend on the particular symbol sequence. In fact, the factor has the mission to normalize the power of the signal to unity.

4.4.1 Sinusoidal Binary Offset Carrier (SOC) Signals

To derive the spectrum of the SOC signals, the most convenient is to use the convolution theorem. According to it, the Fourier transform of the chip waveform can be expressed in terms of a convolution between the modulating carrier and the code bit. The problem reduces then to calculating the Fourier transforms for each signal as shown in [J. Winkel, 2002]. In fact:

$$S_{\mathrm{SOC}}(f) = FT\left\{s_{\mathrm{SOC}}(t)\right\} = FT\left\{\sqrt{2}\sin(2\pi n f_c t)\right\} \otimes FT\left\{c_k(t)\right\} \tag{4.72}$$

which can be further simplified as follows, assuming that the code is ideal:

$$S_{\mathrm{SOC}}(f) = j\frac{\sqrt{2}}{f_c}\left[\mathrm{sinc}\left(\frac{\pi f}{f_c} + n\pi\right) + \mathrm{sinc}\left(\frac{\pi f}{f_c} - n\pi\right)\right] \tag{4.73}$$

Therefore, the power spectral density adopts the following form:

$$G_{\mathrm{SOC}}(f) = \frac{2}{f_c}\left[\mathrm{sinc}\left(\frac{\pi f}{f_c} + n\pi\right) + \mathrm{sinc}\left(\frac{\pi f}{f_c} - n\pi\right)\right]^2 \tag{4.74}$$

It is interesting to note also that the same distinction between even and odd SOCs can also be made here as with the rectangular signals that we have already studied. Furthermore, the maximum of the spectrum is not located at $f = nf_c$ as one might expect, but somewhere close to that point as shown in [J. Winkel, 2002]. Finally, the autocorrelation function of the SOC signal for the sine-phased case is shown to be [J. Winkel, 2002]:

$$\Re_{\mathrm{SOC}}(\tau) = \frac{8}{\pi^2 f_c}\left\{\Lambda(2\tau f_c)\cos\left(\frac{n\pi}{2f_c}\right) - \frac{\sin(2n\pi\tau f)}{2n\pi}\left[\theta(\tau - T_c) + \theta(\tau + T_c) - 2\theta(\tau)\right]\right\} \tag{4.75}$$

where $\Lambda(\tau)$ is the triangular function and $\theta(\tau)$ represents the Heaviside step function. As we know the triangular function is defined as follows:

$$\Lambda(\tau) = \begin{cases} 1-\tau & \|\tau\| < 1 \\ 0 & \|\tau\| > 1 \end{cases} \tag{4.76}$$

and the Heaviside step function is equally shown to be defined as:

$$\theta(\tau) = \begin{cases} 0 & \tau \le 0 \\ 1 & \tau > 0 \end{cases} \tag{4.77}$$

4.4.2 Minimum Shift Keying (MSK)

The MSK modulation is a constant envelope signal with continuous phase that results from modulating the instantaneous frequency with rectangular pulses. MSK is considered to be a special case of Offset QPSK (OQPSK) with half sinusoidal pulse weighting rather than rectangular. Furthermore, MSK presents lower side lobes than QPSK and OQPSK as shown in [S. A. Gronemeyer and A. L. McBride, 1976] and [H. R. Mathwich et al., 1974]. As one can imagine, this could be of great interest for those navigation bands where the Out of Band emission constraints are stringent as in the case of the C-band between 5010 and 5030 MHz.

Assuming that the PRN codes are ideal and making the same assumptions of previous chapters, the MSK modulation can be seen as a particular case of SMCS with sinusoidal pulse waveform. Moreover, since MSK is a particular case of MCS, all the expressions derived in previous chapters can also be used for this particular case.

In the MSK modulation the evolution of the phase over the time is linear. Indeed, recalling the general expression of (4.2) and keeping in mind that MSK is a frequency modulation, it can be shown that the evolution of the frequency over time adopts the following expression:

$$f(t) = \sum_k c_k(t)\, p(t - kT_c) \tag{4.78}$$

where $c_k(t)$ is the PRN code and $p(t)$ is the frequency pulse, defined for period n as follows:

$$p(t) = \begin{cases} \dfrac{1}{2T_c} & nT_c \le t \le (n+1)T_c \\ 0 & \text{elsewhere} \end{cases} \tag{4.79}$$

Accordingly, the variation of the phase over the time will adopt the following form:

$$\phi(t) = 2\pi h \int_{-\infty}^{t} f(\tau)\mathrm{d}\tau \tag{4.80}$$

with $h = 1/2$. Putting now (4.78) and (4.80) together, the evolution of the phase over one period n, that is $nT_c \le t \le (n+1)T$, will be:

$$\phi_n(t) = \pi \sum_k c_k \int_{-\infty}^{t} f(\tau - nT_c)\mathrm{d}\tau \tag{4.81}$$

which can also be expressed as follows:

$$\phi_n(t) = \pi \cdot c_n \cdot \frac{t - nT_c}{2T_c} + \frac{\pi}{2} \sum_{k=-\infty}^{n-1} c_k \tag{4.82}$$

Accordingly, the expression of the MSK will be:

$$s_n(t) = A \cdot \exp\left\{ j\left[\pi \cdot c_n\left(\frac{t - nT_c}{2T_c} \right) + \frac{\pi}{2} \sum_{k=-\infty}^{n-1} c_k \right] \right\} = A \cdot \exp\left\{ j\left[\theta_{n-1} + \pi \cdot c_n\left(\frac{t - nT_c}{2T_c} \right) \right] \right\} \tag{4.83}$$

with $\theta_{n-1} = \dfrac{\pi}{2} \sum_{k=-\infty}^{n-1} c_k$.

Taking now the real and imaginary part of (4.83), the sinusoidal shape of the chip waveform is then observed. Since we assume ideal codes, we only need to work with the chip waveform as described in (4.8). Next figure compares the typical binary pulse with that of MSK:

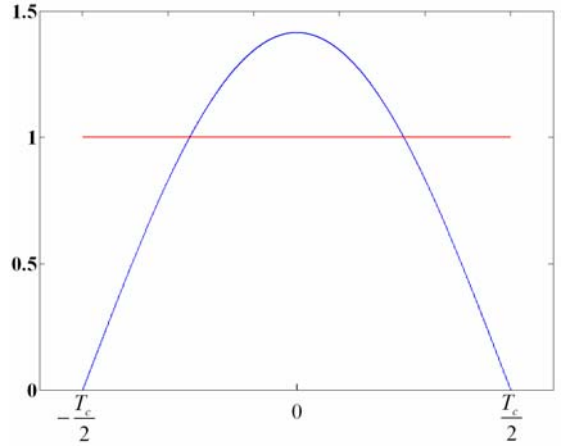

Figure 4.21. Binary and MSK chip waveform

In order the original power of MSK to remain equivalent to that of the ordinary binary signals, the factor $A=\sqrt{2}$ was used in the MSK expression as we can observe. To derive now the PSD according to (4.8), we calculate first the Fourier Transform of the MSK pulse waveform:

$$S_{\text{MSK}}(\omega)=\int_{-T_{sc}/2}^{T_{sc}/2}\sqrt{2}\cos\left(\frac{\pi t}{T_{sc}}\right)e^{-j\omega t}dt=\sqrt{2}\int_{-T_{sc}/2}^{T_{sc}/2}\left[\frac{e^{j\frac{\pi t}{T_{sc}}}+e^{-j\frac{\pi t}{T_{sc}}}}{2}\right]e^{-j\omega t}dt \tag{4.84}$$

which simplifies to:

$$S_{\text{MSK}}(\omega)=j\sqrt{2}\left\{\frac{\sin\left[\left(\frac{\pi}{T_{sc}}-\omega\right)\frac{T_{sc}}{2}\right]}{\left(\frac{\pi}{T_{sc}}-\omega\right)}+\frac{\sin\left[\left(\frac{\pi}{T_{sc}}+\omega\right)\frac{T_{sc}}{2}\right]}{\left(\frac{\pi}{T_{sc}}+\omega\right)}\right\} \tag{4.85}$$

As we can recognize, we are defining the spreading waveform in a *subchip* of length T_{sc} where $T_c=nT_{sc}$, being T_c the duration of a chip and *n* the number of *subchips* in one chip. Accordingly, this is the Fourier transform of the *subchip* part and $f_{sc}=nf_c$. This expression can be further simplified yielding:

$$S_{\text{MSK}}(\omega)=j\sqrt{2}\cos\left(\frac{\omega T_{sc}}{2}\right)\left\{\frac{1}{\left(\frac{\pi}{T_{sc}}-\omega\right)}+\frac{1}{\left(\frac{\pi}{T_{sc}}+\omega\right)}\right\}=j\frac{2\sqrt{2}\pi\cos\left(\frac{\omega T_{sc}}{2}\right)}{T_{sc}\left(\frac{\pi^2}{T_{sc}^2}-\omega^2\right)} \tag{4.86}$$

According to this, the normalized Power Spectral Density of the spreading MSK waveform adopts the following form:

$$G_{\text{MSK}}(\omega)=\frac{1}{T_{sc}}\left\|S_{\text{MSK}}(\omega)\right\|^2=\frac{1}{T_{sc}}\frac{8\pi^2\cos^2\left(\frac{\omega T_{sc}}{2}\right)}{T_{sc}^2\left(\frac{\pi^2}{T_{sc}^2}-\omega^2\right)^2} \tag{4.87}$$

which can also be expressed as follows:

$$G_{\text{MSK}}(f)=\frac{8f_{sc}^3}{\pi^2}\frac{\cos^2\left(\frac{\pi f}{f_{sc}}\right)}{\left(f_{sc}^2-4f^2\right)^2} \tag{4.88}$$

As we can recognize, this expression perfectly coincides with that derived in [S. Pasupathy, 1979].

Once we have derived the pulse waveform for a cosine shape, any SMCS can be obtained using the general formula obtained in (4.28). As an example, in the next lines we derive the expression for a sine-phased BOC(f_s , f_c) with MSK pulses and we will compare it with the original BPSK with MSK pulses. For simplicity in the notation we call MSK(f_s , f_c) to the first one and MSK(f_c) to the second one. As one can imagine, this notation can be generalized to any BOC or arbitrary BCS signal. It is important to note that in this particular case T_{sc} is equal to T_c/n and $f_{sc}=nf_c$ consequently. In addition, it can be shown that $nf_c=2f_s$ for the modulating term as it was also the case for the usual BOC modulation. In conclusion, the PSD of MSK-BOC(f_s , f_c) or MSK(f_s , f_c) for short, will adopt the following form:

$$G_{\text{MSK-BOC}(f_s,f_c)}(f)=G_{\text{MSK pulse}}(f)G_{\text{Mod BOC}(f_s,f_c)}(f) \tag{4.89}$$

where in this particular case:

$$G_{\text{MSK pulse}}(f)=\frac{8f_{sc}^3}{\pi^2}\frac{\cos^2\left(\frac{\pi f}{f_{sc}}\right)}{\left(f_{sc}^2-4f^2\right)^2}=\frac{4f_c^3}{\pi^2}\frac{\cos^2\left(\frac{\pi f}{2f_c}\right)}{\left(f_c^2-f^2\right)^2} \tag{4.90}$$

since $f_{sc}=2f_c$ for the sine-phased MSK-BOC case. On the other hand, for the even case, the modulation spectral term adopts the following form in general:

$$G_{\text{Mod},e}^{\text{BOC}_{\sin}(f_s,f_c)}(f)=\frac{\sin^2\left(\frac{\pi f}{f_c}\right)}{\cos^2\left(\frac{\pi f}{nf_c}\right)}=\frac{\sin^2\left(\frac{\pi f}{f_c}\right)}{\cos^2\left(\frac{\pi f}{2f_s}\right)} \tag{4.91}$$

where n is again the number of *subchips* in one chip. Thus, multiplying now both terms and normalizing the power to integrate to 1 in an infinite bandwidth yields thus the PSD of the MSK(f_s , f_c):

$$G_{\mathrm{MSK}(f_s f_c)}(f) = \frac{4f_c^3}{f_{sc}\pi^2}\frac{\cos^2\left(\frac{\pi f}{2f_c}\right)}{\left(f_c^2 - f^2\right)^2}\frac{\sin^2\left(\frac{\pi f}{f_c}\right)}{\cos^2\left(\frac{\pi f}{2f_s}\right)} = \frac{1}{2f_c}\left[\frac{2f_c^2}{\pi}\frac{\cos\left(\frac{\pi f}{2f_c}\right)}{\left(f_c^2 - f^2\right)}\frac{\sin\left(\frac{\pi f}{f_c}\right)}{\cos\left(\frac{\pi f}{2f_s}\right)}\right]^2 \tag{4.92}$$

For comparison the PSDs of MSK(1,1), MSK(1), BPSK(1) and BOC(1,1) are shown next:

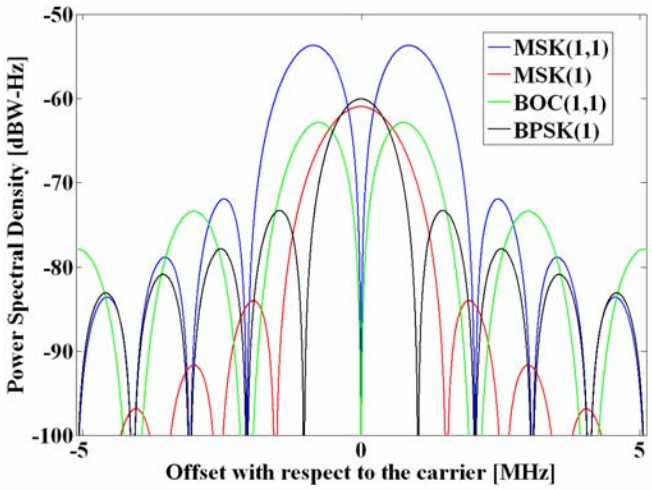

Figure 4.22. PSDs of MSK(1,1), MSK(1), BOC(1,1) and BPSK(1)

As we can recognize from the previous figure, for the same chip rate of 1.023 Mcps, MSK(1) has a main lobe that is 1.5 times wider than that of BPSK(1). On the other hand, MSK(1,1) has a main lobe that is as broad as that of BOC(1,1) but with secondary lobes that are half the width. MSK has a very good spectral confinement and provides at the same time constant envelope.

4.4.3 Gaussian Minimum Shift Keying (GMSK)

In the previous chapter the analytical expression of the MSK modulation was shown to be a particular case of MCS with frequency modulation and sinusoidal pulse. We have also seen that MSK presents a very good spectral confinement in the band of interest but still an important amount of power is allocated on the side lobes of the signal.

This chapter presents a modified version of the previous MSK where the phase is further filtered through a Gaussian filter to smooth the transitions from one point to the next in the constellation. Next figure presents the GMSK generation scheme:

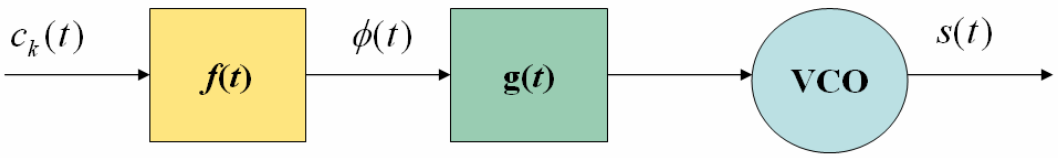

Figure 4.23. GMSK generation scheme

where the Gaussian filter $g(t)$ adopts the following form in the time domain:

$$g(t) = \lambda \sqrt{\frac{2\pi}{\ln 2}} B e^{-\frac{2\pi^2 B^2 t^2}{\ln 2}} \tag{4.93}$$

where λ is a normalization constant to maintain the power and the product BT_c is the -3 dB bandwidth-symbol time product. The higher this value, the cleaner will be the eye diagram of the signal but more power will be transmitted on the side lobes of the spectrum. A typical value in communication applications is $BT_c = 0.3$ which is a good compromise between spectral efficiency and Inter-Symbol interference.

4.5 Generalized Multilevel Coded Symbols (GMCS)

As we saw in the definition of chapter 4.2, Multilevel Coded Symbols consist of spreading waveforms that are divided into an integer number of equal-length segments, each of them with a deterministic value. According to this definition, any imaginable signal can in principle be described as an MCS signal as long as the length of the segments can be expressed as a rational number. In that case, we will always be able to find a finite length *n* to build the MCS vector and define each of the segments with the notation used above. As we saw in previous chapter, also non-rectangular forms are possible to modulate the subchips, as long as they are deterministic. In general, the basic pulse of each of the segments can adopt any arbitrary shape as equation (4.28) reflected.

Let us now extend our definition of MCS to signal waveforms with divisions that are not necessarily rational and thus with non finite *n*. As we will see in the following chapters, this will open new possibilities and further simplify the notation. To do so, it is first necessary to define an intermediate function that we will call Tertiary Coded Symbols or TCS for short. The reason for that is that many of the Generalized MCS signals can be expressed as sum of different TCS. A modified version of the TCS waveform, namely the Unilateral TCS (UTCS), is analyzed in detail in Appendix E.

We further define MCS in a general case as follows:

$$s = \left[s_1^{\rho_1}, s_2^{\rho_2}, s_3^{\rho_3} \ldots s_n^{\rho_n} \right] \tag{4.94}$$

where ρ_i indicates the part of the chip that the symbol occupies such that

$$\sum_{i=1}^{n} \rho_i = 1 \tag{4.95}$$

This can also be seen in the following figure:

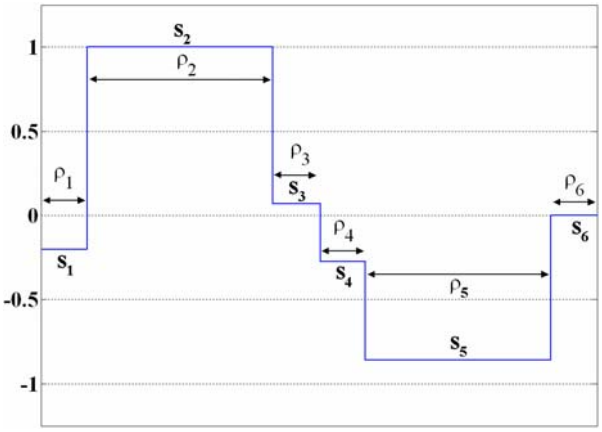

Figure 4.24. Generalized Multilevel Coded Symbols (GMCS)

We can clearly see that in this new definition the duration of every subchip does not necessarily have to be expressed as T_c/n but can adopt any imaginable length. Moreover, the amplitude of that subchip can adopt any amplitude too. Finally, it is important to note that if the MCS generation vector [s] could have an infinite length, the SOC modulation that we saw in the previous chapter could also be considered as a particular case of the generalized MCS (GMCS) signal. In general we can also say that MCS is a particular case of GMCS with segments of equal length.

4.5.1 Tertiary Coded Symbols (TCS)

Tertiary Coded Symbols are a particular case of GMCS with three-state amplitude adopting the values {-1,0,1}. As shown in Appendix D, the power spectral density of a generic TCS signal is shown to be:

$$G_{\mathrm{TCS}([s],f_c)}(f)=\left(\frac{f_c}{1-\rho}\right)\frac{\sin^2\left[\frac{\pi f}{nf_c}(1-\rho)\right]}{(\pi f)^2}\left\{\sum_{l=1}^{n}s_l^2+2\sum_{l=1}^{n-1}\sum_{m=l+1}^{n}s_l s_m\cos\left[(m-l)\frac{\omega T_c}{n}\right]\right\} \tag{4.96}$$

where ρ indicates the dwell time where the function adopts a value 0. As we can see, the expression above is practically identical to (4.23) as derived in chapter 4.2.1 except for the factor (1-ρ). This will help us in finding explicit expressions for particular TCS modulations in the next chapters. Moreover, it must be noted that the definition above is not only valid for binary signals but could be extended to any amplitude in general

4.5.2 Tertiary Offset Carrier (TOC)

A particular case of the TCS signal is the Tertiary Offset Carrier modulation, or TOC for short. As shown in [A.R. Pratt and J.I.R. Owen, 2003b], Tertiary Offset Carrier Signals are 3-level signals, similar in the form to the BOC signals, but with a dwell time ρ of value 0 in each sub-carrier half cycle. As shown by [A.R. Pratt and J.I.R. Owen, 2003b], these signals have appeared in response to the ever demanding needs of compatibility and interoperability of satellite navigation, in particular in the E1/L1 band.

According to this definition, if $\rho/2$ is a rational number it will be possible to express it by means of a fraction and the denominator of the reduced form of this fraction will be half of the minimum required length *n* of the MCS vector that would define the modulation using the MCS notation of chapter 4.2. As we can observe from our assumption that $\rho/2$ is a rational number, the length *n* would be finite too. Indeed, if ρ were irrational, *n* would have to be infinite to represent the signal using the MCS definition. However, the Generalized MCS definition would be in this case more appropriate and the TOC modulation could be seen as a particular case of GMCS. In this chapter we concentrate on the case when $\rho/2$ is rational.

A straightforward approach to derive the general power density of the TOC signals is based on (4.96). Indeed, Tertiary Offset Carrier signals are a particular case of TCS with the same definition vector as that of the BOC signals. Thus, we can use the derived expressions for the modulating factor obtained in chapter 4.3.2 to give the general expression of a generic TOC(f_s, f_c, ρ). Again, we will distinguish between TOC signals in sine phasing, namely $\mathrm{TOC}_{\sin}(f_s, f_c, \rho)$, and TOC signals in cosine phasing or $\mathrm{TOC}_{\cos}(f_s, f_c, \rho)$. We analyze both next.

4.5.2.1 Tertiary Offset Carrier in sine phasing : $\mathrm{TOC}_{\sin}(f_s, f_c, \rho)$

Assuming that ρ is a rational number, the sine-phased TOC signal fulfils the condition that $\rho/2 = 2m/n$ and is shown to follow the pattern below. Indeed, for the particular case of the sine-phased TOC(f_s, f_c, ρ), the TCS vector would adopt the following form:

$$\underbrace{0,0,0,0,0,0,0,\ldots}_{m},\underbrace{1,1,1,1,1,1,1,1\ldots}_{n/2-2m},\underbrace{0,0,0,0,0,0,0,0\ldots}_{2m},\underbrace{-1,-1,-1,-1,-1,-1,-1,-1\ldots}_{n/2-2m},\underbrace{0,0,0,0,0,0,0,0,\ldots}_{m} \tag{4.97}$$

It is clear to see that the concept can be easily generalized to any sine-phased TOC(f_s, f_c, ρ) without great difficulties as far as f_s/f_c delivers an integer number. We would simply have to extend the figure above by the factor f_s/f_c.

Recalling (4.96) and simplifying the terms in the G_{Mod} brackets for the case of a binary code, it can be shown that the PSD of a generic $\mathrm{TOC}_{\sin}(f_s, f_c, \rho)$ signal adopts the following form:

$$G_{\mathrm{TOC}_{\sin}(n,f_c,\rho)} = \left(\frac{f_c}{1-\rho}\right)\frac{\sin^2\left[\frac{\pi f}{nf_c}(1-\rho)\right]}{(\pi f)^2}\left\{n + 2\sum_{i=1}^{n-1}(-1)^i(n-i)\cos\left(i\frac{2\pi f}{nf_c}\right)\right\} \tag{4.98}$$

If we go now one step further using the results obtained in (B.11) for the sine-phased BOC modulation, the power spectral density is shown to simplify to the following expression:

$$G_{\mathrm{TOC}_{\sin}(n,f_c,\rho)} = \left(\frac{f_c}{1-\rho}\right)\frac{\sin^2\left[\frac{\pi f}{nf_c}(1-\rho)\right]}{(\pi f)^2}\frac{\sin^2\left(\frac{\pi f}{f_c}\right)}{\cos^2\left(\frac{\pi f}{nf_c}\right)} \tag{4.99}$$

We can also write it in a more compact way as follows,

$$G_{\mathrm{TOC}_{\sin}(f_s,f_c,\rho)} = \left(\frac{f_c}{1-\rho}\right)\left[\frac{\sin\left(\frac{\pi f}{f_c}\right)\sin\left[\frac{\pi f}{2f_s}(1-\rho)\right]}{\pi f\cos\left(\frac{\pi f}{2f_s}\right)}\right]^2 \tag{4.100}$$

since $n = 2f_s/f_c$, what coincides perfectly with the formulas derived in [A.R. Pratt and J.I.R. Owen, 2005] for the even case.

In the same manner, we can also obtain the expression for the power spectral density of the odd sine-phased TOC modulation as follows:

$$G_{\mathrm{TOC}_{\sin}(f_s,f_c,\rho)} = \left(\frac{f_c}{1-\rho}\right)\left[\frac{\cos\left(\frac{\pi f}{f_c}\right)\sin\left[\frac{\pi f}{2f_s}(1-\rho)\right]}{\pi f\cos\left(\frac{\pi f}{2f_s}\right)}\right]^2 \tag{4.101}$$

Next figure shows the evolution of the signal in the time domain:

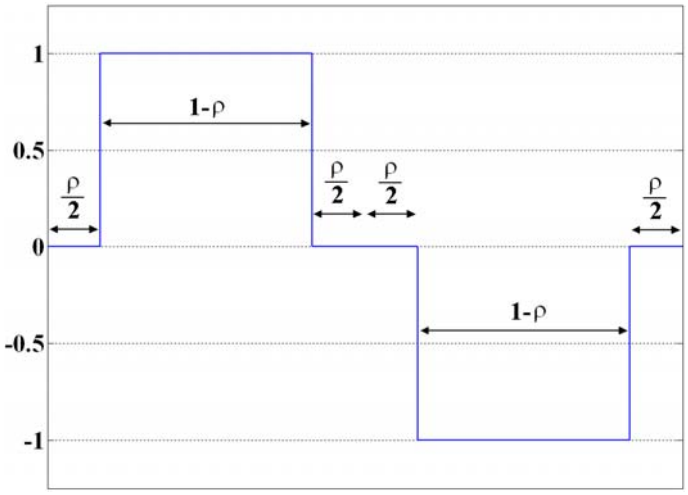

Figure 4.25. Chip waveform of $\mathrm{TOC}_{\sin}(1,1)$ for a dwell time ρ

4.5.2.2 Tertiary Offset Carrier in cosine phasing : $\mathrm{TOC}_{\cos}(f_s, f_c, \rho)$

In a similar way, the PSD of any $\mathrm{TOC}_{\cos}(f_s, f_c, \rho)$ can be expressed as follows,

$$G_{\mathrm{TOC}_{\cos}(n,f_c,\rho)} = \left(\frac{f_c}{1-\rho}\right)\frac{\sin^2\left[\frac{\pi f}{nf_c}(1-\rho)\right]}{(\pi f)^2}G_{\mathrm{Mod\ BOC}_{\cos}(n,f_c)} \tag{4.102}$$

where,

$$G_{\mathrm{Mod}}^{\mathrm{BOC}_{\cos}(nf_c/4,f_c)} = \left\{n + 2\left[\sum_{i=1}^{n/2}(-1)^i\cos\left[(2i-1)\frac{2\pi f}{nf_c}\right] + \sum_{i=1}^{n/2-1}2(-1)^i(n/2-i)\cos\left(2i\frac{2\pi f}{nf_c}\right)\right]\right\} \tag{4.103}$$

As shown in (C.26), this modulating term can be simplified for any n, yielding the following expression for the even cosine-phased TOC modulation:

$$G_{\mathrm{TOC}_{\cos}(n,f_c,\rho)} = \left(\frac{f_c}{1-\rho}\right)\frac{\sin^2\left[\frac{\pi f}{nf_c}(1-\rho)\right]}{(\pi f)^2}\frac{4\sin^2\left(\frac{\pi f}{f_c}\right)\sin^2\left(\frac{\pi f}{nf_c}\right)}{\cos^2\left(\frac{2\pi f}{nf_c}\right)} \tag{4.104}$$

what can also be written in a more compact way as follows,

$$G_{\mathrm{TOC}_{\cos}(n,f_c,\rho)} = \left(\frac{f_c}{1-\rho}\right)\left[\frac{2\sin\left(\frac{\pi f}{f_c}\right)\sin\left(\frac{\pi f}{4f_s}\right)\sin\left[\frac{\pi f}{4f_s}(1-\rho)\right]}{\pi f\cos\left(\frac{\pi f}{2f_s}\right)}\right]^2 \tag{4.105}$$

where we have made the change $n = 4f_s/f_c$ as already seen in chapter 4.3.2.2.

In the same manner, the expression for the power spectral density of the odd cosine-phased TOC modulation is shown to present the following form:

$$G_{\mathrm{TOC}_{\cos}(n,f_c,\rho)} = \left(\frac{f_c}{1-\rho}\right)\left[\frac{2\cos\left(\frac{\pi f}{f_c}\right)\sin\left(\frac{\pi f}{4f_s}\right)\sin\left[\frac{\pi f}{4f_s}(1-\rho)\right]}{\pi f\cos\left(\frac{\pi f}{2f_s}\right)}\right]^2 \tag{4.106}$$

Finally, it is important to comment regarding the time representation of the cosine-phased TOC modulation, that this is similar to the sine-phased version that we studied in the previous chapter, but shifted by a quarter of the phase.

4.5.3 Tertiary Phase Shift Keying TPSK

Tertiary Phase Shift Keying signals or TPSK for short are also a particular case of Tertiary Coded Symbols with a modulation vector that consists of only ones. Next figure shows the chip form of such a signal:

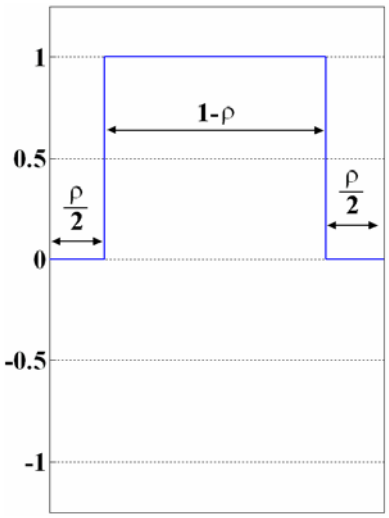

Figure 4.26. Chip waveform of TPSK (1) for a dwell time ρ

According to the definition of previous chapters, it can be shown that the power spectral density adopts the following form in this case:

$$G_{\mathrm{TPSK}(f_c,\rho)} = \left(\frac{f_c}{1-\rho}\right)\frac{\sin^2\left[\dfrac{\pi f}{nf_c}(1-\rho)\right]}{(\pi f)^2}\left\{n + 2\left[\sum_{i=1}^{n-1}(n-i)\cos\left(i\frac{2\pi f}{nf_c}\right)\right]\right\} \tag{4.107}$$

As we already saw in chapter 4.3.1, the term in the brackets can be simplified after some math, and thus the expression for the power spectral density is shown to simplify to:

$$G_{\mathrm{TPSK}(f_c,\rho)} = \left(\frac{f_c}{1-\rho}\right)\frac{\sin^2\left[\dfrac{\pi f}{nf_c}(1-\rho)\right]}{(\pi f)^2}\frac{\sin^2\left(\dfrac{\pi f}{f_c}\right)}{\sin^2\left(\dfrac{\pi f}{nf_c}\right)} \tag{4.108}$$

Or more explicitly:

$$G_{\mathrm{TPSK}(f_c,\rho)} = \left(\frac{f_c}{1-\rho}\right)\left[\frac{\sin\left[\dfrac{\pi f}{n f_c}(1-\rho)\right]\sin\left(\dfrac{\pi f}{f_c}\right)}{\pi f \sin\left(\dfrac{\pi f}{nf_c}\right)}\right]^2 \tag{4.109}$$

4.5.4 Generic m-PSK Coded Symbols

All the modulations that we have analyzed so far in chapter 4.5 are tertiary. However, TCS signals are a particular case of a greater family of signals known as m-PSK Coded Symbols. In addition, m-PSK Coded Symbols are a particular case of MCS.

m-PSK Coded Symbols have as spreading symbol an integer number m of equal-length segments with a castle-like shape of $2\log_2(m)-1$ amplitude levels. Moreover, it can easily be shown that m-PSK Coded Symbols can be expressed as a linear combination of TCS or UTCS signals, where the UTCS signals are Unilateral TCS waveforms, analyzed in Appendix E. A particular case of m-PSK signal that is especially interesting in navigation is the m-PSK Offset Carrier Modulation. We describe this signal waveform in detail in the following chapters.

4.5.5 m-PSK Offset Carrier or m-PSK BOC

The m-PSK Offset Carrier modulation was discussed in [A.R. Pratt and J.I.R. Owen, 2003b] where it was defined as m-PSK BOC modulation. In this thesis we will use the generalized notation to define such a signal. Additionally, we will distinguish between sine-phasing and cosine-phasing. According to this, a sine-phased Offset Carrier with sub-carrier frequency f_s and code frequency f_c corresponds to an m-PSK $\mathrm{BOC}_{\sin}(f_s, f_c)$ in our notation. It is important to recall that whenever we refer to a BOC, we mean the sine-phased version by default. Otherwise we will indicate it.

The interest of this modulation lies in the fact that it allows for a very accurate spectrum control. Given the importance that this topic has had during the design of the Galileo E1 OS signals, specific configurations like 8-PSK BOC(2,2), were seriously considered in the past.

In next chapter, general expressions for the power spectral densities will be derived for this case. As we will see, since the m-PSK Offset Carrier signals can be expressed as a linear combination of TCS and UTCS, we can use the expressions derived above in our derivations.

4.5.5.1 8-PSK Offset Carrier in sine phasing or 8-PSK BOC$_{sin}$(f_s, f_c)

The m-PSK BOC modulation can be expressed as a linear combination of TOCs with their corresponding amplitudes. For the case of the BOC$_8$(f_s , f_c), Figure 4.27 shows in detail how the *castle* chip construction of the chip waveform would look like.

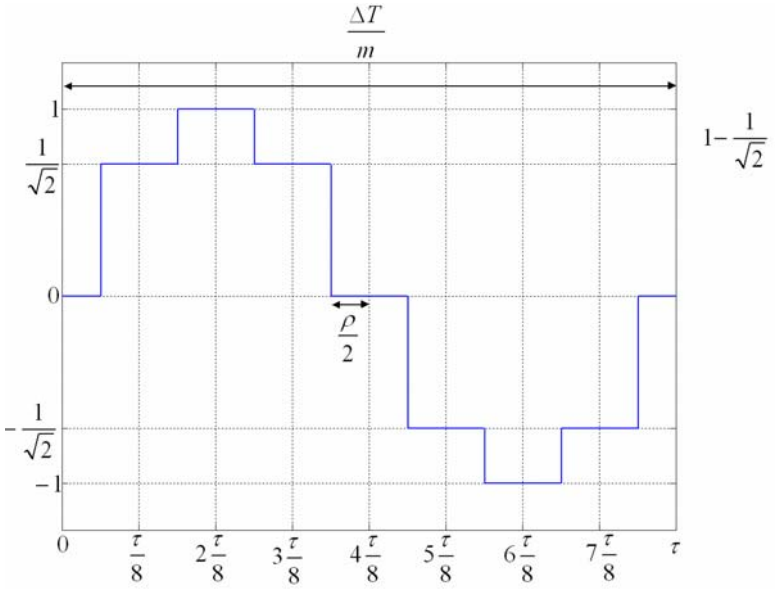

Figure 4.27. Time domain representation of a sine-phased BOC$_8$(f_s , f_c)

It must be noted that *m* refers here to the ratio between the sub-carrier frequency and the code rate according to the figure above. The amplitudes of the different parts of the chip result from projecting the phase points of an 8-PSK modulation as graphically explained in Figure F.2 of the Appendix. Moreover, as we derive in Appendix F, all the points of the constellation present the same probability of occurrence.

Following thus the time definition of Appendix F, the Fourier transform of any 8-PSK sine-phased BOC signal can be expressed as follows,

$$S_{\mathrm{BOC}^8_{\sin}(f_s,f_c)}(f) = \lambda_l S_{\mathrm{TOC}_{\sin}(f_s,f_c,\rho_l)} + \lambda_s S_{\mathrm{TOC}_{\sin}(f_s,f_c,\rho_s)} \qquad (4.110)$$

where ρ_l and ρ_s represent the length of the zero support of the long and short sine-phased TOC modulations as defined in chapter 4.5.2.1. Moreover, λ_l and λ_s are the weighting factors

required to shape the chip waveform as shown in Figure 4.27. Appendix F proves that its power spectral density can be expressed as:

$$G_{\mathrm{BOC}^{8}_{\sin}(f_s,f_c)}(f) = 2f_c\left[\frac{\sin\left(\frac{\pi f}{8f_s}\right)\left[1+\sqrt{2}\cos\left(\frac{\pi f}{4f_s}\right)\right]\sin\left(\frac{\pi f}{f_c}\right)}{\pi f\cos\left(\frac{\pi f}{2f_s}\right)}\right]^2 \tag{4.111}$$

which is graphically shown in the next figure for the particular case of $\mathrm{BOC}_8(2,2)$. As we have already commented in other parts of this thesis, this signal was considered for some time as a potential alternative for the Galileo E1 OS service given its high level of interoperability with GPS. For comparison also the original BOC(2,2) is depicted in the next figure.

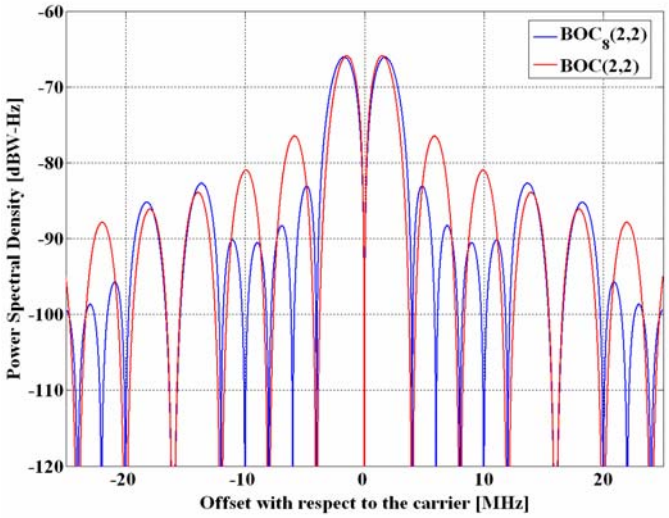

Figure 4.28. Power Spectral Density of BOC(2,2) versus $\mathrm{BOC}_8(2,2)$

As we can recognize, the 8-PSK BOC(2,2) presents a very similar spectrum to that of the original BOC(2,2), especially at low frequencies, with the interesting advantage that it introduces additional zeros at 6 and 10 MHz. Moreover, reducing the power spectrum around the M-Code helps in ensuring higher compatibility with the rest of GPS signals around as identified in [A.R. Pratt and J.I.R. Owen, 2003b].

4.5.5.1.1 ACF of 8-PSK Offset Carrier in sine phasing

Once we have derived the spectral properties of the 8-PSK BOC(2,2) modulation, we spend some time in the next lines deriving the analytical expression of its ideal autocorrelation function for the case of infinite bandwidth.

To derive the general form of the ACF of any 8-PSK Offset Carrier in sine phasing we will make use of the functions derived in chapter 4.3.2.3. To do so, we have to express first the PSD in the oscillation domain of ω in the appropriate form that we saw in previous chapters. According to this, using the spectrum derived in the previous pages, it can be shown that:

$$G_{\mathrm{BOC}^{8}_{\sin}(f_s,f_c)}(\omega)=2f_c\left[\frac{\sin\left(\frac{\omega}{16f_s}\right)\left[1+\sqrt{2}\cos\left(\frac{\omega}{8f_s}\right)\right]\sin\left(\frac{\omega}{2f_c}\right)}{\frac{\omega}{2}\cos\left(\frac{\omega}{4f_s}\right)}\right]^2 \tag{4.112}$$

which can be further developed and expressed as follows for the particular case of the 8-PSK BOC(2,2):

$$R_{\mathrm{BOC}^{8}_{\sin}(2,2)}(\tau)=\frac{1}{\tau\omega^2}\left[\begin{array}{l}\left(8\sqrt{2}-9\right)\cos\left(\frac{1}{4}\omega\tau\right)+\left(-8+4\sqrt{2}\right)\cos(\omega\tau)+\left(3-4\sqrt{2}\right)\cos\left(\frac{3}{4}\omega\tau\right)+\\+\left(-4\sqrt{2}+5\right)\cos\left(\frac{5}{4}\omega\tau\right)+\left(-2\sqrt{2}+2\right)\cos\left(\frac{1}{2}\omega\tau\right)+\\+\left(2\sqrt{2}-2\right)\cos\left(\frac{3}{2}\omega\tau\right)+\cos\left(\frac{7}{4}\omega\tau\right)+\left(8-4\sqrt{2}\right)\end{array}\right] \tag{4.113}$$

where

$$\tau=\frac{\Delta T}{m}=\frac{1}{2f_c} \tag{4.114}$$

From (4.113), we can now obtain an expression for the autocorrelation function in the time domain in a similar form as we did for the BOC signals of previous chapter: ´

$$\begin{aligned}R_{\mathrm{BOC}^{8}_{\sin}(2,2)}(\tau)&=\left(8\sqrt{2}-9\right)T_{\frac{1}{4}}(\tau)+\left(-8+4\sqrt{2}\right)T_1(\tau)+\left(3-4\sqrt{2}\right)T_{\frac{3}{4}}(\tau)+\left(-4\sqrt{2}+5\right)T_{\frac{5}{4}}(\tau)+\\&+\left(-2\sqrt{2}+2\right)T_{\frac{1}{2}}(\tau)+\left(2\sqrt{2}-2\right)T_{\frac{3}{2}}(\tau)+T_{\frac{7}{4}}(\tau)+\left(8-4\sqrt{2}\right)S_1(\tau)\end{aligned} \tag{4.115}$$

where $T_k(\tau)$ and $S_k(\tau)$ were defined in (4.58) and (4.59) respectively. It is important to note that the time unit is the chip.

Figure 4.29 shows graphically the shape of the autocorrelation function for the particular case of the BOC(2,2) modulation.

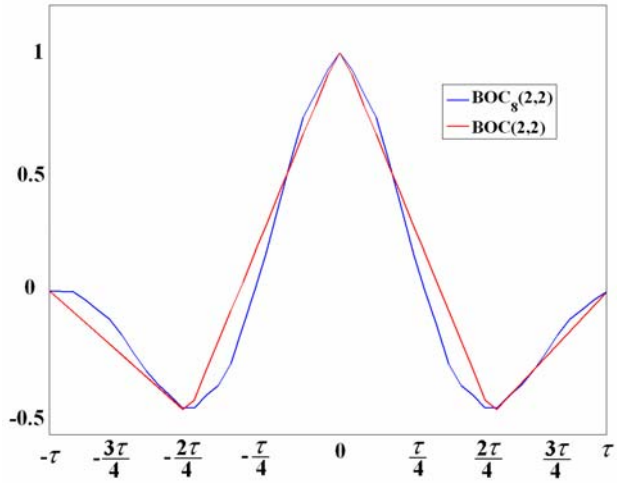

Figure 4.29. Autocorrelation Function of BOC$_8$(2,2)

We analyze in the next chapter the ACF of the cosine-phased version of the 8-PSK BOC(f_s, f_c) modulation. Later we will compare it with its sine-phased counterpart that we have just studied. As an example, we will take the Galileo PRS since this service will make use of the cosine phased $BOC_{cos}(15,2.5)$.

4.5.5.2 8-PSK Offset Carrier in cosine phasing or 8-PSK $BOC_{cos}(f_s, f_c)$

If we express the cosine-phased 8-PSK modulation as a linear combination of TOC signals as we did with its sine-phased counterpart in (4.110), the representation in the time domain is not so easy to accomplish. Therefore, as shown in Appendix E, an alternative expression is employed that is based on a linear combination of unilateral TCS symbols (UTCS).

According to this, the power spectral density of a generic even cosine-phased 8-PSK BOC modulation is shown to adopt the following form:

$$G_{\mathrm{BOC}^{8}_{\cos}(f_s,f_c)}(f) = 2f_c \left[\frac{\left[-1+\cos\left(\frac{\pi f}{8f_s}\right)\left[1-\left(4-2\sqrt{2}\right)\sin^2\left(\frac{\pi f}{8f_s}\right)\right]+8\sin^2\left(\frac{\pi f}{8f_s}\right)\cos^2\left(\frac{\pi f}{8f_s}\right)\right]\sin\left(\frac{\pi f}{f_c}\right)}{\pi f \cos\left(\frac{\pi f}{2f_s}\right)} \right]^2 \tag{4.116}$$

If we particularize now the expression above for the case of the cosine 8-PSK BOC(15,2.5) modulation, we can recognize interesting spectral properties compared with those of the typical $BOC_{sin}(15,2.5)$ case. We show the resulting spectrum in the next figure and compare it with other similar alternatives that were object of study during the design of the Galileo Signal Plan.

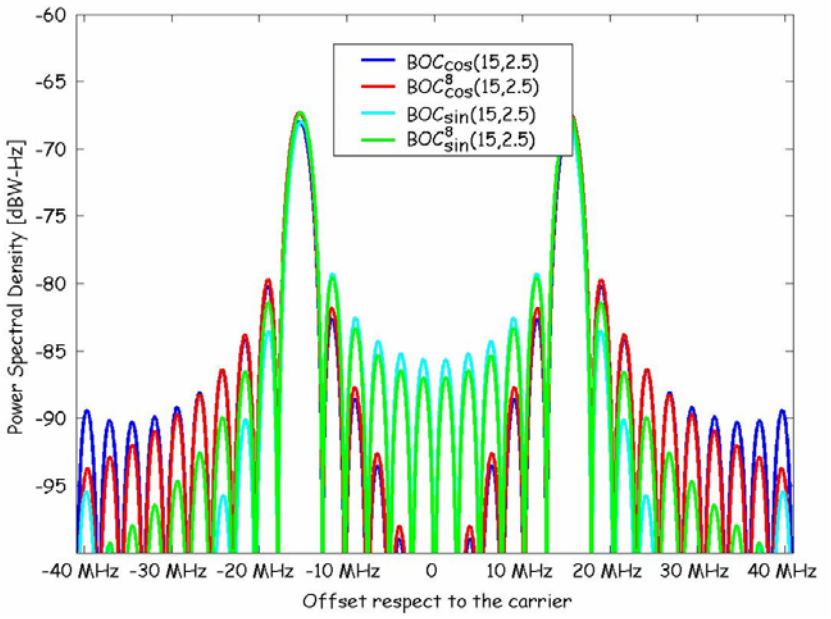

Figure 4.30. Power Spectral Density of some studied PRS alternatives

As we can recognize in the figure above, the cosine-phased 8-PSK BOC(15,2.5) modulation behaves similar to the cosine-phased BOC(15,2.5) in the inner part of the spectrum, while on the outer part it is slightly better regarding the spectral isolation, what would be interesting if we consider the effect on the GLONASS signals. In addition, $BOC_{sin}(15,2.5)$ and 8-PSK $BOC_{sin}(15,2.5)$ are also shown for comparison.

A figure of great interest in analyzing the spectral compatibility between signals in a shared band is the Cross Power Spectral Density (CPSD). The Cross Power Spectral Density is basically the product of the power spectral densities of two signals and gives an idea of how much they overlap with each other. Indeed, the Cross Power Spectral Density between the studied signal and the M-Code is shown in the next figure. We will talk about this figure more in detail in the chapter 5.

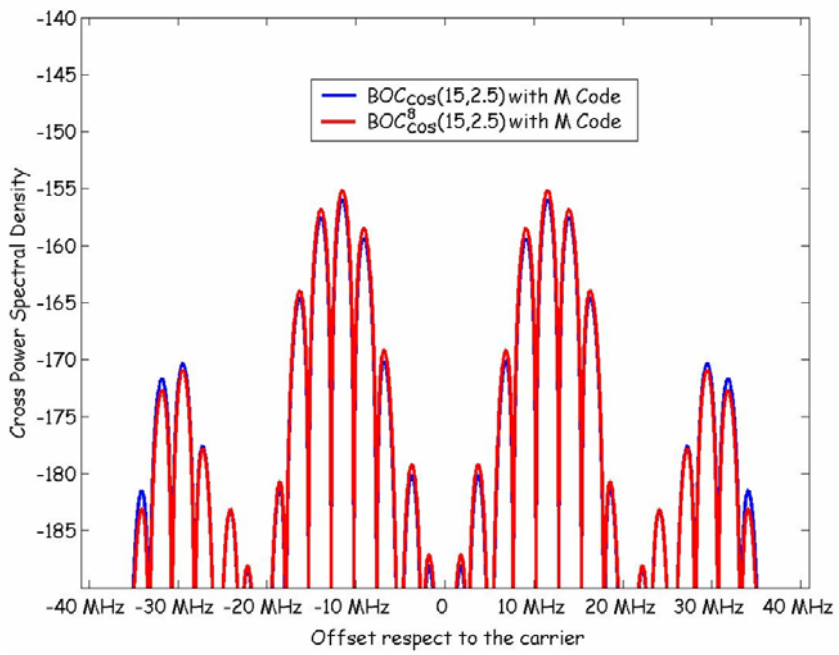

Figure 4.31. Cross Power Spectral Density of PRS alternatives with GPS M-Code

As we can clearly see, while for an offset of less than 20 MHz both analyzed solutions show more or less the same values, $BOC^{8}_{cos}(15,2.5)$ seems to be slightly better above 20 MHz. To conclude our analysis on the cosine-phased 8-PSK modulation, we derive in the next lines some expressions of interest for the autocorrelation function.

4.5.5.2.1 ACF of 8-PSK Offset Carrier in cosine phasing

For the particular case of $BOC^{8}_{cos}(15,2.5)$, the power spectral density is shown to be expressed as follows in the ω domain.

$$
\begin{aligned}
&G_{\mathrm{BOC}^{8}_{\cos}(15,2.5)}(\omega)= \\
&= \frac{1}{\tau\omega^{2}}\left[\begin{array}{l}
4\sqrt{2}\cos\left(\frac{29}{96}\omega\tau\right)-4\sqrt{2}\cos\left(\frac{17}{32}\omega\tau\right)+\left(-60\sqrt{2}+62\right)\cos\left(\frac{19}{48}\omega\tau\right)+ \\
+\left(-4+4\sqrt{2}\right)\cos\left(\frac{1}{24}\omega\tau\right)+\left(-38+36\sqrt{2}\right)\cos\left(\frac{31}{48}\omega\tau\right)+\left(50-52\sqrt{2}\right)\cos\left(\frac{7}{16}\omega\tau\right)+ \\
+\left(4\sqrt{2}-8\right)\cos\left(\frac{7}{96}\omega\tau\right)+\left(60\sqrt{2}-58\right)\cos\left(\frac{17}{48}\omega\tau\right)-4\sqrt{2}\cos\left(\frac{35}{96}\omega\tau\right)+ \\
+\left(-10+12\sqrt{2}\right)\cos\left(\frac{41}{48}\omega\tau\right)+\left(4-4\sqrt{2}\right)\cos\left(\frac{1}{8}\omega\tau\right)+\left(4\sqrt{2}-8\right)\cos\left(\frac{11}{32}\omega\tau\right)+ \\
+\left(-4+4\sqrt{2}\right)\cos\left(\frac{5}{24}\omega\tau\right)+\left(-70+68\sqrt{2}\right)\cos\left(\frac{5}{16}\omega\tau\right)+\left(80-32\sqrt{2}\right)\cos\left(\frac{2}{3}\omega\tau\right)+ \\
+\left(4\sqrt{2}-8\right)\cos\left(\frac{23}{96}\omega\tau\right)-40\cos^{2}\left(\frac{1}{6}\omega\tau\right)+\left(8-4\sqrt{2}\right)\cos\left(\frac{31}{96}\omega\tau\right)+ \\
+4\sqrt{2}\cos\left(\frac{11}{96}\omega\tau\right)+\left(20\sqrt{2}-22\right)\cos\left(\frac{13}{16}\omega\tau\right)+\left(8-4\sqrt{2}\right)\cos\left(\frac{19}{32}\omega\tau\right)+ \\
+\left(4\sqrt{2}-8\right)\cos\left(\frac{1}{96}\omega\tau\right)+4\sqrt{2}\cos\left(\frac{13}{96}\omega\tau\right)+\left(82-84\sqrt{2}\right)\cos\left(\frac{5}{48}\omega\tau\right)+4\sqrt{2}\cos\left(\frac{25}{32}\omega\tau\right)- \\
-4\sqrt{2}\cos\left(\frac{1}{32}\omega\tau\right)+\left(4\sqrt{2}-8\right)\cos\left(\frac{17}{96}\omega\tau\right)+\left(88\sqrt{2}-176\right)\cos\left(\frac{1}{12}\omega\tau\right)+ \\
+\left(-26+28\sqrt{2}\right)\cos\left(\frac{11}{16}\omega\tau\right)+\left(-64\sqrt{2}+160\right)\cos\left(\frac{1}{3}\omega\tau\right)+\left(-90+92\sqrt{2}\right)\cos\left(\frac{1}{48}\omega\tau\right)- \\
-4\sqrt{2}\cos\left(\frac{23}{32}\omega\tau\right)+\left(14-12\sqrt{2}\right)\cos\left(\frac{43}{48}\omega\tau\right)-4\sqrt{2}\cos\left(\frac{53}{96}\omega\tau\right)+\left(-16\sqrt{2}+40\right)\cos\left(\frac{5}{6}\omega\tau\right)- \\
-4\sqrt{2}\cos\left(\frac{85}{96}\omega\tau\right)+\left(2-4\sqrt{2}\right)\cos\left(\frac{15}{16}\omega\tau\right)-4\sqrt{2}\cos\left(\frac{5}{96}\omega\tau\right)+ \\
+\left(-80+40\sqrt{2}\right)\cos\left(\frac{7}{12}\omega\tau\right)+\left(-144+72\sqrt{2}\right)\cos\left(\frac{1}{4}\omega\tau\right)-4\sqrt{2}\cos\left(\frac{83}{96}\omega\tau\right)+ \\
+\left(-54+52\sqrt{2}\right)\cos\left(\frac{23}{48}\omega\tau\right)+\left(18-20\sqrt{2}\right)\cos\left(\frac{37}{48}\omega\tau\right)+4\sqrt{2}\cos\left(\frac{15}{32}\omega\tau\right)+ \\
+\left(46-44\sqrt{2}\right)\cos\left(\frac{9}{16}\omega\tau\right)+\left(8-4\sqrt{2}\right)\cos\left(\frac{3}{32}\omega\tau\right)+4\sqrt{2}\cos\left(\frac{77}{96}\omega\tau\right)-4\sqrt{2}\cos\left(\frac{37}{96}\omega\tau\right)+ \\
+\left(4-4\sqrt{2}\right)\cos\left(\frac{7}{24}\omega\tau\right)+\left(-86+84\sqrt{2}\right)\cos\left(\frac{7}{48}\omega\tau\right)+\left(8-4\sqrt{2}\right)\cos\left(\frac{5}{32}\omega\tau\right)+ \\
+\left(4\sqrt{2}-8\right)\cos\left(\frac{29}{32}\omega\tau\right)+\left(4\sqrt{2}-8\right)\cos\left(\frac{55}{96}\omega\tau\right)+\left(30-28\sqrt{2}\right)\cos\left(\frac{35}{48}\omega\tau\right)+ \\
+\left(-112+56\sqrt{2}\right)\cos\left(\frac{5}{12}\omega\tau\right)-4\sqrt{2}\cos\left(\frac{19}{96}\omega\tau\right)+\left(44\sqrt{2}-42\right)\cos\left(\frac{25}{48}\omega\tau\right)+ \\
+4\sqrt{2}\cos\left(\frac{9}{32}\omega\tau\right)+\left(8-4\sqrt{2}\right)\cos\left(\frac{41}{96}\omega\tau\right)+\left(8-4\sqrt{2}\right)\cos\left(\frac{47}{96}\omega\tau\right)+ \\
+4\sqrt{2}\cos\left(\frac{31}{32}\omega\tau\right)-4\sqrt{2}\cos\left(\frac{7}{32}\omega\tau\right)+4\sqrt{2}\cos\left(\frac{59}{96}\omega\tau\right)
\end{array}\right]+
\end{aligned}
$$

$$+\frac{1}{\tau\omega^2}\left[\begin{array}{l}
+\left(-92\sqrt{2}+94\right)\cos\left(\frac{1}{16}\omega\tau\right)+\left(76\sqrt{2}-74\right)\cos\left(\frac{3}{16}\omega\tau\right)+\left(4\sqrt{2}-8\right)\cos\left(\frac{49}{96}\omega\tau\right)+\\
+\left(-4+4\sqrt{2}\right)\cos\left(\frac{17}{24}\omega\tau\right)+4\sqrt{2}\cos\left(\frac{61}{96}\omega\tau\right)-4\sqrt{2}\cos\left(\frac{67}{96}\omega\tau\right)+\\
+\left(-6+4\sqrt{2}\right)\cos\left(\frac{47}{48}\omega\tau\right)+4\sqrt{2}\cos\left(\frac{43}{96}\omega\tau\right)+\left(4-4\sqrt{2}\right)\cos\left(\frac{5}{8}\omega\tau\right)+\\
+\left(-4+4\sqrt{2}\right)\cos\left(\frac{13}{24}\omega\tau\right)+\left(8-4\sqrt{2}\right)\cos\left(\frac{25}{96}\omega\tau\right)+\left(8-4\sqrt{2}\right)\cos\left(\frac{21}{32}\omega\tau\right)+\\
+4\sqrt{2}\cos\left(\frac{91}{96}\omega\tau\right)+\left(4\sqrt{2}-8\right)\cos\left(\frac{27}{32}\omega\tau\right)-32\cos\left(\frac{1}{6}\omega\tau\right)\cos\left(\frac{1}{3}\omega\tau\right)-16\cos\left(\frac{1}{6}\omega\tau\right)\cos\left(\frac{2}{3}\omega\tau\right)-\\
-8\cos\left(\frac{1}{6}\omega\tau\right)\cos\left(\frac{5}{6}\omega\tau\right)-24\cos\left(\frac{1}{6}\omega\tau\right)\cos\left(\frac{1}{2}\omega\tau\right)+\left(176-80\sqrt{2}\right)\cos\left(\frac{1}{6}\omega\tau\right)+\\
+\left(34-36\sqrt{2}\right)\cos\left(\frac{29}{48}\omega\tau\right)+\left(-4+4\sqrt{2}\right)\cos\left(\frac{3}{8}\omega\tau\right)+\left(8-4\sqrt{2}\right)\cos\left(\frac{79}{96}\omega\tau\right)+\left(-4+4\sqrt{2}\right)\cos\left(\frac{7}{8}\omega\tau\right)+\\
+\left(4-4\sqrt{2}\right)\cos\left(\frac{19}{24}\omega\tau\right)+\left(8-4\sqrt{2}\right)\cos\left(\frac{89}{96}\omega\tau\right)+\\
+\left(4-4\sqrt{2}\right)\cos\left(\frac{11}{24}\omega\tau\right)+\left(4\sqrt{2}-8\right)\cos\left(\frac{65}{96}\omega\tau\right)+\left(4-4\sqrt{2}\right)\cos\left(\frac{23}{24}\omega\tau\right)+\left(4\sqrt{2}-8\right)\cos\left(\frac{71}{96}\omega\tau\right)+\\
+\left(-76\sqrt{2}+78\right)\cos\left(\frac{11}{48}\omega\tau\right)+\left(8-4\sqrt{2}\right)\cos\left(\frac{73}{96}\omega\tau\right)+\\
+\left(-16+8\sqrt{2}\right)\cos\left(\frac{11}{12}\omega\tau\right)+\left(8-4\sqrt{2}\right)\cos\left(\frac{95}{96}\omega\tau\right)+\left(4\sqrt{2}-8\right)\cos\left(\frac{13}{32}\omega\tau\right)+\\
+\left(-68\sqrt{2}+66\right)\cos\left(\frac{13}{48}\omega\tau\right)+\left(-48\sqrt{2}+120\right)\cos\left(\frac{1}{2}\omega\tau\right)+\left(24\sqrt{2}-48\right)\cos\left(\frac{3}{4}\omega\tau\right)+\left(-48\sqrt{2}+120\right)
\end{array}\right] \tag{4.117}$$

with

$$\tau=\frac{\Delta T}{m}=\frac{1}{2f_c} \tag{4.118}$$

From (4.117), we can derive an expression for the autocorrelation function in the time domain. It is important to note that the time variable is expressed in chips.

$$
\begin{aligned}
&R_{\mathrm{BOC}^{8}_{\cos}(15,2.5)}(\tau) = \\
&= 4\sqrt{2}\,T_{\frac{29}{96}}(\tau) - 4\sqrt{2}\,T_{\frac{17}{32}}(\tau) + \left(-60\sqrt{2}+62\right)T_{\frac{19}{48}}(\tau) + \left(-4+4\sqrt{2}\right)T_{\frac{1}{24}}(\tau) + \left(-38+36\sqrt{2}\right)T_{\frac{31}{48}}(\tau) + \\
&+ \left(50-52\sqrt{2}\right)T_{\frac{7}{16}}(\tau) + \left(4\sqrt{2}-8\right)T_{\frac{7}{96}}(\tau) + \left(60\sqrt{2}-58\right)T_{\frac{17}{48}}(\tau) - 4\sqrt{2}\,T_{\frac{35}{96}}(\tau) + \left(-10+12\sqrt{2}\right)T_{\frac{41}{48}}(\tau) + \\
&+ \left(4-4\sqrt{2}\right)T_{\frac{1}{8}}(\tau) + \left(4\sqrt{2}-8\right)T_{\frac{11}{32}}(\tau) + \left(-4+4\sqrt{2}\right)T_{\frac{5}{24}}(\tau) + \left(-70+68\sqrt{2}\right)T_{\frac{5}{16}}(\tau) + \\
&+ \left(80-32\sqrt{2}\right)T_{\frac{2}{3}}(\tau) + \left(4\sqrt{2}-8\right)T_{\frac{23}{96}}(\tau) - 40\,M_{\left(\frac{1}{6},\frac{1}{6}\right)}(\tau) + \left(8-4\sqrt{2}\right)T_{\frac{31}{96}}(\tau) + 4\sqrt{2}\,T_{\frac{11}{96}}(\tau) + \\
&+ \left(20\sqrt{2}-22\right)T_{\frac{13}{16}}(\tau) + \left(8-4\sqrt{2}\right)T_{\frac{19}{32}}(\tau) + \left(4\sqrt{2}-8\right)T_{\frac{1}{96}}(\tau) + 4\sqrt{2}\,T_{\frac{13}{96}}(\tau) + \left(82-84\sqrt{2}\right)T_{\frac{5}{48}}(\tau) + \\
&+ 4\sqrt{2}\,T_{\frac{25}{32}}(\tau) - 4\sqrt{2}\,T_{\frac{1}{32}}(\tau) + \left(4\sqrt{2}-8\right)T_{\frac{17}{96}}(\tau) + \left(88\sqrt{2}-176\right)T_{\frac{1}{12}}(\tau) + \left(-26+28\sqrt{2}\right)T_{\frac{11}{16}}(\tau) + \\
&+ \left(-64\sqrt{2}+160\right)T_{\frac{1}{3}}(\tau) + \left(-90+92\sqrt{2}\right)T_{\frac{1}{48}}(\tau) - 4\sqrt{2}\,T_{\frac{23}{32}}(\tau) + \left(14-12\sqrt{2}\right)T_{\frac{43}{48}}(\tau) - 4\sqrt{2}\,T_{\frac{53}{96}}(\tau) + \\
&+ \left(-16\sqrt{2}+40\right)T_{\frac{5}{6}}(\tau) - 4\sqrt{2}\,T_{\frac{85}{96}}(\tau) + \left(2-4\sqrt{2}\right)T_{\frac{15}{16}}(\tau) - 4\sqrt{2}\,T_{\frac{5}{96}}(\tau) + \left(-80+40\sqrt{2}\right)T_{\frac{7}{12}}(\tau) + \\
&+ \left(-144+72\sqrt{2}\right)T_{\frac{1}{4}}(\tau) - 4\sqrt{2}\,T_{\frac{83}{96}}(\tau) + \left(-54+52\sqrt{2}\right)T_{\frac{23}{48}}(\tau) + \left(18-20\sqrt{2}\right)T_{\frac{37}{48}}(\tau) + 4\sqrt{2}\,T_{\frac{15}{32}}(\tau) + \\
&+ \left(46-44\sqrt{2}\right)T_{\frac{9}{16}}(\tau) + \left(8-4\sqrt{2}\right)T_{\frac{3}{32}}(\tau) + 4\sqrt{2}\,T_{\frac{77}{96}}(\tau) - 4\sqrt{2}\,T_{\frac{37}{96}}(\tau) + \left(4-4\sqrt{2}\right)T_{\frac{7}{24}}(\tau) + \\
&+ \left(-86+84\sqrt{2}\right)T_{\frac{7}{48}}(\tau) + \left(8-4\sqrt{2}\right)T_{\frac{5}{32}}(\tau) + \left(4\sqrt{2}-8\right)T_{\frac{29}{32}}(\tau) + \left(4\sqrt{2}-8\right)T_{\frac{55}{96}}(\tau) + \\
&+ \left(30-28\sqrt{2}\right)T_{\frac{35}{48}}(\tau) + \left(-112+56\sqrt{2}\right)T_{\frac{5}{12}}(\tau) - 4\sqrt{2}\,T_{\frac{19}{96}}(\tau) + \left(44\sqrt{2}-42\right)T_{\frac{25}{48}}(\tau) + 4\sqrt{2}\,T_{\frac{9}{32}}(\tau) + \\
&+ \left(8-4\sqrt{2}\right)T_{\frac{41}{96}}(\tau) + \left(8-4\sqrt{2}\right)T_{\frac{47}{96}}(\tau) + 4\sqrt{2}\,T_{\frac{31}{32}}(\tau) - 4\sqrt{2}\,T_{\frac{7}{32}}(\tau) + 4\sqrt{2}\,T_{\frac{59}{96}}(\tau) + \\
&+ \left(-92\sqrt{2}+94\right)T_{\frac{1}{16}}(\tau) + \left(76\sqrt{2}-74\right)T_{\frac{3}{16}}(\tau) + \left(4\sqrt{2}-8\right)T_{\frac{49}{96}}(\tau) + \left(-4+4\sqrt{2}\right)T_{\frac{17}{24}}(\tau) + \\
&+ 4\sqrt{2}\,T_{\frac{61}{96}}(\tau) - 4\sqrt{2}\,T_{\frac{67}{96}}(\tau) + \left(-6+4\sqrt{2}\right)T_{\frac{47}{48}}(\tau) + 4\sqrt{2}\,T_{\frac{43}{96}}(\tau) + \left(4-4\sqrt{2}\right)T_{\frac{5}{8}}(\tau) + \\
&+ \left(-4+4\sqrt{2}\right)T_{\frac{13}{24}}(\tau) + \left(8-4\sqrt{2}\right)T_{\frac{25}{96}}(\tau) + \left(8-4\sqrt{2}\right)T_{\frac{21}{32}}(\tau) + 4\sqrt{2}\,T_{\frac{91}{96}}(\tau) + \left(4\sqrt{2}-8\right)T_{\frac{27}{32}}(\tau) - \\
&- 32\,M_{\left(\frac{1}{6},\frac{1}{3}\right)}(\tau) - 16\,M_{\left(\frac{1}{6},\frac{2}{3}\right)}(\tau) - 8\,M_{\left(\frac{1}{6},\frac{5}{6}\right)}(\tau) - 24\,M_{\left(\frac{1}{6},\frac{1}{2}\right)}(\tau) + \left(176-80\sqrt{2}\right)T_{\frac{1}{6}}(\tau) + \\
&+ \left(34-36\sqrt{2}\right)T_{\frac{29}{48}}(\tau) + \left(-4+4\sqrt{2}\right)T_{\frac{3}{8}}(\tau) + \left(8-4\sqrt{2}\right)T_{\frac{79}{96}}(\tau) + \left(-4+4\sqrt{2}\right)T_{\frac{7}{8}}(\tau) + \\
&+ \left(4-4\sqrt{2}\right)T_{\frac{19}{24}}(\tau) + \left(8-4\sqrt{2}\right)T_{\frac{89}{96}}(\tau) + \left(4-4\sqrt{2}\right)T_{\frac{11}{24}}(\tau) + \left(4\sqrt{2}-8\right)T_{\frac{65}{96}}(\tau) + \left(4-4\sqrt{2}\right)T_{\frac{23}{24}}(\tau) + \\
&+ \left(4\sqrt{2}-8\right)T_{\frac{71}{96}}(\tau) + \left(-76\sqrt{2}+78\right)T_{\frac{11}{48}}(\tau) + \left(8-4\sqrt{2}\right)T_{\frac{73}{96}}(\tau) + \left(-16+8\sqrt{2}\right)T_{\frac{11}{12}}(\tau) + \\
&+ \left(8-4\sqrt{2}\right)T_{\frac{95}{96}}(\tau) + \left(4\sqrt{2}-8\right)T_{\frac{13}{32}}(\tau) + \left(-68\sqrt{2}+66\right)T_{\frac{13}{48}}(\tau) + \left(-48\sqrt{2}+120\right)T_{\frac{1}{2}}(\tau) + \\
&+ \left(24\sqrt{2}-48\right)T_{\frac{3}{4}}(\tau) + \left(-48\sqrt{2}+120\right)S_1(\tau)
\end{aligned}
\tag{4.119}
$$

The autocorrelation is shown graphically in the next figure.

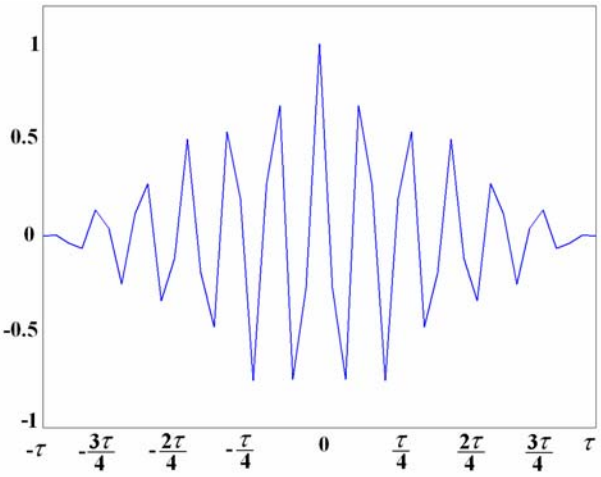

Figure 4.32. Autocorrelation Function of $BOC_8(15,2.5)$

4.5.6 m-PSK Coded Symbols (m-PSK CS)

So far, we have analyzed the case of 8-PSK sine-phased and cosine-phased BOC modulations but as one can imagine, we can extend the idea to any BCS using more levels. Next figure shows some examples:

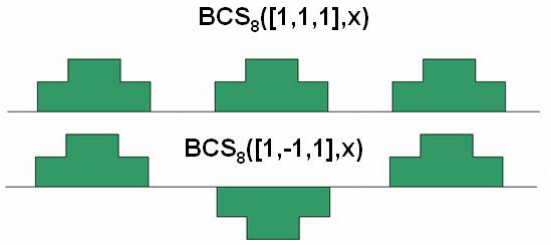

Figure 4.33. Example of waveform for a general 8-PSK BCS signal

In addition, we can recognize again here that the BOC case that we studied above is nothing else than a particular BCS case, as shown next:

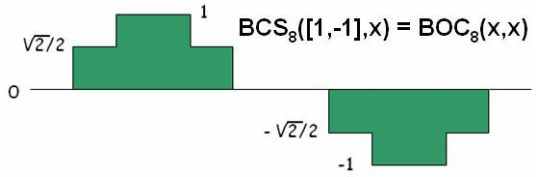

Figure 4.34. Equivalence between 8-PSK BCS(1,-1) and 8-PSK BOC

This rule applies also for the case of other well-known BCS signals as BPSK. Finally, it is important to underline that all the signals we have studied in the preceding chapters are indeed particular cases of the most general MCS definition that we gave at the very beginning. The only distinction to make is whether the MCS segments are of equal length or not.

4.6 CBCS Modulation definition and analysis of performance

On June 26th, 2004, the United States of America and the European Union signed the *Agreement on the promotion, provision and use of Galileo and GPS satellite-based navigation systems and related applications* [G.W. Hein et al., 2005]. Among other topics it was decided to adopt a common baseline signal to be transmitted by both the Galileo E1 Open Service (OS) and the future GPS L1 Civil signal (L1C) on E1/L1. Although the agreement fixed BOC(1,1) as the baseline for both Galileo E1 OS and the GPS future L1C signals, it left the door open for a possible optimization of that signal considering the overall framework conditions of the agreement.

Right after the Agreement was signed, experts on both sides of the Atlantic started to work on possible solutions that would fulfil the criteria set up in the Agreement. The solution would have to clearly outperform the agreed BOC(1,1). Finally, in September 2005 a first temptative solution, known as CBCS(20) was presented by members of the Signal Task Force (STF) of the European Commission (EC) [G.W. Hein et al., 2005]. The proposed solution was highly interoperable with the baseline BOC(1,1) and offered at the same time the possibility to have superior performance to high precision receivers with wider bandwidths.

The CBCS modulation (Composite Binary Coded Symbols) is the result of superposing BOC(1,1) and a BCS (Binary Coded Symbol) waveform with the same chip rate, according to the following expression:

$$G_{\mathrm{CBCS}}(f) = \alpha\, G_{\mathrm{BOC}(1,1)}(f) + \beta\, G_{\mathrm{BCS}([s],1)}(f) \tag{4.120}$$

where α and β indicate the amount of power that is put on BOC(1,1) and on the BCS signal with respect to the total OS power of the signal. Thus, α and β fulfil the condition $\alpha + \beta = 1$. For this same reason, we will use in other parts of the thesis $\beta = \rho$ and $\alpha = 1 - \rho$ instead. Moreover, [s] represents the BCS vector as defined in chapter 4.2. As we saw there, BCS is a generalization of the BPSK and BOC modulations. In addition, it is important to realize that the CBCS definition intrinsically assumes the use of Interplex to multiplex the signals.

The flexibility of the CBCS approach lies in the fact that it could be easily converted into another CBCS by changing the contribution of the BCS part or even choosing different chip rates. In fact, a particular case of the CBCS solution is the pure BCS signal which seems to present the best performance in terms of multipath for selected sequences. Nonetheless, for the EU developers keeping high interoperability with BOC(1,1) receivers was a mandatory from the very beginning and this forced the design to have an important amount of BOC(1,1) in the definition.

We show next graphically the signal generation of CBCS in the time domain. It is important to note that CBCS is not a binary signal but two binary signals in anti-phase in data and pilot.

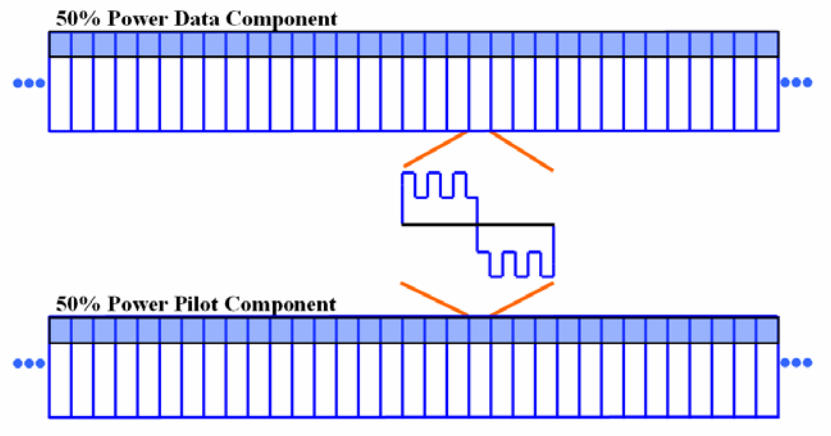

Figure 4.35. CBCS representation in the time domain

As we saw in previous chapters, signal waveforms with a very sharp peak were the goal of the optimization carried out in the past years for both GPS and Galileo. Indeed, as we have shown in chapter 4.1.1, by selecting $p_{T_c}(t)$ with good aperiodic correlation, important improvements in terms of performance can be obtained, especially regarding multipath. In the course of the optimization other interesting solutions were found with even different chip rates than those of the Agreement. Nevertheless, the important constraint to be compliant with BOC(1,1) limited the candidates to have a chip rate of 1 MHz, as we have already underlined.

Unlike the MBOC signal that we will present in the next chapter, the CBCS modulation was proposed alone from the European side. Thus, to the signal definition of the equation (4.120) above the extra constraint to use the Interplex modulation scheme was added in the definition in light with the development of other signals in the Galileo satellites. Indeed, the CBCS modulation is defined *as the superposition of a BOC signal with a BCS using a modified and optimized Interplex scheme in the navigation payload of the satellite.*

4.6.1 CBCS Time Domain Representation and Spectrum

The CBCS signal features a spread-spectrum signal with 4-level sub-carriers, whereas the BOC or BCS signals feature only binary sub-carriers. As we will show in detail in chapter 7, an implementation of the CBCS signals on the Galileo E1 modulation could have been performed using other multiplexing schemes such as the FH-Interplex (Faded-Harmonics) [CNES, 2005], as this also relies on the sum of two 4-level spread-spectrum signals.

Yet, the analysis of the FH-Interplex scheme for the CBCS put in evidence two important drawbacks [G.W. Hein et al., 2005]:

- The inter-modulation product relative power of the FH-Interplex that results from applying CBCS is increased resulting thus in an important loss of efficiency

- The quadrature component suffers from important distortions which may induce unacceptable losses on the receiver, as well as an increased spreading of the quadrature signal in adjacent frequency bands. In the case of Galileo, the degraded signal would be the PRS what supposed an important drawback.

As a solution, a new modulation scheme was developed in [L. Ries et al., 2006] to provide an optimized implementation of the CBCS signals, without the drawbacks described in the preceding lines. The resulting modulation is more efficient than the Modified Hexaphase as it reduces significantly the effect and power of the inter-modulation product.

As shown in Appendix J, the generic CBCS baseband modulation can be expressed mathematically as follows:

$$s(t) = A_1 \left[\begin{array}{l} \frac{c_D(t)}{2}\left(\cos\theta_1 \, s_{\mathrm{BOC}(1,1)}(t) + \cos\theta_2 \, s_{\mathrm{BCS}([\bar{s}],1)}(t)\right) + \\ + \frac{c_P(t)}{2}\left(\cos\theta_1 \, s_{\mathrm{BOC}(1,1)}(t) - \cos\theta_2 \, s_{\mathrm{BCS}([\bar{s}],1)}(t)\right) + \\ + j\, s_{\mathrm{PRS}}(t)\left(\frac{\sin\theta_1 + \sin\theta_2}{2}\right) + s_{\mathrm{IM}}(t) \end{array} \right] \tag{4.121}$$

$$s_{\mathrm{IM}}(t) = -j\, c_D(t)\, c_P(t)\, s_{\mathrm{PRS}}(t)\left(\frac{\sin\theta_1 - \sin\theta_2}{2}\right) \tag{4.122}$$

where:

- A_1 is the amplitude of the modulation envelope, sum of the OS data (D) and pilot (P), PRS and Inter-Modulation product IM. The maximum possible value of A_1 that respects the Agreement of 2004 is a function of the percentage of power put on the BCS component of the signal and the spectral relationship between BOC(1,1) and BCS. Moreover, $A_1 = \sqrt{2P_T}$ where P_T is the total power of the multiplexed signal.
- θ_1 and θ_2 describe the angular distance of points of the 8-PSK modulation as described in Figure 4.36. This depends on the percentage of power that is placed on BCS.
- $s_{\mathrm{BOC}(1,1)}(t)$ represents the BOC(1,1) modulation with chip rate of 1.023 MHz
- $s_{\mathrm{BCS}([s],1)}(t)$ represents the BCS([s],1) modulation with a chip rate of 1.023 MHz and a BCS vector given by [s].
- $s_{\mathrm{PRS}}(t)$ is the PRS modulation $\mathrm{BOC}_{\cos}(15,2.5)$
- $s_{\mathrm{IM}}(t)$ is the Inter-Modulation product signal
- $c_D(t)$ and $c_P(t)$ are the data and pilot codes respectively. It is important to note that $c_D(t)$ also includes the data bits.

The phase points of the resulting constellation are shown in the following figure:

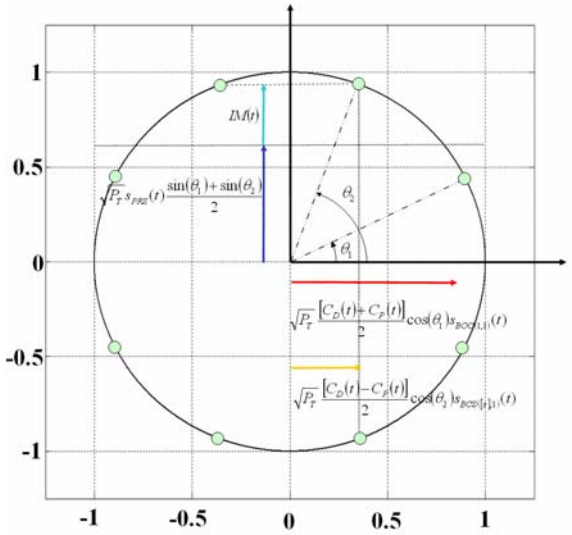

Figure 4.36. Modified 8-PSK modulation with constant envelope for the optimized signal

The modulation can be optimized so as to pseudo-randomly time-multiplex the BOC and BCS sub-carriers on the in-phase component. Rearranging the terms of (4.121) to make this pseudo-random time-multiplexing appear yields to the following expression:

$$s(t) = A_1 \left[\begin{array}{l} \dfrac{c_D(t) + c_P(t)}{2} \cos\theta_1 \; s_{\mathrm{BOC}(1,1)}(t) + \\ + \dfrac{c_D(t) - c_P(t)}{2} \cos\theta_2 \; s_{\mathrm{BCS}([\bar{s}],1)}(t) + \\ + j\, s_{\mathrm{PRS}}(t) \left(\dfrac{\sin\theta_1 + \sin\theta_2}{2} \right) + s_{\mathrm{IM}}(t) \end{array} \right] \tag{4.123}$$

If we look at the previous equation in detail, we can observe that the BOC(1,1) sub-carrier of the OS_D (Data) and OS_P (Pilot) components is transmitted during the same time-slots as it was on the original Hexaphase modulation with only BOC(1,1). This will be further analyzed in chapter 7.7. In addition, the BCS sub-carrier of the OS_D and OS_P components is transmitted in time-slots complementary to those of the BOC sub-carrier (i.e in the time slot when the Modified Hexaphase in-phase component was equal to zero and therefore nothing was transmitted). As a result, the IM product is considerably reduced and 8 phase points appear instead of only 6. Also important to note is that the quadrature component (the PRS signal) is left unaffected by this new scheme, except for its relative amplitude.

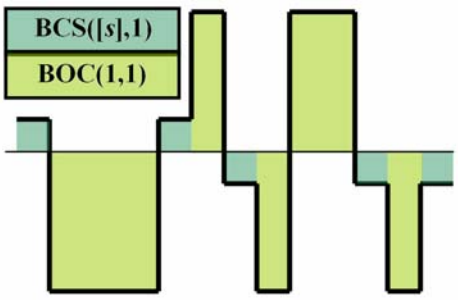

Figure 4.37. Pseudo-random time multiplexing of BCS and BOC(1,1) in CBCS solution

Another important conclusion that we can draw from observing the equation above is that if one optimizes the data and pilot channel codes with each other, the code structure that results from applying the multiplexing scheme of (4.123) does not necessarily have to be also optimized in the general case.

Indeed, we can clearly recognize that the code that actually modulates the BOC(1,1) signal waveform is the semi-sum of the data and pilot codes. Equally, the semi-difference of the data and pilot codes modulates the BCS sequence. Moreover, these codes are not binary since they can take the values +2, 0 and -2 [P.G. Mattos, 2005]. As shown in [F. Soualle et al., 2005] the data and pilot codes were optimized without accounting for the modulation scheme. The consequence of this is that unless the receiver applies a coherent processing of the incoming signal, the codes will show a slight degradation.

Another very important aspect from the CBCS modulation is the power distribution, since this determines in the end the multipath rejection potential of the solutions. As shown in Appendix J, the following expressions for the data and pilot channels can be derived:

$$P_{\mathrm{OS}_D} = A_1^2\left[\frac{\cos^2(\theta_1)+\cos^2(\theta_2)}{4}+\frac{\cos(\theta_1)\cos(\theta_2)}{2}r\right] \tag{4.124}$$

$$P_{\mathrm{OS}_P} = A_1^2\left[\frac{\cos^2(\theta_1)+\cos^2(\theta_2)}{4}-\frac{\cos(\theta_1)\cos(\theta_2)}{2}r\right] \tag{4.125}$$

where the parameter r represents the correlation between BOC(1,1) and the BCS signal:

$$r=\frac{1}{T_c}\int_{T_c} s_{\mathrm{BOC}(1,1)}(t)s_{\mathrm{BCS}([\bar{s}],1)}(t)\mathrm{d}t \tag{4.126}$$

This parameter is of great importance as we will see when we describe the MBOC modulation in the next chapter. In fact, the BCS sequence of the CBCS was selected among other reasons because its value of r is zero. However, the cross-correlation of the CBCS signal with a BOC(1,1) alone receiver is not zero any more and presents a so-called tracking bias. Indeed, this was the main drawback of the CBCS solution with respect to the finally selected MBOC. We show in the next figure the cross-correlation of the CBCS signal with BOC(1,1):

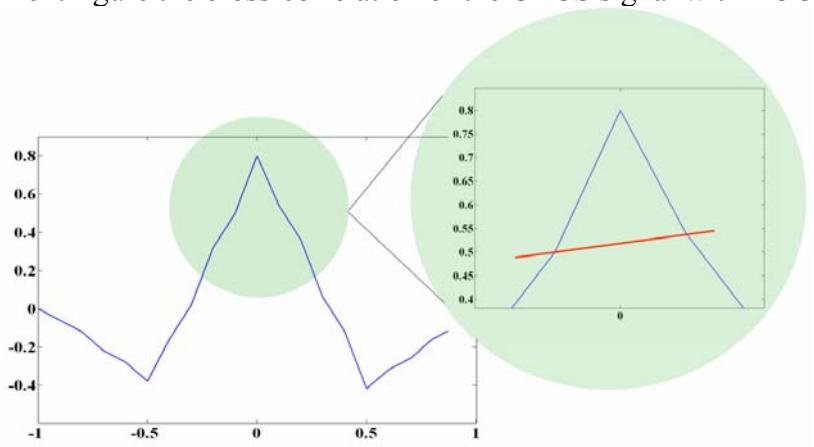

Figure 4.38. Cross-correlation between CBCS and a BOC(1,1) receiver

Indeed, this asymmetry leads to the mentioned tracking bias, as can be seen in the next figure:

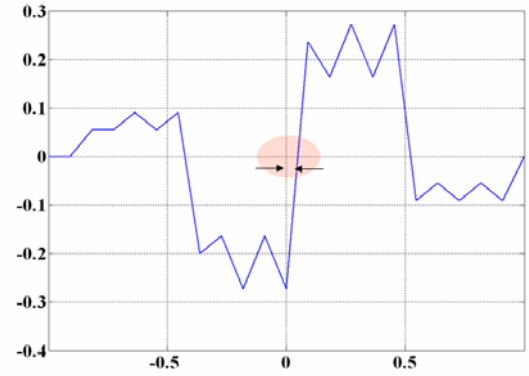

Figure 4.39. CBCS and local BOC(1,1) discriminator function

We will talk a little bit more on this bias at the end of this chapter. Nevertheless, it is important to mention here that although there are solutions to eliminate the tracking bias that results from the non-zero correlation between CBCS and BOC(1,1), the need to have a signal that would not present such a disadvantage was the main reason that lead to moving to the finally selected CBOC solution. CBOC is a particular implementation of MBOC where the Interplex multiplex is part of the definition as shown in chapter 4.6. Furthermore, CBOC can also be seen as a particular case of CBCS where the selected BCS is BOC(6,1). For more details on MBOC and its implementations, refer to chapter 4.7

A figure of great interest to analyze the impact of the CBCS modulation on a BOC(1,1) receiver is given by the cross-correlation that a receiver would suffer if it would only track the BOC(1,1) component of the CBCS signal.

As shown in [G.W. Hein et al., 2005], the delta correlation losses with respect to the baseline BOC(1,1) are the difference between the cross-correlation measured when the input is CBCS and the result of the auto-correlation when the input is a BOC(1,1) signal. Figure 4.40 below shows in detail the scheme assumed to measure the correlation losses.

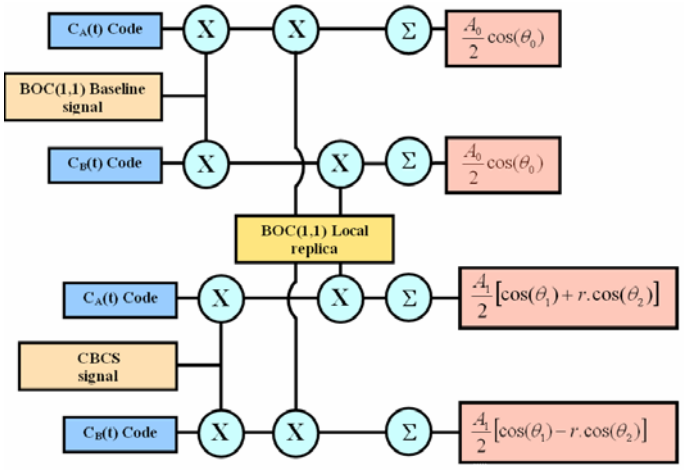

Figure 4.40. Model to measure the delta correlations between CBCS and BOC(1,1)

The driving idea behind this model is to measure the real delta correlation losses that a receiver would experience if instead of the baseline BOC(1,1), the CBCS were emitted. It must be noted that while CBCS will of course not correlate 100 % with a BOC(1,1) replica as BOC(1,1) would do, resulting thus in losses, the more efficient CBCS modulation that results from reducing the IM product allows for higher receiver powers at user level for the same transmitted power from the satellite. Both figures go in opposite directions and must be considered together. Indeed, as shown in [G.W. Hein et al., 2005], the delta correlation losses are shown to be:

$$\Delta L = \left[\frac{A_1}{A_0} \frac{\left(\cos\theta_1 + r\cos\theta_2\right)}{\cos\theta_0} \right]^2 = \left(\frac{A_1}{A_0} \right)^2 \left(\frac{\cos\theta_1}{\cos\theta_0} \right)^2 \left(1 + r\frac{\cos\theta_2}{\cos\theta_1} \right)^2 \tag{4.127}$$

When we express it in dB, the three contributions to the delta correlation losses can be clearly separated as follows:

$$\Delta L_{\text{Total}} = \Delta L_{\text{Envelope Power}} + \Delta L_{\text{BOC(1,1) Power Share}} + \Delta L_{\text{Mismatch Loss}} \tag{4.128}$$

where

$$\Delta L_{\text{Envelope Power}} = 20\log_{10}\left(\frac{A_1}{A_0} \right) \tag{4.129}$$

$$\Delta L_{\text{BOC(1,1) Power Share}} = 20\log_{10}\left(\frac{\cos\theta_1}{\cos\theta_0} \right) \tag{4.130}$$

$$\Delta L_{\text{Mismatch Loss}} = 20\log_{10}\left(1 + r\frac{\cos\theta_2}{\cos\theta_1} \right) \tag{4.131}$$

$\Delta L_{\text{Envelope Power}}$ accounts for the fact that the amplitude of the baseline interplex modulation and that of the optimized signal differ slightly. Additionally, the term $\Delta L_{\text{BOC(1,1) Power Share}}$ represents the losses of power of the BOC(1,1) signal since part of it goes now to the BCS component and finally the third term $\Delta L_{\text{Mismatch Loss}}$ of the correlation losses is a function of the correlation between the chosen BCS([s],1) and BOC(1,1) and gives an idea of how similar to BOC(1,1) the CBCS signal is. If we look at the correlation term more in detail,

$$\Delta L_{\text{Mismatch Loss}} = 1 + r\frac{\cos\theta_2}{\cos\theta_1} \tag{4.132}$$

we can see that this contribution to the correlation losses can be eliminated by two means. The first one is doing $\theta_2 = \pi/2$ what corresponds to the case of pure BOC(1,1). The other possibility and of much more interest is to have $r = 0$ what leads to a CBCS solution with zero mismatch correlation losses. For reasons of implementation due to symmetry, special attention was paid to the solutions with $r = 0$.

Now that we have shown the mathematical background behind the CBCS modulation, we are ready to introduce the signal that for some time was the most interesting candidate of Galileo to substitute BOC(1,1) until CBOC came: namely CBCS. CBOC is the European implementation of MBOC as will be shown in chapter 4.7.3.

4.6.2 CBCS([1,-1,1,-1,1,-1,1,-1,1,1], 1, 20 %)

After signing the Agreement of 2004 and as a result of long months of hard work, a BCS sequence was found to be an interesting candidate for the Galileo E1 OS signal. The selected BCS sequence was compatible to a very high degree with pure BOC(1,1) receivers [G.W. Hein et al., 2005] while it offered at the same time an important potential to improve the positioning performance and to mitigate multipath. Moreover, the selected signal was compliant with the Agreement of 2004 and did not require important changes in the satellite payload. The BCS sequence was [*s*] = [1, -1, 1, -1, 1, -1, 1, -1, 1, 1] and the amount of power on the BCS sequence with respect to the total OS power was selected to be 20 % at user level what would corresponds to approximately 26 % at generation in the satellite. For simplicity, the signal was thus baptized with the name CBCS([1, -1, 1, -1, 1, -1, 1, -1, 1, 1], 1, 20 %) or CBCS(20) for short. The selected BCS sequence can be seen as a *quasi* BOC(5,1). Indeed, in terms of performance it was very similar to a BOC(5,1) but had a more favourable spectral distribution since it did not overlap the M-Code as much as the last one.

As we have said above, the CBCS modulation had a minimum impact on the payload, what made the solution a serious alternative. In addition a number of advantages can be identified:

- Compared with the original Interplex using only BOC(1,1), the CBCS modulation is more efficient, reducing the IM product power by more than 3 dB.
- As a result, the optimized modulation offered an additional margin of 0.26 dB on the link budget, for the same transmitted power at satellite level.
- The modulation is fully compatible with a flexible signal generator implementation based on modulation tables with a high number of bits of quantization.
- Finally, in spite of having two additional phase points closer to each other, the CBCS modulation is less sensitive to payload phase noise than the original modulation.

The following figure shows in detail how the Galileo and GPS Signal Plan would have looked like if the CBCS signal had been selected instead of MBOC.

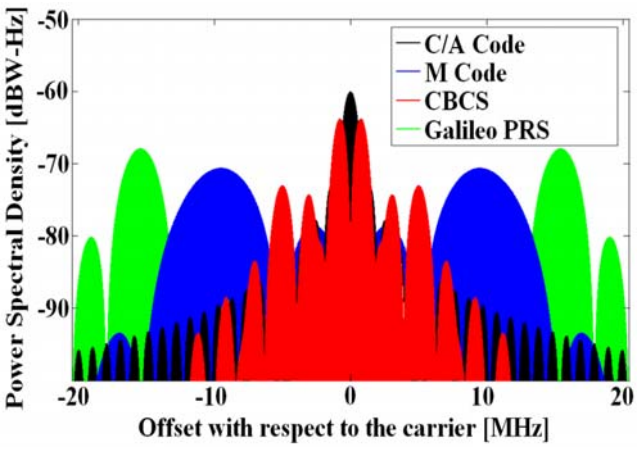

Figure 4.41. Power Spectral Density of Galileo and GPS signals in E1/L1

In the next figure we show in detail the power distribution of the spectra of the different components of the CBCS modulation:

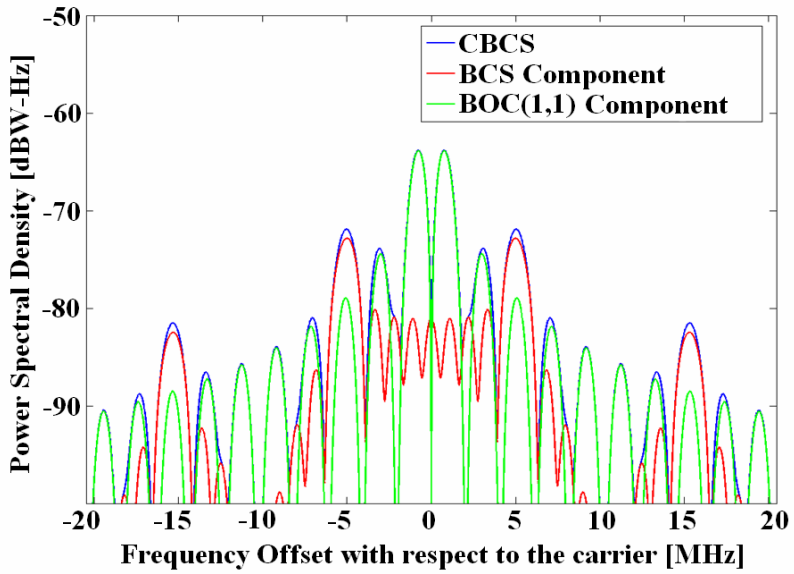

Figure 4.42. Power Spectral Distribution of BOC(1,1) and BCS within CBCS

An important number of constraints were introduced during the search of the best potential signal candidate for the Galileo E1 OS to substitute BOC(1,1). Finally among all the solutions that passed the selected criteria, the best candidate was chosen. One of the most important performance merit figures for the final selection was the multipath performance for a given bandwidth (12 MHz) since this was considered to be the most important source of error due to its unpredictable properties. Furthermore 12 MHz was thought to be a reasonable bandwidth for future receivers even in the field of mass market.

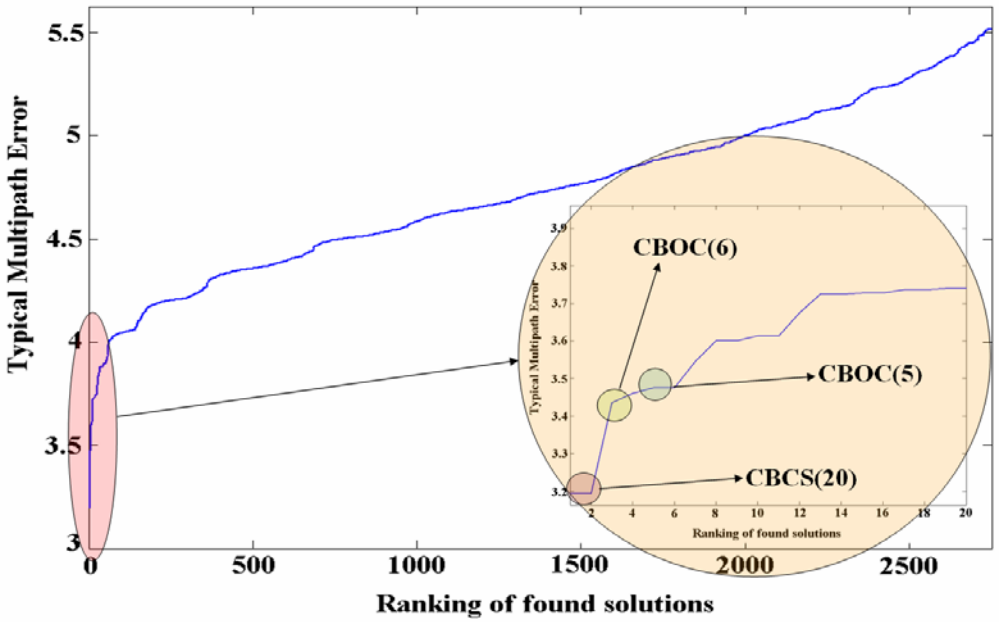

Figure 4.43. Ranking of CBCS solutions in terms of multipath mitigation potential

As we can recognize in the previous figure, CBCS(20) occupies the first place in the ranking, followed by CBOC(6) and CBOC(5). It is interesting to note that other solutions were also found at that time, with performance figures close to those of the CBCS signal. The figure above shows the ranking of the different solutions and the multipath performance of each of them. We can clearly recognize that CBOC(6) performed in second place for 12 MHz. This is indeed the signal finally selected as baseline for Galileo E1 OS and GPS L1C since it presents a better performance over a wider range of receiver bandwidths. We will come back on this point in the next chapter. We can also read from the previous figure that CBOC(5) was an interesting option, but its major drawback was that the coefficient *r*, as defined in (4.126), is not zero and thus the delta correlation losses of this solution would increase very rapidly as we would increase the power on the BOC(5,1) component. As a result, the percentage of the non-BOC(1,1) component was very limited, and consequently the growth potential in terms of multipath mitigation.

4.6.3 CBCS Power Spectral Density

Using the theory developed above for BCS signals and thoroughly explained in chapter 4.3 we will derive here a compact simplified expression for the CBCS signal. As we have seen, the selected BCS sequence was $\bar{s} = [+1,-1,+1,-1,+1,-1,+1,-1,+1,+1]$. Summing now in parallel the terms of the 10 diagonals of the matrix definition of BCS, we have:

$$G_{\text{Mod}}^{\text{BCS}([1,-1,1,-1,1,-1,1,-1,1,1],f_c)}(f) = 10 + 2\left[\begin{array}{l} -7\cos\left(\frac{2\pi f}{10 f_c}\right) + 6\cos\left(2\frac{2\pi f}{10 f_c}\right) - 5\cos\left(3\frac{2\pi f}{10 f_c}\right) + \\ +4\cos\left(4\frac{2\pi f}{10 f_c}\right) - 3\cos\left(5\frac{2\pi f}{10 f_c}\right) + 2\cos\left(6\frac{2\pi f}{10 f_c}\right) - \\ -\cos\left(7\frac{2\pi f}{10 f_c}\right) + \cos\left(9\frac{2\pi f}{10 f_c}\right) \end{array}\right] \quad (4.133)$$

For our particular CBCS case, we have thus:

$$G_{\text{CBCS}}(f) = (1-\rho)G_{\text{BOC}(1,1)} + \rho G_{\text{BCS}}(f) \quad (4.134)$$

being ρ the percentage of power on the BCS component, as we saw above. According to this, we can express the power spectral density of the CBCS([*s*],1,%) modulation as follows:

$$\begin{aligned} &G_{\text{CBCS}}(f) = (1-\rho)G_{\text{BOC}(1,1)} + \rho G_{\text{BCS}}(f) = \\ &= (1-\rho)G_{\text{BPSK}(1)}\, G_{\text{Mod}([+1,-1])} + \rho G_{\text{BPSK}(10)}(f) G_{\text{Mod}([+1,-1,+1,-1,+1,-1,+1,-1,+1,+1])}(f) \end{aligned} \quad (4.135)$$

As derived in Appendix B the power spectral density of BOC(1,1) is shown to be:

$$G_{\mathrm{BOC}_{\sin}(1,1)} = f_c \left[\frac{\sin\left(\frac{\pi f}{f_c}\right)\sin\left(\frac{\pi f}{2f_s}\right)}{\pi f \cos\left(\frac{\pi f}{2f_s}\right)} \right]^2 \Bigg|_{f_c = f_s = 1.023\,MHz} \tag{4.136}$$

Nevertheless, since we are interested in finding a simplified expression for the CBCS Power Spectral Density, it is convenient to express BOC(1,1) as a BCS sequence with a vector of length 10. Indeed, BOC(1,1) can also be expressed as BCS([+1,+1,+1,+1,+1,-1,-1,-1,-1,-1],1).

Another way of describing CBCS in the frequency domain is to realize that the BCS signal can be expressed as the sum of a BOC(5,1) signal and an MCS(0,0,0,0,0,0,0,0,0,2) signal in the time domain. Thus, we have to calculate first the Fourier Transform of both, sum them up and calculate the modulus according to equation (4.8):

As we know, the spectrum of BOC(5,1) is shown to be:

$$S_{\mathrm{BOC}_{\sin}(5,1)}(f) = j \frac{\sin\left(\frac{\pi f}{f_c}\right)\sin\left(\frac{\pi f}{10 f_c}\right)}{\pi f \cos\left(\frac{\pi f}{10 f_c}\right)} \Bigg|_{f_c = 1.023\,MHz} \tag{4.137}$$

Equally, the spectrum of a pulse signal of duration (T_c/10) with the pulse centred on the last subchip can be expressed as follows:

$$S_{\mathrm{Pulse}}(f) = 2 \frac{\sin\left(\frac{\pi f}{10 f_c}\right)}{\pi f} \left[\cos\left(9 \frac{\pi f}{10 f_c}\right) - j \sin\left(9 \frac{\pi f}{10 f_c}\right) \right] \Bigg|_{f_c = 1.023\,MHz} \tag{4.138}$$

Hence the PSDs for the data and pilot signals yields:

$$G_D(f) = f_c \left[\sqrt{1-\rho}\, S_{\mathrm{BOC}(1,1)}(f) + \sqrt{\rho} \left\{ S_{\mathrm{BOC}(5,1)}(f) + S_{pulse}(f) \right\} \right]^2 \tag{4.139}$$

$$G_P(f) = f_c \left[\sqrt{1-\rho}\, S_{\mathrm{BOC}(1,1)}(f) - \sqrt{\rho} \left\{ S_{\mathrm{BOC}(5,1)}(f) + S_{pulse}(f) \right\} \right]^2 \tag{4.140}$$

4.6.4 CBCS Positioning Performance

One of the performance figures used to select the CBCS signal was the multipath error. In order to realistically estimate the multipath that the candidate signals could present in real environments, the methodology presented in [G.W. Hein and J.-A. Avila-Rodriguez, 2005] and [M. Irsigler et al., 2005] was followed. Furthermore, in order to reduce the computations and given the enormous number of potential signals to assess, a simplified model was employed. Nevertheless, [M. Irsigler et al., 2005] and [M. Irsigler, 2008] have shown that more simplified models also give satisfactory results in the same direction at the expense of generalizing the assumptions and simplifying scenarios.

Another important aspect to note with regards to the CBCS modulation is that the data and pilot channels are in anti-phase and present thus different correlation functions as shown in Appendix J. The direct consequence of that is that the data and pilot channels present different performance depending on whether the signal has the BOC(1,1) and BCS in phase or in anti-phase. As we will show in the next pages, the anti-phase signal has got the sharpest ACF and thus better performance. For this reason, this was assigned to the pilot channel.

In the following lines we show the performance of CBCS in terms of multipath using the multipath error envelopes. As we know, its computation relies on the assumptions that the line of sight is always visible, that only one multipath signal is present and that the multipath signal experiences a fixed amplitude attenuation (e.g. coefficient of reflection $\alpha = 0.5$ in our simulations) with respect to the direct signal. In addition, a static environment is commonly assumed.

More sophisticate models to quantify the differences between the multipath performance of different signals for a given receiver architecture or different receiver implementations have been analyzed in [M. Irsigler, 2008].

In the next figures we compare the performance of the CBCS(20) signal with that of other solutions that were also considered in the past. As we can see, the same CBCS with a slight lower power was also object of the analysis. The reason to reduce the power on the BCS component to 15.6 % was to improve the coexistence of the signal with the rest of signals in the E1/L1 band. Of course, this reduction of power on the BCS part implied a slight deterioration of the performance. Note also that the A and B channels perform the same and thus the dotted and continues curves overlap each other.

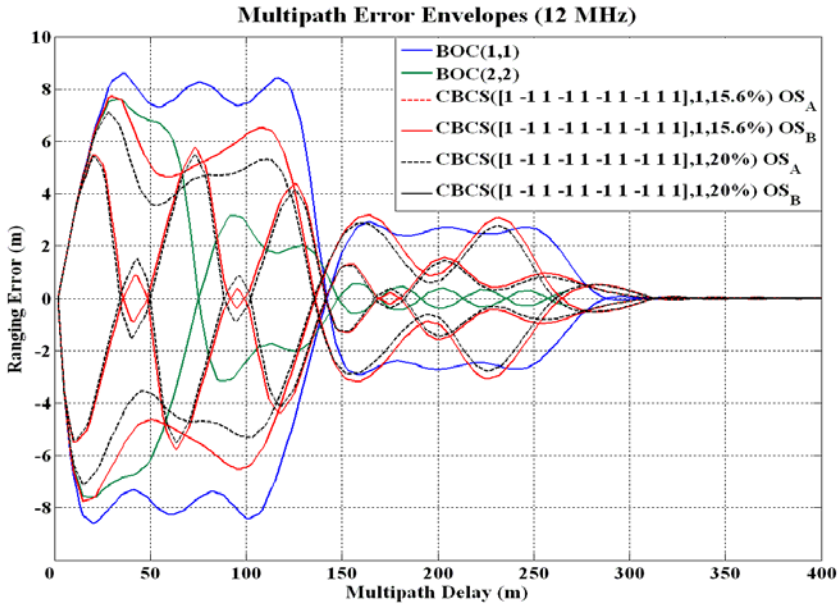

Figure 4.44. Multipath error envelopes for different Galileo signal candidates. A pre-correlation bandwidth of 12 MHz and a chip spacing of δ= 0.1 chips have been assumed

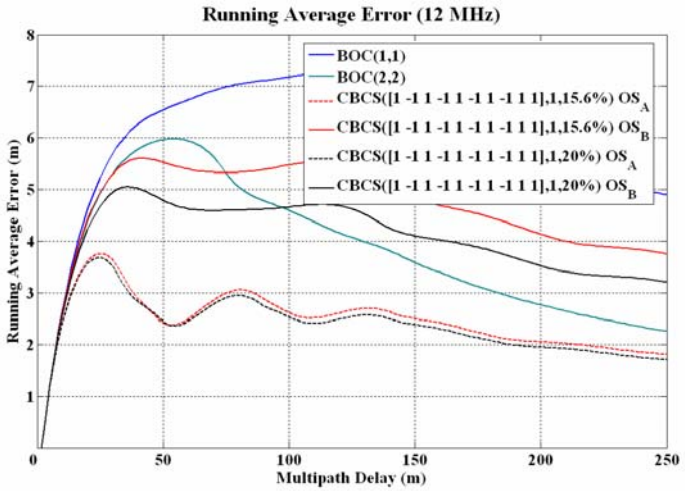

Figure 4.45. Running average multipath errors for different Galileo signal candidates. A pre-correlation bandwidth of 12 MHz and a chip spacing of δ= 0.1 chips were assumed

As analyses have shown, CBCS presented a considerable improvement of more than 25 % with respect to the baseline for a bandwidth of 24 MHz. Furthermore, the improvement was of even 40 % in terms of multipath with 12 MHz as previous figure shows. This was especially relevant in urban and suburban environments. Moreover, for 12 MHz CBCS performed even better than BOC(2,2). This is a direct consequence of the fact that while BOC(1,1) needs a larger bandwidth of 24 MHz to exploit to the limit the possibilities of the modulation, the CBCS modulation needs a lower bandwidth to make an optimum use of the signal in the sense that its Gabor bandwidth for the same receiver bandwidth is higher. A complete analysis of positioning accuracy using the concept of the User Equivalent Range Error (UERE) was presented by [J.-A. Avila-Rodriguez et al., 2005b] where the superiority of CBCS in different baseline scenarios was demonstrated.

Finally, to have a complete insight into the performance of CBCS, the Cramér Rao Lower Bound (CRLB) is shown in the following figure.

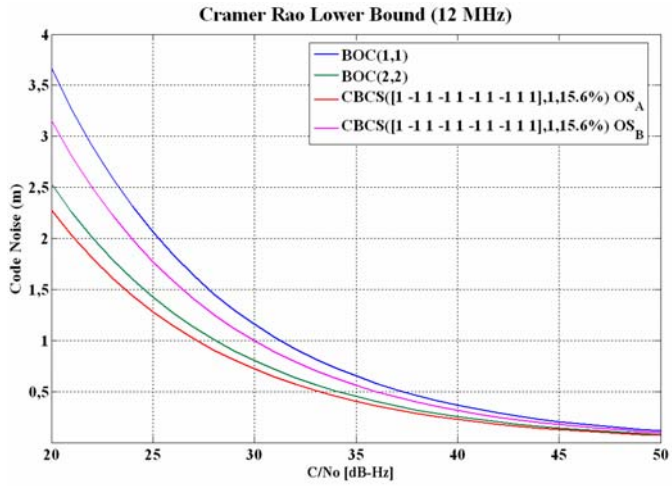

Figure 4.46. Cramér Rao Lower Bound of E1 OS signals. It must be noted that OS_A refers to the data channel while OS_B refers to the pilot channel

The Cramér Rao Lower Bound is defined in (4.141) and is the lower bound of the mean-squared error for any estimate of a non-random parameter as shown by [H. Cramér, 1946] and [J.-A. Avila-Rodriguez et al., 2006b]. The Cramér-Rao lower bound defines the ultimate accuracy of any estimation and shows the minimum code pseudorange variance we would have with the best possible receiver implementation. Indeed, this bound is a different way of expressing the Gabor bandwidth which sets the physical limit of a signal for a given bandwidth. This last one is also known in the literature as the Root Mean Square (RMS) bandwidth. As shown in Appendix K, the Cramér Rao Lower Bound is defined as:

$$\mathrm{CRLB} = -\frac{B_L}{\frac{C}{N_0} R''_{ss}(0)} = \frac{B_L}{\frac{C}{N_0}(2\pi)^2 \int_{-\infty}^{\infty} f^2 \, G_s(f)\mathrm{d}f} \tag{4.141}$$

where B_L refers to the loop bandwidth of the code tracking loop and $R''_{ss}(0)$ and $G_s(f)$ are respectively the autocorrelation and power spectral density of the signal.

The Cramér-Rao lower bound is usually employed to assess the performance of the position estimation based on the delay between the transmitting satellite and the receiver. However, since the function that maps the signal delay to the physical location is not necessarily continuous and differentiable everywhere due to the usual oscillations and discontinuities of the received signal, the Cramér Rao lower bound cannot be applied in all cases. In fact, differentiability is a requirement for the Cramér Rao lower bound to be properly used. As shown in [H. Koorapaty, 2004], it may be feasible to create a continuous approximation of this mapping function although this is discontinuous in reality. However, in order to be accurate, the function would need to have large local variations and the Cramér-Rao bound would then be too inaccurate. In the same manner, if a smooth function without large variations were assumed, the bound would also be inaccurate. In particular, such an approach would be too pessimistic in its performance estimates.

As an alternative, the Barankin bound was proposed in [E. Barankin, 1949]. As shown in [H. Koorapaty, 2004], the Barankin bound does not require the mapping function to be continuous and differentiable being hence better suited for some problems. The Barankin bound is computed by selecting a set of test points $[x_1, x_2, ..., x_N]$ in the area of analysis and defining the following function:

$$\mathrm{L}(r, x_i, x) = \frac{P(r|x_i)}{P(r|x)} \tag{4.142}$$

where $P(r|x)$ denotes the conditional probability density function at the set of chosen test points with $i \in \{1,2,...,N\}$. According to this, the Barankin matrix is defined as follows:

$$B_{i,j}(x) = \int L(r, x_i, x) L(r, x_j, x) \, P(r|x)\mathrm{d}r = E\left\{ \int L(r, x_i, x) L(r, x_j, x) \right\} \tag{4.143}$$

with $(i, j) \in \{1,2,...,N\} \times \{1,2,...,N\}$. Furthermore, the Barankin bound on the covariance $\mathrm{Cov}[\hat{x}(r)]$ for the parameter *x* based on the measurements *r* is given by:

$$\mathrm{Cov}\left[\hat{x}(r)\right] \geq \Lambda B^{-1}(x)\Lambda^{T} \tag{4.144}$$

where

$$\Lambda = \left[\{x_1 - x\}, \{x_2 - x\}, ..., \{x_N - x\}\right]^{T} \tag{4.145}$$

As we can recognize, the computation of the Barankin bound only requires knowledge of the conditional probability density function $P(r|x)$ at the set of chosen test points and no assumption on the differentiability is required. Moreover, it is important to note that the Barankin bound is a lower bound on the covariance matrix of the position errors but it does not say anything about the probability density function of the position errors.

Finally, we must underline that the Barankin bound is more accurate than the Cramér Rao lower bound as shown in [R. McAulay and E. Hofstetter, 1971]. In fact, the Barankin bound can be made tighter than the Cramér-Rao bound provided the correct test points are chosen. Moreover, the Barankin bound can be applied in general to more cases than the Cramér Rao bound under the assumption that we have some a priori knowledge on the conditional probability of some particular points. As one can imagine, this information is not always available and justifies the common use of the Cramér Rao lower bound instead.

4.6.5 CBCS Interference Performance

Another important aspect in the performance of a signal is the interference that the signal suffers and causes from and to the rest of signals in the band. The Spectral Separation Coefficient (SSC), to which we will dedicate the next two chapters, is the key figure to assess the isolation among signals and gives us thus a good insight into this problem. In the next tables different SSCs are given for the case that no filter is used at the satellite. However, it must be noted that in case of filtering the spectral isolation would even improve. For the calculations a transmission bandwidth of 40.92 MHz and a receiver bandwidth of 24.00 MHz were assumed.

Table 4.1. Spectral Separation Coefficients of proposed Open Signals on E1/L1. For the CBCS signal an optimized filter was employed to avoid the third harmonic emissions

SSC [dB-Hz]	C/A Code	BOC(1,1)	CBCS(20%)
C/A Code	-61.8008	-67.7844	-68.1428
BOC(1,1)	-67.7844	-64.7373	-
CBCS(20%)	-68.1428	-	-65.6087

As we will see in detail in chapter 5, the self SSC (SSC of one signal with itself) tells us how the intra-system interference is. From the table above we can also recognize that CBCS has better spectral isolation with itself than BOC(1,1) given its wider spreading. Moreover, the CBCS modulation has better spectral isolation with the GPS C/A Code than BOC(1,1) which is logical since part of the power has been moved to higher frequencies. As a conclusion,

CBCS presented an improvement in the SSC values that lead to an increase of the minimum C/N_0 value (in both Galileo OS and GPS L1C) of up to 0.6 dB, resulting thus in an overall superior link budget.

The interference that we have analyzed so far refers to interference from other GNSS sources. Now we concentrate on the case of non-intentional interference coming from other potential sources. We distinguish between narrowband interference and wideband interference.

- Narrowband interference: The susceptibility to narrow band interference depends on the continuous PSD and on the code structure. Since this latter is not modified by CBCS, and because the continuous PSD of CBCS was wider than that of BOC(1,1), the optimized CBCS presented a higher robustness to narrowband interference.
- Wideband interference: The susceptibility to wide band interference is closely linked to the spreading of the PSD: the more the PSD is spread, the higher the robustness will be. Because CBCS features a PSD which is more spread than that of the BOC(1,1) signal, the CBCS was consequently present a higher robustness than BOC(1,1).

For more details on the mathematical model behind, refer to Appendix J. As we will see, also here CBCS was superior to BOC(1,1).

One final aspect to analyze the performance of a signal is the acquisition. A very straightforward strategy to acquire CBCS was presented in [G.W. Hein et al., 2005], proving that false acquisition should not represent a big problem. In fact, the only degradation observable with respect to BOC(1,1) would be of less than 1 dB, coming from the correlation losses due to processing with a pure BOC(1,1) receiver.

4.6.6 Receiver Options for CBCS

As presented in [G.W. Hein et al., 2005] and [A.R. Pratt et al., 2006] there are several options to receive the CBCS signals. As we will see, some solutions are more efficient while others aim at reducing the receiver complexity as much as possible. We enumerate them next:

- The most straightforward approach is to use a CBCS replica at receiver level for both the data and the pilot channels. As usual, the pilot signal can be used to support data demodulation of the other signal and help in scenarios with poor C/N_0 ratios.
- A simplified model would be to use a BOC(1,1) replica only. Indeed, as we have repeatedly commented in different parts of this thesis, special care was put during the optimization of the E1 OS signals to achieve a modulation that should be as highly interoperable as possible with BOC(1,1). This option results in a slight loss of signal power (-0.97 dB) but the receiver is then enormously simplified.

- Another imaginable configuration would be to only process the BCS channel extracting thus the difference data message as we will describe in chapter 7. However, the BCS signal was not optimized for this application, more due to the high data rate than to the low amount of power that was put on the BCS modulation, which was about -6.97 dB lower. Nevertheless, there could be other interesting benefits in terms of improved performance to multipath given the wider bandwidth BCS.
- Another possibility would be to form composite codes from the sum and the difference of the data and pilot codes. By doing so, we could dispread the BOC(1,1) and BCS channels with the BOC(1,1) and BCS signal waveforms correspondingly. This option could also support data-aiding as identified in [A.R. Pratt and J.I.R. Owen, 2005] but it would not be absolutely necessary.

4.6.7 Drawbacks of the CBCS solution

After describing all the positive aspects of the CBCS modulation, it is time to describe now the two main drawbacks of CBCS with respect to other solutions that were not selected at that time. These are basically the cross-correlation bias and the need of filtering to achieve spectral compatibility with the rest of signals in the band. We concentrate on them now:

4.6.7.1 CBCS Cross-Correlation Bias

The selected CBCS solution presented a non-symmetric correlation function when a BOC(1,1) receiver correlates with the incoming CBCS signal as we saw in Figures 4.38 and 4.39. As a result, a constant bias appears that is a function only of the percentage of power put on the BCS signal with respect to the OS signal, the received power of the desired signal and the receiver bandwidth. In principle this bias could be corrected if manufacturers would calibrate it as another bias in the receiver processing. Additionally, this bias could be avoided with an appropriate correlation at the receiver [A.R. Pratt et al., 2006] and future receivers could consider it as a variable that could be updated at any moment in case future changes in the signal structure would occur. Nevertheless if due to imperfections not all the satellites would be similar, this would introduce a non-negligible complexity that handicapped CBCS.

Different solutions were proposed to avoid the tracking bias, being one of the more interesting the so-called flipping CBCS or CBCS*. This consisted of a BOC(1,1) plus a BCS sequence that alternates its sign from chip to chip. The CBCS* signal would adopt the following form:

$$s(t) = A_1 \left[\begin{array}{l} \frac{c_D(t)}{2}\left[\cos\theta_1 s_{\mathrm{BOC}(1,1)}(t) + (-1)^m \cos\theta_2\, s_{\mathrm{BCS}([\bar{s}],1)}(t)\right] + \\ + \frac{c_P(t)}{2}\left[\cos\theta_1 s_{\mathrm{BOC}(1,1)}(t) - (-1)^m \cos\theta_2\, s_{\mathrm{BCS}([\bar{s}],1)}(t)\right] + \\ + j\, s_{\mathrm{PRS}}(t)\left(\frac{\sin\theta_1 + \sin\theta_2}{2}\right) + s_{\mathrm{IM}}(t) \end{array} \right] \quad (4.146)$$

$$s_{IM}(t) = -j\, c_D(t)\, c_P(t)\, s_{PRS}(t)\left(\frac{\sin\theta_1 - \sin\theta_2}{2}\right) \tag{4.147}$$

where we can recognize that compared to (4.121) the alternating term $(-1)^m$ was introduced to account for the alternation of the BCS sequence from one chip to the other chip. As a result, the cross-correlation between CBCS* and BOC(1,1) would be in average zero as desired. The disadvantage of this approach would be on the other hand that the real length of the BCS would duplicate to all effects due to the phase-alternation.

4.6.7.2 CBCS Satellite Transmission Filter

A second and actually the major drawback of the CBCS solution was the need to introduce a filter in the satellite to get sufficient isolation of the third harmonic of the BCS signal with the Galileo PRS signal. As we mentioned above, the selected BCS sequence is qualitatively very similar to a BOC(5,1) which, as we know from theory, has got harmonics at odd multiples of the sub-carrier frequency of 5 MHz. Thus, the third harmonic would fall directly on the PRS at 15 MHz. As suggested in [G.W. Hein et al., 2005] different measures might have been implemented in the satellite payload without inducing a loss of power at user level. A careful selection of the technique guarantees that the main power stays more or less around 5 MHz offset from the centre frequency so that the resulting waveform does not show any significant impact in the multipath error considerations and subsequent performance of the final signal. Whilst this is true, it is also true that from the moment a filter would have been introduced, the multipath mitigation performance would have been limited saturating for wider bandwidths what was a very undesirable property. Similar arguments have also been used against SRRC signals as we will show at the end of this chapter. This can be shown by means of the Root Mean Square bandwidth in the next figure. For completeness also MBOC is depicted. This modulation (baseline of the Galileo Open Service and GPS Civil signals in E1/L1) will be described in detail in the next chapter.

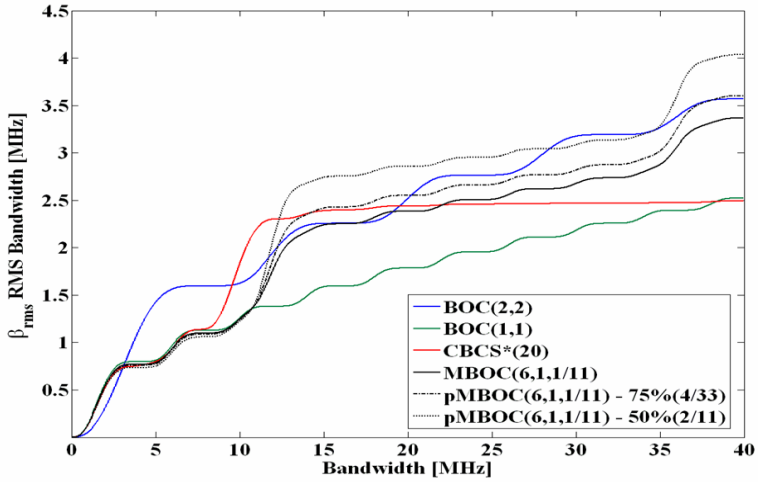

Figure 4.47. Root Mean Square Bandwidth (RMS) of studied OS candidate signals. pMBOC refers to the pilot signal and the percentage to the amount of pilot power

As we know, the Root Mean Square (RMS) bandwidth of a spreading symbol is defined by:

$$BW_{\mathrm{RMS}}(\beta_r) = \sqrt{\int_{-\frac{\beta_r}{2}}^{\frac{\beta_r}{2}} f^2 \, \overline{G}(f) \mathrm{d}f} \tag{4.148}$$

where $\overline{G}(f)$ is normalized for unit power over the signal bandwidth being used, and β_r is the double-sided receiver pre-correlation bandwidth. The RMS bandwidth can also be seen as another way of interpreting the Cramér Rao lower bound or as the Gabor bandwidth of a signal. According to this, the higher the RMS bandwidth, the better the signal will be.

If we observe now the results of Figure 4.47 above, we can clearly see that unlike CBCS*, the potential RMS bandwidth of MBOC does not saturate for higher bandwidths. CBCS* is the phase alternating version of CBCS that we describe in the following lines. Furthermore, not only is MBOC by far better than BOC(1,1), but it presents also a performance comparable to that of BOC(2,2) and even superior for some implementations. It is interesting to note that for bandwidths higher than about 14 MHz the RMS bandwidth of CBCS* does not grow any more due to the necessary filtering, while that of MBOC does.

As a conclusion, the CBCS signal candidate presented in [G.W. Hein et al., 2005] clearly outperformed the baseline BOC(1,1) but presented some inherent limitations that rose some doubts. Especially the two drawbacks explained above were reason of concern since they demanded modification from the receiver manufacturers to get rid of these potential biases. The solution to all those problems would not take much time to come: the name was MBOC and this time, not only Galileo was eager to adopt it, but also GPS for its modernized GPS.

4.7 MBOC modulation definition and analysis

Nearly twenty months after the EU and the US signed the *Agreement on the Promotion, Provision and use of Galileo and GPS Satellite-Based Navigation Systems and Related Applications* an optimized signal waveform named MBOC (Multiplexed Binary Offset Carrier modulation) was proposed by a common group of experts of the EU and US for GPS L1C and Galileo E1 OS [G.W. Hein et al., 2006a], [G.W. Hein et al., 2006b] and [J.-A. Avila-Rodriguez et al., 2006d].

Except for the fact that the CBCS definition requires Interplex to multiplex all the signals, the MBOC modulation can be seen a particular case of the CBCS solution where the BCS sequence adopts the known sine-phased BOC-like form. In this sense, MBOC(6,1,1/11) could also be expressed as CBCS([1,-1,1,-1,1,-1,1,-1,1,-1,1,-1],1,1/11) if the requirement on the Interplex Multiplexing were abandoned. The main objective of the common GPS and Galileo signal design activity was that the PSD of the proposed solution would be identical for GPS

L1C and Galileo E1 OS when the pilot and data components are computed together. This assures a high interoperability between both signals. This normalized (unit power) power spectral density, specified without the effect of bandlimiting filters and payload imperfections, is given by

$$G_{\mathrm{MBOC}(6,1,1/11)}(f)=\frac{10}{11}G_{\mathrm{BOC}(1,1)}(f)+\frac{1}{11}G_{\mathrm{BOC}(6,1)}(f) \tag{4.149}$$

where the high BOC frequency component, that is BOC(6,1), is shown to be:

$$G_{\mathrm{BOC}_{\sin}(6,1)}=f_c\frac{\sin^2\left(\frac{\pi f}{f_c}\right)}{(\pi f)^2}\tan^2\left(\frac{\pi f}{12f_c}\right)=f_c\left[\frac{\sin\left(\frac{\pi f}{f_c}\right)\sin\left(\frac{\pi f}{12f_c}\right)}{\pi f\cos\left(\frac{\pi f}{12f_c}\right)}\right]^2 \tag{4.150}$$

with f_c=1.023 MHz. Equally, the low BOC frequency component, namely BOC(1,1) will be:

$$G_{\mathrm{BOC}_{\sin}(1,1)}=f_c\frac{\sin^2\left(\frac{\pi f}{f_c}\right)}{(\pi f)^2}\tan^2\left(\frac{\pi f}{2f_c}\right)=f_c\left[\frac{\sin\left(\frac{\pi f}{f_c}\right)\sin\left(\frac{\pi f}{2f_c}\right)}{\pi f\cos\left(\frac{\pi f}{2f_c}\right)}\right]^2 \tag{4.151}$$

and thus:

$$\begin{aligned}
&G_{\mathrm{MBOC}(6,1,1/11)}(f)=\frac{10}{11}G_{\mathrm{BOC}(1,1)}(f)+\frac{1}{11}G_{\mathrm{BOC}(6,1)}(f)= \\
&=\frac{10}{11}f_c\left[\frac{\sin\left(\frac{\pi f}{f_c}\right)\sin\left(\frac{\pi f}{2f_c}\right)}{\pi f\cos\left(\frac{\pi f}{2f_c}\right)}\right]^2+\frac{1}{11}f_c\left[\frac{\sin\left(\frac{\pi f}{f_c}\right)\sin\left(\frac{\pi f}{12f_c}\right)}{\pi f\cos\left(\frac{\pi f}{12f_c}\right)}\right]^2= \\
&=\frac{f_c}{11\pi^2f^2}\sin^2\left(\frac{\pi f}{f_c}\right)\left[10\tan^2\left(\frac{\pi f}{2f_c}\right)+\tan^2\left(\frac{\pi f}{12f_c}\right)\right]
\end{aligned} \tag{4.152}$$

Additional conclusions can be drawn from analyzing the spectral shape of MBOC. Indeed, as shown in [J.-A. Avila-Rodriguez et al., 2006b], an interesting interpretation of (4.141) and (4.148) is that an ideal power spectral density regarding the tracking performance should be inversely proportional to the square of the frequency, according to:

$$G(f)\propto\frac{1}{f^2} \tag{4.153}$$

It must be noted that such a spectrum would have nevertheless other non desirable properties with regards to its implementation. However, if we look now at the envelope of the well known power spectral densities of BPSK(1) and BOC(1,1) we can clearly recognize that their envelopes interestingly decay with $1/f^2$, as Figure 4.48 shows next. Moreover, MBOC seems to follow pretty well this desirable pattern too. In fact, this was one of the figures in the mind of all those people involved in the optimization of the Galileo OS in E1.

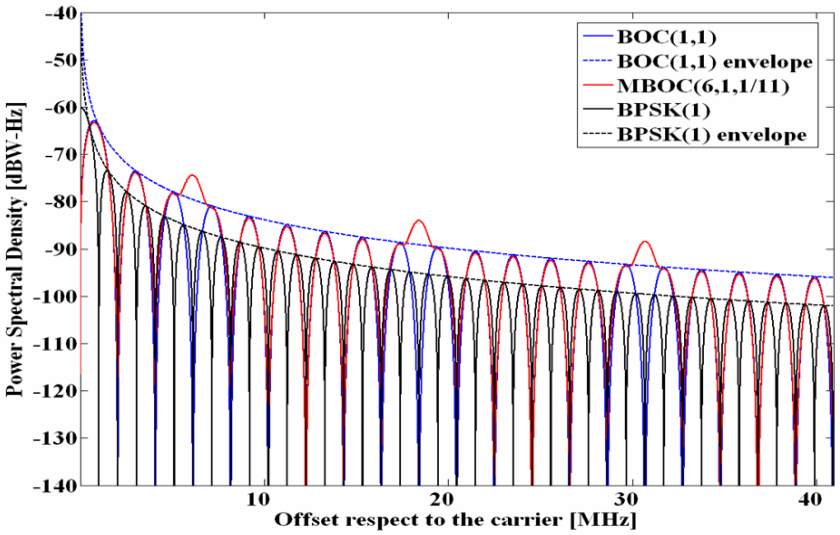

Figure 4.48. Decay of the envelopes of the power spectral densities of BOC(1,1) – in blue – and BPSK(1) – in black. As it can be clearly seen, the selected MBOC signal for GPS L1C and Galileo E1 OS – in red – follows a similar pattern

We show in the next figure all the Galileo and GPS signals in the E1/L1-band.

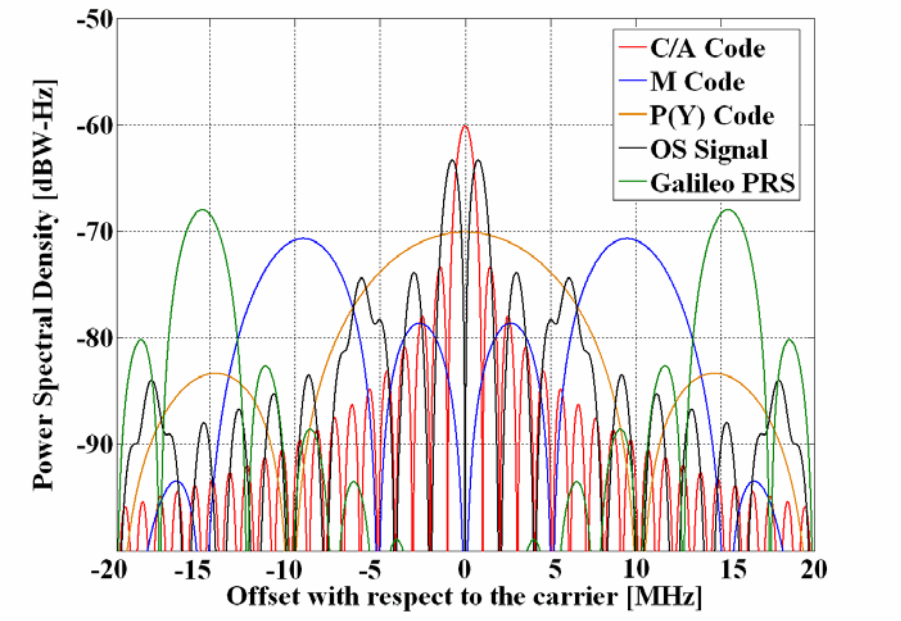

Figure 4.49. GPS and Galileo Spectra in E1/L1

4.7.1 Implementing MBOC

Once we have defined the power spectral density of MBOC, it is the right moment to talk about the implementation. Indeed, different time representations result in the same power spectral density and the Agreement between the EU and the US on MBOC left this freedom to both parties so that each could implement its own solution according to its own conception. Two solutions have been realized to implement MBOC:

- CBOC: The Composite BOC is the solution adopted by Galileo for the Open Service in E1/L1. It is an Interplex multiplexing where the sub-carriers BOC(1,1) and BOC(6,1) are added in anti-phase on each channel.
- TMBOC: The Time-Multiplexed BOC is the solution adopted by GPS for L1C. It is a binary signal where BOC(1,1) and BOC(6,1) are time-multiplexed according to a pre-established pattern that was optimized to improve the correlation properties of the signal when the effect of the PRN code is taken into account.

We describe the two possible implementations in detail in the next chapters. Before that, it is interesting to mention that between CBCS and the final MBOC(6,1) there was an intermediate solution that was object of interest for a short period of time. This was the so called MBOC(4,1) that was shortly described in chapter 3.6.4.

One final but important comment is related to the power allocated on the high frequency component of MBOC, namely BOC(6,1). Indeed, the 1/11 of power refers to the power at generation, without accounting for the effect of the satellite's filter and other imperfections. This is so because as we know, MBOC admits different implementations, being one of them TMBOC. If we would define the exact power split at user level, the power at generation would be different depending on the final implementation. As we have seen, TMBOC accomplishes the required power percentage by time-multiplexing BOC(6,1) and BOC(1,1) so that 1/11 of the time the satellite transmits BOC(6,1) and the rest of the time BOC(1,1). Since the GPS L1C codes have a length of 10,230 chips as we saw in chapter 2.3.2.1, this percentage incorporates the factorial decomposition of 10,230. It is trivial to show that $10{,}230 = 2 \text{ x } 3 \text{ x } 5 \text{ x } 11 \text{ x } 31$ and indeed 11 was found to be the optimum number to divide the transmission periods of the multiplexing signals of GPS L1C. Indeed, 1/11 of the time was long enough to considerably improve the performance with respect to BOC(1,1) but not so long to concentrate too much power on the high frequencies and overlap the M-Code and PRS to non acceptable levels. More details on the exact location of the BOC(6,1) chips are given in chapter 4.7.4 of this chapter.

Finally, it is important to mention that in the case of CBOC, the generation of power presents no limitations since this is achieved by correspondingly modulating the amplitude as described in (4.121).

4.7.2 On MBOC and Antisymmetric sequences

Before we describe the performance of MBOC regarding the characteristics and details of its different implementations, let us first make some final comments on the MBOC spectrum and the ideas behind.

As we have seen some lines above, the Galileo MBOC implementation (CBOC) is the result of an additive and subtractive mixture of two separate spreading symbols. Moreover, we have

already noted that some BCS sequences can potentially cause tracking bias in receivers adapted to receive only one of the spreading symbols. This was indeed one of the main disadvantages of CBCS. The solution to this problem was given by MBOC and the key concept is antisymmetric sequences. These sequences are explained in detail in Appendix K but in the next lines we anticipate some concepts already. Since BOC(1,1) is antisymmetric, receiver biases can be avoided by choosing the correct properties for the partner spreading symbol sequence.

As we have repeatedly mentioned in this chapter, compatibility with BOC(1,1) receivers was a major driver in the design of the optimized Galileo signal. As a result of this, having BOC(1,1) a partner spreading symbol sequence with zero cross-correlation became one of the most important drivers in the design of the Galileo OS in E1.

After CBCS was proposed, a new BCS solution that could avoid all the drawbacks described in chapter 4.6.7 was the objective of the works of US and EU. We can summarize the properties that this desired BCS sequence should present:

- Anti-symmetry
- Balance (zero-sum) for the sequence
- Zero crosscorrelation with the partner sequence

As shown in [A.R. Pratt et al., 2006] a comprehensive search for binary sequences was conducted with some or all of these properties. These are listed below for a variety of sequence lengths n, all divisible by 2, from 2 to 12. Moreover, we show only distinct sequences so that the tables contain $\{x_i\}$ but not the time reversed versions $\{-x_i\}$, $\{x_{n-1-i}\}$ or $\{-x_{n-1-i}\}$. Since the sequences are antisymmetric, they may be considered to be constructed from a base sequence $\{\hat{y}_i\}$ of length n as shown in the following equation:

$$X = \{x_i\} = \{\hat{y}_i, -\hat{y}_{n-1-i}\} \tag{4.154}$$

As shown in Appendix K, all antisymmetric sequences of even length n are balanced. The next tables show the cross-correlation with a BOC(1,1) partner sequence, under the assumption that the spreading symbol durations are common, that is the duration of an $n = 2$ sequence is identical with that of an $n = 12$ sequence, for example.

Moreover, the cross-correlation between $x_0 = \mathrm{BOC}(1,1)$ and the corresponding BCS sequence x_k is shown to be:

$$\Sigma(z_k) = \sum_{i=0}^{n-1} z_{k,i} = \sum_{i=0}^{n-1} x_{0,i}\, x_{k,i} = n\, R^{c}_{x_0,x_k}(0) = n \bmod 4 \tag{4.155}$$

where $n \bmod m$ represents the modulo operation defined as the remainder of the division of n by m. Next pages summarizes the results:

Table 4.2. Tables of Distinct Spreading Symbol Sequences for *n*=2 to 12

$n=2$		$R^c_{x_0,x_k}(0)$
x_0	1,-1	1.0

$n=4$		$R^c_{x_0,x_k}(0)$
x_0	1,1,-1,-1	1.0
x_1	1,-1,1,-1	0.0

$n=6$		$R^c_{x_0,x_k}(0)$
x_0	1,1,1,-1,-1,-1	1.0
x_1	1,1,-1,1,-1,-1	1/3
x_2	1,-1,1,-1,1,-1	1/3

$n=8$		$R^c_{x_0,x_k}(0)$
x_0	1,1,1,1,-1,-1,-1,-1	1.0
x_1	1,1,1,-1,1,-1,-1,-1	0.5
x_2	1,1,-1,1,-1,1,-1,-1	0.5
x_3	1,1,-1,-1,1,1,-1,-1	0
x_4	1,-1,1,-1,1,-1,1,-1	0
x_5	1,-1,-1,1,-1,1,1,-1	0

$n=10$		$R^c_{x_0,x_k}(0)$
x_0	1,1,1,1,1,-1,-1,-1,-1,-1	1.0
x_1	1,1,1,1,-1,1,-1,-1,-1,-1	3/5
x_2	1,1,1,-1,1,-1,1,-1,-1,-1	3/5
x_3	1,1,1,-1,-1,1,1,-1,-1,-1	1/5
x_4	1,1,-1,1,1,-1,-1,1,-1,-1	3/5
x_5	1,1,-1,1,-1,1,-1,1,-1,-1	1/5
x_6	1,1,-1,-1,1,-1,1,1,-1,-1	1/5
x_7	1,-1,1,1,-1,1,-1,-1,1,-1	1/5
x_8	1,-1,1-,1,1,-1,1,-1,1,-1	1/5
x_9	1,-1,-1,-1,1,-1,1,1,1,-1	-1/5

$n=12$		$R^c_{x_0,x_k}(0)$
x_0	1,1,1,1,1,1,-1,-1,-1,-1,-1,-1	1.0
x_1	1,1,1,1,1,-1,1,-1,-1,-1,-1,-1	4/6
x_2	1,1,1,1,-1,1,-1,1,-1,-1,-1,-1	4/6
x_3	1,1,1,1,-1,-1,1,1,-1,-1,-1,-1	2/6
x_4	1,1,1,-1,1,1,-1,-1,1,-1,-1,-1	4/6
x_5	1,1,1,-1,1,-1,1,-1,1,-1,-1,-1	2/6
x_6	1,1,1,-1,-1,1,-1,1,1,-1,-1.-1	2/6
x_7	1,1,1,-1-,1,-1,1,1,1,-1,-1,-1	0
x_8	1,1,-1,1,1-,1,1,-1,-1,1,-1,-1	2/6
x_9	1,1,-1,1,-1,1,-1,1,-1,1,-1,-1	2/6
x_{10}	1,1,-1,1,-1,-1,1,1,-1,1,-1,-1	0
x_{11}	1,1,-1,-1,1,1,-1,-1,1,1,-1,-1	2/6
x_{12}	1,1,-1,-1,1,-1,1,-1,1,1,-1,-1	0
x_{13}	1,1,-1,-1,-1,1,-1,1,1,1,-1,-1	0
x_{14}	1,-1,1,1,1,1,-1,-1,-1,-1,1,-1	4/6
x_{15}	1,-1,1,1,1,-1,1,-1,-1,-1,1,-1	2/6
x_{16}	1,-1,1,1,-1,1,-1,1,-1,-1,1,-1	2/6
x_{17}	1,-1,1,-1,1,-1,1,-1,1,-1,1,-1	0
x_{18}	1,-1,1,-1,-1,1,-1,1,1,-1,1,-1	0
x_{19}	1,-1,-1,-1,-1,1,-1,1,1,1,1,-1	-2/6

From the tables, it can be seen that only tables for $0 = n \bmod 4$, that is $n = 4,8,12$, have any entries with zero crosscorrelation with BOC(1,1). For $n = 4$, there is only 1 sequence corresponding to a BOC(2,1) spreading symbol modulation. For $n = 8$, there are 3 permissible sequences, x_3, x_4, x_5. Of these, x_4 corresponds to the BOC(4,1) modulation that we mentioned some lines above. Finally for $n = 12$, there are 6 possible sequences, x_7, x_{10}, x_{12}, x_{13}, x_{17}, x_{18} where x_{17} corresponds to BOC(6,1), one of the solutions and indeed the best in terms of performance.

4.7.3 CBOC Implementation

The CBOC implementation is a particular case of the CBCS modulation that we studied in chapter 4.6. As we saw there, the CBOC modulation can be expressed as follows

$$s(t) = A_1 \left[\begin{array}{l} \frac{c_D(t)}{2}\left(\cos\theta_1 \, s_{\text{BOC}(1,1)}(t) + \cos\theta_2 \, s_{\text{BOC}(6,1)}(t)\right) + \\ + \frac{c_P(t)}{2}\left(\cos\theta_1 \, s_{\text{BOC}(1,1)}(t) - \cos\theta_2 \, s_{\text{BOC}(6,1)}(t)\right) + \\ + j \, s_{\text{PRS}}(t)\left(\frac{\sin\theta_1 + \sin\theta_2}{2}\right) + s_{\text{IM}}(t) \end{array} \right] \tag{4.156}$$

$$s_{\mathrm{IM}}(t) = -j\, c_D(t)\, c_P(t)\, s_{\mathrm{PRS}}(t)\left(\frac{\sin\theta_1 - \sin\theta_2}{2}\right) \tag{4.157}$$

where we can recognize that in this particular case the BCS component is BOC(6,1) with a percentage of power of 1/11. Furthermore the high frequency signal is placed on both the data and pilot channels and equal power for both channels is assumed. In addition, the total OS power is equal to that of the PRS and the modulation parameters that result of solving the equations system (J.35) of Appendix J are the following:

Table 4.3. Interplex parameters of the CBOC(6,1,1/11) modulation

Percentage ρ	1/11
θ_1	0.1314692798 π
θ_2	0.4064655161 π
A_1	1.0409984082268

4.7.4 TMBOC Implementation

In a TMBOC spreading time series [G.W. Hein et al., 2006a], different BOC spreading symbols are used for different chip values, in either a deterministic or periodic pattern. To produce an MBOC(6,1,1/11) spectrum, the used spreading symbols are BOC(1,1) chips, denoted as $g_{\mathrm{BOC(1,1)}}(t)$, and BOC(6,1) chips, denoted as $g_{\mathrm{BOC(6,1)}}(t)$, where

$$g_{\mathrm{BOC(1,1)}}(t) = \begin{cases} \mathrm{sign}\left[\sin\left(2\pi t / T_c\right)\right] & 0 \le t \le T_c \\ 0 & \text{elsewhere} \end{cases} \tag{4.158}$$

and

$$g_{\mathrm{BOC(6,1)}}(t) = \begin{cases} \mathrm{sign}\left[\sin\left(12\pi t / T_c\right)\right] & 0 \le t \le T_c \\ 0 & \text{elsewhere} \end{cases} \tag{4.159}$$

Since the pilot and data components of a signal can be formed using different spreading time series, and the total signal power can be divided differently between the pilot and data components, many different TMBOC-based implementations are possible.

The selected TMBOC implementation is a signal with 75 % power on the pilot component and 25 % power on the data component, such that all the BOC(1,1) spreading symbols are used for the data, since data demodulation does not benefit from the higher frequency contributions of BOC(6,1). On the other hand, the pilot component time series comprises 29/33 BOC(1,1) spreading symbols and 4/33 BOC(6,1) spreading symbols. This design places all of the higher frequency contributions in the pilot component, providing the greatest possible benefit to signal tracking when only the pilot channel is used to this purpose.

$$\begin{aligned} G_P(f) &= \frac{29}{33} G_{\mathrm{BOC(1,1)}}(f) + \frac{4}{33} G_{\mathrm{BOC(6,1)}}(f) \\ G_D(f) &= G_{\mathrm{BOC(1,1)}}(f) \\ G_{\mathrm{MBOC(6,1,1/11)}}(f) &= \frac{3}{4} G_P(f) + \frac{1}{4} G_D(f) = \frac{10}{11} G_{\mathrm{BOC(1,1)}}(f) + \frac{1}{11} G_{\mathrm{BOC(6,1)}}(f) \end{aligned} \tag{4.160}$$

Figure 4.50 next shows the BOC(6,1) spreading symbols in locations 1, 5, 7, and 30 of each 33 spreading symbol locations. This pattern will be repeated 310 times since the spreading code is 10230 chips long.

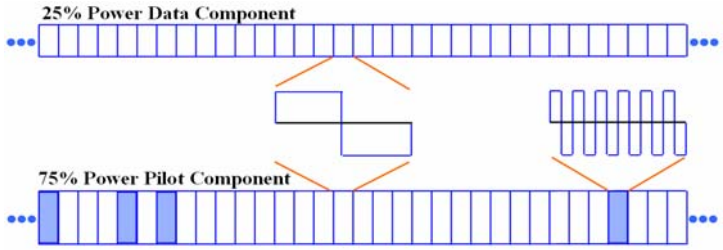

Figure 4.50. TMBOC time representation with all BOC(6,1) Spreading symbols in the 75% Pilot Power Component

Several considerations affect the choice of the specific locations of the BOC(6,1) spreading symbols. For example, if the BOC(6,1) chips were placed in both the pilot and data components, the receiver implementation would be more simple than if these symbols were placed in the same locations in both. In addition, the proper placement of the BOC(6,1) symbols leads to an improvement of the spreading codes' autocorrelation and crosscorrelation properties of approximately 1 dB, compared to those that can be observed when only BOC(1,1) spreading symbols are used. The good results obtained for L1C using the BOC(6,1) locations and the performance of the spreading codes for L1C [G.W. Hein et al., 2006a] confirm the optimality of the described positions of BOC(6,1).

Finally, we show in the next table the correlation losses that result from correlating a BOC(1,1) replica with different implementations of MBOC, included the finally selected for GPS, discussed above. The definition of correlation losses was provided in (4.126):

Table 4.4. Correlation losses of different MBOC implementations

Power in pilot channel	**50%**		**75%**	
Signal	**CBOC(6,1,1/11)**	**TMBOC(6,1,1/11)**	**CBOC(6,1,1/11)**	**TMBOC(6,1,1/11)**
System	**Galileo**	**GPS**	**Galileo**	**GPS**
Pilot losses	1/11 (0.4 dB)	2/11 (0.9 dB)	1/11 (0.4 dB)	4/33 (0.6 dB)
Data losses	1/11 (0.4 dB)	0	1/11 (0.4 dB)	0

After having analyzed the two possible implementations of MBOC, namely CBOC and TMBOC, we can conclude that there are no significant differences of performance between both as this depends actually on the final user configuration. Indeed, how good or bad placing all the high frequency BOC(6,1) component on both data and pilot or only on the pilot channel is depends on the particular application. In addition, from the point of view of the correlation characteristics, we have seen that TMBOC provides an additional improvement of 1 dB in terms of reduced correlation if the BOC(6,1) component is placed at proper locations, what futher improves the noise input.

4.7.5 Optimal Tracking of CBOC

As one can imagine, until the final Galileo implementation of MBOC was selected, different CBOC implementations were under consideration. In the next lines we summarize the main results of the analyses carried out to optimally track CBOC each of the proposed solutions.

Following the results from [O. Julien et al., 2006] we will show in this chapter the tracking performance of the CBOC modulation when only one channel of the Galileo E1 OS (data or pilot) is used. As we have seen above, there are many ways of implementing MBOC and even if we would constrain our analysis to CBOC, it can be shown that the variety of solutions is still broad. Indeed, the high frequency BOC(6,1) component could go in principle on both data and pilot channels, only on the pilot, only on the data, the power splits could change, and they all would still fulfil the MBOC definition that we gave above. To simplify thus our analysis, the three main cases are exposed next. These correspond basically to the three CBOC implementations that were considered for the Galileo E1 OS:

- The use of a CBOC(6,1,1/11) where both the data and pilot channels have a BOC(6,1) component in anti-phase. In this case, the power of the BOC(6,1) part is 1/11 of the channel total power. This is the implementation finally selected for Galileo E1 OS.
- The use of a CBOC(6,1,2/11) where only one of the channels, the pilot or the data, has a BOC(6,1) component with alternating sign, while the other channel is a pure BOC(1,1). In this case, the power of the BOC(6,1) part is 2/11 of the pilot channel total power. Moreover, it is important to note that the alternation of BOC(6,1) is necessary to get rid of the cross spectral terms that would result otherwise. This will be shown in the following lines.
- CBOC(6,1,1/11) is used on both the data and pilot channels, being BOC(6,1) in both channels with alternating sign. In this case, the data and pilot channels have a BOC(6,1) power of 1/11 of the channel total power.

Recalling now the general CBCS definition from (4.121) and substituting BCS by BOC(6,1) we can define the general CBOC model as follows:

$$s(t) = A_1 \left[\begin{array}{l} \frac{c_D(t)}{2}\left[\cos\theta_1 \, s_{\mathrm{BOC}(1,1)}(t) \pm \cos\theta_2 \, s_{\mathrm{BOC}(6,1)}(t)\right] + \\ + \frac{c_P(t)}{2}\left[\cos\theta_1 \, s_{\mathrm{BOC}(1,1)}(t) \pm \cos\theta_2 \, s_{\mathrm{BOC}(6,1)}(t)\right] + \\ + j\, s_{\mathrm{PRS}}(t)\left(\frac{\sin\theta_1 + \sin\theta_2}{2}\right) + s_{\mathrm{IM}}(t) \end{array} \right] \tag{4.161}$$

$$s_{\mathrm{IM}}(t) = -j\, c_D(t) c_P(t)\, s_{\mathrm{PRS}}(t)\left(\frac{\sin\theta_1 - \sin\theta_2}{2}\right) \tag{4.162}$$

and looking only at the pilot channel for the three cases described above, we have:

$$\text{CBOC}(6,1,\rho,\text{'+'})(t) = c_P(t)\left\{k_1\, s_{\text{BOC}(1,1)}(t) + k_2\, s_{\text{BOC}(6,1)}(t)\right\} \quad (4.163)$$

$$\text{CBOC}(6,1,\rho,\text{'-'})(t) = c_P(t)\left\{k_1\, s_{\text{BOC}(1,1)}(t) - k_2\, s_{\text{BOC}(6,1)}(t)\right\} \quad (4.164)$$

where ρ indicates the amount of power on the high frequency BOC(6,1) component:

$$\rho = \frac{k_2^2}{k_1^2 + k_2^2} \quad (4.165)$$

The last model to introduce is the alternating model, which is shown to be:

$$\text{CBOC}(6,1,\rho,\text{'+/-'})(t) = c_P(t)\left\{k_1\, s_{\text{BOC}(1,1)}(t) + k_2\, s_{\text{BOC}(6,1)}(t)\right\} \quad (4.166)$$

for even chips, and

$$\text{CBOC}(6,1,\rho,\text{'+/-'})(t) = c_P(t)\left\{k_1\, s_{\text{BOC}(1,1)}(t) - k_2\, s_{\text{BOC}(6,1)}(t)\right\} \quad (4.167)$$

for odd chips. The autocorrelation function of the three models is shown next:

$$\Re_{\text{CBOC}(6,1,\rho,\text{'-'})}(\tau) = k_1^2\,\Re_{\text{BOC}(1,1)}(\tau) + k_2^2\,\Re_{\text{BOC}(6,1)}(\tau) - 2k_1 k_2\,\Re_{\text{BOC}(1,1)/\text{BOC}(6,1)}(\tau) \quad (4.168)$$

$$\Re_{\text{CBOC}(6,1,\rho,\text{'+'})}(\tau) = k_1^2\,\Re_{\text{BOC}(1,1)}(\tau) + k_2^2\,\Re_{\text{BOC}(6,1)}(\tau) + 2k_1 k_2\,\Re_{\text{BOC}(1,1)/\text{BOC}(6,1)}(\tau) \quad (4.169)$$

$$\Re_{\text{CBOC}(6,1,\rho,\text{'+/-'})}(\tau) = k_1^2\,\Re_{\text{BOC}(1,1)}(\tau) + k_2^2\,\Re_{\text{BOC}(6,1)}(\tau) \quad (4.170)$$

As we can see, the two first auto-correlations present an additional cross-term due to the existence of cross-correlation between BOC(1,1) and BOC(6,1). As we mentioned above, this cross-term is not desirable and must be eliminated to generate a spectrum according to the MBOC definition. This is possible if data and pilot are in anti-phase (each with a different sign) or if the BOC(6,1) component alternates its sign. Nonetheless, we will keep these signals for reference in the following figures to show the performance. We show next the autocorrelation functions of the different analyzed solutions compared with the TMBOC solution for a receiver bandwidth of 24 MHz:

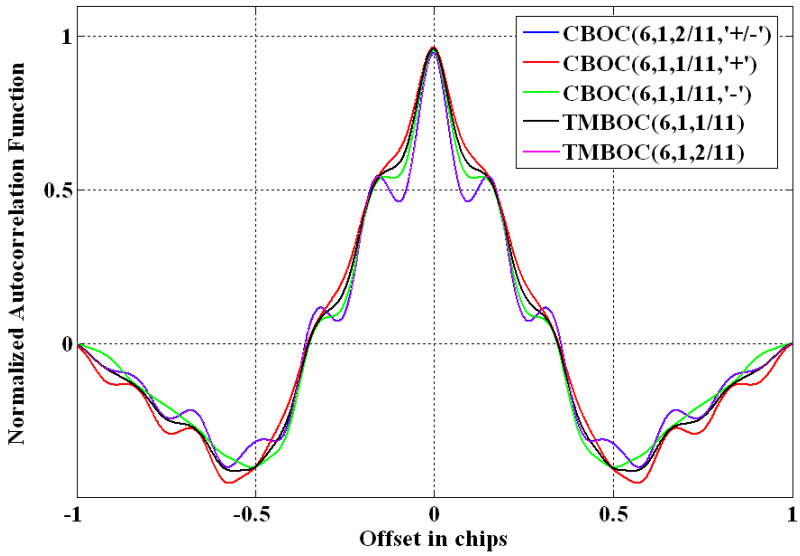

Figure 4.51. CBOC and TMBOC Autocorrelation Function

As we can recognize in the figure above, the shape of the auto-correlation function highly depends on the amount of power on BOC(6,1). Indeed, the higher the value of ρ, the more ripples the auto-correlation will present and the better the potential performance will be. Furthermore, it is interesting to see that the sharpest slope around the origin is shown by TMBOC and the CBOC$('-')$ version while TMBOC(6,1,2/11) and CBOC$(6,1,2/11,'+/-')$ perform similar. MBOC is analyzed next regarding the following three criteria:

- False tracking points
- Code tracking noise
- Multipath-induced code tracking error

4.7.5.1 False Tracking Points

If we take a closer look at the auto-correlation function of Figure 4.51 above, it is clear to recognize the existence of secondary peaks that could lead to stable false locks. Indeed, the more ripples the function presents and the more accentuated the undulations are, the higher the probability that we lock on a non desired but stable tracking point. Fortunately, not all the solutions are equally susceptible to suffering from this effect, since this depends actually on how the auto-correlation function looks like. In fact, while the selected CBOC(1/11) for Galileo E1 OS is not likely to lead to stable false lock points as shown in [J.-A. Avila-Rodriguez et al., 2006c], the existence of false lock points would be nearly unavoidable for the CBOC$(6,1,2/11,'+/-')$ implementation, implying thus a higher complexity to detect the right peak. This is in fact the prize for allocating more BOC(6,1) power on the channel. Finally, it is important to note that no matter which of the implementations we look at, since BOC(1,1) is the dominant signal in all of them, a false lock detector is still necessary in order to make sure that the receiver is tracking the signal based on the correct autocorrelation main peak, and not the secondary of BOC(1,1).

4.7.5.2 Thermal Noise-Induced Code Tracking Error

In order to understand how the code tracking noise behaves for the different implementations of MBOC discussed above, we present in the next figure the Cramér Rao Lower Bound.

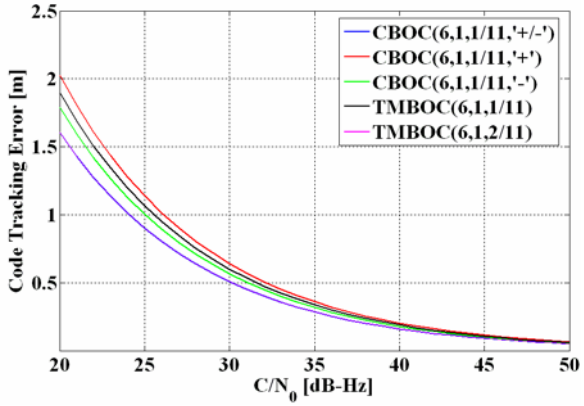

Figure 4.52. BOC(1,1), CBOC and TMBOC Cramér Rao Lower Bound with 1 Hz Loop Bandwidth, 1/12 Chip E-L Spacing, 4 ms Integration and 12 MHz One-Sided Filter

As we can see, the best performance corresponds to the alternating CBOC$('+/-')$ version with 2/11 of power on BOC(6,1) or to its equivalent TMBOC version, since these can take advantage of the high frequency components of the signal the best. Moreover, among the different CBOC solutions with the 1/11 of average power that results from considering data and pilot together, the worst performance is shown to be that of the in-phase CBOC$(1/11,'+')$ solution while the anti-phase CBOC$(1/11,'-')$ is the best. This was to expect since its autocorrelation function's main peak has the steepest slope. We can also see this if we compare both phase and anti-phase versions in the time domain.

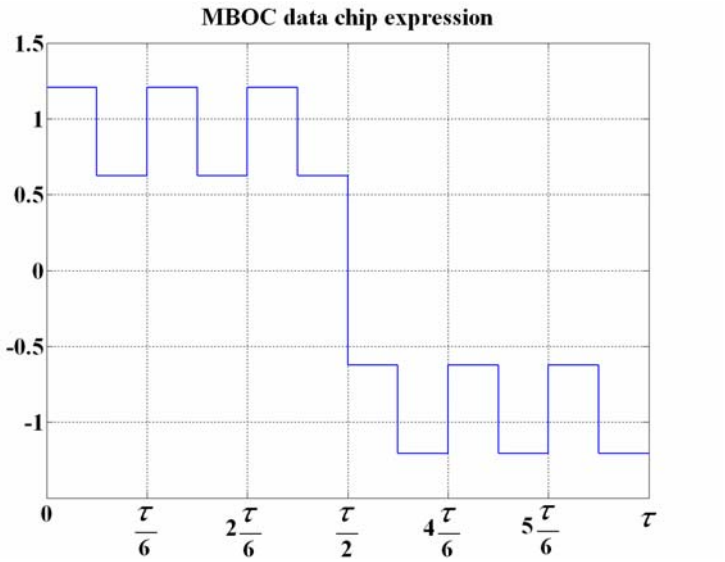

Figure 4.53. CBOC data chip with BOC(1,1) and BOC(6,1) in-phase

Equally, the pilot channel would present the following shape for a chip.

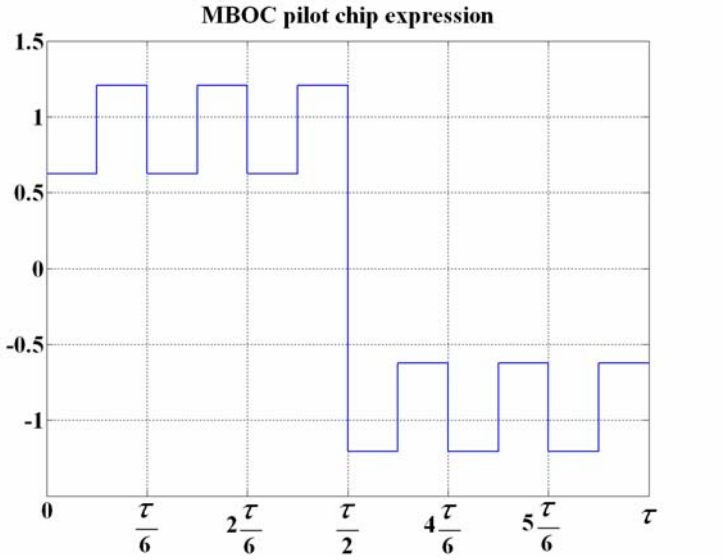

Figure 4.54. CBOC pilot chip with BOC(1,1) and BOC(6,1) in anti-phase

From the previous figures it is easy to recognize that the pilot channel will have more components at higher frequencies since at 0.5 chips the amplitude variation is higher.

Furthermore, the alternating CBOC solution with 1/11 of power on BOC(6,1) performs as the average of the phase and anti-phase solutions shown above. To avoid any confusion, it is important to underline that the solutions studied above correspond to MBOC implementations that were object of study during the design of Galileo E1 OS and GPS L1C. The finally selected CBOC implementation of Galileo has BOC(6,1) on both data and pilot, being these in anti-phase with respect to each other. According to the previous notation, this means that the pilot channel of Galileo E1 OS will be $\mathrm{CBOC}(1/11,'-')$ and the data channel $\mathrm{CBOC}(1/11,'+')$.

4.7.5.3 Multipath Induced Tracking Error

The multipath performance of a signal highly depends on the shape of the auto-correlation function, as we saw in chapter 4.1.1. Indeed, this was one of the aspects that were more seriously taken into consideration during the optimization of the Galileo Open Service and GPS Civil signals in E1/L1. We show in the next figures the multipath performance of different MBOC implementations by means of the multipath envelopes and the multipath running average error as done in [G.W. Hein et al., 2006a] and [G.W. Hein et al., 2006b]. Note that TMBOC(6,1,1/11) and $\mathrm{CBOC}(6,1,1/11,'+/-')$ perform the same and therefore are overlapped in the next figures.

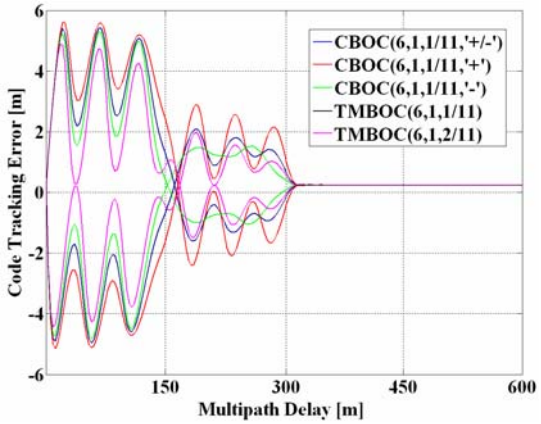

Figure 4.55. MBOC Multipath Envelopes with an E-L Spacing of 0.1 chips and a Double-Sided Filter of 24 MHz

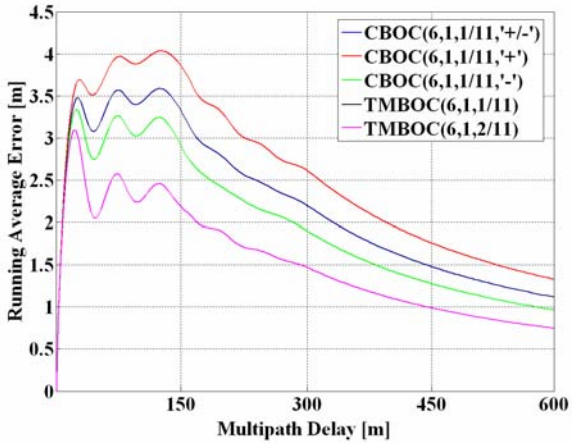

Figure 4.56. MBOC Multipath Running Average Error with an E-L Spacing of 0.1 chips and a Double-Sided Filter of 24 MHz

As we can see, for an early-late spacing of 0.1 chips and a one-sided front-end filter of 12 MHz, the best performance is exhibited by $\mathrm{CBOC}(6,1,2/11,'+/-')$, followed by $\mathrm{CBOC}(6,1,1/11,'-')$, $\mathrm{CBOC}(6,1,1/11,'+/-')$ and $\mathrm{CBOC}(6,1,1/11,'+')$. Moreover, it is clear to see that all the solutions clearly outperform BOC(1,1). In addition, it is important to note that $\mathrm{CBOC}(6,1,1/11,'+/-')$ and TMBOC(6,1,1/11) perform the same in average when both data and pilot are processed in the receiver.

4.7.5.4 Conclusions on Optimal CBOC Tracking

As we have seen in previous lines, the best CBOC implementation of MBOC in terms of performance is the anti-phase $\mathrm{CBOC}(6,1,1/11,'-')$ solution. Nevertheless, as demonstrated in (4.169), this solution presents the great inconvenient of showing a non desired cross-term that can only be eliminated if the other channel adopts the counterpart $\mathrm{CBOC}(6,1,1/11,'+')$. This is indeed the case in the finally selected CBOC implementation of Galileo E1 OS. Then, the total performance of this CBOC implementation, seen as data and pilot together, is equivalent to that of the alternating $\mathrm{CBOC}(6,1,1/11,'+/-')$ solution.

Another studied option was to use directly the $\mathrm{CBOC}(6,1,1/11,'+/-')$ solution on both the data and pilot channels, in which case both channels would have the same tracking performance. This implementation would perfectly fulfil the MBOC spectrum too but the drawback was be the extra complexity required for the implementation of the alternation. Equally, the option of using a $\mathrm{CBOC}(6,1,2/11,'+/-')$ on one channel and a pure BOC(1,1) on the other channel would permit to have one channel with excellent tracking performance, while the other channel would just use a pure BOC(1,1) modulation. This signal would be of interest for some types of receivers with a philosophy behind very much in line with how TMBOC is conceived.

All the figures that we have shown above rely on the assumption that a CBOC replica signal has to be locally generated by the receiver. Indeed, CBOC is a linear combination of two sub-carriers and has thus more than two levels, so that 2 bits are needed to encode the signal. While this should not be a great challenge as some works have already shown [P.G. Mattos, 2007], we will study in the next chapter a suboptimal tracking of CBOC using local replicas encoded with only 1 bit, as shown in [J.-A. Avila-Rodriguez et al., 2006c] and [O. Julien et al., 2006]. One could of course think of separating the correlation of the incoming CBOC signal with a pure BOC(1,1) replica and, on the other side, with a pure BOC(6,1) replica. Then a simple linear combination of the outputs of both correlators would be sufficient to obtain the same result as if we had correlated directly with the CBOC replica of two bits. However, this processing requires twice as many correlators as the traditional CBOC tracking. In the next lines we present a solution that avoids to have to pay this prize [O. Julien et al., 2006] and [J.-A. Avila-Rodriguez et al., 2006c].

4.7.6 Suboptimal Tracking of CBOC: TMBOC like approach

As shown in [J.-A. Avila-Rodriguez et al., 2006c], the idea behind the 1-bit receiver technique is to correlate the incoming CBOC signal with a locally generated signal obtained by time-multiplexing a BOC(1,1) sub-carrier and a BOC(6,1) sub-carrier. We can model this replica as follows:

$$\mathrm{TM}_{61}(t) = \begin{cases} c_k(t)\, s_{\mathrm{BOC}(1,1)}(t), & \text{if } t \in S_1 \\ c_k(t)\, s_{\mathrm{BOC}(6,1)}(t), & \text{if } t \in S_2 \end{cases} \tag{4.171}$$

where S_1 is the union of the segments of time when a BOC(1,1) sub-carrier is used. Equally, S_2, the complement of S_1 in the time domain, is the union of the segments of time when a BOC(6,1) sub-carrier is generated. In addition, we write TM_{61} in order to distinguish this technique from the typical CBOC replica approach studied above. The advantage of this approach is that by using such a replica we only need to encode with 1 bit reducing thus the complexity of the receiver. Moreover, time-multiplexing reduces the number of correlators.

Let us define α to designate the percentage of time that the BOC(6,1) sub-carrier is used in one code length, and $\beta = 1 - \alpha$ to represent the amount of time reserved for the BOC(1,1) local sub-carrier part. Furthermore, we will assume that the sign of the BOC(6,1) local sub-carrier in the local replica is taken according to the sign of the BOC(6,1) used in the CBOC signal. This means that for the case the CBOC channel is in-phase, we have a positive sign and thus the percentage of BOC(6,1) time is given by $\alpha^+ = 1 - \beta^+$. Equally, for the anti-phase CBOC component the percentage of BOC(6,1) time is given by $\alpha^- = 1 - \beta^-$. It must be noted that α^+ and α^- can be different in general. As a result, the cross-correlation that results from using the TM_{61} replica with the different CBOC implementations of previous chapter is given by the following expressions:

$$\Re_{\mathrm{CBOC}('-')/\mathrm{TM}_{61}(\alpha^-)}(\tau) = \beta^- k_1 \Re_{\mathrm{BOC}(1,1)}(\tau) + \alpha^- k_2 \Re_{\mathrm{BOC}(6,1)}(\tau) - \left(\beta^- k_1 + \alpha^- k_2\right)\Re_{\mathrm{BOC}(1,1)/\mathrm{BOC}(6,1)}(\tau) \tag{4.172}$$

$$\Re_{\mathrm{CBOC}('+')/\mathrm{TM}_{61}(\alpha^+)}(\tau) = \beta^+ k_1 \Re_{\mathrm{BOC}(1,1)}(\tau) + \alpha^+ k_2 \Re_{\mathrm{BOC}(6,1)}(\tau) + \left(\beta^+ k_1 + \alpha^+ k_2\right)\Re_{\mathrm{BOC}(1,1)/\mathrm{BOC}(6,1)}(\tau) \tag{4.173}$$

$$\Re_{\mathrm{CBOC}('+/-')/\mathrm{TM}_{61}(\alpha)}(\tau) = \frac{1}{2}\left[\left(\beta^- + \beta^+\right)k_1 \Re_{\mathrm{BOC}(1,1)}(\tau) + \left(\alpha^- + \alpha^+\right)k_2 \Re_{\mathrm{BOC}(6,1)}(\tau) + \left(\alpha^- - \alpha^+\right)\left(k_2 - k_1\right)\right] \tag{4.174}$$

As we can see in the expressions above, the correlation functions of BOC(1,1) and BOC(6,1) are also weighted as was also the case for the CBOC replica, with the difference that the weights are in this case controlled by the factors α and β and the cross-correlation between TM_{61} and CBOC induces additional correlation losses as shown in [O. Julien et al., 2006] and [J.-A. Avila-Rodriguez et al., 2006c].

It is also interesting to see in [O. Julien et al., 2006] and [J.-A. Avila-Rodriguez et al., 2006c] that if the Dot Product (DP) discriminator is employed, different TM_{61} replicas could be used for the prompt correlator and for the early and late correlators. Indeed, for the particular case of the DP discriminator, the prompt correlator only affects the tracking noise squaring losses and is thus recommendable to choose a local prompt replica that minimizes the correlation loss with the incoming CBOC signal. As shown in [J.-A. Avila-Rodriguez et al., 2006c], this can be achieved by selecting $\alpha = 0$ or what is equivalent, by using a pure BOC(1,1) sub-carrier as proposed in [J.-A. Avila-Rodriguez et al., 2006c].

On the other hand, the early and late correlator outputs determine the gain of the discriminator as well as the noise correlation between the early and late correlators' output. Next table shows the tracking noise degradation that results from the use of the TM_{61} technique for the different studied CBOC cases and we compare it with the optimal TMBOC tracking for the same BOC(6,1) power [O. Julien et al., 2006].

Table 4.5. TM61(α) Tracking Noise Degradation with respect to TMBOC in Terms of Equivalent C/N_0 for Different CBOC Configurations

Value of α for Early and Late $TM_{61}(\alpha)$ Local Replicas	$TM_{61}(\alpha)$ Tracking Noise Degradation w.r.t. TMBOC in Terms of Equivalent C/N_0 [dB]			
	CBOC(6,1,1/11,'x') vs TMBOC(6,1,1/11)			CBOC(6,1,2/11,'x') vs TMBOC(6,1,2/11)
	+	-	+/-	+/-
0	4	2	2.9	5
0.2	5.1	2.9	3.6	4.2
0.4	5.1	2.8	3.4	3.3
0.6	4.9	2.6	3.3	2.6
0.8	4.6	2.3	3.2	2.1
1	4.3	1.9	3	1.6

As we can see, for CBOC(1/11) the most interesting values are either a high or a low value of α, since for those cases the equivalent C/N_0 degradation of the tracking noise is the lowest with a value of 1.9 dB for the $\text{CBOC}(6,1,1/11,'-')$, of 3 dB for the $\text{CBOC}(6,1,1/11,'+/-')$ and of 4 dB for the $\text{CBOC}(6,1,1/11,'+')$. It is important to note that $\alpha = 0$ implies to use a pure BOC(1,1) replica and $\alpha = 1$ a pure BOC(6,1) replica.

In the same manner, the best option for $\text{CBOC}(6,1,2/11,'+/-')$ and TMBOC(6,1,2/11) would be to take a value of α as high as possible. This means, a pure BOC(6,1) replica for the E-L correlators would be the ideal choice in this case. As a conclusion, in order to have a common architecture for CBOC(6,1,1/11), CBOC(6,1,2/11) and TMBOC(6,1,2/11), the best would be to select a TM_{61} tracking technique that would only use pure local replicas: BOC(1,1) for the prompt correlator and BOC(6,1) for the E-L correlators. Moreover, no time-multiplexing

would be needed any more, simplifying thus the complexity of the receiver. As one can imagine, if this approach is valid for the different MBOC implementations discussed in previous pages, it is also valid for the particular CBOC and TMBOC solutions adopted by Galileo and GPS.

Another aspect that we have not touched yet is the multipath rejection of the different discussed TM_{61} options. As shown in [O. Julien et al., 2006] for both the CBOC(1/11) and the CBOC(2/11) cases, a value of α around 0.5 would lead to the best results. Nevertheless, values of α close to 1 would also deliver performances close to the optimum. In addition, using $\alpha = 0$ is shown to be suboptimal in terms of multipath rejection since the performance is then that of BOC(1,1) [J.-A. Avila-Rodriguez et al., 2006c].

As a conclusion, it seems that a sub-optimum implementation of a CBOC-TMBOC receiver based on a 1 bit architecture could use a pure local BOC(1,1) replica for the prompt correlator and a pure local BOC(6,1) replica for the early and late correlators. Moreover, we have seen that this scheme provides with relatively low degradation in terms of code tracking noise compared to the optimal TMBOC tracking.

The preceding derivations pursued to show that processing CBOC with a1 bit receiver is possible already today at the cost of some degradation. However, 2-bit receivers are already reality as shown in [P.G. Mattos, 2007] and an optimal processing with 2 bits would be thus preferred. This would additionally imply some superiority of CBOC with respect to the TMBOC implementation since no blanking would be needed any more. Indeed, blanking of the BOC(6,1) pulses to avoid correlation losses is equivalent to reducing the equivalent code length by a factor 29/33 of the total length (10230). It must be noted though that this supposes a minimum additional complexity.

4.7.7 MBOC Tracking Sensitivity

As shown in [O. Julien, 2005], we can distinguish two types of tracking sensitivity:

- Code Tracking Sensitivity (DLL)
- Carrier Tracking Sensitivity (PLL)

We describe the MBOC properties regarding Code Tracking sensitivity in detail.

4.7.7.1 Code Tracking Sensitivity

Following the definition from [O. Julien, 2005], the tracking sensitivity can be defined as the minimum pre-correlation Signal to Noise Ratio (SNR) that is necessary to correctly track a desired signal. To correctly track, the post-correlation SNR should be as high as possible, what can be achieved by different means. Whatever the followed approach is, the main objective is always to increase the correlation gain, which is the ratio between the post-correlation SNR and pre-correlation SNR.

According to [O. Julien, 2005], the post-correlation SNR_{post} is shown to be

$$SNR_{\text{post}} = \frac{2PT_I\widetilde{R}^2(\varepsilon_\tau)}{N_0\widetilde{R}(0)} \tag{4.175}$$

where

- ε_τ is the code delay
- $\widetilde{R}$ is the correlation of the filtered incoming signal with the local replica
- N_0 is the noise power density
- P is the power of the desired signal
- and T_I is the coherent integration time.

On the other hand, the pre-correlation SNR adopts the following form:

$$SNR_{\text{pre}} = \frac{P\widetilde{R}(0)}{N_0\beta_r} \tag{4.176}$$

where β_r is the pre-correlation bandwidth.

Therefore the correlation gain can be expressed as [R. Watson, 2005]

$$G = \frac{SNR_{\text{post}}}{SNR_{\text{pre}}} = \frac{2T_I\beta_r\,\widetilde{R}^2(\varepsilon_\tau)}{\widetilde{R}^2(0)} \tag{4.177}$$

which can be further simplified to

$$G = 2T_I\beta_r \tag{4.178}$$

as also shown in [O. Julien, 2005].

4.7.7.2 Effect of longer integrations on code tracking sensitivity

If we take a closer look into the expressions above, we can clearly see that the most straightforward way of improving the tracking sensitivity is to increase the coherent integration T_I as much as possible. Unfortunately, this is not always possible due to the presence of data bits or secondary codes. Additionally, even though it were possible to integrate for long periods of time in the absence of data, other major problems coming from the code and phase delay variation during the integration would appear.

The best known solution to overcome this problem is the use of standard non-coherent summations according to the following expression

$$Y_{\text{st}} = \sum_{k=1}^{M} Z_k = \sum_{k=1}^{M} \left\| \sqrt{I_k^2 + Q_k^2} \right\| \tag{4.179}$$

where I_k and Q_k correspond to the in-phase and quadrature non-coherent correlation inputs obtained over a coherent integration time T_I. Moreover M is the number of values used for the non-coherent integration and Y_{st}, as defined in (4.179), can be used to apply the Neumann-Pearson lemma, as this lemma allows one to obtain a powerful test in the case of two simple alternative hypotheses H_1 and H_2.

By doing so, further correlation gain can be reached but due to the squaring in the expression above the process is subject to the so-called squaring losses that reduce the total gain [M.M. Chansarkar and L. Garin, 2000] and [G.D. MacGougan, 2003]. The squaring loss depends on the SNR before the non-coherent integration is realized and is higher the lower the SNR. Thus, long coherent integration is desirable before the non-coherent correlation is applied, in order to reach a good SNR before accumulating. Indeed, by non-coherent integrating we increase the power of our desired signal but since the noise is not eliminated as with the coherent integration, the gain in power is lower than the increase of noise.

According to this scheme, depending on whether the desired signal is or is not present in the searching bin, the variable Z_k will present a Ricean or Rayleigh distribution correspondingly. Indeed, it can be shown that if the desired signal is present, a Ricean distribution holds, which has the following probability density function [J.-A. Avila-Rodriguez et al., 2006b]:

$$\mathrm{pdf}(z) = \frac{z}{\sigma^2} \mathrm{e}^{-\frac{z^2+A^2}{2\sigma^2}} I_0\left(\frac{Az}{\sigma^2}\right) \tag{4.180}$$

where z is the test variable, A is the signal amplitude, σ^2 the noise power and $I_0(\ )$ the zero-order modified Bessel function of the first kind. According to this, if the output SNR is defined as:

$$\mathrm{SNR}_z = \frac{\mathrm{E}(z) - \mathrm{E}(z)\big|_{s=0}}{\sigma_z\big|_{s=0}} \tag{4.181}$$

where

$$\mathrm{E}(z) = \sigma\sqrt{\frac{\pi}{2}} \mathrm{e}^{-\frac{z^2}{4\sigma^2}} \left[\left(1+\frac{z^2}{2\sigma^2}\right) I_0\left(\frac{z^2}{4\sigma^2}\right) + \frac{z^2}{2\sigma^2} I_1\left(\frac{z^2}{4\sigma^2}\right)\right] \tag{4.182}$$

the squaring loss can be obtained according to [G. Lachapelle, 2004] as follows:

$$S_L(\mathrm{dB}) = 20\log_{10}\left(\frac{A}{z}\right) - 20\log_{10}(\mathrm{SNR}_z) \tag{4.183}$$

as shown graphically in the following figure:

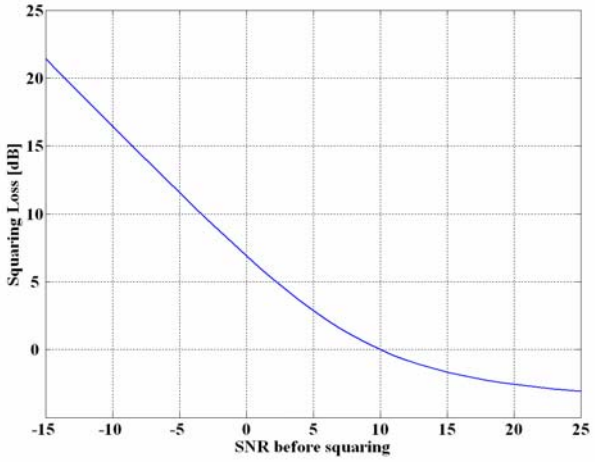

Figure 4.57. Squaring Loss as a function of the SNR after coherent integration (before the non-coherent accumulation)

Reading the squaring losses from the figure above, the total processing gain with respect to the pre-correlation SNR can be easily calculated [J.-A. Avila-Rodriguez et al., 2006b]:

$$G = 10\log_{10}(\beta_r T_I) + G_{\mathrm{NC}} = 10\log_{10}(\beta_r T_I) + 10\log_{10}(M) - S_L \quad (4.184)$$

where

- G is the total processing gain (dB) with respect to the pre-correlation SNR,
- G_{NC} is the non-coherent signal gain from the non-coherent integration alone,
- β_r is the pre-detection bandwidth,
- T_I is the total coherent integration time,
- M is the number of non-coherent integrations,
- and S_L are the squaring losses that we defined above.

The main drawback from the standard non-coherent integration comes from the fact that the noise is squared. Alternative expressions have been studied in the literature to sort out this problem as explained in [J.-A. Avila-Rodriguez et al., 2005c] and [G. Lachapelle, 2004]. One of those is the non-coherent differential correlation dc, also known as dot-product correlation, which is based on multiplying consecutive samples. One of its multiple expressions is:

$$Y_{\mathrm{dc}} = \sum_{i=1}^{K/2}\left(I_{2i}I_{2i-1} + Q_{2i}Q_{2i-1}\right) = I_2I_1 + Q_2Q_1 + I_4I_3 + Q_4Q_3 + \ldots + I_KI_{K-1} + Q_KQ_{K-1} \quad (4.185)$$

where I_i and Q_i denote again the output of the coherent integration process. Since now the input i is multiplied with the input i-1, better results are expected in the ideal case, given that the noise is uncorrelated in the time with itself. This is in fact what the simulations show. However, this algorithm presents a main drawback due to its high sensitivity to Doppler.

In the previous lines we have briefly discussed the most straightforward way of increasing tracking sensitivity by increasing the total integration time. Additionally, there exist other ways of increasing the post-correlation SNR such as increasing the signal power at the satellite. Unfortunately, this would have extremely negative effects on interference with already existing terrestrial systems.

4.7.7.3 Signal structure and DLL code tracking error

Fortunately, there is another way of increasing the *per se* tracking sensitivity of a receiver, which is based on the signal structure of the desired signal. As we know, any DLL configuration is usually based on the combination of early and late correlators, so that the noise correlation of each output is also important to the resulting combined noise. Here plays the signal structure an outstanding role since the DLL tracking sensitivity will be affected by the selection of the signal waveform. In the next lines, we will show the theoretical tracking performance of MBOC and we will compare it with that of BOC(1,1) and the C/A Code.

If perfect normalization is assumed and the loop bandwidth is negligible compared with the bandwidth of the discriminator noise, [J.K. Holmes, 2000] and [O. Julien, 2005] have shown that the DLL estimated code delay tracking error variance with Gaussian noise yields:

$$\sigma^2_{\text{disc},\varepsilon_\tau,t} = \frac{2B_L\left(1-\frac{1}{2}B_L T_I\right)S_{N_{\text{disc}}}(0)}{K^2_{\text{disc}}} \tag{4.186}$$

where

- disc refers to the type of discriminator,
- $S_{N_{\text{disc}}}$ is the discriminator noise PSD,
- B_L is the loop bandwidth,
- T_I is the integration time, and
- K_{disc} is the loop gain associated to the discriminator, with $K_{\text{disc}} = \left.\frac{\mathrm{d}D_{\text{disc}}}{\mathrm{d}\varepsilon_\tau}\right|_{\varepsilon_\tau=0}$, where D_{disc} is the discriminator function.

Additionally, since the noise power spectral density that results from multiplying the incoming signal with the local replica is very wide band, we can approximate the expression above by the following [O. Julien, 2005]:

$$\sigma^2_{\text{disc},\varepsilon_\tau,t} = \frac{2B_L\left(1-\frac{1}{2}B_L T_I\right)T_I\,\sigma^2_{D_{\text{disc}}}}{K^2_{\text{disc}}} \tag{4.187}$$

where $\sigma^2_{D_{\text{disc}}}$ represents the discriminator output standard deviation without normalizing. This expression is very close to that of the PLL, with the difference that the effect of the normalization (through K_{disc}) has been introduced here. This means in other words, that the DLL tracking error is directly dependent upon the discriminator resistance to noise, and thus on the signal structure.

If perfect normalization is assumed again, no frequency uncertainty is considered, a front-end filter with ideal unity gain and receiver bandwidth β_r and a code delay error remaining small, the DLL tracking error variance produced by use of an EMLP discriminator is shown to be [O. Julien, 2005] and [J.W. Betz and K.R. Kolodziejski, 2000]:

$$\sigma^2_{\text{EMLP}} = \frac{B_L\left(1-\frac{1}{2}B_L T_I\right)\int_{-\frac{\beta_r}{2}}^{\frac{\beta_r}{2}} G(f)\sin^2(\pi f\delta)\mathrm{d}f}{\frac{C}{N_0}\left[2\pi\int_{-\frac{\beta_r}{2}}^{\frac{\beta_r}{2}} f\,G(f)\sin(\pi f\delta)\mathrm{d}f\right]^2}\left[1+\frac{\int_{-\frac{\beta_r}{2}}^{\frac{\beta_r}{2}} G(f)\cos^2(\pi f\delta)\mathrm{d}f}{\frac{C}{N_0}T_I\left[2\pi\int_{-\frac{\beta_r}{2}}^{\frac{\beta_r}{2}} G(f)\cos(\pi f\delta)\mathrm{d}f\right]^2}\right] \tag{4.188}$$

where β_r is the receiver bandwidth and δ the correlator spacing of the receiver.

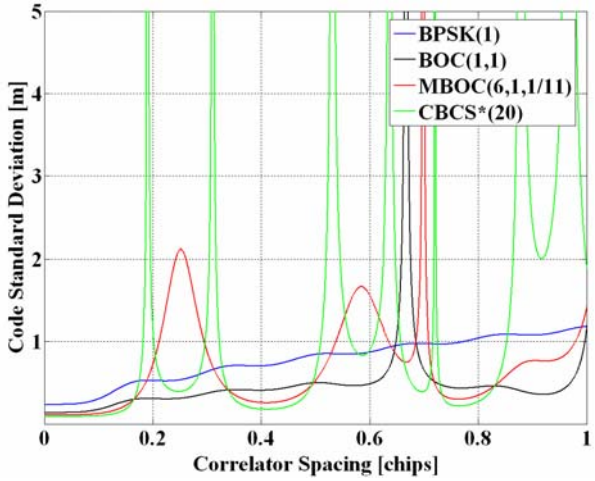

Figure 4.58. Pseudorange Code Measurement Accuracy as a function of the discriminator spacing

In the figure above, derived according to [J.W. Betz and K.R. Kolodziejski, 2000], a receiver bandwidth β_r of 24 MHz, a loop bandwidth B_L of 1 Hz, a C/N_0 of 45 dB-Hz and a coherent integration time T_I of 4 ms were used for BOC(1,1) and MBOC(6,1,11). For BPSK(1), 20 ms coherent integration were assumed. It is important to note that other alternative models have been derived to describe the behaviour of the code tracking noise for spacing values close to zero as shown in [T. Pany et al., 2002]. In addition, similar figures could also be obtained for different receiver discriminators. One final comment on the figure above is that MBOC has got less *dangerous* regions than CBCS* regarding the code spacing what was also an important advantage in favour of MBOC.

Equally, as derived in [O. Julien, 2005], the DLL tracking error variance using a Dot Product (DP) discriminator presents the following expression:

$$\sigma^2_{\mathrm{DP}} = \frac{B_L\left(1-\frac{1}{2}B_L T_I\right)\int_{-\frac{\beta_r}{2}}^{\frac{\beta_r}{2}} G(f)\sin^2(\pi f \delta)\mathrm{d}f}{\frac{C}{N_0}\left[2\pi\int_{-\frac{\beta_r}{2}}^{\frac{\beta_r}{2}} f\,G(f)\sin(\pi f \delta)\mathrm{d}f\right]^2}\left[1+\frac{1}{\frac{C}{N_0}T_I\int_{-\frac{\beta_r}{2}}^{\frac{\beta_r}{2}} G(f)\mathrm{d}f}\right] \tag{4.189}$$

which simplifies for the case that an infinite receiver bandwidth is assumed, yielding:

$$\sigma^2_{\mathrm{EMLP}} = \frac{B_L\left(1-\frac{1}{2}B_L T_I\right)\delta}{2\alpha\frac{C}{N_0}}\left[1+\frac{2}{(2-\delta\alpha)\frac{C}{N_0}T_I}\right] \tag{4.190}$$

$$\sigma^2_{\mathrm{DP}} = \frac{B_L\left(1-\frac{1}{2}B_L T_I\right)\delta}{2\alpha\frac{C}{N_0}}\left[1+\frac{1}{\frac{C}{N_0}T_I}\right] \tag{4.191}$$

where α is the slope of the autocorrelation function around the main peak. The above derived expressions are in consonance with the results obtained in [L. Ries et al., 2003] and

[O. Julien, 2005] and confirm the fact that depending on the slope of the autocorrelation function of the signal waveform around the main peak, the tracking performance and achievable sensitivity will be better or worse, as we expected. Indeed, the steeper the autocorrelation function around the main peak is, the better the performance of the signal will be in terms of standard error. This result underlines the conclusions that we drew in chapter 4.1.1 on how an optimized signal should be designed.

Additionally, we can see from the expressions above that if an infinite front-end filter bandwidth is assumed, the squaring losses for the Dot Product (DP) discriminator do not depend on the signal structure any more, while for case of the Early Minus Late Power (EMLP) discriminator they do depend, being these larger the steeper the autocorrelation function around the main peak.

If we take a look now at Figure 4.59 next, we can recognize that while the GPS C/A code presents a slope value of $\alpha = 1$, for BOC(1,1) the slope around the main peak is of $\alpha = 3$, resulting thus in an improvement of the tracking error standard deviation of 2.4 dB approximately (without accounting for the squaring effects).

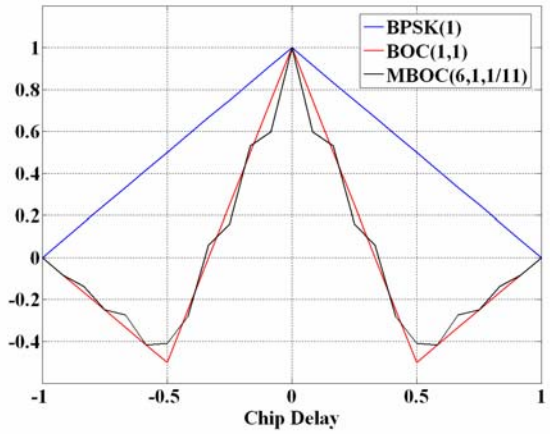

Figure 4.59. Autocorrelation Function of BPSK(1), BOC(1,1) and MBOC(6,1,1/11)

The improvement is still more spectacular if we take a look at the MBOC autocorrelation function, where the average slope around the main peak, considering data and pilot together, is shown to be 53/11. This represents an improvement of the tracking performance of approximately 1.03 dB with respect to BOC(1,1) and of 3.41 dB with respect to BPSK(1). The slope of the main peak can be easily computed from (4.149).

In fact, the slope of the autocorrelation function of BOC(6,1) takes a value of 23 around the main peak for infinite bandwidth. Equally, for BOC(1,1) the slope has a value 3 and the resulting slope of MBOC around the main peak will be $23 \cdot 1/11 + 3 \cdot 10/11 = 53/11$. In general, the slope of the main peak of a BOC(x,1) is shown to be $4x - 1$ for the case of infinite bandwidth. It is important to note that the MBOC ACF shown above (CBOC implementation) corresponds to the mean ACF that results from averaging the data and pilot channel. In the

case that both data and pilot would alternate the phase of the BOC(6,1) signal every chip, a similar result could be obtained. For the TMBOC case, it would represent the case when BOC(6,1) is on both data and pilot with the same power on both. This is equivalent to saying that the cross-correlation between BOC(1,1) and BOC(6,1) does not show up in the figures above since they average to zero.

We can see this more clearly if we recall the equations derived in chapter 4.6 for the CBOC implementation of MBOC. Indeed,

$$R_{\mathrm{CBOC('+/-')}}(\tau) = k_1^2 \, R_{\mathrm{BOC(1,1)}}(\tau) + k_2^2 \, R_{\mathrm{BOC(6,1)}}(\tau) \tag{4.192}$$

so that the cross-term between the BOC(1,1) and BOC(6,1) does not appear in the expression, unlike for the $\mathrm{CBOC}('+')$ and $\mathrm{CBOC}('-')$ cases.

If we take a look now into the performance of the data and pilot channels separately, we can see that for the case of GPS L1C, the TMBOC implementation of MBOC puts all the high frequency power on the pilot channel for tracking purposes. This results in a steeper slope of the autocorrelation function around the main peak. Recalling the GPS power split between data and pilot of 25/75 in L1C, the slope will have a value of $23 \cdot 4/33 + 3 \cdot 29/33 = 179/33$, bringing thus an improvement for the pilot channel of approximately 3.67 dB with respect to BPSK(1) and of 1.28 dB with respect to BOC(1,1). On the other hand, the data channel will present a performance equivalent to that of BOC(1,1).

Equivalently, its counterpart Galileo will have a performance 3.41 dB better than BPSK(1) and will be 1.03 dB better than BOC(1,1) since BOC(6,1) is placed on both data an pilot with a power split 50/50. This can also be seen if we take a look at the ACFs of the data and pilot channels separately.

Finally, it is important to note that although MBOC(6,1,1/11) and BOC(1,1) present improved performance with respect to BPSK(1), the tracking region is smaller if we track the whole MBOC. In fact, the linear region around the main peak will be six times narrower.

4.7.7.4 Signal structure and DLL sensitivity

Now that we have calculated the code tracking error for MBOC and the rest of Open signals in E1, the next step is to obtain the necessary C/N_0 to ensure a correct tracking. This will give us an idea of the potential DLL sensitivity of the different analyzed signal structures.

Following [P. Ward, 1996] and [O. Julien, 2005] to study the PLL sensitivity, the rule of thumb we will use is to have a 3-sigma of the errors within the linear tracking region, which is in theory $\pm \frac{\delta}{2}$. This can also be expressed as follows:

$$3\sigma_{\varepsilon_\tau,\mathrm{TH}} \leq \frac{\delta}{2} \tag{4.193}$$

It must be noted that actually not all the errors are included in the expression above, and thus the multipath-induced tracking error must be studied separately. The reason for this is that the multipath error does not imply a tracking error in the sense that it would push the tracking loop away from its stability point as explained in detail in [O. Julien, 2005].

Recalling now the equations for the tracking error of (4.190) and (4.191) above, we can see that (4.190) can be simplified for the EMLP as follows:

$$\sigma^2_{\text{EMLP}} = \frac{A_1}{\frac{C}{N_0}}\left[1+\frac{1}{\frac{C}{N_0}A_2}\right] \tag{4.194}$$

where

$$A_1 = \frac{B_L\left(1-\frac{1}{2}B_L T_I\right)\int_{-\frac{\beta_r}{2}}^{\frac{\beta_r}{2}} G(f)\sin^2(\pi f \delta)\mathrm{d}f}{\left[2\pi\int_{-\frac{\beta_r}{2}}^{\frac{\beta_r}{2}} f\, G(f)\sin(\pi f \delta)\mathrm{d}f\right]^2} \tag{4.195}$$

and

$$A_2 = \frac{T_I\left[2\pi\int_{-\frac{\beta_r}{2}}^{\frac{\beta_r}{2}} G(f)\cos(\pi f \delta)\mathrm{d}f\right]^2}{\int_{-\frac{\beta_r}{2}}^{\frac{\beta_r}{2}} G(f)\cos^2(\pi f \delta)\mathrm{d}f} \tag{4.196}$$

Equally for the Dot Product Discriminator, (4.191) can also be expressed as:

$$\sigma^2_{\text{DP}} = \frac{A_1}{\frac{C}{N_0}}\left(1+\frac{1}{\frac{C}{N_0}A_3}\right) \tag{4.197}$$

with

$$A_3 = T_I\int_{-\frac{\beta_r}{2}}^{\frac{\beta_r}{2}} G(f)\mathrm{d}f \tag{4.198}$$

According to this, if we assume as mentioned above that $3\sigma_{\varepsilon_\tau,\text{TH}} \le \delta/2$ for the case of the EMLP discriminator, the EMLP tracking threshold results to be:

$$\left.\frac{C}{N_0}\right|_{\text{TH,DP}} = 18\,A_1\frac{\left(1+\sqrt{1+\frac{\delta^2}{9A_1A_2}}\right)}{\delta^2} \tag{4.199}$$

and for the DP we have equally:

$$\left.\frac{C}{N_0}\right|_{\text{TH,DP}} = 18\,A_1\frac{\left(1+\sqrt{1+\frac{\delta^2}{9A_1A_3}}\right)}{\delta^2} \tag{4.200}$$

Using the expressions above, the tracking thresholds are computed in the next figures as a function of the coherent integration time and the DLL loop bandwidth. For the case of infinite

bandwidth the expressions for the standard delay error simplify considerably adopting A_1, A_2 and A_3 the following values:

$$A_1 = \frac{B_L\left(1-\frac{1}{2}B_L T_I\right)\delta}{2\alpha} \tag{4.201}$$

$$A_2 = \frac{(2-\delta\alpha)T_I}{2} \tag{4.202}$$

$$A_3 = T_I \tag{4.203}$$

For comparison, a spacing of 0.1 chips (left) and a spacing of 0.2 chips (right) will be used.

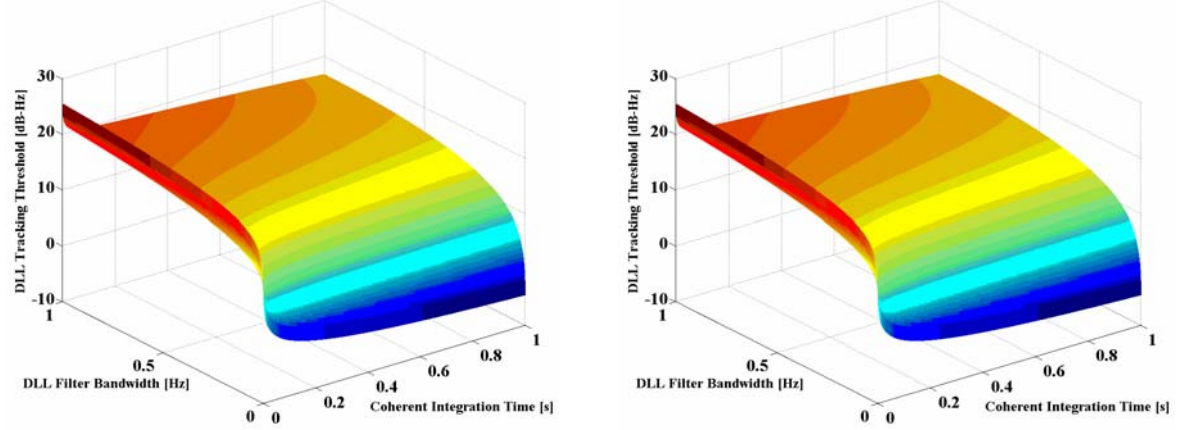

Figure 4.60. DLL Tracking Threshold of BPSK(1) for the DP Discriminator

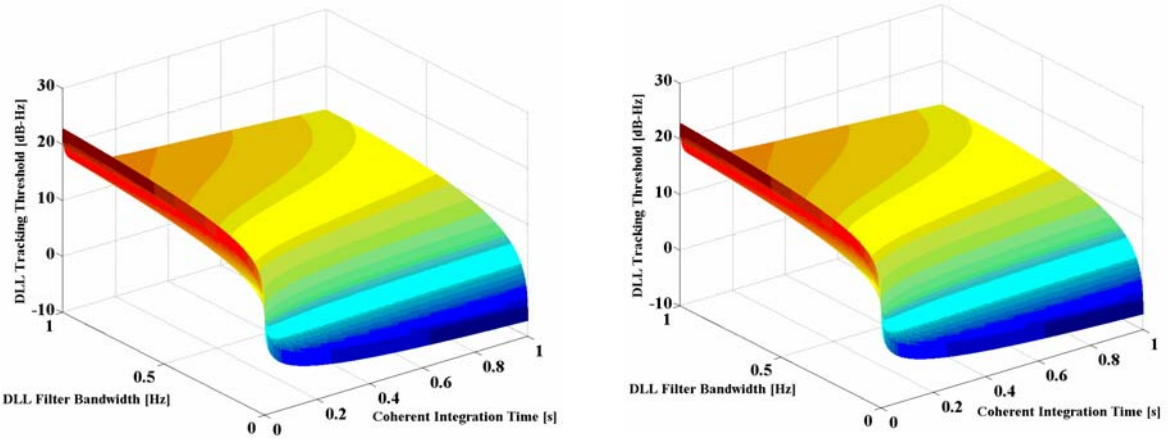

Figure 4.61. DLL Tracking Threshold of BOC(1,1) for the DP Discriminator

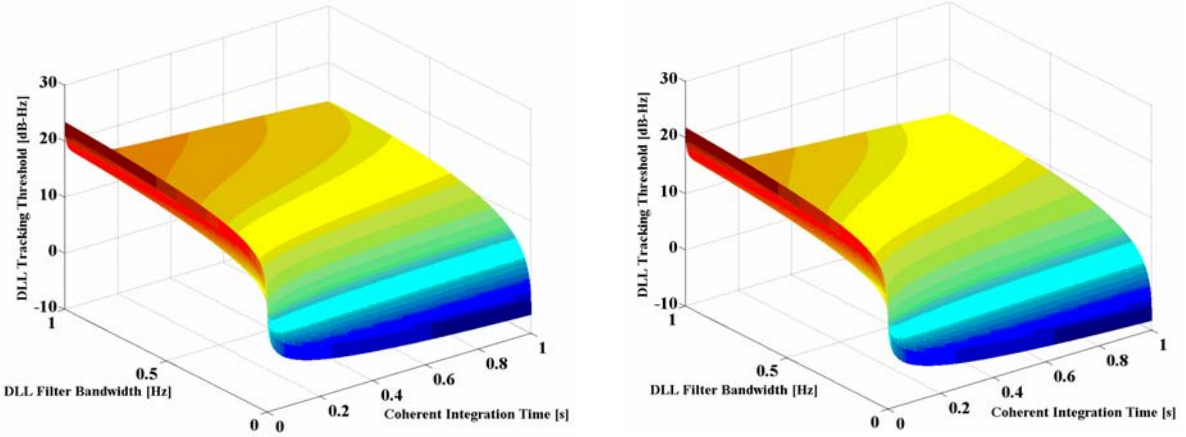

Figure 4.62. DLL Tracking Threshold of MBOC(6,1,1/11) for the DP

As we can recognize, using a chip spacing of 0.1 or 0.2 chips does not really make a big difference.

If we take a close look at the results shown in the figures above, we can see that MBOC presents the lowest tracking threshold and thus the best sensitivity, followed by BOC(1,1) and BPSK(1). It is also interesting to see that the results of the simulations show an even higher improvement of the C/N_0 sensitivity of MBOC with respect to BOC(1,1) and BPSK(1) than that predicted in chapter 4.7.7.3. Indeed, while we saw there that MBOC was expected to have a tracking threshold 1 dB lower than that of BOC(1,1) and 3.4 dB better with respect to BPSK(1), the results of the figures above account for higher improvements. This could be due to filtering effects in the loop bandwidth and coherent integration that are not reflected in the analytical expressions for infinite bandwidth and that would positively favour MBOC against the other studied options.

Another important comment is that for the simulation of MBOC, a slope of 53/11 was assumed around the main peak. This is actually the average of data and pilot as we saw above. If we concentrate on the pilot performance of GPS L1C, the slope will be steeper since it has all the BOC(6,1) contribution, and even better results are expected.

In order to be able to compare the three signals more efficiently, the next figures show again the tracking thresholds for specific DLL configurations and chip spacing values.

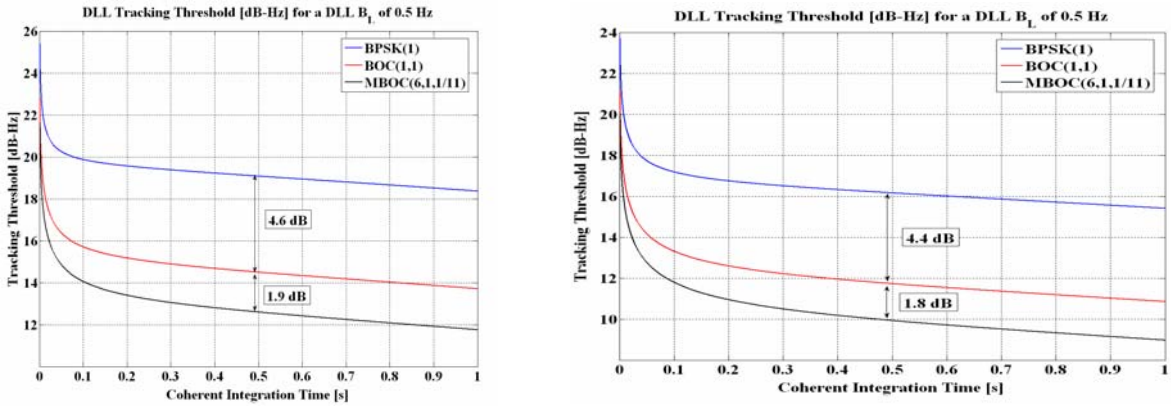

Figure 4.63. DLL tracking threshold for the DP Discriminator with a DLL loop bandwidth of 0.5 Hz and a chip spacing of δ=0.1 (left) and δ=0.2 (right)

It is interesting to note that for a coherent integration time of 0.5 seconds and a spacing of 0.1 chips, the improvement in sensitivity of BOC(1,1) and MBOC(6,1,1/11) with respect to BPSK(1) is even more spectacular. Indeed, BOC(1,1) performs approximately 4.6 dB better than BPSK(1), while MBOC outperforms BPSK(1) by 6.5 dB.

If we repeat the figures above for a DLL loop bandwidth of 0.1 Hz, we can see that although the difference in sensitivity of the various signals reduces, for a coherent integration of 0.5 seconds and a spacing of 0.1 chips, BOC(1,1) is still 4.2 dB better than BPSK(1) and MBOC(6,1,1/11) approximately 1.7 dB better than BOC(1,1).

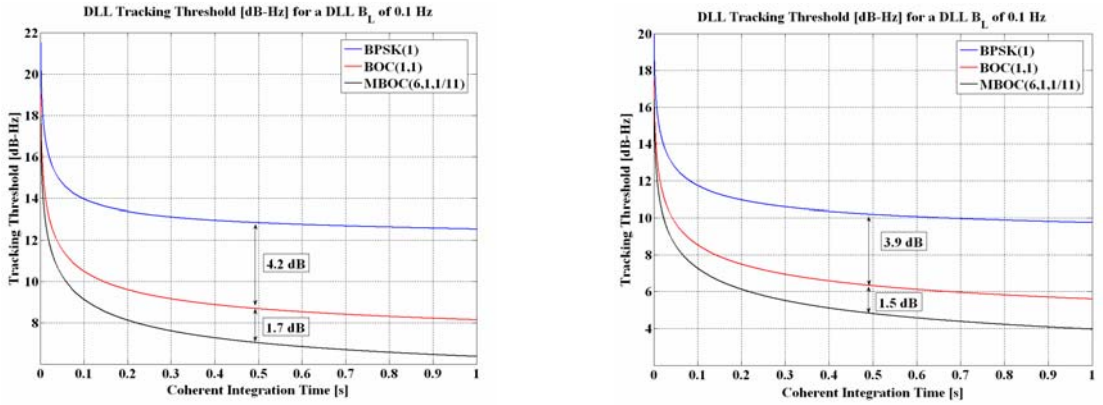

Figure 4.64. DLL tracking threshold for the DP Discriminator with a DLL loop bandwidth of 0.1 Hz and a chip spacing of δ=0.1 (left) and δ=0.2 (right)

Once the sensitivity performance of the different signals has been compared as a function of the DLL loop bandwidth and the spacing, the next step is to assess the behaviour of these signals as a function of the coherent integration time.

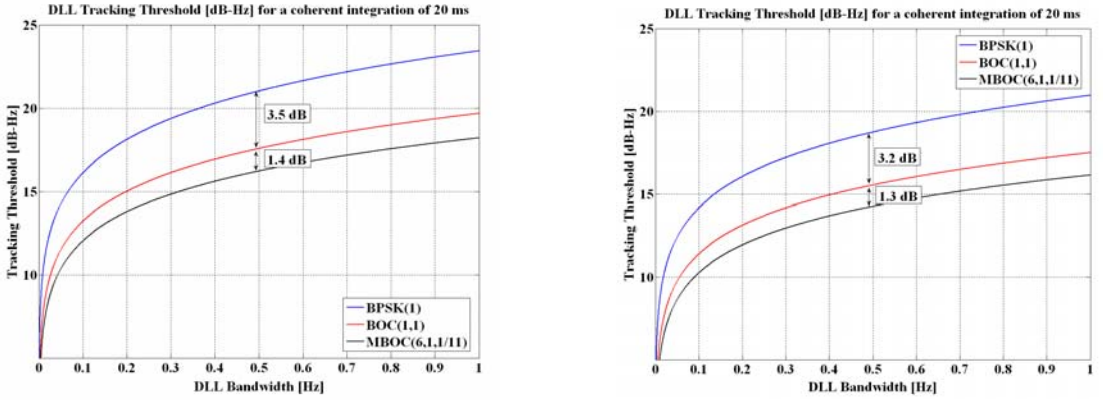

Figure 4.65. DLL tracking threshold for the DP Discriminator with a coherent integration time of 20 ms and a chip spacing of δ=0.1 (left) and δ=0.2 (right)

As we can see, for a DLL loop bandwidth of 0.5 Hz and a chip spacing of 0.1, BOC(1,1) has a sensitivity approximately 3.5 dB higher than that of BPSK(1) while MBOC(6,1,1/11) is better than BOC(1,1) by 1.4 dB.

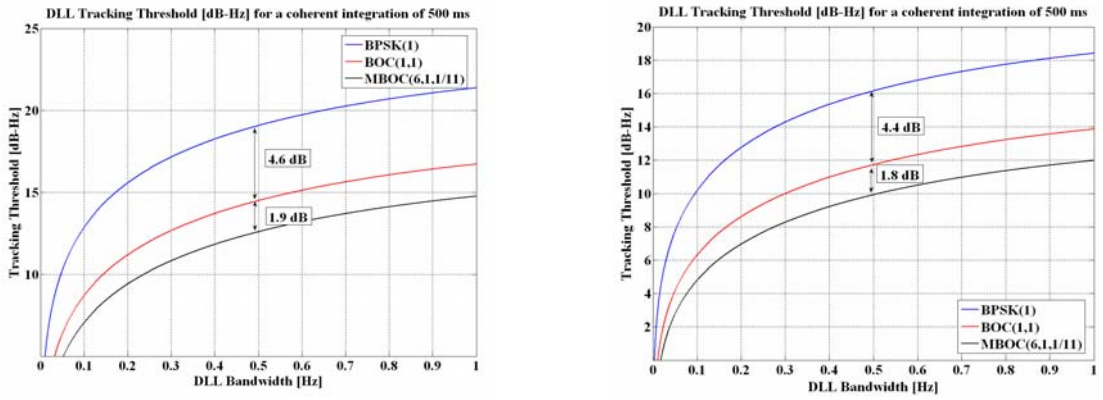

Figure 4.66. DLL tracking threshold for the DP Discriminator with a coherent integration time of 500 ms and a chip spacing of δ=0.1 (left) and δ=0.2 (right)

Furthermore, when the coherent integration time is increased to 500 ms, the sensitivity improvement of BOC(1,1) turns to be even clearer, resulting in a improvement of approximately 4.6 dB for BOC(1,1) with respect to BPSK(1) and of 1.9 dB for MBOC with respect to BOC(1,1).

From the figures above we can clearly recognize that the tracking threshold decreases as the integration time increases and the DLL loop bandwidth decreases. We can also see that the obtained values seem to be very low compared to those obtained in real applications. However, it must be noted that ideal conditions were assumed in the simulations.

The following tables summarize the results for a chip spacing of 0.1 chips with DP and EMLP discriminators. Similar tables could have also been derived for a spacing of 0.2 chips showing always the superiority of MBOC against BOC(1,1) and C/A Code.

Table 4.6. DLL Tracking Threshold [dB-Hz] using the DP discriminator δ= 0.1 chips

DP discriminator		DLL Tracking Threshold [dB-Hz]			
		Loop bandwidth [Hz]			
Coherent integration time [ms]	**Signal**	**0.1**	**0.25**	**0.5**	**1**
10	**BPSK(1)**	17.1896	19.6931	21.7531	23.9894
	BOC(1,1)	14.4201	16.7131	18.5537	20.5185
	MBOC(6,1,1/11)	13.2798	15.5096	17.2816	19.1553
20	**BPSK(1)**	16.0525	18.7428	20.9791	23.4025
	BOC(1,1)	13.1316	15.5434	17.5082	19.6268
	MBOC(6,1,1/11)	11.9461	14.2713	16.1450	18.1493
100	**BPSK(1)**	13.9894	17.2301	19.8594	22.5642
	BOC(1,1)	10.5185	13.3552	15.6970	18.1742
	MBOC(6,1,1/11)	9.1553	11.8369	14.0460	16.3974
500	**BPSK(1)**	12.8697	16.4445	19.0688	21.3663
	BOC(1,1)	8.7073	11.9971	14.4897	16.7134
	MBOC(6,1,1/11)	7.0563	10.1846	12.5878	14.7558
1000	**BPSK(1)**	12.5642	16.0585	18.3560	19.5899
	BOC(1,1)	8.1742	11.4794	13.7031	14.9092
	MBOC(6,1,1/11)	6.3974	9.5775	11.7455	12.9294

Once we have computed the DLL tracking threshold for the case of infinite bandwidth, the next step should be to employ different assumptions on the receiver bandwidth. Different configurations have been analyzed delivering however similar results to those provided in previous lines.

The previous results show the ideal sensitivity values when all the potential sources of error are eliminated. As we know, increasing the total integration time does not only require extra complexity but implies other real challenges. Indeed, there are several problems inherent to longer coherent integration times, which are mainly related to the fact that the longer the coherent integration is, the more likely it will be that the signal conditions change during the integration period. Among others, the existence of frequency errors, non-ideal normalizations in the discriminator and the change of signal power during the integration would be the main sources of additional errors. They were not considered in the simulations above, since we are interested here in finding the theoretical limit, no matter how this is realized in reality. The same comment applies for the normalization of the discriminator. In fact, as explained in [O. Julien, 2005], the effect of normalization in the discriminator would be another factor to take into account for more realistic simulations.

Table 4.7. DLL Tracking Threshold [dB-Hz] for an EMLP discriminator with δ= 0.1

EMLP discriminator with a spacing of 0.2 chips		**DLL Tracking Threshold [dB-Hz]**			
		Loop bandwidth [Hz]			
Integration time [ms]	**Signal**	**0.1**	**0.25**	**0.5**	**1**
10	**BPSK(1)**	17.2781	19.7695	21.8173	24.0394
	BOC(1,1)	14.7318	17.0015	18.8170	20.7487
	MBOC(6,1,1/11)	13.8245	16.0236	17.7618	19.5899
20	**BPSK(1)**	16.1323	18.8070	21.0291	23.4380
	BOC(1,1)	13.4266	15.8067	17.7384	19.8161
	MBOC(6,1,1/11)	12.4688	14.7515	16.5796	18.5248
100	**BPSK(1)**	14.0394	17.2612	19.8788	22.5755
	BOC(1,1)	10.7487	13.5301	15.8260	18.2612
	MBOC(6,1,1/11)	9.5899	12.1906	14.3255	16.6008
500	**BPSK(1)**	12.8891	16.4539	19.0742	21.3695
	BOC(1,1)	8.8363	12.0725	14.5367	16.7432
	MBOC(6,1,1/11)	7.3358	10.3650	12.7075	14.8350
1000	**BPSK(1)**	12.5755	16.0639	16.0639	19.5924
	BOC(1,1)	8.2612	11.5264	13.7329	14.9323
	MBOC(6,1,1/11)	6.6008	9.6972	11.8247	12.9918

The figures obtained above extend over very long coherent integrations. In fact, no data channel could in reality reach such values unless external sources were used, what shows clearly the superiority of the pilot channel for these purposes. Indeed, the introduction of pilot channels by Galileo and the modernized GPS can be considered as one of the main contributions to the navigation. Navigation and communication applications require of different needs and the use of pilot signals in GNSS in the future is clear proof of that.

4.7.8 MBOC Interference with other GNSSes

Interoperability and compatibility have been hot issues in the design of Galileo since the beginning. Indeed, as more systems join the select club of countries with their own navigation system, the more important these concepts have become. As we have seen in chapter 2, the global system of systems that GPS, GLONASS, Galileo, the Japanese Quasi Zenith Satellite System (QZSS), the Chinese Compass and the Indian Regional Navigation Satellite System (IRNSS) might become one day makes this chapter of major interest.

As defined in, [S. Wallner et al., 2005] and [S. Wallner et al., 2006] and, interoperability refers to the *ability of civil U.S. and foreign space-based PNT services to be used together to provide better capabilities compared with those that would be achieved relying solely on one service or signal*.

In June 2004, the United States and the European Union signed a historical Agreement on the common use of shared frequencies, setting up a complete methodology to assess the GPS/Galileo radio frequency compatibility. More details on the theoretical framework can be found in Appendix M. Based on the mathematical ideas gathered in the work, [S. Wallner et al., 2005] have carried out simulations with smooth spectra and with real codes. According to the results, the degradation from GPS on Galileo and of Galileo on GPS is lower than 0.25 dB proving thus that both systems can perfectly coexist. Moreover, the introduction of QZSS will lead to an increase of the intersystem interference in the visibility region of QZSS that will never be higher than 0.07 dB. We show next the degradation values for BOC(1,1) when the analytical model is employed.

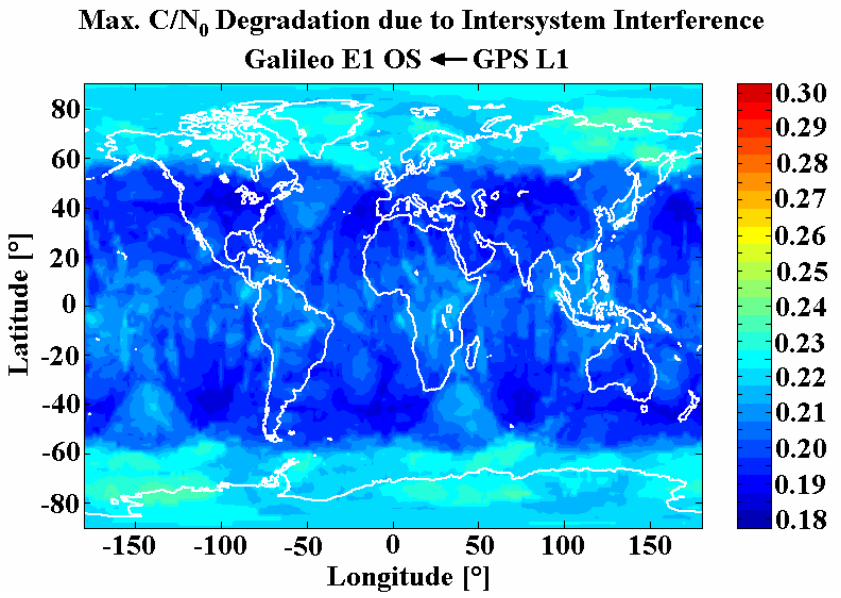

Figure 4.67. Maximum C/N_0 Degradation due to Intersystem Interference caused by the GPS L1 Signals on Galileo [S. Wallner et al., 2005]. Minimum: 0.186 dB, mean 0.214 dB and maximum 0.243 dB

If the same model is applied to the MBOC baseline, we can see that this contributes to an easier compatibility since the interference reduces in all considered scenarios. In fact, for average scenarios the typical figures are far lower than the 0.25 dB mentioned above.

The additional reduction of interference that MBOC provides is direct consequence of the better Spectral Separation Coefficients (SSC) of the signal. This confirms the great importance of this instrument to assess the degradation and overlapping among different signals. In the next figure we show the reduction of the maximum C/N_0 degradation that resulted from changing the baseline from BOC(1,1) to the final MBOC(6,1,1/11).

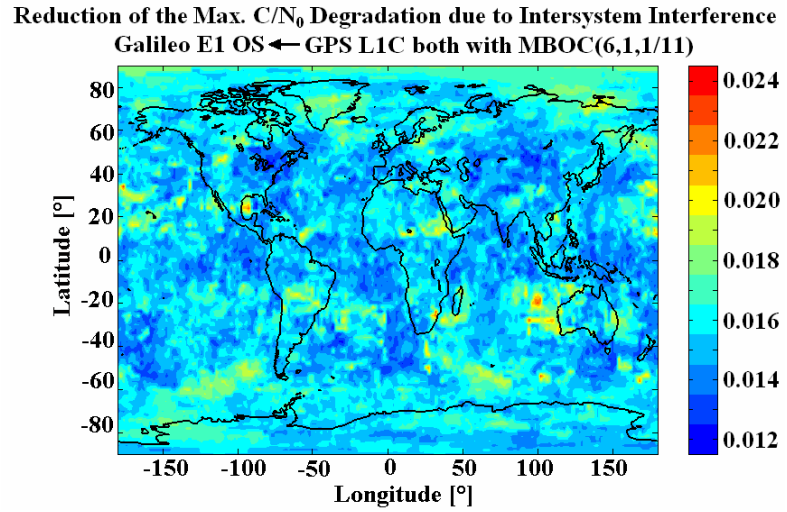

Figure 4.68. Reduction of the maximum C/N_0 Degradation due to Intersystem Interference when MBOC is used instead of BOC(1,1) [S. Wallner et al., 2005]. Minimum: 0.016 dB, mean 0.018 dB and maximum 0.023 dB

Equally, if we include the effect of QZSS, the following results are obtained.

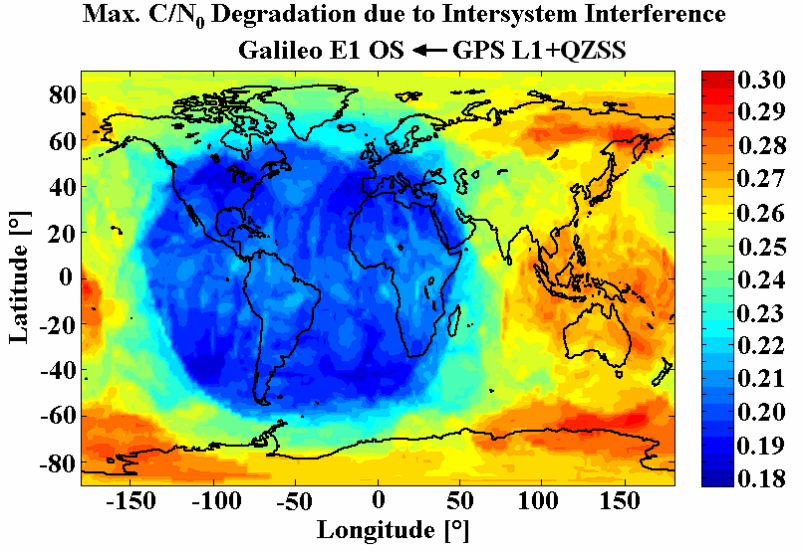

Figure 4.69. Maximum C/N_0 Degradation due to Intersystem Interference caused by the GPS L1 and QZSS Signals on Galileo [S. Wallner et al., 2005]. Minimum: 0.187 dB, mean 0.247 dB and maximum 0.310 dB

The mathematical framework of the methodology described in Appendix M can be easily expanded to other bands as for example E5-L5 or to other SBAS systems as done in [S. Wallner et al., 2005] where the results with smooth spectra and real codes were compared. One final comment on the figures above is that the minimum power levels were used for the simulations resulting thus in significantly higher values of interference than those we will observe in a typical scenario. Nonetheless, it must be kept in mind that the purpose of an interference methodology is to assess compatibility in all the cases, and therefore looking at the worst cases is thus of major interest.

4.8 Other Modulation Schemes

4.8.1 AltBOC Modulation

The Alternative BOC modulation (AltBOC) is conceptually very similar to the BOC modulation but with an important difference, since contrary to BOC, AltBOC provides high spectral isolation between the two upper main lobes and the two lower main lobes (considering the I and Q phases separately). This is accomplished by using different codes for each main lobe. We can clearly see this if we remember how single band processing works [J. W. Betz, 1999]. Indeed, any BOC signal could be correlated with a BPSK replica having as chip rate the sub-carrier frequency of the original BOC signal. Of course the prize is the loss of power, but processing the upper or lower main lobe would make no difference since both are modulated with the same PRN code. On the other hand, if we would do the same with the AltBOC signal, we could still receive each main lobe separately since different codes would be needed. This is very interesting because AltBOC allows thus keeping the BOC implementation simple while permitting to differentiate the lobes [E. Rebeyrol et al., 2005]. Similar to the BOC modulation, for simplicity the AltBOC modulation is generally referred to as AltBOC(f_s, f_c) with $f_s = m \cdot 1.023$ and $f_c = n \cdot 1.023$ so that commonly one only says AltBOC(m, n) for simplicity.

The Alternative BOC modulation uses a *complex* sub-carrier so that the spectrum is not split up, as is the case of BOC, but simply shifted to higher or lower frequencies. We already analyzed in chapter 4.3.2 the problematic of using different conventions to represent the BOC signals, and indeed the same conclusions are also valid here for the AltBOC modulation. In order to avoid this, we will make use of the definition presented in [L. Ries et al., 2003] where the AltBOC signal is defined as the product of a PRN code sequence with a complex sub-carrier. This convention covers even and odd ratios with no necessary modification.

The AltBOC signal can be formed by two (only data signals) or four codes (data and pilot). If we have only two codes, the signal is composed of only data and can be expressed as follows:

$$s_{\text{AltBOC}}(t) = c_L \, c_s(t) + c_U \, c_s^*(t) \tag{4.204}$$

where $c_s(t)$ is the complex sub-carrier, complex sum of the rectangular cosine and sine-phased rectangular waveform. As we can see, this is the binary version of the complex exponential function and can be defined as follows

$$c_s(t) = \text{sign}\left[\cos\left(2\pi f_s t\right)\right] + j\,\text{sign}\left[\sin\left(2\pi f_s t\right)\right] = c_r(t) + j\,s_r(t) \tag{4.205}$$

where c_L and c_U are the lower and upper codes respectively. As we can recognize from (4.204), what we are basically doing by multiplying the lower code and the upper code by the complex sub-carrier and its conjugate is approximately to shift the lower code to $-f_s$ and the upper code to $+f_s$. In fact, this would be the case if we would multiply with the exponential function:

$$e^{j2\pi f_s t} = \cos\left(2\pi f_s t\right) + j\sin\left(2\pi f_s t\right) \tag{4.206}$$

Although not exactly the same, the binary complex function is indeed a good approximation. Furthermore, AltBOC can be seen as a particular case of MCS with complex chip waveform. The following figure shows the spectrum (in units of Watts) of the complex sub-carrier and its conjugate. As we can see, most of the power is concentrated at the coefficients +1 and -1 and only the first 10 negative and positive coefficients are depicted in the figure (a repetition interval of 20 samples was assumed for the simulation). It is important to note that +1 and -1 corresponds in general to $+f_s$ and $-f_s$ after normalizing by the repetition period of the exponential function. Moreover, we can recognize that the spectrum, indeed the square of the Fourier coefficients $\|c_k\|^2$, is normalized to integrate to 2 W of power.

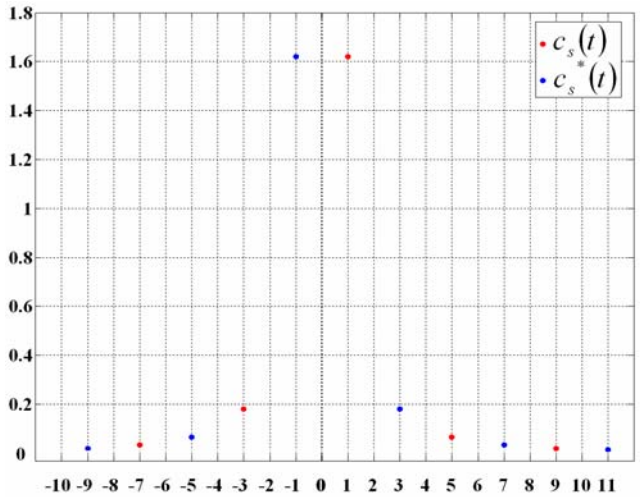

Figure 4.70. Spectrum $\|c_k\|^2$ [W] of the complex sub-carrier

If we add now the pilot channel to the definition, the general expression of the AltBOC modulation will adopt the following form:

$$s_{\text{AltBOC}}(t) = \left(c_L^D + j\,c_L^P\right)c_s(t) + \left(c_U^D + j\,c_U^P\right)c_s^*(t) \tag{4.207}$$

where c_L^D is the data lower code, c_L^P the pilot lower code, c_U^D the data upper code and c_U^P the pilot upper code.

The signal defined above corresponds to the general case of the AltBOC modulation. The only problem is that by introducing a complex sub-carrier and complex codes for the data and pilot channels, the composite signal looses the constant envelope that the original BOC modulation possessed. As we have seen when we analyzed the MBOC modulation, having a constant envelope is a must since otherwise the distortion caused by the High Power Amplifier (HPA) in the satellite would not be tolerable.

In order to solve this problem, a constant envelope modified version of the AltBOC modulation was presented in [J. Godet, 2001]. The idea behind is to bring the phase points of the constellation back to the circle so that the amplitude of the envelope remains constant. This is achieved by introducing a new signal called Inter-Modulation (IM) product whose new terms do not contain any usable information. The modified constant envelope AltBOC [M. Soellner et al., 2003] and [E. D. Kaplan and C. Hegarty, 2006], yields:

$$s_{\text{AltBOC}}(t) = \begin{cases} \left(c_L^D + j\,c_L^P\right)\left[sc_d(t) - j\;sc_d\left(t - \frac{T_s}{4}\right)\right] + \\ \left(c_U^D + j\,c_U^P\right)\left[sc_d(t) + j\;sc_d\left(t - \frac{T_s}{4}\right)\right] + \\ \left(\overline{c_L^D} + j\,\overline{c_L^P}\right)\left[sc_p(t) - j\,sc_p\left(t - \frac{T_s}{4}\right)\right] + \\ \left(\overline{c_U^D} + j\,\overline{c_U^P}\right)\left[sc_p(t) + j\,sc_p\left(t - \frac{T_s}{4}\right)\right] \end{cases} \tag{4.208}$$

where T_s is the period of the sub-carrier. Moreover,

$$\overline{c_L^D} = c_U^P\,c_U^D\,c_L^P \qquad \overline{c_L^P} = c_U^D\,c_U^P\,c_L^D \qquad \overline{c_U^D} = c_L^D\,c_U^P\,c_L^P \qquad \overline{c_U^P} = c_U^D\,c_L^D\,c_L^P \tag{4.209}$$

and the following data and pilot sub-carriers

$$sc_d(t) = \left\{\frac{\sqrt{2}}{4}\text{sign}\left[\cos\left(2\pi f_s t - \frac{\pi}{4}\right)\right] + \frac{1}{2}\text{sign}\left[\cos\left(2\pi f_s t\right)\right] + \frac{\sqrt{2}}{4}\text{sign}\left[\cos\left(2\pi f_s t + \frac{\pi}{4}\right)\right]\right. \tag{4.210}$$

$$sc_p(t) = \left\{-\frac{\sqrt{2}}{4}\text{sign}\left[\cos\left(2\pi f_s t - \frac{\pi}{4}\right)\right] + \frac{1}{2}\text{sign}\left[\cos\left(2\pi f_s t\right)\right] - \frac{\sqrt{2}}{4}\text{sign}\left[\cos\left(2\pi f_s t + \frac{\pi}{4}\right)\right]\right. \tag{4.211}$$

As we can see, while in our original conception the complex sub-carrier was composed of a cosine-phased rectangular signal for the real part and a sine-phased rectangular signal for the complex part, now both the real and complex part are a mixture of both sine and cosine delayed and early rectangular waveforms.

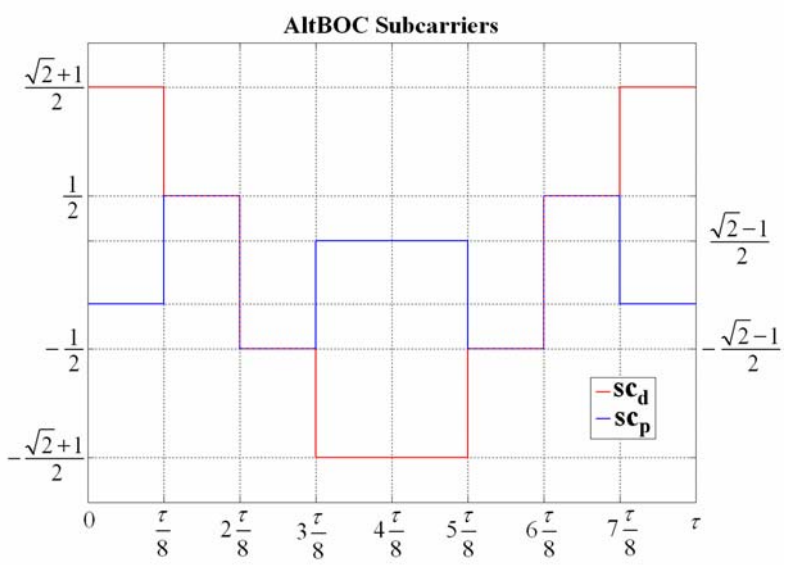

Figure 4.71. Shapes of data and pilot sub-carriers

Another interesting observation is that if we take a look at the phase plots of the constant envelope AltBOC signal, we can clearly recognize that it is a classical 8-PSK modulation with a non-constant allocation of the 8 phase-states.

As shown in Appendix I, the power spectral density for the modified even AltBOC modulation with constant envelope is shown to be:

$$G_{\text{AltBOC}}^{\Phi_{\text{even},c}}(f)=\frac{4f_c}{\pi^2 f^2}\frac{\sin^2\left(\frac{\pi f}{f_c}\right)}{\cos^2\left(\frac{\pi f}{2f_s}\right)}\left[\cos^2\left(\frac{\pi f}{2f_s}\right)-\cos\left(\frac{\pi f}{2f_s}\right)-2\cos\left(\frac{\pi f}{2f_s}\right)\cos\left(\frac{\pi f}{4f_s}\right)+2\right] \tag{4.212}$$

while for the odd case, we have:

$$G_{\text{AltBOC}}^{\Phi_{\text{odd},c}}(f)=\frac{4f_c}{\pi^2 f^2}\frac{\cos^2\left(\frac{\pi f}{f_c}\right)}{\cos^2\left(\frac{\pi f}{2f_s}\right)}\left[\cos^2\left(\frac{\pi f}{2f_s}\right)-\cos\left(\frac{\pi f}{2f_s}\right)-2\cos\left(\frac{\pi f}{2f_s}\right)\cos\left(\frac{\pi f}{4f_s}\right)+2\right] \tag{4.213}$$

Finally, it is important to underline that the AltBOC modulation in its most general form does not have a constant envelope as shown in Appendix I. As shown in chapter 7.7, due to the need to have a constant envelope, slight changes were made in the multiplexing scheme and the result was the modified AltBOC modulation that we have shown in the previous lines.

AltBOC can not only be understood as a signal waveform but also as a multiplexing scheme as those that we will see in chapter 7. The same comment is indeed also valid for the BOC modulation that we studied in previous chapters.

4.8.2 Square-Root Raised Cosine Signals (SRRC)

One of the main drawbacks of all the signal waveforms studied so far is that although they can very well control the power emissions within the bandwidth of interest, they send relatively high amounts of power out of this one. A practical way of reducing the side-lobes of the spectrum of the navigation signals could be to use a Raised Cosine Filter (RCF) since this has a limited bandwidth. The Raised Cosine Filter is a particular case of Nyquist filter and is defined in the frequency domain as follows

$$H_{\mathrm{RC}}(f)=\begin{cases}1 & \text{for } |f|<2W_0-W \\ \cos^2\left[\dfrac{\pi}{4}\dfrac{|f|+W-2W_0}{W-W_0}\right] & \text{for } 2W_0-W<|f|<W \\ 0 & \text{for } |f|>W\end{cases} \tag{4.214}$$

where $W-W_0$ is defined as the excess bandwidth and indicates how much the spectrum of the Raised Cosine spills over a given bandwidth W_0. As we know, Nyquist pulses (filters) are pulses that result in no Inter Symbol Interference (ISI) at the sampling time. The Nyquist pulse-shaping criterion or Nyquist condition for zero ISI is fulfilled if

$$x(kT_c)=\delta(k) \tag{4.215}$$

where

$$\delta(k)=\begin{cases}1 & k=0 \\ 0 & k\neq 0\end{cases} \tag{4.216}$$

Indeed, this is a necessary and sufficient condition which can also be expressed as follows:

$$\sum_{m=-\infty}^{\infty} X\left(f+\frac{m}{T_c}\right)=T_c \tag{4.217}$$

where $X(f)$ is the Fourier transform of a generic signal $x(t)$ and T_c the time period of the pulse. The Raised Cosine filter that we described some lines above has an equivalent representation in the time domain. This is shown to be:

$$h_{\mathrm{RC}}(t)=2W_0\,\mathrm{sinc}(2W_0t)\frac{\cos[2\pi(W-W_0)t]}{1-[4(W-W_0)t]^2} \tag{4.218}$$

Another way of expressing the excess bandwidth is by means of the roll-off factor, which is defined as follows:

$$\alpha=\frac{W-W_0}{W_0} \tag{4.219}$$

The roll-off factor indicates how much power the Raised Cosine emits above a given bandwidth W_0. Therefore $0\leq\alpha\leq 1$. This can be clearly seen in the following figure for different roll-off factors:

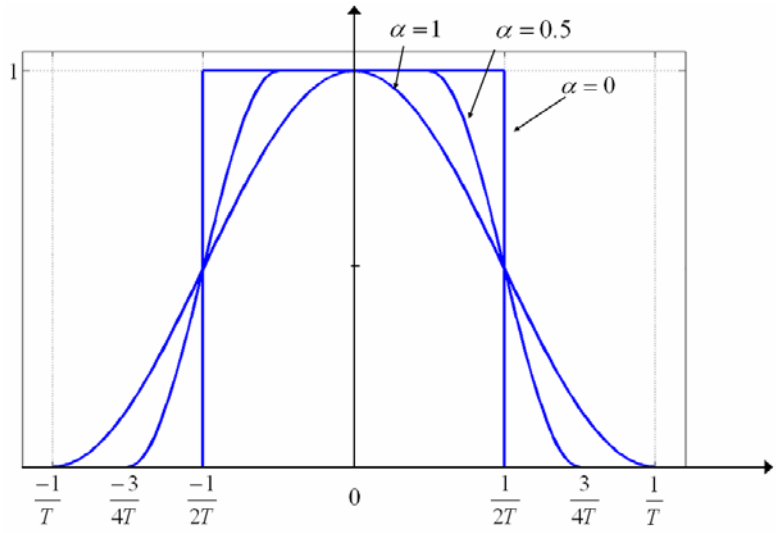

Figure 4.72. Raised Cosine Filter for different roll-off factors

We show next the time representation $h_{RC}(t)$ of the Raised Cosine pulses of the previous figure for different roll-off factors:

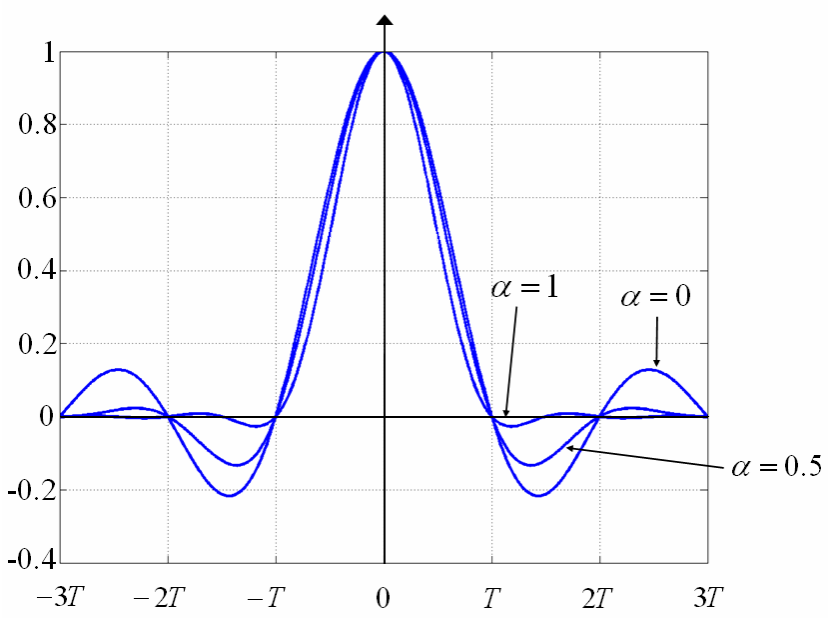

Figure 4.73. Raised Cosine pulses for different roll-off factors

As we can recognize, the raised cosine pulse waveform with the optimum spectrum occupation ($\alpha = 0$) is the pulse that also presents more oscillations in the time domain, what is a non desired characteristic in principle. In fact, low values of α allow for a more efficient use of the spectrum but increase the ISI. Moreover, we have to keep in mind that none of the filters of the figures above could correspond to a real implementation since they are not causal as $h(t) \neq 0$ for $t < 0$. To avoid this, a minimum delay should be added for the pulse to gain causality. Indeed, real implementations already add a delay of some chips from the moment the signal enters the filter and leaves it. This is observed in the Raised Cosine filters too.

It is important to note that a band-limited Nyquist pulse cannot avoid by itself the ISI unless the channel is ideal. This means that the RC pulses have got to be implemented together with an equalizer at the receiver for the correct identification of the symbols at the sampling time. We can express this in the following expression:

$$H_{\mathrm{RC}}(f) = H_{\mathrm{TX}}(f)H_{\mathrm{C}}(f)H_{\mathrm{RX}}(f)H_{\mathrm{E}}(f) \tag{4.220}$$

where $H_{\mathrm{TX}}(f)$ is the transmission filter, $H_{\mathrm{C}}(f)$ is the channel frequency response, $H_{\mathrm{RX}}(f)$ is the receiver filter and $H_{\mathrm{E}}(f)$ is the equalizer. The usual approach is to design the transmitter and receiver filters such that

$$\begin{aligned} H_{\mathrm{RC}}(f) &= H_{\mathrm{TX}}(f)H_{\mathrm{RX}}(f) \\ H_{\mathrm{TX}}(f) &= H_{\mathrm{RX}}(f) = \sqrt{H_{\mathrm{RC}}(f)} = H_{\mathrm{SRRC}}(f) \end{aligned} \tag{4.221}$$

and leave the equalizer filter to take care of the imperfections and ISI caused by the channel:

$$H_{\mathrm{E}}(f) = \frac{1}{H_{\mathrm{C}}(f)} \tag{4.222}$$

According to this, the square-root raised cosine (SRRC) pulses are Nyquist pulses of finite bandwidth with power spectral density given by:

$$G_{\mathrm{SRRC}}(\alpha, f) = \begin{cases} T_c & \|f\| \le \dfrac{1-\alpha}{2T_c} \\ \dfrac{T_c}{2}\left\{1+\cos\left[\dfrac{\pi T_c}{\alpha}\left(\|f\| - \dfrac{1-\alpha}{2T_c}\right)\right]\right\} & \dfrac{1-\alpha}{T_c} \le \|f\| \le \dfrac{1+\alpha}{2T_c} \\ 0 & \|f\| > \dfrac{1+\alpha}{2T_c} \end{cases} \tag{4.223}$$

Moreover, it can be shown that

$$\int_{-\infty}^{\infty} G_{\mathrm{SRRC}}(\alpha, f)\mathrm{d}f = 1 \tag{4.224}$$

where we can recognize that the bilateral bandwidth is finite and of value $(1+\alpha)/T_c$. In the same manner, the time representation of such SRRC pulses is shown to adopt the following form [E.A. Lee and D.B. Messerschmitt, 1994]:

$$s(t) = \frac{4\alpha}{\pi\sqrt{T_c}} \frac{\cos\left[\dfrac{(1+\alpha)}{T_c}\pi t\right] + \dfrac{T_c}{4\alpha t}\sin\left[\dfrac{(1-\alpha)}{T_c}\pi t\right]}{1-\left(\dfrac{4\alpha t}{T_c}\right)^2} \tag{4.225}$$

which is indeed a pulse shape with infinite support as we expected, since bandlimited signals extend to infinity in the time-domain. The interesting aspect of this waveform is that it satisfies the Nyquist condition for zero Inter-Symbol interference (ISI), so that the bit-error

probability is identical to that of BPSK with Non Return to Zero (NRZ) pulses if the receiver samples at zero-ISI locations.

In spite of its interesting properties, the Raised Cosine Signals proposed by [R. De Gaudenzi et al., 2000] for Galileo presented a series of major problems that made it not recommendable for satellite navigation applications:

- One of the most important disadvantages is the fact that the RC signal is handicapped from the beginning regarding its potential improvement of performance. We have seen that the SRRC modulation makes a very efficient use of the assigned spectrum. This remains true. However, the signal is by definition band-limited to a very narrow bandwidth so that the performance could never be as good as that of other signals sharing the band with wider bandwidths. A SRRC would have been maybe the best for a narrowband receiver of around 3 MHz as we commented in chapter 3 but Galileo would have lost the race in competitiveness as soon as other signals would have made use of wider bandwidths.
- Another consequence of the fact that the SRRC modulation is bandlimited is that its auto-correlation function has a very rounded peak. As we have seen at the beginning of this chapter, the quality of a signal improves as the slope of the ACF becomes steeper around the main peak. In the case of the Raised Cosine Signal no matter how wide the receiver bandwidth would be, we would not be able to do anything to improve the quality of our measurements. If there is something that technology shows us permanently, that is the fact that we cannot design systems thinking of today's limitations but we must challenge our potentials.
- As shown in [R. De Gaudenzi et al., 2000] the receiver complexity could have profited from simplified receivers with lower complexity. While this might be true, an inherent degradation would be introduced in the system per definition since the replica signals in the receivers would be band-limited and thus *handicapped*. Furthermore, techniques like the narrow correlator would have brought no improvement due to the band-limited property of the SRRC pulse.
- The Raised Cosine solutions that were proposed in [R. De Gaudenzi et al., 2000] presented another very serious inherent problem: namely a worse antijamming protection compared with other signals, due to its spectrum concentrated in a relatively narrow bandwidth. As we can see in Appendix M and in chapter 4.7.8, the more spread the frequency components of a signal are, the better the resistance against narrowband and wideband interference will be.
- Finally, the original proposal of [R. De Gaudenzi et al., 2000] did not contemplate the possibility of having a military signal as the PRS. Such a signal would need wide bandwidths per definition and using SRRC would have also implied important risks due to its weakness against all sources of interference.

4.8.3 Prolate Spheroidal Wave Functions (PSWF)

Another family of waveforms that have gained in interest in the past months is that of the so-called Prolate Spheroidal Wave Functions (PSWF). The PSWF family offers an infinite base of orthogonal functions $\{\psi_1(t),\psi_2(t),...,\psi_i(t),...\}$ with associated Eigenvalues $\{\lambda_1,\lambda_2,...,\lambda_i,...\}$ that are real and positive. Similar to the SRRC signal that we saw in the previous chapter, they also show ideal bandlimiting within $[-\beta_r/2,\beta_r/2]$, making the PSWF signals very interesting to fulfil stringent demands on band-limitation.

As the name well indicates, the Prolate Spheroidal Wave Functions are the result of solving the Helmholtz equation or wave equation in Prolate Spheroidal coordinates. This electromagnetic identity is shown to adopt the following form:

$$\Delta\varphi(x,y,z)+k^2\varphi(x,y,z)=0 \tag{4.226}$$

where k defines the wave number in prolate spheroidal coordinates. The Prolate Spheroidal coordinates can be expressed in Cartesian coordinates according to the following transformation [M. Abramovitz and I.A. Stegun, 1965]:

$$\begin{aligned} x &= f\sqrt{(1-\eta^2)(\xi^2-1)}\cos\phi \\ y &= f\sqrt{(1-\eta^2)(\xi^2-1)}\sin\phi \\ z &= f\eta\xi \end{aligned} \tag{4.227}$$

with

$$-1\le\eta\le 1,\ 1\le\xi\le\infty,\quad 0\le\phi\le 2\pi \tag{4.228}$$

where:

- f is the semifocal distance,
- η is the angular coordinate,
- ξ is the radial coordinate, and
- ϕ is the azimuthal coordinate.

Furthermore, the Laplace operator in the new coordinate system adopts the following form:

$$\Delta h=\frac{1}{h_\xi h_\eta h_\phi}\left[\frac{\partial}{\partial\xi}\left(\frac{h_\eta h_\phi}{h_\xi}\frac{\partial}{\partial\xi}\right)+\frac{\partial}{\partial\eta}\left(\frac{h_\xi h_\phi}{h_\eta}\frac{\partial}{\partial\eta}\right)+\frac{\partial}{\partial\phi}\left(\frac{h_\xi h_\eta}{h_\phi}\frac{\partial}{\partial\phi}\right)\right] \tag{4.229}$$

Thus the scalar wave equation can be written in prolate spheroidal coordinates as follows:

$$\Delta\psi+k^2\psi=\frac{\partial}{\partial\xi}\left[(\xi^2-1)\frac{\partial\psi}{\partial\xi}\right]+\frac{\partial}{\partial\eta}\left[(1-\eta^2)\frac{\partial\psi}{\partial\eta}\right]+\frac{\xi^2-\eta^2}{(\xi^2-1)(1-\eta^2)}\frac{\partial^2\psi}{\partial\phi^2}+c^2(\xi^2-\eta^2)\psi=0 \tag{4.230}$$

being $c=fk/2$ per definition. As it can be shown in [M. Abramovitz and I.A. Stegun, 1965], this partial differential equation of second order can be solved by variables separation as

follows:

$$\psi = R_{mn}(c,\xi)S_{mn}(c,\eta)\begin{Bmatrix}\cos(m\phi)\\ \sin(m\phi)\end{Bmatrix} \tag{4.231}$$

where $R_{mn}(c,\xi)$ represents the radial part and $S_{mn}(c,\xi)$ depicts the angular component of the solution. According to this, the radial solution is shown to comply with the following equation

$$\frac{\partial}{\partial\xi}\left[\left(\xi^2-1\right)\frac{\partial}{\partial\xi}R_{mn}(c,\xi)\right]-\left(\lambda_{mn}(c)-c^2\xi^2+\frac{m^2}{\xi^2-1}\right)R_{mn}(c,\xi)=0 \tag{4.232}$$

while the angular part needs to be a solution of the differential equation shown next

$$\frac{\partial}{\partial\eta}\left[\left(1-\eta^2\right)\frac{\partial}{\partial\eta}S_{mn}(c,\eta)\right]+\left(\lambda_{mn}(c)-c^2\eta^2-\frac{m^2}{1-\eta^2}\right)S_{mn}(c,\eta)=0\,. \tag{4.233}$$

In the radial as well as in the angular differential equations shown above, the eigenvalues are denoted as $\lambda_{mn}(c)$. In addition, since both differential equations are identical except for their respective definition supports, a transformation from the radial to the angular expression is possible without great difficulties. Furthermore, if we particularize the previous equations for $c=0$, both the radial and the angular differential equations are shown to result in the same expression. The resulting homogeneous equation presents as solutions the so-called Legendre Functions, which can be expressed as follows:

$$\frac{d}{dz}\left[\left(1-z^2\right)\frac{dP_\nu^\mu}{dz}\right]+\left(\nu(\nu+1)-\frac{\mu^2}{1-z^2}\right)P_\nu^\mu=0\,, \tag{4.234}$$

being $P_\nu^\mu(z)$ the Legendre function of degree ν and order μ. In analogy to other similar problems that can be found in the literature, the homogeneous solutions can be used to solve the radial and angular differential equations. In fact, the particular prolate angular solution $S_{mn}(c,\eta)$ can be expressed as an infinite series of Legendre functions in the following way:

$$S_{mn}(c,\eta)=\sum_{r=0,1}^{\infty\,*}d_r^{mn}(c)P_{m+r}^m(\eta) \tag{4.235}$$

where the symbol * indicates that the index *r* of the summation is even if *n-m* is even and that the index *r* is odd if *n-m* is odd. If we further introduce the homogeneous solution of the prolate angular function $S_{mn}(c,\eta)$ into the general differential equation we obtain the following recursive relationship [S. Wallner 2007]:

$$\alpha_r^m(c)d_{r+2}^{mn}(c)+\left[\beta_r^m(c)-\lambda_{mn}(c)\right]d_r^{mn}(c)+\gamma_r^m(c)d_{r-2}^{mn}(c)=0 \tag{4.236}$$

with

$$\alpha_r^m(c)=\frac{(2m+r+2)(2m+r+1)}{(2m+2r+3)(2m+2r+5)c^2}$$
$$\beta_r^m(c)=\frac{2(m+r)(m+r+1)-2m^2-1}{(2m+2r+3)(2m+2r-1)}c^2+(m+r)(m+r+1) \quad (4.237)$$
$$\gamma_r^m(c)=\frac{r(r-1)}{(2m+2r-3)(2m+2r-1)}c^2$$

If we apply now the following recurrence relation, valid for all Legendre functions in general:

$$(\nu-\mu+1)P_{\upsilon+1}^{\mu}(z)=(2\nu+1)z\,P_{\upsilon}^{\mu}(z)-(\upsilon+\mu)P_{\upsilon-1}^{\mu}(z) \quad (4.238)$$

and rewrite it in the following matrix form [S. Wallner 2007]:

$$\begin{pmatrix} \beta_0 & \alpha_0 & & & & \\ \gamma_2 & \beta_2 & \alpha_2 & & & \\ & \ddots & \ddots & \ddots & & \\ & & \gamma_{2k} & \beta_{2k} & \alpha_{2k} & \\ & & & \ddots & \ddots & \ddots \end{pmatrix} \cdot \begin{pmatrix} d_0^{mn}(c) \\ d_2^{mn}(c) \\ \vdots \\ d_{2k}^{mn}(c) \\ \vdots \end{pmatrix} = \lambda_{mn} \begin{pmatrix} d_0^{mn}(c) \\ d_2^{mn}(c) \\ \vdots \\ d_{2k}^{mn}(c) \\ \vdots \end{pmatrix} \text{ for } m\text{-}n \text{ even} \quad (4.239)$$

$$\begin{pmatrix} \beta_1 & \alpha_1 & & & & \\ \gamma_3 & \beta_3 & \alpha_3 & & & \\ & \ddots & \ddots & \ddots & & \\ & & \gamma_{2k+1} & \beta_{2k+1} & \alpha_{2k+1} & \\ & & & \ddots & \ddots & \ddots \end{pmatrix} \cdot \begin{pmatrix} d_1^{mn}(c) \\ d_3^{mn}(c) \\ \vdots \\ d_{2k+1}^{mn}(c) \\ \vdots \end{pmatrix} = \lambda_{mn} \begin{pmatrix} d_1^{mn}(c) \\ d_3^{mn}(c) \\ \vdots \\ d_{2k+1}^{mn}(c) \\ \vdots \end{pmatrix} \text{ for } m\text{-}n \text{ odd.} \quad (4.240)$$

we can recognize that the problem to solve is in fact the well known Eigenvalue equation with Eigenvector $d^{mn}(c)$ and associated Eigenvalue λ_{mn}. According to this, the general prolate angular function is shown to adopt the following form:

$$S_{mn}(c,\eta)=\sum_{r=0,1}^{\infty}{}^{*}\,d_r^{mn}(c)P_{m+r}^{m}(\eta) \quad (4.241)$$

where P_{ν}^{μ} refers to the Legendre function as defined previously. A very interesting property of these functions is that they have a limited domain, i.e. $P_{\nu}^{\mu}:[-1,1]\rightarrow I\!R$ and so do also have all Prolate Spheroidal Wave Functions. It is important to say that this property cannot only be used in the frequency domain but also in the time domain, what could also be of interest in some applications. That is to say, that the Prolate Spheroidal Wave Functions could be used to either define the Power Spectral Density directly or the time chips.

Another way of expressing the Prolate Spheroidal Wave Functions is as solution of the following integral equation:

$$\lambda_i\psi_i(t)=\int_{-T_c/2}^{T_c/2}\frac{\sin[\pi\beta_r(t-s)]}{\pi(t-s)}\psi_i(s)\mathrm{d}s \quad (4.242)$$

where T_c represents the chip duration and β_r the double-sided bandwidth. An analytical expression is not easy to derive but [F. Antreich and J. A. Nossek, 2007] have shown that

interesting signal waveforms can be derived using only a few vectors of the functions base. It must be noted though that the proposed solutions do not take into account important constraints related to spectrum compatibility and implementation aspects.

It is interesting to note that the previous integral equation (4.242) can also be interpreted as a Karhunen-Loève transform. The Karhunen-Loève is a representation of a stochastic process by means of a linear combination of orthogonal functions on a finite support of definition. The coefficients are random variables and the expansion basis takes a form that depends on the specific problem. For example, for the Wiener process the basis functions are sinusoidals. If we take a close look at equation (4.242), we can recognize the similarity of:

$$\frac{\sin\left[\pi \beta_r \left(t-s\right)\right]}{\pi\left(t-s\right)} \tag{4.243}$$

to the Dirichlet kernel. This kernel can be further expressed in terms of Legendre prolynomials which are in fact the basis functions of the Prolate Spheroidal Wave Functions as we saw in previous pages. It is also interesting to see that the integral equation above implicitly describes the problem of maximizing the power of a signal in the frequency domain when this signal is also highly localized in time. As a matter of fact, the continuous PSWFs are highly confined simultaneously in time and frequency, what makes them also of great interest for modeling periodic phenomena if they are used as wavelet functions.

Related to the discussion of previous chapters on signals with good spectral confinement, it is of interest to note that while the Fourier and Shannon bandwidths are normally used to estimate what the effective bandwidth of a process is, also other figures such as the Campbell bandwidth equally provide valuable information. The Campbell bandwidth indicates the process spectral entropy and is defined as follows:

$$B_{Campbell} = e^{-\int_{-\infty}^{\infty} G(f)\log[G(f)]\mathrm{d}f} \tag{4.244}$$

4.8.4 Faded Harmonics (FH) Interplex Modulation

Faded Harmonics (FH) is an Interplex modulation that uses non-binary signals to better control the spectral emissions of the open signals of Galileo. For more details on Interplex refer to chapter 7.7. Using tertiary modulation waveforms is a way of achieving this objective. Tertiary Offset carrier signals have been introduced in [A.R. Pratt and J.I.R. Owen, 2003] and are conceptually equivalent to the TCS and TOC modulations that we described in chapter 4.5. The main driver of the work presented in [A.R. Pratt and J.I.R. Owen, 2003] was to find an alternative signal to the original BOC(2,2) baseline of 2002. that would overlay the military signals less while it should perform as good as the reference BOC(2.2) signal. The proposed solution received the name of 8-PSK BOC(2,2) or $BOC_8(2,2)$. The idea behind, as we already pointed out in chapters 4.5.1 and 4.5.2, is to suppress specific secondary lobes by

zeroing one pair of harmonics in the sub-carrier spectra. This can be easily accomplished by building up multilevel signals which can be expressed as the sum of other elementary sub-carriers. Indeed, as shown in Appendix F, by properly selecting the parameters ρ_l and ρ_s we could completely suppress any specific secondary lobe.

We can generalize the results that we obtained in chapter 4.5.4 if we realize that any BOC sub-carrier is indeed a periodic signal and can thus be expressed as a Fourier series:

$$s_s(t) = \sum_{k=1}^{\infty} b_k \sin(2\pi k f_c t) \tag{4.245}$$

where

$$b_k = \frac{1}{T_c}\int_0^{T_c/2} e^{jk\frac{2\pi}{T_c}t}\,dt - \frac{1}{T}\int_{T_c/2}^{T_c} e^{jk\frac{2\pi}{T_c}t}\,dt = \frac{e^{jk\pi}}{jk\pi}\left[1-\cos(k\pi)\right] = \frac{2}{jk\pi} \tag{4.246}$$

for k odd. Furthermore, since $c_k - c_k^* = jb_k$, if we define the Fourier sum between 1 and infinity, the odd coefficients in sine will adopt the following form:

$$b_k = \frac{4}{k\pi} \tag{4.247}$$

while all the cosine terms are zero.

If we simply subtract now to the BOC signal above a sub-carrier of frequency and amplitude equal to that of the harmonic we want to suppress, for example the n^{th} harmonic, that harmonic of the sub-carrier will be eliminated. This means, a faded harmonic sub-carrier that has suppressed the n^{th} harmonic would ideally look as follows:

$$s_s^n(t) = s_s(t) - \frac{4}{n\pi}\sin(2\pi n f_c t) = \sum_k b_k \sin(2\pi k f_c t) - \frac{4}{n\pi}\sin(2\pi n f_c t) \tag{4.248}$$

Such a signal would not be practical since it has an infinite number of levels due to the sine term on the right. Therefore a rectangular approximation to the sine function is more appropriate and instead of subtracting a sinusoid we will subtract another BOC signal with frequency and amplitude equal to that of the lobe we want to annulate as shown next:

$$\hat{s}_s^n(t) = s_s(t) - \frac{4}{n\pi}s_s^n(t) = \sum_k b_k \sin(2\pi k f_c t) - \frac{4}{n\pi}\left[b_{k-n+1} + b_{n+k-1}\right]\sin(2\pi n f_c t) \tag{4.249}$$

This is shown graphically next. In the example, we have taken BOC(1,1) and we have suppressed the 9$^{\text{th}}$ and 11$^{\text{th}}$ harmonic respectively. These harmonics were selected given their proximity to the M-Code. As we can clearly recognize, the spectrum is very close to that of the original BOC(1,1) with the only difference that those components of the corresponding faded harmonics are lower. As one can expect, this will clearly contribute to reaching a better spectral separation with the rest of signals around. Moreover, this effect is more important the higher the sub-carrier frequency we want to cancel in the original spectrum.

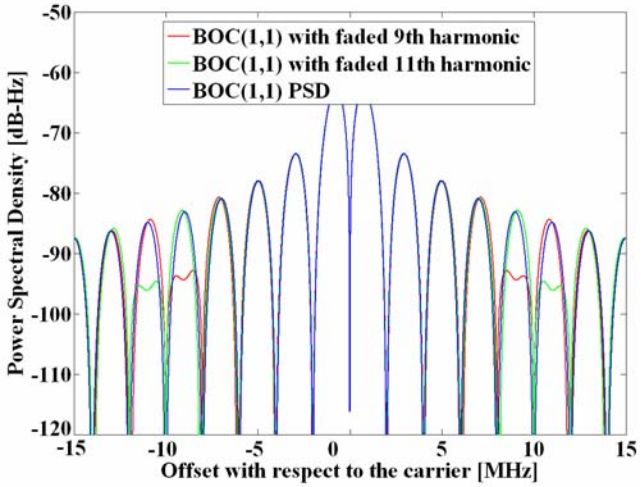

Figure 4.74. Harmonic fading of BOC(1,1) using a 4-level sub-carrier

This is indeed the idea behind the faded-harmonics modulation. As we can also recognize from the expression above, the number of harmonics or lobes that are suppressed is directly related to the number of levels of the resulting sub-carrier. For exemplification, we show next the power spectral density that an even sine-phased BOC signal with suppressed lobes would have if only one harmonic is eliminated. Generalizing the result to more signals and with more cancelled lobes is trivial.

$$G^{n}_{\mathrm{BOC}(f_s,f_c)} = f_c \left[\frac{\sin\left(\frac{\pi f}{f_c}\right)\sin\left(\frac{\pi f}{2f_s}\right)}{\pi f \cos\left(\frac{\pi f}{2f_s}\right)} - \frac{4}{n\pi} \frac{\sin\left(\frac{\pi f}{f_c}\right)\sin\left(\frac{\pi f}{2nf_s}\right)}{\pi f \cos\left(\frac{\pi f}{2nf_s}\right)} \right]^2 \tag{4.250}$$

This can also be expressed as follows:

$$G^{n}_{\mathrm{BOC}(f_s,f_c)} = f_c \left[\frac{\sin\left(\frac{\pi f}{f_c}\right)}{\pi f} \right]^2 \left[\frac{\sin\left(\frac{\pi f}{2f_s}\right)}{\cos\left(\frac{\pi f}{2f_s}\right)} - \frac{4}{n\pi} \frac{\sin\left(\frac{\pi f}{2nf_s}\right)}{\pi f \cos\left(\frac{\pi f}{2nf_s}\right)} \right]^2 \tag{4.251}$$

where the super index n indicates that we have suppressed the n–th lobe. It must be noted that the lobe n to suppress must be a multiple of the sub-carrier f_s of the signal. Another interesting comment is that not only the lobe we want to suppress is eliminated but also other secondary lobes or harmonics are slightly attenuated. Nonetheless this effect is practically negligible.

As we mentioned above, we can generalize this procedure to more lobes and harmonics to suppress. The only problem is that the number of levels grows very quickly as more harmonics are eliminated. As we can imagine, this could make the implementation more difficult in the end. A solution to this problem has been proposed in chapter 4.5.5 and by [L. Ries and J.-L. Issler 2003] based on the principle that completely removing one lobe or a few of them is sometimes not absolutely necessary since attenuating them by some dBs might be enough. Indeed, if we work with four level signals but do not constrain ourselves to

dividing the code chip waveform in equal length segments as done in chapter 4.5, we gain a degree of freedom that compensates that one that we lose by fixing the number of possible amplitude levels to only four. Let us imagine a four-level signal as depicted below:

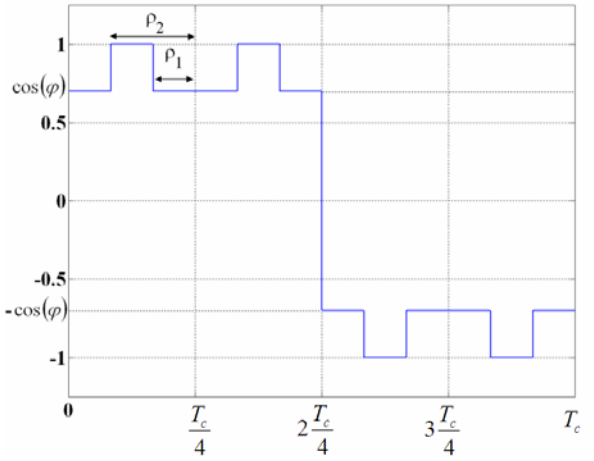

Figure 4.75. Four-Level Waveform to realize the fading effect

In spite of being the segments in principle of any arbitrary length, we create however a reference framework by dividing the chip in *n* subchips. To further provide flexibility in the location, the parameters ρ_1 and ρ_2 are then introduced.

As we can recognize, the location of the different pieces of the chip waveform is not at positions T_c/n but could adopt any imaginable place determined by ρ_1 and ρ_2. To account for changes in sign in the general Coded Symbol (CS) sequence, we will further use the general notation of chapter 4.2 and define the signal as follows within a sub-chip $s_c(t)$. In fact, we can define our signal for the general case of faded-harmonic CS of four levels as follows:

$$p(t)=\sum_{i=1}^{n} p_i\; p_{T_c/n}\left(t-i\frac{T_c}{n}\right)=\sum_{i=1}^{n} p_i(t)p_{T_c/n}(t)\otimes\delta\left(t-\frac{iT_c}{n}\right)=p_{T_c/n}(t)\otimes\sum_{i=1}^{n} p_i(t)\delta\left(t-\frac{iT_c}{n}\right) \tag{4.252}$$

As we can recognize in the expression above, the code symbols start with a delay T_c/n when $i=1$. Thus, an extra shift of half a sub-chip to the left is necessary if we define $p_{T_c/n}(t)$ between $-T_c/2n$ and $T_c/2n$. As we know this is equivalent to multiplying by $\exp(j\omega T_c/2n)$. Moreover, if we want our time definition to start at zero and define $p_{T_c/n}(t)$ between 0 and T_c/n, a shift of one whole sub-chip T_c/n to the left would be necessary, what in the frequency domain is equivalent to multiplying by the factor $\exp(j\omega T_c/n)$. No matter how we do, the final result is the factor $\exp(j\omega T_c/n)$ that we have seen in the Appendix. Using the symmetric definition around 0, we have:

$$p_{T_c/n}(t)=\begin{cases}\cos(\varphi) & -\dfrac{T_c}{2n}<t\le-\rho_2\\ 1 & -\rho_2<t\le-\rho_1\\ \cos(\varphi) & -\rho_1<t\le\rho_1\\ 1 & \rho_1<t\le\rho_2\\ \cos(\varphi) & \rho_2<t\le\dfrac{T_c}{2n}\end{cases} \tag{4.253}$$

and the Fourier Transform of this generic faded-harmonic CS is thus shown to be

$$P_{\mathrm{CS}}^{\mathrm{FH}}(j\omega) = P_c(j\omega)\,\mathrm{e}^{\frac{j\omega T_c}{2n}} \sum_{k=1}^{n} p_k \mathrm{e}^{-\frac{jk\omega T_c}{n}} \tag{4.254}$$

where

$$P_{T_c/n}(j\omega) = \int_{-\frac{T_c}{2n}}^{-\rho_2} \cos(\varphi)\mathrm{e}^{-j\omega t}\mathrm{d}t + \int_{-\rho_2}^{-\rho_1} \mathrm{e}^{-j\omega t}\mathrm{d}t + \int_{-\rho_1}^{\rho_1} \cos(\varphi)\mathrm{e}^{-j\omega t}\mathrm{d}t + \int_{\rho_1}^{\rho_2} \mathrm{e}^{-j\omega t}\mathrm{d}t + \int_{\rho_2}^{\frac{T_c}{2n}} \cos(\varphi)\mathrm{e}^{-j\omega t}\mathrm{d}t \tag{4.255}$$

which can be further developed to the following expression

$$P_{T_c/n}(j\omega) = \frac{2}{\omega}\left[\sin\left(\frac{\omega T_c}{2n}\right)\cos(\varphi) + \sin(\omega\rho_1)\left[\cos(\varphi)-1\right] + \sin(\omega\rho_2)\left[1-\cos(\varphi)\right]\right] \tag{4.256}$$

or in the frequency domain:

$$P_{T_c/n}(f) = \frac{1}{\pi f}\left[\sin\left(\frac{\pi f}{nf_c}\right)\cos(\varphi) + \sin(2\pi f\rho_1)\left[\cos(\varphi)-1\right] + \sin(2\pi f\rho_2)\left[1-\cos(\varphi)\right]\right] \tag{4.257}$$

Therefore, the power spectral density of any Coded Symbol of four levels as defined above, would present the following form

$$G_{\mathrm{CS}}^{\mathrm{FH}}(f) = \frac{f_c}{\cos^2\varphi + (\rho_2-\rho_1)\sin^2\varphi}\left\| e^{j\frac{\pi fk}{nf_c}} P_{T_c/n}(f)\right\|^2 \left\|\sum_{k=1}^{n} p_k \mathrm{e}^{-j\frac{2\pi fk}{nf_c}}\right\|^2 \tag{4.258}$$

or equivalently,

$$G_{\mathrm{CS}}^{\mathrm{FH}}(f) = \frac{f_c\left[\sin\left(\frac{\pi f}{nf_c}\right)\cos(\varphi) + \sin(2\pi f\rho_1)\left[\cos(\varphi)-1\right] + \sin(2\pi f\rho_2)\left[1-\cos(\varphi)\right]\right]^2 \left\|\sum_{k=1}^{n} p_k \mathrm{e}^{-j\frac{2\pi fk}{nf_c}}\right\|^2}{\cos^2\varphi + (\rho_2-\rho_1)\sin^2\varphi} \tag{4.259}$$

where the modulating term on the right is common to the MCS definition and therefore all the results that we obtained in the previous chapters can be used here too. Finally, it is interesting to see that playing with the parameters ρ_1, ρ_2 and φ, we can select the lobe we want to suppress and how much we want to attenuate it. Furthermore, it is trivial to see that this technique can be further generalized to more lobes if new parameters are introduced, according to the previously discussed scheme.

Regarding the multiplex, it is important to note that, as we will see in chapter 7, we cannot apply the Interplex modulation directly since such a signal is not binary and slight changes in the multiplex scheme are thus required. Nonetheless, the theory that we will derive in chapter 7.7.10 on the Modified Interplex could also be applied here too. To show a potential application of this modulation, next figure compares different solutions to implement CBCS using Faded Harmonics and the Modified Interplex. For more details on Interplex and the Modified Interplex, refer to chapter 7.7.9.

In-Phase Component						
Code A	**1**	**-1**	**-1**	**-1**	**1**	**-1**
Code B	**1**	**-1**	**1**	**-1**	**-1**	**1**

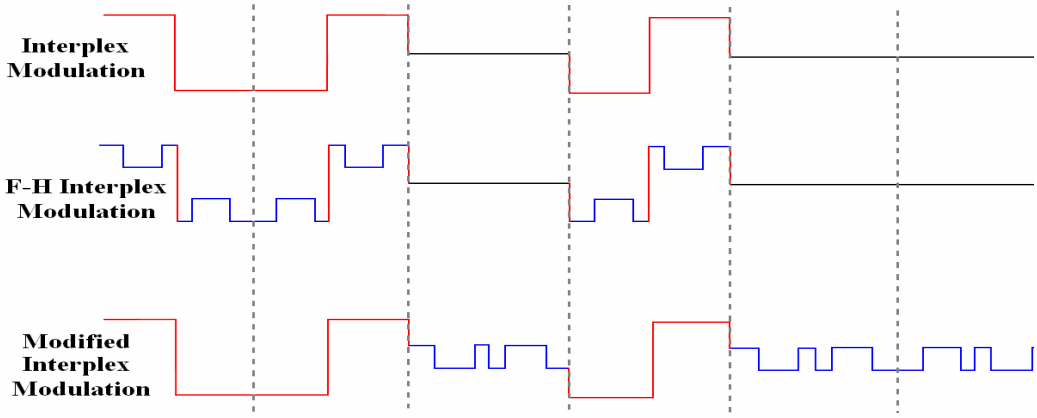

Figure 4.76. Pseudo-random multiplexing of BCS and BOC using Interplex, Faded Harmonics Interplex and modified Interplex for CBCS

As shown in [G.W. Hein et al., 2005], the implementation of any CBCS signal, and in particular of CBOC, could have also been performed using the Faded Harmonics (FH) Interplex scheme since this one also relies on the sum of two 4-level spread-spectrum signals. However, the analysis of FH-Interplex for CBCS put in evidence two important drawbacks:

- The relative power of the Inter-Modulation product is increased, resulting in a loss of efficiency
- The modulation results in significant distortions on the quadrature signals, for example the PRS signal. These distortions may induce unacceptable losses on the receiver, as well as an increased spreading of the PRS signal in adjacent frequency bands.

5. Spectral Separation Coefficient (SSC)

5.1 Definition

The Spectral Separation Coefficients, or SSCs for short, are a very powerful figure to indicate and measure the degree of interference that a signal suffers due to other signals sharing the band. This degradation is evaluated in terms of reduction of the Signal to Noise plus Interference Ratio (SNIR) of the desired signal, measured at the output of a receiver's correlator that uses an ideal matched filter to receive the navigation signals as described by [J.-L. Issler et al., 2003], [J.W. Betz, 2001b] and [A.R. Pratt and J.I.R. Owen, 2003a]. Indeed, the methodology to compute the SSCs relies on the idea of measuring the power of the desired signal and its reduction due to all the interfering signals, at the correlator's output. This can graphically be shown in the following scheme

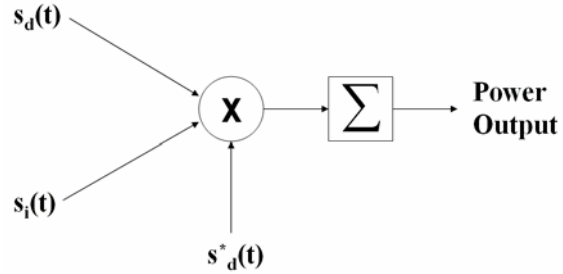

Figure 5.1. SSC Correlator Model for the Spectral Separation Coefficients calculations

where $s_d(t)$ refers to the desired signal, $s_i(t)$ to the interfering signal and $s^*_d(t)$ is the matched spreading waveform of the desired signal. Moreover, the sum module represents the integration and dump function. This is the general model that we can find in the literature [J.J. Spilker, 1997b]. It is also important to note that this model implies that the receiver does not make use of any cancellation technique.

Another interesting interpretation of the SSC is to see it as the mean power of the crosscorrelation function between the desired and the interfering signal [J.-L. Issler et al., 2003]. For this reason, also expressions for the crosscorrelation function in the frequency and time domain are derived in the next lines.

As shown in [A.R. Pratt and J.I.R. Owen, 2003a], the SSC provides a measure of the noise power output by a receiver when certain signals are incident at its input. As one can imagine, the better the isolation of a signal with the rest of signals in the band, the lower will be the equivalent noise caused by them, resulting thus the concept of cross power spectral density here of special interest.

If we take a closer look at Figure 5.1, it is possible to see that the power spectrum at the output of the correlator of a filter $H(\omega)$ matched to the desired signal – being thus $H(\omega)$ equal to the conjugate of the desired signal spectrum $S_d^*(\omega)$ – can be expressed as follows:

$$S_o(\omega) = \left\{\sqrt{P_i}\, S_i(\omega) + \sqrt{P_d}\, S_d(\omega)\right\} H(\omega) = \left\{\sqrt{P_i}\, S_i(\omega) + \sqrt{P_d}\, S_d(\omega)\right\} S_d^*(\omega) \tag{5.1}$$

where P_i refers to the power level of the interfering signal and P_d that of the desired signal. Moreover, in a general case a protection filter can also be included in the expression as shown in [A.R. Pratt and J.I.R. Owen, 2003a]. It is also important to see that the spectral definition above encompasses both the spreading codes as well as the spreading waveform of the desired and interfering signals, being thus valid for the most general case.

The power spectral density can thus be expressed as follows:

$$P_o(\omega) = \|S_o(\omega)\|^2 = \left\{P_i \|S_i(\omega)\|^2 + P_d \|S_d(\omega)\|^2 + 2\sqrt{P_i P_d}\, \mathrm{Re}\left\{S_i(\omega) S_d^*(\omega)\right\}\right\} \|S_d(\omega)\|^2 \tag{5.2}$$

what can be further simplified yielding:

$$P_o(\omega) = \|S_o(\omega)\|^2 = \left\{P_i \|S_i(\omega)\|^2 + P_d \|S_d(\omega)\|^2\right\} \|S_d(\omega)\|^2 = \left[P_i G_i(\omega) + P_d G_d(\omega)\right] \|S_d(\omega)\|^2 \tag{5.3}$$

if we assume that the interfering signal and the desired signal are uncorrelated, averaging thus the cross-spectrum term to zero. This can be achieved either by means of the signal structure or the code structure being thus this assumption also true even if we work with signals of the same family, as long as all the codes are ideally orthogonal. As we can imagine, this is a very strong assumption since especially for the case of intra-system interference of signals with short codes this approximation could lead to wrong results as we will show in chapter 6.2.2. Nonetheless, we will still consider it as valid in this chapter.

Moreover, it is important to note that the functions $G_i(\omega)$ and $G_d(\omega)$ are both normalized Power Spectral Densities as those defined in chapter 4.1.1. Thus, the total power at the output of the correlator will be the integral of the output spectrum, expressed as follows:

$$P_o = \int_{-\infty}^{\infty} P_o(f)\mathrm{d}f = P_i \kappa_{id} + P_d \kappa_{dd} = P_i \int_{-\infty}^{\infty} G_i(f) G_d(f)\mathrm{d}f + P_d \int_{-\infty}^{\infty} G_d^2(f)\mathrm{d}f \tag{5.4}$$

where we can recognize the spectral separation coefficient κ_{dd} of the desired signal with itself and between the desired signal and the interfering signal κ_{id}. These are defined as:

$$\begin{aligned} \kappa_{dd} &= \int_{-\infty}^{\infty} G_d^2(f)\mathrm{d}f \\ \kappa_{id} &= \int_{-\infty}^{\infty} G_i(f) G_d(f)\mathrm{d}f \end{aligned} \tag{5.5}$$

where the receiver and transmitter are assumed to have infinite bandwidth. If this is not the case, either the integration limits require adjustment or corrections to the SSCs must be made to include the effects of the finite bandwidths of receiver and transmitter, as we saw in (4.13).

We can obtain the same expressions reasoning in a different way. If we assume that the undesired signal is stochastic and Gaussian with a normalized power spectral density $G_i(f)$ and that the desired signal can also be characterized adequately as an independent stochastic

process with normalized $G_d(f)$, then the multiplier output will be Gaussian and it is shown to be the convolution of both power spectral densities, according to:

$$S_m(f) = \int_{-\infty}^{\infty} G_i(f_1) G_d(f - f_1) \mathrm{d}f_1 \tag{5.6}$$

such that after the Integrate and Dump (I&D) operator we will have:

$$S_m(f) \left| T_I \, H_{ID}(f) \right|^2 \tag{5.7}$$

where $H_{ID}(f) = \mathrm{sinc}(\pi f T_I)$ being T_I the coherent integration time.

According to this, if the interference is Additive White Gaussian Noise (AWGN) then the I&D output will be $N_0 \left| T_I \, H_{ID}(f) \right|^2$ and thus the correlation sum variance will adopt the value $N_0 T_I$. On the other hand, for the interesting case of non-white interference the output is shown to be:

$$\overline{\Psi}_{id} = T_I \int_{-\infty}^{\infty} \int_{-\infty}^{\infty} G_i(f_1) G_d(f_2 - f_1) \mathrm{d}f_1 \left| H_{ID}(f_2) \right|^2 \mathrm{d}f_2 \tag{5.8}$$

For the case that the multiplier output Power Spectral Density is sufficiently flat across the I&D filter, that is for very long pseudorandom noise codes, the computation of the spectral separation is shown to approximate to the following expression:

$$\overline{\Psi}_{id} \approx T_I \int_{-\infty}^{\infty} G_i(f_2) \otimes G_d(f_2) \left| H_{ID}(f_2) \right|^2 \mathrm{d}f_2 \Big|_{f=0} = \int_{-\infty}^{\infty} G_i(f) G_d(f) \mathrm{d}f \tag{5.9}$$

where $\otimes$ represents the convolution operator. Moreover, if we include the effect of the filtering at the receiver, the simplified SSC will adopt the following form:

$$\kappa_{id} = \int_{-\beta_r/2}^{\beta_r/2} G_i(f) G_d(f) \left| H_{\mathrm{RX}}(f) \right|^2 \mathrm{d}f \tag{5.10}$$

where

- $G_i(f)$ stands for the normalized power spectral density of the aggregate interference,
- $G_d(f)$ is the normalized power spectral density of the desired signal, and
- $H_{\mathrm{RX}}(f)$ is the receiver transfer function

This equation is not applicable when the desired signal and aggregate interference are *line-like*. In the next chapters we will work with this approximation but in chapter 6 we will analyze the particular case of the C/A code where the short integrations make this approximation incorrect.

The inner product is not generally applicable when desired signals and interference have line-like spectra. Therefore, for each particular problem we have to see if the multiplier output PSD is smooth enough to justify the approximation above.

Furthermore, if we normalize the power spectral densities of the desired and interfering

signals as defined in (4.13), the SSC adopts the following form for the case of an infinite integration time, as a function of Doppler:

$$\kappa_{id}(\Delta f) = \int_{-\beta_r/2}^{\beta_r/2} \overline{G}_i(f-\Delta f)\overline{G}_d(f)\left|H_{\mathrm{RX}}(f)\right|^2 \mathrm{d}f \tag{5.11}$$

where Δf indicates the Doppler difference at receiver level between the desired signal and the interfering signal. In addition, if an ideal filter of amplitude 1 is considered, we can express (5.11) also as follows:

$$\kappa_{id}(\Delta f) = \overline{G}_i(f) \otimes \overline{G}_d(f) = \Re_{\overline{G}_i,\overline{G}_d}(\Delta f) \tag{5.12}$$

Once we have derived a general expression for the Spectral Separation Coefficient and found useful approximations, we further analyze the cross power spectra terms that we have already anticipated in chapter 4. As we have seen in (5.4), there is a fundamental element of the SSC that is defined as:

$$G_{id}(f) = G_i(f)G_d(f) \tag{5.13}$$

This expression is of great interest since it will help us in finding the main interactions between the interfering spectrum and the desired signal spectrum by simply observing its behaviour in the frequency domain. Moreover, if we expand (5.13) expressing the power spectral density of each of the signals in terms of their autocorrelation, we see that:

$$G_{id}(\omega) = \int_{-\infty}^{\infty} \Re_{s_i}(\tau)\mathrm{e}^{-j\omega\tau}\,\mathrm{d}\tau \int_{-\infty}^{\infty} \Re_{s_d}(\tau)\mathrm{e}^{-j\omega\tau}\,\mathrm{d}\tau = \int_{-\infty}^{\infty}\int_{-\infty}^{\infty} \Re_{s_i}(\tau_1)\Re_{s_d}(\tau_2)\mathrm{e}^{-j\omega(\tau_1+\tau_2)}\,\mathrm{d}\tau_1\mathrm{d}\tau_2 \tag{5.14}$$

and therefore

$$\Re_{s_i,s_d}(\eta) = \frac{1}{2\pi}\int_{-\infty}^{\infty}\int_{-\infty}^{\infty}\int_{-\infty}^{\infty} \Re_{s_i}(\tau_1)\Re_{s_d}(\tau_2)\mathrm{e}^{-j\omega(\tau_1+\tau_2-\eta)}\,\mathrm{d}\tau_1\,\mathrm{d}\tau_2\,\mathrm{d}\omega \tag{5.15}$$

which is shown [A.R. Pratt and J.I.R. Owen, 2003a] to reduce to the simplified form:

$$\Re_{s_i,s_d}(\eta) = \int_{-\infty}^{\infty} \Re_{s_i}(\tau_1)\Re_{s_d}(\eta-\tau_1)\mathrm{d}\tau_1 = \Re_{s_i}(\eta) \otimes \Re_{s_d}(\eta) \tag{5.16}$$

In other words, the autocorrelation function of the cross power is the convolution of the interfering and desired signals. In addition, applying the Weiner-Kinchine spectrum theorem as shown in [A.R. Pratt and J.I.R. Owen, 2003a], yields:

$$\Re_{s_i,s_d}(\eta) = \int_{-\infty}^{\infty} G_{id}(f)\mathrm{e}^{j2\pi f\eta}\,\mathrm{d}f \tag{5.17}$$

Using this expression, we can calculate the cross SSC, namely κ_{id}, in the same manner:

$$\kappa_{id} = \Re_{s_i,s_d}(0) = \int_{-\infty}^{\infty} \Re_{s_i}(\tau_1)\Re_{s_d}(-\tau_1)\mathrm{d}\tau_1 \tag{5.18}$$

5.1.1 SSC between two QPSK signals

The spectral separation coefficient between two signals that we have derived above applies for the case that both signals are in-phase. Although this is a common case, many of the GNSSes today have also navigation signals that are in quadrature with each other, sharing the same frequency. It is thus necessary to find an expression for this important case too. Fortunately, the results that were obtained in the previous chapter can be reutilized here. Indeed, as shown in Appendix N and by [J.-L. Issler et al., 2003], the SSC between two QPSK navigation signals sharing the same frequency can be expressed as the sum of 4 SSCs of two BPSK elementary signal components, according to the expression below:

$$\mathrm{SSC}\left(s_I, s_Q\right) = \mathrm{SSC}\left(s_I^D, s_Q^D\right) + \mathrm{SSC}\left(s_I^P, s_Q^P\right) + \mathrm{SSC}\left(s_I^D, s_Q^P\right) + \mathrm{SSC}\left(s_I^P, s_Q^D\right) \quad (5.19)$$

where:

- $\mathrm{SSC}\left(s_I, s_Q\right)$ is the SSC between the interfering in-phase signal s_I and the quadrature signal s_Q.
- $\mathrm{SSC}\left(s_I^D, s_Q^D\right)$ is the SSC between the data component of the interfering signal and the data component of the quadrature signal.
- $\mathrm{SSC}\left(s_I^P, s_Q^P\right)$ is the SSC between the pilot component of the interfering signal and the pilot component of the quadrature signal.
- $\mathrm{SSC}\left(s_I^D, s_Q^P\right)$ is the SSC between the data component of the interfering signal and the pilot component of the quadrature signal.
- $\mathrm{SSC}\left(s_I^P, s_Q^D\right)$ is the SSC between the pilot component of the interfering signal and the data component of the quadrature signal.

5.2 Derivation of analytical expressions

In the next lines analytical expressions for the SSC with an infinite period of integration, and thus no Doppler error, will be presented. Moreover, we will further assume ideal code properties. Later in chapter 6 we will revisit our assumptions and we will assess the effect of real codes on the measured SSC. Equally, the impact of the data on the spectral fine structure of the navigation signals will be investigated.

5.2.1 SSC between two generic BCS signals

As demonstrated in Appendix O, the Spectral Separation Coefficient between two arbitrary BCS signals, namely $\mathrm{BCS}\left([\bar{r}], f_c^1\right)$ and $\mathrm{BCS}\left([\bar{s}], f_c^2\right)$, can be expressed as follows:

$$\mathrm{SSC}_{\mathrm{BCS}\left([\bar{r}],f_c^1\right)-\mathrm{BCS}\left([\bar{s}],f_c^2\right)} = \begin{cases} n_1 n_2 f_c^1 f_c^2\, \Xi\left(f_c^1, n_1, f_c^2, n_2, 0, 0\right) + \\ + 2n_1 f_c^1 f_c^2 \sum_{i'=1}^{n_2-1} \sum_{j'=i'+1}^{n_2} s_{i'} s_{j'}\, \Xi\left(f_c^1, n_1, f_c^2, n_2, 0, j'-i'\right) + \\ + 2n_2 f_c^1 f_c^2 \sum_{i=1}^{n_1-1} \sum_{j=i+1}^{n_1} r_i r_j\, \Xi\left(f_c^1, n_1, f_c^2, n_2, j-i, 0\right) + \\ + 4 f_c^1 f_c^2 \sum_{i'=1}^{n_2-1} \sum_{j'=i'+1}^{n_2} \sum_{i=1}^{n_1-1} \sum_{j=i+1}^{n_1} r_i r_j s_{i'} s_{j'}\, \Xi\left(f_c^1, n_1, f_c^2, n_2, j-i, j'-i'\right) \end{cases} \tag{5.20}$$

where we have assumed that the receiver integrates for an infinite period of time, there is no Doppler error and the receiver has a front-end with infinite bandwidth. The function $\Xi\left(f_c^1, n_1, f_c^2, n_2, j-i, j'-i'\right)$ is defined in (O.15) of a Appendix O. Moreover, n_1 is the length of the generation vector $\bar{r} = \left\{r_1, r_2, ..., r_{n_1}\right\}$ of the first BCS signal and n_2 the length of the generation vector $\bar{s} = \left\{s_1, s_2, ..., s_{n_2}\right\}$ of the second BCS signal.

As we commented in chapter 4.7, during the optimization of the Open and Civil Signals in E1/L1, the spectral overlay with the rest of signals sharing the band was one of the most important constraints to take into account. Therefore, the spectral separation coefficient of the selected MBOC signal with the C/A Code, M-Code and PRS was a figure of major importance. Now that we have derived the general expression for the SSC between two BCS signals, we will particularize the expression to derive some cases of interest. As one can imagine, this reduces time and computation since the function $\Xi\left(f_c^1, n_1, f_c^2, n_2, j-i, j'-i'\right)$ can be saved in tensorial form for all possible input parameters. Then, calculating an SSC would be just a matter of reading from the tensor and combining the outputs according to (5.20).

5.2.2 SSC between a generic BCS signal and the M-Code

Before deriving the general expression of the SSC between a generic BCS signal and the M-Code, let us begin with the example of the SSC between BOC(1,1) and the GPS M-Code. As we know, BOC(1,1) can be expressed as BCS([1 -1],1) and BOC(10,5) as BCS([1 -1 1 -1],5). Moreover, following the matrix notation of chapter 4.3, we can further express our signals of study as follows:

$$M^2_{\mathrm{BOC}(1,1)}\left([+1,-1]\right) = \begin{pmatrix} 1\{0\} & -1\{1\} \\ & 1\{0\} \end{pmatrix} \tag{5.21}$$

and for the M-Code we have equally:

$$M^2_{\text{M-Code}}\left([+1,-1,+1,-1]\right)=\begin{pmatrix} 1\{0\} & -1\{1\} & 1\{2\} & -1\{3\} \\ & 1\{0\} & -1\{1\} & 1\{2\} \\ & & 1\{0\} & -1\{1\} \\ & & & 1\{0\} \end{pmatrix} \tag{5.22}$$

From the matrices above we can extract the following parameters:

$$\begin{aligned} \mathrm{s}^1 &= [+1\text{-}1] \qquad f_c^1 = 1.023\,\text{MHz} \quad n_1 = 2 \\ \mathrm{s}^2 &= [+1\text{-}1+1\text{-}1] \quad f_c^2 = 5.115\,\text{MHz} \quad n_2 = 4 \end{aligned} \tag{5.23}$$

and therefore, we can express the SSC between BOC(1,1) and M-Code as follows:

$$\text{SSC}_{\text{BOC(1,1)–BOC(10,5)}} = \int_{-\infty}^{\infty} G_{\text{BOC(1,1)}}(f)\,G_{\text{BOC(10,5)}}(f)\,\mathrm{d}f \tag{5.24}$$

with

$$\text{SSC}_{\text{BOC(1,1)–BOC(10,5)}} = \left\{ \begin{array}{l} n_1 n_2 f_c^1 f_c^2 \Xi\left(f_c^1, n_1, f_c^2, n_2, 0, 0\right) + 2 n_1 f_c^1 f_c^2 \left(\begin{array}{l} -3\Xi\left(f_c^1, n_1, f_c^2, n_2, 0, 1\right) + \\ +2\Xi\left(f_c^1, n_1, f_c^2, n_2, 0, 2\right) - \\ -\Xi\left(f_c^1, n_1, f_c^2, n_2, 0, 3\right) \end{array} \right) - \\ -2 n_2 f_c^1 f_c^2 \Xi\left(f_c^1, n_1, f_c^2, n_2, 1, 0\right) - 4 f_c^1 f_c^2 \left(\begin{array}{l} -3\Xi\left(f_c^1, n_1, f_c^2, n_2, 1, 1\right) + \\ +2\Xi\left(f_c^1, n_1, f_c^2, n_2, 1, 2\right) - \\ -\Xi\left(f_c^1, n_1, f_c^2, n_2, 1, 3\right) \end{array} \right) \end{array} \right\} \tag{5.25}$$

As it can be shown, the theoretical value obtained from the expression above is in this case $\text{SSC}_{BOC(1,1)-BOC(10,5)} = -83.1091$ dB-Hz. We can graphically show the validity of the result obtained above if we numerically compute the SSC between BOC(1,1) and the M-Code increasing the bandwidth of integration progressively. As we can see, our analytical value matches very well the results of the simulations.

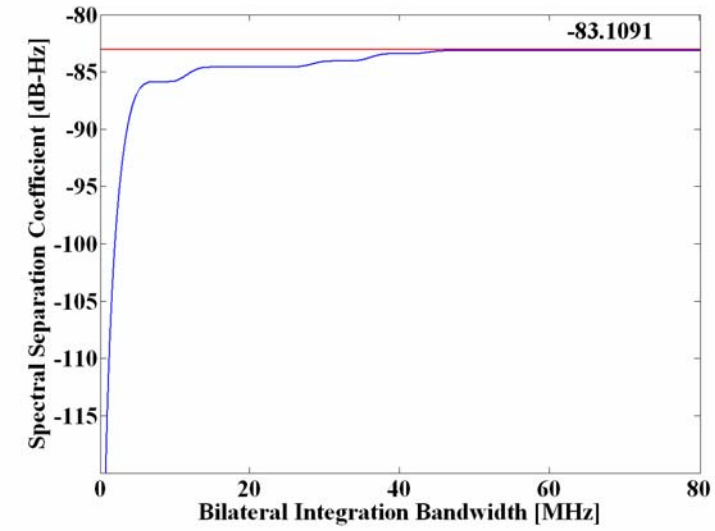

Figure 5.2. Spectral Separation Coefficient between BOC(1,1) and M-Code as a function of the Integration Bandwidth. It must be noted that the PSD of both signals is normalized to 1 W in an infinite bandwidth. The analytical value is shown in red

In general, the SSC between an arbitrary signal and the M-Code can be further expressed as follows, according to (O.46) in Appendix O:

$$\mathrm{SSC}_{\mathrm{BCS}\left([\bar{r}],f_c^1\right)\text{-}\mathrm{BOC}(10,5)}=\begin{cases} n_1 f_c^1 f_c^2\left[\begin{array}{l} n_2\,\Phi\left(n_1,0,0\right)+\\ 2\left[-3\Phi\left(n_1,0,1\right)+2\Phi\left(n_1,0,2\right)-\Phi\left(n_1,0,3\right)\right]\end{array}\right]+\\ 2f_c^1 f_c^2\sum_{l=1}^{n_1-1}\bar{r}\left[\theta\left(\bar{r},l\right)\right]^T\left[\begin{array}{l} n_2\Phi\left(n_1,l,0\right)+\\ +2\left\{-3\Phi\left(n_1,l,1\right)+2\Phi\left(n_1,l,2\right)-\Phi\left(n_1,l,3\right)\right\}\end{array}\right]\end{cases} \tag{5.26}$$

where $\Phi\left(n,l_1,l_2\right)=\Xi\left(f_c,n,f_c,n,l_1,l_2\right)$ as shown in detail in the Appendix.

5.2.3 Self SSC of a generic BCS signal

After having obtained an analytical expression for the SSC between a BCS signal and the M-Code we solve next the case of the SSC of a generic BCS signal with itself. Indeed, this spectral separation coefficient is of great importance too as it gives an idea of how robust a signal is to interference coming from the same family of signals or from adapted jammers that match its power spectral density.

After some manipulation of the original SSC between two arbitrary BCS sequences, it can be shown that the self SSC adopts the following form:

$$\mathrm{SSC}_{\mathrm{BCS}}^{\mathrm{Self}}=\mathrm{SSC}_{\mathrm{BCS}\left([\bar{r}],f_c^1\right)-\mathrm{BCS}\left([\bar{s}],f_c^2\right)}\Big|_{\bar{r}=\bar{s},\,f_c^1=f_c^2,\,n_1=n_2=n}=\begin{cases} n^2 f_c^2\,\Xi\left(f_c,n,f_c,n,0,0\right)+\\ +2nf_c^2\sum_{i'=1}^{n-1}\sum_{j'=i'+1}^{n}s_{i'}s_{j'}\,\Xi\left(f_c,n,f_c,n,0,j'-i'\right)+\\ +2nf_c^2\sum_{i=1}^{n-1}\sum_{j=i+1}^{n}r_i r_j\,\Xi\left(f_c,n,f_c,n,j-i,0\right)+\\ +4f_c^2\sum_{i'=1}^{n-1}\sum_{j'=i'+1}^{n}\sum_{i=1}^{n-1}\sum_{j=i+1}^{n}r_i r_j s_{i'}s_{j'}\,\Xi\left(f_c,n,f_c,n,j-i,j'-i'\right)\end{cases} \tag{5.27}$$

which is only a function of *n*, that is the length of the generation vector $\bar{r}=\bar{s}$, and the chip form of the particular BCS sequence as we can clearly recognize. Moreover, as shown in Appendix O.2, the different sum terms of the SSC simplify to the following expression:

$$\mathrm{SSC}_{\mathrm{BCS}([\bar{s}],f_c)}^{Self}=\begin{cases} n^2 f_c^2\,\Psi\left(n,0,0\right)+\\ 4f_c^2\sum_{l_1=1}^{n-1}\left\{n\bar{s}\left[\theta\left(\bar{s},l_1\right)\right]^T\Psi\left(n,l_1,0\right)+\sum_{l_2=1}^{n-1}\bar{s}\left[\theta\left(\bar{s},l_1\right)\right]^T\bar{s}\left[\theta\left(\bar{s},l_2\right)\right]^T\Psi\left(n,l_1,l_2\right)\right\}\end{cases} \tag{5.28}$$

We show in the next figure as an example the value of the self SSC of the C/A Code as a function of the integration bandwidth. As we can see, the theoretical prediction matches perfectly with the results of the simulations even for narrow receiver bandwidths.

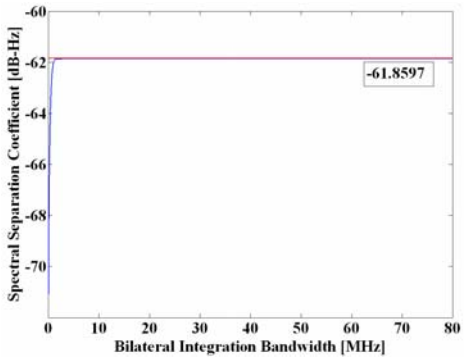

Figure 5.3. Self Spectral Separation Coefficient of C/A Code as a function of the Integration Bandwidth. The analytical value is shown in red

5.2.4 SSC between a generic BCS signal and a sine-phased BOC signal

As shown in Appendix O.3, the SSC between a generic BCS signal $\mathrm{BCS}\left([\bar{r}], f_c^1\right)$ and a sine-phased BOC with chip rate f_c^2 and subcarrier frequency $f_s^2 = n_2 f_c^2/2$ is:

$$\begin{aligned}
&\mathrm{SSC}_{\mathrm{BCS}\left([\bar{r}], f_c^1\right)-\mathrm{BOC}_{\sin}\left(f_s^2=\frac{n_2 f_c^2}{2}, f_c^2\right)} = \\
&\begin{cases}
n_1 n_2 f_c^1 f_c^2\, \Xi\left(f_c^1, n_1, f_c^2, n_2, 0, 0\right) + \\
+ 2 n_1 f_c^1 f_c^2 \sum_{i=1}^{n_2-1} (-1)^i (n_2 - i) \Xi\left(f_c^1, n_1, f_c^2, n_2, 0, i\right) + \\
+ 2 n_2 f_c^1 f_c^2 \sum_{l=1}^{n_1-1} [r_1, r_2, \ldots r_{n_1}] \left[\theta\left([r_1, r_2, \ldots r_{n_1}], l\right)\right]^T \Xi\left(f_c^1, n_1, f_c^2, n_2, l, 0\right) + \\
+ 4 f_c^1 f_c^2 \sum_{l=1}^{n_1-1} \left\{ [r_1, r_2, \ldots r_{n_1}] \left[\theta\left([r_1, r_2, \ldots r_{n_1}], l\right)\right]^T \sum_{i=1}^{n_2-1} (-1)^i (n_2 - i) \Xi\left(f_c^1, n_1, f_c^2, n_2, l, i\right) \right\}
\end{cases}
\end{aligned} \tag{5.29}$$

5.2.5 SSC between a generic BCS signal and a cosine-phased BOC signal

Equally, the SSC between a generic BCS signal and a cosine-phased BOC is shown to be:

$$\begin{aligned}
&\mathrm{SSC}_{\mathrm{BCS}\left([\bar{r}], f_c^1\right)-\mathrm{BOC}_{\cos}\left(f_s^2=\frac{n_2 f_c^2}{4}, f_c^2\right)} = \\
&\begin{cases}
n_1 n_2 f_c^1 f_c^2\, \Xi\left(f_c^1, n_1, f_c^2, n_2, 0, 0\right) + \\
+ 2 n_1 f_c^1 f_c^2 \left[\sum_{i=1}^{n_2/2} (-1)^i\, \Xi\left(f_c^1, n_1, f_c^2, n_2, 0, 2i-1\right) + \sum_{i=1}^{n_2/2-1} 2(-1)^i (n_2/2 - i) \Xi\left(f_c^1, n_1, f_c^2, n_2, 0, 2i\right) \right] + \\
+ 2 n_2 f_c^1 f_c^2 \sum_{l=1}^{n_1-1} [r_1, r_2, \ldots r_{n_1}] \left[\theta\left([r_1, r_2, \ldots r_{n_1}], l\right)\right]^T \Xi\left(f_c^1, n_1, f_c^2, n_2, l, 0\right) + \\
+ 4 f_c^1 f_c^2 \sum_{l=1}^{n_1-1} \left\{ [r_1, r_2, \ldots r_{n_1}] \left[\theta\left([r_1, r_2, \ldots r_{n_1}], l\right)\right]^T \times \left[\sum_{i=1}^{n_2/2} (-1)^i \Xi\left(f_c^1, n_1, f_c^2, n_2, l, 2i-1\right) + \right. \right. \\
\left. \left. + \sum_{i=1}^{n_2/2-1} 2(-1)^i (n_2/2 - i) \Xi\left(f_c^1, n_1, f_c^2, n_2, l, 2i\right) \right] \right\}
\end{cases}
\end{aligned} \tag{5.30}$$

5.2.6 SSC between a generic BCS signal and BPSK

Finally, the SSC between an arbitrary BCS signal and BPSK simplifies as shown next:

$$\mathrm{SSC}_{\mathrm{BCS}\left([\bar{r}],f_c^1\right)-\mathrm{BPSK}(f_c^2)}=\begin{cases} n_1 n_2 f_c^1 f_c^2\,\Xi\left(f_c^1,n_1,f_c^2,n_2,0,0\right)+ \\ +2n_1 f_c^1 f_c^2\sum_{i=1}^{n_2-1}(n_2-i)\Xi\left(f_c^1,n_1,f_c^2,n_2,0,i\right)+ \\ +2n_2 f_c^1 f_c^2\sum_{l=1}^{n_1-1}[r_1,r_2,...r_{n_1}]\left[\theta\left([r_1,r_2,...r_{n_1}],l\right)\right]^T\Xi\left(f_c^1,n_1,f_c^2,n_2,l,0\right)+ \\ +4f_c^1 f_c^2\sum_{l=1}^{n_1-1}\left\{[r_1,r_2,...r_{n_1}]\left[\theta\left([r_1,r_2,...r_{n_1}],l\right)\right]^T\sum_{i=1}^{n_2-1}(n_2-i)\Xi\left(f_c^1,n_1,f_c^2,n_2,l,i\right)\right\} \end{cases} \tag{5.31}$$

5.2.7 MBOC Theoretical SSCs

As shown in chapter 3.7, the selection of MBOC(6,1,1/11) was the result of long research works carried out by Working Group A members of the EU and US. Given the importance that the spectral separation of MBOC played at that time, we show next the analytical expressions for the SSC between an arbitrary BCS signal and MBOC(6,1,1/11). The driver of studying this variable is that if a new signal is proposed in the future for this band, the spectral separation with the MBOC(6,1,1/11), as well as with the rest of signals, will have to be carefully studied to make sure that the new signal would be compatible with the Galileo E1 OS and GPS L1C. It is important to note that this potential signal does not necessarily have to be from GPS and Galileo, but could be from any other system.

MBOC(6,1,1/11) is a particular case of the MBCS signals analyzed in chapter 3.6.2 and represents the multiplexing of BOC(1,1) and BOC(6,1) with 1/11 of power on the high frequency BOC component. As we have shown in chapter 4, while the CBOC implementation reaches this percentage modifying the amplitude of the modulation in the time domain, TMBOC obtains the desired percentage by repeating the BOC(6,1) component in the time domain correspondingly.

To calculate the SSC between a given signal and MBOC, we calculate separately the SSC with BOC(1,1) and BOC(6,1) given that the multiplexed GPS L1C and Galileo E1 OS signals are a lineal combination of both. General expressions were derived in Appendix O.

In the case of BOC(6,1), the BCS vector is shown to be s = [1,-1,1,-1,1,-1,1,-1,1,-1,1,-1] and from its M generation matrix, it can be shown that the SSC between an arbitrary BCS signal $\mathrm{BCS}\left([\bar{r}],f_c^1\right)$ and BOC(6,1) can be expressed as follows:

$$\mathrm{SSC}_{\mathrm{BCS}\left([\bar{r}],f_c^1\right)-\mathrm{BOC}(6,1)}=\mathrm{SSC}_1+\mathrm{SSC}_2+\mathrm{SSC}_3+\mathrm{SSC}_4 \tag{5.32}$$

where:

$$\mathrm{SSC}_1\left(n_1, f_c^1\right) = n_1 n_2 f_c^1 f_c^2\, \Xi\left(f_c^1, n_1, f_c^2, n_2, 0, 0\right)$$

$$\mathrm{SSC}_2\left(n_1, f_c^1\right) = 2 n_1 f_c^1 f_c^2 \begin{bmatrix} -11\Xi\left(f_c^1, n_1, f_c^2, n_2, 0, 1\right) + 10\Xi\left(f_c^1, n_1, f_c^2, n_2, 0, 2\right) - 9\Xi\left(f_c^1, n_1, f_c^2, n_2, 0, 3\right) + \\ +8\Xi\left(f_c^1, n_1, f_c^2, n_2, 0, 4\right) - 7\Xi\left(f_c^1, n_1, f_c^2, n_2, 0, 5\right) + 6\Xi\left(f_c^1, n_1, f_c^2, n_2, 0, 6\right) - \\ -5\Xi\left(f_c^1, n_1, f_c^2, n_2, 0, 7\right) + 4\Xi\left(f_c^1, n_1, f_c^2, n_2, 0, 8\right) - 3\Xi\left(f_c^1, n_1, f_c^2, n_2, 0, 9\right) + \\ +2\Xi\left(f_c^1, n_1, f_c^2, n_2, 0, 10\right) - \Xi\left(f_c^1, n_1, f_c^2, n_2, 0, 11\right) \end{bmatrix}$$

$$\mathrm{SSC}_3\left(n_1, f_c^1\right) = 2 n_2 f_c^1 f_c^2 \sum_{l=1}^{n_1 - 1} [r_1, r_2, \ldots r_{n_1}] \left[\theta\left([r_1, r_2, \ldots r_{n_1}], l\right)\right]^T \Xi\left(f_c^1, n_1, f_c^2, n_2, l, 0\right)$$

$$\mathrm{SSC}_4\left(n_1, f_c^1\right) = 4 f_c^1 f_c^2 \sum_{l=1}^{n_1 - 1} [r_1, r_2, \ldots r_{n_1}] \left[\theta\left([r_1, r_2, \ldots r_{n_1}], l\right)\right]^T \begin{Bmatrix} -11\Xi\left(f_c^1, n_1, f_c^2, n_2, l, 1\right) + 10\Xi\left(f_c^1, n_1, f_c^2, n_2, l, 2\right) - \\ -9\Xi\left(f_c^1, n_1, f_c^2, n_2, l, 3\right) + 8\Xi\left(f_c^1, n_1, f_c^2, n_2, l, 4\right) - \\ -7\Xi\left(f_c^1, n_1, f_c^2, n_2, l, 5\right) + 6\Xi\left(f_c^1, n_1, f_c^2, n_2, l, 6\right) - \\ -5\Xi\left(f_c^1, n_1, f_c^2, n_2, l, 7\right) + 4\Xi\left(f_c^1, n_1, f_c^2, n_2, l, 8\right) - \\ -3\Xi\left(f_c^1, n_1, f_c^2, n_2, l, 9\right) + 2\Xi\left(f_c^1, n_1, f_c^2, n_2, l, 10\right) - \\ -\Xi\left(f_c^1, n_1, f_c^2, n_2, l, 11\right) \end{Bmatrix} \tag{5.33}$$

with

$$\begin{aligned} f_c^2 &= 1.023 MHz \\ n_2 &= 12 \end{aligned} \tag{5.34}$$

In a similar way the parameters for the SSC with BOC(1,1) could be derived.

5.2.8 Analytical Power of a generic BCS signal in a given Bandwidth β_r

Once we have the general expression for the SSC of any possible combination of signals, we concentrate now on another figure: namely the power that falls in a given bandwidth. Indeed, sometimes SSCs are not computed in an infinite but in a finite bandwidth and the power spectral densities are normalized to the transmission bandwidth. As shown in Appendix O.5, the general expression of the power of a BCS signal is shown to be given by:

$$P = \begin{Bmatrix} nf_c \dfrac{\dfrac{2\left[-1+\cos\left(\dfrac{\pi\beta_r}{f_c n}\right)\right]}{\beta_r} + \dfrac{2\pi\, Si\left(\dfrac{\pi\beta_r}{f_c n}\right)}{f_c n}}{\pi^2} + \\ + \dfrac{2}{\beta_r\, n\, \pi^2} \displaystyle\sum_{i=1}^{n-1} \sum_{j=i+1}^{n} s_i s_j \begin{bmatrix} -2 f_c n \cos\left(\dfrac{\beta_r\, k\pi}{f_c n}\right) + 2 f_c n \cos\left(\dfrac{\beta_r \pi}{f_c n}\right) \cos\left(\dfrac{\beta_r k\pi}{f_c n}\right) + \\ \beta_r (k-1)\pi\, Si\left[\dfrac{\beta\pi(k-1)}{f_c n}\right] - 2\beta_r\, k\pi\, Si\left[\dfrac{\beta_r \pi k}{f_c n}\right] + \\ +\beta_r (1+k)\pi\, Si\left[\dfrac{\beta_r \pi (1+k)}{f_c n}\right] \end{bmatrix}_{k=j-i} \end{Bmatrix} \tag{5.35}$$

In the next pages the spectral separation coefficients of different signals of interest are shown in detail. To calculate them, the general SSC definition as well as the expressions derived in previous chapters will be employed to study the effects of filtering and normalization with respect to the transmission bandwidth. It must be noted that the bandwidth must be read exactly as it appears on the table. Thus 24 MHz must be interpreted as 24.00 MHz. For the rest a factor 1.023 is explicitly multiplying.

5.2.9 Efficiency Parameters

Together with the SSC derivations of previous chapters, we present here some other figures of interest that help in understanding the power distribution profile of a particular signal.

As we saw in (4.13), sometimes it is of interest to normalize the power spectral density to the transmission bandwidth β_T to compensate for the power that goes lost outside the transmission bandwidth. As we saw there, to keep the transmitted power constant after applying filtering, the power has to be raised by the corresponding factor:

$$\varepsilon = \int_{-\frac{\beta_T}{2}}^{\frac{\beta_T}{2}} G(f)\mathrm{d}f \tag{5.36}$$

This parameter indicates how much of the PSD normalized in an infinite bandwidth falls within a given bandwidth and thus the correction that must be made to have a normalized power spectral density of 1 W within the transmission bandwidth. The more energy the signal concentrates at low frequencies, the less significative will be the necessary correction as table 5.1 next clearly shows for different signals. As we can recognize, the parameter ε is equivalent to P in (5.35).

Once we have realized the necessary correction on the normalized PSD to accomplish the desired power emission, we can see that in general the receiver bandwidth will be much narrower than the emission bandwidth, resulting thus in an additional reduction of power at user level versus that emitted by the satellite. This is a figure of great importance for the correct design of a system, since as we have seen, all the power specifications are given at user level and correspondingly the powers must be adjusted in the satellite. To the object of analyzing this effect for different signals, we define an additional efficiency parameter:

$$\eta = \int_{-\frac{\beta_R}{2}}^{\frac{\beta_R}{2}} \overline{G}(f)\mathrm{d}f \tag{5.37}$$

where

$$\overline{G}(f) = \frac{G(f)}{\int_{-\frac{\beta_T}{2}}^{\frac{\beta_T}{2}} G(f)\mathrm{d}f} \tag{5.38}$$

This parameter indicates how much power falls within the receiver bandwidth. In the next table, the above defined efficiency parameters are calculated for the GPS and Galileo signals in E1/L1. For simplicity, the same bandwidths as in [S. Wallner et al., 2005] are assumed.

Table 5.1. Efficiency Parameters of GPS L1 signals

	BPSK(1)	BPSK(10)	BOC(10,5)	BOC(1,1)	MBOC
TX BW [MHz]	**30.69**	**30.69**	**30.69**	**30.69**	**30.69**
RX BW [MHz]	**24.00**	**24.00**	**24.00**	**24.00**	**24.00**
ε	-0.0294	-0.3101	-0.8023	-0.0890	-0.1545
η	-0.0077	-0.1216	-0.3727	-0.0222	-0.0207

Table 5.2. Efficiency Parameters of Galileo E1 signals

	BOC(1,1)	MBOC	$BOC_{cos}(15,2.5)$
TX BW [MHz]	**40.92**	**40.92**	**40.92**
RX BW [MHz]	**24.00**	**24.00**	**40.92**
ε	-0.0665	-0.0989	-1.1069
η	-0.0448	-0.0762	$-\infty$

As we can recognize, Galileo presents better values than GPS due to the wider transmission and receiver bandwidth that we have assumed. These are indeed standard figures that can be found today in the hardware specifications of any receiver and signal generator manufacturer. Furthermore, for GPS a bandwidth of 30.69 MHz was selected so as to have the main lobe of the widest signal inside, namely the M-Code. In the same manner, we have assumed a transmission bandwidth of 40.92 for the PRS for at least one of the secondary lobes to fall inside. As one can imagine, real emissions will considerably differ from the assumptions of previous and next pages.

Table 5.3. Spectral Separation Coefficients in E1/L1. The Power Spectral Densities are normalized to the transmission bandwidth and integrated in the bandwidth of the receiver

SSC in L1 [dB-Hz]				RECEPTION							
				GPS					Galileo		
				BPSK(1)	BOC(1,1)	MBOC	P-Code	M-Code	BOC(1,1)	MBOC	PRS
			Tx_2 BW	30.69 MHz	30.69 MHz	30.69 MHz	30.69 MHz	30.69 MHz	40.92 MHz	40.92 MHz	40.92 MHz
			Rx BW / Tx_1 BW	24 MHz	24 MHz	24 MHz	24 MHz	24 MHz	24 MHz	24 MHz	40.92 MHz
EMISSION	GPS	BPSK(1)	30.69 MHz	-61.8008	-67.7619	-68.0983	-69.9070	-87.1118	-67.7844	-68.1539	-99.0884
		BOC(1,1)	30.69 MHz	-67.7619	-64.6921	-65.0346	-70.1590	-82.2681	-64.7147	-65.0901	-94.3047
		MBOC	30.69 MHz	-68.0983	-65.0346	-65.3483	-70.3936	-81.9455	-65.0572	-65.4039	-94.2558
		P-Code	30.69 MHz	-69.9070	-70.1590	-70.3936	-71.2521	-79.9042	-70.1816	-70.4492	-86.4481
		M-Code	30.69 MHz	-87.1118	-82.2681	-81.9455	-79.9042	-71.6920	-82.2906	-82.0010	-86.7214
	Galileo	BOC(1,1)	40.92 MHz	-67.7844	-64.7147	-65.0572	-70.1816	-82.2906	-64.7373	-65.1127	-91.6095
		MBOC	40.92 MHz	-68.1539	-65.0901	-65.4039	-70.4492	-82.0010	-65.1127	-65.4594	-91.3435
		PRS	40.92 MHz	-108.6953	-103.1826	-101.4261	-100.5956	-88.8814	-103.2052	-101.4817	-68.4503

As we can recognize from the table above, MBOC presents better spectral separation with the rest of signals in the band, making thus the compatibility considerably easier. For instance, the spectral overlapping of the GPS MBOC with the GPS C/A code is approximately 0.34 dB better than that of BOC(1,1) and even 0.37 dB in the case of Galileo. In addition, since the Self SSC of MBOC is around 0.7 dB lower than that of BOC(1,1) for both GPS and Galileo, resulting in better intrasystem interference figures as the results of chapter 4.7.8 clearly showed.

Table 5.4. Spectral Separation Coefficients in E6. The Power Spectral Densities are normalized to the transmission bandwidth and integrated in the receiver bandwidth

SSC in E6 [dB-Hz]				RECEPTION		
				QZSS	Galileo	
				BPSK(5)	BPSK(5)	$BOC_{cos}(10,5)$
			Tx_2 BW	40.92MHz	40.92 MHz	40.92 MHz
			Rx BW / Tx_1 BW	24 MHz	24 MHz	40.92 MHz
EMISSION	QZSS	BPSK(5)	40.92 MHz	-68.6289	-68.6289	-85.7897
	Galileo	BPSK(5)	40.92 MHz	-68.6289	-68.6289	-85.7897
		$BOC_{cos}(10,5)$	40.92 MHz	-86.9659	-86.9659	-71.3410

Table 5.5. Spectral Separation Coefficients in E5. The Power Spectral Densities are normalized to the transmission bandwidth and integrated in the receiver bandwidth

SSC in E5 [dB-Hz]				RECEPTION		
				QZSS	GPS	Galileo
				BPSK(10)	BPSK(10)	AltBOC(15,10)
			Tx_2 BW	24 MHz	30.69 MHz	92.07 MHz
			Rx BW / Tx_1 BW	24 MHz	24 MHz	92.07 MHz
EMISSION	QZSS	BPSK(10)	24 MHz	-71.0089	-71.1305	-74.5742
	GPS	BPSK(10)	30.69 MHz	-71.1305	-71.2521	-74.6958
	Galileo	AltBOC(15,10)	92.07 MHz	-74.5742	-74.6851	-75.0696

We repeat now the computation of the SSCs of QZSS, GPS and Galileo signals but this time without normalizing at the satellite and thus assuming an infinite transmission bandwidth. The purpose of this exercise is to show the difference with respect to the values of the tables calculated above. Since analytical expressions have been derived for infinite bandwidth, to compute the band-limited versions of the SSCs their analytical counterparts could be employed applying the corresponding corrections from the efficiency parameters. As one can imagine, this would imply an enormous simplification. We see this more in detail in the next tables.

Table 5.6. Spectral Separation Coefficients in E1/L1. The PSDs are normalized to infinite bandwidth and integrated in the receiver bandwidth

SSC in L1 [dB-Hz]				RECEPTION							
				GPS					Galileo		
				BPSK(1)	BOC(1,1)	MBOC	P-Code	M-Code	BOC(1,1)	MBOC	PRS
			Tx_2 BW	∞ MHz	∞ MHz	∞ MHz	∞ MHz	∞ MHz	∞ MHz	∞ MHz	∞ MHz
			Rx BW / Tx_1 BW	24 MHz	24 MHz	24 MHz	24 MHz	24 MHz	24 MHz	24 MHz	40.92 MHz
EMISSION	GPS	BPSK(1)	∞ MHz	-61.8597	-67.8803	-68.2823	-70.2466	-87.9436	-67.8803	-68.2823	-97.5478
		BOC(1,1)	∞ MHz	-67.8803	-64.8702	-65.2781	-70.5581	-83.1594	-64.8702	-65.2781	-92.7828
		MBOC	∞ MHz	-68.2823	-65.6573	-65.2781	-70.8582	-82.9023	-65.2781	-65.6573	-92.5493
		P-Code	∞ MHz	-70.2466	-70.5581	-70.8582	-71.8723	-81.0166	-70.5581	-70.8582	-85.0854
		M-Code	∞ MHz	-87.9436	-83.1594	-82.9023	-81.0166	-73.2967	-83.1594	-82.9023	-88.3768
	Galileo	BOC(1,1)	∞ MHz	-67.8803	-64.8702	-65.2781	-70.5581	-83.1594	-64.8702	-65.2781	-92.7828
		MBOC	∞ MHz	-68.2823	-65.6573	-65.2781	-70.8582	-82.9023	-65.2781	-65.6573	-92.5493
		PRS	∞ MHz	-109.8317	-104.3785	-102.6875	-102.0126	-90.7907	-104.3785	-102.6875	-70.6641

If we compare now tables 5.3 and 5.6 we can clearly see that the SSCs normalized to the transmission bandwidth and to infinite bandwidth can significantly differ from one another being the difference more significant the more power the signal concentrates at higher frequencies. In fact, it is trivial to recognize that the SSC that results from normalizing to the transmission bandwidth and integrating in the receiver bandwidth (Table 5.3) can be easily obtained from the sum of the non-normalized SSC integrated in infinite bandwidth (Table 5.6) minus the efficiency factors of the signals. For example, $\mathrm{SSC}_{BPSK,Tx}(-61.8008) = \mathrm{SSC}_{BPSK,\infty}(-61.8597) - 2\varepsilon_{BPSK,Tx}(-0.0294)$. Equally for the SSC between the C/A Code and BOC(1,1) we have $\mathrm{SSC}^{Tx_1,Tx_2}_{BPSK,BOC(1,1)}(-67.7619) = \mathrm{SSC}^{\infty,\infty}_{BPSK,BOC(1,1)}(-67.8803) - \varepsilon_{BPSK,Tx_1}(-0.0294) - \varepsilon_{BPSK,Tx_2}(-0.0890)$. We can express this as follows:

$$\mathrm{SSC}^{T_x^1,T_x^2}_{s_1,s_2} = \mathrm{SSC}^{\infty,\infty}_{s_1,s_2} - \varepsilon_{s_1} - \varepsilon_{s_2} \tag{5.39}$$

Table 5.7. Spectral Separation Coefficients in E6. The PSDs are normalized to infinite bandwidth and integrated in the receiver bandwidth

SSC in E6 [dB-Hz]				RECEPTION		
				QZSS	Galileo	
				BPSK(5)	BPSK(5)	$BOC_{cos}(10,5)$
			Tx_2 BW	∞ MHz	∞ MHz	∞ MHz
			Rx BW / Tx_1 BW	24 MHz	24 MHz	40.92 MHz
EMISSION	QZSS	BPSK(5)	∞ MHz	-68.8510	-68.8510	-87.0217
	Galileo	BPSK(5)	∞ MHz	-68.8510	-68.8510	-87.0217
		$BOC_{cos}(10,5)$	∞ MHz	-88.1979	-88.1979	-73.5827

Table 5.8. Spectral Separation Coefficients in E5. The PSDs are normalized to infinite bandwidth and integrated in the receiver bandwidth

SSC in E5 [dB-Hz]				RECEPTION		
				QZSS	GPS	Galileo
				BPSK(10)	BPSK(10)	AltBOC(15,10)
			Tx_2 BW	∞ MHz	∞ MHz	∞ MHz
			Rx BW / Tx_1 BW	24 MHz	24 MHz	92.07 MHz
EMISSION	QZSS	BPSK(10)	∞ MHz	-71.8723	-71.8723	-83.6088
	GPS	BPSK(10)	∞ MHz	-71.8723	-71.8723	-83.6088
	Galileo	AltBOC(15,10)	∞ MHz	-86.0782	-86.0782	-75.4304

We can still go one step further and not only work with non-normalized Power Spectral Densities as we did in the previous tables, but also integrate in an infinite bandwidth at receiver level. This is of enormous interest because if we find out that there are no significant differences in the obtained values, we could apply the analytical expressions derived in this chapter to easily calculate the values also for the band-limited case. As we saw, the analytical values are only valid for the infinite bandwidth case, but as we will see, this is a very good approximation for most of the signals.

Table 5.9. Spectral Separation Coefficients in E1/L1. The PSDs are normalized to infinite bandwidth and integrated in an infinite bandwidth. The numbers were obtained using the analytical expressions derived in chapter 5.2

SSC in L1 [dB-Hz]				RECEPTION							
				GPS					Galileo		
				BPSK(1)	BOC(1,1)	MBOC	P-Code	M-Code	BOC(1,1)	MBOC	PRS
			Tx_2 BW	∞ MHz	∞ MHz	∞ MHz	∞ MHz	∞ MHz	∞ MHz	∞ MHz	∞ MHz
			Rx BW / Tx_1 BW	∞ MHz	∞ MHz	∞ MHz	∞ MHz	∞ MHz	∞ MHz	∞ MHz	∞ MHz
EMISSION	GPS	BPSK(1)	∞ MHz	-61.8597	-67.8803	-68.2821	-70.2460	-87.8803	-67.8803	-68.2821	-97.4229
		BOC(1,1)	∞ MHz	-67.8803	-64.8700	-65.2779	-70.5563	-83.1091	-64.8700	-65.2779	-92.6514
		MBOC	∞ MHz	-68.2821	-65.2779	-65.6566	-70.8559	-82.8373	-65.2779	-65.6566	-92.4166
		P-Code	∞ MHz	-70.2460	-70.5563	-70.8559	-71.8597	-80.8906	-70.5563	-70.8559	-84.9924
		M-Code	∞ MHz	-87.8803	-83.1091	-82.8373	-80.8906	-73.1091	-83.1091	-82.8373	-88.2146
	Galileo	BOC(1,1)	∞ MHz	-67.8803	-64.8700	-65.2779	-70.5563	-83.1091	-64.8700	-65.2779	-92.6514
		MBOC	∞ MHz	-68.2821	-65.2779	-65.6566	-70.8559	-82.8373	-65.2779	-65.6566	-92.4166
		PRS	∞ MHz	-97.4229	-92.6514	-92.4166	-84.9924	-88.2146	-92.6514	-92.4166	-70.5939

If we compare now tables 5.6 and 5.9, we can clearly see that the derived SSCs are practically identical for most of the cases of interest, in particular for the Self SSCs. While for the case of the Self C/A Code SSC similar results to those obtained with the analytical expressions are achieved using the infinite bandwidth approximation and integrating in 24.00 MHz, for the Self SSC of the PRS the difference is lower than 0.1 dB. For the rest of combinations, the differences are normally not higher than 0.25 dB except for the particular case of the PRS. Since this signal concentrates an important amount of power at higher frequencies due to its high sub-carrier frequency and cosine phasing, considerable differences are observed here. This corresponds to the worst case and thus, unless very accurate figures are required, the derived analytical expressions corrected by the efficiency parameters seem to be accurate enough for most of the purposes. Note that the goodness of the approximation will depend on how true the approximation is that the receiver bandwidth is large enough compared with the main lobe of the signal.

Table 5.10. Spectral Separation Coefficients in E6. The PSDs are normalized to infinite bandwidth and integrated in an infinite bandwidth. The figures were obtained using the analytical expressions derived in chapter 5.2

SSC in E6 [dB-Hz]				RECEPTION		
				QZSS	Galileo	
				BPSK(5)	BPSK(5)	$BOC_{cos}(10,5)$
			Tx_2 BW	∞ MHz	∞ MHz	∞ MHz
			Rx BW / Tx_1 BW	∞ MHz	∞ MHz	∞ MHz
EMISSION	QZSS	BPSK(5)	∞ MHz	-68.8494	-68.8494	-86.9112
	Galileo	BPSK(5)	∞ MHz	-68.8494	-68.8494	-86.9112
		$BOC_{cos}(10,5)$	∞ MHz	-86.9112	-86.9112	-73.4870

Table 5.11. Spectral Separation Coefficients in E5. The PSDs are normalized to infinite bandwidth and integrated in an infinite bandwidth. The figures were obtained using the analytical expressions derived in chapter 5.2

SSC in E5 [dB-Hz]				RECEPTION		
				QZSS	GPS	Galileo
				BPSK(10)	BPSK(10)	AltBOC(15,10)
			Tx_2 BW	∞ MHz	∞ MHz	∞ MHz
			Rx BW / Tx_1 BW	∞ MHz	∞ MHz	∞ MHz
EMISSION	QZSS	BPSK(10)	∞ MHz	-71.8597	-71.8597	-84.0291
	GPS	BPSK(10)	∞ MHz	-71.8597	-71.8597	-84.0291
	Galileo	AltBOC(15,10)	∞ MHz	-84.0291	-84.0291	-76.2645

For E5 and E6 we can see that again the analytical approximation corrected by the efficiency parameters are a good approximation except for the case of the cosine-phase BOC(10,5) and AltBOC.

Now that we have calculated the SSCs of some of the GPS, Galileo and QZSS signals, we analyze next the particular case of GLONASS. As we thoroughly described in chapter 2.5, GLONASS makes use of FDMA instead of CDMA yet. Let us see the robustness of the approach in regards to the Spectral Separation Coefficients. For exemplification, the Self SSC of the GLONASS L1 C/A Code and P-Code for SVNs with indexes from -7 to -1 are presented in the following tables:

Table 5.12. L1 GLONASS C/A Code Self SSCs. The PSDs are normalized to the main lobe of the C/A Code and integrated in a receiver with infinite bandwidth

GLONASS C/A Code SSC [dB-Hz]							
SVN	**-7**	**-6**	**-5**	**-4**	**-3**	**-2**	**-1**
-7	-57.9700	-69.5604	-∞	-∞	-∞	-∞	-∞
-6	-69.5604	-57.9700	-69.5604	-∞	-∞	-∞	-∞
-5	-∞	-69.5604	-57.9700	-69.5604	-∞	-∞	-∞
-4	-∞	-∞	-69.5604	-57.9700	-69.5604	-∞	-∞
-3	-∞	-∞	-∞	-69.5604	-57.9700	-69.5604	-∞
-2	-∞	-∞	-∞	-∞	-69.5604	-57.9700	-69.5604
-1	-∞	-∞	-∞	-∞	-∞	-69.5604	-57.9700

In the same manner, the Self SSCs of the L1 GLONASS P-Code signals for SVNs with index ranging between -7 to -1 are shown next:

Table 5.13. L1 GLONASS P-Code Self SSCs. The PSDs are normalized to the main lobe of the P-Code and integrated in a receiver with infinite bandwidth

GLONASS P-Code SSC [dB-Hz]							
SVN	**-7**	**-6**	**-5**	**-4**	**-3**	**-2**	**-1**
-7	-67.9700	-68.0732	-68.3840	-68.9060	-69.6454	-70.6122	-71.8202
-6	-68.0732	-67.9700	-68.0732	-68.3840	-68.9060	-69.6454	-70.6122
-5	-68.3840	-68.0732	-67.9700	-68.0732	-68.3840	-68.9060	-69.6454
-4	-68.9060	-68.3840	-68.0732	-67.9700	-68.0732	-68.3840	-68.9060
-3	-69.6454	-68.9060	-68.3840	-68.0732	-67.9700	-68.0732	-68.3840
-2	-70.6122	-69.6454	-68.9060	-68.3840	-68.0732	-67.9700	-68.0732
-1	-71.8202	-70.6122	-69.6454	-68.9060	-68.3840	-68.0732	-67.9700

As we can see from the tables above, the FDMA concept that GLONASS employs does not really bring alone a clear improvement of the spectral isolation among signals. In fact, the figures are in the same order of magnitude of the Self SSCs of the CDMA signals we have analyzed in previous pages. CDMA provides the capability to introduce an additional isolation among signals of the same family and other family by means of well selected codes while GLONASS uses the same code for all the satellites. The final superiority .of CDMA considering also the effect of the codes would be thus in the order of 20 dB or even more.

To have an idea of how GLONASS interferes with other systems in the vicinity, the next table presents the SSC between Galileo E6 and GLONASS L3 (option 2) for the different GLONASS SVNs. For more details on the signal definition, refer to chapter 2.5.3. As we saw there, this option has BPSK(8) for the I channel and BPSK(2) for the quadrature channel. In addition, for completeness not only the SSC between the GLONASS L3 signals and the

whole Galileo AltBOC modulation are shown, but also separately between GLONASS and E5a on the one side and between GLONASS and E5b on the other side. In this case, the assumption is that the receiver will correlate each of the main lobes of the AltBOC signal with a BPSK(10) replica. As we mentioned already in chapter 4.3.2.4, AltBOC signals can be processed as BPSK signals if only the main lobes are used. For the simulations, the GLONASS PSDs were normalized to the main lobe while the Galileo signals were normalized to a transmission bandwidth of 92.07 MHz, that 90 x 1.023 MHz. In addition, the assumed receiver bandwidth was of 92.07 MHz for the AltBOC receiver while for the E5a and E5b receivers a bandwidth of 40.92 MHz was assumed.

Table 5.14. SSC between Galileo E5 and GLONASS L3

SSC [dB-Hz] between Galileo E5 and GLONASS L3						
Phase	**L3 I**	**L3 Q**	**L3 I**	**L3 Q**	**L3 I**	**L3 Q**
SVN	**AltBOC receiver**		**E5a receiver**		**E5b receiver**	
-7	-81.4014	-86.2399	-95.3234	-138.3102	-78.5145	-83.7132
-6	-80.7037	-84.4147	-96.6860	-∞	-77.7527	-81.8166
-5	-80.0278	-82.8656	-98.1793	-∞	-77.0261	-80.1968
-4	-79.3815	-81.5332	-99.8186	-∞	-76.3387	-78.7953
-3	-78.7700	-80.3744	-101.6237	-∞	-75.6925	-77.5702
-2	-78.1961	-79.3582	-103.6194	-∞	-75.0887	-76.4908
-1	-77.6614	-78.4619	-105.8386	-∞	-74.5273	-75.5348
0	-77.1666	-77.6685	-108.3247	-∞	-74.0081	-74.6854
+1	-76.7116	-76.9651	-111.1382	-∞	-73.5306	-73.9297
+2	-76.2961	-76.3416	-114.3651	-∞	-73.0940	-73.2577
+3	-75.9195	-75.7903	-118.1350	-∞	-72.6975	-72.6616
+4	-75.5811	-75.3050	-122.6559	-∞	-72.3403	-72.1349
+5	-75.2802	-74.8807	-128.2930	-∞	-72.0217	-71.6728
+6	-75.0162	-74.5135	-135.7847	-∞	-71.7409	-71.2710
+7	-74.7883	-74.2001	-147.0266	-∞	-71.4972	-70.9264
+8	-74.5960	-73.9381	-170.6288	-∞	-71.2900	-70.6362

As we can recognize, an important overlapping can be observed between the Galileo signals and GLONASS L3 for some particular combinations, making thus the compatibility of both systems more difficult. The final decision on the GLONASS final signal selection is still open and subject to discussion.

To conclude it is important to recall the definition of SSC that we presented at the beginning of this chapter. As we saw there, the SSC can be seen as the mean power of the crosscorrelation function between the desired and the interfering signals. We have repeatedly

seen in the preceding lines that in reality the signal coming from the satellite is filtered to avoid interference with other services around. This was reflected by the efficiency parameter ε. But on the side of the replica generation at receiver level the issue is not so unambiguous. While in our previous tables it was assumed that the Power Spectral Density of the desired signal was also normalized to the transmission bandwidth of the receiver, we could have also assumed that the replica signal at receiver level is generated with no significant filtering effects. The corresponding SSC would adopt the following form:

$$\kappa_{id} = \int_{-\beta_r/2}^{\beta_r/2} \overline{G_i}(f) G_d(f) \left| H_{\mathrm{RX}}(f) \right|^2 \mathrm{d}f \tag{5.40}$$

where we can recognize that only the interfering signal is normalized this time. The idea behind this SSC notation is in fact that the receiver generates the desired replica signal digitally while the interfering incoming signal will present in reality filtered values. To see the effect of considering the desired signal without normalization, some SSCs are calculated in the next table for comparison.

Table 5.15. Spectral Separation Coefficients of some signals of interest when the Power Spectral Density of the replica signal is normalized to the TX Bandwidth and when it is not (Infinite Bandwidth). All the indicated bandwidths are assumed to be in MHz

SSC [dB-Hz]	Des. Signal	BPSK(1)		BOC(1,1)		MBOC	
	Tx_2 BW	30.69	∞	30.69	∞	30.69	∞
Int. Signal	Rx BW / Tx_1 BW	24	24	24	24	24	24
BPSK(1)	30.69	-61.8008	-61.8303	-67.7619	-67.8509	-68.0983	-68.2528
BOC(1,1)	30.69	-67.7619	-67.7913	-64.6921	-64.7812	-65.0346	-65.1891
MBOC	30.69	-68.0983	-68.1278	-65.0346	-65.1236	-65.3483	-65.5028

As we can see, slight differences can be observed depending on the notation that is followed. These differences are more notable the more energy is concentrated on higher frequencies being even higher than 1 dB in the case of the SSC between GPS M-Code and Galileo PRS.

6. Spectral Separation Coefficients with data and non ideal codes

So far we have derived expressions for the Spectral Separation Coefficients between two signals when ideal codes are assumed. In this chapter we will derive expressions for the case when the data is also considered and we will study the effect of non-ideal codes on the resulting spectra.

As we have seen above, the analytical expressions for the spectral separation coefficients (SSC) and power spectral densities (PSD) that we have derived above are valid under the assumption that the chip waveform is modulated by ideal random codes which behave like noise and that we integrate for a infinite period of time. This implies that $H_{ID}(f) \to \delta(f)$.

If we recall now (5.9) again,

$$\overline{\Psi}_{ks} \approx T\int_{-\infty}^{\infty} G_k(f) \otimes G_s(f)\left|H_{ID}(f)\right|^2 \mathrm{d}f\Big|_{f=0} \approx \int_{-\infty}^{\infty} G_k(f) G_s(f) \mathrm{d}f \tag{6.1}$$

we can clearly see that depending on the integration in the receiver and the properties of the codes, the results could differ much from those expected from assuming ideal random codes. Experimental results on the goodness of the Galileo and GPS codes have been presented in [S. Wallner et al., 2006a].

The question that arises now is how true the assumptions on ideal random codes are for real receiver implementations and the effect that non-idealities in the codes have on the final power spectral density and, correspondingly, on the SSC values. We concentrate first on the effect of the data bits and the non ideality of the codes on the spectra of the signals to study later the effect of having limited integration times versus infinite integrations as assumed in chapter 5.

6.1 Analytical expressions when data is present

Until now the effect of the data bits has not been considered yet, but as we know well, GPS and Galileo will both have data channels. This will affect on the shape of the spectrum.

As we know from theory, when the chip waveform of a signal is modulated with a non-ideal PRN code, and ideal random data is placed on top of the signal, the power spectral density of the resulting modulated signal is obtained by replacing every spike of the code by a sinc of bandwidth equal to the bit data rate. Indeed, this is equivalent to the convolution of the data sinc with the non continuous line-like spectrum of the non-ideal primary code.

For the case of the GPS C/A code, the BPSK(1) waveform is modulated by a Gold code of length 1023 and the bit data rate is of 50 symbols per second (sps) resulting thus in the repetition of 20 code sequences within every data bit. Thus, the analytical way of computing the PSD would be to obtain first the spectrum of the sequence of 1 millisecond and substitute every spike by a sinc of 50 Hz. In fact, the code is 1 millisecond of duration and repeats 20 times. Moreover, since the GPS C/A primary code has a length of 1 ms, the spectral lines will present a separation with each other of 1 kHz.

Figure 6.1 next shows the PSD that would result from modulating our original signal with data on top. For our analysis a one-sided bandwidth of 15.345 MHz was assumed and thus a sampling frequency of 30.69 MHz was employed for the simulations. As a result, every chip is sampled with 30 values. No filtering is employed in the simulation and for exemplification only the spectrum of SVN 1 is shown. Moreover, the smooth spectrum of the C/A Code with ideal random codes is also shown in red for comparison.

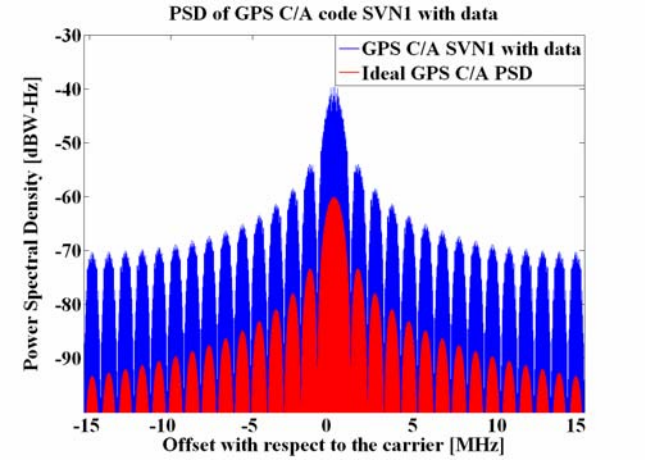

Figure 6.1. Power spectral density of GPS C/A code SVN 1 with data for a bandwidth of 30.69 MHz versus ideal PSD of a BPSK(1) modulated with an ideal random code

If we look now into the fine structure of the spectrum, we can recognize the data sincs separated by 1 kHz with respect to each other that we can predict from theory.

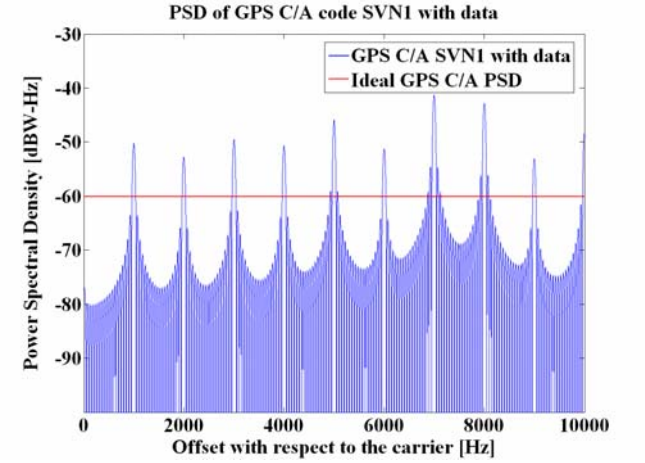

Figure 6.2. Power spectral density of GPS C/A code SVN 1 with data at low frequencies. A transmission bandwidth of 30.69 MHz was assumed

Now that we have derived the analytical expression for the power spectral density of a signal waveform modulated with ideal random data and non-ideal codes, we analyze the difference with respect to the ideal case when the signal waveform is modulated with ideal codes.

As we have seen, if data is supposed to be ideally random, the spectrum of the modulated signal with data results from the convolution of both power spectral densities, what is equivalent to substituting every spike by a sinc of the form:

$$\frac{1}{f_d}\text{sinc}\left(\frac{f}{f_d}\right) \tag{6.2}$$

where f_d refers to the data rate. As a result, the spikes of the code are spread over a wider bandwidth, increasing the amplitude as Figure 6.1 has shown. For the case of GPS C/A code with a data rate of 50 sps, this increase in the amplitude with respect to the ideal smooth spectrum is of $10\log_{10}(50) \approx 17$ dB.

If we plot now the product of the ideal PSDs of SVN 1 and SVN 2 with data and 0 Hz offset and compare it with the product of the ideal PSDs without data, we can recognize that in the ideal smooth case the product lies around 34 dB below. This is due to the fact that each PSD is 17 dB below with respect to the case with data as we saw above. Indeed, this is the reason that the SSCs, result of the integrate of both spectra with data, are around 12 dB higher than for the ideal case that we calculated in chapter 5 (-61.8597 dB-Hz).

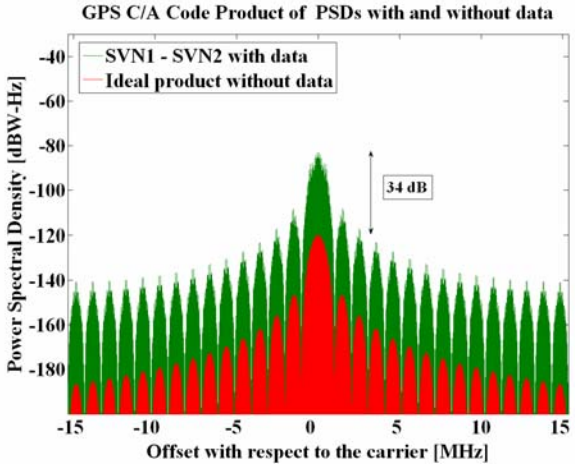

Figure 6.3. Product of C/A Code Spectra modulated with codes SVN 1 and SVN 2 with and without data

In the next table we present for comparison the SSCs of different GNSS signals when there is data and when an ideal spectrum is assumed.

Table 6.1. Spectral Separation Coefficients with and without data

SSC [dB-Hz]	Ideal SSC without data	Ideal SSC with random data	TX Bandwidth	Rx Bandwidth
BPSK(1)	-61.8008	-50.5460	30.69	30.69
BOC(1,1)	-64.6920	-64.6920	30.69	30.69
MBOC(6,1,1/11)	-65.3070	-65.3070	24.5520	24.5520

Once we have studied the problematic of calculating spectra when data or non-ideal codes are accounted, it is time to make a classification of the different types of spectra depending on the fine structure that they present. Indeed, we distinguish the following three classes according to [F. Soualle and T. Burger, 2002]:

- Type 1: Signals with smooth power spectral density (non periodical codes)
- Type 2: Signals with periodic codes and no data modulation (pilot signals)
- Type 3: Signals with periodic codes and data modulation.

As we will show next, the SSCs differ in value depending on the type of signals that are considered and the data rate. Moreover, it can be shown that if one of the signals is of type 1 (non periodical code) and the other one of type 2 or 3 the value of the spectral separation coefficient is similar to that of considering both signals of type 1.

We show an example now. The following figure depicts the product of the Power Spectral Densities of the M-Code and BOC(1,1) assuming ideal random codes and ideal random data for the M-Code (thus smooth spectrum) while for the BOC(1,1) we have smooth spectrum in one case (type 1) and the effect of ideal random data in the other case (type 3).

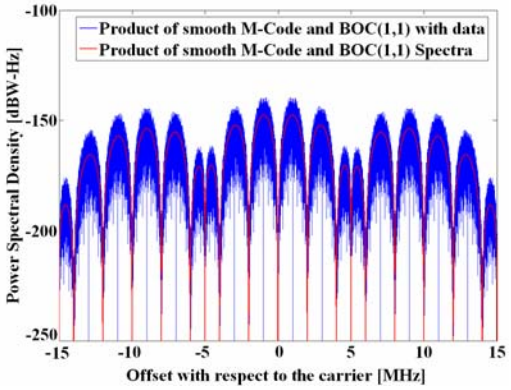

Figure 6.4. Product of BOC(1,1) Code Spectrum modulated with SVN 1 and M-Code smooth spectrum. In blue the effect of the data on BOC(1,1) is considered while in red ideal smooth fine structure is assumed

We can see the difference between both curves in detail in the next figure:

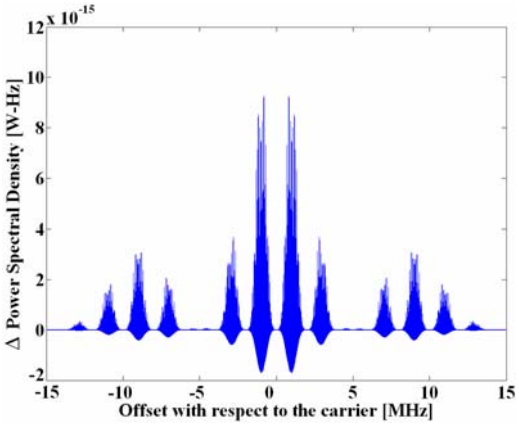

Figure 6.5. Comparison of the product of PSDs between BOC(1,1) and M-Code when data modulation is present or not

If we measure now the resulting SSCs between the M-Code and BOC(1,1) when no data is considered and when data is considered, we obtain the following results:

Table 6.2. Spectral Separation Coefficients between BOC(1,1) and M-Code with and without data

SSC [dB-Hz]	Data
-82.6566	Yes
-83.1241	No

If we sum up now the difference of Figure 6.5 and divide by the interference coefficient with data and without data, we obtain a value of approximately -9.9113 dB and -9.4437 dB respectively, confirming thus that the interference coefficient or SSC is about of the same order of magnitude as when we consider two non-periodical PSDs (SSC = -83.1241 dB-Hz), and when only the non periodic properties of BOC(1,1) are taken into account (SSC = -82.6566 dB-Hz). While this is true for these types of signals, others like the C/A Code require special attention since the fine structure is considerably affected by the code structure.

6.2 Computation of non-ideal Spectral Separation Coefficients

Once we have derived the ideal PSD that a signal with a non-ideal pseudorandom code but completely random data will have, it is important to revisit the assumptions that we have made. Indeed, assuming that the data is completely random is equivalent to saying that our receiver integrates over an infinite period of time, what is of course impossible.

This means that the integration time for the computation of the SSC plays an outstanding role in the estimation of the power spectral density. Indeed, even though our signal were ideally modulated with random data, since our observation window is limited, the partial integration of the data will result in a non-ideal partial correlation different to the ideal Dirac delta. This is deeply connected with the ideas gathered in [G.W. Hein et al., 2006c] where the concept of random codes was discussed concluding that time-limited codes and ideal random noise are contradictory *per se*.

In order to see the effect that the number of bits taken into account in the integration plays in the composition of the spectrum at receiver level, simulations were run for different integration times, averaging the resulting spectra over all possible bit combinations to derive general consequences from the results of the computations. Indeed, for n bits, 2^n possible bit combinations are possible, of which only a few have to be considered due to existing symmetries. Furthermore, (6.1) was employed to compute the SSC, not accounting thus for the filtering effect of the time-windowing. Additionally, it was assumed that the DLL behaves

as a filter and thus the power spectral density that is formed could be seen as the average of preceding bit combinations. Following these ideas, non ideal SSCs have been computed in this chapter and compared with the SSCs that would result from using the ideal power spectral density of chapter 4. This process was repeated for different bandwidths and for each of them the results are shown next. As we can see, for every considered receiver bandwidth, averaging over all data combinations results in mean SSCs that are virtually equal to those obtained using ideal PSDs. However, if we take a closer look into the fine structure (see Figure 6.6) we can recognize that the spectra are slightly different.

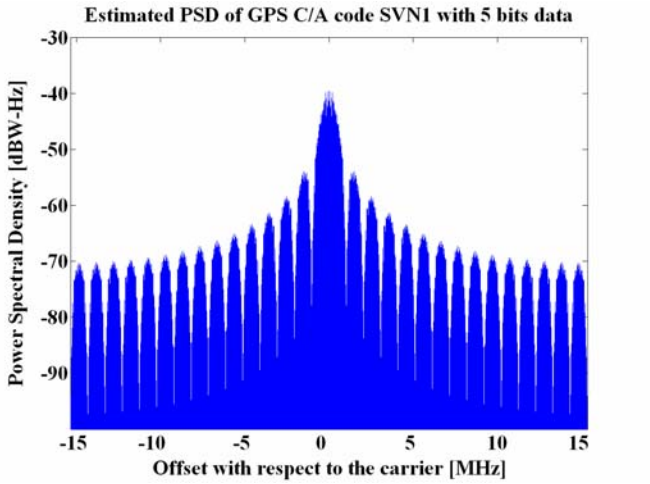

Figure 6.6. Averaged PSD of GPS C/A code SVN 1 that results from averaging all possible code sequences with 5 data bits

For the particular case of the C/A Code, we can recognize the 50 Hz sinc with already 100 milliseconds of coherent integration. However, the amplitude of the side lobes is lower in the case of the spectra estimated from simulations. Nevertheless, the amplitude of the main lobes is approximately equal in both ideal and simulated power spectral densities, and since this part of the spectrum is the main contributor to the SSC, the difference is considered negligible.

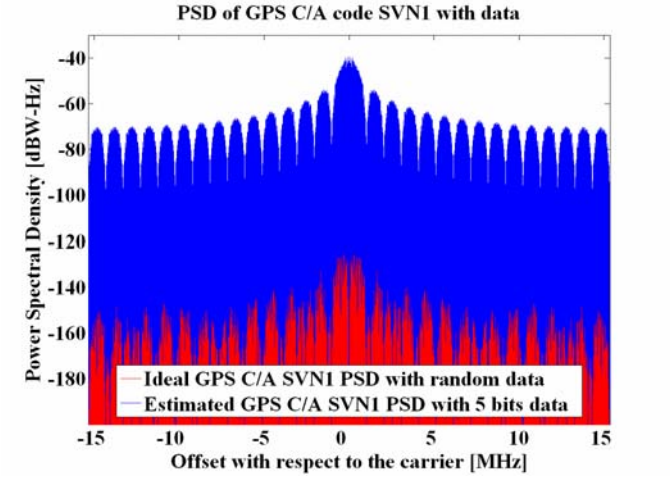

Figure 6.7. Comparison between the ideal PSD of BPSK(1) with random data at 50 sps and the averaged PSD that results from taking all combinations of 5 data bits

Moreover, if we take a look now at the fine structure that results from averaging the spectra of all possible combinations of five bits and compare it with the ideal spectrum with ideal data, we obtain the following figure:

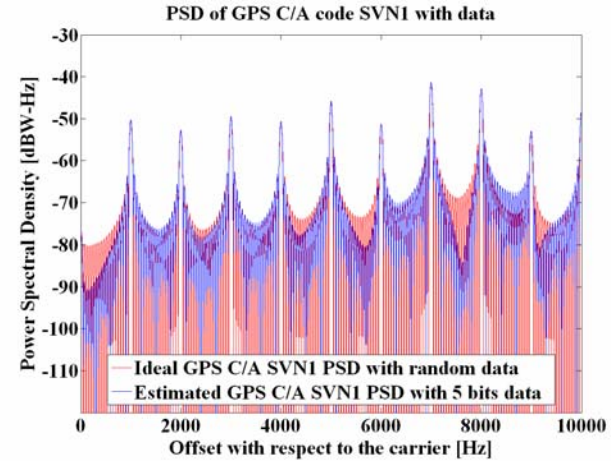

Figure 6.8. Low frequencies comparison between the ideal PSD of BPSK(1) with data at 50 sps and the averaged PSD of all 5 data bit combinations

Table 6.3. BPSK(1) SSC [dB-Hz] computed between the averaged spectra of SVN 1 and SVN 2 for a data rate of 50 sps. A spectral resolution of 5 Hz was assumed

Signal	BPSK(1)		
Double-Sided Bandwidth [MHz]	**30.69**	**4.092**	**2.046**
Self SSC with ideal primary random codes and no data	-61.8008	-61.4155	-60.9845
SSC with ideal primary random codes and ideal data	-50.5460	-50.1607	-49.7297
SSC with SVN 1-SVN 2 primary codes and ideal data	-50.3370	-49.8988	-49.4649
1 bit	-51.1024	-50.9993	-50.6490
2 bits	-50.9997	-51.1065	-50.7282
3 bits	-50.3370	-50.2056	-49.8273
4 bits	-50.8283	-50.6059	-50.2275
5 bits	-50.3370	-50.2056	-49.8273
10 bits	-50.3370	-50.2056	-49.8273

It must be noted that the SSCs are normalized and integrated to the same bandwidth. That means that for the 30.69 MHz column, the normalization of the PSD is done to 30.69 MHz and the SSC computation integrates equally in 30.69 MHz.

The interest of these results lies in the fact that no matter what the actual code selected for the simulation is, the values will not vary significantly in reality. Thus we could easily estimate the SSCs between two C/A codes by just adding a constant offset of approximately 11.25 dB to the smooth spectrum SSC since this is the difference between the constant value SSC (smooth spectrum, random codes, no data) and the peak of the repetitive codes (random or

selected data sequences). Keep in mind that the average of the SSC values for C/A codes over all possible Doppler values leads to the smooth SSC. Moreover, using the previous figures, one does not require to know the exact data sequence or satellite interfering since the results are an average of all cases. As one can imagine, this can simplify computations enormously what is of great interest for example with interference computations.

Furthermore, if we work with the spectrum normalized to 30.69 MHz and integrate it within a narrow bandwidth of 4.092 MHz, only 95.05% of the power falls within the considered bandwidth, and a correction of 0.2203 dB would be necessary in the PSD. To compare the results, this corresponds approximately to the difference of 0.4429 dB that we can observe between the ideal SSC for 30.69 MHz and that with 4.092 MHz. For narrower bandwidths like 2.046 MHz a larger correction of 0.8862 dB should be applied following the reasoning above. This value is very close to that obtained from the simulations. As a conclusion, the narrower the bandwidth, the higher the power spectral density and the higher will be the SSC as we can observe in Table 6.3.

Additionally, we can see from the table above that when a wide bandwidth is considered, already 5 bits, thus 100 ms, seem to be sufficient in average to estimate correctly the PSD of the signal with data. In other words, 5 bits seem to be enough to consider the ideal spectrum as a good approximation. However, for narrower bandwidths more bits have to be considered to correctly estimate the SSC.

This is important because many analyses on interference are highly dependant on the SSCs between the interfering and the desired signals. In fact, if a brute force approach were followed and all the possible SSCs for all possible combinations of satellites, data and receiver implementations had to be computed, the computational load would be unaffordable.

As a conclusion, if we compare the results that come from assuming ideal PSD with random data and those obtained from the simulations for a relatively low number of chips, we can see that the difference in dB is always smaller than 1 dB.

As we mentioned above and the previous figure for the combination of 5 data bits shows in detail, a close look into the fine structure reveals that the spectra are only slightly different. Indeed, the amplitude of the main lobes of the data sinc are nearly equal in both ideal and simulated power spectral densities, being the main difference the amplitude of the secondary lobes of the data sinc. It is also interesting to note that if the number of considered bits is increased from 5 to 10, the shape of the estimated PSD does not significantly change and the difference still remains. Furthermore, the previous figures were calculated for a bandwidth of 30.69 MHz but similar can be obtained for the case of 2.046 MHz. The results are the same except for the fact that the ideal spectrum and the averaged spectrum are higher by 0.55 dB due to the normalization of the power in a narrower bandwidth.

It is also interesting to compare the estimated PSDs that result from integrating for very short periods with the ideal PSD with ideal data. Indeed, as next figure shows, if only 1 data bit is considered, although the peaks in steps of 1 kHz can already be localized, the side lobes cannot be distinguished yet. Moreover, the amplitude of the peaks is something different to that of the ideal PSD, what explains the difference in the SSCs.

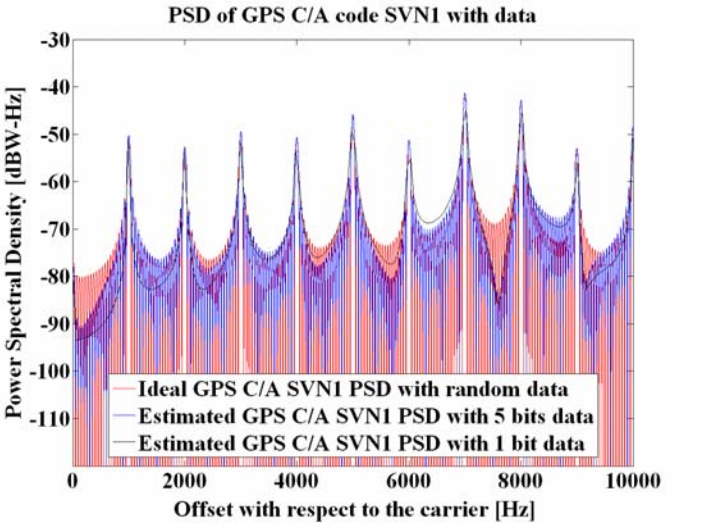

Figure 6.9. Power Spectral Density of GPS C/A Code SVN 1 with data and different number of bits considered

The figures that have been shown above correspond to the average of all the possible spectrum combinations of 5 bits of data. As we can clearly see, the spectrum is already very smooth. However, for this short coherent integration, if a specific combination of bits is considered, the resulting spectrum is in the general case relatively spiky.

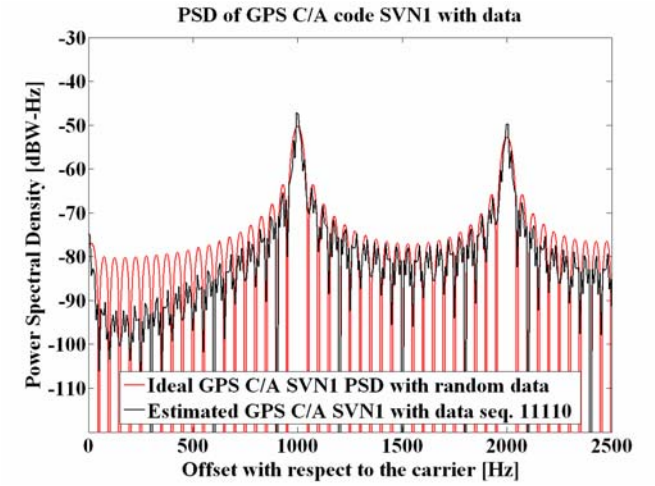

Figure 6.10. PSD of GPS C/A code SVN 1 that results from taking the 5 bits combination [1 1 1 1 -1] at low frequencies

We conclude that although the average of 2^5 bit combinations results in a pretty smooth estimation of the PSD, when we analyze a specific data sequence, the spectrum will present in the general case a pretty abrupt shape.

Once we have graphically shown the results for the C/A Code, we repeat next the analysis for other signals of interest and for different bandwidths. We begin with BOC(1,1). The results are summarized in Table 6.4.

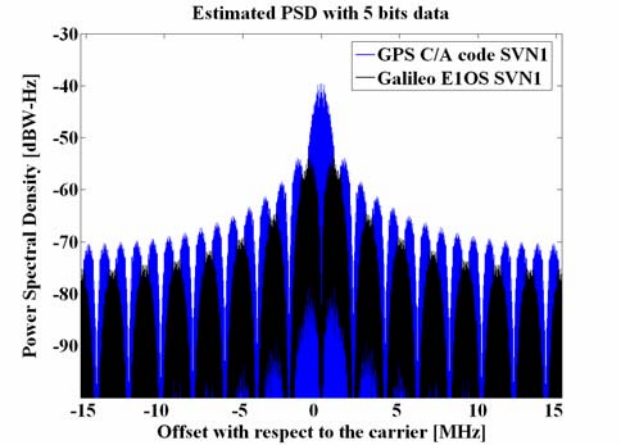

Figure 6.11. Averaged PSD of GPS C/A code and BOC(1,1) with SVN 1 that results from averaging all possible combinations of 5 bits

For the case of BOC(1,1), 5 bits of integration correspond to a different total integration time than for the GPS C/A Code. Indeed, while for GPS C/A code 5 bits correspond to 100 ms, for the Galileo E1 OS these correspond to only 20 ms. For a correct comparison, the estimated Power Spectral Densities were normalized to have unity power in the corresponding time frame of the simulation.

Table 6.4. BOC(1,1) SSC [dB-Hz] computed between the averaged spectra of SVN 1 and SVN 2 for a data rate of 250 sps. A spectral resolution of 5 Hz was assumed

Signal	BOC(1,1)			
Double-Sided Bandwidth [MHz]	**30.69**	**24.5520**	**4.092**	**2.046**
SSC with ideal primary random codes and no data	-64.6920	-64.6477	-63.5526	-61.8483
SSC with ideal primary random codes and ideal random data	-64.6920	-64.6477	-63.5526	-61.8483
SSC with SVN 1-SVN 2 primary codes and ideal data	-64.8997	-64.8863	-63.7495	-61.4179
1 bit	-64.9102	-64.9446	-63.8386	-61.5051
2 bits	-64.9721	-67.9954	-63.7993	-64.3390
3 bits	-64.9886	-64.8525	-64.3102	-61.9844
4 bits	-65.1495	-64.7102	-63.9080	-61.6450
5 bits	-64.9000	-64.7954	-63.7208	-61.5104
10 bits	-64.9253	-64.9313	-63.7977	-61.4719

It is important to note that as we also did with BPSK(1) in Table 6.3 and unlike in the tables of chapter 5, the SSCs are integrated and normalized in the same bandwidth.

An interesting conclusion that results from comparing Table 6.3 and Table 6.4 is that, while the ideal PSDs of the GPS C/A Code and BOC(1,1) in the case of ideal codes and no data have only a difference of approximately 3 dB, the PSD of the GPS C/A Code grows more than that of BOC(1,1) when non random codes are considered and data is modulated on top. As a result, much higher SSCs are obtained for the GPS C/A Code as the simulations of the tables above clearly show. Indeed, for Galileo E1 OS it seems that the smooth spectrum approach is a good approximation while for the C/A Code this is not the case. This is due to the fact that the data rate of the C/A Code is significantly lower than that of BOC(1,1). Furthermore, we can also recognize that BOC(1,1) presents similar SSCs to those of ideal spectrum when ideal random codes are considered no matter whether the data is present or not. On the contrary, we saw in Table 6.4 for BPSK(1) that the SSC with ideal random codes and no data and the SSC for ideal random codes with data can differ by even 11 dB.

Another interesting result from the comparison between the structure of BPSK(1) and BOC(1,1) with data comes from analyzing the fine structure. As an example, the low frequency region of Figure 6.11 is shown next.

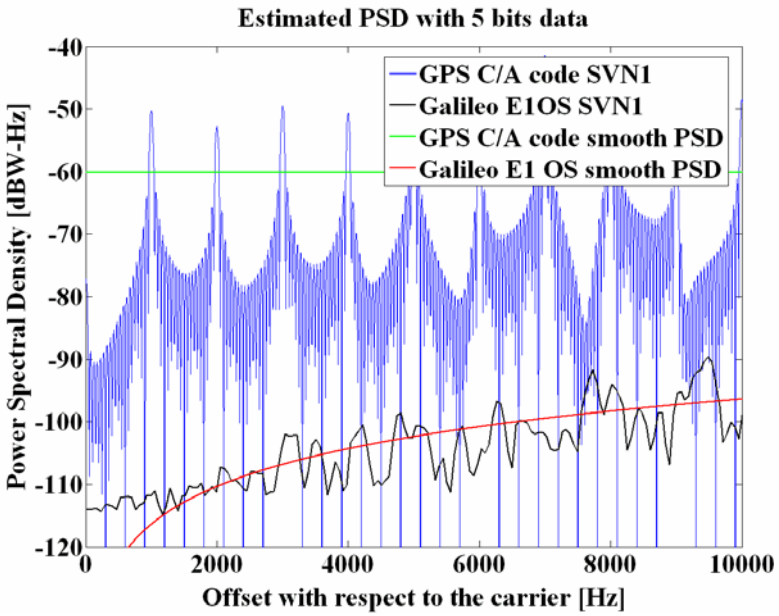

Figure 6.12. Comparison between the averaged (all combinations of 5 bits) PSD of GPS C/A code and BOC(1,1) with SVN 1 at low frequencies. For completeness also the smooth BPSK(1) and BOC(1,1) spectra are depicted

As we can recognize, the low frequency region until 10 kHz shows that while the GPS C/A Code has sincs of width 50 Hz every 1 kHz, Galileo presents sincs of 250 Hz every 250 Hz as predicted in theory. This is shown more in detail in the next figure. If we take a closer look into the fine structure of the ideal PSD of Galileo E1 OS for SVN 1 with data, we can observe the interesting effect that even though the sincs of 250 Hz are located in steps of 250 Hz, in general the local maxima are not necessarily situated at multiples of the data rate.

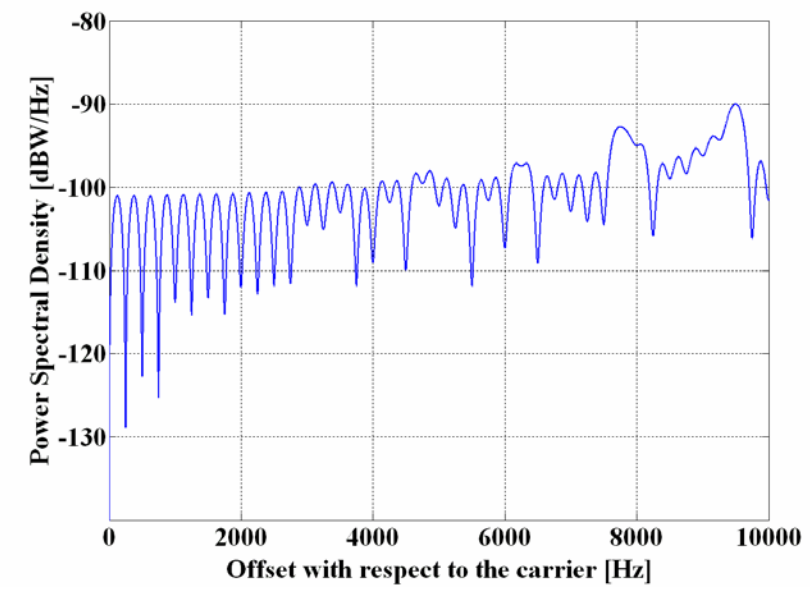

Figure 6.13. Averaged (5 bits) PSD of BOC(1,1) with SVN 1 at low frequencies

As an example of this, there is a local maximum at 125 Hz which is caused by the particular spectral characteristics of the Galileo E1 OS code number 1. For this particular sequence, the second harmonic is higher than the first, so that the first secondary left lobe of the sinc at 500 Hz (located at 125 Hz) summed up with the tails of other sincs around is higher than the main lobe of the sinc at 250 Hz. Such effects can be observed for Galileo E1OS spectra but not so easily for GPS C/A code because the Galileo E1 OS codes are first longer and secondly posses a higher data rate.

In fact, the spectrum of the Galileo E1 OS code number 1 takes the following values for the first harmonics:

Table 6.5. Galileo E1 OS SVN 1 first harmonics

Harmonic	**0**	**1**	**2**	**3**	**4**
Amplitude [x10^{-11}]	0	0.013	0.052	0.030	0.419

where we can see that the second harmonic at 500 Hz is nearly five times higher (approximately 7 dB higher) than the first at 250 Hz. Furthermore, we know from theory that a sinc of 250 Hz has a main lobe that is 13.4648 dB higher than the first secondary lobe, 17.9018 dB higher than the second secondary lobe and 20.8244 dB higher than the third secondary lobe. Considering the code structure and the properties of the sinc together, one can derive in theory all relative amplitudes.

Finally, we present in the next lines similar SSC analyses for the case of MBOC.

Table 6.6. Data MBOC(6,1,1/11) SSC [dB-Hz] between the averaged spectra of SVN 1 and SVN 2 for a data rate of 250 sps. A spectral resolution of 5 Hz was assumed

Signal	MBOC(6,1,1/11) data ('+')	
Double-Sided Bandwidth [MHz]	**24.5520**	**12.2760**
SSC with ideal primary random codes and no data	-65.3070	-64.8149
SSC with ideal primary random codes and ideal data	-65.3070	-64.8149
SSC with SVN 1-SVN 2 primary codes and ideal data	-65.3214	-65.1860
1 bit	-65.3794	-65.2440
2 bits	-65.3695	-65.2343
3 bits	-65.2749	-65.1783
4 bits	-65.1700	-65.7362
5 bits	-65.3133	-65.2934
10 bits	-65.3721	-65.2328

As we can recognize in the table above, only the in-phase channel (data '+') was shown. However, simulations were run for the pilot channel too. Indeed, as explained in chapter 3.6.2, MBOC will be implemented by Galileo as a CBOC signal which is a four level sequence according to the definition of chapter 3.6.2. Furthermore, a power split of 50/50 between data and pilot was considered as well as equal power for the open signals (E1 OS) and the protected signals (PRS). We show the spectra of the in-phase and anti-phase components in the following figure:

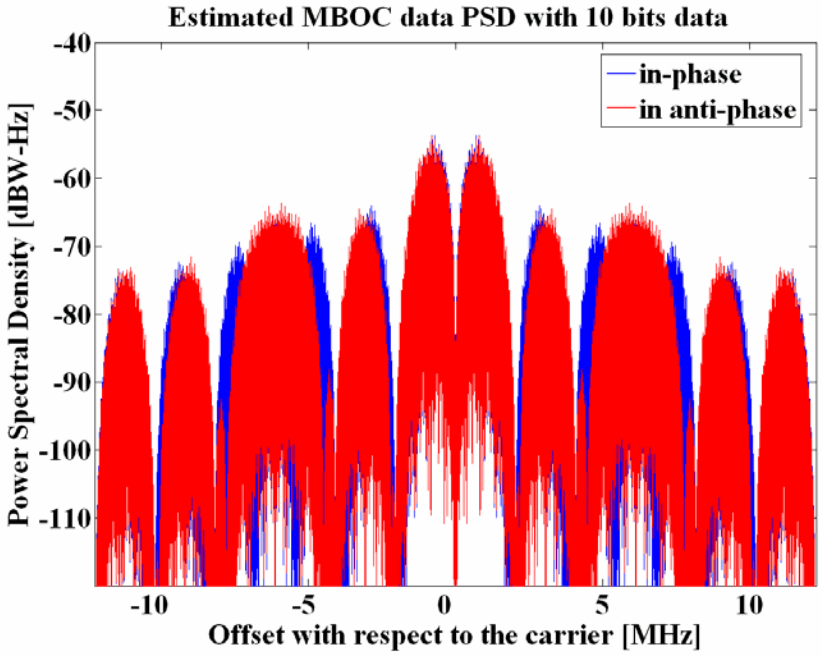

Figure 6.14. Averaged PSDs of MBOC(6,1,1/11) in phase and anti-phase channels with SVN 1 that result from taking 10 data bits into account

If we take a look now at the previous figure, we can clearly see that neither the data channel nor the pilot channel fulfil completely the MBOC spectrum as defined in (4.149) if considered independently. Actually we can recognize that the phase signal (data) places power at frequencies where the pilot (anti-phase) does not. Similarly, the pilot concentrates power at frequencies where the data does not. This is especially evident in the small lobes around 4.092 and 8.184 MHz, which actually merge into broader lobes when data and pilot are computed together. If we add now the data and pilot spectra of the previous figures, we have:

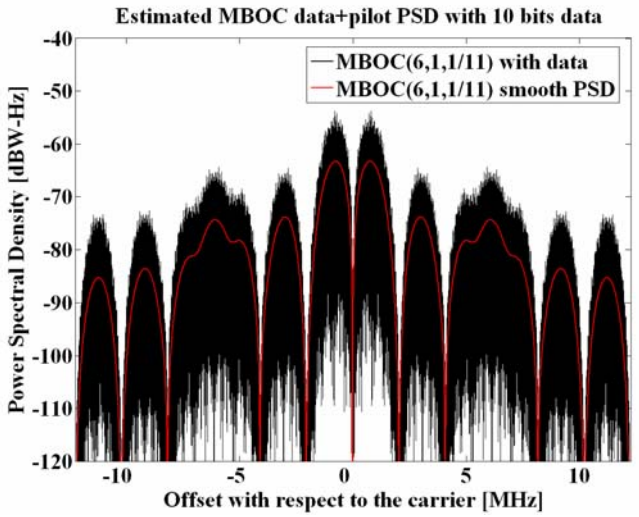

Figure 6.15. Averaged SVN 1 PSD of MBOC(6,1,1/11) – Data + Pilot – that results from taking 10 bits into account. For comparison the smooth spectrum is shown in red

When data and pilot are added, we can clearly recognize the MBOC theoretical shape of (4.149). It must be noted that this is only an approximation to prove that the sum of data and pilot results in the agreed MBOC PSD. Indeed, for a correct calculation of the total MBOC PSD, the pilot channel should be computed using only the secondary code and no data on top. Then we would have to sum them up as we have also done here. However, since the Galileo E1 OS secondary code of the pilot component has a length of 25 bits, the effect is very much like that of random data and therefore the resulting PSD is approximately similar to the one that we have calculated above. In the previous figures we have considered the average of all combinations of 10 bits but no big qualitative difference can be observed. For correctness though, the anti-phase signal with the pilot should be modulated with the unique sequence of 25 bits as defined in [Galileo SIS ICD, 2008].

Additionally, to be more accurate, the effect of the signal structure and the multiplex should be taken into account considering the theory of chapter 7.7.

The main objective of this chapter was to see and analyze how many data bits must be taken into account to consider the analytical approach as a good approximation. As shown in previous pages, the figures derived above could help in developing simplified average models to assess the compatibility among different systems.

6.2.1 Spectral Separation Coefficients for quasi ideal codes

In the previous chapter we have computed the SSCs that result from using the real codes of GPS and Galileo. Now we want to go one step further and compare the results obtained above with those we would observe in the case that we would use ideal codes of a given length. It must be noted that there exist no ideal codes of finite length as this is impossible per definition. Indeed, random codes require an infinite length to have ideal properties.

Codes are digital sequences that, in order to behave ideally, must be as long and as random as possible. That is equivalent to saying that they must appear as *noise-like* as possible. Only then the spreading and dispreading operations will work optimally [G.W. Hein et al., 2006c]. However, the codes must remain reproducible. Otherwise, the receiver would not be able to extract the message that was sent. This is the reason why these sequences are said to be *nearly random* or pseudo-random. As [J. Von Neumann et al., 1951] memorably stated referring to the possibility of generating codes with finite machines, *"Anyone who considers arithmetical methods of producing random digits is, of course, in a state of sin."*

Now that we have seen the limitations of our approach, we can set up the model with which we will assess the effects of the ideal line structure of a code on the SSCs. In this chapter we will use what we describe as *ideal code of a given length*. This consists basically in using the desired properties of the spreading sequence of that length in the frequency domain. The code sequence power spectral density will represent then the average of all possible code sequence spectra for the chosen repetition interval.

6.2.1.1 Signal Model with ideal codes

If we recall the model that we defined in chapter 4.1.1, a DSSS signal that is stationary in wide sense can be expressed as follows:

$$s(t) = \sum_k c_k \; p(t - kT_c) = c(t) \otimes p(t) \tag{6.3}$$

where the code sequence waveform $s(t)$ can be seen as the convolution of the PRN code $c(t)$ with the spreading symbol waveform $p(t)$. Moreover, the spreading symbol waveform $p(t)$ is defined over a specific finite time period T_s, normally equal to the code duration T_c (even case). In the same manner, the code c_k is composed of N elements and repeats in reality every T_p units of time, so that each code element has a duration Δt of

$$\Delta t = \frac{T_p}{N} \tag{6.4}$$

The spreading symbol is normally designed to have the duration of exactly one code element Δt, so that in general $p\,(t) = 0$ for $t \notin [0, \Delta t)$. However, if we take a close look at the model defined by (6.3), the general spreading symbol waveform covers also the case where the

support of the function extends beyond the duration of a single code element and beyond a single repetition of the code sequence. This effect is known as Inter-Symbol Interference (ISI) and can be observed when the real effects of the satellite transmission filters are considered. The principal effect of finite bandwidth is that the effective impulse response of the spreading symbol extends to durations longer than Δt. This is in fact what happens when a finite impulse response filter (FIR) is used in the spreading symbol generator.

On the other hand, the PRN code is assumed to be binary with $c_k \in \{-1,+1\}$ being $k \in [0, N-1]$ and repetitive with N code elements. Thus:

$$\begin{aligned} c_k(t) &= c_k\, \delta(t - k\,\Delta t) \\ c_{k+lN} &= c_k \quad \text{for all integer } l \end{aligned} \tag{6.5}$$

As we can recognize, the PRN code is separated from the chipping waveform in the previous expressions. In conclusion, the Fourier Transform of equation (6.3) is shown to be

$$S(f) = C_k(f)P(f) \tag{6.6}$$

and its power spectral density adopts the following form

$$\Gamma(f) = S^*(f)S(f) = C_k^*(f)C_k(f)P^*(f)P(f) = |C_k(f)|^2 |P(f)|^2 \tag{6.7}$$

If we normalize for the total power to integrate to one,

$$\int_{-\infty}^{\infty} \overline{\Gamma}(f)\,\mathrm{d}f = 1 \tag{6.8}$$

where the following relationship must remain valid:

$$\overline{\Gamma}(f) = \frac{|C_k(f)|^2 |P(f)|^2}{\int_{-\infty}^{\infty} |C_k(f)|^2 |P(f)|^2\,\mathrm{d}f} \tag{6.9}$$

The formula derived above is of enormous interest because by expressing the satellite signal generator function as a function of the power spectral density, the requirement for specific code families can be bypassed. In fact, we just have to substitute the code spectrum by its ideal representation in the frequency domain, no matter whether this is realizable or not.

Once the expressions for the power spectral density of a signal waveform modulated with an ideal code have been derived, it is time to compute the spectrum of the spreading symbol and of the ideal spreading code sequence of length N.

For simplicity we will use in the next lines the BPSK signal for exemplification. As can be seen in Appendix O, its normalized power spectral density is shown to be:

$$\overline{\Gamma}_S(f) = G_{BPSK(f_c)} = f_c \frac{\sin^2\left(\dfrac{\pi f}{f_c}\right)}{(\pi f)^2} \tag{6.10}$$

which has the well known spectrum of the figure below for a chip rate of 1.023 MHz:

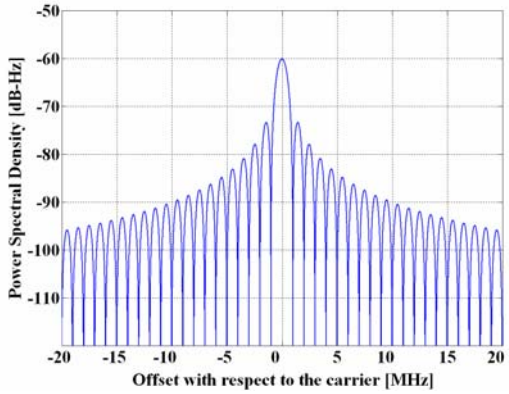

Figure 6.16. Power Spectral Density of the BPSK(1) modulation

As we mentioned above, we will avoid the use of specific codes in our analysis by taking the properties that an *ideal code of a given length* will present. Indeed, an idealized version of the aperiodic code sequence auto-correlation function would present the following form:

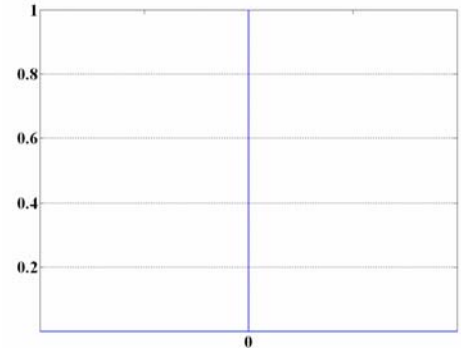

Figure 6.17. ACF of an *ideal code of finite length*

It is important to note that while the idealized autocorrelation can not be shown to be the average of all possible code sequence choices, except for specific code families, it is representative of the expectation for the behaviour of specific code families. Moreover, this is true for any code length in general, although there exist lengths where there is no set of codes that would fulfil the desired properties shown above.

In order to account for the continuous repetition of the code sequence, we will employ the circular autocorrelation function in the next lines. This provides the correct result if the data or pseudodata are of the same phase as is the case in the even autocorrelation. On the contrary, when the data sequence flips its elements, the resulting ACF is then called *odd*. The odd correlation is more difficult to compute since it depends on the particular data.

As shown by [F. Soualle et al., 2005] the data modulation can cause the chip values over the integration time to flip resulting thus in the mentioned difference between the even and odd correlation. If we further assume that the Doppler shift was perfectly eliminated and there is no data flip, the even crosscorrelation between two codes c_1 and c_2 is then shown to be:

$$CC^e(\tau) = C_{1,2}(\tau) + C_{1,2}(\tau - N) \tag{6.11}$$

Equally, for the odd case when the data changes during the coherent integration, the correlation adopts the following expression:

$$CC^{o}(\tau) = C_{1,2}(\tau) - C_{1,2}(\tau - N) \tag{6.12}$$

where in both cases $C_{1,2}(\tau)$ represents the aperiodic correlation function defined as:

$$C_{1,2}(p) = \begin{cases} \sum_{j=0}^{N-1-p} c_1(j)c_2(j+p) & 0 \le p \le N-1 \\ \sum_{j=0}^{N-1+p} c_1(j-p)c_2(j) & 1-N \le p \le 0 \\ 0 & |p| \ge N \end{cases} \tag{6.13}$$

We can see the difference of both in the following figure:

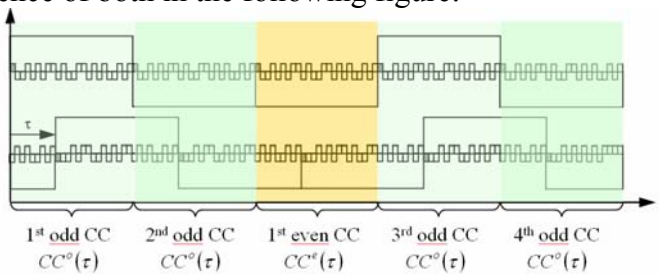

Figure 6.18. Difference between the even and odd ACFs (Courtesy of Stefan Wallner)

6.2.1.2 Even Autocorrelation Function of Quasi Ideal Codes

The normalized periodic even autocorrelation function ACF is shown to be

$$\gamma_{\text{circ}}(\tau) = \lim_{T_c \to \infty} \left\{ \frac{\int_0^{T_c} c_i(t)c_i(t+\tau)\mathrm{d}t \Big|_{\text{circ}}}{\int_0^{T_c} c_i^{\,2}(t)\,\mathrm{d}t} \right\} = \lim_{T_c \to \infty} \left\{ \frac{\int_0^{T_c-\tau} c_i(t)c_i(t+\tau)\,\mathrm{d}t + \int_{T_c-\tau}^{T_c} c_i(t)c_i\left[(t-T_c)+\tau\right]\mathrm{d}t}{\int_0^{T_c} c_i^{\,2}(t)\,\mathrm{d}t} \right\} \tag{6.14}$$

where *circ* stands for circular. We can recognize that the integration in the numerator is taken as circular (auto) correlation over an interval of T_c given the repetitive nature of $c_i(t)$. Moreover we can see that this integration time tends to infinity. Since in reality the integration intervals are longer than the code period but not infinite, we propose an alternative version of the autocorrelation function. For the even case, this can be expressed as follows:

$$\gamma_{even}^{M}(\tau) = \frac{\int_0^{MT_c} c_i(t)c_i(t+\tau)\mathrm{d}t}{M\int_0^{T_c} c_i^{\,2}(t)\,\mathrm{d}t} \quad \text{valid for } |\tau| \le MT_c \tag{6.15}$$

where for simplicity a total coherent integration equal to a multiple M of the code repetition interval was assumed. Additionally, since now the code sequence is only defined in the observation interval MT_c, no circular correlation is needed any more.

Following the thoughts of previous chapter, let us assume now an ideal random code of length T_c (or in a relaxed form, the average of the codes of the set). The linear autocorrelation sequence in this case is not periodic and adopts the following form:

$$\gamma_{even}^{M}(\tau)=\begin{cases}\dfrac{M-|n|}{M} & \text{for } \tau=nT_c \text{ and } n \text{ integer with } |n|\le M\\ 0 & \text{for all other } \tau\end{cases} \tag{6.16}$$

This is shown graphically in the next figure for the specific case that the code repeats 20 times within one data chip as is the case with the GPS C/A Code.

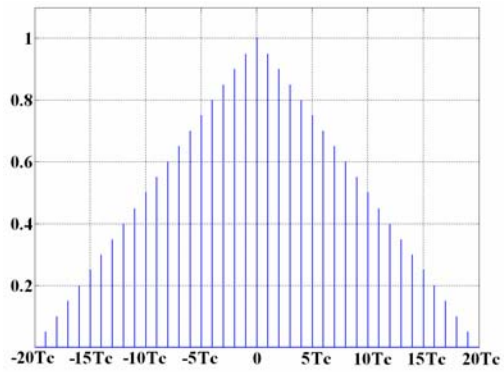

Figure 6.19. GPS C/A Code Autocorrelation Function

Since the power spectral density is the Fourier Transform of the autocorrelation, we have:

$$\Gamma_{even}^{M}(\omega)=\int_{-\infty}^{\infty}\gamma_{even}^{M}(\tau)\,\mathrm{e}^{-j\omega\tau}\mathrm{d}\tau=\int_{-MT}^{MT}\sum_{n=-M}^{M}\left\{\frac{M-|n|}{M}\right\}\delta(\tau-nT_c)\,\mathrm{e}^{-j\omega\tau}\mathrm{d}\tau \tag{6.17}$$

This expression can be further expanded into three parts since the integral above can be evaluated at values of $\tau=nT_c$, including $n=0$, as follows:

$$\Gamma_{even}^{M}(\omega)=\begin{cases}\displaystyle\int_{0^-}^{0^+}\delta(\tau)\,\mathrm{e}^{-j\omega\tau}\mathrm{d}\tau\\ \displaystyle+\int_{-MT}^{0^-}\sum_{n=-M}^{-1}\left\{\frac{M-|n|}{M}\right\}\delta(\tau-nT_c)\,\mathrm{e}^{-j\omega\tau}\mathrm{d}\tau\\ \displaystyle+\int_{0^+}^{MT}\sum_{n=1}^{M}\left\{\frac{M-|n|}{M}\right\}\delta(\tau-nT_c)\,\mathrm{e}^{-j\omega\tau}\mathrm{d}\tau\end{cases} \tag{6.18}$$

$$\Gamma_{even}^{M}(\omega)=1+\int_{0^+}^{MT}\sum_{n=1}^{M-1}\left\{\frac{M-n}{M}\right\}\delta(\tau-nT_c)\left\{\mathrm{e}^{j\omega\tau}+\mathrm{e}^{-j\omega\tau}\right\}\mathrm{d}\tau=1+2\sum_{n=1}^{M-1}\left\{\frac{M-n}{M}\right\}\cos(n\omega T_c) \tag{6.19}$$

where we have assumed positive values of n with $n\le M$. It is important to note that when the code rate and the data rate are equal, $M=1$ and the code spectrum is flat.

If we take a closer look at equation (6.19), we can clearly recognize that the function $\Gamma_{even}^{M}(\omega)$ is not square integrable and would thus be difficult to use alone. As we know, a real or complex function is square-integrable if the integral of the square of its absolute value over

the interval is finite and thus belongs to the Hilbert space L^2. This is a necessary condition to apply the Fourier theory with correctness. Accordingly $\Gamma_{even}^{M}(\omega)$ can not, on its own, represent a PSD since the integral over frequency is not finite. However, as we will see next, used in combination with other functions offering appropriate frequency behaviour, we will be allowed to use it.

The origin of this effect lies in the definition of the ACF for periodic functions. There are ways to circumvent this problem using, for example, the ACF of m-sequences. Indeed, these can be taken as an approach to purely random sequences since the ACF could be arranged to have an integrated value of zero, that is 1 in phase and -1/*n* out of phase. This could also be arranged for the periodic ACF by ensuring that the average of the ACF over all delays is exactly 0 and there is thus no DC component. The result would be then a function that would be square integrable but the conclusions would remain unaffected.

The power spectral density for $\Gamma_{even}^{M}(\omega)$ with $M = 20$, is shown in the next figure. It must be noted that it is not normalized and thus the maxima have a value of $10\log_{10}(20)$.

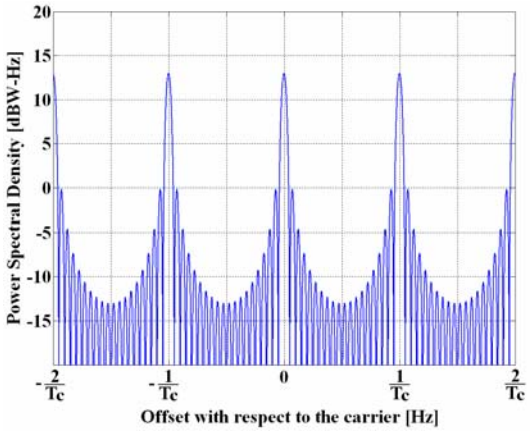

Figure 6.20. Power Spectral Density (not normalized) of an ideal code sequence that repeats 20 times within one data bit

It is interesting to note that the obtained power spectral density is the result of convoluting a Dirac comb with separation 1 kHz, with a sinc of $f_d = 50\,\text{Hz}$. Indeed, equation (6.19) can be rewritten as shown next:

$$\Gamma_{even}^{M}(f) = 1 + 2\sum_{n=1}^{M-1}\left\{\frac{M-n}{M}\right\}\cos\left(\frac{2\pi n f}{f_c}\right) = f_d\left[\frac{\sin\left(\frac{\pi f}{f_d}\right)}{(\pi f)}\right]^2 \otimes \sum_{l=-\infty}^{\infty}\delta(f - l\,\Delta f_c) \qquad (6.20)$$

being Δf the separation of the deltas of the Dirac comb or 1 kHz in our particular example. Next, the Dirac comb is shown in detail.

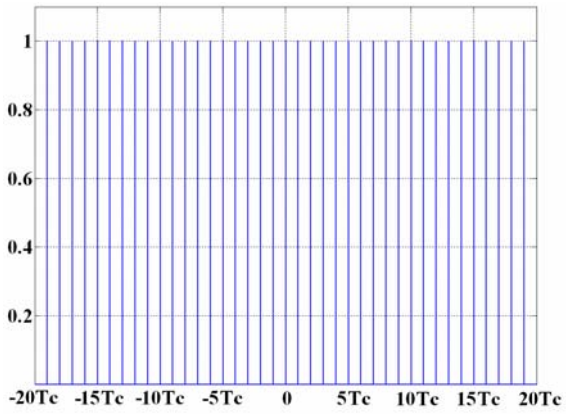

Figure 6.21. Power spectral Density for ideal code sequence with *M*=20

As we can see, the frequency components repeat at intervals of $1/T_c$, being $T_c = 1$ ms since this is the period of the C/A code. As it is trivial to show, this Dirac frequency comb is the Fourier transformation of a similar comb in the time domain according to the following expression:

$$F\left\{\sum_{l=-\infty}^{\infty}\delta(\tau - nT_c)\right\} = \frac{1}{T_c}\sum_{l=-\infty}^{\infty}\delta\left(f - \frac{l}{T_c}\right) \tag{6.21}$$

More important even, the magnitude of each line component is the same, unlike in actual C/A sequences where the magnitude of the lines can be larger or smaller than the average value due to specific non-zero values of the autocorrelation function for $\tau \neq 0$.

A very important conclusion can also be obtained from Figure 6.21. In fact, The Dirac comb with separation T_c, being T_c the duration of the C/A code and thus 1 millisecond, results from the convolution of the linear autocorrelation function of Figure 6.19 with a train of Dirac deltas separated by 20 milliseconds. This value comes from the fact that *M*=20 is the number of times that the C/A code repeats within one data bit. This is shown in the next figure:

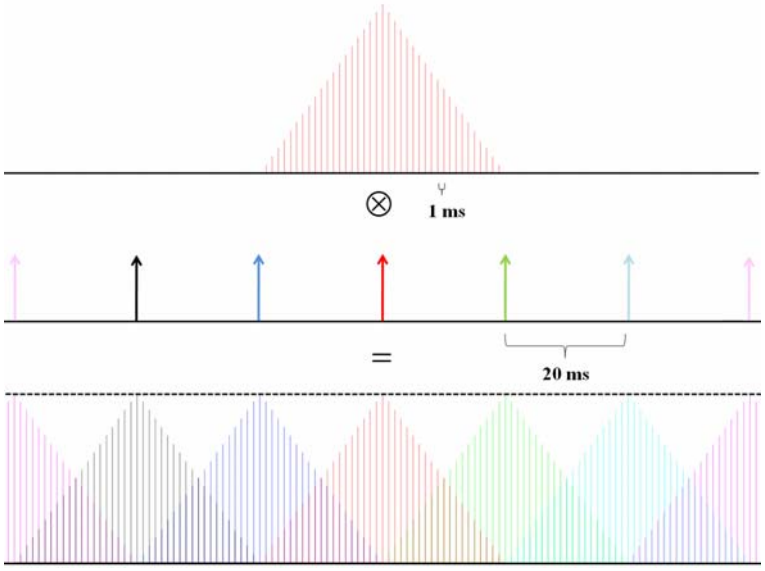

Figure 6.22. Convolution between the linear even correlation and the *even train of Dirac pulses* to form the even periodic correlation

Since this function is the key to form the PSD of the signal modulated with data and a short code in the even correlation case, it is important to remember it when we work with its odd counterpart. Moreover, since the train of Dirac deltas in the case of the odd correlation will be slightly different, we denote this train in the even case as *even train of Dirac deltas*.

In addition, although for both even and odd correlations we have to work with periodic correlations, we have shown in previous lines that the linear correlation in conjunction with the particular train of Dirac deltas contains all the necessary information to derive the correlation that is seen by the receiver at the output. Indeed, the previous Figure 6.22 reflects nothing else than the following mathematical identity:

$$\sum_{n=-M}^{M}\left\{\frac{M-|n|}{M}\right\}\delta(\tau-nT_c)\otimes\sum_{n=-\infty}^{\infty}\delta(\tau-MnT_c)=\sum_{n=-\infty}^{\infty}\delta(\tau-nT_c) \tag{6.22}$$

being thus the result of the convolution a constant discrete function with pulses separated 1 millisecond. As in previous chapters, the operator $\otimes$ refers to the convolution.

6.2.1.3 Odd Autocorrelation Function of Quasi Ideal Codes

As we have seen in Figure 6.18, the even correlation occurs when the data bits do not change of sign during the integration, while the odd corresponds to the case that the bits flip during the coherent integration. This case would happen indeed, when the data bits are not perfectly aligned at receiver level.

In the previous pages we have shown that the even correlation can be expressed by means of the linear correlation of the code sequence that results from replicating the primary code twenty times one after each other with the same data sign. This is so because the interfering signal is assumed not to flip any of its data bits during the correlation integration as the correlation is even.

Now, for the case of the odd correlation, the situation is similar but additional care has to be paid since the odd correlation implies by definition that the data bit flips within the integration time. Given the fact that the primary C/A code repeats twenty times within one data bit, the position of the data flip can adopt in principle any of the twenty possible positions. Accordingly, the linear correlation can also adopt twenty different shapes. As a conclusion, since the distribution of the data flip over the 20 possible locations p is uniformly distributed, the odd linear correlation will be the average of the 20 linear correlations that are possible depending on where the data flip actually occurs.

The twenty possible cases are summarized in the following table:

Table 6.7. Relative position of the data flip of the interfering signal with respect to the desired replica

Delay τ \ p	1	2	3	4	5	6	7	8	9	10	11	12	13	14	15	16	17	18	19	20
$s(\tau=1)$	1	1	1	1	1	1	1	1	1	1	1	1	1	1	1	1	1	1	1	1
$s(\tau=2)$	1	1	1	1	1	1	1	1	1	1	1	1	1	1	1	1	1	1	1	-1
$s(\tau=3)$	1	1	1	1	1	1	1	1	1	1	1	1	1	1	1	1	1	1	-1	-1
$s(\tau=4)$	1	1	1	1	1	1	1	1	1	1	1	1	1	1	1	1	1	-1	-1	-1
$s(\tau=5)$	1	1	1	1	1	1	1	1	1	1	1	1	1	1	1	1	-1	-1	-1	-1
$s(\tau=6)$	1	1	1	1	1	1	1	1	1	1	1	1	1	1	1	-1	-1	-1	-1	-1
$s(\tau=7)$	1	1	1	1	1	1	1	1	1	1	1	1	1	1	-1	-1	-1	-1	-1	-1
$s(\tau=8)$	1	1	1	1	1	1	1	1	1	1	1	1	1	-1	-1	-1	-1	-1	-1	-1
$s(\tau=9)$	1	1	1	1	1	1	1	1	1	1	1	1	-1	-1	-1	-1	-1	-1	-1	-1
$s(\tau=10)$	1	1	1	1	1	1	1	1	1	1	1	-1	-1	-1	-1	-1	-1	-1	-1	-1
$s(\tau=11)$	1	1	1	1	1	1	1	1	1	1	-1	-1	-1	-1	-1	-1	-1	-1	-1	-1
$s(\tau=12)$	1	1	1	1	1	1	1	1	1	-1	-1	-1	-1	-1	-1	-1	-1	-1	-1	-1
$s(\tau=13)$	1	1	1	1	1	1	1	1	-1	-1	-1	-1	-1	-1	-1	-1	-1	-1	-1	-1
$s(\tau=14)$	1	1	1	1	1	1	1	-1	-1	-1	-1	-1	-1	-1	-1	-1	-1	-1	-1	-1
$s(\tau=15)$	1	1	1	1	1	1	-1	-1	-1	-1	-1	-1	-1	-1	-1	-1	-1	-1	-1	-1
$s(\tau=16)$	1	1	1	1	1	-1	-1	-1	-1	-1	-1	-1	-1	-1	-1	-1	-1	-1	-1	-1
$s(\tau=17)$	1	1	1	1	-1	-1	-1	-1	-1	-1	-1	-1	-1	-1	-1	-1	-1	-1	-1	-1
$s(\tau=18)$	1	1	1	-1	-1	-1	-1	-1	-1	-1	-1	-1	-1	-1	-1	-1	-1	-1	-1	-1
$s(\tau=19)$	1	1	-1	-1	-1	-1	-1	-1	-1	-1	-1	-1	-1	-1	-1	-1	-1	-1	-1	-1
$s(\tau=20)$	1	-1	-1	-1	-1	-1	-1	-1	-1	-1	-1	-1	-1	-1	-1	-1	-1	-1	-1	-1

where s denotes the data sequence of the interfering signal. As we can see, τ=1 denotes that the flip transition takes place in the very last primary code and consequently the sequence s consists of only 1s.

As we can recognize from the previous table, we can make use of symmetry properties to simplify the number of linear autocorrelations that we have to consider. In fact, there are only 9+2 different linear autocorrelations since it is trivial to prove that

$$ACF_{linear}\{s(\tau=21-i)\}=ACF_{linear}\{s(\tau=i+1)\} \tag{6.23}$$

with $i\in(1,2,...,9)$. Moreover, $ACF_{linear}\{s(\tau=1)\}$ and $ACF_{linear}\{s(\tau=11)\}$ repeat only one time. Taking this into account, it can be shown that the average autocorrelation function for the odd case adopts the following form:

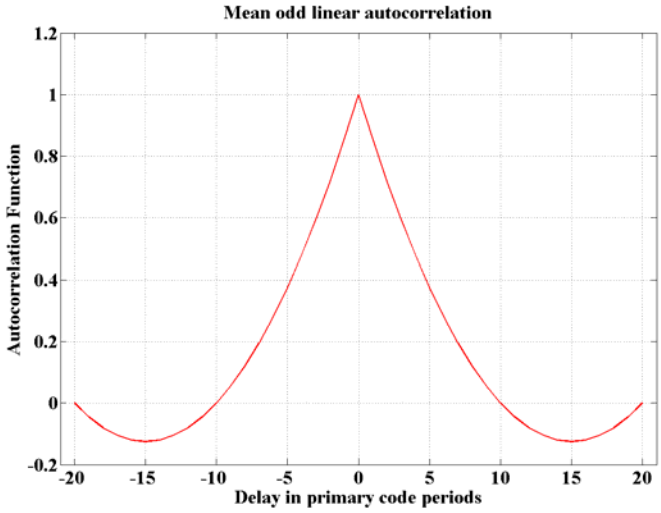

Figure 6.23. Average odd linear autocorrelation

Once we have the average linear autocorrelation for the odd case in all its possible cases, we can follow the same logic as for the even case. To do so, we correlate next the average linear odd autocorrelation with the *odd train of Dirac pulses*. As we remember, the even train of Dirac pulses was characterized by having all pulses of the same normalized amplitude +1 since there was no change in data bit. The odd case, however, is actually characterized by the fact that the data bit alternates from one bit to the other in order to always have odd correlation. Accordingly, the *odd train of Dirac pulses* adopts the following form:

$$\sum_{n=-\infty}^{\infty}(-1)^n \delta(\tau - MnT_c) \tag{6.24}$$

such that pulses of amplitude +1 and -1 alternate in a separation of M=20 milliseconds. As a result, the convolution between the *odd train of Dirac pulses* and the average odd correlation adopts the following form:

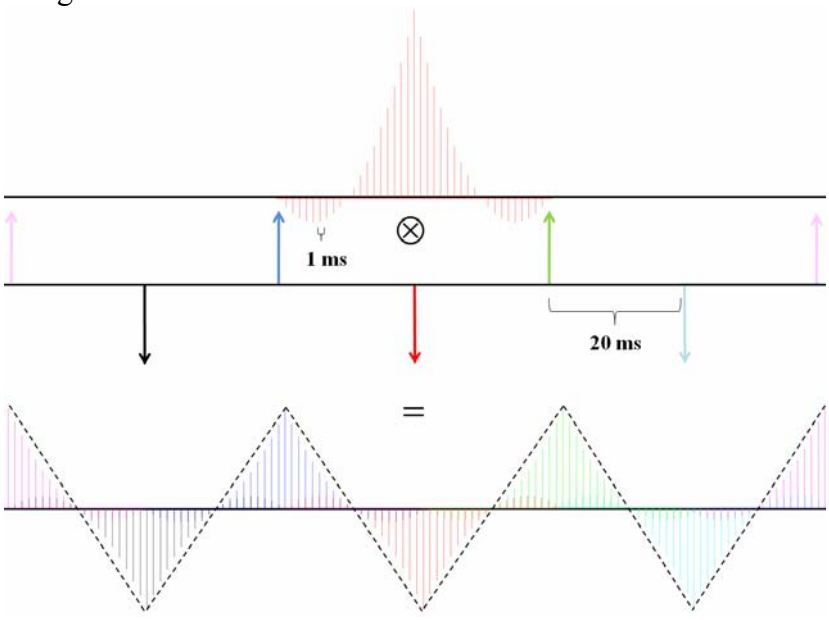

Figure 6.24. Convolution between the linear odd correlation and the *odd train of Dirac pulses* to form the odd periodic correlation

As a result, the convoluted function adopts the following form:

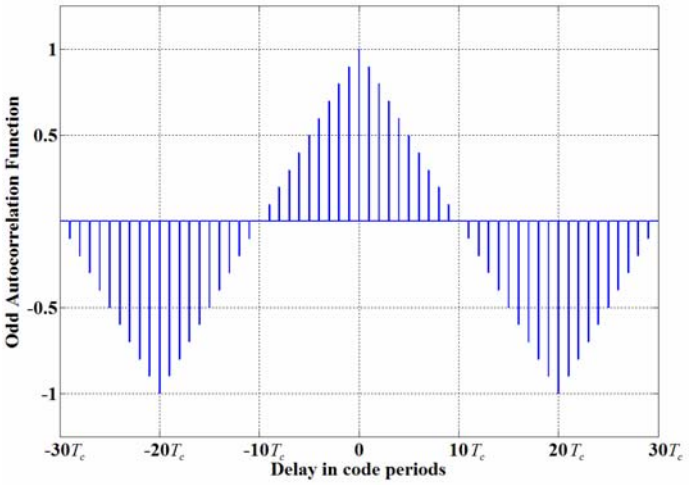

Figure 6.25. Normalized periodic odd correlation with *M*=20

If we calculate now the Fourier transform of this signal, we can observe that while the spectrum of the even correlation allocates all its power around frequencies multiple of 1 kHz, most of the power is concentrated in the case of the odd correlation at ± 50 Hz around frequencies multiple of 1 kHz. We can also recognize that the Odd Code Spectrum also has power at other frequencies $\pm 50k$ with $k = \pm[2,...10]$ but of considerably lower amount. Indeed, the spectral lines at ± 50 Hz amount slightly more than 81% of the total power, being the rest distributed among the other spectral lines. Accordingly, we can state that while the Even Code spectrum places all its power at multiples of 1 kHz, the Odd concentrates most of it at ± 50 Hz around frequencies multiple of 1 kHz.

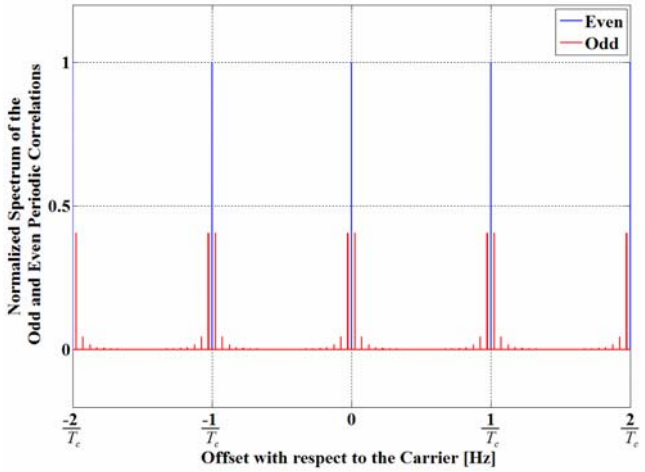

Figure 6.26. Normalized Even and Odd Code Power spectral Density for *M*=20

The spectral coefficients of the previous figure can be easily obtained if we recall that the odd autocorrelation function for GPS C/A is periodic with period $T_0 = 40T_c$, being T_c the period of the primary code, that is 1 millisecond for the C/A code. Indeed, the odd autocorrelation can be expressed by means of a Fourier series as shown next:

$$ACF_{odd}(\tau) = \frac{1}{T_0}\sum_{k=-\infty}^{\infty} a_k e^{jk\omega_0\tau} \tag{6.25}$$

where $\omega_0 = 2\pi/T_0 = \pi/20T_c$ since $T_0 = 40T_c$. Accordingly, the complex coefficients of the Fourier series are shown to adopt the following form:

$$a_k = \int_{\tau=-20T_c}^{20T_c} ACF_{odd}(\tau) e^{-jk\omega_0\tau} \tag{6.26}$$

Since the odd autocorrelation function is shown to be expressed as follows:

$$ACF_{odd}(\tau) = \sum_{n=-M}^{M-1} \frac{M-2\|n\|}{M} \delta(\tau - nT_c) \tag{6.27}$$

with $M = 20$, the spectral coefficients are then further shown to simplify to:

$$a_k = 2 + \sum_{l=1}^{9} \frac{4l}{10} \cos\left[k(10-l)\frac{\pi}{20}\right] \tag{6.28}$$

for odd values of k, where k adopts values between -19 and 19, with $a_k = a_{-k}$. In general:

$$a_k = 2 + \sum_{l=1}^{\frac{M}{2}-1} \frac{8l}{M} \cos\left[\frac{k}{2}(M-2l)\frac{\pi}{M}\right] \tag{6.29}$$

It is also trivial to show that all the even coefficients are of value 0. Normalizing now the coefficients to the total power of the signal,

$$\bar{a}_k = \frac{2 + \sum_{l=1}^{9} \frac{4l}{10} \cos\left[k(10-l)\frac{\pi}{20}\right]}{\sum_{\substack{k=-19 \\ k\,odd}}^{19} a_k} = \frac{2 + \sum_{l=1}^{9} \frac{4l}{10} \cos\left[k(10-l)\frac{\pi}{20}\right]}{40} \tag{6.30}$$

we obtain the normalized spectrum. For a generic value M, this expression is shown to adopt the following form:

$$\bar{a}_k = \frac{2 + \sum_{l=1}^{\frac{M}{2}-1} \frac{8l}{M} \cos\left[\frac{k}{2}(M-2l)\frac{\pi}{20}\right]}{\sum_{\substack{k=-M \\ k\,odd}}^{M} a_k} = \frac{2 + \sum_{l=1}^{\frac{M}{2}-1} \frac{8l}{M} \cos\left[\frac{k}{2}(M-2l)\frac{\pi}{20}\right]}{2M} \tag{6.31}$$

Convoluting now the previous odd code spectrum with the ideal data sinc of 50 Hz, we obtain the following shape for the odd code spectrum with data:

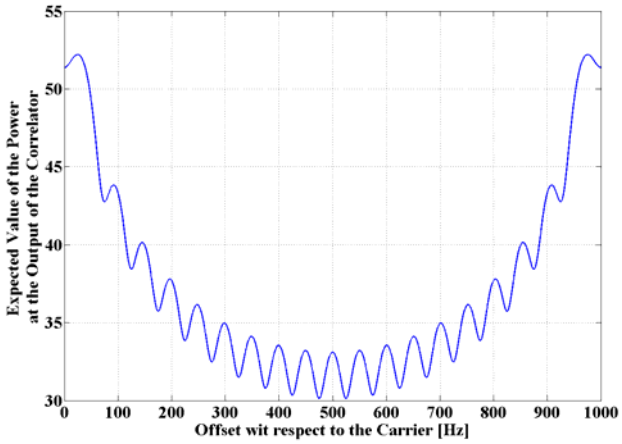

Figure 6.27. Odd Power Spectral Density [dB] of an ideal code sequence that repeats 20 times in one data bit

6.2.1.4 Combined Spreading Waveform PSD

Now that we have obtained the expressions for the chip waveform PSD and for the code spectrum, the PSD of a BPSK(f_c) with ideal PRN codes will be:

$$\Gamma(f) = \Gamma^M(f)\Gamma_S(f) \tag{6.32}$$

where we have seen that:

$$\Gamma_S(f) = G_{BPSK(f_c)} = f_c \frac{\sin^2\left(\frac{\pi f}{f_c}\right)}{(\pi f)^2} \tag{6.33}$$

and

$$\Gamma^M(f) = f_d \left[\frac{\sin\left(\frac{\pi f}{f_d}\right)}{(\pi f)}\right]^2 \otimes \sum_{l=-\infty}^{\infty} \delta(\omega - 2\pi l \Delta f) \tag{6.34}$$

6.2.2 Spectral Separation coefficients for short PRN codes

As we have seen at the beginning of this chapter, the approximation of using the inner product to calculate the spectral separation coefficient is only valid if the code modulating the signal is sufficiently long to smooth the spectrum. Otherwise, the correct definition to use should be the one derived in (5.8). We recall it to help the understanding in the next pages:

$$\overline{\Psi}_{id} = T_I \int_{-\infty}^{\infty}\int_{-\infty}^{\infty} G_i(f_1) G_d(f_2 - f_1) \mathrm{d}f_1 \left|H_{ID}(f_2)\right|^2 \mathrm{d}f_2 = T_I \int_{-\infty}^{\infty} G_i(f_2) \otimes G_d(f_2) \left|H_{ID}(f_2)\right|^2 \mathrm{d}f_2 \tag{6.35}$$

where the filter function is given by:

$$\left|H_{ID}(f_2)\right|^2 = \frac{\left\|FT\{w(t)\}\right\|^2}{T_I} = \frac{1}{T_I^2}\left[\frac{\sin(\pi f T_I)}{\pi f}\right]^2 \tag{6.36}$$

Moreover we have assumed a perfect windowing of the incoming signal by means of the rectangular function $w(t)$, defined as follows:

$$w(t) = \begin{cases} 1 & 0 \le t \le T_I \\ 0 & \text{otherwise} \end{cases} \tag{6.37}$$

Graphically, the filter function adopts the following form:

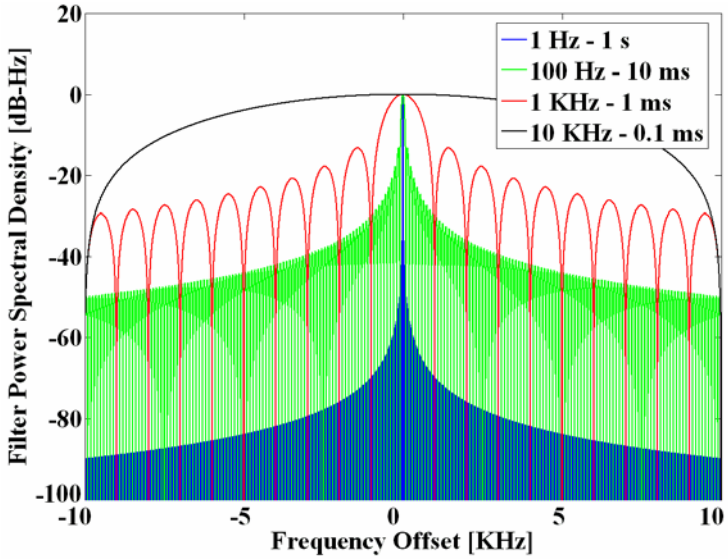

Figure 6.28. Power Spectral Density Convolution of the integration filter function

Equally, we show in the next figure the result of convoluting two BOC(1,1) signals with SVN 1 and SVN 2.

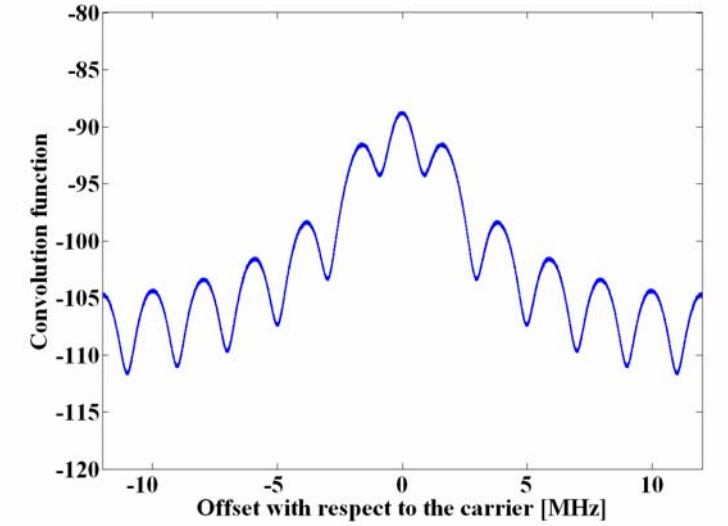

Figure 6.29. Power Spectral Density Convolution of two BOC(1,1) signals modulated respectively by SVN 1 and SVN 2

In addition, if we plot the convolution density function together with the filter function of 1 second of coherent integration, we obtain a sinc function with a frequency rate of 1 Hz as shown in the next figure. As we can recognize, the bandwidth of this last signal compared with that of the convolution function is significantly narrower.

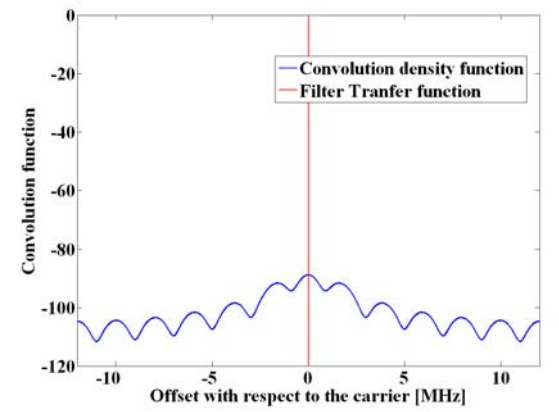

Figure 6.30. Power Spectral Density of the Convolution of two BOC(1,1) signals with SVN 1 and SVN 2 and a receiver filter function of 1 ms of coherent integration

Furthermore, if we integrate the product of the convolution function shown above and the integration filter of 250 Hz (4 ms of integration), we obtain an SSC value of -64.9505 dB-Hz which is very close to the one that we would obtain applying the SSC simplified model of (6.38). Indeed, when we integrate for relatively long periods of time, the filter function gets narrower tending to a Dirac delta. Accordingly, (6.35) converges to the value we would obtain if we would take the value of the convolution at zero offset. In such a case, the SSC general definition from above simplifies to the well known expression that we used in chapter 5:

$$\overline{\Psi}_{id} \approx T_I \int_{-\infty}^{\infty} G_i(f) G_d(f) \left| H_{ID}(f) \right|^2 \mathrm{d}f \Big|_{f_I=0} = \int_{-\infty}^{\infty} G_i(f) G_d(f) \mathrm{d}f \qquad (6.38)$$

Equally, for the C/A code we show in the next figure the convolution density function together with the filter transfer function for an integration of 1 second. As we can recognize, the sinc function is already very narrow and (6.38) is a good approximation to the real SSC computed using (6.35). In fact, the real SSC takes a value of -61.5915 dB-Hz while the approximation of (6.38) yields -61.8597 dB-Hz. It is important to note that no normalization was made. The result of convoluting two C/A Code spectra with different codes is shown in the following figure together with the filter transfer function:

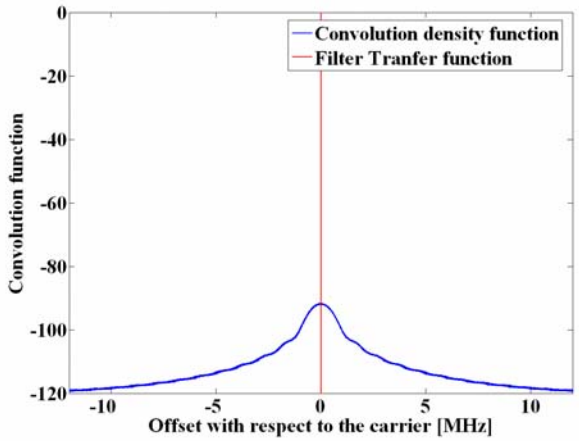

Figure 6.31. Power Spectral Density Convolution of two BPSK(1) signals modulated respectively by SVN 1 and SVN 2 and receiver filter function

The C/A Code is a particular case due to its low data rate. If we now account for the effect of the data, similar figures can be obtained:

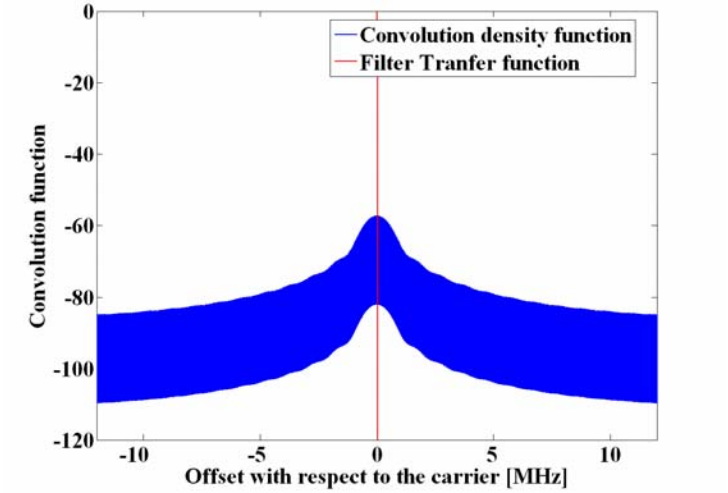

Figure 6.32. Power Spectral Density Convolution of two BPSK(1) signals modulated respectively by SVN 1 and SVN 2 with ideal random data on top

If we use now a filter of 1 kHz (integration of 1 ms instead of 1 s), the resulting spectral separation coefficient of (6.35) seems to deliver results close to those of the SSC approximation of (6.38). We conclude that even for very short integrations, the approximation seems to remain valid. Moreover, the transfer filter has to be multiplied by the factor T_I because otherwise the filter would amplify or attenuate.

Now that we have already studied the effect of data, non-ideal codes and coherent integration on the power spectral densities, it is time to assess the effect of the Doppler shift between the desired signal and the interfering signal on the Spectral Separation Coefficients. To begin we show in the next figure the self SSC of the C/A Code (SVN 1 and SVN 2) as a function of Doppler when a data stream of 50 sps is considered. As we can see, the worst cases occur at shifts multiple of 1 kHz.

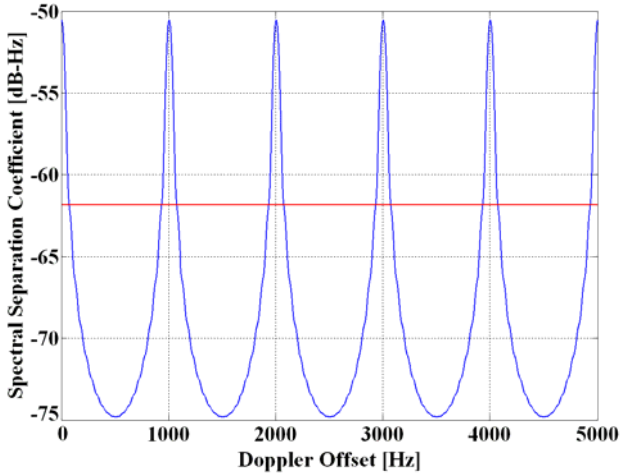

Figure 6.33. C/A Code Self SSC between SVN 1 and SVN 2 as a function of Doppler. For comparison the ideal smooth spectrum SSC is shown in red

As we can see, the value of the Self SSC at Doppler shifts multiple of 1 kHz is not always equal since it depends on the particular two codes of the example. Nevertheless, the difference is negligible and proves that the high Self SSC value of the C/A Code is actually due to the low data rate and not to the C/A Code structure. In fact, as we can see in the next figure there is no significant difference to note if we use the approach of quasi ideal codes as defined in chapter 6.2.1:

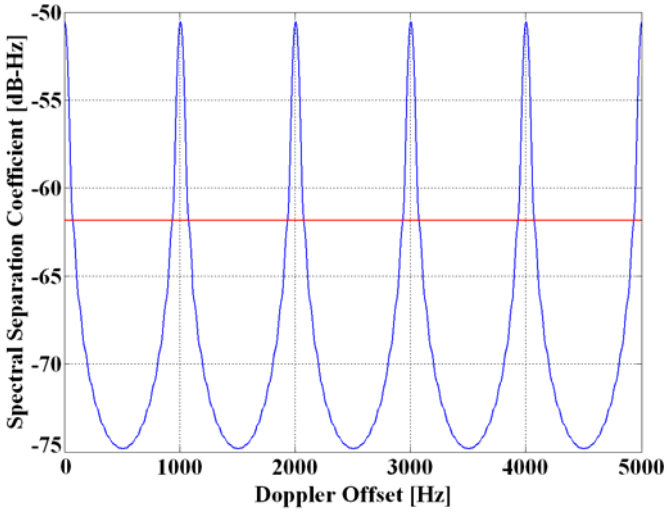

Figure 6.34. C/A Code Self SSC with quasi ideal codes as a function of Doppler. For comparison the ideal smooth spectrum SSC is also shown in red

As we can see, the maxima of the SSC (located every multiple of 1 kHz) are constant in this case. To generalize our results, we calculate in the next figure the Self SSC of BOC(1,1) as a function of the Doppler offset, when two codes are considered and when ideal code properties are assumed. It must be noted that the spectra of the codes were normalized to 24 MHz and not to 40.92 MHz as done in chapter 5. Moreover the SSC were integrated in 24 MHz. If the correct normalization to the transmission bandwidth were done, the result would be a shift of the curves but from a qualitative point of view there would be no difference.

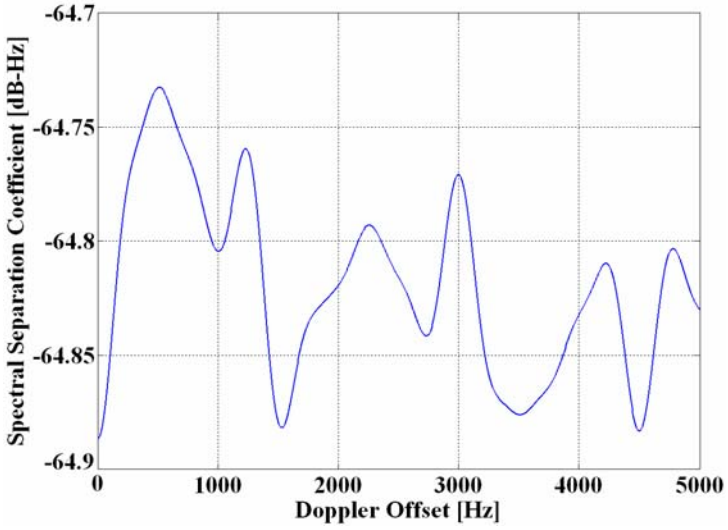

Figure 6.35. BOC(1,1) Self SSC between SVN 1 and SVN 2 as a function of Doppler

It is interesting to see now, that if we repeat the previous computation for quasi ideal codes, the SSC presents the following smooth structure:

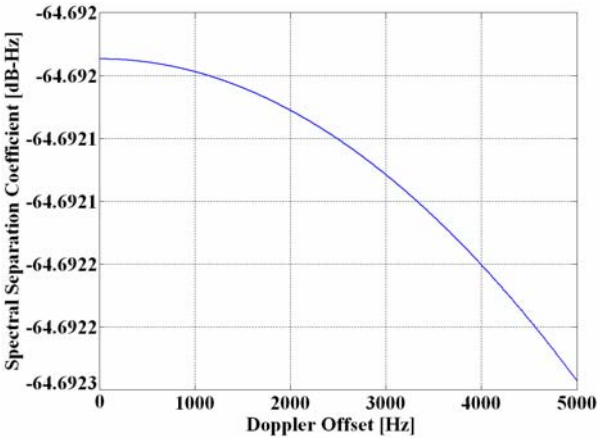

Figure 6.36. BOC(1,1) Self SSC with quasi ideal codes as a function of Doppler

As we can clearly recognize, the variation of the self SSC of BOC(1,1) with data on top hardly varies within the Doppler range that we have studied, showing that the smooth spectrum approach is a good approximation when the data rate is high enough. Indeed, for the C/A code, even with quasi ideal codes, the low data rate was responsible for the important variation of the SSC over the Doppler range. To conclude it is important to mention that similar conclusions can be drawn for the case of MBOC.

6.2.3 Final comments on the SSCs

As we know from [J.W. Betz, 2000b] and [J.W. Betz and K.R. Kolodziejski, 2000], the effective C/N_0 of a desired signal subject to interference is shown to be:

$$\left.\frac{C}{N_0}\right|_{\text{eff}} = \frac{C_d \int_{-\frac{\beta_r}{2}}^{\frac{\beta_r}{2}} G_d(f)\mathrm{d}f}{\left[\begin{array}{c} N_0 \int_{-\frac{\beta_r}{2}}^{\frac{\beta_r}{2}} G_d(f)\mathrm{d}f + \\ + \sum_{k=1}^{N_{\text{intra}}^{\text{interfering}}} C_{i,k} \int_{-\infty}^{\infty} G_{i,k}(f) G_d\left(f - f_{Doppler,k}\right)\mathrm{d}f + \\ + \sum_{l=1}^{N_{\text{inter}}^{\text{interfering}}} C_{i,l} \int_{-\infty}^{\infty} G_{i,l}(f) G_d\left(f - f_{Doppler,l}\right)\mathrm{d}f \end{array}\right]} \tag{6.39}$$

where

- β_r is the two-sided bandwidth of the front-end filter,
- N_0 is the Power Spectral Density of the thermal noise,
- C_d and $G_d(f)$ are respectively the power and the PSD of the desired signals, normalized to the transmission bandwidth of the satellite,
- $C_{i,k}$ and $G_{i,k}(f)$ are respectively the power and the PSD of the interfering signals, normalized equally to the transmission bandwidth. These interfering signals can be

from the same system or from another system in the band. In the case of $C_{i,k}$ and $G_{i,k}(f)$, the interference comes from the same system as that of the desired signal. Moreover $N_{\text{intra}}^{\text{interfering}}$ refers to the number of interfering signals from the same system that can be seen in the receiver.

- Finally, $C_{i,l}$ and $G_{i,l}(f)$ are respectively the power and the PSD of interfering signals from another GNSS interfering system, being $N_{\text{inter}}^{\text{interfering}}$ the number of interfering signals from another GNSS system that can be seen in the receiver.

As we can clearly recognize in the expression above, the impact of the interference onto the $\left.\frac{C}{N_0}\right|_{\text{eff}}$ is directly related to the Spectral Separation Coefficient (SSC), as defined at the beginning of this chapter. Moreover, the expressions above refer to acquisition and data demodulation. Thus we can say that the SSC as defined in this chapter is an acquisition Spectral Separation Coefficient, or SSC_{acq} for short.

The SSC indicates the degree of degradation that a desired signal suffers during acquisition due to the interference of other signals present in the band, no matter whether this comes from the same system or from another system.

Similarly to the acquisition SSC, it is equally possible to propose an effective $C/N_0|_{\text{eff}}$ for the tracking performance [F. Soualle et al., 2007]. This equivalent figure is computed by estimating the equivalent new noise level $N_0|_{\text{eff}}$ that leads to the same jitter that would be obtained in the presence of an equivalent pure thermal noise level. Furthermore, we can distinguish between the coherent and non-coherent DLL cases. As we saw in chapter 4, the tracking error of the EMLP discriminator with only noise is shown to be (4.188):

$$\sigma_{\text{EMLP}}^2 = \frac{B_L\left(1-\frac{1}{2}B_L T_I\right)\int_{-\frac{\beta_r}{2}}^{\frac{\beta_r}{2}} G_d(f)\sin^2(\pi f\delta)\mathrm{d}f}{\frac{C_d}{N_0}\left[2\pi\int_{-\frac{\beta_r}{2}}^{\frac{\beta_r}{2}} f\,G_d(f)\sin(\pi f\delta)\mathrm{d}f\right]^2}\left[1+\frac{\int_{-\frac{\beta_r}{2}}^{\frac{\beta_r}{2}} G_d(f)\cos^2(\pi f\delta)\mathrm{d}f}{\frac{C_d}{N_0}T_I\left[2\pi\int_{-\frac{\beta_r}{2}}^{\frac{\beta_r}{2}} G_d(f)\cos(\pi f\delta)\mathrm{d}f\right]^2}\right] \tag{6.40}$$

If we further develop this idea, it can be shown that an equivalent figure to the SSC is present in the expressions of the degradation of the tracking performance of the desired signal. Moreover, since this figure is very similar in its form to the SSC_{acq} but applies only for tracking, we will call it tracking SSC. The tracking SSC is shown to adopt the following form [F. Soualle et al., 2007]:

$$k_{d,i}^{\text{Tracking}} = \frac{\int_{-\frac{\beta_r}{2}}^{\frac{\beta_r}{2}} G_i(f)G_d(f)\sin^2(\pi f\delta)\mathrm{d}f}{\int_{-\frac{\beta_r}{2}}^{\frac{\beta_r}{2}} G_d(f)\sin^2(\pi f\delta)\mathrm{d}f} \tag{6.41}$$

If we recall now the expression of the acquisition SSC for comparison:

$$k_{d,i}^{\text{Acquisition}} = \frac{\int_{-\frac{\beta_r}{2}}^{\frac{\beta_r}{2}} G_i(f)G_d(f)\mathrm{d}f}{\int_{-\frac{\beta_r}{2}}^{\frac{\beta_r}{2}} G_d(f)\mathrm{d}f} \tag{6.42}$$

We can recognize that except for the squared sine function multiplying the power spectral density, both figures are nearly identical. We show them now in the next figure as a function of the spacing:

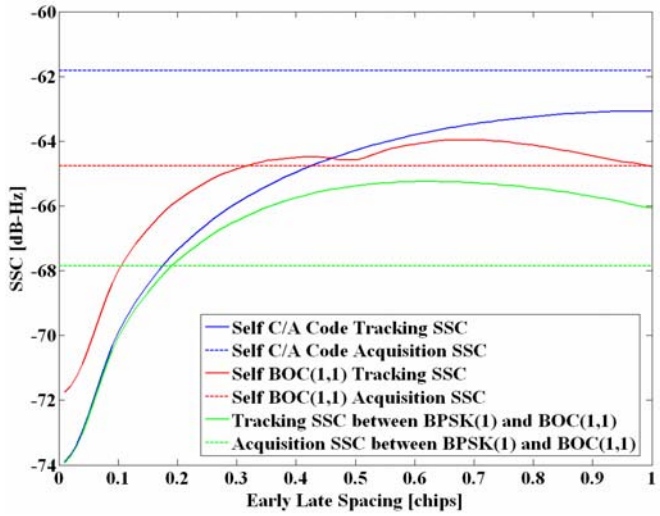

Figure 6.37. Variation of the Acquisition SSC and Tracking SSC with the spacing

Similar figures can be equally derived for MBOC as shown in the following figure

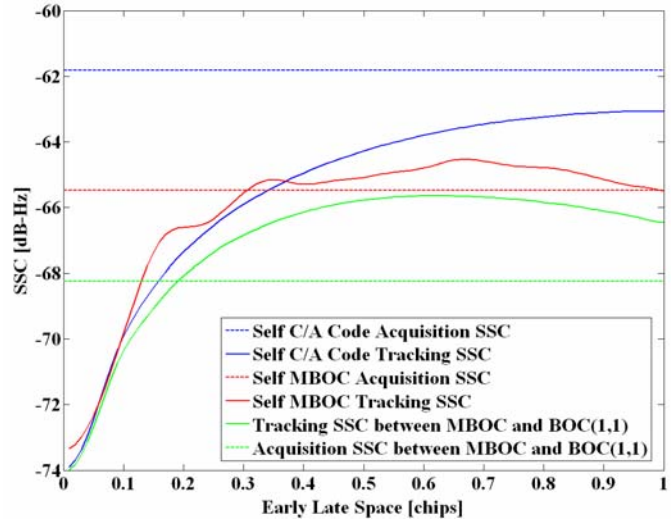

Figure 6.38. Acquisition SSC and Tracking SSC as a function of the spacing

To conclude, it is important to mention that the squared sine function that we have seen in the lines above converges to $1/f^2$ when the spacing tends to zero according to (4.153). This is indeed deeply related to the ideas that were gathered in chapter 4.7 on MBOC where we mentioned that a signal whose spectrum envelope decays with $1/f^2$ would be optimum in terms of tracking performance. As we saw, MBOC follows this pattern too.

7. Signal Multiplex Techniques for GNSS

7.1 Introduction

As we have seen in chapter 2, all the existing and planned Global Satellite Navigation Systems will be transmitting more than two services in each transmission band.

- In E1/L1
  - GPS plans to transmit at least four signals: The old C/A Code and P(Y) Code, the modernized military M-Code and the new L1 Civil signal (L1C).
  - Similarly, Galileo will provide on E1 the Public Regulated Service (PRS) and the E1 OS data and pilot signals.
  - GLONASS transmits the C/A Code and P-Code, and plans new CDMA signals
  - and Compass plans to provide two additional signals with services that are still to be specified.
- In L2
  - GPS will be transmitting the L2 Civil Signal (L2C) together with the P(Y) Code and M-Code,
  - and GLONASS transmits the C/A Code and P-Code.
- In E5/L5
  - GPS L5 will provide data and pilot signals, while
  - Galileo plans to transmit four signals using the Alt-BOC modulation,
  - GLONASS plans to transmit new open CDMA signals in the L5 band,
  - and Compass plans to provide two additional signals with services that are still to be specified.
- In E6
  - Galileo plans to transmit the Public Regulated Service (PRS) and a Commercial Service (CS) with improved characteristics with respect to the free Open Service (OS),
  - and Compass plans to provide two additional signals with services that are still to be specified.
- Finally in L3
  - GLONASS will also transmit one civil signal (C/A Code) and the military P-Code.

The availability of spectrum allocations is a limited resource as we have seen in previous chapters and thus the existing bands have to be reused. As new services are demanded, new signals are also required to fulfil needs that did not exist previously. Moreover it is highly desirable and of greatest importance that the new navigation signals that are introduced do not

cause significant distortion on other signals sharing the frequency. In other words, they have to be compatible with the already existing ones. Additional constraints are that we can transmit the new signals through the same High Power Amplifier (HPA), to be able to accommodate new data messages and new Pseudo Random Noise (PRN) code families, to have spectral isolation with the rest of signals in the band and to be capable of providing flexibility to control the distribution of power between the signals in and outside of the allocated band.

If we take a look at all these constraints, we can clearly recognize the importance of developing good signal multiplex techniques based on a high efficiency constant-envelope. Multiplexing aims at providing a multiplicity of signals that must coexist on the same carrier without mutual interference [A.R. Pratt and J.I.R. Owen, 2005]. Moreover, we cannot ignore that there are clear constraints to fulfil at payload level and that the multiplex technique must therefore be carefully selected to avoid undesirable sources of degradation. In this chapter we will study the characteristics of current and future multiplexing techniques and the recently proposed modifications for GPS and Galileo in order to be capable of accommodating the optimized MBOC signal modulation.

Finally, it is interesting to note that, as shown in [A.R. Pratt and J.I.R. Owen, 2005], alternative multiplexing methods to those discussed in this chapter could be used. In fact, separate antenna and amplifier chains (that is separate aperture) which allow for signal combination in the far field of the satellite antenna system could be employed. In addition, different signals could be multiplexed on the carrier frequency on several different antenna beams as suggested in [G.L. Cangiani, 2005]. Nevertheless, the extra complexity that the spacecraft payload would have to deal with would be of consideration and the antenna design would suffer from poor efficiency and important cost and weight drawbacks. Moreover, the more challenging problem of transmitting these signals would be the development of a general modulation approach with a single modulator, up-converter, power amplifier chain and antenna aperture [P.A. Dafesh et al., 2006].

7.2 Multiplexing Schemes

The first multiplexing technique used in navigation (GPS) was employed to send the C/A Code and the P(Y) Code providing two bi-phase signals on the same carrier frequency in phase quadrature (QPSK). Demultiplexing was relatively simple. However, the need to have more navigation signals has made this multiplexing scheme obsolete for future modernized implementations. In fact, the possible solution of adding another signal slightly offset in frequency would give rise to a non-constant envelope with the consequent distortion after passing through the High Power Amplifier (HPA). The following multiplexing techniques

will be studied in the next pages:

- Linear Modulation (Spatial Combining)
  - Tri-code Hexaphase Modulation
- Majority signal voting
- Hard Limiting
- Quadrature Product Sub-carrier Modulation (QPSM)
  - Interplex and CASM
  - Modified Interplex Modulation
- Intervoting

In spite of the important advances realized in the past years, the research field on signal multiplex is still subject to active studies as shown in [T. Fan et al, 2005]. Out of all the multiplex techniques presented above, the Linear Modulation and the Tri-code Hexaphase Modulation have maximum efficiencies limited to roughly seventy-one percent [P.A. Dafesh et al., 2006], what is an important disadvantage. Moreover, they are limited to multiplexing only binary signals. The rest of multiplex techniques offer a superior performance as we will see in next chapters. The efficiency is defined as the sum of the effective transmitted power P_{useful} plus any band limiting losses, divided by the total transmitted power P_{total}.

$$\eta = \frac{P_{\text{useful}}}{P_{\text{total}}} \tag{7.1}$$

We describe next all the techniques in detail.

7.3 Linear Modulation (Spatial Combining)

The Linear Modulation, also known as additive or spatial modulation, basically consists in the addition of a new ranging signal to either the I or Q phases of a carrier where already at least other two signals are present. A well documented case in navigation is that of the GPS IIR Modernization or GPS IIR-M [P.A. Dafesh et al., 1999a] and [P.A. Dafesh et al., 2000]. In fact, GPS investigated at some point during its modernization the possibility of adding the M-Code in phase with the C/A Code or the P(Y) Code using this technique as shown by [J. W. Betz, 1999] and [S. H. Raghavan et al., 1997].

Let as suppose that we want to linearly add a new binary signal $s_N(t)$ to a baseband waveform modulated with other two binary signals $s_O^I(t)$ and $s_O^Q(t)$, where the subindex N refers to the new signal, O indicates the old signals that were already on the carrier in quadrature (QPSK) and I and Q are the respective phase. The In-phase and Quadrature components of the new multiplexed signal may be represented by

$$s(t) = I(t)\cos(2\pi f_c t) - Q(t)\sin(2\pi f_c t) \tag{7.2}$$

where the In-phase and quadrature components of the carrier, that is $I(t)$ and $Q(t)$, are defined as follows:

$$I(t) = \sqrt{2P_O^I}\, s_O^I(t) + \sqrt{2P_N}\, s_N(t) \tag{7.3}$$

and,

$$Q(t) = \sqrt{2P_O^Q}\, s_O^Q(t) \tag{7.4}$$

As we can recognize, the new signal has been added in-phase without loss of generality. If we define now the total power of the signal as

$$P_T = P_O^I + P_O^Q + P_N \tag{7.5}$$

it can be shown that the envelope of the composite signal will adopt the following form:

$$A(t) = \sqrt{2P_T + 4\sqrt{P_O^I P_N}\, s_O^I(t) s_N(t)} \tag{7.6}$$

which is not constant due to the presence of a time-varying component in addition to the constant $2P_T$. This is in principle negative because the result is AM-to-AM and AM-to-PM distortions when the signal is filtered through a nonlinear High Power Amplifier (HPA) unless we work in the linear region, far away from saturation. If this were the case, the operating point of the amplifier would be backed off from its saturation point to the linear region of the amplifier, making in principle this multiplexing approach a suitable alternative.

However, such a back-off is not of interest most of the times due to the high power inefficiency that results. Indeed, as early GPS modernization studies have clearly shown, the back-off functioning of an amplifier working in the linear region can result in several dB of power losses. We will show this in the next section with a particular example of the Linear Modulation, namely the Tri-code Hexaphase Modulation.

Last but not the least, it is important to mention that a Linear modulation is equivalent to spatially combining the signals to multiplex, where a separate amplifier chain and antenna aperture are used to modulate the existing signals and the new signals. This so-called separate aperture implementation results in a significant loss of overall power efficiency since a second power amplifier would be required for the new signals to be modulated.

7.3.1 Tri-code Hexaphase Modulation

The tri-code Hexaphase modulation is a particular implementation of the Linear Modulation described above. Let us assume as an example that the GPS M-Code and P(Y) Code would have the same power level, being this half of that of the C/A Code. [P.A. Dafesh et al., 2000] have shown that as a result of applying the Linear Modulation, the envelope of the multiplexed signal would not be constant. This is shown in the following figure, where the constellation diagram is depicted.

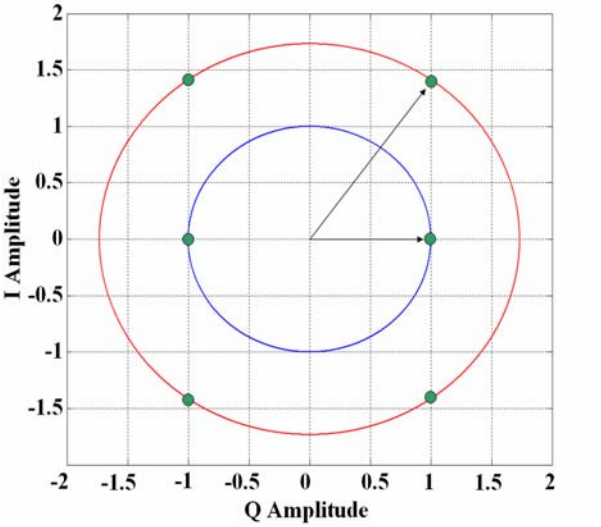

Figure 7.1. Constellation diagram for the Linear Modulation

As we can clearly see, the plot presents two distinct amplitudes since the constellation points lie on two different constant circles. This results in an hexaphase modulation as the name well indicates. In this particular example, the new M-Code was added to the P(Y) Code in-phase (vertical axis in the figure) following the mathematical scheme of (7.3).

Let us assume now a GPS transmission bandwidth of 30.69 MHz. This results in a filtering loss of approximately 0.03 dB for the C/A Code, 0.31 dB for the P(Y) Code and 0.80 dB for the M-Code. If we further assume same transmission powers as [P.A. Dafesh et al., 2000], the power efficiency of the linear modulation applied to GPS would adopt a value of approximately 93.23 %. This is indeed very close to the figure of the 92.80 % derived by [P.A. Dafesh et al., 2000] under similar assumptions.

Table 7.1. Power Efficiency of Linear Modulation

Signal and Carrier Phase	Percentage of Power before filtering and combining	Filtering Loss (dB)	Transmitted Power after filtering (dBW)
C/A (Q)	46.88 %	-0.03	-155
P(Y) Code (I)	25.06 %	-0.31	-158
M-Code (I)	28.06 %	-0.80	-158
Total	100 %		-151.6

This means a 0.30 dB power loss in the total signal power due to filtering and the Linear modulation. Although this might seem a good number in principle, the fact is that the overall power efficiency is in reality significantly reduced due to the amplifier back-off operation (unless we employ a separate power amplifier and work with a separate aperture) required to amplify the linearly modulated signals without causing AM-AM or AM-PM distortions. In fact, the 93.23 % power efficiency obtained in the previous analysis does not include the modulator inefficiency that amplifiers present in real world.

In order to avoid the disadvantages of this modulation, constant envelope solutions have been proposed to at least reduce the degradation effects that result from the High Power Amplifier as shown in the patent of [P.A. Dafesh et al., 2006]. We describe them in following chapters.

7.4 Majority Signal Voting

7.4.1 History of Majority Voting

The majority combining technique dates back to those days when communication engineers relied on increased power levels and redundancy to improve the reliability of a communication link. The basic form of redundancy consisted in transmitting each data symbol an odd number of times, demodulating each symbol individually and deciding in favour of the symbol value that occurred more frequently [R. S. Orr and B. Veytsman, 2002]. In fact, this is the simplest implementation of the majority vote multiplex as we will discuss in the next chapters. It is important to note however that while the majority voting that we will describe in the following chapters is realized at the transmitter, the combination that we referred to in the previous lines is carried out at the receiver.

The type of redundancy that we have mentioned has long been introduced in most of the digital circuits today. As a good example of it the Triple Modular Redundancy (TMR) is a standard design practice in systems where stringent availability and tolerance are required. Other systems with even higher requirements such as manned space missions use accordingly a higher level of redundancy.

As shown by [R. S. Orr and B. Veytsman, 2002], another field where majority voting has attracted the interest of researchers in the past has been that of using the combination of binary codes for ranging applications. References dating to as early as 1962 can be found in works from [M. F. Easterling, 1962], [D.J. Braverman, 1963], [R.C. Tausworthe, 1971] and [J.J. Spilker, 1977]. These works describe how long codes with particularly well selected properties can be developed on the basis of shorter codes that are combined in an intelligent way. As it is well known, long codes are desirable to obtain good auto- and cross-correlation properties. However, for acquisition, shorter codes are preferred to accelerate the process. Majority voting provides an efficient way to multiplex several short codes into a long code with good properties. The interest of this technique is that although the code presents a majority voted length that is in general by far longer than that of the individual codes it consists of, there exists a substructure that can be used to quickly acquire one of the codes. This principle is in fact described by [M. F. Easterling, 1962]. In this work it is shown how several Pseudo Random Noise (PRN) sequences with prime periods can be majority voted to form a code with period the product of the individual components. This longer code presents improved correlation characteristics but still preserves the substructure of the individual codes of shorter length, facilitating thus the acquisition.

It seems that, as shown in [A.R. Pratt and J.I.R. Owen, 2005], the majority voting multiplexing technique has not been implemented yet in any real navigation system. Nonetheless we can find patents where this technique is employed combined with more sophisticated schemes such as the Interplex [G.L. Cangiani et al., 2004]. We will refer to these in chapter 7.8. Majority voting could play indeed an important role in the future, not only for navigation, but also for terrestrial networks. The transmission of voice and data at higher rates than those that are possible today could be reality someday. As described by [R. S. Orr and B. Veytsman, 2002], the idea would be to transmit more than one code per service in such a way that different code channels could be assigned to different functions such as pilot, paging, synchronization, control and traffic. In addition, different power allocations could be assigned to different services to avoid the dominance of one or a few.

In addition, not only more services or channels could be transmitted multiplexed by the majority voted signal. In fact, different codes could be used too to transmit the same one service, enabling the operation of this service at higher data rates by splitting its data across the different codes as shown by [R. S. Orr and B. Veytsman, 2002]. Indeed, if N codes are used to transmit the same service, each code could carry part of the data message and the total data rate would increase. Of course care has to be taken in making the code sufficiently long. The reason for this is that by having several codes running in parallel multiplexed within the majority voted signal, each code will suffer a slight degradation that will make the demodulation more complicated. However, this is by far compensated by the increase of the data rate that can be achieved and by the fact that the correlation losses of any individual channel are limited even when the number of signals to multiplex increases.

Another interesting application that derives from the previous discussion could be the use of majority voting to transmit different codes with different lengths from the same satellite. The different codes could have prime lengths and would be selected in such a way that they would be optimum to serve specific applications. One can think, for example, of an indoor code, an urban-canyon code, codes with good acquisition properties or with good tracking characteristics. They would all be sent from the same satellite in an unique majority voted code. From the receiver point of view, the particular user would only have to care about the particular family of codes of interest being the rest of codes sent in the majority voted signal invisible to him. For example, indoor receivers would have to correlate in the receiver with the particular indoor codes of the constellation. These should be optimized in terms of correlation properties. In the end, an indoor receiver working on indoor codes would not see the effect of the other codes transmitted on the same satellite, except for a correlation loss of never more than 1.96 dB as we will show next.

To conclude, it is of interest to mention that another highly desirable property of the subject multiplex method is its transparency to the receiver equipment in the sense that this does not need to care about how the multiplex of the different signals looks like.

7.4.2 Definition of Majority Voting

The Majority Voting modulation, also known as Majority Combining, is a constant-envelope multiplex technique based on majority-vote logic [J.J. Spilker Jr. and R.S. Orr, 1998]. The majority vote approach is basically a time-multiplexing of either the I or Q phases (scalar) or of both of them (vectorial) at the same time, where multiple signals are transmitted in a single constant envelope. The basic idea is that the time-multiplexed signal to transmit is selected following a particular logic based on the input signals. In its simplest form, namely the *uniform weighting scalar distribution* or *equal weighting* that will be described in chapter 7.4.4, the number of signals to multiplex must be odd to ensure majority in all possible cases. In this approach, the majority vote logic produces a multiplex where each component signal is equally weighted. In its most general form, namely the Generalized Majority Voting (GMV), any odd and even number of signals can be multiplexed in principle with any possible weighting.

Majority voting is a non-linear multiplex technique that provides a convenient and flexible method to multiplex several signals into one constant envelope without multiplexing losses [J.J. Spilker Jr. and R.S. Orr, 1998]. Moreover, it elegantly circumvents the peak versus average power trade that the lossless linear superposition presents when applied through a common aperture, as we showed in previous chapter 7.3. The Majority Voting technique is also of particular interest to secure acquisition of codes such as the M-Code where the insertion of particularly well selected sequences would accelerate its detection. In the next chapters, the true relevance of majority voting will be underlined by comparing this multiplexing scheme with other better known techniques.

7.4.3 Theory on Majority Voting

Let an odd number of binary spread spectrum codes be multiplexed as proposed by [J.J. Spilker Jr. and R.S. Orr, 1998]. Majority logic operates on the principle that at a given time point the value to transmit is that of the majority of the codes. For this reason, the number of component codes must be odd. According to this, if the codes share a common chip rate, the majority voting operation will be done once per chip, while for the case that the rates differ, the majority combination will occur at their least common multiple.

If we think about the functioning of the majority logic, we can see that the majority combination rule is equivalent to computing the numerical sum of the code chips and taking its algebraic sign as shown by [J.J. Spilker Jr. and R.S. Orr, 1998]. Indeed, for the combination of three binary codes (c_1, c_2 and c_3) the majority code, c_{Maj}, can be as:

$$c_{\mathrm{Maj}} = \frac{c_1 + c_2 + c_3 - c_1 c_2 c_3}{2} \tag{7.7}$$

Of course similar expressions can be derived for more codes, but the complexity increases with the number of signals to multiplex. Furthermore, it is interesting to note that the previous equation can be used to derive the autocorrelation function of the majority voted signal and correspondingly the total spectrum as a function of the individual PSDs.

The case that we have described in the previous lines is the simplest implementation of the majority voting logic. A generalization can be easily accomplished by means of *interlacing*, which is the insertion of chips of one or more of the component codes into the output chip stream as replacement for the corresponding majority chips as explained by [J.J. Spilker Jr. and R.S. Orr, 1998]. Interlacing is an intelligent way to achieve non-uniform effective power distribution among the codes as we will see in the next chapters.

7.4.4 Majority Voting: Scalar Combination with Uniform Weighting

Let us assume, as we also did in previous lines, that we want to multiplex an odd number of $2N+1$ statistically independent binary signals using majority logic. Furthermore, let us assume that the codes are statistically balanced, so that the chip values can be modelled as independent, identically distributed binary random variables. According to this, the majority voted signal that will result of multiplexing the $2N+1$ individual signals can be expressed as:

$$c_{\text{Maj}} = \text{Maj}\left(c_1, c_2, c_3, ..., c_{2N+1}\right) = \text{sign}\left(\sum_{i=1}^{2N+1} c_i\right) \tag{7.8}$$

where the Majority operator Maj indicates the sign of the majority of the signals. This signal receives the name of majority voted signal and is the one that will be transmitted instead of the $2N+1$ signals. As one can imagine, in order the correlation losses not to be very high, the majority vote signal should somehow represent each of the $2N+1$ individual signals that form it. To measure how true this assumption is, the correlation between the majority voted signal c_{Maj} and a particular reference code has to be calculated.

The result of a single chip correlation, denoted χ in the following lines, equals +1 or -1 depending on the coincidence of the majority voting chip and the replica chip of the particular code we correlate with, assuming perfect alignment. In fact, the majority chip matches the reference chip (thus $\chi = +1$) if and only if at least N chips from the other remaining $2N$ codes also match it [J.J. Spilker Jr. and R.S. Orr, 1998]. Otherwise the correlation will be -1. According to this, the average correlation between any particular code c_i and the majority voting signal c_{Maj} will be

$$\overline{\chi} = \begin{cases} +1 \cdot p\left(c_i = +1, c_{\text{Maj}} = +1\right) + 1 \cdot p\left(c_i = -1, c_{\text{Maj}} = -1\right) - \\ -1 \cdot p\left(c_i = +1, c_{\text{Maj}} = -1\right) - 1 \cdot p\left(c_i = -1, c_{\text{Maj}} = +1\right) \end{cases} \tag{7.9}$$

what can also be expressed as follows:

$$\overline{\chi} = \begin{cases} +1 \cdot p(c_i = +1) \cdot p(c_{\text{Maj}} = +1 \,|\, c_i = +1) + 1 \cdot p(c_i = -1) \cdot p(c_{\text{Maj}} = -1 \,|\, c_i = -1) - \\ -1 \cdot p(c_i = +1) \cdot p(c_{\text{Maj}} = -1 \,|\, c_i = +1) - 1 \cdot p(c_i = -1) \cdot p(c_{\text{Maj}} = +1 \,|\, c_i = -1) \end{cases} \tag{7.10}$$

We assume that

$$p(c_i = +1) = p(c_i = -1) = \frac{1}{2} \tag{7.11}$$

Furthermore, it is trivial to see that

$$p(c_{\text{Maj}} = +1 \,|\, c_i = +1) = p_N^{2N}(+1) + p_{N+1}^{2N}(+1) + \ldots + p_{2N}^{2N}(+1) \tag{7.12}$$

where $p_N^{2N}(+1)$ is the probability that exactly N codes out of $2N$ adopt the value +1. As it can be shown, this probability is also equal to that of having N codes out of $2N$ with value -1 and adopts the following form:

$$p_N^{2N}(+1) = p_N^{2N}(-1) = \frac{1}{2^{2N}} \binom{2N}{N} \tag{7.13}$$

being thus the following identity true:

$$p(c_{\text{Maj}} = +1 \,|\, c_i = +1) = pp(c_{\text{Maj}} = -1 \,|\, c_i = -1) \tag{7.14}$$

In the same manner, it can be shown that:

$$p(c_{\text{Maj}} = -1 \,|\, c_i = +1) = p(c_{\text{Maj}} = +1 \,|\, c_i = +1) = p_{N+1}^{2N}(-1) + p_{N+2}^{2N}(-1) + \ldots + p_{2N}^{2N}(-1) \tag{7.15}$$

If we further develope (7.10), we can see that the mean correlation $\overline{\chi}$ between any particular code c_i and the majority voting code c_{Maj} simplifies to:

$$\overline{\chi} = \begin{cases} +\frac{1}{2} \cdot \left[p_N^{2N}(+1) + p_{N+1}^{2N}(+1) + \ldots + p_{2N}^{2N}(+1) \right] + \\ +\frac{1}{2} \cdot \left[p_N^{2N}(-1) + p_{N+1}^{2N}(-1) + \ldots + p_{2N}^{2N}(-1) \right] - \\ -\frac{1}{2} \cdot \left[p_{N+1}^{2N}(-1) + p_{N+2}^{2N}(-1) + \ldots + p_{2N}^{2N}(-1) \right] - \\ -\frac{1}{2} \cdot \left[p_{N+1}^{2N}(+1) + p_{N+2}^{2N}(+1) + \ldots + p_{2N}^{2N}(+1) \right] \end{cases} \tag{7.16}$$

or equivalently

$$\overline{\chi} = \frac{1}{2} p_N^{2N}(+1) + \frac{1}{2} p_N^{2N}(-1) = p_N^{2N}(+1) = \frac{1}{2^{2N}} \binom{2N}{N} \tag{7.17}$$

This expression can be further simplified using an approximation based on the Stirling bounds of the factorial function as shown by [W. Feller, 1957]:

$$\overline{\chi}^* = \frac{e^{-\frac{1}{8N}}}{\sqrt{\pi N}} \approx \overline{\chi} = \frac{1}{2^{2N}} \binom{2N}{N} \tag{7.18}$$

which is a good approximation even for low values of N.

If we normalize now the amplitude of the majority code to the summed power of the component codes, that is $\sqrt{2N+1}$, the normalized mean correlation $\overline{\rho}$ between any particular code c_i and the majority voting code c_{Maj} will be

$$\overline{\rho} = \frac{\sqrt{2N+1}}{2^{2N}}\binom{2N}{N} \approx \sqrt{\frac{2N+1}{\pi N}}\mathrm{e}^{-\frac{1}{8N}} \tag{7.19}$$

The problem of this implementation of the majority voting is that since all the signals are equally weighted in power, there appear relatively large majority combining losses per signal, resulting in relatively poor overall power efficiencies. In fact, for the case of three transmitted signals, the majority vote multiplexing is shown to result in a 1.25 dB multiplexing loss (what corresponds to an efficiency of approximately 75 %). It is important to keep in mind that when three signal are majority voted, *N* adopts the value 1 in the previous equations ($3 = 2\cdot 1+1$). Next table exemplifies the possible chip combinations for majority combining of three codes and the correlation between each of the three codes and the majority voted code

Table 7.2. Chip combinations and correlation for majority combining of three codes

Code 1	+	+	+	+	-	-	-	-
Code 2	+	+	-	-	+	+	-	-
Code 3	+	-	+	-	+	-	+	-
Majority Voting Code	+	+	+	-	+	-	-	-
χ **Code 1 – MV Code**	+	+	+	-	-	+	+	+
χ **Code 2 – MV Code**	+	+	-	+	+	-	+	+
χ **Code 3 – MV Code**	+	-	+	+	+	+	-	+

As we can see, the unnormalized mean correlation between any particular code and the majority voting code adopts the value + in 18 cases and – in 6 cases. Probabilistically speaking, this implies that:

$$\begin{aligned} p(\chi = +) &= \frac{3}{4} \\ p(\chi = -) &= \frac{1}{4} \end{aligned} \tag{7.20}$$

so that the unnormalized mean correlation will be $\overline{\chi} = 1/2$, resulting in an apparent loss of 6.02 dB. If we consider now the power of the three codes, the total loss will be $\overline{\rho} = \sqrt{3}/2$ which corresponds to the 1.25 dB we mentioned some lines above. This result coincides perfectly with the predictions of the theory developed in previous equations.

The correlation power loss factor *L*(*N*) is defined by [J.J. Spilker Jr. and R.S. Orr, 1998] as the fraction of power of any code in the majority voted signal measured at the correlator output and is shown to adopt the following form:

$$L(N) = \overline{\rho}^2 \tag{7.21}$$

or expressed in dB,

$$L_{\mathrm{dB}}(N) = -20\log_{10}\left[2^{-2N}\sqrt{2N+1}\binom{2N}{N}\right] \tag{7.22}$$

It is interesting to analyze this equation when the number of equal-weighted inputs increases. In fact, when $N \to \infty$, (7.19) shows that the achievable per-code correlation asymptotically approaches $\sqrt{2/\pi}$, so that the correlation losses will increase as the number of signals to multiplex increases, but will never be higher than 1.96 dB. In fact, when the receiver performs a correlation among all the possibilities, some of the received chips will be wrong but limited in number according to the above derived expressions. The following figure shows the losses as a function of the number of multiplexed signals. To compute the curve, the exact formula of the majority losses was employed. However, the difference with respect to the Stirling approximation is minimum even for low numbers of signals.

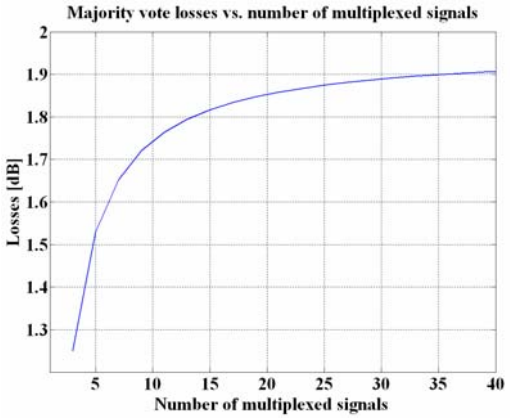

Figure 7.2. Majority voting losses

Another important drawback of this simple implementation of the majority vote multiplexing is that it is difficult to control the relative power levels between the different multiplexed signals without incurring in additional losses as shown in [P.A. Dafesh et al., 2006]. Indeed, in the previous derivations all codes or signals are assigned the same power levels. Furthermore, this multiplexing technique does not provide sufficient spectral separation and has limited inherent flexibility in adjusting the amplitude of generated harmonics, being all these great disadvantages.

A way to achieve an arbitrary weighting of the power of the signals to multiplex is using a statistical mix of majority vote rules operating on appropriately chosen subsets of the input chips of each signal [P.A. Dafesh et al., 2006]. Here, the power distribution is realised playing with the relative frequency of use of the various majority vote rules. As we can imagine, a particular power distribution can be accomplished with different majority vote rules and thus the optimum of all the possible solutions will be that one with the smallest multiplexing losses. This will be further clarified in the next chapters.

To conclude this chapter it is important to mention that the correlation loss can also be interpreted as the additional fraction of transmit power ΔP that is required to neutralize the receiver performance loss, so that it can be defined as follows:

$$\Delta P = L^{-1} \tag{7.23}$$

7.4.5 Majority Voting: Scalar Combination with Non-Uniform Weighting

In the previous chapter we have analyzed the simplest realization of the majority voting technique, namely the uniformly weighted version, where all the signals contribute with the same power to the majority voted signal. As we saw there, this solution presents limitations with respect to the flexibility to meet the power requirements in normal GNSS systems. To cope with this, this chapter describes the non-uniform solution.

The non-uniform weighting can be likened to shareholder voting as graphically described by [R. S. Orr and B. Veytsman, 2002]. In fact, based on a targeted power allocation, each of the signals to multiplex is allocated a number of votes, which may be fractional in the most general case. Then, at each chip epoch, the transmitted majority voted value is selected by taking the sign of the sum of the weighted chips of each individual code. Without loss of generality, the codes or channels are assumed to be binary. This is shown in the expression next proposed by [R. S. Orr and B. Veytsman, 2002]:

$$c_{\text{Maj}} = \text{sign}\left(\sum_{i=1}^{N} \lambda_i c_i \right) \tag{7.24}$$

where λ_i is the number of votes allocated to the i-th of the N signals, c_i represents the chip value of the i-th signal and c_{Maj} is the majority voted chip value. As we can see in the expression above, this generalized form of majority voting also includes the particular case of (7.8) where all the weights are equal. Moreover, it is easy to recognize that this adaptation of majority logic enables a constant-envelope multiplexing of an arbitrary distribution of chip-synchronous CDMA signals. In addition, there is no constraint on the number of signals that can be multiplexed so that also an even number of codes could be majority voted using this general approach. One final comment on the previous equation is that the weighting factors must be selected in such a way that the summation is different than zero at any time.

As we can read from (7.24), the key to achieve an efficient multiplexing is the correct selection of the weighting factors so that the resulting composite signal does indeed reflect the desired power distribution among the various user signals. As shown by [R. S. Orr and B. Veytsman, 2002], if all the chips of the signals to multiplex were weighted as in a linear multiplexer in proportion to the square root of their power allocation, (7.24) would not reflect in general the desired power distribution. In fact, those signals with small amounts of power could become suppressed relative to more powerful codes.

Let us assume that we want to majority vote two signals with power ratios 20 % and 80 % of the total power respectively. This means that one signal will be four times stronger than the other one. As we mentioned in the previous lines, a linear multiplexer would assign coefficients 1 and 2 to the weak and strong signals according to:

$$c_{\text{Maj}} = c_1 + 2 \cdot c_2 \tag{7.25}$$

If we show now the possible chip combinations of this scheme and the correlation between each of the two codes and the majority voted code, we have:

Table 7.3. Chip combinations and correlation for linear majority combining of the majority rule $c_{\text{Maj}} = c_1 + 2 \cdot c_2$

Code 1	+	+	-	-
Code 2	+	-	+	-
Majority Voting Code	+	-	+	-
χ Code 1 – MV Code	+	-	-	+
χ Code 2 – MV Code	+	+	+	+

As we can recognize, while the mean correlation of code 1 with the majority voting signal is zero, code 2 presents a perfect correlation of 100 %.

As we can see, the weakest signal is not reflected at all in the majority voted signal at the end as the information from code 1 has gone lost in the majority voted signal. This small signal suppression or capture is a well known result of non-linear signal processing operation and reflects indeed the fact that *no coalition of minority stockholders can ever outvote a 51 % majority interest* as graphically expressed by [R. S. Orr and B. Veytsman, 2002].

With the previous example, we have demonstrated that a faithful representation of a commanded power distribution can not be achieved in the most general case using a linear multiplexer. Indeed, the signal weight cannot be the square root of the power allocation unless the signals to multiplex were Gaussian distributed.

[R. S. Orr and B. Veytsman, 2002] have derived a set of equations that give an elegant solution to this problem. According to the algorithm presented in their work, the cross-correlation between the majority voted code and a particular component code is constraint by a set of equations in such as way that the power allocated to the particular signal is equal to the square of the value of the corresponding correlation between this signal and the majority vote signal. In addition, a coefficient of proportionality is also introduced in the model in order to control the efficiency or multiplexing losses common to each code. The solution of the equations provides the appropriate weighting of each signal maximizing the efficiency for the desired power ratio. The model is extremely non-linear and therefore, to minimize the resolution of the algorithm, [R. S. Orr and B. Veytsman, 2002] propose to assign each of the component codes to one of two groups, designated as *Gaussian* and *non-Gaussian*.

The components assigned to the Gaussian group *G* are typically small in power but numerous in number. As one can imagine, the division between Gaussian and not Gaussian (*NG*) is not always so straightforward. Normally, the criterion to define a group of signals as Gaussian is that the weighted sum of their chips, with the weight being proportional to the square root of the power allocation, will have a power that is less than a specified fraction of the total power,

typically 5 % to 10 %. It must be underlined that, in spite of existing well defined statistical tests to decide on the Gaussianness of a group of signals, the determination of this decision threshold is relatively flexible and up to the designer. Indeed, the threshold value for this test is a parameter that permits some flexibility. [R. S. Orr and B. Veytsman, 2002] have shown that still in cases where the Gaussian group does not ideally behave as it should according to theory, the algorithm delivers good solutions.

Taking (7.24), the majority voted signal will be formed in this case as follows:

$$c_{\text{Maj}} = \text{sign}\left(S^G + S^{NG}\right) = \text{sign}\left(\sum_{i=1}^{N^G} \lambda_i^G c_i^G + \sum_{j=1}^{N^{NG}} \lambda_j^{NG} c_j^{NG}\right) \tag{7.26}$$

where G refers to the Gaussian group of signals, NG to the non-Gaussian group and N^G and N^{NG} are respectively the number of Gaussian and non-Gaussian signals.

The commanded power distribution is described by a set of non-decreasing ratios $\{R_i\}$ with $0 \le i \le N^{NG}$, where the lowest ratio, R_0, describes the power of the Gaussian group and is normalized to 1 as shown by [R. S. Orr and B. Veytsman, 2002]. Accordingly, the remaining signals $1 \le i \le N^{NG}$ will represent the non-Gaussian group. Following this notation, R_i would indicate that the non-Gaussian signal c_{i} has a power R_i times that of the Gaussian group.

The Gaussian group signals have assigned weighting factors that are equal to the root square of the power allocation. Therefore, if all the N^G signals had the same power and given that the whole power of the Gaussian group is normalized to unity, each code of the group would be allocated a power $1/N^G$ being consequently the weighting factor of all the signals in the Gaussian group $1/\sqrt{N^G}$. The composite Gaussian group S^G is normalized to have power 1 and mean zero being therefore its probability density function defined as follows.

$$f_{S^G}\left(S^G\right) = \frac{1}{\sqrt{2\pi}} \text{e}^{-\frac{\left(S^G\right)^2}{2}} \tag{7.27}$$

Since in the next lines the probability of S^G to be in an arbitrary region $-x < S^G < x$ will appear relatively often, it is worth to recall the value of this probability

$$p\left(-x < S^G < x\right) = \int_{-x}^{x} f_{S^G}\left(S^G\right) \text{d}S^G = \int_{-x}^{x} \frac{1}{\sqrt{2\pi}} \text{e}^{-\frac{\left(S^G\right)^2}{2}} \text{d}S^G = \frac{2}{\sqrt{\pi}} \int_0^{\frac{x}{\sqrt{2}}} \text{e}^{-\left(S'^G\right)^2} \text{d}S'^G \tag{7.28}$$

This result can be further simplified, at least regarding the notation, if we express it in terms of the mathematical error function, which is defined as follows:

$$\text{erf}(x) = \frac{2}{\sqrt{\pi}} \int_0^x \text{e}^{-t^2} dt \tag{7.29}$$

According to this, the probability that the Gaussian group variable S^G is between –x and x can also be expressed as follows:

$$p\left(-x < S^G < x\right) = \operatorname{erf}\left(\frac{x}{\sqrt{2}}\right) \tag{7.30}$$

As we have emphasized in previous lines, the collective power ratio R_0 of the Gaussian signal codes must be unity. This means that the commanded distribution power allocations of the Gaussian signals $P_1^G, P_2^G, ..., P_{N^G}^G$ must be normalized as follows:

$$\overline{P}_i^G = \frac{P_i^G}{\sum_{i=1}^{N^G} P_i^G} \tag{7.31}$$

and the corresponding weighting coefficients will thus adopt the following form:

$$\lambda_i^G = \sqrt{\overline{P}_i^G} \quad 1 \le i \le N^G \tag{7.32}$$

For the non-Gaussian group codes, the power ratios of the N^{NG} non-Gaussian signal codes are equally determined as shown next [R. S. Orr and B. Veytsman, 2002]:

$$R_i = \frac{P_i^{NG}}{\sum_{i=1}^{N^G} P_i^G} \quad 1 \le i \le N^{NG} \tag{7.33}$$

As we can see, the ratio R_i indicates the relative power between the non-Gaussian code *i* and the power of the Gaussian group.

In line with the derivations of chapter 7.4.4, we have to derive now the correlation equations to find the optimum weighting factors. Indeed, the power allocated to each non-Gaussian signal should be the square of the correlation between that code and the majority voted signal.

Since each chip in the multiplex can adopt two values, there is a total of $2^{N^{NG}}$ possibilities at any time for the N^{NG} non-Gaussian chips [R. S. Orr and B. Veytsman, 2002]. Let us define $\overline{c}^{NG}$ as a combination of N^{NG} non-Gaussian chips such that

$$S^{NG}\left(\overline{c}^{NG}\right) = \sum_{j=1}^{N^{NG}} \lambda_j^{NG} c_j^{NG} \tag{7.34}$$

and $S_i^{NG}\left(\overline{c}^{NG}\right)$ equals (7.34) except for the exclusion of the *i*-th chip,

$$S_i^{NG}\left(\overline{c}^{NG}\right) = \sum_{j=1, j\neq i}^{N^{NG}} \lambda_j^{NG} c_j^{NG} \tag{7.35}$$

If we recall (7.24), the Majority Vote (MV) signal in its general form is shown to be:

$$c_{\text{Maj}} = \operatorname{sign}\left[S^G\left(\overline{c}^G\right) + S^{NG}\left(\overline{c}^{NG}\right)\right] = \operatorname{sign}\left[S^G + S^{NG}\left(\overline{c}^{NG}\right)\right] \tag{7.36}$$

If we have a look at a particular non-Gaussian code c_i^{NG}, the value of the sum $S^G + S^{NG}\left(\overline{c}^{NG}\right)$ can adopt the two following values:

$$S^G + S^{NG}\left(\overline{c}^{NG}\right) = \begin{cases} S^G + S_i^{NG}\left(\overline{c}^{NG}\right) + \lambda_i^{NG} & \text{for } c_i^{NG} = +1 \\ S^G + S_i^{NG}\left(\overline{c}^{NG}\right) - \lambda_i^{NG} & \text{for } c_i^{NG} = -1 \end{cases} \tag{7.37}$$

being thus the correlation between the replica desired signal c_i^{NG} and c_{Maj} as follows:

$$\overline{\chi}_i = \begin{cases} +1 \cdot p\left(c_i^{NG} = +1\right) \cdot p\left[S_i^{NG}\left(\overline{c}^{NG}\right)\right] \cdot p\left(S^G + S_i^{NG}\left(\overline{c}^{NG}\right) + \lambda_i^{NG} \geq 0\right) + \\ +1 \cdot p\left(c_i^{NG} = -1\right) \cdot p\left[S_i^{NG}\left(\overline{c}^{NG}\right)\right] \cdot p\left(S^G + S_i^{NG}\left(\overline{c}^{NG}\right) - \lambda_i^{NG} < 0\right) + \\ -1 \cdot p\left(c_i^{NG} = +1\right) \cdot p\left[S_i^{NG}\left(\overline{c}^{NG}\right)\right] \cdot p\left(S^G + S_i^{NG}\left(\overline{c}^{NG}\right) + \lambda_i^{NG} < 0\right) - \\ -1 \cdot p\left(c_i^{NG} = -1\right) \cdot p\left[S_i^{NG}\left(\overline{c}^{NG}\right)\right] \cdot p\left(S^G + S_i^{NG}\left(\overline{c}^{NG}\right) - \lambda_i^{NG} \geq 0\right) \end{cases} \tag{7.38}$$

where $p\left[S_i^{NG}\left(\overline{c}^{NG}\right)\right]$ indicates the probability that the Non-Gaussian sum adopts a particular value determined by $\overline{c}^{NG}$. Furthermore, the sign function is defined as:

$$\text{sign}(x) = \begin{cases} 1 & \text{for } x \geq 0 \\ -1 & \text{for } x < 0 \end{cases} \tag{7.39}$$

It is important to note, that the coefficients must be selected such that the sum of all the weighted signals is never zero. Moreover, the probability to have a specific combination of Non-Gaussian codes is shown to adopt the following form:

$$p\left[S_i^{NG}\left(\overline{c}^{NG}\right)\right] = \frac{1}{2^{N^{NG}-1}} \tag{7.40}$$

If we further develope (7.38), we have a mean correlation:

$$\overline{\chi}_i = \begin{cases} 1 \cdot \frac{1}{2} \cdot \frac{1}{2^{N^{NG}-1}} \cdot p\left(S^G \geq -S_i^{NG}\left(\overline{c}^{NG}\right) - \lambda_i^{NG}\right) + \\ +1 \cdot \frac{1}{2} \cdot \frac{1}{2^{N^{NG}-1}} \cdot p\left(S^G < -S_i^{NG}\left(\overline{c}^{NG}\right) + \lambda_i^{NG}\right) - \\ -1 \cdot \frac{1}{2} \cdot \frac{1}{2^{N^{NG}-1}} \cdot p\left(S^G < -S_i^{NG}\left(\overline{c}^{NG}\right) - \lambda_i^{NG}\right) - \\ -1 \cdot \frac{1}{2} \cdot \frac{1}{2^{N^{NG}-1}} \cdot p\left(S^G \geq -S_i^{NG}\left(\overline{c}^{NG}\right) + \lambda_i^{NG}\right) \end{cases} \tag{7.41}$$

which can also be expressed as:

$$\overline{\chi}_i = \begin{cases} \frac{1}{2^{N^{NG}}} \cdot p\left(S^G \leq S_i^{NG}\left(\overline{c}^{NG}\right) + \lambda_i^{NG}\right) + \frac{1}{2^{N^{NG}}} \cdot p\left(S^G > S_i^{NG}\left(\overline{c}^{NG}\right) - \lambda_i^{NG}\right) - \\ -\frac{1}{2^{N^{NG}}} \cdot p\left(S^G > S_i^{NG}\left(\overline{c}^{NG}\right) + \lambda_i^{NG}\right) - \frac{1}{2^{N^{NG}}} \cdot p\left(S^G \leq S_i^{NG}\left(\overline{c}^{NG}\right) - \lambda_i^{NG}\right) \end{cases} \tag{7.42}$$

If we have a look now at the next figure representing the probability density function of the Gaussian group,

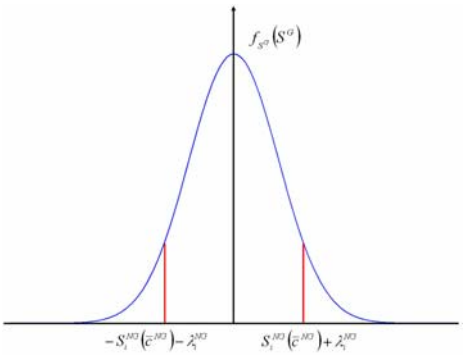

Figure 7.3. Probability density function of the Gaussian sum S^G

it is clear to recognize that

$$p\left(S^G \le S_i^{NG}\left(\bar{c}^{NG}\right)+\lambda_i^{NG}\right)-p\left(S^G > S_i^{NG}\left(\bar{c}^{NG}\right)+\lambda_i^{NG}\right)=\operatorname{erf}\left(\frac{S_i^{NG}\left(\bar{c}^{NG}\right)+\lambda_i^{NG}}{\sqrt{2}}\right) \quad (7.43)$$

and

$$p\left(S^G > S_i^{NG}\left(\bar{c}^{NG}\right)-\lambda_i^{NG}\right)-p\left(S^G \le S_i^{NG}\left(\bar{c}^{NG}\right)-\lambda_i^{NG}\right)=-\operatorname{erf}\left(\frac{S_i^{NG}\left(\bar{c}^{NG}\right)-\lambda_i^{NG}}{\sqrt{2}}\right) \quad (7.44)$$

Therefore, the mean correlation can be simplified to:

$$\bar{\chi}_i=\frac{1}{2^{N^{NG}}}\cdot\left[\operatorname{erf}\left(\frac{S_i^{NG}\left(\bar{c}^{NG}\right)+\lambda_i^{NG}}{\sqrt{2}}\right)-\operatorname{erf}\left(\frac{S_i^{NG}\left(\bar{c}^{NG}\right)-\lambda_i^{NG}}{\sqrt{2}}\right)\right] \quad (7.45)$$

The expression derived above corresponds to a particular combination of $N^{NG}-1$ non-Gaussian chips $\bar{c}_i^{NG}$ where all non-Gaussian codes, except for code c_i^{NG}, were considered. To extend the result to all the code combinations and have thus the mean correlation for any component signal, we only have to sum over $\bar{c}_i^{NG}$ as shown next:

$$\bar{\chi}_i^{NG}=\frac{1}{2^{N^{NG}}}\cdot\sum_{\bar{c}_i^{NG}}\left[\operatorname{erf}\left(\frac{S_i^{NG}\left(\bar{c}^{NG}\right)+\lambda_i^{NG}}{\sqrt{2}}\right)-\operatorname{erf}\left(\frac{S_i^{NG}\left(\bar{c}^{NG}\right)-\lambda_i^{NG}}{\sqrt{2}}\right)\right] \quad (7.46)$$

This expression can be further simplified if we recall that integrating (7.45) over $\bar{c}_i^{NG}$ and $\bar{c}^{NG}$ (that is over all code combinations including that of code *i*) will be similar except for a factor 2. In fact, it can be shown that

$$\begin{aligned}\bar{\chi}_i^{NG} &=\frac{1}{2^{N^{NG}}}\cdot\sum_{\bar{c}_i^{NG}}\left[\operatorname{erf}\left(\frac{S_i^{NG}\left(\bar{c}^{NG}\right)+\lambda_i^{NG}}{\sqrt{2}}\right)-\operatorname{erf}\left(\frac{S_i^{NG}\left(\bar{c}^{NG}\right)-\lambda_i^{NG}}{\sqrt{2}}\right)\right]= \\ &=\frac{1}{2^{N^{NG}+1}}\cdot 2\sum_{\bar{c}_i^{NG}}\left[\operatorname{erf}\left(\frac{S_i^{NG}\left(\bar{c}^{NG}\right)+\lambda_i^{NG}}{\sqrt{2}}\right)-\operatorname{erf}\left(\frac{S_i^{NG}\left(\bar{c}^{NG}\right)-\lambda_i^{NG}}{\sqrt{2}}\right)\right]= \\ &=\frac{1}{2^{N^{NG}+1}}\cdot\sum_{\bar{c}^{NG}}\left[\operatorname{erf}\left(\frac{S_i^{NG}\left(\bar{c}^{NG}\right)+\lambda_i^{NG}}{\sqrt{2}}\right)-\operatorname{erf}\left(\frac{S_i^{NG}\left(\bar{c}^{NG}\right)-\lambda_i^{NG}}{\sqrt{2}}\right)\right]\end{aligned} \quad (7.47)$$

As we can see, the last line of the previous equation integrates over $\bar{c}^{NG}$ and not $\bar{c}_i^{NG}$.

In the same manner, the correlation between the Gaussian group and the majority voted signal can be approximated as follows:

$$\bar{\chi}^G=\frac{1}{2^{N^{NG}}}\cdot\sum_{\bar{c}^{NG}}\sqrt{\frac{2}{\pi}}\cdot e^{-\frac{\left[S^{NG}\left(\bar{c}^{NG}\right)\right]^2}{2}} \quad (7.48)$$

An example confirming the validity of the previous expression is briefly depicted in the next lines. Let us imagine that our majority voting signal adopts the following form:

$$c_{\text{Maj}}=\operatorname{sign}\left(S^G+S^{NG}\right)=\operatorname{sign}\left(S^G+5\cdot c_1+10\cdot c_2\right) \quad (7.49)$$

As we can recognize, the majority voted multiplexed signal consists of the Gaussian group and two non-Gaussian codes c_1 and c_2 weighted with 5 and 10 respectively. We analyze next all possible cases:

For the particular combination $(c_1,c_2)=(-1,-1)$, the mean value of the sum of the Gaussian and non-Gaussian signals S^G+S^{NG} will be -15 adopting the probability density function the following form:

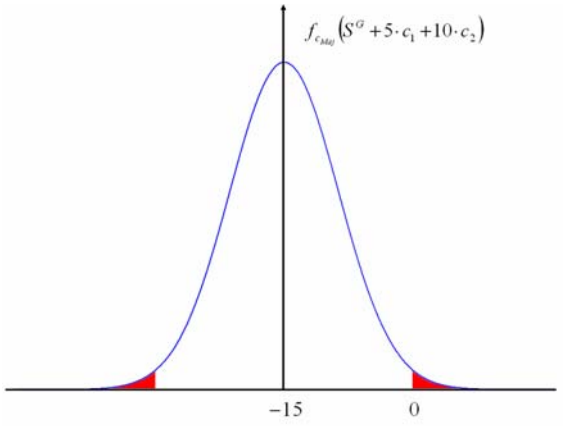

Figure 7.4. Probability density function of S^G+S^{NG} for $(c_1,c_2)=(-1,-1)$

where the area in red indicates the value of the mean correlation for this particular combination of non-Gaussian codes. Indeed, the mean correlation in this case is shown to adopt the following value:

$$\chi^{G}_{\bar{c}^{NG}=(-1,-1)}=\frac{1}{4}\cdot\begin{bmatrix}+1\cdot p(G<0)+\\+1\cdot p(G\geq 15)-\\-1\cdot p(0\leq G<15)\end{bmatrix}=\frac{1}{4}\cdot p\{G\notin(-15,15)\}=\frac{1}{4}\cdot\operatorname{erfc}\left(\frac{15}{\sqrt{2}}\right) \tag{7.50}$$

where $\operatorname{erfc}(x)=1-\operatorname{erf}(x)$ This can also be expressed as a function of the weightings:

$$\chi^{G}_{\bar{c}^{NG}=(-1,-1)}=\frac{1}{4}\cdot\operatorname{erfc}\left(\frac{\|+\lambda_1+\lambda_2\|}{\sqrt{2}}\right)\Bigg|_{(\lambda_1,\lambda_2)=(5,10)} \tag{7.51}$$

As one can observe, this is the unnormalized correlation between the Gaussian group and the majority voted signal for this particular combination of non-Gaussian codes. To normalize the expression, we only have to multiply by $\|+\lambda_1+\lambda_2\|$ resulting thus

$$\rho^{G}_{\bar{c}^{NG}=(-1,-1)}=\frac{1}{4}\cdot\|+\lambda_1+\lambda_2\|\operatorname{erfc}\left(\frac{\|+\lambda_1+\lambda_2\|}{\sqrt{2}}\right)\Bigg|_{(\lambda_1,\lambda_2)=(5,10)} \tag{7.52}$$

In the same manner, for the combination of non-Gaussian codes $(c_1,c_2)=(-1,+1)$, the mean value of the sum of the Gaussian and non-Gaussian signals S^G+S^{NG} will be 5 in this case, yielding the mean unnormalized correlation:

$$\chi^{G}_{\bar{c}^{NG}=(-1,+1)}=\frac{1}{4}\cdot\begin{bmatrix}+1\cdot p(G\geq 0)+\\+1\cdot p(G<-5)-\\-1\cdot p(-5\leq G<0)\end{bmatrix}=\frac{1}{4}\cdot p\{G\notin(-5,5)\}=\frac{1}{4}\cdot\operatorname{erfc}\left(\frac{5}{\sqrt{2}}\right) \tag{7.53}$$

or again for any arbitrary two weighting factors:

$$\chi^{G}_{\bar{c}^{NG}=(-1,+1)}=\frac{1}{4}\cdot\operatorname{erfc}\left(\frac{\|-\lambda_1+\lambda_2\|}{\sqrt{2}}\right) \tag{7.54}$$

so that the normalized expression will be:

$$\rho^{G}_{\bar{c}^{NG}=(-1,+1)} = \frac{1}{4}\cdot\left\|-\lambda_1+\lambda_2\right\|\operatorname{erfc}\left(\frac{\left\|-\lambda_1+\lambda_2\right\|}{\sqrt{2}}\right) \tag{7.55}$$

In the same manner, the mean normalized correlation for the code combination $(c_1,c_2)=(+1,-1)$ will be:

$$\rho^{G}_{\bar{c}^{NG}=(+1,-1)} = \frac{1}{4}\cdot\left\|+\lambda_1-\lambda_2\right\|\operatorname{erfc}\left(\frac{\left\|+\lambda_1-\lambda_2\right\|}{\sqrt{2}}\right) \tag{7.56}$$

and for $(c_1,c_2)=(+1,+1)$,

$$\rho^{G}_{\bar{c}^{NG}=(+1,+1)} = \frac{1}{4}\cdot\left\|-\lambda_1-\lambda_2\right\|\operatorname{erfc}\left(\frac{\left\|-\lambda_1-\lambda_2\right\|}{\sqrt{2}}\right) \tag{7.57}$$

Grouping now all the previous normalized correlations, the mean value will be then:

$$\overline{\rho}^{G}_{\bar{c}^{NG}} = \frac{1}{4}\cdot\sum_{\bar{c}^{NG}}\left\|S^{NG}\right\|\operatorname{erfc}\left(\frac{\left\|S^{NG}\right\|}{\sqrt{2}}\right) \tag{7.58}$$

where $S^{NG}=5\cdot c_1+10\cdot c_2$ in this particular example. Moreover, the erfc function can be well approximated as follows when the argument is higher than 3 (as it is the case in Majority Vote combinations) [M. Abramovitz and I.A. Stegun, 1965]:

$$\operatorname{erfc}(x)\approx\frac{1}{x\sqrt{\pi}}\mathrm{e}^{-x^2} \tag{7.59}$$

For our particular case, this implies that the correlation between the Gaussian group and the majority voted signal can be approximated for any generic non-Gaussian code combination $\bar{c}^{NG}$ as follows:

$$\overline{\rho}^{G}_{\bar{c}^{NG}} = \frac{1}{2^{N^{NG}}}\cdot\sum_{\bar{c}^{NG}}\sqrt{\frac{2}{\pi}}\cdot\mathrm{e}^{-\frac{\left[S^{NG}\left(\bar{c}^{NG}\right)\right]^2}{2}} \tag{7.60}$$

which is the expression presented in (7.48).

Dividing now (7.47) by (7.60) and squaring, the power ratio of code c_i^{NG} will adopt the following form:

$$R_i=\left\{\frac{\overline{\chi}_i^{NG}}{\overline{\rho}^{G}_{\bar{c}^{NG}}}\right\}^2=\frac{\pi}{8}\left\{\frac{\sum_{\bar{c}^{NG}}\left[\operatorname{erf}\left(\frac{S_i^{NG}\left(\bar{c}^{NG}\right)+\lambda_i^{NG}}{\sqrt{2}}\right)-\operatorname{erf}\left(\frac{S_i^{NG}\left(\bar{c}^{NG}\right)-\lambda_i^{NG}}{\sqrt{2}}\right)\right]}{\sum_{\bar{c}^{NG}}\mathrm{e}^{-\frac{\left[S^{NG}\left(\bar{c}^{NG}\right)\right]^2}{2}}}\right\}^2 \tag{7.61}$$

which coincides with the formula derived by [R. S. Orr and B. Veytsman, 2002]. Once we have the ratio of the power of any code c_i^{NG} of the non-Gaussian group with respect to the Gaussian group, the power loss factor of all the signals multiplexed can be expressed in terms of the losses of the Gaussian group multiplied by the total power of the signal since all the power ratios are normalized to the power of the Gaussian group:

$$L=\left(1+\sum_{i=1}^{N^{NG}}R_i\right)\left(\overline{\rho}^{G}_{\bar{c}^{NG}}\right)^2=\left(1+\sum_{i=1}^{N^{NG}}R_i\right)\left[\frac{1}{2^{N^{NG}}}\cdot\sum_{\bar{c}^{NG}}\sqrt{\frac{2}{\pi}}\cdot\mathrm{e}^{-\frac{\left[S^{NG}\left(\bar{c}^{NG}\right)\right]^2}{2}}\right]^2 \tag{7.62}$$

or simplified:

$$L = \left(\frac{1 + \sum_{i=1}^{N^{NG}} R_i}{2^{N^{NG}-1}\pi} \right) \left[\sum_{\bar{c}^{NG}} \mathrm{e}^{-\frac{\left[S^{NG}\left(\bar{c}^{NG}\right)\right]^2}{2}} \right]^2 \tag{7.63}$$

which also coincides with the expression derived by [R. S. Orr and B. Veytsman, 2002].

Once we have derived the general expressions for the losses of the majority vote multiplex and thus the efficiency of the modulation for a targeted power distribution, the next step is to find the optimum weighting factors. This problem is basically a minimization exercise that consists in finding the weighting factors that minimize the total losses subject to the envisaged power division between the different signals. This can be expressed as follows:

$$\begin{aligned} &\min_{\left\{\lambda_i^{NG}\right\}} \{L\} \\ &\text{subject to } \{R_i\} \end{aligned} \tag{7.64}$$

where

$$L = \left(\frac{1 + \sum_{i=1}^{N^{NG}} R_i}{2^{N^{NG}-1}\pi} \right) \left[\sum_{\bar{c}^{NG}} \mathrm{e}^{-\frac{\left[S^{NG}\left(\bar{c}^{NG}\right)\right]^2}{2}} \right]^2 \tag{7.65}$$

and

$$R_i = \frac{\pi}{8} \left\{ \frac{\sum_{\bar{c}^{NG}} \left[\operatorname{erf}\left(\frac{S_i^{NG}\left(\bar{c}^{NG}\right) + \lambda_i^{NG}}{\sqrt{2}} \right) - \operatorname{erf}\left(\frac{S_i^{NG}\left(\bar{c}^{NG}\right) - \lambda_i^{NG}}{\sqrt{2}} \right) \right]}{\sum_{\bar{c}^{NG}} e^{-\frac{\left[S^{NG}\left(\bar{c}^{NG}\right)\right]^2}{2}}} \right\}^2 \tag{7.66}$$

[R. S. Orr and B. Veytsman, 2002] have proposed an efficient way to solve this problem where the set of weighting factors $\left\{\lambda_i^{NG}\right\}$ is efficiently calculated.

7.4.6 Generalized Majority Voting (GMV): Cyclostationary Solutions

In the previous chapter different majority vote solutions have been derived for the case that the weighting rule applied to each instantaneous set of component channels is constant over time. Furthermore, theory was presented to derive the weighting factors required to obtain a desired power distribution. However, as shown by [R. S. Orr and B. Veytsman, 2002], not always the targeted power allocation of the different services can be accomplished on the basis of an stationary approach and a cyclostationary solution is required then. In this case, the weighted majority voting rules exhibit time variation varying the weighting coefficients over time. The time variation is applied periodically over the largest available processing interval as shown by [R. S. Orr and B. Veytsman, 2002], being this interval normally the shortest data symbol of any of the component codes of the multiplexing. The cyclostationary power allocation can be further tuned by averaging different weighting schemes over time.

7.4.7 Generalized Majority Voting (GMV): Sub-Majority Voting

As shown by [R. S. Orr and B. Veytsman, 2002], the stationary solutions that result from applying the theory of previous chapters to the commanded powers of the majority voted signal present a quantized behaviour in the sense that the achieved gains do not automatically change when sufficiently small changes in the vote allocation are realized. Indeed, a break point only occurs when a slight change in the vote allocation permits some coalition of votes to dominate in a situation when they previously could not. In this sense, if an accurate allocation of the powers on the different signals is required, this can only be achieved on the basis of a cyclostationary solution as introduced in the previous lines.

Based on this idea, a simple way of decreasing the effective power allocated to a particular channel is to omit this code from a certain number of majority votes resulting in the so-called sub-majority voting. When this occurs, certain codes or signals do not participate in the sub-majority voting, changing thus the weightings of the different codes or channels over the time (thus a cyclostationary solution). It must be noted that while the weighting might change relatively often, it will however be constant for a relatively long period of time, in the order of the length of a bit. This can also be understood as time-multiplexing different signals according to a predefined scheme. In the following lines we analyze the implementation proposed by [G. L. Cangiani et al., 2002]. To illustrate the functioning of this cyclostationary solution, we take as an example the case when three signal codes are majority voted.

As shown by [G. L. Cangiani et al., 2002], when three signals are combined using Generalized Majority Voting (GMV) on a sub-majority voting basis, there are four possible elements to consider: the majority vote of the three chips and the three individual chips themselves. As it can be demonstrated, if one of the codes is smaller than the other two, the transmission of *solo* chips from that code will never result in an efficient solution. According to this, if the targeted power distribution is $\{G_1, G_2, G_3\}$, being the gains listed in non-decreasing order, the majority vote $\mathrm{Maj}\{c_1, c_2, c_3\}$ and the *solo* chips c_2 and c_3 should be transmitted the following fractions of time [R. S. Orr and B. Veytsman, 2002]:

$$\begin{aligned} t_{\mathrm{Maj}} &= \frac{2}{\sqrt{G_2}+\sqrt{G_3}} \\ t_{c_2} &= \frac{\sqrt{G_2}-1}{\sqrt{G_2}+\sqrt{G_3}} \\ t_{c_3} &= \frac{\sqrt{G_3}-1}{\sqrt{G_2}+\sqrt{G_3}} \end{aligned} \tag{7.67}$$

where the three time fractions sum to unity as one could expect. The resulting signal with interlacing of the majority vote of c_1, c_2 and c_3 and the *solo* chips c_2 and c_3 will be referred to as $\{\mathrm{Maj}(c_1, c_2, c_3), c_2, c_3\}$ in following chapters.

The interpretation of the time fractions is as follows. Let us assume that each data bit contains 100 chips and that the commanded power distribution is $\{G_1, G_2, G_3\} = \{1,4,9\}$. According to (7.67), the fraction of time values will be $\{t_{\text{Maj}}, t_{c_2}, t_{c_3}\} = \{2/5, 1/5, 2/5\}$. This means that out of the 100 chips of a bit, 40 of them will directly correspond to the highest gain code c_3. In the same manner other 20 will be devoted to the medium gain code c_2 and the final 40 chips are determined following the true majority vote of the chips of the three codes as described in chapters 7.4.4 and 7.4.5.

As shown by [G. L. Cangiani et al., 2002], the interest of this approach is that the combining losses are distributed uniformly over the three original signals in such a way that all the signals will suffer the same percentage loss of power at the end. The efficiency of the three-code multiplex is shown to adopt the following form:

$$\eta_{\text{MV}} = \frac{G_1 + G_2 + G_3}{\left(\sqrt{G_2} + \sqrt{G_3}\right)^2} \tag{7.68}$$

which can also be expressed as follows taking as power reference the signal with the lowest gain, namely c_1

$$\eta_{\text{MV}} = \frac{1 + \frac{G_2}{G_1} + \frac{G_3}{G_1}}{\left(\sqrt{\frac{G_2}{G_1}} + \sqrt{\frac{G_3}{G_1}}\right)^2} \tag{7.69}$$

Next figure depicts the efficiency of the majority vote as a function of the power ratios G_2/G_1 and G_3/G_1:

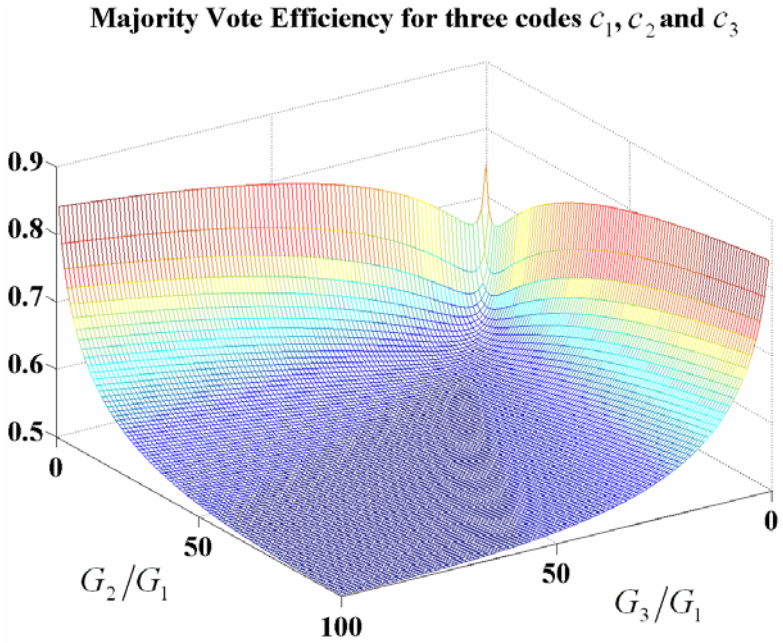

Figure 7.5. Majority Vote Efficiency for three codes c_1, c_2 and c_3

As we can recognize in the previous figure, when the power of one of the codes is much larger than that of either of the other two, the multiplex efficiency approaches 100 %. However, in the case that one code is much smaller that the other two, the efficiency deteriorates to approximately 50 %. If the three codes are of similar power levels, the efficiency is then close to 75 %. Although the previous values are only valid for the three-code multiplexing case, similar behaviours are found when the number of codes to multiplex increases. Indeed, majority voting presents the great inconvenience that in presence of a few codes monopolizing the total power, the efficiency reduces considerably.

In the previous three-code case, the solution for the time fraction of each individual code or majority voted code was unique. Indeed, the number of target parameters was two (since the three power ratios sum to unity there are only two free ratios) and the number of free variables was also two (since the three time fractions also sum to unity, only two are free). However this is not the case always. Indeed, when the number of signals to multiplex increases, so does also increase the number of possible solutions of the fractions of time that deliver the targeted power ratios. As an example, in the five-code case, the Generalized Majority Vote (GMV) signal could consist of the following signals [G. L. Cangiani et al., 2002]:

- One five majority-vote code
- $\binom{5}{3}$ three-way code combinations
- Four *solo* chips. It must be noted that the weakest code is not used as shown above
- $\binom{5}{4}$ four-way code combinations where one of the codes is weighted twice.

If we consider all the potential components of the GMV signal described above, there are a total of 20 elements to consider. Nevertheless, since the fraction times must sum to unity, the real number of free variables is actually 19. This number is however by far greater than the commanded powers (four in the case of five multiplexed signals) so that at the end the most efficient multiplex can only be discovered by a search technique of all potential combinations.

Last but not the least, it is important to mention that the cyclostationary solutions depicted in previous lines also fall in the general mathematical description given by (7.24). In fact, recalling the general equation of GMV, the majority voted code will adopt the following form

$$c_{\text{Maj}}(k) = \text{sign}\left(\sum_{i=1}^{N} \lambda_i(k) c_i(k) \right) \tag{7.70}$$

taking on the sub-majority vote factors $\lambda_i(k)$ values of 0 or 1 in this case. It is important to mention here that while in the approach of previous lines the weighting was achieved by averaging over the time, in chapter 7.4.5 this effect was mainly reached by selecting a proper weighting factor.

7.5 Hard Limiting

As we have already mentioned in previous chapters, during the design of the GPS M-Code different multiplexing options were considered to achieve a constant envelope [P.A. Dafesh et al., 2006]. Together with the majority voting that we saw above, hard-limiting of the C/A Code, P(Y) Code and M-Code signals was another considered option.

The hard-limiting approach basically forces the non-constant envelope of the sum of C/A Code and M-Code on one phase and P(Y) on the orthogonal phase (assuming we want to place the M-Code on the same phase as the C/A Code) to be constant by limiting the variation of the amplitude to its minimum value. The problem though is that the C/A Code and M-Code suffer from significant power losses and distortions. Indeed, the total efficiency of the hard-limiting modulation is roughly of 83 % as shown in [P.A. Dafesh et al., 2006], what corresponds to approximately 0.8 dB of overall combining losses. Moreover, as also described in this paper, the power split between the different signals is not easy to achieve.

7.6 Quadrature Product Sub-carrier Modulation

The quadrature product sub-carrier modulation (QPSM) enables the transmission of a quadrature multiplexed carrier modulation with one or more sub-carrier signals in the same constant envelope waveform as shown in [P.A. Dafesh, 1999] and [P.A. Dafesh et al., 2006]. Moreover, in its generalized form, QPSM is capable of applying sub-carrier modulation to already existing systems with Quadrature Phase Shift Keying (QPSK) or Minimum Shift Keying (MSK). In fact, one of its main advantages is that it can easily introduce new additional spread signals with excellent spectral isolation to those already in the band, using the same transmitter power amplifier. This is accomplished using multiple rate product codes that cause minimal interference to the existing ones. Finally, the power control and energy distribution between the carrier and sub-carrier signals can be accomplished selecting the desired modulation index.

In the next lines we show how the QPSM modulation can be represented mathematically. However, let us begin first with a simplified model. Let us assume a pair of quadrature components I_0 and Q_0 onto a carrier signal as follows,

$$s(t) = I_0(t)\cos(2\pi f_c t) - Q_0(t)\sin(2\pi f_c t) \tag{7.71}$$

where f_c denotes the carrier frequency. As we can clearly recognize, the magnitude is constant and can be expressed as follows [S. Butman and U. Timor, 1972]:

$$s(t) = A_0(t)\cos\left[2\pi f_c t + \phi(t)\right] \tag{7.72}$$

where

$$A_0(t) = \sqrt{I_0^2(t) + Q_0^2(t)} \tag{7.73}$$

and

$$\phi(t) = \arctan\left(\frac{Q_0(t)}{I_0(t)}\right) \tag{7.74}$$

From the equations above we can recognize that the resulting composite signal has a constant magnitude A_0 and does not depend on time as long as $I_0^2(t)$ and $Q_0^2(t)$ do not vary, what is always satisfied if I_0 and Q_0 are binary sequences.

Indeed this is the basic idea of the QPSM modulation. If we generalize now this principle, we can further add new signals modulating the phase part according to the following approach [S. Butman and U. Timor, 1972]:

$$s(t) = I_0(t)\cos[2\pi f_c t + \phi_s(t)] - Q_0(t)\sin[2\pi f_c t + \phi_s(t)] \tag{7.75}$$

with

$$\phi_s(t) = \sum_j m_j \, s_j(t)\varphi_j(t) \tag{7.76}$$

where

- m_j is the modulation index of the *j*-th signal. It determines the power allocation of each component,
- $s_j(t)$ is the *j*-th signal to modulate. It can be expressed as the product of the respective data message and the PRN code.
- and $\varphi_j(t)$ is the periodic sub-carrier, which may be any regular signal as for example sine, square or triangular, for example.

It is trivial to see that the envelope also remains constant in this modulated carrier signal. Moreover, the sub-carrier signal can be made up of many components being the limit only the phase noise that appears when the states of the constellation come too close to each other, as we will see later. Furthermore, the model is not only valid for binary sequences. In fact, the periodic sub-carrier could adopt any form in principle as long as it is regular. This is very important, because as we saw in chapter 4.6.1, the CBCS and CBOC signals are not binary.

The conventional sub-carrier modulation presents so-called cross-product inter-modulation components which can be considered as signal losses, resulting thus in a loss of efficiency. The conventional constant envelope Sub-carrier Modulation is used today on the Space Ground Link Subsystem (SGLS) and other terrestrial and space systems as shown by [P.A. Dafesh et al., 1999a], [Philco-Ford Corp., 1968], [J.K. Holmes, 1982] and [M. M. Shihabbi et al., 1994]. A generalization of the Sub-carrier modulation that has gained in interest over the past years is the Coherent Adaptive Sub-Carrier, which is presented in the following chapter.

Finally, it is important to note that the spectral separation of the different signals to modulate depends on the sub-carrier signal in particular allowing thus for spectral control as desired.

7.7 Coherent Adaptive Sub-Carrier Modulation (CASM) and Interplex

7.7.1 Origins of CASM and Interplex

The CASM Modulation is very similar to Interplex [S. Butman and U. Timor, 1972]. It receives also the name of Modified Tri-code Hexaphase modulation since it can be seen as a constant envelope modification of the Tri-code Hexaphase modulation described in chapter 7.3.1. CASM was first proposed in [M. Ananda et al., 1993] and later patented by [P.A. Dafesh, 2002] while Interplex was patented by [G.L. Cangiani, 2005].

In spite of CASM and Interplex being mathematically very similar, an important distinction must be made regarding the implementation. In fact, while Interplex uses exclusively additive methods to multiplex the signals, CASM employs a combination of angle modulation and additive methods. In the end, both of these techniques require the addition of an Inter-Modulation (IM) component that is necessary to maintain constant carrier magnitude [A. R. Pratt and J. I. R. Owen, 2007]. It is therefore important to keep in mind that while in the next pages we will refer indistinctly to CASM and Interplex since they are very similar from the mathematical point of view, they are realized and implemented in two very different ways, with two associated patents. In fact, CASM is described in [P.A. Dafesh, 2002], while Interplex was presented later by [G.L. Cangiani, 2005]. The slight differences between both implementations are also reflected in the performance during the amplification, where CASM is more subject to non desired effects.

CASM and Interplex are constant envelope modulations with added sub-carriers that do not distort the existing ones when the composite signal is passed through a high-power amplifier operating close to saturation. Moreover, they provide additional control on the power and the spectral separation of the different quadrature multiplexed signals through the use of different sub-carrier frequencies, a particular sub-carrier code rate and a sub-carrier modulation index. As we have emphasized in the previous chapters, this is especially interesting when a high number of signals must be transmitted on the same band. In addition, the modulation of orthogonal pairs of sub-carrier signals on the I and Q phases is also possible with reduced distortion and losses.

The CASM and Interplex implementations provide a means to multiplex all the signals that is equivalent to the spatially combined transmitter implementation that we described in chapter 7.3, where the Linear Modulation was described. In fact, CASM and Interplex have only slightly higher modulation losses than the Linear Modulation, but can work in saturation achieving thus in the end a superior efficiency for the same total required power. It is also important to keep in mind that although using a separate aperture would in principle provide

the cleanest transmission of all the signals, the simplification in the modulator design that using an unique constant envelope allows is more than offset by the impact on the satellite of adding an independent antenna and amplifier.

Finally, it is interesting to note that as stated in the CASM patent [P.A. Dafesh, 2002] the Inter-Modulation (IM) signals could be used as additional ranging or communication signals, transmitting thus additional information to that of the data channels. This is indeed the point where some people make another difference between CASM and Interplex. According to this, CASM would use the Inter-Modulation signals as another useful signal to transmit, while the Interplex implementation would allocate such a low power on this component that can be seen as lost power. Finally it is important to underline that the patent of [G.L. Cangiani, 2005] incorporates CASM but it is actually directed to a multi-beam/multi-antenna invention.

7.7.2 CASM, Interplex and Modified Tri-Code Hexaphase

CASM and Interplex can be seen as particular cases of the QPSM modulation or as an evolution of the conventional constant-envelope sub-carrier modulation that we saw in chapter 7.7. It is important to stress again that while Interplex uses exclusively additive methods to multiplex the signals, CASM employs a combination of angle modulation and additive methods. Moreover, CASM can utilize the cross-product inter-modulation (IM) terms as an additional useful signal. These terms can be considered as new ranging communication signals in some applications and not only as noise in the most general case. Nevertheless, for our navigation applications these terms will not be desired.

This modulation is extremely flexible and efficient, offering additionally the possibility to provide modes of operation with civilian and military signals together. This makes the approach of great interest. In addition, CASM and Interplex provide high efficiency with values greater than 90 % and inherent flexibility to fine tune the modulation architecture maintaining an ability to provide backward compatibility with current signals [G.L. Cangiani, 2005]. Also of great interest is that they may be generated using both square-wave and sine-wave sub-carriers although employing square-wave signals is normally preferred.

As shown in [A.R. Pratt and J.I.R. Owen, 2005] and [G.L. Cangiani, 2005], the CASM and Interplex techniques are able to support altogether more complex solutions than any of the techniques studied so far. In fact, if we work with equation (7.71) derived above for the general QPSM case, and assume that there is a single sub-carrier, the expression can be rewritten as follows:

$$s(t) = I_0(t)\cos\left[2\pi f_c t + m\, s_c(t)\varphi_s(t)\right] - Q_0(t)\sin\left[2\pi f_c t + m\, s_c(t)\varphi_s(t)\right] \qquad (7.77)$$

where m is the modulation index of the multiplex, $s_c(t)$ the modulating signal and $\varphi_s(t)$ the periodic sub-carrier. This expression can be further developed as follows:

$$s(t)=\begin{cases} I_0(t)\cos(2\pi f_c t)\cos[m\,s_c(t)\varphi_s(t)]-I_0(t)\sin[m\,s_c(t)\varphi_s(t)]\sin(2\pi f_c t) \\ -Q_0(t)\sin(2\pi f_c t)\cos[m\,s_c(t)\varphi_s(t)]-Q_0(t)\sin[m\,s_c(t)\varphi_s(t)]\cos(2\pi f_c t) \end{cases} \tag{7.78}$$

yielding:

$$s(t)=\begin{cases} \{I_0(t)\cos[m\,s_c(t)\varphi_s(t)]-Q_0(t)\sin[m\,s_c(t)\varphi_s(t)]\}\cos(2\pi f_c t) \\ -\{I_0(t)\sin[m\,s_c(t)\varphi_s(t)]+Q_0(t)\cos[m\,s_c(t)\varphi_s(t)]\}\sin(2\pi f_c t) \end{cases} \tag{7.79}$$

This can also be expressed in a simplified form as follows:

$$s(t)=I(t)\cos(2\pi f_c t)-Q(t)\sin(2\pi f_c t) \tag{7.80}$$

with

$$\begin{aligned} I(t)&=I_0(t)\cos[m\,s_c(t)\varphi_s(t)]-Q_0(t)\sin[m\,s_c(t)\varphi_s(t)] \\ Q(t)&=I_0(t)\sin[m\,s_c(t)\varphi_s(t)]+Q_0(t)\cos[m\,s_c(t)\varphi_s(t)] \end{aligned} \tag{7.81}$$

where the in-phase and quadrature components have been isolated. Moreover, if we carefully look at the equation above, we can recognize that the envelope is constant, as it could not be different since the single sub-carrier case is a particular case of the general QPSM modulation where we have shown that this is true.

In navigation the in-phase I_0 and quadrature Q_0 signals are modulated with data and pseudorandom codes as we saw in chapter 4. The signal modulated with data and code is called data channel while the other one has only code and is thus known as data-less or pilot channel. According to this, we have:

$$\begin{aligned} I_0(t)&=\sqrt{2P_I}\,d_I(t)c_I(t) \\ Q_0(t)&=\sqrt{2P_Q}\,d_Q(t)c_Q(t) \end{aligned} \tag{7.82}$$

In addition, the sub-carrier modulating signal $s_c(t)$ can be considered to contain data $d_s(t)$ and spreading code $c_s(t)$. Moreover, this signal is further modulated by the so-called data and code partitioning functions $\alpha_d(t)$ and $\beta_c(t)$ correspondingly [A.R. Pratt and J.I.R. Owen, 2005], depending on whether the term modulates the data or the code. We can write thus:

$$s_c(t)=[d_s(t)\alpha_d(t)][c_s(t)\beta_c(t)] \tag{7.83}$$

These two partitioning functions are of great importance since they control the type of QPSM modulation that we will have, as shown in [P.A. Dafesh, 1999 and P.A. Dafesh, 1999b]. If we assume, a square-wave sub-carrier we have then:

$$\varphi_s(t)=\text{sign}[\sin(2\pi f_s t)] \tag{7.84}$$

where we have to note that the square-wave works with a frequency f_s. In addition, if the signal $s_c(t)$ is binary, we can simplify for this particular case as follows:

$$\begin{aligned}\cos\left[m\,s_c(t)\varphi_s(t)\right] &= \cos(m)\\ \sin\left[m\,s_c(t)\varphi_s(t)\right] &= \sin(m)s_c(t)\,\mathrm{sign}\left[\sin(2\pi f_s t)\right]\end{aligned} \tag{7.85}$$

If we substitute now in (7.80) we have then:

$$s(t)=\begin{cases}\left[\sqrt{2P_I}\cos(m)d_I(t)c_I(t)-\sqrt{2P_Q}\sin(m)d_{QS}(t)c_{QS}(t)\,\mathrm{sign}\left[\sin(2\pi f_s t)\right]\right]\cos(2\pi f_c t)\\ -\left[\sqrt{2P_Q}\cos(m)d_Q(t)c_Q(t)-\sqrt{2P_I}\sin(m)d_{IS}(t)c_{IS}(t)\,\mathrm{sign}\left[\sin(2\pi f_s t)\right]\right]\sin(2\pi f_c t)\end{cases} \tag{7.86}$$

where

$$\begin{aligned}d_{IS}(t) &= d_I(t)d_S(t)\alpha_d(t)\\ d_{QS}(t) &= d_Q(t)d_S(t)\alpha_d(t)\\ c_{IS}(t) &= c_I(t)c_S(t)\beta_c(t)\\ c_{QS}(t) &= c_Q(t)c_S(t)\beta_c(t)\end{aligned} \tag{7.87}$$

As we have already commented above, depending on the values that the functions $\alpha_d(t)$ and $\beta_c(t)$ adopt, we will have the different QPSM options identified by [A.R. Pratt and J.I.R. Owen, 2005] and [P.A. Dafesh et al., 2006]. If we take a closer look at the equations, we can recognize the desired in-phase and quadrature components of $s(t)$ multiplied by $\cos(m)$ while the additional non-desired components added by the sub-carrier modulation appear multiplying $\sin(m)$. We have assumed from the very beginning that the data and code spreading codes are binary, and thus a useful multiplex option is shown to be the one that results from further assuming the following values for the partitioning functions:

$$\begin{aligned}\alpha_d(t) &= d_I(t)\\ \beta_c(t) &= c_I(t)\end{aligned} \tag{7.88}$$

These partitioning functions make use of the binary characteristics of the codes and data to separate them. In fact, substituting in (7.86), we obtain the following identities:

$$\begin{aligned}d_{IS}(t) &= d_S(t)\\ d_{QS}(t) &= d_I(t)d_Q(t)d_S(t)\\ c_{IS}(t) &= c_S(t)\\ c_{QS}(t) &= c_I(t)c_Q(t)c_S(t)\end{aligned} \tag{7.89}$$

Moreover, assuming that the codes $c_I(t)$ and $c_Q(t)$ are optimized to be orthogonal with each other, as it is the case, and that the I and Q data signals are also independent and thus ideally orthogonal, we can rename the terms $c_{QS}(t)$ and $d_{QS}(t)$ as $c_{S,\mathrm{IM}}(t)$ and $d_{S,\mathrm{IM}}(t)$ correspondingly, where the term *IM* denotes the Inter-Modulation signal. Finally, applying the changes described above, our multiplexed signal $s(t)$ can be expressed as follows:

$$s(t)=\begin{cases}\left[\sqrt{2P_I}\cos(m)d_I(t)c_I(t)-\sqrt{2P_Q}\sin(m)d_{S,IM}(t)c_{S,\mathrm{IM}}(t)\,\mathrm{sign}\left[\sin(2\pi f_s t)\right]\right]\cos(2\pi f_c t)\\ -\left[\sqrt{2P_Q}\cos(m)d_Q(t)c_Q(t)-\sqrt{2P_I}\sin(m)d_S(t)c_S(t)\,\mathrm{sign}\left[\sin(2\pi f_s t)\right]\right]\sin(2\pi f_c t)\end{cases} \tag{7.90}$$

It is interesting to note from the expression above that the original quadrature product components are reduced by a factor cos(*m*). We recall that these quadrature product components could correspond to two already existing orthogonal signals as could be the C/A Code and the P(Y) Code in GPS (CASM implementation) before the M-Code was introduced. But also Galileo with Interplex follows a similar pattern with the OS signals in-phase and the PRS in quadrature. In addition, we can see a new sub-carrier component with a BOC modulation and data $d_S(t)$ and code $c_S(t)$. Finally, we can equally recognize a fourth component with the codes and data signals $c_{S,\mathrm{IM}}(t)$ and $d_{S,\mathrm{IM}}(t)$. Since this last signal does not transmit any useful information in the general case as it is modulated by the cross-correlation of two codes that are ideally orthogonal and two data streams that in an ideal case are also independent, this term is further called inter-modulation component. Nonetheless, it must be noted that if an appropriate structure were found for the 3 spreading codes $c_I(t)$, $c_Q(t)$ and $c_S(t)$, this could be used as a fourth channel to transmit an additional signal.

In summary, CASM and Interplex offer a QPSK signal and an additional BOC, all of them forming a constant envelope multiplexed signal. The phase constellation diagram is given by the following 8 points:

$$\theta(m) = \pm\left(\pi \pm m \pm \arctan\left(\sqrt{\frac{P_Q}{P_I}}\right)\right) \tag{7.91}$$

and the power of the different channels is thus:

Table 7.4. Power Distribution of the CASM and Interplex multiplexing

I Channel	$P_I \cos^2(m)$
Q Channel	$P_Q \cos^2(m)$
S Channel	$P_I \sin^2(m)$
IM Channel	$P_Q \sin^2(m)$

We can further analyze the equations if we recall again the equation that we derived above:

$$s(t) = \begin{cases} \left[\sqrt{2P_I}\cos(m)d_I(t)c_I(t) - \sqrt{2P_Q}\sin(m)d_{QS}(t)c_{QS}(t)\mathrm{sign}\left[\sin(2\pi f_s t)\right]\right]\cos(2\pi f_c t) \\ -\left[\sqrt{2P_Q}\cos(m)d_Q(t)c_Q(t) - \sqrt{2P_I}\sin(m)d_{IS}(t)c_{IS}(t)\mathrm{sign}\left[\sin(2\pi f_s t)\right]\right]\sin(2\pi f_c t) \end{cases} \tag{7.92}$$

where

$$\begin{aligned} d_{IS}(t) &= d_I(t)d_S(t)\alpha_d(t) \\ d_{QS}(t) &= d_Q(t)d_S(t)\alpha_d(t) \\ c_{IS}(t) &= c_I(t)c_S(t)\beta_c(t) \\ c_{QS}(t) &= c_Q(t)c_S(t)\beta_c(t) \end{aligned} \tag{7.93}$$

We can further project the amplitudes of each of the signals on the I and Q axes, such that:

$$\begin{aligned} \sqrt{2P_I} &= \sqrt{2P}\cos(\beta) \\ \sqrt{2P_Q} &= \sqrt{2P}\sin(\beta) \end{aligned} \tag{7.94}$$

where P is the total power of the signal and β an additional variable to link the I and Q powers, P_I and P_Q respectively. Furthermore, we rename the variables β and m as follows:

$$\begin{aligned} \beta_2 &= \beta - \frac{\pi}{2} \Rightarrow \begin{cases} \sin(\beta) = -\cos(\beta_2) \\ \cos(\beta) = \sin(\beta_2) \end{cases} \\ \beta_3 &= m \end{aligned} \tag{7.95}$$

and redefine the signals as follows:

$$\begin{aligned} s_1(t) &= d_Q(t) c_Q(t) \\ s_2(t) &= d_I(t)\, c_I(t) \\ s_3(t) &= d_{QS}(t)\, c_{QS}(t) = d_Q(t) d_S(t) \alpha_d(t) c_Q(t) c_S(t) \beta_c(t) \end{aligned} \tag{7.96}$$

We can show that then:

$$s_2(t) s_3(t) = d_S(t) \alpha_d(t) c_S(t) \beta_c(t) \tag{7.97}$$

yielding thus,

$$d_{IS}(t) c_{IS}(t) = d_I(t) d_S(t) \alpha_d(t) c_I(t) c_S(t) \beta_c(t) \tag{7.98}$$

which can be further simplified to:

$$d_{IS}(t) c_{IS}(t) = [d_I(t) c_I(t)][d_S(t) \alpha_d(t) c_S(t) \beta_c(t)] = s_1(t) s_2(t) s_3(t) \tag{7.99}$$

If we introduce these expressions in (7.92), we have then:

$$s(t) = \begin{cases} \left[\sqrt{2P}\sin(\beta_2)\cos(\beta_3) s_2(t) + \sqrt{2P}\cos(\beta_2)\sin(\beta_3) s_3(t)\right]\cos(2\pi f_c t) + \\ + \left[\sqrt{2P}\cos(\beta_2)\cos(\beta_3) s_1(t) - \sqrt{2P}\sin(\beta_2)\sin(\beta_3) s_1(t) s_2(t) s_3(t)\right]\sin(2\pi f_c t) \end{cases} \tag{7.100}$$

which coincides with the form derived by [E. Rebeyrol et al., 2005]. In fact, it is not difficult to show that after some math this expression can be further simplified to:

$$s(t) = \sqrt{2P}\cos\left(2\pi f_c t - \frac{\pi}{2} s_1(t) + \beta_2 s_1(t) s_2(t) + \beta_3 s_1(t) s_3(t)\right) \tag{7.101}$$

where the factor multiplying the signal $s_1(t)$, namely β_1, is equal to $-\pi/2$ so that this signal is in quadrature with the other two we want to modulate, namely $s_2(t)$ and $s_3(t)$. Moreover, the normalized powers of the different signals can be expressed as follows:

$$\begin{aligned} P_1(\beta_2, \beta_3) &= P\cos^2(\beta_2)\cos^2(\beta_3) \\ P_2(\beta_2, \beta_3) &= P\sin^2(\beta_2)\cos^2(\beta_3) \\ P_3(\beta_2, \beta_3) &= P\cos^2(\beta_2)\sin^2(\beta_3) \\ P_4(\beta_2, \beta_3) &= P\sin^2(\beta_2)\sin^2(\beta_3) \end{aligned} \tag{7.102}$$

According to this, the modulated signal could be generated following the scheme shown in [G.L. Cangiani and J.A. Rajan, 2002]:

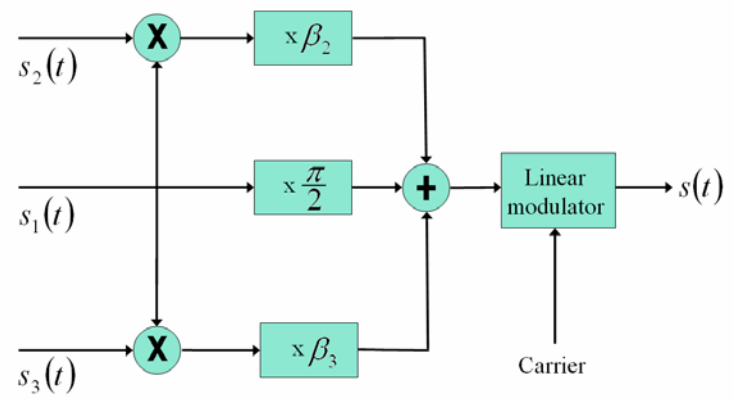

Figure 7.6. Interplex schematic generation

The generation scheme presented above is conceptually useful to derive the theoretical expressions of this chapter but presents a series of limitations in a real implementation as identified by [G. L. Cangiani et al., 2002].

While common practice in the design of the architecture dictates generating the entire composite signal at baseband first to further up-convert it later to the desired carrier frequency, for the frequencies of interest in GNSS (microwave systems) this is a problem. In fact, the baseband frequency is too low to avoid harmonic and intermodulation interference with the desired output during the up-conversion. Moreover, the time jitter of the Digital-to-Analog Converters (DAC) adds phase noise onto the desired output signal and the up-conversion process requires band-pass filters at each mixing stage that destroy the original constant envelope of the signal.

A solution to this problem is the implementation proposed by [G. L. Cangiani et al., 2002] where the Interplex signal at the desired carrier frequency is generated as depicted in the following figure.

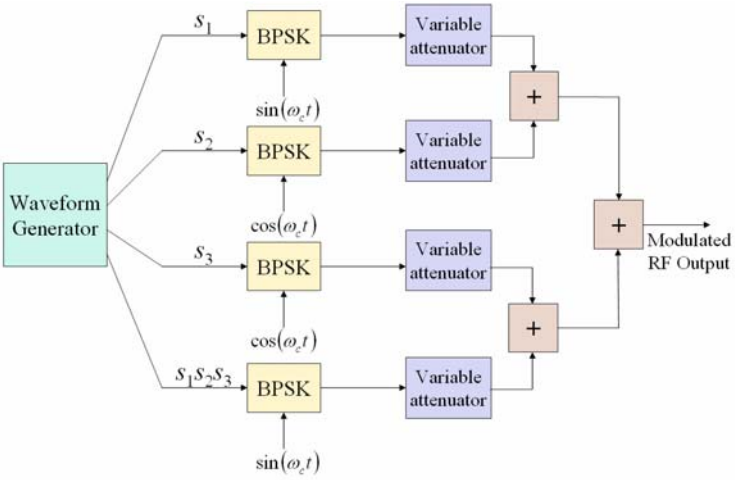

Figure 7.7. Alternative Interplex scheme proposed by [G. L. Cangiani et al., 2002]

As an example, the variation of the signal power of s_1 as a function of the two interplex modulation angles β_2 and β_3 is shown in the following figure:

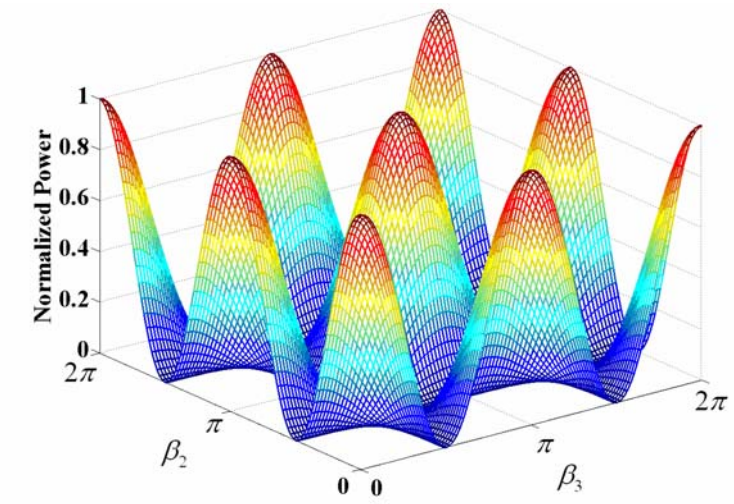

Figure 7.8. Variation of the P_1 power of the signal s_1 as a function of β_2 and β_3

As we can see, the optimum combination of β_2 and β_3 depends on how much power we want to place on each of the desired signals. In fact, the principle is to minimize the amount of power of the IM channel since this does not bring any information.

It must be noted that the equations derived above do not make use of the data and code partitioning functions. We express now the equivalent form for baseband as follows:

$$s_{\mathrm{BB}}(t)=\sqrt{P_2}\,s_2(t)+\sqrt{P_3}\,s_3(t)+j\left[\sqrt{P_1}\,s_1(t)-\sqrt{\frac{P_2\,P_3}{P_1}}\,s_1(t)s_2(t)s_3(t)\right] \tag{7.103}$$

As we can recognize, the equations derived above are based on the assumption of binary data and spreading codes, and a square-wave sub-carrier signal (BOC). Accordingly, the results are not valid for the most general case but can be easily generalized to other types of signal waveforms at the extent of some extra terms in the final expressions. Indeed, as we will show next, adapting this multiplexing to include the CBOC implementation of the MBOC signal is trivial. Furthermore, the derived expressions are only valid for infinite bandwidth, being thus the real power split among all the signals slightly different after filtering.

If we further normalize (7.103) to have unit power, the previous expression adopts the following form:

$$s_{\mathrm{BB}}(t)=\frac{\sqrt{P_2}\,s_2(t)+\sqrt{P_3}\,s_3(t)+j\left[\sqrt{P_1}\,s_1(t)-\sqrt{\frac{P_2\,P_3}{P_1}}\,s_1(t)s_2(t)s_3(t)\right]}{\sqrt{P_1+P_2+P_3+\frac{P_2\,P_3}{P_1}}} \tag{7.104}$$

which can be further simplified as follows:

$$s_{\mathrm{BB}}(t)=\frac{\sqrt{P_1P_2}\,s_2(t)+\sqrt{P_1P_3}\,s_3(t)+j\left[P_1\,s_1(t)-\sqrt{P_2\,P_3}\,s_1(t)s_2(t)s_3(t)\right]}{\sqrt{P_1^2+P_1P_2+P_1P_3+P_2\,P_3}} \tag{7.105}$$

For simplicity we refer next all the powers to P_3. In fact, to define uniquely the multiplex with three signals, two power ratios are necessary if the powers are referred to a third signal and the total power sums to unity. According to this, the three-signal interplex is defined by:

$$\begin{aligned} I &= \frac{\sqrt{P_1 P_2}\, s_2(t) + \sqrt{P_1}\, s_3(t)}{\sqrt{P_1^2 + P_1 P_2 + P_1 + P_2}} = \frac{\sqrt{P_1 P_2}\, s_2(t) + \sqrt{P_1}\, s_3(t)}{\sqrt{(1+P_1)(P_1+P_2)}} \\ Q &= \frac{P_1\, s_1(t) - \sqrt{P_2}\, s_1(t) s_2(t) s_3(t)}{\sqrt{P_1^2 + P_1 P_2 + P_1 + P_2}} = \frac{P_1\, s_1(t) - \sqrt{P_2}\, s_1(t) s_2(t) s_3(t)}{\sqrt{(1+P_1)(P_1+P_2)}} \end{aligned} \tag{7.106}$$

being the efficiency of the interplex modulation as follows:

$$\eta_{\text{Interplex}} = \frac{P_1^2 + P_1 + P_1 P_2}{(1+P_1)(P_1+P_2)} = \frac{P_1(1+P_1+P_2)}{(1+P_1)(P_1+P_2)} \tag{7.107}$$

This is the percentage of power with respect to the total transmitted power that is employed for the useful signal.

Finally, it is important to mention that additional signals can be incorporated into the CASM and Interplex schemes because the desirable constant envelope characteristic remains unchanged independent from the shape of the sub-carrier modulation. The drawback is the extra complexity that is needed to separate spectrally the additional signals, as pointed out in [A.R. Pratt and J.I.R. Owen, 2005] and developed in [T. Fan et al, 2005]. A particular realization with non-binary sub-carriers is discussed in the next chapter, where a sinewave sub-carrier is employed instead of the usual square-wave version.

7.7.3 Single Sinewave Sub-carrier CASM

The Single Sinewave Sub-carrier version was originally proposed as a constant-envelope Multi-Mode Spread-Spectrum Sub-carrier Modulation (MMSSS) for GPS [P.A. Dafesh et al., 1999a]. This sub-carrier is shown to adopt the following form:

$$\varphi_s(t) = \sin(2\pi f_s t) \tag{7.108}$$

If we introduce now the sine-wave sub-carrier in equations (7.75) and (7.76) the multiplexed signal is shown to approximate to the following [P.A. Dafesh et al., 1999a]:

$$\begin{aligned} & s(t) \approx \\ & \approx \left[\begin{array}{l} \sqrt{2P_I}\, J_0(m) d_I(t) c_I(t) - \\ -\sqrt{2P_Q}\, 2J_1(m) d_Q(t) c_Q(t) d_s(t) c_s(t) \alpha_d(t) \beta_c(t) \sin(2\pi f_s t) \end{array} \right] \cos(2\pi f_c t) - \\ & - \left[\begin{array}{l} \sqrt{2P_Q}\, J_0(m) d_Q(t) c_Q(t) + \\ +\sqrt{2P_I}\, 2J_1(m) d_I(t) c_I(t) d_s(t) c_s(t) \alpha_d(t) \beta_c(t) \sin(2\pi f_s t) \end{array} \right] \sin(2\pi f_c t) + \\ & + \sqrt{2P_I}\, 2J_2(m) d_I(t) c_I(t) \cos(4\pi f_s t) \cos(2\pi f_c t) - \\ & - \sqrt{2P_Q}\, 2J_2(m) d_Q(t) c_Q(t) \cos(4\pi f_s t) \sin(2\pi f_c t) \end{aligned} \tag{7.109}$$

where $J_n(m)$ is the Bessel function of order n and m the modulation index of the signal. As we can recognize, the previous expression is only approximate as an infinite number of carrier harmonics (J_0, J_2, J_4,…) and sub-carrier harmonics (J_1, J_3, J_5, …) would be required to define the multiplexed signal completely. However, only the first carrier and sub-carrier harmonics need to be considered if $m \le \pi/2$. This will be assumed in the following lines. Furthermore, for this range of modulation index the sinewave CASM approach presents a high efficiency of approximately 95 % as shown in [P.A. Dafesh et al., 1999a].

We can further develop the previous expression if we realize the same transformation as in (7.93). In fact, after some math (7.109) is shown to simplify to [P.A. Dafesh, 1999]:

$$\begin{aligned} s(t) \approx & \begin{bmatrix} \sqrt{2P_I}\,J_0(m)\,d_I(t)\,c_I(t) - \\ -\sqrt{2P_Q}\,2J_1(m)\,d_{IS}(t)\,c_{QS}(t)\sin(2\pi f_s t) \end{bmatrix} \cos(2\pi f_c t) - \\ & - \begin{bmatrix} \sqrt{2P_Q}\,J_0(m)\,d_Q(t)\,c_Q(t) + \\ +\sqrt{2P_I}\,2J_1(m)\,d_{QS}(t)\,c_{IS}(t)\sin(2\pi f_s t) \end{bmatrix} \sin(2\pi f_c t) \end{aligned} \tag{7.110}$$

It is interesting to note that by appropriately selecting the sub-carrier and code partitioning functions we may employ $c_{IS}(t)$ and $c_{QS}(t)$ as coherently military acquisition and tracking signals as suggested by [P.A. Dafesh et al., 1999a]. Moreover, if different partitioning functions are selected, the I/Q phasing of these military signals can be reversed.

7.7.4 Generalization to any number of Sub-carriers

In the previous chapter, general expressions were derived for CASM and Interplex with only three ranging signals. However, they can be easily extended to any number n of signals in the most general case. Furthermore, the sub-carriers do not necessarily have to be square-wave but could also be sinewaves as shown by [P.A. Dafesh et al., 1999a]. In fact, if we recall the general expression:

$$s(t) = \sqrt{2P_T}\cos\left[2\pi f_c t + \phi_s(t)\right] \tag{7.111}$$

with

$$\phi_s(t) = \sum_{i=1}^{n} m_i\, d_i(t)\,\alpha_d^i(t)\,\beta_c^i(t)\,s_j(t)\,\varphi_i(t) \tag{7.112}$$

we can see that the number of sub-carriers n that can be multiplexed is in principle unlimited. As we can recognize from the previous expression,

- m_i indicates the modulation index of the i-th sub-carrier,
- $d_i(t)$ is the data sequence of the i-th multiplexed sub-carrier,
- $\alpha_d^i(t)$ is the data partition function of the i-th multiplexed sub-carrier,
- $\beta_c^i(t)$ is the code partition function of the i-th multiplexed sub-carrier and
- $\varphi_i(t)$ is the i-th sub-carrier.

After appropriate selection of the data and code partition functions, (7.112) can be further modified and expressed as follows for the case of square-wave sub-carriers:

$$\phi_s(t) = m_1 s_1(t) + \sum_{i=2}^{n} m_i\, s_1(t) s_i(t) \tag{7.113}$$

with

$$s_i(t) = c_i(t)\, d_i(t) \varphi_i(t) \tag{7.114}$$

being

- $\varphi_i(t)$ the square-wave sub-carrier,
- $d_i(t)$ is the data message of the i-th signal to multiplex, and
- $c_i(t)$ is the spreading code of the i-th multiplexed signal.

As we can recognize, this is the same notation that we followed in (7.101) for the particular case of only three signals to multiplex.

Once we have described CASM and Interplex, it is the right moment to talk a little bit more on the Galileo multiplex needs. Indeed, sometimes we are not free to choose how we want our system to be and in the case of Galileo there were clear requirements and constraints on how the signals should interact with each other. As we will see, this determines already to a high degree the multiplex scheme to choose.

To conclude, it is important to mention that the names Interplex and CASM are ambiguously used to define a similar idea. Nonetheless, we can find slight differentiations in addition to the implementation aspects we have mentioned. In [E. Rebeyrol et al., 2006], for example, we can see CASM defined as a three components Interplex modulation with a particular and optimal choice of the modulation indexes. However, nothing is said about what signals are in phase or in quadrature. In fact, although [P.A. Dafesh et al., 1999] and [P.A. Dafesh et al., 2000] proposed to have the C/A Code and M-Code in phase with the P(Y) Code in quadrature, other works have explored alternative configurations [G.H. Wang et al., 2004]. The same applies to Galileo as we see next.

7.7.5 Galileo Multiplex Needs

As shown in [A.R. Pratt and J.I.R. Owen, 2005], Galileo has to use an additive multiplexing technique that produces a constant envelope by means of an inter-modulation signal. We have shown that this is possible with the Interplex or CASM techniques provided that the modulating signals remain binary. Moreover, as we saw in chapter 2.4.1, the Galileo system aims at having the following signals on E1, for example:

- E1 OS data signal,
- E1 OS pilot signal,
- E1 Public Regulated Service (PRS), and
- an Inter-Modulation (IM) signal.

Interplex fulfils these requirements and it is in fact the multiplex baseline for the Galileo signals transmitted on E1 as shown in [G.W. Hein et al., 2002] and [G.H. Wang et al., 2004].

The Interplex modulation consists of one In-phase and one quadrature signal. In the particular case of Galileo:

- The In-phase signal is the linear sum of the two Open Signal components, OS_D and OS_P where D stands for data and P for pilot.
- The quadrature signal carries the Public Regulated Service (PRS) signal and an additional signal, named inter-modulation product, whose role is to provide the modulation with a constant envelope.

Moreover, according to [Galileo SIS ICD, 2008], the power split of the OS_D, OS_P and PRS must be 25 %, 25 % and 50 % respectively.

As we have seen in chapter 4.6.1, the mathematical expression of the interplex modulation for the old BOC(1,1) baseline of 2004, it is shown to be :

$$s(t) = A_0\left[\frac{c_D(t)+c_P(t)}{2}\cos\theta_0\, s_{\mathrm{BOC(1,1)}}(t) + j\left(\frac{1+\sin\theta_0}{2}\right)s_{\mathrm{PRS}}(t) + s_{\mathrm{IM}}(t)\right] \tag{7.115}$$

$$s_{\mathrm{IM}}(t) = -j\,c_D(t)\,c_P(t)\left(\frac{\sin\theta_0 - 1}{2}\right)s_{\mathrm{PRS}}(t) \tag{7.116}$$

where,

- A_0 is the amplitude of the modulation envelope,
- θ_0 is the angle of four of the six phase states of the 6-PSK modulation. It corresponds to half the angular distance between 2 states across the real axis,
- $s_{\mathrm{BOC(1,1)}}(t)$ represents the BOC(1,1) modulation,
- $s_{\mathrm{PRS}}(t)$ is the PRS $\mathrm{BOC_{cos}}(15,2.5)$ modulation,
- $s_{\mathrm{IM}}(t)$ is the Inter-Modulation product, used to keep the amplitude constant, and
- $c_D(t)$ and $c_P(t)$ are the codes for the E1 OS data and pilot channels respectively.

The baseband equations above can also be expressed as follows for the particular case of the Galileo signals on E1:

$$s_{E1}(t) = \alpha\left[s_{E1_D^{\mathrm{OS}}}(t) - s_{E1_P^{\mathrm{OS}}}(t)\right]\cos(2\pi f_{E1}t) - \left[\beta\, s_{E1_{\mathrm{PRS}}}(t) - \gamma\, s_{E1_{\mathrm{IM}}}(t)\right]\sin(2\pi f_{E1}t) \tag{7.117}$$

being

$$\begin{aligned}
s_{E1_D^{\mathrm{OS}}}(t) &= d_{\mathrm{OS}}^{E1}(t)\,c_D^{E1_{\mathrm{OS}}}(t)\,s_D^{E1_{\mathrm{OS}}}(t)\\
s_{E1_P^{\mathrm{OS}}}(t) &= c_P^{E1_{\mathrm{OS}}}(t)\,s_P^{E1_{\mathrm{OS}}}(t)\\
s_{E1_{\mathrm{PRS}}}(t) &= d_{\mathrm{PRS}}^{E1}(t)\,c_{\mathrm{PRS}}^{E1}(t)\,s_{\mathrm{PRS}}^{E1}(t)\\
s_{E1_{\mathrm{IM}}}(t) &= s_{E1_D^{\mathrm{OS}}}(t)\,s_{E1_P^{\mathrm{OS}}}(t)\,s_{E1_{\mathrm{PRS}}}(t)
\end{aligned} \tag{7.118}$$

Here the coefficients α, β and γ play the same role as the phase angles θ_0 and the amplitude A_0 in the equations of previous chapters. Moreover, D stands for data, P for pilot, $d(t)$ is the data signal, $c(t)$ is the PRN code and $s(t)$ is the modulated signal. As it can be shown, the resulting modulation is a 6-PSK or Hexaphase modulation with constant envelope, also known as Modified Hexaphase for this reason. Next figure shows the phase plot:

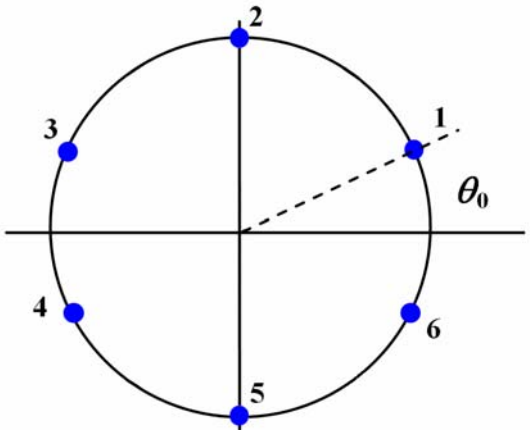

Figure 7.9. Modified Hexaphase modulation with BOC(1,1)

where the angle θ_0 is chosen so as to provide the appropriate power ratio as described in the Appendix J. In our case, in order to have the power ratios given in [Galileo SIS ICD, 2008], the value must be of:

$$\theta_0 = 0.1082\,\pi = 0.3399 \text{ radians} \tag{7.119}$$

To have a better understanding on the location of the phase states, we show next the different probabilities of the constellation phase points by means of the following truth table. It must be noted that the amplitudes were not corrected to account for the loss of efficiency that results from the inter-modulation signal IM.

Table 7.5. Phase states of the Interplex modulation as a function of code and data inputs

{E1 OS_D, E1 OS_P, PRS}	E1 OS_D+E1 OS_P	Phase state	Inter-Modulation
+1,+1,+2	+2	1	-0.5
+1,-1,+2	0	2	+0.5
-1,-1,+2	-2	3	-0.5
-1,+1,+2	0	2	+0.5
+1,+1,-2	+2	6	+0.5
+1,-1,-2	0	5	-0.5
-1,-1,-2	-2	4	+0.5
-1,+1,-2	0	5	-0.5

We can graphically see this also as follows:

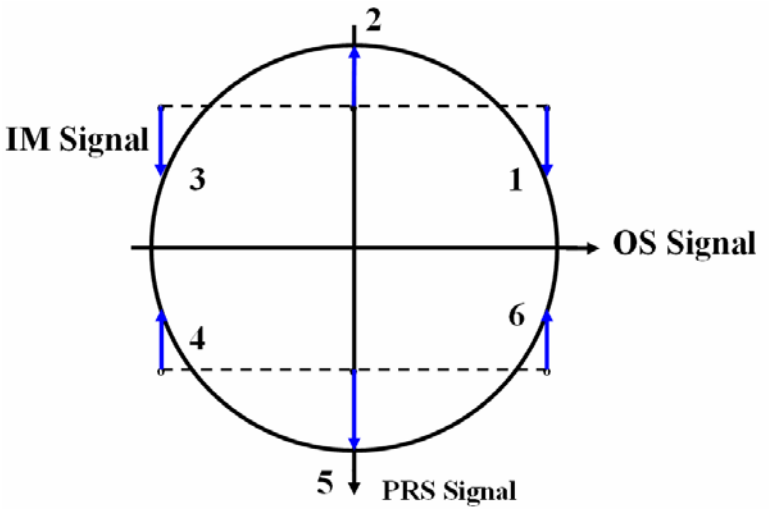

Figure 7.10. Modified Hexaphase modulation

As we can see from the figure and table above, states 2 and 5 occur each with a probability of 25 %. As a result, the OS channel transmits no signal 50 % of the time. Moreover, binary codes were assumed with values {+1,-1} of equal probability. In addition, the PRS has 3 dB more power than the OS signals in consonance with [Galileo SIS ICD, 2008]. As we can see, the mission of the Inter-Modulation signal IM is to bring the phase points back to the circle as depicted by the arrows of the figure above.

The final power distribution inside the modulation takes thus the following values for the baseline of 2004 (see chapter 3.5 for more details):

Table 7.6. Power distribution of Interplex with OS and PRS

BOC(1,1)	OS_A	OS_B	PRS	IM
Relative Power	2/9	2/9	4/9	1/9
	-6.53 dB	-6.53 dB	-3.53 dB	-9.54 dB

As we can observe, the IM term has a power level of -9.54 dB with respect to the total transmitted power and 6 dB below the PRS. It is important to note that in a real application the values derived above should be further compensated to account for the different losses of every signal through the satellite filter.

Moreover, the amplitude of the envelope, A_0, must be modified to compensate the loss of efficiency of the modulation due to the presence of the Inter-Modulation product. In the present case, A_0 is set to $\sqrt{9/8} = 1.0607$. After applying the amplitude compensation, the power distribution adopts the following form:

Table 7.7. Compensated power distribution to match the baseline values

BOC(1,1)	OS_A	OS_B	PRS	IM
Relative Power	1/4	1/4	1/2	1/8
	-6 dB	-6 dB	-3 dB	-9.04 dB

Finally, it is interesting to note that the power split between the OS and PRS channels can be easily modified playing with the parameters A_0 and θ_0 . In terms of phase states, the effect would be a movement of the phase angle θ_0 within the circle of the constellation.

7.7.6 Power Spectral Density of CASM and Interplex

Although CASM and Interplex correspond to two different implementations, the simplified mathematical description is very similar, being only the Inter-Modulation components slightly different. As we have seen in the lines above, the baseband expression can be expressed as:

$$s_{\mathrm{BB}}(t) = \sqrt{P_2}\, s_2(t) + \sqrt{P_3}\, s_3(t) + j\left[\sqrt{P_1} s_1(t) - \sqrt{P_{\mathrm{IM}}}\, s_1(t) s_2(t) s_3(t)\right] \tag{7.120}$$

where

$$P_{\mathrm{IM}} = \frac{P_2 P_3}{P_1} \tag{7.121}$$

Moreover, as shown in [E. Rebeyrol et al., 2006],

$$s_{\mathrm{BB}}(t) = \mathrm{Re}\left\{ s_{\mathrm{BB}}(t) \mathrm{e}^{j 2\pi f_c t} \right\} \tag{7.122}$$

such that:

$$\Re_s(\tau) = \frac{1}{2} \Re_{s_{\mathrm{BB}}}(\tau) \cos(2\pi f_c \tau) \tag{7.123}$$

As shown in Appendix I, the autocorrelation of the baseband signal adopts the form:

$$\Re_{s_{\mathrm{BB}}}(\tau) = E\left\{ s_{\mathrm{BB}}(t)\, s_{\mathrm{BB}}(t-\tau) \right\} \tag{7.124}$$

If we further assume ideal codes, the expression for the autocorrelation function will be:

$$\Re_{s_{\mathrm{BB}}}(\tau) = P_1 \Re_{s_1}(\tau) + P_2 \Re_{s_2}(\tau) + P_3 \Re_{s_3}(\tau) + P_{\mathrm{IM}} \Re_{s_{\mathrm{IM}}}(\tau) \tag{7.125}$$

In addition, since the power spectral density is the Fourier Transform of the autocorrelation function, we have:

$$G_{s_{\mathrm{BB}}}(f) = FT\left\{ \Re_{s_{\mathrm{BB}}}(\tau) \right\} = P_1 G_{s_1}(f) + P_2 G_{s_2}(f) + P_3 G_{s_3}(f) + P_{\mathrm{IM}} G_{s_{\mathrm{IM}}}(f) \tag{7.126}$$

Equally, for the whole signal including carrier frequency, we would have:

$$G_{\mathrm{Interplex}}(f) = \frac{1}{4} G_{s_{\mathrm{BB}}}(f - f_c) + \frac{1}{4} G_{s_{\mathrm{BB}}}(f + f_c) \tag{7.127}$$

7.7.7 CASM Modulation in GPS

As we saw in chapter 7.7, if we apply CASM to all the GPS signals except for GPS L1C, the Power Spectral Density is shown to adopt the following form:

$$G_{s_{\mathrm{BB}}}^{\mathrm{GPS}}(f) = P_{\mathrm{C/A}}\, G_{\mathrm{C/A}}(f) + P_{\mathrm{P(Y)}}\, G_{\mathrm{P(Y)}}(f) + P_{\mathrm{M-Code}}\, G_{\mathrm{M-Code}}(f) + P_{\mathrm{IM}}\, G_{\mathrm{IM}}(f) \qquad (7.128)$$

where the power spectral densities of the C/A Code, P(Y) Code and M-Code were already shown in chapter 4.3.2. In the case of the IM component, the signal presents the spectrum of a BOC(10,10) modulation. In fact, as we have already seen, the Inter-Modulation signal is formed by multiplying the three signals we want to modulate. In this case, $s_1(t)$ is BPSK(1), $s_2(t)$ is BPSK(10) and $s_3(t)$ is BOC(10,5). Since the three signals are binary, the product of them will be a sine or cosine-phased $\mathrm{BOC}(f_s, f_c)$ modulation with f_s the highest offset carrier frequency of the three and with code rate f_c the highest of the three. In this particular case the chipping rate of the P(Y) code and the offset carrier frequency of the M-Code.

Moreover, as presented in [P.A. Dafesh et al., 2000], the GPS CASM modulation defines its angle β_2 as follows:

$$\begin{aligned} \cos(\beta_2) &= \sqrt{\frac{P_Q}{P}} \\ \sin(\beta_2) &= \sqrt{\frac{P_I}{P}} \end{aligned} \qquad (7.129)$$

being thus the only variable to play with the angle β_3 which is renamed as m in this particular case. Consequently, in line with the derivations of chapter 7.7.2, the power of each particular signal depends only on m:

$$\begin{aligned} P_1(m) &= P_Q \cos^2(m) \\ P_2(m) &= P_I \cos^2(m) \\ P_3(m) &= P_Q \sin^2(m) \\ P_{IM}(m) &= P_I \sin^2(m) \end{aligned} \qquad (7.130)$$

so that

$$P = P_1 + P_2 + P_3 + P_{IM} = P_I + P_Q \qquad (7.131)$$

As a conclusion, the CASM GPS signal can thus be expressed as follows:

$$s(t) = \sqrt{2}\left\{ \begin{aligned} &\left[\sqrt{P_I}\cos(m)s_2(t) + \sqrt{P_Q}\sin(m)s_3(t)\right]\cos(2\pi f_c t) - \\ &-\left[\sqrt{P_Q}\cos(m)s_1(t) - \sqrt{P_I}\sin(m)s_1(t)s_2(t)s_3(t)\right]\sin(2\pi f_c t) \end{aligned} \right\} \qquad (7.132)$$

As we can see, the desired powers and relationships between the different signals, can be well adjusted by appropriately selecting the values of β_2 and m. The corresponding diagram of the modulation constellation is shown in the following figure from [E. Rebeyrol et al., 2006].

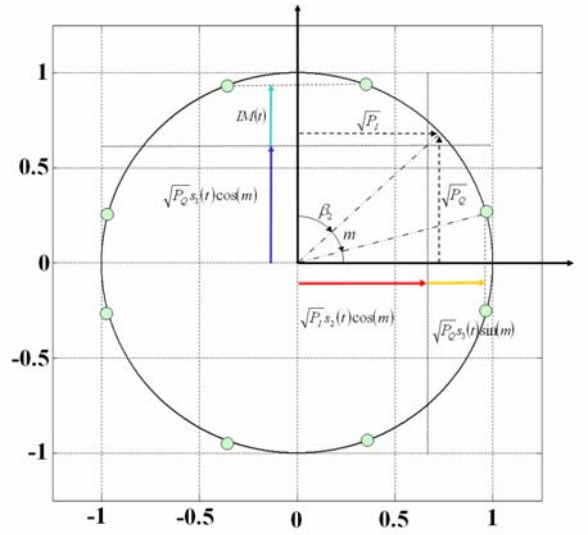

Figure 7.11. GPS CASM modulation constellation

As we can recognize from equation (7.132), the phase rotation of the sub-carrier signal onto the carrier can be implemented in very different ways. Apart from implementations of proprietary nature, two main realizations of the CASM modulation have been identified for GPS as identified in [P.A. Dafesh et al., 2000]:

- The most straightforward approach is to process the sub-carrier signal in baseband. According to this, the new signal to add in the multiplexing produces a digital rotation of the phase of the carrier as shown in Figure 7.12 below:

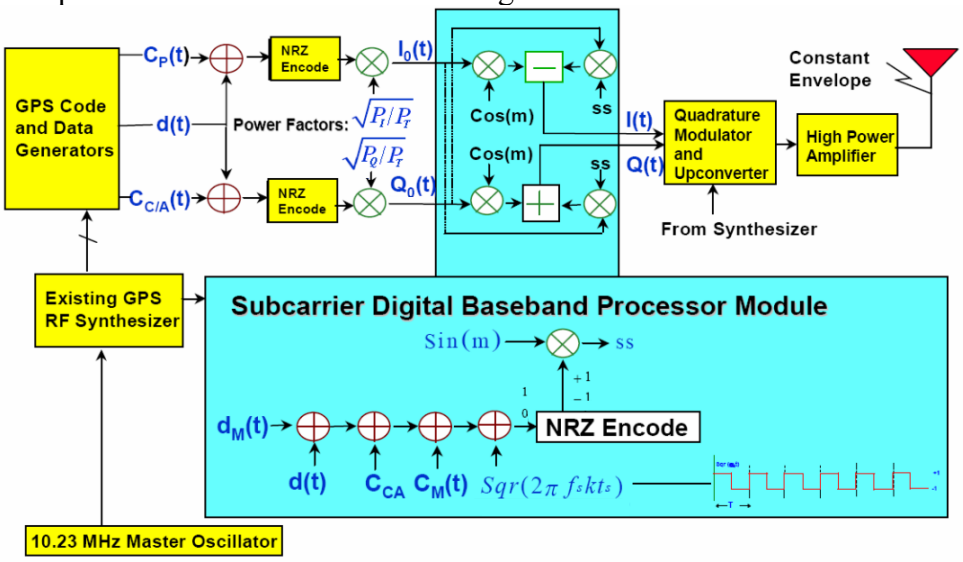

Figure 7.12. Flexible digital CASM modulator implementation [P.A. Dafesh et al., 2000]

- An alternative implementation is to phase modulate the local oscillator as described in [P.A. Dafesh, 1999b]. This approach is very similar to that followed on the Space Ground Link Subsystem (SGLS. In this case we would only need an additional bi-phase modulator to modulate the cross-term. It must be noted that depending on the sub-carrier frequency of the new signal to multiplex one approach or the other will be more appropriate.

In the previous lines a CASM implementation was applied to multiplex all the GPS baseline signals except for the new GPS L1C. However, the original CASM modulation method for GPS pursued the transmission of not only one military signal, but actually two. In fact, the CASM technique proposed by [P.A. Dafesh et al., 1999a] was applicable to the transmission of Military Acquisition (MA) and Military Tracking (MT) signals in a flexible and efficient manner. The high efficiency approach presented there for combined aperture, that is C/A, P(Y), MA and MT sent through the same upconverter amplifier chain and antenna, was shown to be equivalent to that of the separate aperture, where MA and MT would be transmitted with a separate upconverter, amplifier and antenna from that of C/A and P(Y).

One final point to discuss is the power efficiency of the resulting multiplex. As an example, we show the case of the C/A Code, P(Y) Code and M-Code signals and assume that the Inter-Modulation signal is 2 dB lower power than the M-Code and the P(Y) Code as also done in [P.A. Dafesh et al., 2000]. Furthermore, if we recall the filtering losses derived in Table 7.1, the power efficiency of CASM in GPS will be:

Table 7.8. Power Efficiency of CASM

Signal and Carrier Phase	Percentage of Power before filtering and combining	Filtering Loss (dB)	Transmitted Power after filtering (dBW)
C/A (Q)	39.96 %	-0.03	-156
P(Y) Code (I)	21.36 %	-0.31	-159
M-Code (I)	23.91 %	-0.80	-159
IM (10,10) (Q)	14.78 %	-0.71	-161
Total	100 %		-152.0

As we can see, the total transmitted power is approximately the same as that of the Linear Modulation in chapter 7.3.1 (-151.6 dBW). However, here the result of applying CASM to GPS results in a final efficiency of approximately 79.45 %, or 0.99 dB loss in total power due to the CASM Multiplexing and filtering of the IM signal when only the useful signals are considered. That results in 0.69 dB higher losses than in the case of the Linear Modulation, which had 0.30 dB losses or 93.23 % power efficiency. The efficiency of the CASM approach can be further improved if the Inter-Modulation signal is tracked reaching then a final efficiency of approximately 92 %, or 0.36 dB losses. This means only 0.06 dB higher losses than in the case of the Linear Modulation.

We can conclude that the CASM implementation of GPS presents slightly higher modulation losses than the Linear Modulation in general. However, the overall power efficiency when all the contributions are taken into account is significantly greater for CASM than for the Linear Modulation since in this case it is not required that the amplifier works at back-off or that a separate high power amplifier chain is used.

It is important to note that the conclusion from the example above results from a very simplified approach as it is not possible to complete all the modulation at baseband and have just one up-conversion to the transmission frequency. As a result of distributed signal filtering, in reality there are differences in the signal trajectory between the phase plane plots, what has a significant effect on the requirement for HPA back-off. Ideally, a desirable feature would be that all transients lie along the unit circle. However, this does not happen in real implementations in any case.

7.7.8 Interplex Modulation for Galileo: BOC(1,1) + $BOC_{cos}(15,2.5)$

If we apply the Interplex Modulation to the Galileo signals baseline of 2004 as described in chapter 2.4.2, the general expression of the Power Spectral Density is shown to adopt the following expression:

$$G_{s_{BB}}^{\text{Galileo}}(f) = P_{\text{OS}_D}\, G_{\text{OS}_D}(f) + P_{\text{OS}_P}\, G_{\text{OS}_P}(f) + P_{\text{PRS}}\, G_{\text{PRS}}(f) + P_{\text{IM}}\, G_{\text{IM}}(f) \qquad (7.133)$$

where the power spectral densities of the OS and PRS signals were derived in chapter 4.3.2. Moreover, the IM signal will have the same spectrum as the PRS $BOC_{cos}(15,2.5)$ as shown by [E. Rebeyrol et al., 2006] . It must be noted that these expressions are only valid for the case of having BOC(1,1) as open signal, since as we have repeatedly mentioned in this chapter, the standard Interplex equations are not valid when we consider the CBOC implementation of MBOC, as this is not binary.

As stated in [Galileo SIS ICD, 2008], the total power of the Galileo E1 signals should be equally divided between the in-phase and quadrature components. Furthermore, the power of the data and pilot channels should be equal. Using (7.102), this leads to the following relationship:

$$\left.\begin{aligned} P_1 &= P\cos^2(\beta_2)\cos^2(\beta_3) \\ P_2 = P_3 &= P\sin^2(\beta_2)\cos^2(\beta_3) = P\cos^2(\beta_2)\sin^2(\beta_3) \end{aligned}\right\} \Rightarrow \beta_2 = -\beta_3 = m \qquad (7.134)$$

For the Galileo Interplex modulation with BOC(1,1) and $BOC_{cos}(15,2.5)$, that is the old baseline of 2004, the modulation index m adopts the value $m = 0.1959\pi$ and the expression of the transmitted signal is shown to be [E. Rebeyrol et al., 2006]:

$$s(t) = \sqrt{2P_T}\left\{\begin{aligned} &\left[\sin(m)\cos(m)s_{\text{BOC}(1,1)}(t) - \sin(m)\cos(m)s_{\text{BOC}(1,1)}(t)\right]\cos(2\pi f_c t) + \\ &+\left[\cos^2(m)s_{\text{BOC}_{\cos}(15,2.5)}(t) + \sin^2(m)s_{\text{BOC}_{\cos}(15,2.5)}(t)s_{\text{BOC}(1,1)}(t)s_{\text{BOC}(1,1)}(t)\right]\sin(2\pi f_c t) \end{aligned}\right. \qquad (7.135)$$

where

- P is the total power of the signal,

- $s_{\mathrm{BOC}_{\cos}(15,2.5)}(t)$ represents the cosine-phased $\mathrm{BOC}_{\cos}(15,2.5)$ signal waveform of the Public Regulated Service (PRS),
- $s_{\mathrm{BOC}(1,1)}(t)$ is the BOC(1,1) modulation that was used for the data and pilot Open Service in the baseline of 2004, and
- $s_{\mathrm{BOC}_{\cos}(15,2.5)}(t)s_{\mathrm{BOC}(1,1)}(t)s_{\mathrm{BOC}(1,1)}(t)$ is the Inter-Modulation term that keeps the constant envelope of the multiplexed signal.

According to this:

$$\begin{aligned} P_1 &= P\cos^4(m) \\ P_2 &= P_3 = P\cos^2(m)\sin^2(m) \\ P_{\mathrm{IM}}(m) &= P\sin^4(m) \end{aligned} \tag{7.136}$$

Equation (7.135) can be further simplified if we employ the general notation of equations (7.111) and (7.113) as shown next:

$$s(t) = \sqrt{2P}\cos\left(2\pi f_c t - \frac{\pi}{2}s_1(t) + m\,s_1(t)s_2(t) - m\,s_1(t)s_3(t)\right) \tag{7.137}$$

The resulting diagram of the modulation constellation is shown in the next figure:

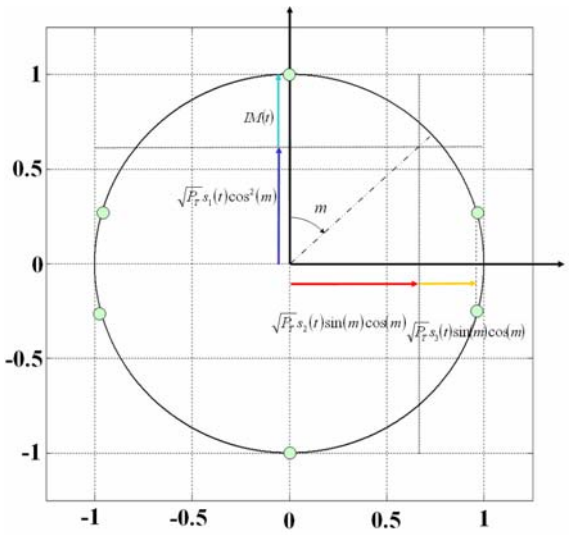

Figure 7.13. Galileo Interplex phase constellation for the Galileo baseline of 2004 [E. Rebeyrol et al., 2006]

7.7.9 Modified Interplex and Modified CASM

As a result of the changes proposed in [G.W. Hein et al., 2005], slight modifications had to be made to the multiplex schemes presented above in order to be able to transmit the CBOC signal for the Galileo E1 OS service. As we have seen in detail in chapter 4.6.4, the CBOC modulation was selected due to its great multipath mitigation potential and spectral compatibility with the rest of signals in the band, among other characteristics of interest. The data and pilot channels are in anti-phase and the difference or additive components are not binary. Indeed, CBOC in particular and CBCS in general, are formed by adding BOC(1,1)

with a new sub-carrier, $s_{\mathrm{BOC}(6,1)}(t)$ for CBOC and $s_{\mathrm{BCS}}(t)$ in general, of relative amplitude μ. This means that the Inter-Modulation component does not obey to the equations that we saw in the previous lines for Interplex and CASM. However, the Interplex and CASM analytical expressions can be easily modified to account for the new signal waveform. In fact, the composite multiplexed signal should present for CBOC the following form:

$$s_{E1}(t)=\alpha\left[s_{E1_D^{\mathrm{OS}}}(t)-s_{E1_P^{\mathrm{OS}}}(t)\right]\cos(2\pi f_{E1}t)-\left[\beta s_{E1_{\mathrm{PRS}}}(t)-\gamma s_{E1_{\mathrm{IM}}}(t)\right]\sin(2\pi f_{E1}t) \tag{7.138}$$

being

$$\begin{aligned}
s_{E1_D^{\mathrm{OS}}}(t)&=d_{\mathrm{OS}}^{E1}(t)\,c_D^{E1_{\mathrm{OS}}}(t)\left[s_{\mathrm{BOC}(1,1)}^{E1_{\mathrm{OS}}}(t)+\mu s_{\mathrm{BOC}(6,1)}^{E1_{\mathrm{OS}}}(t)\right]\\
s_{E1_P^{\mathrm{OS}}}(t)&=c_P^{E1_{\mathrm{OS}}}(t)\left[s_{\mathrm{BOC}(1,1)}^{E1_{\mathrm{OS}}}(t)-\mu s_{\mathrm{BOC}(6,1)}^{E1_{\mathrm{OS}}}(t)\right]\\
s_{E1_{\mathrm{PRS}}}(t)&=d_{\mathrm{PRS}}^{E1}(t)\,c_{\mathrm{PRS}}^{E1}(t)\,s_{\mathrm{PRS}}^{E1}(t)
\end{aligned} \tag{7.139}$$

As we can clearly recognize from the equations above, this modulation scheme is generally more efficient. Indeed, as we saw in chapter 4.6.1, the OS channel is in this case transmitting signal all the time and not only 50 % of the time as was the case with the BOC(1,1) signal. The equation above can be further expressed as follows:

$$s_{E1}(t)=\begin{cases}
\alpha\left[d_{\mathrm{OS}}^{E1}(t)c_D^{E1_{\mathrm{OS}}}(t)-c_P^{E1_{\mathrm{OS}}}(t)\right]s_{\mathrm{BOC}(1,1)}^{E1_{\mathrm{OS}}}(t)\cos(2\pi f_{E1}t)+\\
+\alpha\mu\left[d_{\mathrm{OS}}^{E1}(t)c_D^{E1_{\mathrm{OS}}}(t)+c_P^{E1_{\mathrm{OS}}}(t)\right]s_{\mathrm{BOC}(6,1)}^{E1_{\mathrm{OS}}}(t)\cos(2\pi f_{E1}t)-\\
-\left[\beta s_{\mathrm{PRS}}^{E1}(t)-\gamma s_{\mathrm{IM}}^{E1}(t)\right]\sin(2\pi f_{E1}t)
\end{cases} \tag{7.140}$$

where the emission of BOC(1,1) and the BOC(6,1) signal are shown separately. As it is trivial to recognize, the two emissions are time disjoint and satisfy the requirement to be orthogonal. Another important observation is that now we have 8 phase points instead of only 6. From a quick inspection of the phase diagram one might find analogies with the CASM and Interplex schemes that we saw above. Nonetheless, the CASM and Interplex cannot be applied directly since we do not have binary signals any more.

Finally, it is important to mention that the more signals are multiplexed in the general scheme, the more phase constellation points are needed to achieve the constant envelope. This raises some concerns on the complexity of the signal generator and the identification of the phase points as shown in [A.R. Pratt and J.I.R. Owen, 2005]. Indeed, after filtering at the receiver some phase states might be difficult to distinguish if they are too close to each other.

For more details on the modified interplex modulation, refer to Appendix J where all the analytical expressions for the general CBCS modulation and CBOC are derived.

7.7.10 Interesting Aspects of the Modified Interplex

In all the modulations studied so far, the most typical case was to multiplex binary signals. Nevertheless, there are cases of interest that cannot be described by the original version of the Interplex modulation unless slight modifications are made. In fact, CBOC has data and pilot in anti-phase. This results in an additive/subtractive combination of BOC(1,1) and BOC(6,1) that is not binary any more. Nonetheless, a careful look into the equations shows that for these cases, the inter-modulation still remains binary and thus, except for the amplitude, it can be predicted with the Interplex equations as shown in [G.W. Hein et al., 2005].

As we saw in chapter 4.7.3, CBOC requires to form the sum and difference of the data and pilot channels. The conditions for the BOC(1,1) and BOC(6,1) can be stated as follows:

$$\begin{aligned} d_{\mathrm{OS}}^{E1}(t)\, c_D^{E1_{\mathrm{OS}}}(t) - c_P^{E1_{\mathrm{OS}}}(t) \neq 0 \quad \mathrm{BOC}(1,1) \\ d_{\mathrm{OS}}^{E1}(t)\, c_D^{E1_{\mathrm{OS}}}(t) + c_P^{E1_{\mathrm{OS}}}(t) \neq 0 \quad \mathrm{BOC}(6,1) \end{aligned} \tag{7.141}$$

where the BOC(1,1) and BOC(6,1) channels are time disjoint and could be thus separately decoded. The equation above is subject to further interesting interpretations. In fact, since two time multiplexed channels are created, one could use the difference channel to carry additional signals or services as proposed in [A.R. Pratt and J.I.R. Owen, 2005]. If we assume that 20 % of the total signal power is on the BCS channel and 80 % on the BOC(1,1) channel, this makes a difference of 6 dB in power. For the bit error rate not to be affected with these power levels, the reduced power of the difference channel BOC(6,1) could be compensated by a reduction of the data rate from 250 symbols per second to 50 as shown next:

$$s_{E1}(t) = \alpha\left[s_{E1_D^{\mathrm{OS}}}(t) - s_{E1_P^{\mathrm{OS}}}(t)\right]\cos(2\pi f_{E1}\, t) - \left[\beta\, s_{E1_{PRS}}(t) - \gamma\, s_{E1_{\mathrm{IM}}}(t)\right]\sin(2\pi f_{E1}\, t) \tag{7.142}$$

being

$$\begin{aligned} s_{E1_D^{\mathrm{OS}}}(t) &= d_{\mathrm{OS}}^{E1}(t)\, c_D^{E1_{\mathrm{OS}}}(t)\left[s_{\mathrm{BOC}(1,1)}^{E1_{\mathrm{OS}}}(t) + \mu\, d_{\mathrm{Diff}}^{E1}(t)\, s_{\mathrm{BOC}(6,1)}^{E1_{\mathrm{OS}}}(t)\right] \\ s_{E1_P^{\mathrm{OS}}}(t) &= c_P^{E1_{\mathrm{OS}}}(t)\left[s_{\mathrm{BOC}(1,1)}^{E1_{\mathrm{OS}}}(t) - \mu\, d_{\mathrm{Diff}}^{E1}(t)\, s_{\mathrm{BOC}(6,1)}^{E1_{\mathrm{OS}}}(t)\right] \\ s_{E1_{\mathrm{PRS}}}(t) &= d_{\mathrm{PRS}}^{E1}(t)\, c_{\mathrm{PRS}}^{E1}(t)\, s_{\mathrm{PRS}}^{E1}(t) \end{aligned} \tag{7.143}$$

which is very similar to the expressions derived in previous chapters, but with the slight difference that in this case an additional signal with information $d_{\mathrm{Diff}}^{E1}(t)$ accompanies BOC(6,1). This additional signal has no effect on the time-multiplexing as we can see, since the phase inversion of this data does only cause a change of the sign of the BOC(6,1) signal at every data symbol transition of the difference channel. Finally, it must be noted that as commented in [A.R. Pratt and J.I.R. Owen, 2005], the presence of a data signal on the difference channel, namely BOC(6,1), definitely has an effect on the global signal characteristics equalizing the average spectra, the multipath sensitivity envelope and the DLL tracking characteristics. A method for modulating data for the BOC(6,1) signal and to dispread this data message have been proposed in [A.R. Pratt and J.I.R. Owen, 2005].

7.8 Intervoting (Interplex + Majority Voting)

In chapter 7.4 we saw that majority voting presents interesting characteristics with respect to current known multiplexing techniques, being majority voting an extremely efficient technique when the number of signals to multiplex increases. On the other hand, it can be shown that while the number of signals to multiplex is not higher than three, interplex is optimum in the sense of presenting minimum multiplex losses, especially when the power distribution of the different signals varies considerably. For more than three signals, however, majority voting is shown to outperform interplex.

When both multiplex techniques are compared, one comes to the natural question of whether it would not be possible to have the best of both techniques in one single multiplexing. The answer to this is that it is in fact possible. Such a modulation receives the name of Intervoting (Interplex + Majority Voting). We dedicate this chapter to study its mathematical properties.

7.8.1 Origins of Intervoting

[G. L. Cangiani et al., 2002] have proved that the interplex modulation can be further exploited and generalized to the intervote multiplex, where elementary majority voting techniques are combined with the interplex modulation. Next figure shows schematically how the intervoting modulation works.

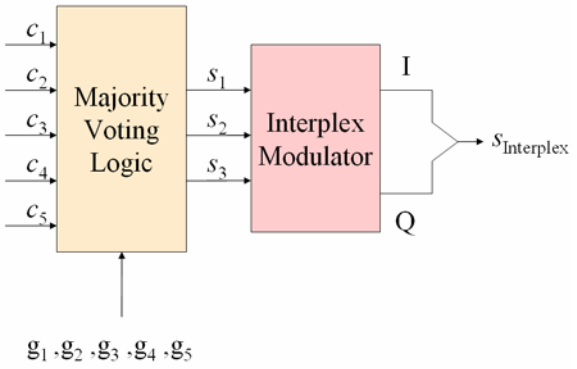

Figure 7.14. Scheme of the intervote multiplex

As we can recognize, an intervote modulator includes a majority voting logic unit and an interplex modulator. The majority voting logic receives as input a number of signal codes with the commanded power ratios and delivers as output three signals that result from majority voting the inputs. In a particular implementation, two of the original input signals remain unchanged and are directly output, being the third output signal the majority vote of the rest of input signals. The majority vote signal and the other two uncombined signals are then fed into the interplex modulator as signals s_1, s_2 and s_3 to form the in-phase and quadrature components of the final composite signal.

7.8.2 Theory on Intervoting

The intervoting multiplex takes advantage of the positive aspects of both interplex and majority voting while it gives a solution to the disadvantages that both present separately. In fact, while majority voting degrades its performance when the power difference between the different signals is considerable (this is the so-called small signal suppression problem that we saw in chapter 7.4.5), interplex reduces its efficiency as the number of signals increases. The combination of both techniques, is capable of elegantly coping with the drawbacks of the two multiplexing schemes, providing an efficient modulation for any number of signals and any arbitrary power distribution.

The particular intervoting multiplex that we analyze in this chapter combines five different signals, being three of them previously multiplexed using Majority Voting. It is important to mention that intervote could in principle be constructed with an interplex scheme that could accommodate more than three signals. Moreover, the total number of signals to multiplex could be in principle also higher. Without loss of generality, we will concentrate however in the following on this particular case given its simplicity and optimum combination of performance and flexibility.

As we can recognize from Figure 7.14, three of the signals are aggregated using majority voting and the resulting majority voted signal is then further multiplexed with the other two uncombined codes using interplex. This solution is especially optimum if the commanded power distribution could change during operation or would adopt any arbitrary set of values not necessarily fixed at the beginning. It is important to note that for a particular power distribution, a particular five signal interplex solution could possibly outperform intervote. Nevertheless, intervote will result in general in an improved efficiency for the majority of power distributions, bringing an additional flexibility in the design.

Let us assume five binary signals $\{c_1, c_2, c_3, c_4, c_5\}$ with target commanded power distribution $\{g_1, g_2, g_3, g_4, g_5\}$, being the gains defined in non-decreasing order such that $g_{n+1} \geq g_n$. As graphically depicted in Figure 7.14, each time there is a change in the target gains of the different signals, the majority voting logic of the intervote multiplexer has to determine which of the five signals is to be mapped [G. L. Cangiani et al., 2002] to which of the three interplex modulator inputs s_1, s_2 or s_3 during the period in which the particular targeted gains apply. Furthermore, the intervote logic has to decide which three codes are majority voted and where the two remaining codes input the interplex multiplexer such as to obtain the maximum global efficiency.

Since intervote bases on interplex to combine all the signals, we recall the general expression of the interplex multiplexing for the I and Q channels as presented in (7.106) of chapter 7.7.2:

$$I = \frac{\sqrt{P_1 P_2}\, s_2(t) + \sqrt{P_1}\, s_3(t)}{\sqrt{P_1^2 + P_1 P_2 + P_1 + P_2}} = \frac{\sqrt{P_1 P_2}\, s_2(t) + \sqrt{P_1}\, s_3(t)}{\sqrt{(1+P_1)(P_1+P_2)}}$$
$$Q = \frac{P_1 s_1(t) - \sqrt{P_2}\, s_1(t) s_2(t) s_3(t)}{\sqrt{P_1^2 + P_1 P_2 + P_1 + P_2}} = \frac{P_1 s_1(t) - \sqrt{P_2}\, s_1(t) s_2(t) s_3(t)}{\sqrt{(1+P_1)(P_1+P_2)}} \quad (7.144)$$

where $s_1(t)$, $s_2(t)$ and $s_3(t)$ are the input interplex components and the powers are all expressed in terms of P_3 with $P_3 = 1$. Furthermore, the efficiency of the interplex modulation was shown to be:

$$\eta_{\text{Interplex}} = \frac{P_1(1 + P_1 + P_2)}{(1+P_1)(P_1+P_2)} \quad (7.145)$$

As we mentioned above, all the permutations of five codes and all locations of the majority vote have to be tested to find the best global efficiency. Indeed, analysis shows that although a particular three-code combination could result in an optimum GMV solution for three particular codes, it is not always true that placing these three codes as input of the interplex and the other two uncombined in the other two interplex inputs would result in the best global intervote efficiency. This means in other words, that all possible $5! = 120$ combinations have to be tried to select the optimum configuration.

Fortunately, the number of efficiency evaluations significantly reduces if symmetry considerations are taken into account. In fact, a careful look at (7.144) reveals that only three logical possibilities for the majority vote placement are to be considered, namely s_1, s_2 or s_3. In this manner, the number of combinations to try is of only $3\binom{5}{3} = 30$. Moreover, positions s_2 and s_3 are interchangeable so that the order does not affect the efficiency formulas as we will also prove next. According to this, only two placement options are possible for the majority vote signal:

- Majority Vote on I: As we have mentioned, placing the majority vote signal on either s_2 or s_3 is arbitrary in terms of the total efficiency. Therefore, the default majority vote signal will be taken to be s_2 in the following pages.
- Majority Vote on Q: In this case, the majority vote signal will be s_1.

7.8.3 Intervoting with Majority Vote on I

In the case that the majority voted signal is placed on I, the generic transmitted binary signals $\{c_1, c_2, c_3, c_4, c_5\}$ can be assigned as follows [G. L. Cangiani et al., 2002]:

$$\begin{aligned} s_1 &= c_4 \\ s_2 &= \{\text{Maj}(c_1, c_2, c_3), c_2, c_3\} \\ s_3 &= c_5 \end{aligned} \quad (7.146)$$

where the majority vote was arbitrarily placed on s_2 as we discussed above. Furthermore, the notation $s_2 = \{\text{Maj}(c_1, c_2, c_3), c_2, c_3\}$ indicates that s_2 is an interlace of the majority vote of c_1, c_2 and c_3 with solo chips of c_2 and c_3, as described in chapter 7.4.7.

We further assume that the code set $\{c_1, c_2, c_3, c_4, c_5\}$ has as target commanded power distribution $\{g_1, g_2, g_3, g_4, g_5\}$. According to this, the normalized interplex gain of s_1 and s_3 should be then g_4 and g_5 respectively. Taking now (7.144) into consideration this implies:

$$\begin{aligned} g_4 &= g(s_1) = \frac{P_1^2}{(1+P_1)(P_1+P_2)} \\ g_5 &= g(s_3) = \frac{P_1}{(1+P_1)(P_1+P_2)} \end{aligned} \tag{7.147}$$

so that

$$P_1 = g_4 / g_5 \tag{7.148}$$

Recalling the efficiency expression of the general interplex modulation as given in (7.107), the total efficiency of Intervoting with majority vote on I will be then as follows:

$$\eta^I_{\text{Intervote}} = \frac{P_1(1+P_1+P_2\eta_{\text{GMV}})}{(1+P_1)(P_1+P_2)} \tag{7.149}$$

It is important to note that this expression is slightly different to that presented in (7.107) for the general interplex case. Indeed, the power allocated on the signal s_2 in the numerator has been corrected by the efficiency of the majority vote multiplex as not all the power allocated on s_2 corresponds in reality to the useful binary signals c_1, c_2 and c_3. In fact, as shown in (7.68), part of the power goes lost in the majority voting reducing the efficiency from 1 to η_{GMV}. For the denominator, however, the whole power allocated on s_2 has to be considered including also the non-desired multiplex losses.

As we have mentioned above, signal s_2 is the majority vote of c_1, c_2 and c_3. According to this, for the targeted power gains g_1, g_2 and g_3, the power gain of s_2 should be

$$g(s_2) = \frac{P_1 P_2}{(1+P_1)(P_1+P_2)} = \frac{g_1+g_2+g_3}{\eta_{\text{GMV}}} = P_2 g_5 \tag{7.150}$$

or equivalently,

$$P_2 \eta_{\text{GMV}} = \frac{g_1+g_2+g_3}{g_5} \tag{7.151}$$

This can be further simplified if we recall that

$$\eta_{\text{GMV}} = \frac{g_1+g_2+g_3}{\left(\sqrt{g_2}+\sqrt{g_3}\right)^2} \tag{7.152}$$

Consequently,

$$g(s_2) = \left(\sqrt{g_2}+\sqrt{g_3}\right)^2 = P_2 g_5 \tag{7.153}$$

or in a similar form

$$P_2 = \frac{\left(\sqrt{g_2}+\sqrt{g_3}\right)^2}{g_5} \tag{7.154}$$

Using now equations (7.149), (7.148), (7.154) and (7.151) together, the total intervote efficiency when the majority vote is placed on I will be:

$$\eta^{I}_{\text{Intervote}} = \frac{P_1\left(1+P_1+P_2\eta_{\text{GMV}}\right)}{\left(1+P_1\right)\left(P_1+P_2\right)} = \frac{\dfrac{g_4}{g_5}\left(1+\dfrac{g_4}{g_5}+\dfrac{g_1+g_2+g_3}{g_5}\right)}{\left(1+\dfrac{g_4}{g_5}\right)\left(\dfrac{g_4}{g_5}+\dfrac{\left(\sqrt{g_2}+\sqrt{g_3}\right)^2}{g_5}\right)} \tag{7.155}$$

which can be further simplified and perfectly coincides with the expression shown by [G. L. Cangiani et al., 2002]:

$$\eta^{I}_{\text{Intervote}} = \frac{g_4\left(g_1+g_2+g_3+g_4+g_5\right)}{\left(g_4+g_5\right)\left[\left(\sqrt{g_2}+\sqrt{g_3}\right)^2+g_4\right]} \tag{7.156}$$

It is interesting to note from the expression above that the position of s_2 and s_3 is insignificant what reinforces the comments we made in chapter 7.8.2 as we anticipated that positions s_2 and s_3 are arbitrarily interchangeable. This is also valid for the case of Intervoting with Majority Vote on Q as we show next.

7.8.4 Intervoting with Majority Vote on Q

In the previous lines we have derived the analytical expression for the intervote efficiency when the majority vote signal is placed on I. In this chapter, we will repeat the same exercise for the case that the majority signal is placed on Q.

In this case, the transmitted signals can be assigned as follows [G. L. Cangiani et al., 2002]:

$$\begin{aligned} s_1 &= \left\{\text{Maj}\left(c_1,c_2,c_3\right),c_2,c_3\right\} \\ s_2 &= c_4 \\ s_3 &= c_5 \end{aligned} \tag{7.157}$$

Since the code set $\left\{c_1,c_2,c_3,c_4,c_5\right\}$ has as target commanded power distribution $\left\{g_1,g_2,g_3,g_4,g_5\right\}$, the normalized interplex gain of s_2 and s_3 should be then g_4 and g_5 respectively. Taking (7.144) into consideration, this implies:

$$\begin{aligned} g_4 &= g\left(s_2\right) = \frac{P_1P_2}{\left(1+P_1\right)\left(P_1+P_2\right)} \\ g_5 &= g\left(s_3\right) = \frac{P_1}{\left(1+P_1\right)\left(P_1+P_2\right)} \end{aligned} \tag{7.158}$$

so that

$$P_2 = g_4/g_5 \tag{7.159}$$

Recalling now the expression for the efficiency of the intervote multiplex on I, the total efficiency with majority vote on Q adopts a slightly different form:

$$\eta_{\text{Intervote}}^{Q} = \frac{P_1\left(1 + P_1\eta_{\text{GMV}} + P_2\right)}{\left(1 + P_1\right)\left(P_1 + P_2\right)} \tag{7.160}$$

As we can recognize, the power allocated on signal s_1 in the numerator has been corrected by the efficiency of the majority vote multiplex following the same logic as in the case of majority vote on I. On the other hand, the whole power allocated on s_1 is considered for the denominator including also the non-desired multiplex losses as explained in previous chapter.

Signal s_1 is the majority vote of c_1, c_2 and c_3. According to this, for the targeted power gains g_1, g_2 and g_3, the power gain of s_1 will be:

$$g\left(s_1\right) = \frac{P_1^2}{\left(1 + P_1\right)\left(P_1 + P_2\right)} = \frac{g_1 + g_2 + g_3}{\eta_{\text{GMV}}} = P_1 g_5 \tag{7.161}$$

or

$$P_1\eta_{\text{GMV}} = \frac{g_1 + g_2 + g_3}{g_5} \tag{7.162}$$

This can be further simplified as follows:

$$g\left(s_1\right) = \left(\sqrt{g_2} + \sqrt{g_3}\right)^2 = P_1 g_5 \tag{7.163}$$

or equivalently

$$P_1 = \frac{\left(\sqrt{g_2} + \sqrt{g_3}\right)^2}{g_5} \tag{7.164}$$

Putting now (7.160), (7.159), (7.151) and (7.154) together, the total intervote efficiency when the majority vote is placed on Q will be then:

$$\eta_{\text{Intervote}}^{Q} = \frac{P_1\left(1 + P_1\eta_{\text{GMV}} + P_2\right)}{\left(1 + P_1\right)\left(P_1 + P_2\right)} = \frac{\frac{\left(\sqrt{g_2} + \sqrt{g_3}\right)^2}{g_5}\left(1 + \frac{g_1 + g_2 + g_3}{g_5} + \frac{g_4}{g_5}\right)}{\left(1 + \frac{\left(\sqrt{g_2} + \sqrt{g_3}\right)^2}{g_5}\right)\left(\frac{\left(\sqrt{g_2} + \sqrt{g_3}\right)^2}{g_5} + \frac{g_4}{g_5}\right)} \tag{7.165}$$

which can be simplified coinciding with the expression of [G. L. Cangiani et al., 2002]:

$$\eta_{\text{Intervote}}^{Q} = \frac{\left(\sqrt{g_2} + \sqrt{g_3}\right)^2\left(g_1 + g_2 + g_3 + g_4 + g_5\right)}{\left[\left(\sqrt{g_2} + \sqrt{g_3}\right)^2 + g_5\right]\left[\left(\sqrt{g_2} + \sqrt{g_3}\right)^2 + g_4\right]} \tag{7.166}$$

In the previous lines we have derived the efficiency of the intervote multiplex for the case that the majority vote signal is either on I or on Q for a particular code set $\{c_1, c_2, c_3, c_4, c_5\}$ with target commanded power distribution $\{g_1, g_2, g_3, g_4, g_5\}$. However, as we mentioned in chapter 7.8.2, to find the optimum code allocation it would be necessary to evaluate (7.149) and (7.160) for all the possible permutations.

Fortunately, since the gains of the different codes are defined in non-decreasing order and the signal with the lowest power c_1 will never have solo chips in the majority vote signal, the number of permutations to assess reduces to ten for the case that we multiplex five signals.

The ten standard permutations, as defined by [G. L. Cangiani et al., 2002] are presented next:

$$\{g_1,g_2,g_3,g_4,g_5\}=\begin{cases}\{G_1,G_2,G_3,G_4,G_5\}\\ \{G_1,G_2,G_4,G_3,G_5\}\\ \{G_1,G_2,G_5,G_3,G_4\}\\ \{G_1,G_3,G_4,G_2,G_5\}\\ \{G_1,G_3,G_5,G_2,G_4\}\\ \{G_1,G_4,G_5,G_2,G_3\}\\ \{G_2,G_3,G_4,G_1,G_5\}\\ \{G_2,G_3,G_5,G_1,G_4\}\\ \{G_2,G_4,G_5,G_1,G_3\}\\ \{G_3,G_4,G_5,G_1,G_2\}\end{cases} \tag{7.167}$$

where $\{g_1,g_2,g_3,g_4,g_5\}=\{G_1,G_2,G_3,G_4,G_5\}$ is the particular case that we covered in the previous two chapters. As underlined by [G. L. Cangiani et al., 2002], the indexes are increasing in positions 1, 2 and 3 of (7.167) in order to assure that the majority vote will never transmit the signal with the lowest power as solo chip. However, the situation for positions 4 and 5 is definitely different since here the order is significant. Indeed, depending on which signal occupies positions 4 and 5, this signal could be on I and Q resulting thus in different efficiency values as we have shown. According to this, twenty permutations are to be evaluated: the ten given by (7.167) plus another ten with positions four and five interchanged.

Once the previous equations determine with code set results in the optimum total efficiency, we would only have to form the majority vote of the three selected signals according to the theory presented in chapter 7.4.7. In a next step, the resulting majority vote signal would be further interplex-multiplexed with the other two uncombined signals.

Last but not the least, it is important to mention that in principle any interplex solution could be employed in the intervote scheme to multiplex all the signals as defended and emphasized by [G. L. Cangiani et al., 2002]. In the particular but illustrating case of previous pages five signals were intervote-multiplexed using a three-input interplex. Nevertheless, as one can imagine, when the signals to multiplex increase, other interplex solutions could also be used. However, three seems to be a good compromise as then interplex behaves optimally.

7.9 FDMA vs. CDMA

We have seen in chapter 2 that GPS, Galileo and Compass are or will be using CDMA while GLONASS is the only one that still employs FDMA for the transmission of its navigation signals. However, as we have seen in chapter 2.5.3 it seems that the Russian Navigation System is moving in the direction of achieving higher interoperability with the American, European and Chinese systems as GLONASS is already taking the first steps to CDMA.

In spite of the promising benefits that this change would bring, the main reasons that the Russian GLONASS has used as argument in the past against CDMA are summarized next:

- Existence of single point of failure if all signals are located at E1/L1,
- FDMA offers improved security protection (not any more true as we explain next),
- The issue of paying for the new civil signal design,
- The historical reasons that lead to FDMA

The improved robustness of FDMA versus CDMA has usually been justified by the improved SSCs that FDMA can achieve. If we take as an example the C/A Codes of GPS and GLONASS, we can see that the Self SSC of the GLONASS C/A Code is of approximately -57.9700 dB-Hz while for GPS we obtain -61.8008 dB-Hz. The favourable difference for the GPS C/A Code comes from the different employed transmission filters and the lower code rate of the GLONASS C/A Code. However, if we take a look at the SSC between spectral adjacent GLONASS C/A Codes, we can recognize than the spectral separation improves to -69.5604 dB-Hz, providing thus nearly 12 dB of additional protection with respect to CDMA. Moreover, if we take a look at non-adjacent spectra the theoretical isolation is infinite and thus the average of the adjacent SSCs would be of -80.6999 dB-Hz or nearly 22 dB better (considering 14 frequency slots).

CDMA achieves higher protection by means of the cross-correlation of the employed codes. These provide in the case of the GPS C/A Gold Codes an additional protection of 24 dB when no Doppler is considered and of approximately 21 dB when also Doppler is taken into account. In the case of FDMA there is only one code and thus we have to talk about auto-correlation instead of cross-correlation. Nonetheless, although all the GLONASS satellites employ the same code for all the satellites, since the relative Doppler and delay among them can be considered as random, the final autocorrelation value that two FDMA satellites present is that of the secondary peaks of the ACF, also in the order of 21 dB with respect to the main peak, and thus close to the cross-correlation of GPS C/A Codes. The randomization effect through Doppler is similar to the principle of Doppler Division Multiple Access (DDMA).

If we consider now the spectral separation and code separation effects together, we can see that from this point of view FDMA would provide an additional protection of 22 dB with

respect to the CDMA approach. This has been indeed the main argument used by GLONASS experts until now. As we can recognize, the implicit assumption behind is that the jammers are narrowband.

While the protection against jammers was at the beginning of GNSS of particular importance and drove most of the decisions that Russia and the USA took to build their respective satellite navigation systems, nowadays it is possible to build very wideband jammers. Thus, the protection that FDMA was supposed to offer against narrowband interferers is not any more an advantage against CDMA.

We can imagine it with a simple example. If we jam a satellite in a CDMA system with a narrowband interferer, we automatically jam all the other satellites since they are on the same carrier. On the contrary, in an FDMA system the other satellites would result in principle unaffected. Wideband jammers are however not an issue or at least not as they were at the beginning when GLONASS argued the FDMA goodness on the basis of its superior jamming protection. As a result, unless the different satellites used carriers very separated in frequency, with today's technology one could jam all the FDMA signals at the same time disabling the extra protection that FDMA was supposed to bring.

In addition, FDMA is a clear show-stopper for mass market applications since having different carriers for each satellite poses an important challenge in the design of the receivers. As one can imagine, this makes FDMA less competitive than its CDMA competitor. Moreover, filter design and other synchronization aspects difficult the design of an FDMA receiver. Although the problem can be solved as many manufacturers have shown in the past years, there is no doubt that if GLONASS wants to really provide mass-market signals, its civil signals will have to slowly migrate to CDMA.

8. Conclusions and Recommendations

In this last chapter, the conclusions from the research work of this thesis are presented. Furthermore, recommendations for future work activities are proposed.

8.1 Conclusions

This thesis provides a theoretical framework to describe analytically the characteristics of any generic navigation signal waveform. Generalized expressions have been derived and fundamental theoretical concepts have been proposed to represent a signal waveform in both the time and frequency domains. The analyzed theory on Multilevel Coded Symbols (MCS) provides a powerful means to mathematically model any of the current navigation signals and, what is of even greater interest, of potential alternative signal schemes that could be proposed in the future.

The thesis starts with a complete description of all existing and planned Global, Regional and Augmentation Satellite Navigation Systems. Special attention has been paid to all the aspects related to signal structure with particular focus on the European Galileo system. The evolution of the Galileo frequency and signal plan was a case of intensive study given its novelty.

The main relevant parameters in the signal design of any navigation system have been further discussed and generally valid formulas have been obtained. A family of generalized waveforms has been proposed and investigated in detail. Furthermore, potential applications and the performance of alternative solutions were studied and compared with other well known solutions.

Given the fact that the number of navigation systems sharing the currently available Radio-Navigation frequency bands is dramatically increasing, this thesis has discussed the relevant aspects related to the spectral compatibility and interoperability among signals. To achieve this objective, the Spectral Separation Coefficients were object of profound analysis. Building on generalized theoretical models to describe any chipping waveform, analytical expressions have been derived for the case of smooth spectra. In addition, the effect of non idealities related to the imperfections of the Pseudo Random Noise (PRN) codes and the existence of data were also modelled in detail. Simulations have shown that numerical computations deliver exactly the same results predicted by the analytical formulas.

To conclude, the different signals introduced in this thesis have been briefly analyzed regarding their implementation in the payload. Here, already implemented and new multiplexing techniques were presented and studied in light of their feasibility to accommodate optimized signal waveforms in the future. This is a field which is expected to attract attention in coming years.

8.2 Recommendations for Future Work

This thesis has provided the theory and mathematical tools with which any present and future navigation signal could be represented. The present work should serve as fundament for future research activities in the field signal design. As this thesis has shown, payload limitations practically reduce today the number of palette signals to binary solutions. However, other families of signals could become reality in the coming years.

In order to guarantee a peaceful coexistence of all existing, planned and potential future signals a correct understanding of compatibility and interoperability is a fundamental requirement. This thesis provides the analytical models and expressions required to support future studies in the field. This work has shown that backward compatibility with other existing signals is possible if some constraints are introduced in the signal design. This concept has proved to work as it has been recently demonstrated with the design of MBOC in E1/L1 and should be further exploited using the models of this thesis.

While this work provides the fundamental models and theory required to design a signal plan from the point of view of the signal waveforms. Further research is found necessary in several other fields of comparable relevance. Next lines describe those aspects of the signal design where further work is recommended in the future:

- **New frequency allocations for navigation services:** The efforts invested by all Satellite Navigation Systems have mainly concentrated on placing new services in the very few frequency bands that are already allocated to Radio-Navigation Satellite Services (RNSS) today. However, the present RNSS bands are scarce and overcrowded. Moreover, they provide very limited physical performance given the relatively narrow band they possess. Future efforts should be dedicated to finding new frequency resources with the required protection to provide any potential service.
- **RNSS C-band and S-band for navigation:** In consonance with the previous paragraph and keeping in mind that these two bands are already accepted as RNSS either on a global or a regional basis, they should be further explored in coming years:

    - The C-band range from 5000 MHz to 5030 MHz is an RNSS band in the whole world and could provide improved navigation services given its higher carrier frequency. The main contributions to the error budget, namely ionospheric errors and multipath, are in this band considerably lower. This band could give answer to those limitations that the L-band shows today. However, the technology in C-band poses important challenges that are still to be well understood.

  - The S-band range from 2483.5 MHz to 2500 MHz is already a navigation band in many Asian countries (ITU Region 3). In fact, The Chinese Beidou GEO satellites use as carrier frequency 2491 MHz and the Japanese Engineering Test Satellite Number 8 (ETS/8) too. In addition, the Indian IRNSS system also plans navigation signals in this band for the near future as we have seen in chapter 2.8.2. For this band to be used for a global satellite navigation service further work is required in understanding the advantages and limitations of this frequency allocation. Given its proximity to communication services, important synergies are to be expected. Further work could use this thesis as fundament to understand the potential of this band.

- **New signal waveforms for navigation:** While the BOC, AltBOC and MBOC modulations have represented important innovations in the signal design, this thesis has shown that there are still other signal options of great interest, not necessarily binary, that should be further investigated in the future. The current payload limitations to have binary signals will soon be overcome and future work is thus required to identify new signals. This thesis offers the mathematical framework under which these new signals could be investigated.
- **Relative reduction in the importance of backward compatibility:** In the design and modernization of all current navigation systems, backward compatibility with legacy signals has played an outstanding role. However, as software receivers gain in importance, this constraint could lose part of its weight in future decisions. New and more powerful signals could thus be designed. Future work should also be carried out using the guidelines proposed in this thesis.
- **Need of improved multiplexing techniques:** As the number of signals increases, new techniques will be required in the future to accommodate new services and targeted applications. Today, the same navigation signal serves completely different users. However, as suggested in this thesis, several signals optimized to particular users of interest could be multiplexed using advanced multiplexing techniques already present today in the literature. Further work is found to be required in coming years to give an answer to the ever increasing needs of the different user communities. In particular for services that require improved robustness, combinations of CDMA with frequency hopping and Orthogonal Frequency Division Multiplexing (OFDM) could provide promising solutions.
- **New code families:** Significant progress has been made in the field of code theory over the past years. However, much of these developments have not yet been applied to satellite navigation. While the modernized GPS and Galileo will make use of new code concepts, it is clear that further research will still be required in the future. In addition, new encryption methods should be further explored to give an answer to the needs of certain services.

- **Modernized Message Structure:** Message structure is one of the aspects in the signal design that has less evolved in the past years. While GPS III will introduce some slight modifications to the actual designs, it is clear that still further improvements can be achieved. Fundamental research should thus be realized in coming years to elaborate optimized message designs for new satellite navigation signals. The use of dynamic messages with data rates that change depending on the needs of the system is a field where future work is required. Some of these ideas could be well answered using the theory presented in this thesis, exploiting the multiplexing characteristics.
- **Compatibility and Interoperability:** This thesis has underlined the importance of the signal design to achieve compatibility. Future work will be required in coming years to understand how the coexistence between all the different services of the various Global and Regional Satellite Navigation Systems could be guaranteed as new systems come into play.
- **Interoperable Integrity:** In line with the previous paragraph, interoperability in the integrity concept of the different navigation systems should equally be further investigated. The user will only be capable of really profiting from the different integrity concepts that exist today if harmonized statistical models are developed.

A Appendix. PSD of BPSK signals

As shown in chapter 4.3.1, BPSK is a particular case of MCS. Thus, the power spectral density of a generic BPSK(f_c) can be described using the theory on MCS signals as follows:

$$G_{\text{BPSK}}(f_c) = G_{\text{Subchip pulse}}^{\text{BPSK}(nf_c)}(f)\,G_{\text{Mod}}^{\text{BPSK}(f_c)}(f) = f_c\,\frac{\sin^2\left(\frac{\pi f}{nf_c}\right)}{(\pi f)^2}\left\{n + 2\left[\sum_{i=1}^{n-1}(n-i)\cos\left(i\frac{2\pi f}{nf_c}\right)\right]\right\} \tag{A.1}$$

In this Appendix we will show that after some math this expression leads to the well known form of the BPSK Power Spectral Density that can be found in the literature. To do so, we will concentrate on the term in the brackets, namely the modulating factor. For simplicity in the manipulations we will express the cosine as a function of complex exponentials using the Euler´s formula. According to this, the modulating term to simplify is as follows:

$$G_{\text{Mod}}^{\text{BPSK}(f_c)}(f) = n + 2\left[\sum_{i=1}^{n-1}(n-i)\cos\left[i\frac{2\pi f}{nf_c}\right]\right] = n + \sum_{i=1}^{n-1}(n-i)\left(\mathrm{e}^{iA} + \mathrm{e}^{-iA}\right)\Big|_{A=j\frac{2\pi f}{nf_c}} \tag{A.2}$$

As we can recognize from the expression above, the problem to solve reduces to calculating the following sum:

$$\sum_{i=1}^{n-1}(n-i)\mathrm{e}^{iA} = n\sum_{i=1}^{n-1}\mathrm{e}^{iA} - \sum_{i=1}^{n-1} i\,\mathrm{e}^{iA} \tag{A.3}$$

Let us define the following function:

$$f(A) = \sum_{i=1}^{n-1}\mathrm{e}^{iA} = \sum_{i=1}^{n-1}\left(\mathrm{e}^{A}\right)^i = \frac{\mathrm{e}^{An} - \mathrm{e}^{A}}{\mathrm{e}^{A} - 1} \tag{A.4}$$

which shows the interesting property that

$$\frac{\mathrm{d}f(A)}{\mathrm{d}A} = \sum_{i=1}^{n-1} i\,\mathrm{e}^{iA} \tag{A.5}$$

From (A.4) we can also see that

$$\frac{\mathrm{d}f(A)}{\mathrm{d}A} = \frac{\left(n\,\mathrm{e}^{An} - \mathrm{e}^{A}\right)\left(\mathrm{e}^{A} - 1\right) - \mathrm{e}^{A}\left(\mathrm{e}^{An} - \mathrm{e}^{A}\right)}{\left(\mathrm{e}^{A} - 1\right)^2} \tag{A.6}$$

Using the previous results, we define now the function $\Phi(A)$ as follows:

$$\Phi(A) = \sum_{i=1}^{n-1}(n-i)\mathrm{e}^{iA} = n\sum_{i=1}^{n-1}\mathrm{e}^{iA} - \sum_{i=1}^{n-1} i\,\mathrm{e}^{iA} = n\,f(A) - \frac{\mathrm{d}f(A)}{\mathrm{d}A} \tag{A.7}$$

Combining now (A.4) and (A.6) according to (A.7) yields then:

$$\Phi(A) = \sum_{i=1}^{n-1}(n-i)\mathrm{e}^{iA} = \frac{\mathrm{e}^{A}(n-1) + \mathrm{e}^{A(n+1)} - n\,\mathrm{e}^{2A}}{\left(\mathrm{e}^{A} - 1\right)^2} \tag{A.8}$$

We can further express the original expression of (A.2) as follows in terms of $\Phi(A)$:

$$G_{\text{Mod}}^{\text{BPSK}(f_c)}(f)=n+2\left[\sum_{i=1}^{n-1}(n-i)\cos\left[i\frac{2\pi f}{nf_c}\right]\right]=\left\{n+\Phi(A)+\Phi(-A)\right\}\Big|_{A=j\frac{2\pi f}{nf_c}}=$$
$$=n+\frac{e^{A}(n-1)+e^{A(n+1)}-ne^{2A}}{\left(e^{A}-1\right)^2}+\frac{e^{-A}(n-1)+e^{-A(n+1)}-ne^{-2A}}{\left(e^{-A}-1\right)^2} \quad \text{(A.9)}$$

This can be simplified after extracting the common factor e^{An} and e^{-An} respectively and forming squares, as shown next:

$$G_{\text{Mod}}^{\text{BPSK}(f_c)}(f)=\frac{\left\{\begin{array}{l} n\left[\left(e^{-A}-1\right)\left(e^{A}-1\right)\right]^2+(4n-2)\left(e^{A}+e^{-A}\right)- \\ -6n+4-n\left(e^{2A}+e^{-2A}\right)+\left(e^{\frac{A}{2}}-e^{-\frac{A}{2}}\right)^2\left(e^{An}+e^{-An}\right) \end{array}\right\}}{\left[\left(e^{-A}-1\right)\left(e^{A}-1\right)\right]^2} \quad \text{(A.10)}$$

Moreover, since A can also be expressed as $A=jB$, the modulating term simplifies to

$$G_{\text{Mod}}^{\text{BPSK}(f_c)}(f)=\frac{\left[\begin{array}{l} 16n\sin^4\left(\frac{B}{2}\right)+(8n-4)\left[1-2\sin^2\left(\frac{B}{2}\right)\right]-6n+4- \\ -2n\left[1-8\sin^2\left(\frac{B}{2}\right)\cos^2\left(\frac{B}{2}\right)\right]-8\sin^2\left(\frac{B}{2}\right)\cos(nB) \end{array}\right]}{16\sin^4\left(\frac{B}{2}\right)}\Bigg|_{B=\frac{2\pi f}{nf_c}} \quad \text{(A.11)}$$

resulting in the next expression:

$$G_{\text{Mod}}^{\text{BPSK}(f_c)}(f)=\frac{\left[8\sin^2\left(\frac{B}{2}\right)\left[1-\cos(nB)\right]\right]}{16\sin^4\left(\frac{B}{2}\right)}\Bigg|_{B=\frac{2\pi f}{nf_c}}=\frac{\sin^2\left(\frac{nB}{2}\right)}{\sin^2\left(\frac{B}{2}\right)}\Bigg|_{B=\frac{2\pi f}{nf_c}}=\frac{\sin^2\left(\frac{\pi f}{f_c}\right)}{\sin^2\left(\frac{\pi f}{nf_c}\right)} \quad \text{(A.12)}$$

Now that we have the BCS modulating factor of BPSK(f_c), it can be shown that the power spectral density is the well known expression we saw in chapter 4.3.1:

$$G_{\text{BPSK}}(f_c)=G_{\text{Subchip pulse}}^{\text{BPSK}(nf_c)}(f)G_{\text{Mod}}^{\text{BPSK}(f_c)}(f)=f_c\frac{\sin^2\left(\frac{\pi f}{nf_c}\right)}{(\pi f)^2}\frac{\sin^2\left(\frac{\pi f}{f_c}\right)}{\sin^2\left(\frac{\pi f}{nf_c}\right)}=f_c\frac{\sin^2\left(\frac{\pi f}{f_c}\right)}{(\pi f)^2} \quad \text{(A.13)}$$

B Appendix. PSD of sine-phased BOC signals

As we saw in chapter 4.3.2.1 the power spectral density of any BOC(f_s, f_c) in sine phasing can be expressed using the theory on MCS signals as follows:

$$G^{e}_{\mathrm{BOC}_{\sin}(f_s,f_c)} = G^{\mathrm{BPSK}(2f_c)}_{\mathrm{pulse}}(f)\,G^{\mathrm{BOC}_{\sin}(f_s,f_c)}_{\mathrm{Mod},e}(f) = f_c\,\frac{\sin^2\left(\frac{\pi f}{nf_c}\right)}{(\pi f)^2}\left\{n + 2\sum_{i=1}^{n-1}(-1)^i(n-i)\cos\left[i\frac{2\pi f}{nf_c}\right]\right\} \tag{B.1}$$

where the superindex *e* indicates the even case. Moreover, the modulating factor for the even case presents the following form:

$$G^{\mathrm{BOC}_{\sin}(f_s,f_c)}_{\mathrm{Mod},e}(f) = n + 2\left[\sum_{i=1}^{n-1}(-1)^i(n-i)\cos\left[i\frac{2\pi f}{nf_c}\right]\right] = n + \sum_{i=1}^{n-1}(-1)^i(n-i)\left(\mathrm{e}^{iA} + \mathrm{e}^{-iA}\right)\Big|_{A=j\frac{2\pi f}{nf_c}} \tag{B.2}$$

As we can see, the problem to calculate can be reduced into an easier one by means of the following auxiliary function $\Phi(A)$:

$$\Phi(A) = \sum_{i=1}^{n-1}(-1)^i(n-i)\mathrm{e}^{iA} = n\sum_{i=1}^{n-1}(-1)^i\mathrm{e}^{iA} - \sum_{i=1}^{n-1}i(-1)^i\mathrm{e}^{iA} \tag{B.3}$$

and also with the auxiliary function $f(A)$, defined as follows:

$$f(A) = \sum_{i=1}^{n-1}(-1)^i\mathrm{e}^{iA} = \sum_{i=1}^{n-1}\left(-\mathrm{e}^{A}\right)^i = \frac{\left(-\mathrm{e}^{A}\right)^n + \mathrm{e}^{A}}{-\mathrm{e}^{A} - 1} = \frac{(-1)^n\mathrm{e}^{An} + \mathrm{e}^{A}}{-\mathrm{e}^{A} - 1} \tag{B.4}$$

where we have made the change

$$\sum_{i=1}^{n-1}x^i = \frac{x^n - x}{x - 1} \tag{B.5}$$

The interesting property about the above defined function $f(A)$ is shown in the next relationship:

$$\frac{\mathrm{d}f(A)}{\mathrm{d}A} = \sum_{i=1}^{n-1}i(-1)^i\mathrm{e}^{iA} \tag{B.6}$$

In fact, taking (B.4) we can see that

$$\frac{\mathrm{d}f(A)}{\mathrm{d}A} = \frac{-\left[n(-1)^n\mathrm{e}^{An} + \mathrm{e}^{A}\right]\left(\mathrm{e}^{A} + 1\right) + \mathrm{e}^{A}\left[(-1)^n\mathrm{e}^{An} + \mathrm{e}^{A}\right]}{\left(\mathrm{e}^{A} + 1\right)^2} \tag{B.7}$$

Thus (B.3) can be rewritten as follows

$$\Phi(A) = \sum_{i=1}^{n-1}(-1)^i(n-i)\mathrm{e}^{iA} = n\sum_{i=1}^{n-1}(-1)^i\mathrm{e}^{iA} - \sum_{i=1}^{n-1}i(-1)^i\mathrm{e}^{iA} = nf(A) - \frac{\mathrm{d}f(A)}{\mathrm{d}A} \tag{B.8}$$

Combining now (B.4) and (B.6) according to (B.8) we obtain the following expression:

$$\Phi(A) = \sum_{i=1}^{n-1}(-1)^i(n-i)\mathrm{e}^{iA} = \frac{\mathrm{e}^{A}(1-n) - n\mathrm{e}^{2A} + (-1)^{n+1}\mathrm{e}^{A(n+1)}}{\left(\mathrm{e}^{A} + 1\right)^2} \tag{B.9}$$

And the modulating function simplifies thus to:

$$G_{\mathrm{Mod},e}^{\mathrm{BOC}_{\sin}(f_s,f_c)}(f)=n+2\left[\sum_{i=1}^{n-1}(-1)^i(n-i)\cos\left[i\frac{2\pi f}{nf_c}\right]\right]=\left\{n+\Phi(A)+\Phi(-A)\right\}\Big|_{A=j\frac{2\pi f}{nf_c}}=$$

$$=n+\frac{\mathrm{e}^{A}(1-n)+(-1)^{n+1}\mathrm{e}^{A(n+1)}-n\mathrm{e}^{2A}}{\left(\mathrm{e}^{A}+1\right)^2}+\frac{\mathrm{e}^{-A}(1-n)+(-1)^{n+1}\mathrm{e}^{-A(n+1)}-n\mathrm{e}^{-2A}}{\left(\mathrm{e}^{-A}+1\right)^2}= \tag{B.10}$$

$$n+\frac{-\left(\mathrm{e}^{An}+\mathrm{e}^{-An}\right)+2(1-n)-n\left(\mathrm{e}^{A}+\mathrm{e}^{-A}\right)}{\left(\mathrm{e}^{A}+\mathrm{e}^{-A}+2\right)}=\frac{-\left(\mathrm{e}^{An}+\mathrm{e}^{-An}\right)+2}{\left(\mathrm{e}^{\frac{A}{2}}+\mathrm{e}^{-\frac{A}{2}}\right)^2}=-\frac{\left(\mathrm{e}^{\frac{An}{2}}-\mathrm{e}^{-\frac{An}{2}}\right)^2}{\left(\mathrm{e}^{\frac{A}{2}}+\mathrm{e}^{-\frac{A}{2}}\right)^2}$$

where we have also taken into account that according to the definition of the BOC modulation in terms of a BCS vector, n is even in the even version. Additionally, since A can also be expressed as $A=jB$ the expression above simplifies to

$$G_{\mathrm{Mod},e}^{\mathrm{BOC}_{\sin}(f_s,f_c)}(f)=-\frac{\left[2j\sin\left(\frac{nB}{2}\right)\right]^2}{4\cos^2\left(\frac{B}{2}\right)}\Bigg|_{B=\frac{2\pi f}{nf_c}}=\frac{\sin^2\left(\frac{nB}{2}\right)}{\cos^2\left(\frac{B}{2}\right)}\Bigg|_{B=\frac{2\pi f}{nf_c}}=\frac{\sin^2\left(\frac{\pi f}{f_c}\right)}{\cos^2\left(\frac{\pi f}{nf_c}\right)} \tag{B.11}$$

Once a simplified form has been derived for the BCS modulating factor of BOC(f_s, f_c), we substitute in (B.1) yielding the well known expression for the Power Spectral Density that we saw in chapter 4.3.2.1:

$$G_{\mathrm{BOC}\left(f_s=\frac{nf_c}{2},f_c\right)}=f_c\frac{\sin^2\left(\frac{\pi f}{nf_c}\right)}{(\pi f)^2}\frac{\sin^2\left(\frac{\pi f}{f_c}\right)}{\cos^2\left(\frac{\pi f}{nf_c}\right)}=f_c\frac{\sin^2\left(\frac{\pi f}{f_c}\right)}{(\pi f)^2}\tan^2\left(\frac{\pi f}{nf_c}\right)=f_c\left[\frac{\sin\left(\frac{\pi f}{f_c}\right)\sin\left(\frac{\pi f}{nf_c}\right)}{\pi f\cos\left(\frac{\pi f}{nf_c}\right)}\right]^2 \tag{B.12}$$

Moreover, in chapter 4.3.2.1 we also saw that $n=2f_s/f_c$ so that (B.12) can also be expressed as follows:

$$G_{\mathrm{BOC}(f_s,f_c)}=f_c\left[\frac{\sin\left(\frac{\pi f}{f_c}\right)\sin\left(\frac{\pi f}{2f_s}\right)}{\pi f\cos\left(\frac{\pi f}{2f_s}\right)}\right]^2 \tag{B.13}$$

This is the well known expression that we find everywhere in the literature. Now that we have solved the case of the even BOC modulation in sine phasing, we calculate next its odd counterpart. For the case of the odd BOC modulation in sine phasing, we have to derive first a general expression for any odd n. We will proceed by generalizing over n.

For $n = 3$, $\mathrm{BOC}_{\sin}(f_s, f_c)$ can also be expressed as BCS([+1,-1,+1], f_c), such that the generation matrix will adopt the following form:

$$M^3\left(\left[+1,-1,+1\right]\right)=\begin{pmatrix} s_1s_1\{0\} & s_1s_2\{1\} & s_1s_3\{2\} \\ & s_2s_2\{0\} & s_2s_3\{1\} \\ & & s_3s_3\{0\} \end{pmatrix}=\begin{pmatrix} 1\{0\} & -1\{1\} & 1\{2\} \\ & 1\{0\} & -1\{1\} \\ & & 1\{0\} \end{pmatrix} \tag{B.14}$$

Thus, the odd modulating term yields this time:

$$G_{\mathrm{Mod},o}^{\mathrm{BOC}_{\sin}(f_s,f_c)}(f)=3+2\left[-2\cos\left(\frac{2\pi f}{3f_c}\right)+\cos\left(2\frac{2\pi f}{3f_c}\right)\right] \tag{B.15}$$

where *o* indicates the odd case, and

$$G_{\mathrm{pulse}}^{\mathrm{BPSK}(2f_c)}(f)=f_c\frac{\sin^2\left(\frac{\pi f}{3f_c}\right)}{(\pi f)^2} \tag{B.16}$$

In the same manner, for $n=5$, $\mathrm{BOC}_{\sin}(f_s, f_c)$= $\mathrm{BOC}_{\sin}(2f_c, f_c)$ what can also be defined as in the general form BCS([+1,-1,+1,-1,+1], f_c) with generation matrix given by:

$$M^5\left(\left[+1,-1,+1,-1,+1\right]\right)=\begin{pmatrix} 1\{0\} & -1\{1\} & 1\{2\} & -1\{3\} & 1\{4\} \\ & 1\{0\} & -1\{1\} & 1\{2\} & -1\{3\} \\ & & 1\{0\} & -1\{1\} & 1\{2\} \\ & & & 1\{0\} & -1\{1\} \\ & & & & 1\{0\} \end{pmatrix} \tag{B.17}$$

Thus, for the case of $n=5$, we will have:

$$G_{\mathrm{Mod},o}^{\mathrm{BOC}_{\sin}(f_s,f_c)}(f)=5+2\left[-4\cos\left(\frac{2\pi f}{5f_c}\right)+3\cos\left(2\frac{2\pi f}{5f_c}\right)-2\cos\left(3\frac{2\pi f}{5f_c}\right)+\cos\left(4\frac{2\pi f}{5f_c}\right)\right] \tag{B.18}$$

If we continue by induction we can find the expression for any odd *n*:

$$G_{\mathrm{Mod},o}^{\mathrm{BOC}_{\sin}(f_s,f_c)}(f)=n+2\sum_{i=1}^{n-1}(-1)^i(n-i)\cos\left[i\frac{2\pi f}{nf_c}\right] \tag{B.19}$$

As we can recognize, (B.19) is equal to (B.2) except that *n* is odd now with $n\in\{3,5,7,...\}$ Moreover, it can be shown that for the odd $n=2f_s/f_c$ is still valid. For simplicity, we express the modulating factor above using its exponential equivalent expression:

$$G_{\mathrm{Mod},o}^{\mathrm{BOC}_{\sin}(f_s,f_c)}(f)=n+\sum_{i=1}^{n-1}(-1)^i(n-i)\left(\mathrm{e}^{iA}+\mathrm{e}^{-iA}\right)\Big|_{A=j\frac{2\pi f}{nf_c}} \tag{B.20}$$

Using now the expressions derived above for the sum term $\Phi(A)$, it can be shown that:

$$\Phi(A)=\sum_{i=1}^{n-1}(-1)^i(n-i)\mathrm{e}^{iA}=\frac{\mathrm{e}^A(1-n)-n\mathrm{e}^{2A}+(-1)^{n+1}\mathrm{e}^{A(n+1)}}{\left(\mathrm{e}^A+1\right)^2}=\frac{\mathrm{e}^A(1-n)-n\mathrm{e}^{2A}+\mathrm{e}^{A(n+1)}}{\left(\mathrm{e}^A+1\right)^2} \tag{B.21}$$

Again, this expression is similar to that obtained for the even case, but with a slight

difference. Indeed, since n is odd, the second summand in the numerator has a changed sign with respect to (B.9). The modulating function is thus shown to present the following form:

$$G_{\mathrm{Mod},o}^{\mathrm{BOC}_{\sin}(f_s,f_c)}(f) = n + 2\left[\sum_{i=1}^{n-1}(-1)^i(n-i)\cos\left[i\frac{2\pi f}{nf_c}\right]\right] = \left\{n+\Phi(A)+\Phi(-A)\right\}\Big|_{A=j\frac{2\pi f}{nf_c}} =$$

$$= n + \frac{\mathrm{e}^{A}(1-n)+(-1)^{n+1}\mathrm{e}^{A(n+1)}-n\mathrm{e}^{2A}}{\left(\mathrm{e}^{A}+1\right)^2} + \frac{\mathrm{e}^{-A}(1-n)+(-1)^{n+1}\mathrm{e}^{-A(n+1)}-n\mathrm{e}^{-2A}}{\left(\mathrm{e}^{-A}+1\right)^2} = \tag{B.22}$$

$$= n + \frac{\left(\mathrm{e}^{An}+\mathrm{e}^{-An}\right)+2(1-n)-n\left(\mathrm{e}^{A}+\mathrm{e}^{-A}\right)}{\left(\mathrm{e}^{A}+\mathrm{e}^{-A}+2\right)} = \frac{\mathrm{e}^{An}+\mathrm{e}^{-An}+2}{\left(\mathrm{e}^{\frac{A}{2}}+\mathrm{e}^{-\frac{A}{2}}\right)^2} = \frac{\left(\mathrm{e}^{\frac{An}{2}}+\mathrm{e}^{-\frac{An}{2}}\right)^2}{\left(\mathrm{e}^{\frac{A}{2}}+\mathrm{e}^{-\frac{A}{2}}\right)^2}$$

Additionally, since A can also be expressed as $A=jB$, (B.22) simplifies to

$$G_{\mathrm{Mod},o}^{\mathrm{BOC}_{\sin}(f_s,f_c)}(f) = \frac{\left[2\cos\left(\frac{nB}{2}\right)\right]^2}{4\cos^2\left(\frac{B}{2}\right)}\Bigg|_{B=\frac{2\pi f}{nf_c}} = \frac{\cos^2\left(\frac{nB}{2}\right)}{\cos^2\left(\frac{B}{2}\right)}\Bigg|_{B=\frac{2\pi f}{nf_c}} = \frac{\cos^2\left(\frac{\pi f}{f_c}\right)}{\cos^2\left(\frac{\pi f}{nf_c}\right)} \tag{B.23}$$

Once we have the BCS modulating factor of an arbitrary odd BOC(f_s ,f_c) it can be shown that the power spectral density is the well known expression we saw in chapter 4.3.2.1:

$$G^{o}_{\mathrm{BOC}\left(f_s=\frac{nf_c}{2},f_c\right)} = f_c\frac{\sin^2\left(\frac{\pi f}{nf_c}\right)}{(\pi f)^2}\frac{\cos^2\left(\frac{\pi f}{f_c}\right)}{\cos^2\left(\frac{\pi f}{nf_c}\right)} = f_c\left[\frac{\sin\left(\frac{\pi f}{nf_c}\right)\cos\left(\frac{\pi f}{f_c}\right)}{\pi f\cos\left(\frac{\pi f}{nf_c}\right)}\right]^2 \tag{B.24}$$

which coincides perfectly with the expressions found in the literature [J. W. Betz, 1999], [A.R. Pratt and J.I.R. Owen, 2003a] and [E. Rebeyrol et al., 2005].

Furthermore, since $n = 2f_s/f_c$, the previous expression can also be shown as follows:

$$G^{o}_{\mathrm{BOC}\left(f_s=\frac{nf_c}{2},f_c\right)} = f_c\left[\frac{\cos\left(\frac{\pi f}{f_c}\right)\sin\left(\frac{\pi f}{2f_s}\right)}{\pi f\cos\left(\frac{\pi f}{2f_s}\right)}\right]^2 \tag{B.25}$$

C Appendix. PSD of cosine-phased BOC signals

The derivation of the power spectral density of the BOC modulation in cosine phasing is a little bit more complicated, but it can be accomplished in a similar way as we have done with its sine-phased counterpart. If we recall (4.54), the Power Spectral Density of the even cosine-phased BOC is shown to be:

$$G^{e}_{\mathrm{BOC}_{\cos}(f_s,f_c)} = f_c \frac{\sin^2\left(\frac{\pi f}{nf_c}\right)}{(\pi f)^2}\left\{ n + 2\left[\sum_{i=1}^{n/2}(-1)^i \cos\left[(2i-1)\frac{2\pi f}{nf_c}\right] + \sum_{i=1}^{n/2-1} 2(-1)^i (n/2-i)\cos\left[2i\frac{2\pi f}{nf_c}\right]\right]\right\} \tag{C.1}$$

or equivalently,

$$G^{e}_{\mathrm{BOC}_{\cos}\left(f_s=\frac{nf_c}{4},f_c\right)} = G^{\mathrm{BPSK}(nf_c)}_{\mathrm{pulse}}(f)\, G^{\mathrm{BOC}_{\cos}(nf_c/4,f_c)}_{\mathrm{Mod},e}(f) \tag{C.2}$$

where $n \in \{4,8,12,16...\}$. In order to use the results obtained in the previous Appendixes, we will expand the modulation term $G^{\mathrm{BOC}_{\cos}(nf_c/4,f_c)}_{\mathrm{Mod},e}(f)$ in the brackets using the Euler´s formula:

$$\cos\left[(2i-1)\frac{2\pi f}{nf_c}\right] = \frac{e^{j(2i-1)\frac{2\pi f}{nf_c}} + e^{-j(2i-1)\frac{2\pi f}{nf_c}}}{2} \tag{C.3}$$

$$\cos\left[2i\frac{2\pi f}{nf_c}\right] = \frac{e^{j2i\frac{2\pi f}{nf_c}} + e^{-j2i\frac{2\pi f}{nf_c}}}{2} \tag{C.4}$$

According to this, $G^{\mathrm{BOC}_{\cos}(nf_c/4,f_c)}_{\mathrm{Mod}}(f)$ can be expressed as follows:

$$G^{\mathrm{BOC}_{\cos}(nf_c/4,f_c)}_{\mathrm{Mod},e}(f) = n + 2\left[\sum_{i=1}^{n/2}(-1)^i \cos\left[(2i-1)\frac{2\pi f}{nf_c}\right] + \sum_{i=1}^{n/2-1} 2(-1)^i (n/2-i)\cos\left[2i\frac{2\pi f}{nf_c}\right]\right] \tag{C.5}$$

or equivalently,

$$G^{\mathrm{BOC}_{\cos}(nf_c/4,f_c)}_{\mathrm{Mod},e}(f) = n + \sum_{i=1}^{n/2}(-1)^i\left[e^{-A}e^{2iA} + e^{A}e^{-2iA}\right] + \sum_{i=1}^{n/2-1}(-1)^i (n-2i)\left[e^{2iA} + e^{-2iA}\right]\Big|_{A=j\frac{2\pi f}{nf_c}} \tag{C.6}$$

what can also be expressed as:

$$G^{\mathrm{BOC}(nf_c/4,f_c)}_{\mathrm{Mod},e}(f) = n + \left\{\begin{array}{l} +\sum_{i=1}^{n/2}(-1)^i\left[e^{-A}e^{2iA} + e^{A}e^{-2iA}\right] + \\ +n\sum_{i=1}^{n/2-1}(-1)^i\left[e^{2iA} + e^{-2iA}\right] - \\ -\sum_{i=1}^{n/2-1}2i(-1)^i\left[e^{2iA} + e^{-2iA}\right] \end{array}\right|_{A=j\frac{2\pi f}{nf_c}} \tag{C.7}$$

Decomposing the different terms of the sum, we have:

$$G^{\mathrm{BOC}(nf_c/4,f_c)}_{\mathrm{Mod},e}(f) = n + \Phi_1(A) + \Phi_2(A) - \Phi_3(A) \tag{C.8}$$

where,

$$\begin{aligned}\Phi_1(A) &= \Phi_1^+(A) + \Phi_1^-(A) = \sum_{i=1}^{n/2}(-1)^i\left[\mathrm{e}^{-A}\mathrm{e}^{2iA} + \mathrm{e}^{A}\mathrm{e}^{-2iA}\right] \\ \Phi_2(A) &= \Phi_2^+(A) + \Phi_2^-(A) = n\sum_{i=1}^{n/2-1}(-1)^i\left[\mathrm{e}^{2iA} + \mathrm{e}^{-2iA}\right] \\ \Phi_3(A) &= \Phi_3^+(A) + \Phi_3^-(A) = \sum_{i=1}^{n/2-1}2i(-1)^i\left[\mathrm{e}^{2iA} + \mathrm{e}^{-2iA}\right]\end{aligned} \tag{C.9}$$

As we can observe, $\Phi_1^-(A) = \Phi_1^+(-A)$ remaining this identity true also for the other two summands $\Phi_2^-(A)$ and $\Phi_3^-(A)$. Furthermore, if we look in detail at (C.9), we can see that it can be simplified again using the methodology of previous Appendixes. Indeed,

$$\Phi_1^+(A) = \sum_{i=1}^{n/2}(-1)^i\mathrm{e}^{-A}\left(\mathrm{e}^{2A}\right)^i = \mathrm{e}^{-A}\sum_{i=1}^{n/2}\left(-\mathrm{e}^{2A}\right)^i = \mathrm{e}^{-A}\frac{\left(-\mathrm{e}^{2A}\right)^{n/2+1} - \left(-\mathrm{e}^{2A}\right)}{-\mathrm{e}^{2A}-1} = \mathrm{e}^{-A}\frac{\left(\mathrm{e}^{2A}\right)^{n/2+1} - \mathrm{e}^{2A}}{\mathrm{e}^{2A}+1} \tag{C.10}$$

what can also be expressed as follows:

$$\Phi_1^+(A) = \sum_{i=1}^{n/2}(-1)^i\mathrm{e}^{-A}\left(\mathrm{e}^{2A}\right)^i = \frac{\left[\mathrm{e}^{An}-1\right]}{\mathrm{e}^{A}+\mathrm{e}^{-A}} = \frac{\left[\mathrm{e}^{An}-1\right]}{2\cosh(A)} \tag{C.11}$$

It must be noted, that according to the definition of the BOC modulation in cosine phasing as a BCS signal, $n \in \{4,8,12,...\}$ and the term $(-1)^{n/2+1}$ can be further simplified since $n/2+1$ will always be odd. In the same manner:

$$\Phi_1^-(A) = \Phi_1^+(-A) = \sum_{i=1}^{n/2}(-1)^i\mathrm{e}^{A}\left(\mathrm{e}^{-2A}\right)^i = \frac{\left[\mathrm{e}^{-An}-1\right]}{\mathrm{e}^{A}+\mathrm{e}^{-A}} = \frac{\left[\mathrm{e}^{-An}-1\right]}{2\cosh(A)} \tag{C.12}$$

and consequently,

$$\Phi_1(A) = \Phi_1^+(A) + \Phi_1^-(A) = \sum_{i=1}^{n/2}(-1)^i\left[\mathrm{e}^{(2i-1)A} + \mathrm{e}^{-(2i-1)A}\right] = \frac{\left[\mathrm{e}^{An} + \mathrm{e}^{-An} - 2\right]}{\mathrm{e}^{A}+\mathrm{e}^{-A}} \tag{C.13}$$

Furthermore, $\Phi_2(A)$ is shown to simplify to:

$$\Phi_2(A) = \Phi_2^+(A) + \Phi_2^-(A) = n\sum_{i=1}^{n/2-1}(-1)^i\left[\mathrm{e}^{2iA} + \mathrm{e}^{-2iA}\right] = -n\left[\frac{\mathrm{e}^{2A}+\mathrm{e}^{An}}{1+\mathrm{e}^{2A}} + \frac{\mathrm{e}^{-2A}+\mathrm{e}^{-An}}{1+\mathrm{e}^{-2A}}\right] \tag{C.14}$$

or equivalently,

$$\Phi_2(A) = -n\frac{\left(\mathrm{e}^{2A}+\mathrm{e}^{-2A}\right) + \left(\mathrm{e}^{An}+\mathrm{e}^{-An}\right) + 2 + \left[\mathrm{e}^{A(n-2)} + \mathrm{e}^{-A(n-2)}\right]}{\left(\mathrm{e}^{A}+\mathrm{e}^{-A}\right)^2} \tag{C.15}$$

For the third sum term, namely $\Phi_3(A)$, we have to solve first the following intermediate problem:

$$\Phi_3^+(A) = \sum_{i=1}^{n/2-1}2i(-1)^i\mathrm{e}^{2iA} = \sum_{i=1}^{n/2-1}2i\left(-\mathrm{e}^{2A}\right)^i \tag{C.16}$$

To do so, we define the following auxiliary function:

$$f(A) = \sum_{i=1}^{n/2-1}(-1)^i\mathrm{e}^{2iA} = \sum_{i=1}^{n/2-1}\left(-\mathrm{e}^{2A}\right)^i = \frac{\left(-\mathrm{e}^{2A}\right)^{n/2} + \mathrm{e}^{2A}}{-\mathrm{e}^{2A}-1} = \frac{(-1)^{n/2}\mathrm{e}^{An} + \mathrm{e}^{2A}}{-\mathrm{e}^{2A}-1} \tag{C.17}$$

Since $n/2$ is even, we can further simplify the expression above as follows:

$$f(A)=\sum_{i=1}^{n/2-1}(-1)^i e^{2iA}=-\frac{e^{An}+e^{2A}}{e^{2A}+1} \tag{C.18}$$

being the derivative of $f(A)$ the function $\Phi_3^+(A)$ as shown next:

$$\Phi_3^+(A)=\frac{df(A)}{dA}=\sum_{i=1}^{n/2-1}2i(-1)^i e^{2iA}=\frac{(2-n)e^{A(n+2)}-n e^{An}-2e^{2A}}{\left(e^{2A}+1\right)^2} \tag{C.19}$$

In an analogue way, substituting A by $-A$ in (C.19) we can see that

$$\Phi_3^-(A)=\Phi_3^+(-A)=\sum_{i=1}^{n/2-1}2i(-1)^i e^{-2iA}=\frac{(2-n)e^{-A(n+2)}-n e^{-An}-2e^{-2A}}{\left(e^{-2A}+1\right)^2} \tag{C.20}$$

and therefore,

$$\Phi_3(A)=\Phi_3^+(A)+\Phi_3^-(A)=\frac{(2-n)e^{A(n+2)}-n e^{An}-2e^{2A}}{\left(e^{2A}+1\right)^2}+\frac{(2-n)e^{-A(n+2)}-n e^{-An}-2e^{-2A}}{\left(e^{-2A}+1\right)^2} \tag{C.21}$$

what can be further simplified according to:

$$\Phi_3(A)=\Phi_3^+(A)+\Phi_3^-(A)=\frac{(2-n)\left(e^{An}+e^{-An}\right)-n\left[e^{A(n-2)}+e^{-A(n-2)}\right]-4}{\left(e^{A}+e^{-A}\right)^2} \tag{C.22}$$

Now that we have calculated all the sum terms $\Phi_1(A)$, $\Phi_2(A)$ and $\Phi_3(A)$, we can have a simplified expression for the modulating term of the power spectral density of the cosine-phased BOC modulation. In fact,

$$G_{\text{Mod},e}^{\text{BOC}(nf_c/4,f_c)}(f)=\begin{cases}n+\\+\Phi_1(A)+\\+\Phi_2(A)-\\-\Phi_3(A)\end{cases}=\begin{cases}n+\\+\dfrac{\left[e^{An}+e^{-An}-2\right]}{e^{A}+e^{-A}}+\\+\dfrac{-n\left(e^{2A}+e^{-2A}\right)-n\left(e^{An}+e^{-An}\right)-2n-n\left[e^{A(n-2)}+e^{-A(n-2)}\right]}{\left(e^{A}+e^{-A}\right)^2}+\\+\dfrac{(n-2)\left(e^{An}+e^{-An}\right)+n\left[e^{A(n-2)}+e^{-A(n-2)}\right]+4}{\left(e^{A}+e^{-A}\right)^2}\end{cases} \tag{C.23}$$

If we further develop it, we obtain:

$$G_{\text{Mod},e}^{\text{BOC}(nf_c/4,f_c)}(f)=\frac{\left(e^{An}+e^{-An}\right)\left(e^{A}+e^{-A}\right)-2\left(e^{An}+e^{-An}\right)-2\left(e^{A}+e^{-A}\right)+4}{\left(e^{A}+e^{-A}\right)^2} \tag{C.24}$$

or equivalently,

$$G_{\text{Mod},e}^{\text{BOC}(nf_c/4,f_c)}(f)=\left.\frac{\left(e^{\frac{An}{2}}-e^{-\frac{An}{2}}\right)^2\left(e^{\frac{A}{2}}-e^{-\frac{A}{2}}\right)^2}{\left(e^{A}+e^{-A}\right)^2}\right|_{A=j\frac{2\pi f}{nf_c}} \tag{C.25}$$

Finally, since $A=jB$, we can simplify this expression as follows:

$$G_{\text{Mod},e}^{\text{BOC}(nf_c/4,f_c)}(f)=\left.\frac{\left[2j\sin\left(\frac{Bn}{2}\right)\right]^2\left[2j\sin\left(\frac{B}{2}\right)\right]^2}{\left[2\cos(B)\right]^2}\right|_{B=\frac{2\pi f}{nf_c}}=\frac{4\sin^2\left(\frac{\pi f}{f_c}\right)\sin^2\left(\frac{\pi f}{nf_c}\right)}{\cos^2\left(\frac{2\pi f}{nf_c}\right)} \quad \text{(C.26)}$$

so that the power spectral density of $\text{BOC}_{\cos}(f_s = nf_c/4, f_c)$ is shown to be:

$$G_{\text{BOC}_{\cos}(f_s=nf/4_c,f_c)}=f_c\frac{\sin^2\left(\frac{\pi f}{nf_c}\right)}{(\pi f)^2}\frac{4\sin^2\left(\frac{\pi f}{f_c}\right)\sin^2\left(\frac{\pi f}{nf_c}\right)}{\cos^2\left(\frac{2\pi f}{nf_c}\right)}=4f_c\frac{\sin^2\left(\frac{\pi f}{f_c}\right)\sin^4\left(\frac{\pi f}{nf_c}\right)}{(\pi f)^2\cos^2\left(\frac{2\pi f}{nf_c}\right)} \quad \text{(C.27)}$$

Finally since $n = 4f_s/f_c$, it is trivial to see that the expression of the Power Spectral Density of an arbitrary cosine-phased BOC reduces in the even case to:

$$G_{\text{BOC}_{\cos}(f_s,f_c)}=G_{\text{pulse}}^{\text{BPSK}(nf_c)}(f)G_{\text{Mod},e}^{\text{BOC}_{\cos}(nf_c/4,f_c)}(f)=f_c\left[\frac{2\sin\left(\frac{\pi f}{f_c}\right)\sin^2\left(\frac{\pi f}{4f_s}\right)}{\pi f\cos\left(\frac{\pi f}{2f_s}\right)}\right]^2 \quad \text{(C.28)}$$

Once we have obtained the expression for the even BOC modulation in cosine phasing, we calculate its odd counterpart next.

For the case of the odd BOC modulation in cosine phasing, we have to derive a general expression for any *n*. As done in previous chapters, we will generalize over *n*. As in (C.2), the general expression for the odd case will be:

$$G^{o}_{\text{BOC}_{\cos}\left(f_s=\frac{nf_c}{4},f_c\right)}=G_{\text{pulse}}^{\text{BPSK}(nf_c)}(f)G_{\text{Mod},o}^{\text{BOC}_{\cos}(nf_c/4,f_c)}(f) \quad \text{(C.29)}$$

We begin with $n = 2\cdot 3 = 6$, where $\text{BOC}_{\cos}(f_s, f_c) = \text{BOC}_{\cos}(f_c, f_c)$ can also be expressed as $\text{BCS}([+1,-1,-1,+1,+1,-1], f_c)$, being the generation matrix as follows:

$$M^6\left([+1,-1,-1,+1,+1,-1]\right)=\begin{pmatrix}1\{0\} & -1\{1\} & -1\{2\} & 1\{3\} & 1\{4\} & 1\{5\}\\ & 1\{0\} & 1\{1\} & -1\{2\} & -1\{3\} & 1\{4\}\\ & & 1\{0\} & -1\{1\} & -1\{2\} & 1\{3\}\\ & & & 1\{0\} & 1\{1\} & -1\{2\}\\ & & & & 1\{0\} & -1\{1\}\\ & & & & & 1\{0\}\end{pmatrix} \quad \text{(C.30)}$$

In this case, the modulating term will adopt the following form,

$$G_{\text{Mod},o}^{\text{BOC}_{\cos}(nf_c/4,f_c)}(f)=6+2\left[-\cos\left(\frac{2\pi f}{3f_c}\right)-4\cos\left(2\frac{2\pi f}{3f_c}\right)+\cos\left(3\frac{2\pi f}{3f_c}\right)+2\cos\left(4\frac{2\pi f}{3f_c}\right)+\cos\left(5\frac{2\pi f}{3f_c}\right)\right] \quad \text{(C.31)}$$

while

$$G_{\text{pulse}}^{\text{BPSK}(6f_c)}(f)=f_c\frac{\sin^2\left(\frac{\pi f}{6f_c}\right)}{(\pi f)^2} \quad \text{(C.32)}$$

In the same manner, for $n = 2 \cdot 5 = 10$, $\mathrm{BOC_{cos}}(f_s, f_c) = \mathrm{BOC_{cos}}(2f_c, f_c)$ what can also be defined in the general form as BCS([+1,-1,-1,+1,+1,-1,-1,+1,+1,-1], f_c). Thus

$$G_{\mathrm{Mod},o}^{\mathrm{BOC_{cos}}(nf_c/4,f_c)}(f) = 10 + 2\left[\begin{array}{l} -\cos\left(\frac{2\pi f}{10f_c}\right) - 8\cos\left(2\frac{2\pi f}{10f_c}\right) + \cos\left(3\frac{2\pi f}{10f_c}\right) + \\ +6\cos\left(4\frac{2\pi f}{10f_c}\right) - \cos\left(5\frac{2\pi f}{10f_c}\right) - 4\cos\left(6\frac{2\pi f}{10f_c}\right) + \\ +\cos\left(7\frac{2\pi f}{10f_c}\right) + 2\cos\left(8\frac{2\pi f}{10f_c}\right) - \cos\left(9\frac{2\pi f}{10f_c}\right) \end{array}\right] \quad \text{(C.33)}$$

if we continue by induction we can see that the expression for any n adopts the form:

$$G_{\mathrm{BOC_{cos}}(f_s,f_c)} = f_c \frac{\sin^2\left(\frac{\pi f}{nf_c}\right)}{(\pi f)^2}\left\{n + 2\left[\sum_{i=1}^{n/2}(-1)^i \cos\left[(2i-1)\frac{2\pi f}{nf_c}\right] + \sum_{i=1}^{n/2-1} 2(-1)^i (n/2-i)\cos\left[2i\frac{2\pi f}{nf_c}\right]\right]\right\} \quad \text{(C. 34)}$$

with $n \in \{6,10,14,18,...\}$ and $n = 2f_s/f_c$. Again, the modulating factor can be expressed as:

$$G_{\mathrm{Mod},o}^{\mathrm{BOC_{cos}}(nf_c/4,f_c)}(f) = n + \Phi_1(A) + \Phi_2(A) - \Phi_3(A) \quad \text{(C.35)}$$

with

$$\begin{aligned} \Phi_1(A) &= \Phi_1^+(A) + \Phi_1^-(A) \\ \Phi_2(A) &= \Phi_2^+(A) + \Phi_2^-(A) \\ \Phi_3(A) &= \Phi_3^+(A) + \Phi_3^-(A) \end{aligned} \quad \text{(C.36)}$$

which is indeed the same expression we obtained in (C.7). However, since n is now twice an odd number, the results will vary slightly. Indeed it can be shown that:

$$\Phi_1^+(A) = \sum_{i=1}^{n/2}(-1)^i \mathrm{e}^{-A}\left(\mathrm{e}^{2A}\right)^i = \mathrm{e}^{-A}\sum_{i=1}^{n/2}\left(-\mathrm{e}^{2A}\right)^i = \mathrm{e}^{-A}\frac{\left(-\mathrm{e}^{2A}\right)^{n/2+1} - \left(-\mathrm{e}^{2A}\right)}{-\mathrm{e}^{2A}-1} = -\mathrm{e}^{-A}\frac{\left(\mathrm{e}^{2A}\right)^{n/2+1} + \mathrm{e}^{2A}}{\mathrm{e}^{2A}+1} \quad \text{(C.37)}$$

since $n \in \{6,10,14,18,...\}$ and $n/2+1$ will always be even. Thus we can simplify (C.37) as follows:

$$\Phi_1^+(A) = \sum_{i=1}^{n/2}(-1)^i \mathrm{e}^{-A}\left(\mathrm{e}^{2A}\right)^i = -\frac{\left[1+\mathrm{e}^{An}\right]}{\mathrm{e}^{A}+\mathrm{e}^{-A}} = -\frac{\left[1+\mathrm{e}^{An}\right]}{2\cosh(A)} \quad \text{(C.38)}$$

Therefore:

$$\Phi_1(A) = \sum_{i=1}^{n/2}(-1)^i\left[\mathrm{e}^{(2i-1)A} + \mathrm{e}^{-(2i-1)A}\right] = \sum_{i=1}^{n/2}(-1)^i\left[\mathrm{e}^{-A}\left(\mathrm{e}^{2A}\right)^i + \mathrm{e}^{A}\left(\mathrm{e}^{-2A}\right)^i\right] = -\frac{\left[\mathrm{e}^{An} + \mathrm{e}^{-An} + 2\right]}{\mathrm{e}^{A}+\mathrm{e}^{-A}} \quad \text{(C.39)}$$

We can proceed in a similar way with $\Phi_2(A)$ and $\Phi_3(A)$. To do so, we will use the already derived expressions for the even case and take into account that this time $n \in \{6,10,14,18,...\}$. According to this,

$$\Phi_2(A)=\Phi_2^{+}(A)+\Phi_2^{-}(A)=n\sum_{i=1}^{n/2-1}(-1)^i\left[\mathrm{e}^{2iA}+\mathrm{e}^{-2iA}\right]=n\left[\frac{\mathrm{e}^{An}-\mathrm{e}^{2A}}{1+\mathrm{e}^{2A}}+\frac{\mathrm{e}^{-An}-\mathrm{e}^{-2A}}{1+\mathrm{e}^{-2A}}\right] \quad \text{(C.40)}$$

which can be further simplified to:

$$\Phi_2(A)=-n\frac{\left(\mathrm{e}^{2A}+\mathrm{e}^{-2A}\right)-\left(\mathrm{e}^{An}+\mathrm{e}^{-An}\right)+2-\left[\mathrm{e}^{A(n-2)}+\mathrm{e}^{-A(n-2)}\right]}{\left(\mathrm{e}^{A}+\mathrm{e}^{-A}\right)^2} \quad \text{(C.41)}$$

Similarly, to calculate now $\Phi_3(A)$ we will make use of the function $f(A)$ defined above. Nevertheless, since now $n/2$ is always odd, the expression simplifies as follows:

$$f(A)=\sum_{i=1}^{n/2-1}(-1)^i\mathrm{e}^{2iA}=\sum_{i=1}^{n/2-1}\left(-\mathrm{e}^{2A}\right)^i=\frac{\mathrm{e}^{An}-\mathrm{e}^{2A}}{\mathrm{e}^{2A}+1} \quad \text{(C.42)}$$

and thus, for the odd case $\Phi_3(A)$ is shown to be:

$$\Phi_3(A)=\sum_{i=1}^{n/2-1}2i(-1)^i\left[\mathrm{e}^{2iA}+\mathrm{e}^{-2iA}\right]=\frac{(n-2)\left(\mathrm{e}^{An}+\mathrm{e}^{-An}\right)+n\left[\mathrm{e}^{A(n-2)}+\mathrm{e}^{-A(n-2)}\right]-4}{\left(\mathrm{e}^{A}+\mathrm{e}^{-A}\right)^2} \quad \text{(C.43)}$$

Once we have calculated all the sum terms, it is time to obtain the expression for the modulating term of the power spectral density of the odd cosine-phased BOC modulation:

$$G_{\mathrm{Mod},o}^{\mathrm{BOC}_{\cos}(nf_c/4,f_c)}(f)=\begin{cases}n+\\+\Phi_1(A)+\\+\Phi_2(A)-\\-\Phi_3(A)\end{cases}=\begin{cases}n+\\+\dfrac{-\left[\mathrm{e}^{An}+\mathrm{e}^{-An}+2\right]}{\mathrm{e}^{A}+\mathrm{e}^{-A}}+\\+\dfrac{-n\left(\mathrm{e}^{2A}+\mathrm{e}^{-2A}\right)+n\left(\mathrm{e}^{An}+\mathrm{e}^{-An}\right)-2n+n\left[\mathrm{e}^{A(n-2)}+\mathrm{e}^{-A(n-2)}\right]}{\left(\mathrm{e}^{A}+\mathrm{e}^{-A}\right)^2}+\\+\dfrac{-(n-2)\left(\mathrm{e}^{An}+\mathrm{e}^{-An}\right)-n\left[\mathrm{e}^{A(n-2)}+\mathrm{e}^{-A(n-2)}\right]+4}{\left(\mathrm{e}^{A}+\mathrm{e}^{-A}\right)^2}\end{cases} \quad \text{(C.44)}$$

or equivalently:

$$G_{\mathrm{Mod},o}^{\mathrm{BOC}_{\cos}(nf_c/4,f_c)}(f)=\frac{\left[\begin{array}{l}n\left(\mathrm{e}^{2A}+\mathrm{e}^{-2A}+2\right)-\left(\mathrm{e}^{An}+\mathrm{e}^{-An}\right)\left(\mathrm{e}^{A}+\mathrm{e}^{-A}\right)-n\left(\mathrm{e}^{2A}+\mathrm{e}^{-2A}\right)-\\-2n+2\left(\mathrm{e}^{An}+\mathrm{e}^{-An}\right)-2\left(\mathrm{e}^{A}+\mathrm{e}^{-A}\right)+4\end{array}\right]}{\left(\mathrm{e}^{A}+\mathrm{e}^{-A}\right)^2} \quad \text{(C.45)}$$

The modulation term can also be expressed as follows:

$$G_{\mathrm{Mod},o}^{\mathrm{BOC}_{\cos}(nf_c/4,f_c)}(f)=\left.\frac{-\left(\mathrm{e}^{An}+\mathrm{e}^{-An}\right)\left(\mathrm{e}^{A}+\mathrm{e}^{-A}\right)+2\left(\mathrm{e}^{An}+\mathrm{e}^{-An}\right)-2\left(\mathrm{e}^{A}+\mathrm{e}^{-A}\right)+4}{\left(\mathrm{e}^{A}+\mathrm{e}^{-A}\right)^2}\right|_{A=j\frac{2\pi f}{nf_c}} \quad \text{(C.46)}$$

or

$$G_{\mathrm{Mod},o}^{\mathrm{BOC}_{\cos}(nf_c/4,f_c)}(f)=\left.-\frac{\left(\mathrm{e}^{\frac{An}{2}}+\mathrm{e}^{-\frac{An}{2}}\right)^2\left(\mathrm{e}^{\frac{A}{2}}-\mathrm{e}^{-\frac{A}{2}}\right)^2}{\left(\mathrm{e}^{A}+\mathrm{e}^{-A}\right)^2}\right|_{A=j\frac{2\pi f}{nf_c}} \quad \text{(C.47)}$$

In addition, since $A=jB$, we can simplify this expression as follows:

$$G_{\text{Mod},o}^{\text{BOC}_{\cos}(nf_c/4,f_c)}(f) = -\left.\frac{\left[2\cos\left(\frac{Bn}{2}\right)\right]^2\left[2j\sin\left(\frac{B}{2}\right)\right]^2}{\left[2\cos(B)\right]^2}\right|_{B=\frac{2\pi f}{nf_c}} = \frac{4\cos^2\left(\frac{\pi f}{f_c}\right)\sin^2\left(\frac{\pi f}{nf_c}\right)}{\cos^2\left(\frac{2\pi f}{nf_c}\right)} \quad \text{(C.48)}$$

Thus the power spectral density of $\text{BOC}_{\cos}(f_s=nf_c/4, f_c)$ is shown to be in the odd case:

$$G_{\text{BOC}_{\cos}(f_s=nf_c/4,f_c)} = G_{\text{pulse}}^{\text{BPSK}(nf_c)}(f)\,G_{\text{Mod},o}^{\text{BOC}_{\cos}(nf_c/4,f_c)}(f) = 4f_c\,\frac{\cos^2\left(\frac{\pi f}{f_c}\right)\sin^4\left(\frac{\pi f}{nf_c}\right)}{(\pi f)^2\cos^2\left(\frac{2\pi f}{nf_c}\right)} \quad \text{(C.49)}$$

and since $n = 4f_s/f_c$, we can also express it as follows:

$$G_{\text{BOC}_{\cos}(f_s,f_c)} = 4f_c\,\frac{\cos^2\left(\frac{\pi f}{f_c}\right)\sin^4\left(\frac{\pi f}{4f_s}\right)}{(\pi f)^2\cos^2\left(\frac{\pi f}{2f_s}\right)} = f_c\left[\frac{2\cos\left(\frac{\pi f}{f_c}\right)\sin^2\left(\frac{\pi f}{4f_s}\right)}{\pi f\cos\left(\frac{\pi f}{2f_s}\right)}\right]^2 \quad \text{(C.50)}$$

As a conclusion, the normalized power spectral density of the cosine-phased BOC modulation is shown to be for n even:

$$G_{\text{BOC}_{\cos}(f_s,f_c)} = 4f_c\,\frac{\sin^2\left(\frac{\pi f}{f_c}\right)\sin^4\left(\frac{\pi f}{4f_s}\right)}{(\pi f)^2\cos^2\left(\frac{\pi f}{2f_s}\right)} = f_c\left[\frac{2\sin\left(\frac{\pi f}{f_c}\right)\sin^2\left(\frac{\pi f}{4f_s}\right)}{\pi f\cos\left(\frac{\pi f}{2f_s}\right)}\right]^2 \quad \text{(C.51)}$$

and for n odd,

$$G_{\text{BOC}_{\cos}(f_s,f_c)} = 4f_c\,\frac{\cos^2\left(\frac{\pi f}{f_c}\right)\sin^4\left(\frac{\pi f}{4f_s}\right)}{(\pi f)^2\cos^2\left(\frac{\pi f}{2f_s}\right)} = f_c\left[\frac{2\cos\left(\frac{\pi f}{f_c}\right)\sin^2\left(\frac{\pi f}{4f_s}\right)}{\pi f\cos\left(\frac{\pi f}{2f_s}\right)}\right]^2 \quad \text{(C.52)}$$

Now that we have derived the expressions of the power spectral density of the sine and cosine-phased BOC modulations, it is interesting to note the following relationship:

$$G_{\text{BOC}_{\sin}(f_s,f_c)}(f) = f_c\left(\frac{\sin\left(\frac{\pi f}{2f_s}\right)\sin\left(\frac{\pi f}{f_c}\right)}{\pi f\cos\left(\frac{\pi f}{2f_s}\right)}\right)^2 = f_c\left(\frac{2\sin^2\left(\frac{\pi f}{4f_s}\right)\sin\left(\frac{\pi f}{f_c}\right)}{\pi f\cos\left(\frac{\pi f}{2f_s}\right)\tan\left(\frac{\pi f}{4f_s}\right)}\right)^2 = \frac{G_{\text{BOC}_{\cos}(f_s,f_c)}(f)}{\tan^2\left(\frac{\pi f}{4f_s}\right)} \quad \text{(C.53)}$$

that allows us to go from the sine-phased expression to the other one. We show in the next figure the sine-phased BOC modulation together with its cosine-phased counterpart and the inverse tangent term of the expression above that relates both. For simplicity a sub-carrier frequency f_s of 1.023 MHz and a carrier frequency f_c of 1.023 MHz were assumed.

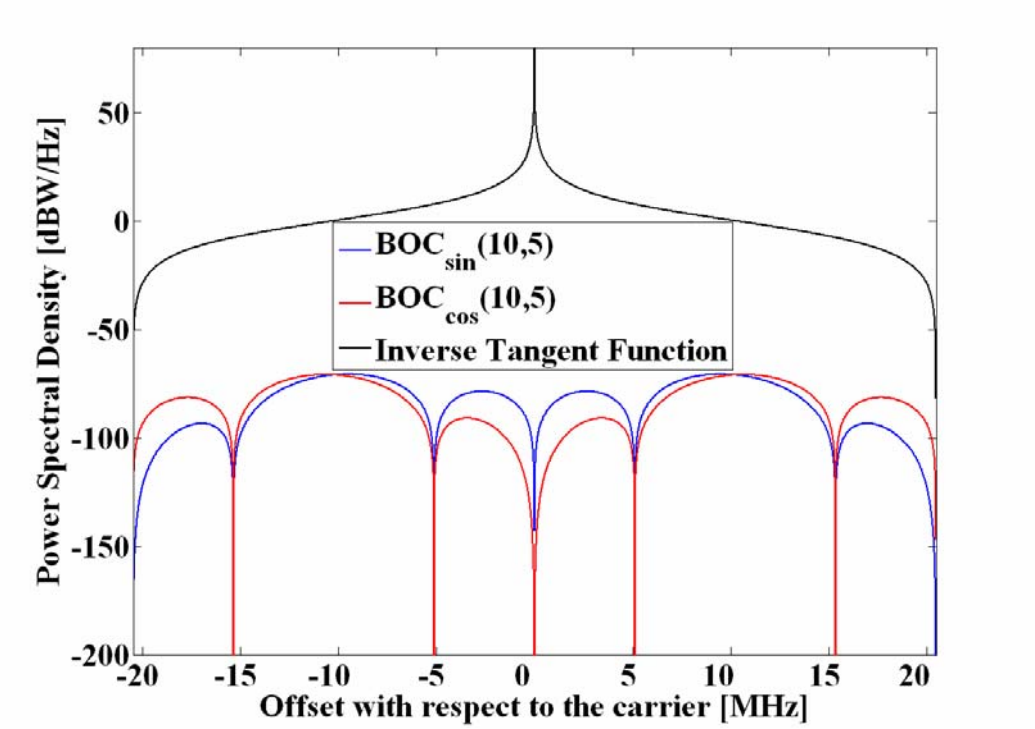

Figure C.1. Power Spectral Density of Sine-phased, Cosine-phased and Inverse Tangent Function of BOC(10,5)

D Appendix. PSD of TCS Signals

The TCS signal waveform has been introduced in chapter 4.5.1. In the next lines we will derive the power spectral density of an arbitrary TCS(f_s, f_c,ρ) with ρ allocated symmetrically around the borders of the sub-chip. To facilitate the understanding, refer to Figure 4.25 in chapter 4.5.1.

For the most general case, the Fourier transform of the signal is shown to be:

$$S_{\mathrm{TCS}}(j\omega)=\sum_{k=1}^{n}\int_{\frac{(k-1+\rho/2)T_c}{n}}^{\frac{(k-\rho/2)T_c}{n}} s_k\,\mathrm{e}^{-j\omega t}\mathrm{d}t=\frac{2}{\omega}\sin\left[\frac{\omega T_c}{2n}(1-\rho)\right]\mathrm{e}^{\frac{j\omega T_c}{2n}}\sum_{k=1}^{n}s_k\,\mathrm{e}^{-\frac{jk\omega T_c}{n}} \tag{D.1}$$

or in the frequency domain

$$S_{\mathrm{TCS}}(f)=\frac{1}{\pi f}\sin\left[\frac{\pi f}{nf_c}(1-\rho)\right]\mathrm{e}^{\frac{j\pi f}{nf_c}}\sum_{k=1}^{n}s_k\mathrm{e}^{-\frac{j2k\pi f}{nf_c}} \tag{D.2}$$

Thus, the general expression for the power spectral density of the TCS adopts the following form:

$$G_{\mathrm{TCS}([\bar{s}],f_c)}(f)=G_{\mathrm{pulse}}^{\mathrm{TCS}}(f)G_{\mathrm{Mod}}^{\mathrm{BCS}([\bar{s}],f_c)}(f)=\left(\frac{f_c}{1-\rho}\right)\frac{\sin^2\left[\frac{\pi f}{nf_c}(1-\rho)\right]}{(\pi f)^2}\left\|\sum_{k=1}^{n}s_k\mathrm{e}^{-j\frac{2\pi fk}{nf_c}}\right\|^2 \tag{D.3}$$

As we can recognize from (D.3), the modulating term on the right is common to the MCS definition and therefore all the results that we obtained in the previous Appendixes apply here too. This will allow us derive general expression for all possible cases of TCS signals. Indeed, the PSD of the TCS modulation can also be expressed as:

$$G_{\mathrm{TCS}([\bar{s}],f_c)}(f)=\left(\frac{f_c}{1-\rho}\right)\frac{\sin^2\left[\frac{\pi f}{nf_c}(1-\rho)\right]}{(\pi f)^2}\left\{\sum_{i=1}^{n}s_i^2+2\sum_{i=1}^{n-1}\sum_{j=i+1}^{n}s_is_j\cos\left[(j-i)\frac{\omega T_c}{n}\right]\right\} \tag{D.4}$$

Since TOC([s],f_c) is a particular case of TCS, we can distinguish the following cases:

- Even $\mathrm{TOC}_{\sin}([s],\ f_c)$: In this case the modulating term coincides with that of $\mathrm{BOC}_{\sin}(f_s\,,f_c)$ for the even case, which was already shown in (B.11) and thus:

$$G_{\mathrm{TCS}([s],f_c)}(f)=\left(\frac{f_c}{1-\rho}\right)\frac{\sin^2\left[\frac{\pi f}{nf_c}(1-\rho)\right]}{(\pi f)^2}\frac{\sin^2\left(\frac{\pi f}{f_c}\right)}{\cos^2\left(\frac{\pi f}{nf_c}\right)}=\left(\frac{f_c}{1-\rho}\right)\left[\frac{\sin\left[\frac{\pi f}{nf_c}(1-\rho)\right]\sin\left(\frac{\pi f}{f_c}\right)}{\pi f\cos\left(\frac{\pi f}{nf_c}\right)}\right]^2 \tag{D.5}$$

- Odd $\mathrm{TOC}_{\sin}([s],\ f_c)$: In this case the modulating term coincides with that of $\mathrm{BOC}_{\sin}(f_s\,,f_c)$ for the odd case, which was already shown in (B.23). Thus:

$$G_{\mathrm{TCS}([s],f_c)}(f)=\left(\frac{f_c}{1-\rho}\right)\frac{\sin^2\left[\frac{\pi f}{nf_c}(1-\rho)\right]}{(\pi f)^2}\frac{\cos^2\left(\frac{\pi f}{f_c}\right)}{\cos^2\left(\frac{\pi f}{nf_c}\right)}=\left(\frac{f_c}{1-\rho}\right)\left[\frac{\sin\left[\frac{\pi f}{nf_c}(1-\rho)\right]\cos\left(\frac{\pi f}{f_c}\right)}{\pi f\cos\left(\frac{\pi f}{nf_c}\right)}\right]^2 \tag{D.6}$$

- Even $\mathrm{TOC}_{\cos}([s],\ f_c)$: In this case the modulating term coincides with that of $\mathrm{BOC}_{\cos}(f_s, f_c)$ for n even. This was already shown in (C.26). Accordingly,

$$G_{\mathrm{TCS}([s],f_c)}(f)=\left(\frac{f_c}{1-\rho}\right)\frac{\sin^2\left[\frac{\pi f}{nf_c}(1-\rho)\right]}{(\pi f)^2}\frac{4\sin^2\left(\frac{\pi f}{f_c}\right)\sin^2\left(\frac{\pi f}{nf_c}\right)}{\cos^2\left(\frac{2\pi f}{nf_c}\right)}=$$

$$=\left(\frac{f_c}{1-\rho}\right)\left[\frac{2\sin\left[\frac{\pi f}{nf_c}(1-\rho)\right]\sin\left(\frac{\pi f}{f_c}\right)\sin\left(\frac{\pi f}{nf_c}\right)}{\pi f\cos\left(\frac{\pi f}{nf_c}\right)}\right]^2 \tag{D.7}$$

- Odd $\mathrm{TOC}_{\cos}([s],\ f_c)$: In this case the modulating term coincides with that of $\mathrm{BOC}_{\cos}(f_s, f_c)$ for n odd which was already shown in (C.48). As a result:

$$G_{\mathrm{TCS}([s],f_c)}(f)=\left(\frac{f_c}{1-\rho}\right)\frac{\sin^2\left[\frac{\pi f}{nf_c}(1-\rho)\right]}{(\pi f)^2}\frac{4\cos^2\left(\frac{\pi f}{f_c}\right)\sin^2\left(\frac{\pi f}{nf_c}\right)}{\cos^2\left(\frac{2\pi f}{nf_c}\right)}=$$

$$=\left(\frac{f_c}{1-\rho}\right)\left[\frac{2\sin\left[\frac{\pi f}{nf_c}(1-\rho)\right]\cos\left(\frac{\pi f}{f_c}\right)\sin\left(\frac{\pi f}{nf_c}\right)}{\pi f\cos\left(\frac{\pi f}{nf_c}\right)}\right]^2 \tag{D.8}$$

which coincides with the well known expressions that can be found in the literature.

E Appendix. PSD of UTCS Signals

A sub-carrier waveform of great interest to model a generic signal is studied in this Appendix. In the next lines we will derive the power spectral density of an arbitrary Unilateral TCS(f_s, f_c, ρ) or UTCS for short. Unlike the TCS case that we studied in Appendix D, here the zero support is only on one of the sides of the sub-chips and not symmetrically placed.

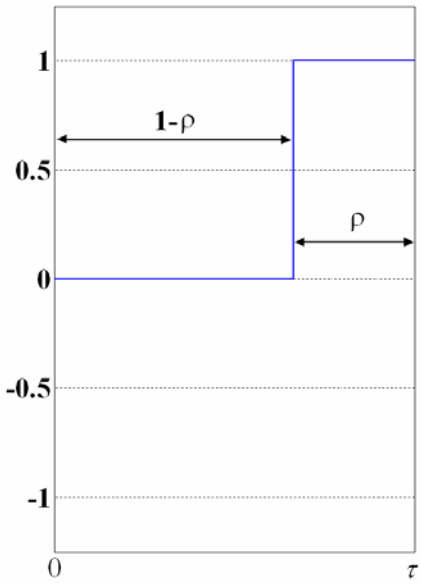

Figure E.1. Chip waveform of the UTCS modulation

According to the figure above, the Fourier transform of the signal is shown to be:

$$S_{\mathrm{UTCS}}(j\omega)=\sum_{k=1}^{n}\int_{\frac{(k-\rho)T_c}{n}}^{\frac{kT_c}{n}} s_k\, \mathrm{e}^{-j\omega t}\mathrm{d}t=\frac{2}{\omega}\sin\left[\rho\frac{\omega T_c}{2n}\right]\mathrm{e}^{\frac{j\omega\rho T_c}{2n}}\sum_{k=1}^{n}s_k\mathrm{e}^{-\frac{jk\omega T_c}{n}} \tag{E.1}$$

and in the frequency domain

$$S_{\mathrm{UTCS}}(f)=\frac{1}{\pi f}\sin\left[\rho\frac{\pi f}{nf_c}\right]\mathrm{e}^{\frac{j\pi f\rho}{nf_c}}\sum_{k=1}^{n}s_k\,\mathrm{e}^{-\frac{j2k\pi f}{nf_c}} \tag{E.2}$$

Thus, the general expression for the power spectral density of a generic UTCS signal will be:

$$G_{\mathrm{UTCS}([s],f_c)}(f)=\left(\frac{f_c}{1-\rho}\right)\frac{\sin^2\left[\rho\frac{\pi f}{nf_c}\right]}{(\pi f)^2}\left\|\sum_{k=1}^{n}s_k\mathrm{e}^{-j\frac{2\pi fk}{nf_c}}\right\|^2 \tag{E.3}$$

It must be noted that in the definition of the unilateral tertiary coded symbols, the parameter ρ represents the period of time with no zero dwell as was the case of the TCS. Again, we can recognize from (E.3) that the Power Spectral Density can be separated in the two usual terms, namely the pulse term and the modulation term:

$$G_{\mathrm{UTCS}([s],f_c)}(f)=G_{\mathrm{pulse}}^{\mathrm{UTCS}}(f)G_{\mathrm{Mod}}^{\mathrm{BCS}([s],f_c)}(f) \tag{E.4}$$

This expression is very convenient, since all the modulating terms derived in previous Appendixes can also be applied here.

F Appendix. PSD of 8-PSK sine-phased BOC Signals

In this Appendix we will derive the power spectral density of an 8-PSK signal in sine phasing. As we will see, the same expression derived by [A.R. Pratt and J.I.R. Owen, 2003] is obtained here using the more general definition of MCS that we have presented in this thesis.

As we saw in chapter 4.5.5.1 the Fourier transform of an arbitrary 8-PSK BOC_{sin} can be expressed as follows:

$$S_{BOC^8_{sin}(f_s,f_c)}(f) = \lambda_l S_{TOC_{sin}(f_s,f_c,\rho_l)} + \lambda_s S_{TOC_{sin}(f_s,f_c,\rho_s)} \tag{F.1}$$

with

$$\begin{aligned} \lambda_s &= 1 - \frac{1}{\sqrt{2}} \quad \rho_s = \frac{3}{4} \\ \lambda_l &= \frac{1}{\sqrt{2}} \quad \rho_l = \frac{1}{4} \end{aligned} \tag{F.2}$$

This function is graphically shown next:

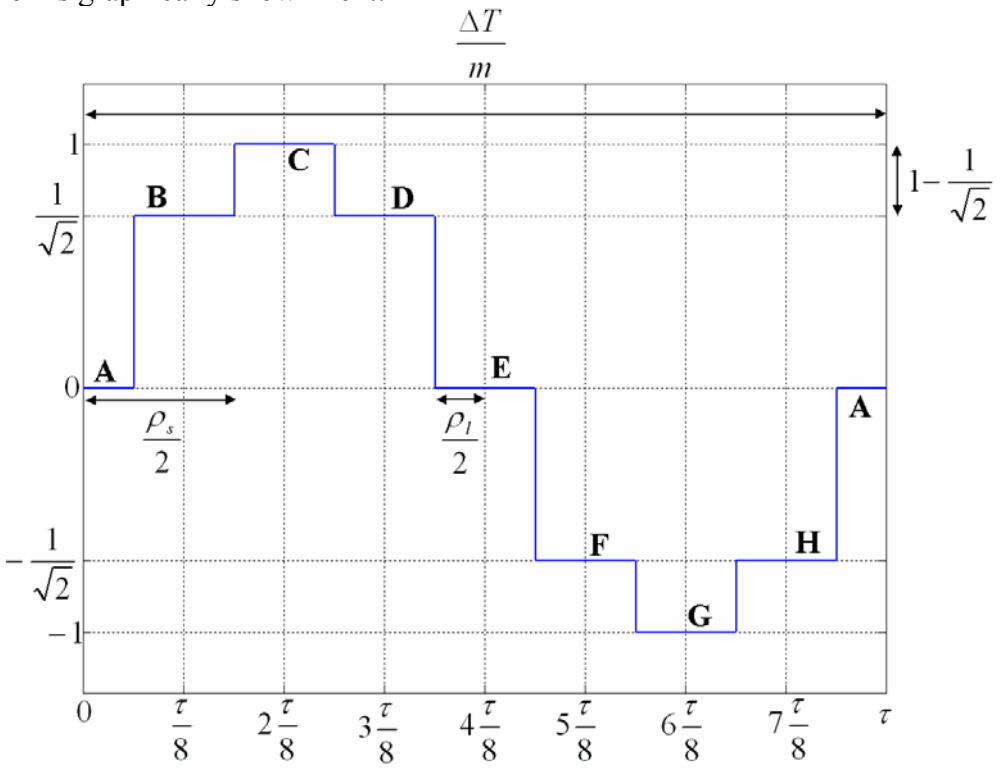

Figure F.1. Signal waveform of the sine-phased 8-PSK BOC(f_s, f_c) modulation

As we can recognize, the different amplitudes of the signal waveform correspond to the phase states of an 8-PSK modulation according to the next figure. Moreover, all the states of the constellation present the same probability of occurrence.

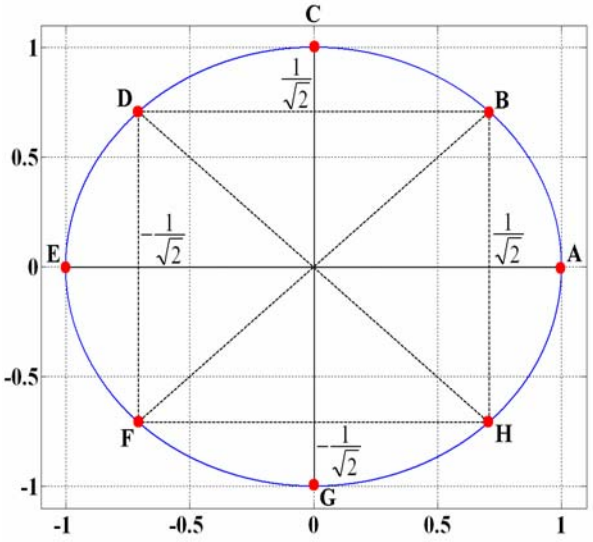

Figure F.2. Constellation points of the sine-phased 8-PSK BOC(f_s,f_c) modulation

Furthermore, the time series of the 8-PSK modulation can be expressed as the sum of the following two functions:

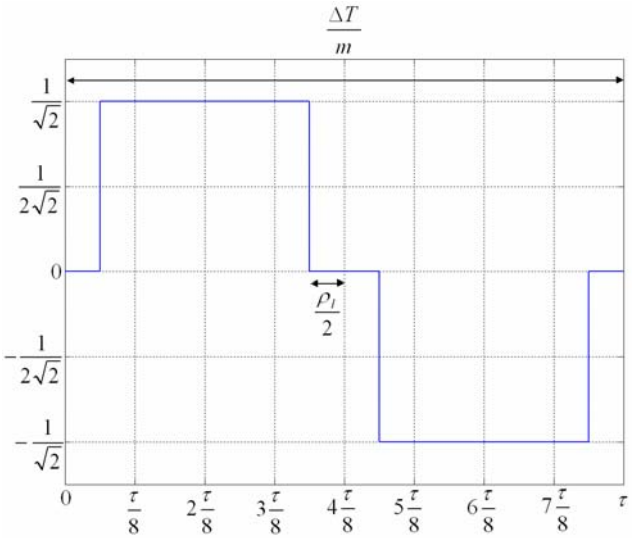

Figure F.3. Long Chip $S_{\mathrm{TOC}_{\sin}(f_s,f_c,\rho_l)}$ Function required to form 8-PSK BOC$_{sin}$(f_s, f_c)

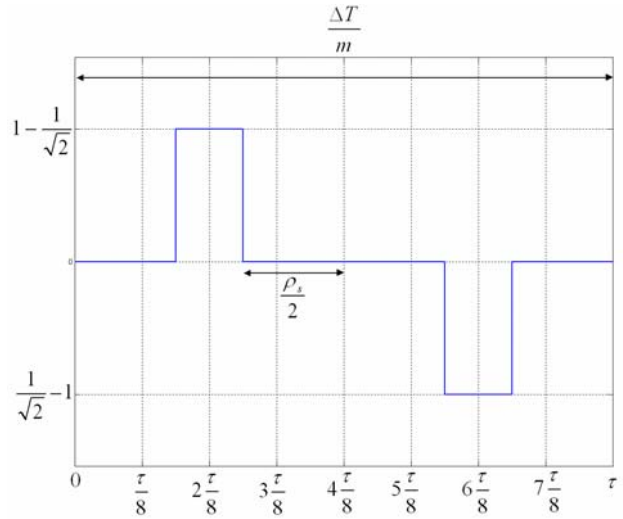

Figure F.4. Short Chip $S_{\mathrm{TOC}_{\sin}(f_s,f_c,\rho_s)}$ Function required to form 8-PSK BOC$_{sin}$(f_s, f_c)

For simplicity, we recall again the Fourier transform of the arbitrary TCS(f_s, f_c, δ):

$$S_{\mathrm{TCS}\left(f_s=\frac{nf_c}{2},f_c,\delta\right)}(f)=\frac{1}{\pi f}\sin\left[\frac{\pi f}{nf_c}(1-\rho)\right]\mathrm{e}^{\frac{j\pi f}{nf_c}}\sum_{k=1}^{n}s_k\,\mathrm{e}^{-\frac{j2k\pi f}{nf_c}} \tag{F.3}$$

Particularizing now (F.2) in (F.3), we obtain the following expression for the Fourier transform of the 8-PSK BOC modulation in sine phasing. As we can see, we have made use of the long and short chip functions $S_{\mathrm{TOC}_{\sin}(f_s,f_c,\rho_l)}$ and $S_{\mathrm{TOC}_{\sin}(f_s,f_c,\rho_s)}$, defined above.

$$S_{\mathrm{BOC}^8_{\sin}\left(f_s=\frac{nf_c}{2},f_c\right)}(f)=\left\{\lambda_l\sin\left[\frac{\pi f}{nf_c}(1-\rho_l)\right]+\lambda_s\sin\left[\frac{\pi f}{nf_c}(1-\rho_s)\right]\right\}\frac{1}{\pi f}\mathrm{e}^{\frac{j\pi f}{nf_c}}\sum_{k=1}^{n}s_k\,\mathrm{e}^{-\frac{j2k\pi f}{nf_c}} \tag{F.4}$$

As a result, the power spectral density of the sine-phased BOC$_8$(f_s,f_c) will be:

$$G_{\mathrm{BOC}^8_{\sin}\left(f_s=\frac{nf_c}{2},f_c\right)}(f)=\frac{f_c}{\rho'}\frac{\left\{\lambda_l\sin\left[\frac{\pi f}{nf_c}(1-\rho_l)\right]+\lambda_s\sin\left[\frac{\pi f}{nf_c}(1-\rho_s)\right]\right\}^2}{(\pi f)^2}\left\|\sum_{k=1}^{n}s_k\mathrm{e}^{-j\frac{2\pi fk}{nf_c}}\right\|^2 \tag{F.5}$$

or equivalently:

$$G_{\mathrm{BOC}^8_{\sin}\left(f_s=\frac{nf_c}{2},f_c\right)}(f)=\frac{f_c}{\rho'}\frac{\left\{\lambda_l\sin\left[\frac{\pi f}{nf_c}(1-\rho_l)\right]+\lambda_s\sin\left[\frac{\pi f}{nf_c}(1-\rho_s)\right]\right\}^2}{(\pi f)^2}\frac{\sin^2\left(\frac{\pi f}{f_c}\right)}{\cos^2\left(\frac{\pi f}{nf_c}\right)} \tag{F.6}$$

where we have used the results of Appendix B for the modulating term. Indeed, the square of the absolute value of the sum term is common to the usual BOC modulation in sine phasing. This term was derived in (B.11) for the even case. Additionally, the correction factor ρ' is shown to be:

$$\rho'=\frac{\rho_l+\rho_s}{2}=0.5 \tag{F.7}$$

According to this,

$$G_{\mathrm{BOC}^8_{\sin}\left(f_s=\frac{nf_c}{2},f_c\right)}(f)=2f_c\frac{\left\{\frac{1}{\sqrt{2}}\sin\left[\frac{3\pi f}{4nf_c}\right]+\left(1-\frac{1}{\sqrt{2}}\right)\sin\left[\frac{\pi f}{4nf_c}\right]\right\}^2}{(\pi f)^2}\frac{\sin^2\left(\frac{\pi f}{f_c}\right)}{\cos^2\left(\frac{\pi f}{nf_c}\right)} \tag{F.8}$$

and since in the case of the sine-phased TOC modulation $n=2f_s/f_c$, we can also express it as follows:

$$G_{\mathrm{BOC}^8_{\sin}(f_s,f_c)}(f)=2f_c\frac{\left\{\frac{1}{\sqrt{2}}\sin\left[\frac{3\pi f}{8f_s}\right]+\left(1-\frac{1}{\sqrt{2}}\right)\sin\left[\frac{\pi f}{8f_s}\right]\right\}^2}{(\pi f)^2}\frac{\sin^2\left(\frac{\pi f}{f_c}\right)}{\cos^2\left(\frac{\pi f}{2f_s}\right)} \tag{F.9}$$

which can be further simplified as:

$$G_{\mathrm{BOC}^{8}_{\mathrm{sin}}(f_s,f_c)}(f) = 2f_c\left[\frac{\sin\left(\frac{\pi f}{8f_s}\right)\left[1+\sqrt{2}\cos\left(\frac{\pi f}{4f_s}\right)\right]\sin\left(\frac{\pi f}{f_c}\right)}{\pi f\cos\left(\frac{\pi f}{2f_s}\right)}\right]^2 \qquad \text{(F.10)}$$

For the case of the odd sine-phased $\mathrm{BOC}_8(f_s,f_c)$ modulation, only the modulating term changes with respect to the above derived expression. Thus, since this is common to that of any $\mathrm{BOC}_{\mathrm{sin}}$ modulation with n odd, the general expression is shown to be:

$$G_{\mathrm{BOC}^{8}_{\mathrm{sin}}(f_s,f_c)}(f) = 2f_c\left[\frac{\sin\left(\frac{\pi f}{8f_s}\right)\left[1+\sqrt{2}\cos\left(\frac{\pi f}{4f_s}\right)\right]\cos\left(\frac{\pi f}{f_c}\right)}{\pi f\cos\left(\frac{\pi f}{2f_s}\right)}\right]^2 \qquad \text{(F.11)}$$

These expressions coincide perfectly with equivalent expressions that can be found in [A.R. Pratt and J.I.R. Owen, 2003].

G Appendix. PSD of 8-PSK cosine-phased BOC Signals

We derive in this Appendix the power spectral density of a generic 8-PSK BOC modulation with cosine phasing in an analogue way as we have done with its sine-phased counterpart. Indeed any 8-PSK signal can be expressed as a linear combination of TCS signals in the domain of the Fourier Transform as we have seen in Appendix F. This will be of course also the case for the 8-PSK BOC cosine-phased modulation, although as we will see next, the linear combination to build here is a little bit more complex since we need UTCS.

As we have seen in Appendix F, any sine-phased 8-PSK BOC modulation can be expressed as the sum of two sine-phased TOC signals. For the case of the cosine-phased 8-PSK BOC modulation however, five UPSK functions are needed. UPSK is the unilateral version of TPSK, which is a particular case of UTCS with BPSK-like shape. Indeed, an arbitrary 8-PSK $\mathrm{BOC}_{\cos}$ can be defined as:

$$S_{\mathrm{BOC}^8_{\cos}(f_s,f_c)}(f)=\sum_{i=1}^{5}\lambda_i\, S_{\mathrm{UTCS}(f_c,\rho_i)} \tag{G.1}$$

where

$$\begin{aligned}&\lambda_1=-1 \quad \lambda_2=1-\frac{1}{\sqrt{2}} \quad \lambda_3=\frac{1}{\sqrt{2}} \quad \lambda_4=\frac{1}{\sqrt{2}} \quad \lambda_5=1-\frac{1}{\sqrt{2}}\\ &\rho_1=1 \qquad \rho_2=\frac{7}{8} \qquad \rho_3=\frac{5}{8} \qquad \rho_4=\frac{3}{8} \qquad \rho_5=\frac{1}{8}\end{aligned} \tag{G.2}$$

being the chip waveform for the even case as follows:

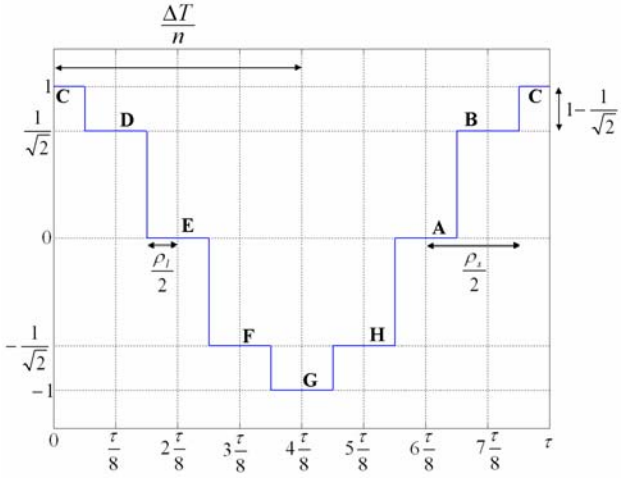

Figure G.1. Signal waveform of the cosine-phased 8-PSK BOC(f_s, f_c) modulation

Using now the general expression of the Fourier transform of an UTCS signal as given by (E.1), since $\mathrm{BOC}^8_{\cos}(f_s,f_c)$ can be expressed as the linear combination of UTCS signals, its Fourier transform will adopt the following form:

$$S_{\mathrm{BOC}^8_{\cos}\left(f_s=\frac{nf_c}{2},f_c\right)}(f)=\left\{-\sum_{i=1}^{5}\lambda_i \sin\left(\rho_i\frac{\pi f}{nf_c}\right)\mathrm{e}^{\frac{j\pi f\rho_i}{nf_c}}\right\}\frac{1}{\pi f}\sum_{k=1}^{n}s_k\,\mathrm{e}^{-\frac{j2k\pi f}{nf_c}} \tag{G.3}$$

yielding the power spectral density of the cosine-phased $\mathrm{BOC}_8(f_s,f_c)$ thus:

$$G_{\mathrm{BOC}^8_{\cos}\left(f_s=\frac{nf_c}{2},f_c\right)}(f)=\frac{f_c}{\rho'}\frac{\left\|-\sum_{i=1}^{5}\lambda_i\sin\left(\rho_i\frac{\pi f}{nf_c}\right)\mathrm{e}^{\frac{j\pi f\rho_i}{nf_c}}\right\|^2}{(\pi f)^2}\left\|\sum_{k=1}^{n}s_k\mathrm{e}^{-j\frac{2\pi fk}{nf_c}}\right\|^2 \tag{G.4}$$

This can be further simplified as shown next:

$$G_{\mathrm{BOC}^8_{\cos}\left(f_s=\frac{nf_c}{2},f_c\right)}(f)=\frac{f_c}{\rho'}\frac{\left\|\sum_{i=1}^{5}\lambda_i\sin\left(\rho_i\frac{\pi f}{nf_c}\right)\mathrm{e}^{\frac{j\pi f\rho_i}{nf_c}}\right\|^2}{(\pi f)^2}\frac{\sin^2\left(\frac{\pi f}{f_c}\right)}{\cos^2\left(\frac{\pi f}{nf_c}\right)} \tag{G.5}$$

since the square of the absolute value of the sum term, namely the modulating factor, is common to the even sine-phased BOC modulation, whose expression was derived in (B.11). Additionally, the correction factor ρ' is shown to be this time $1/2$ too. Consequently,

$$G_{\mathrm{BOC}^8_{\cos}\left(f_s=\frac{nf_c}{2},f_c\right)}(f)=2f_c\frac{\left\|\begin{array}{l}-\sin\left(\frac{\pi f}{nf_c}\right)\mathrm{e}^{j\frac{\pi f}{nf_c}}+\left(1-\frac{1}{\sqrt{2}}\right)\sin\left(\frac{7\pi f}{8nf_c}\right)\mathrm{e}^{j\frac{7\pi f}{8nf_c}}+\\+\frac{1}{\sqrt{2}}\sin\left(\frac{5\pi f}{8nf_c}\right)\mathrm{e}^{j\frac{5\pi f}{8nf_c}}+\frac{1}{\sqrt{2}}\sin\left(\frac{3\pi f}{8nf_c}\right)\mathrm{e}^{j\frac{3\pi f}{8nf_c}}+\\+\left(1-\frac{1}{\sqrt{2}}\right)\sin\left(\frac{\pi f}{8nf_c}\right)\mathrm{e}^{j\frac{\pi f}{8nf_c}}\end{array}\right\|^2}{(\pi f)^2}\frac{\sin^2\left(\frac{\pi f}{f_c}\right)}{\cos^2\left(\frac{\pi f}{nf_c}\right)} \tag{G.6}$$

Moreover, since $n=2f_s/f_c$, the previous expression can be further simplified as follows:

$$G_{\mathrm{BOC}^8_{\cos}(f_s,f_c)}(f)=2f_c\frac{\left\|\begin{array}{l}-\sin\left(\frac{\pi f}{2f_s}\right)\mathrm{e}^{j\frac{\pi f}{2f_s}}+\left(1-\frac{1}{\sqrt{2}}\right)\sin\left(\frac{7\pi f}{16f_s}\right)\mathrm{e}^{j\frac{7\pi f}{16f_s}}+\\+\frac{1}{\sqrt{2}}\sin\left(\frac{5\pi f}{16f_s}\right)\mathrm{e}^{j\frac{5\pi f}{16f_s}}+\frac{1}{\sqrt{2}}\sin\left(\frac{3\pi f}{16f_s}\right)\mathrm{e}^{j\frac{3\pi f}{16f_s}}+\\+\left(1-\frac{1}{\sqrt{2}}\right)\sin\left(\frac{\pi f}{16f_s}\right)\mathrm{e}^{j\frac{\pi f}{16f_s}}\end{array}\right\|^2}{(\pi f)^2}\frac{\sin^2\left(\frac{\pi f}{f_c}\right)}{\cos^2\left(\frac{\pi f}{2f_s}\right)} \tag{G.7}$$

We can further simplify this expression a little bit more yielding finally:

$$G_{\mathrm{BOC}^8_{\cos}(f_s,f_c)}(f)=2f_c\left[\frac{\left\{-1+\cos\left(\frac{\pi f}{8f_s}\right)\left[1-\left(4-2\sqrt{2}\right)\sin^2\left(\frac{\pi f}{8f_s}\right)\right]+2\sin^2\left(\frac{\pi f}{4f_s}\right)\right\}\sin\left(\frac{\pi f}{f_c}\right)}{\pi f\cos\left(\frac{\pi f}{2f_s}\right)}\right]^2 \tag{G.8}$$

Once we have obtained the expression for the even 8-PSK cosine-phased BOC modulation, we can easily derive the form for the odd one too using the results from other parts of this thesis. Indeed, the main advantage of expressing our signal as a linear combination of UTCS is that we can also derive the odd version using a modulating factor as suggested in this work.

Recalling thus the definition of even and odd in chapter 4.3.2, if for the even form we had a vector [-1,+1,+1,-1] for the odd case we should have [-1,1,1,-1,-1,1]. However, since we are expressing our signal with a sine-phased function whose generating vector is [-1,1], for the odd case we should then take [-1,1,-1]. Therefore, to calculate the expression for *n* odd, we simply have to look at the modulating term of the odd sine-phased BOC modulation. Additionally, since the sine-phased is a linear combination of sine-phased TOC modulations, *n* will adopt the value $n = 2f_s / f_c$. Taking into account all these considerations, the power spectral density of $G_{\mathrm{BOC}^8_{\cos}(f_s,f_c)}(f)$ for *n* odd is shown to adopt the following form:

$$G_{\mathrm{BOC}^8_{\cos}(f_s,f_c)}(f) = 2f_c \left[\frac{\left\{ -1 + \cos\left(\frac{\pi f}{8f_s}\right)\left[1 - \left(4 - 2\sqrt{2}\right)\sin^2\left(\frac{\pi f}{8f_s}\right)\right] + 2\sin^2\left(\frac{\pi f}{4f_s}\right)\right\}\cos\left(\frac{\pi f}{f_c}\right)}{\pi f \cos\left(\frac{\pi f}{2f_s}\right)} \right]^2 \tag{G.9}$$

H Appendix. Equivalent C/N_0 in presence of Interference

This Appendix derives some expressions of interest for the Equivalent Carrier to Noise Ratio in presence of RF interference. As we know, one of the main effects of RF interference is to reduce the C_d/N_0 of the desired signal *d*, as shown next:

$$\left(\frac{C_d}{N_0}\right)_{eff} = \frac{\frac{C_d}{N_0}\int_{-\beta_r/2}^{\beta_r/2} G_d(f)\,\mathrm{d}f}{\int_{-\beta_r/2}^{\beta_r/2} G_d(f)\,\mathrm{d}f + \frac{C_i}{N_0}\int_{-\beta_r/2}^{\beta_r/2} G_i(f)\,G_d(f)\,\mathrm{d}f} \tag{H.1}$$

where the subindex *i* refers to the interfering signal and *d* to the desired signal. We can further simplify this expression if we assume that all the power of the desired satellite fits into the bandwidth of the receiver, simplifying the effective C_d/N_0 to:

$$\left(\frac{C_d}{N_0}\right)_{eff} = \frac{\frac{C_d}{N_0}}{1 + \frac{C_i}{N_0}\int_{-\beta_r/2}^{\beta_r/2} G_i(f)\,G_d(f)\,\mathrm{d}f} \tag{H.2}$$

We can classify RF interference sources into narrowband interference and wideband interference. For the case of narrowband interference, the power spectral density of the interfering signal can be approximated as rectangular, such that:

$$G_i(f) = \frac{1}{2(f_u - f_l)} \quad \|f_l\| \le f \le \|f_u\| \tag{H.3}$$

Furthermore, if we assume that the whole interfering narrowband signal is in-band, then the effective C_d/N_0 will be:

$$\left(\frac{C_d}{N_0}\right)_{eff} = \frac{\frac{C_d}{N_0}}{1 + \frac{C_i}{N_0}\int_{-\beta_r/2}^{\beta_r/2} G_i(f)\,G_d(f)\,\mathrm{d}f} = \frac{\frac{C_d}{N_0}}{1 + \frac{C_i}{2N_0}\left[G_d(\frac{f_u+f_l}{2}) + G_d(-\frac{f_u+f_l}{2})\right]} \tag{H.4}$$

In addition, since the PSD is even,

$$G_d(\frac{f_u+f_l}{2}) = G_d(-\frac{f_u+f_l}{2}) \tag{H.5}$$

and assuming that the narrowband interference has a low frequency relative to the chip rate, we can use the following approximation for the particular case of BPSK(f_c):

$$G_{\mathrm{BPSK}(f_c)}\left(\frac{f_u+f_l}{2}\right) = f_c \left.\frac{\sin^2\left(\frac{\pi f}{f_c}\right)}{(\pi f)^2}\right|_{f=\frac{f_u+f_l}{2}} \approx \frac{1}{f_c} \tag{H.6}$$

Finally, as shown in [P. Ward, 1994], the effective C_d/N_0 will be for the case of a narrowband interferer:

$$\left(\frac{C_d}{N_0}\right)_{eff} \approx \frac{\frac{C_d}{N_0}}{1+\frac{C_i}{N_0 f_c}} = \frac{1}{\frac{1}{C_d/N_0}+\frac{C_i/C_d}{f_c}} \tag{H.7}$$

On the other hand, for the case of a wideband interferer, the expression to apply is the following:

$$\left(\frac{C_d}{N_0}\right)_{eff} = \frac{\frac{C_d}{N_0}\int_{-\beta_r/2}^{\beta_r/2} G_d(f)\,\mathrm{d}f}{\int_{-\beta_r/2}^{\beta_r/2} G_d(f)\,\mathrm{d}f + \frac{C_i}{N_0}\int_{-\beta_r/2}^{\beta_r/2} G_i(f)G_d(f)\,\mathrm{d}f} \tag{H.8}$$

where we can recognize the spectral separation coefficient (SSC) in the denominator as defined in chapter 5. In fact, the lower the value the SSC adopts, the more robust will be the signal against wideband and narrowband interferers as shown in the expressions above.

Using again the example of a BPSK signal, the multiple access interference will adopt the following form:

$$I_{ma}(f) = C_i\int_{-\beta_r/2}^{\beta_r/2} G_i(f)G_d(f)\,\mathrm{d}f \tag{H.9}$$

where for the particular case of the intra-system interference or for the case of an interferer matching the spectrum of the desired signal, BPSK in our example, we have:

$$G_i(f) = G_d(f) = f_c\frac{\sin^2\left(\frac{\pi f}{f_c}\right)}{(\pi f)^2} \tag{H.10}$$

As we can recognize, this term appears in the denominator of (H.8). Moreover, if we assume a large processing gain, the multiple access interference will only be significant around zero as we have shown in chapter 5 simplifying the interference to the following [J.J. Spilker, 1997a]:

$$I_{ma}(0) \approx C_i\int_0^{\infty}\left[f_c\frac{\sin^2\left(\frac{\pi f}{f_c}\right)}{(\pi f)^2}\right]^2\mathrm{d}f = \frac{2C_i}{3f_c} \tag{H.11}$$

As we expected, if we express now $2/3f_c$ in dB for a chip rate of 1.023 MHz, we obtain the famous figure of -61.8597 for the C/A Code Self SSC that we obtained in the simulations of chapter 5.

I Appendix. PSD of the AltBOC Modulation

In the next lines the power spectral density of the AltBOC modulation will be derived. We will analyze the most general expressions that apply when data and pilot are considered, using thus four different codes. First the expressions with no constant envelope are obtained and then the modified constant envelope version is studied and compared with that derived in [E. Rebeyrol et al., 2005].

As we have done in previous chapters and Appendixes, we will assume that the AltBOC signal is stationary in wide sense and that the PRN codes are ideal. As we saw in chapter 4.3.2, a slight modification of the codes is necessary to consider that the sub-carrier is included in the chip waveform when the ratio $\Phi = 2f_s/f_c$. Since Galileo will be transmitting AltBOC(15,10) in E5 and thus the ratio Φ is odd, we will pay special attention to this particular case deriving the expressions of AltBOC for both the even and odd cases.

The AltBOC modulation can be defined as follows [E. Rebeyrol et al., 2005]:

$$s_{\text{AltBOC}}(t) = \left(c_L^D + j\,c_L^P\right)c_s(t) + \left(c_U^D + j\,c_U^P\right)c_s^*(t) \tag{I.1}$$

where c_L^D is the lower data code, c_L^P is the lower pilot code, c_U^D the upper data code and c_U^P the upper pilot code. $s_{\text{AltBOC}}(t)$ can also be expressed as follows:

$$s_{\text{AltBOC}}(t) = C_u(t)\,m(t) + C_l(t)\,n(t) \tag{I.2}$$

where

$$\begin{aligned} C_u(t) &= c_U^D(t) + j\,c_U^P(t) \\ C_l(t) &= c_L^D(t) + j\,c_L^P(t) \end{aligned} \tag{I.3}$$

and

$$\begin{aligned} m(t) &= a(t) + j\,b(t) = \text{sign}\left[\cos(2\pi f_S t)\right] + j\,\text{sign}\left[\sin(2\pi f_S t)\right] \\ n(t) &= a(t) - j\,b(t) = \text{sign}\left[\cos(2\pi f_S t)\right] - j\,\text{sign}\left[\sin(2\pi f_S t)\right] \end{aligned} \tag{I.4}$$

Using now the expressions above, the autocorrelation of AltBOC yields:

$$\Re_{s_{\text{AltBOC}}}(\tau) = \begin{cases} \Re_{c_U^D}(\tau)\Re_a(\tau) + \Re_{c_U^D}(\tau)\Re_b(\tau) + \\ \Re_{c_U^P}(\tau)\Re_a(\tau) + \Re_{c_U^P}(\tau)\Re_b(\tau) + \\ \Re_{c_L^D}(\tau)\Re_a(\tau) + \Re_{c_L^D}(\tau)\Re_b(\tau) + \\ \Re_{c_L^P}(\tau)\Re_a(\tau) + \Re_{c_L^P}(\tau)\Re_b(\tau) \end{cases} \tag{I.5}$$

If we assume now again that the crosscorrelation between the different codes is equal to zero and that the complex crosscorrelations cancel each other out, the power spectral density of the AltBOC modulation is then shown to be:

$$G_{\text{AltBOC}}(f) = 4f_c\left|A(f)\right|^2 + 4f_c\left|B(f)\right|^2 = 4\left[G_A(f) + G_B(f)\right] \tag{I.6}$$

where $A(f)$ and $B(f)$ are the Fourier Transforms of $\text{sign}[\cos(2\pi f_s t)]$ and $\text{sign}[\sin(2\pi f_s t)]$ within a chip of length T_c. This means in other words that $G_A(f)$ and $G_B(f)$ are the power spectral densities of the cosine-phased and sine-phased BOC modulations that we have derived in Appendixes B and C. As we know, the expression of $G_A(f)$ and $G_B(f)$ depends on whether the ratio Φ is even or odd and thus to have the general expression of the AltBOC signal we also have to distinguish between these two cases.

If we recall now the results of (C.51) and (C.52) in Appendix C, for the ratio Φ even the normalized power spectral density of the cosine-phased BOC modulation was shown to be:

$$f_c\left|A(f)\right|^2 = G_{\text{BOC}_{\cos}(f_s,f_c)} = f_c\left[\frac{2\sin\left(\frac{\pi f}{f_c}\right)\sin^2\left(\frac{\pi f}{4f_s}\right)}{\pi f\cos\left(\frac{\pi f}{2f_s}\right)}\right]^2 \tag{I.7}$$

and for Φ odd

$$f_c\left|A(f)\right|^2 = G_{\text{BOC}_{\cos}(f_s,f_c)} = f_c\left[\frac{2\cos\left(\frac{\pi f}{f_c}\right)\sin^2\left(\frac{\pi f}{4f_s}\right)}{\pi f\cos\left(\frac{\pi f}{2f_s}\right)}\right]^2 \tag{I.8}$$

Equally, from Appendix B we know that for Φ even the normalized power spectral density of the sine-phased BOC modulation is shown to be:

$$f_c\left|B(f)\right|^2 = G_{\text{BOC}(f_s,f_c)} = f_c\left[\frac{\sin\left(\frac{\pi f}{f_c}\right)\sin\left(\frac{\pi f}{2f_s}\right)}{\pi f\cos\left(\frac{\pi f}{2f_s}\right)}\right]^2 \tag{I.9}$$

and for Φ odd

$$f_c\left|B(f)\right|^2 = G_{\text{BOC}(nf_c,f_c)} = f_c\left[\frac{\cos\left(\frac{\pi f}{f_c}\right)\sin\left(\frac{\pi f}{2f_s}\right)}{\pi f\cos\left(\frac{\pi f}{2f_c}\right)}\right]^2 \tag{I.10}$$

Using these results, the normalized power spectral density of the AltBOC modulation is then shown to adopt the following expression for Φ even:

$$G_{\text{AltBOC}}^{\Phi_{\text{even}}}(f) = 4\left[G_A^{\Phi_{even}}(f) + G_B^{\Phi_{even}}(f)\right] = 4f_c\left[\frac{\sin\left(\frac{\pi f}{f_c}\right)}{\pi f\cos\left(\frac{\pi f}{2f_s}\right)}\right]^2\left[4\sin^4\left(\frac{\pi f}{4f_s}\right) + \sin^2\left(\frac{\pi f}{2f_s}\right)\right] \tag{I.11}$$

which can be further simplified as follows:

$$G_{\text{AltBOC}}^{\Phi_{\text{even}}}(f) = 8f_c\left[\frac{\sin\left(\frac{\pi f}{f_c}\right)}{\pi f\cos\left(\frac{\pi f}{2f_s}\right)}\right]^2\left\{1-\cos\left(\frac{\pi f}{2f_s}\right)\right\} \tag{I.12}$$

which coincides perfectly with the expression derived in [E. Rebeyrol et al., 2005]. If we do the same now for the odd case, we obtain the following expression:

$$G_{\text{AltBOC}}^{\Phi_{\text{odd}}}(f) = 4\left[G_A^{\Phi_{odd}}(f)+G_B^{\Phi_{odd}}(f)\right] = 4f_c\left[\frac{\cos\left(\frac{\pi f}{f_c}\right)}{\pi f\cos\left(\frac{\pi f}{2f_s}\right)}\right]^2\left[4\sin^4\left(\frac{\pi f}{4f_s}\right)+\sin^2\left(\frac{\pi f}{2f_s}\right)\right] \tag{I.13}$$

or equivalently,

$$G_{\text{AltBOC}}^{\Phi_{\text{odd}}}(f) = 8f_c\left[\frac{\cos\left(\frac{\pi f}{f_c}\right)}{\pi f\cos\left(\frac{\pi f}{2f_s}\right)}\right]^2\left\{1-\cos\left(\frac{\pi f}{2f_s}\right)\right\} \tag{I.14}$$

Once we have derived the general AltBOC expressions for the case of non-constant envelope, we concentrate now on the modified AltBOC modulation with constant envelope. In order to distinguish it from the general form, we will write the superindex *c* for constant envelope. As we have shown in chapter 4.8.1 the modified AltBOC signal waveform with constant envelope can be expressed as follows:

$$s_{\text{AltBOC}}^{c}(t) = \begin{cases} \left(c_L^D + j\,c_L^P\right)\left[sc_d(t) - j\,sc_d\left(t-\frac{T_s}{4}\right)\right] + \\ \left(c_U^D + j\,c_U^P\right)\left[sc_d(t) + j\,sc_d\left(t-\frac{T_s}{4}\right)\right] + \\ \left(\overline{c_L^D} + j\,\overline{c_L^P}\right)\left[sc_p(t) - j\,sc_p\left(t-\frac{T_s}{4}\right)\right] + \\ \left(\overline{c_U^D} + j\,\overline{c_U^P}\right)\left[sc_p(t) + j\,sc_p\left(t-\frac{T_s}{4}\right)\right] \end{cases} \tag{I.15}$$

where the superindex indicates constant envelope. Furthermore, T_s is the in inverse of the sub-carrier frequency. According to this expression, $s_{\text{AltBOC}}(t)$ can be further expanded as

$$s_{\text{AltBOC}}^{c}(t) = \begin{cases} c_L^D\,sc_d(t) - j\,c_L^D\,sc_d\left(t-\frac{T_s}{4}\right) + j\,c_L^P\,sc_d(t) + c_L^P\,sc_d\left(t-\frac{T_s}{4}\right) + \\ c_U^D\,sc_d(t) + j\,c_U^D\,sc_d\left(t-\frac{T_s}{4}\right) + j\,c_U^P\,sc_d(t) - c_U^P\,sc_d\left(t-\frac{T_s}{4}\right) + \\ \overline{c_L^D}\,sc_p(t) - j\,\overline{c_L^D}\,sc_p\left(t-\frac{T_s}{4}\right) + j\,\overline{c_L^P}\,sc_p(t) + \overline{c_L^P}\,sc_p\left(t-\frac{T_s}{4}\right) + \\ \overline{c_U^D}\,sc_p(t) + j\,\overline{c_U^D}\,sc_p\left(t-\frac{T_s}{4}\right) + j\,\overline{c_U^P}\,sc_p(t) - \overline{c_U^P}\,sc_p\left(t-\frac{T_s}{4}\right) \end{cases} \tag{I.16}$$

where

$$\overline{c_L^D} = c_U^D c_U^P c_L^P \qquad \overline{c_L^P} = c_U^D c_U^P c_L^D \qquad \overline{c_U^D} = c_L^D c_U^P c_L^P \qquad \overline{c_U^P} = c_U^D c_L^D c_L^P \tag{I.17}$$

and the data and pilot sub-carriers can be expressed as:

$$sc_d(t) = \left\{ \frac{\sqrt{2}}{4}\text{sign}\left[\cos\left(2\pi f_S t - \frac{\pi}{4}\right)\right] + \frac{1}{2}\text{sign}\left[\cos\left(2\pi f_S t\right)\right] + \frac{\sqrt{2}}{4}\text{sign}\left[\cos\left(2\pi f_S t + \frac{\pi}{4}\right)\right] \right. \tag{I.18}$$

$$sc_p(t) = \left\{ -\frac{\sqrt{2}}{4}\text{sign}\left[\cos\left(2\pi f_S t - \frac{\pi}{4}\right)\right] + \frac{1}{2}\text{sign}\left[\cos\left(2\pi f_S t\right)\right] - \frac{\sqrt{2}}{4}\text{sign}\left[\cos\left(2\pi f_S t + \frac{\pi}{4}\right)\right] \right. \tag{I.19}$$

To facilitate now the analyses in the next lines let us rename the following signals in line with the approach followed in [E. Rebeyrol et al., 2005]. Thus:

$$\begin{aligned} sc_d^*(t) &= sc_d(t) \\ sc_d^{**}(t) &= sc_d\left(t - \frac{T_s}{4}\right) \\ sc_p^*(t) &= sc_p(t) \\ sc_p^{**}(t) &= sc_p\left(t - \frac{Ts}{4}\right) \end{aligned} \tag{I.20}$$

If we calculate now the autocorrelation function of $\Re^c_{\text{AltBOC}}(\tau)$, we can clearly recognize that most of the terms cancel out since we have assumed that the codes are ideally orthogonal with each other. Additionally, the cross-correlation between the data and pilot sub-carriers, namely sc_d and sc_p, will also be zero. In addition, the cross-correlations of each data and pilot sub-carrier correlates to zero with a delayed version of themselves by $T_s / 4$ (and actually also with $3T_s / 4$). As a result, $\Re^c_{\text{AltBOC}}(\tau)$ will simplify as follows:

$$\Re^c_{\text{AltBOC}}(\tau) = \begin{cases} \Re_{c_L^D sc_d^*}(\tau) + \Re_{c_L^D sc_d^{**}}(\tau) + \Re_{c_L^P sc_d^*}(\tau) + \Re_{c_L^P sc_d^{**}}(\tau) + \\ \Re_{c_U^D sc_d^*}(\tau) + \Re_{c_U^D sc_d^{**}}(\tau) + \Re_{c_U^P sc_d^*}(\tau) + \Re_{c_U^P sc_d^{**}}(\tau) + \\ \Re_{\overline{c}_L^D sc_p^*}(\tau) + \Re_{\overline{c}_L^D sc_p^{**}}(\tau) + \Re_{\overline{c}_L^P sc_p^*}(\tau) + \Re_{\overline{c}_L^P sc_p^{**}}(\tau) + \\ \Re_{\overline{c}_U^D sc_p^*}(\tau) + \Re_{\overline{c}_U^D sc_p^{**}}(\tau) + \Re_{\overline{c}_U^P sc_p^*}(\tau) + \Re_{\overline{c}_U^P sc_p^{**}}(\tau) \end{cases} \tag{I.21}$$

Since all the codes are of the same length and they do ideally correlate as expected from ideal random codes, the power spectral density of the modified constant envelope AltBOC modulation can be expressed as shown next:

$$G^c_{\text{AltBOC}}(f) = 4f_c\left|SC_d^*(f)\right|^2 + 4f_c\left|SC_d^{**}(f)\right|^2 + 4f_c\left|SC_p^*(f)\right|^2 + 4f_c\left|SC_p^{**}(f)\right|^2 \tag{I.22}$$

or also

$$G^c_{\text{AltBOC}}(f) = 4\left[G_d^*(f) + G_d^{**}(f) + G_p^*(f) + G_p^{**}(f)\right] \tag{I.23}$$

where $SC_d^*(f)$, $SC_d^{**}(f)$, $SC_p^*(f)$ and $SC_p^{**}(f)$ are the Fourier Transforms of $sc_d^*, sc_d^{**}, sc_p^*$ and sc_p^{**} respectively and consequently $G_d^*(f), G_d^{**}(f), G_p^*(f)$ and $G_p^{**}(f)$ are the respective power spectral densities. We recall that the subindexes *d* and *p* indicate whether we refer to the data or pilot carrier and the super-index whether we work with the prompt or the delayed version. To make progress in our derivations it is necessary to calculate first the Fourier Transforms of the data and pilot sub-carriers. Let us begin now with the calculation of the Fourier Transform of sc_d^* over [0, T_c]. To facilitate the understanding, we show again the shape of the AltBOC sub-carriers in the next figures:

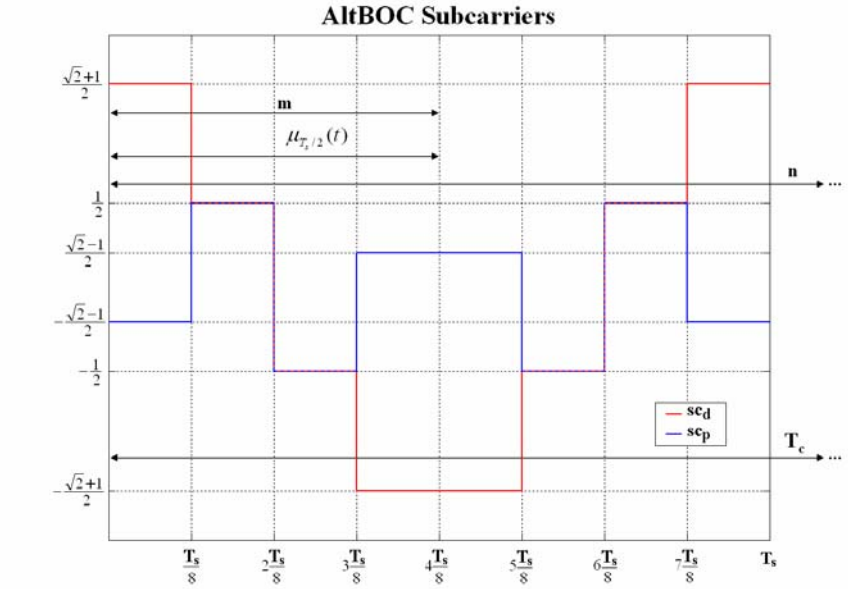

Figure I.1. Shapes of data and pilot sub-carriers

We can define now the prompt data sub-carrier piecewise as follows:

$$sc_d^*(t) = \sum_{m=0}^{n-1} (-1)^m \mu_{T_s/2}\left(t - m\frac{T_s}{2}\right) \tag{I.24}$$

where

$$\mu_{T_s/2}(t) = \begin{cases} \dfrac{\sqrt{2}+1}{2} & \left[0, \dfrac{T_s}{8}\right] \\ \dfrac{1}{2} & \left[\dfrac{T_s}{8}, \dfrac{T_s}{4}\right] \\ -\dfrac{1}{2} & \left[\dfrac{T_s}{4}, \dfrac{3T_s}{8}\right] \\ -\dfrac{\sqrt{2}+1}{2} & \left[\dfrac{3T_s}{8}, \dfrac{T_s}{2}\right] \end{cases} \tag{I.25}$$

It is important to remember that depending on whether the number of times that *m* fits in *n* (see previous Figure) is even or odd we will have the even version of the constant envelope AltBOC modulation or the odd version. Indeed, we can employ here again the figure $\Phi = 2 f_s / f_c$ to make this distinction, where Φ can be seen as the number of half periods within a chip.

To obtain the Fourier Transform of the prompt data sub-carrier, we derive first the Fourier Transform of the auxiliary signal $\mu_{T_s/2}$. This is shown to be:

$$FT\left\{\mu_{T_s/2}\left(t-m\frac{T_s}{2}\right)\right\}=\int_{m\frac{T_s}{2}}^{(m+1)\frac{T_s}{2}}\mu_{T_s/2}\left(t-m\frac{T_s}{2}\right)\mathrm{e}^{-2j\pi ft}\mathrm{d}t \tag{I.26}$$

which can be expanded as follows:

$$FT\left\{\mu_{T_s/2}\left(t-m\frac{t_s}{2}\right)\right\}=\begin{cases}\displaystyle\int_{m\frac{T_s}{2}}^{m\frac{T_s}{2}+\frac{T_s}{8}}\frac{\sqrt{2}+1}{2}\,\mathrm{e}^{-2j\pi ft}\mathrm{d}t+\int_{m\frac{T_s}{2}+\frac{T_s}{8}}^{m\frac{T_s}{2}+\frac{T_s}{4}}\frac{1}{2}\mathrm{e}^{-2j\pi ft}\mathrm{d}t- \\ \displaystyle-\int_{m\frac{T_s}{2}+\frac{T_s}{4}}^{m\frac{T_s}{2}+\frac{3T_s}{8}}\frac{1}{2}\mathrm{e}^{-2j\pi ft}\mathrm{d}t-\int_{m\frac{T_s}{2}+\frac{T_s}{4}}^{m\frac{T_s}{2}+\frac{3T_s}{8}}\frac{\sqrt{2}+1}{2}\mathrm{e}^{-2j\pi ft}\mathrm{d}t\end{cases} \tag{I.27}$$

Fortunately this complex expression can be further simplified and adopts the following form:

$$FT\left\{\mu_{T_s/2}\left(t-m\frac{t_s}{2}\right)\right\}=-\frac{\mathrm{e}^{-2j\pi fm\frac{T_s}{2}}}{2j\pi f}\mathrm{e}^{-j\pi f\frac{T_s}{2}}\left[-\left(\sqrt{2}+1\right)\cos\left(\pi f\frac{T_s}{2}\right)+\sqrt{2}\cos\left(\pi f\frac{T_s}{4}\right)+1\right] \tag{I.28}$$

As a result, the Fourier Transform of the prompt data sub-carrier can be expressed in terms of the equation above as:

$$SC_d^*(f)=-\frac{\mathrm{e}^{-j\pi f\frac{T_s}{2}}}{2j\pi f}\left[-\left(\sqrt{2}+1\right)\cos\left(\pi f\frac{T_s}{2}\right)+\sqrt{2}\cos\left(\pi f\frac{T_s}{4}\right)+1\right]\sum_{m=0}^{n-1}(-1)^m\,\mathrm{e}^{-2j\pi fm\frac{T_s}{2}} \tag{I.29}$$

As we can immediately recognize, the sum term will be different depending on whether Φ is even or odd. In order to have first the most general expression of the constant envelope AltBOC modulation we will not develop this expression any further until all the terms contributing to the computation of AltBOC are obtained.

Summarizing, the power spectral density of the prompt data sub-carrier can be expressed for the general case as follows:

$$G_d^*(f)=\frac{f_c}{4\pi^2f^2}\left[-\left(\sqrt{2}+1\right)\cos\left(\pi f\frac{T_s}{2}\right)+\sqrt{2}\cos\left(\pi f\frac{T_s}{4}\right)+1\right]^2\left\|\sum_{m=0}^{n-1}(-1)^m\,\mathrm{e}^{-2j\pi fm\frac{T_s}{2}}\right\|^2 \tag{I.30}$$

It is interesting to note that a similar formulation is obtained using the MCS definitions of chapter 4.2.1. If we repeat now for the delayed data sub-carrier $sc_d^{**}(t)$ we have then:

$$sc_d^{**}(t)=\sum_{m=0}^{n-1}(-1)^m\mu_{T_s/2}\left(t-m\frac{T_s}{2}\right) \tag{I.31}$$

where in this case the $\mu_{T_s/2}$ function is defined as follows:

$$\mu_{T_s/2}(t)=\begin{cases}\dfrac{1}{2} & \left[0,\dfrac{T_s}{8}\right)\\ \dfrac{\sqrt{2}+1}{2} & \left(\dfrac{T_s}{8},\dfrac{3T_s}{8}\right)\\ \dfrac{1}{2} & \left(\dfrac{3T_s}{8},\dfrac{T_s}{2}\right]\end{cases} \tag{I.32}$$

so that,

$$FT\left\{\mu_{T_s/2}\left(t-m\frac{T_s}{2}\right)\right\}=\int_{m\frac{T_s}{2}}^{(m+1)\frac{T_s}{2}}\mu_{t_s/2}\left(t-m\frac{T_s}{2}\right)\mathrm{e}^{-2j\pi ft}dt=-\frac{\mathrm{e}^{-2j\pi fm\frac{T_s}{2}}}{2j\pi f}\mathrm{e}^{-j\pi f\frac{T_s}{2}}\begin{bmatrix}-j\sin\left(\pi f\dfrac{T_s}{2}\right)\\ -j\sqrt{2}\sin\left(\pi f\dfrac{T_s}{4}\right)\end{bmatrix} \tag{I.33}$$

and therefore

$$SC_d^{**}(f)=-\frac{\mathrm{e}^{-j\pi f\frac{T_s}{2}}}{2j\pi f}\left[-j\sin\left(\pi f\frac{T_s}{2}\right)-j\sqrt{2}\sin\left(\pi f\frac{T_s}{4}\right)\right]\sum_{m=0}^{n-1}(-1)^m\mathrm{e}^{-2j\pi fm\frac{T_s}{2}} \tag{I.34}$$

As we can see, the sum term of the expression above is similar to that of the prompt data sub-carrier adopting the power spectral density of the delayed data sub-carrier the following form in the general case:

$$G_d^{**}(f)=\frac{f_c}{4\pi^2f^2}\left[\sin\left(\pi f\frac{T_s}{2}\right)+\sqrt{2}\sin\left(\pi f\frac{T_s}{4}\right)\right]^2\left\|\sum_{m=0}^{n-1}(-1)^m\mathrm{e}^{-2j\pi fm\frac{T_s}{2}}\right\|^2 \tag{I.35))}$$

We repeat now for the prompt pilot sub-carrier $sc_p^*(t)$ in a similar way:

$$sc_p^*(t)=\sum_{m=0}^{n-1}(-1)^m\mu_{T_s/2}\left(t-m\frac{T_s}{2}\right) \tag{I.36}$$

with

$$\mu_{T_s/2}(t)=\begin{cases}-\dfrac{\sqrt{2}-1}{2} & \left[0,\dfrac{T_s}{8}\right)\\ \dfrac{1}{2} & \left(\dfrac{T_s}{8},\dfrac{T_s}{4}\right)\\ -\dfrac{1}{2} & \left(\dfrac{T_s}{4},\dfrac{3T_s}{8}\right)\\ \dfrac{\sqrt{2}-1}{2} & \left(\dfrac{3T_s}{8},\dfrac{T_s}{2}\right]\end{cases} \tag{I.37}$$

According to this, the Fourier Transform can be obtained from:

$$FT\left\{\mu_{T_s/2}\left(t-m\frac{T_s}{2}\right)\right\}=-\frac{\mathrm{e}^{-2j\pi fm\frac{T_s}{2}}}{2j\pi f}\mathrm{e}^{-j\pi f\frac{T_s}{2}}\left[\left(\sqrt{2}-1\right)\cos\left(\pi f\frac{T_s}{2}\right)-\sqrt{2}\cos\left(\pi f\frac{T_s}{4}\right)+1\right] \tag{I.38}$$

yielding thus:

$$SC_p^*(f) = -\frac{\mathrm{e}^{-j\pi f\frac{T_s}{2}}}{2j\pi f}\left[\left(\sqrt{2}-1\right)\cos\left(\pi f\frac{T_s}{2}\right)-\sqrt{2}\cos\left(\pi f\frac{T_s}{4}\right)+1\right]\sum_{m=0}^{n-1}(-1)^m\,\mathrm{e}^{-2j\pi fm\frac{T_s}{2}} \quad \text{(I.39)}$$

As we can recognize, the sum term is fortunately again the same and thus the power spectral density will be:

$$G_p^*(f) = \frac{f_c}{4\pi^2 f^2}\left[\left(\sqrt{2}-1\right)\cos\left(\pi f\frac{T_s}{2}\right)-\sqrt{2}\cos\left(\pi f\frac{T_s}{4}\right)+1\right]^2\left\|\sum_{m=0}^{n-1}(-1)^m\,\mathrm{e}^{-2j\pi fm\frac{T_s}{2}}\right\|^2 \quad \text{(I.40)}$$

Finally, we calculate the Fourier Transform of the delayed pilot sub-carrier. This can be defined as follows:

$$sc_p^{**}(t) = \sum_{m=0}^{n-1}(-1)^m\mu_{T_s/2}\left(t-m\frac{T_s}{2}\right) \quad \text{(I.41)}$$

with

$$\mu_{T_s/2}(t) = \begin{cases} \frac{1}{2} & \left[0,\frac{T_s}{8}\right) \\ -\frac{\sqrt{2}-1}{2} & \left(\frac{T_s}{8},\frac{3T_s}{8}\right) \\ \frac{1}{2} & \left(\frac{3T_s}{8},\frac{T_s}{2}\right] \end{cases} \quad \text{(I.42)}$$

being its Fourier Transform defined as follows:

$$FT\left\{\mu_{T_s/2}\left(t-m\frac{T_s}{2}\right)\right\} = -\frac{\mathrm{e}^{-2j\pi fm\frac{T_s}{2}}}{2j\pi f}\,\mathrm{e}^{-j\pi f\frac{T_s}{2}}\left[-j\sin\left(\pi f\frac{T_s}{2}\right)+j\sqrt{2}\sin\left(\pi f\frac{T_s}{4}\right)\right] \quad \text{(I.43)}$$

such that:

$$SC_p^{**}(f) = -\frac{e^{-j\pi f\frac{T_s}{2}}}{2j\pi f}\left[-j\sin\left(\pi f\frac{T_s}{2}\right)+j\sqrt{2}\sin\left(\pi f\frac{T_s}{4}\right)\right]\sum_{m=0}^{n-1}(-1)^m\,\mathrm{e}^{-2j\pi fm\frac{T_s}{2}} \quad \text{(I.44)}$$

Once again, the sum term is the same as that of the previous derivations and we can easily express the power spectral density for the general case as:

$$G_p^{**}(f) = \frac{f_c}{4\pi^2 f^2}\left[-\sin\left(\frac{\pi f}{2f_s}\right)+\sqrt{2}\sin\left(\frac{\pi f}{4f_s}\right)\right]^2\left\|\sum_{m=0}^{n-1}(-1)^m\,\mathrm{e}^{-2j\pi fm\frac{T_s}{2}}\right\|^2 \quad \text{(I.45)}$$

Once we have obtained the individual elements that form the constant envelope AltBOC modulation, we can express the power spectral density for the general case as follows:

$$G_{\mathrm{AltBOC}}^c(f)(f) = 4\left[G_d^*(f)+G_d^{**}(f)+G_p^*(f)+G_p^{**}(f)\right] \quad \text{(I.46)}$$

or equivalently,

$$G^{c}_{\mathrm{AltBOC}}(f)=\frac{f_c}{\pi^2 f^2}\left\{\begin{array}{l}\left[-\left(\sqrt{2}+1\right)\cos\left(\frac{\pi f}{2f_s}\right)+\sqrt{2}\cos\left(\frac{\pi f}{4f_s}\right)+1\right]^2+\\ +\left[\sin\left(\frac{\pi f}{2f_s}\right)+\sqrt{2}\sin\left(\frac{\pi f}{4f_s}\right)\right]^2+\\ +\left[\left(\sqrt{2}-1\right)\cos\left(\frac{\pi f}{2f_s}\right)-\sqrt{2}\cos\left(\frac{\pi f}{4f_s}\right)+1\right]^2+\\ +\left[-\sin\left(\frac{\pi f}{2f_s}\right)+\sqrt{2}\sin\left(\frac{\pi f}{4f_s}\right)\right]^2\end{array}\right\}\left\|\sum_{m=0}^{n-1}(-1)^m \mathrm{e}^{-2j\pi f m\frac{T_s}{2}}\right\|^2 \tag{I.47}$$

what can be further simplified to:

$$G^{c}_{\mathrm{AltBOC}}(f)=\frac{4}{\pi^2 f^2 T_c}\left[\cos^2\left(\frac{\pi f}{2f_s}\right)-\cos\left(\frac{\pi f}{2f_s}\right)-2\cos\left(\frac{\pi f}{2f_s}\right)\cos\left(\frac{\pi f}{4f_s}\right)+2\right]\left\|\sum_{m=0}^{n-1}(-1)^m \mathrm{e}^{-2j\pi f m\frac{T_s}{2}}\right\|^2 \tag{I.48}$$

Until now, all the derived expressions are valid for both the even and odd case. However, as we can immediately recognize from the expression derived above, the common sum term will be different depending on whether Φ is even or odd. In order to have a clearer view of the two cases to analyze, we present in the next figures how one could integrate the sub-carrier in the chip waveform for the two cases of Φ.

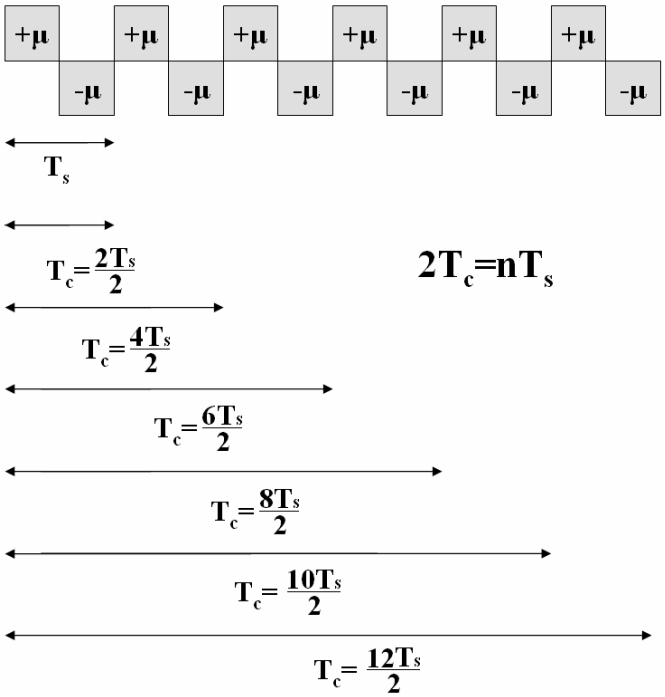

Figure I.2. Relationship between the sub-carrier frequency and the code frequency for the even AltBOC

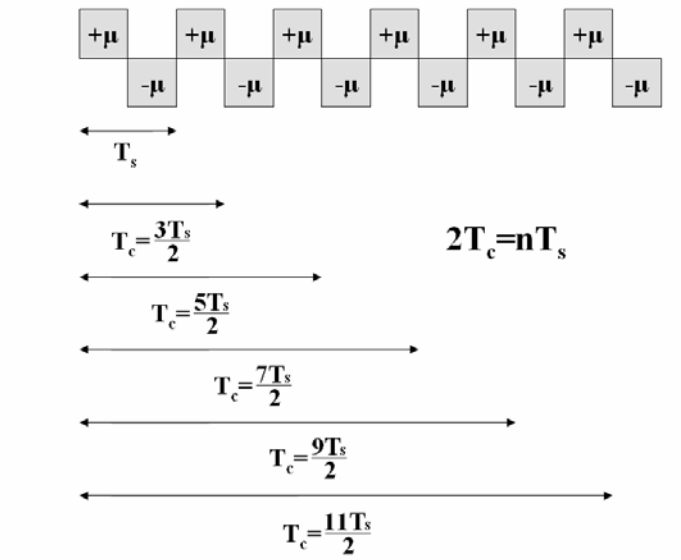

Figure I.3. Relationship between the sub-carrier frequency and the code frequency for the odd AltBOC

As we can see, for both cases the following relationship remains true:

$$n = 2 f_s / f_c \tag{I.49}$$

If we solve the sum term first for Φ even we have:

$$\sum_{m=0}^{n-1} (-1)^m \mathrm{e}^{-2j\pi f m\frac{T_s}{2}} = \frac{(-1)^n \mathrm{e}^{-j\pi f T_s n} - 1}{-\mathrm{e}^{-j\pi f T_s} - 1} = j\,\mathrm{e}^{-j(n-1)\pi f\frac{T_s}{2}} \frac{\sin\left(n\pi f\dfrac{T_s}{2}\right)}{\cos\left(\pi f\dfrac{T_s}{2}\right)} \tag{I.50}$$

since $(-1)^n$ for n even is always 1. We can further simplify the expression above if we recall the relationship between the sub-carrier and the code frequency. In fact, the square of the absolute value adopts the following form if Φ is even:

$$\left\| \sum_{m=0}^{n-1} (-1)^m \mathrm{e}^{-2j\pi f m\frac{T_s}{2}} \right\|^2 = \frac{\sin^2\left(\dfrac{\pi f}{f_c}\right)}{\cos^2\left(\dfrac{\pi f}{2f_s}\right)} \tag{I.51}$$

Equally, for the case of Φ odd we have:

$$\sum_{m=0}^{n-1} (-1)^m \mathrm{e}^{-2j\pi f m\frac{T_s}{2}} = \frac{(-1)^n \mathrm{e}^{-j\pi f T_s n} - 1}{-\mathrm{e}^{-j\pi f T_s} - 1} = \mathrm{e}^{-j(n-1)\pi f\frac{T_s}{2}} \frac{\cos\left(n\pi f\dfrac{T_s}{2}\right)}{\cos\left(\pi f\dfrac{T_s}{2}\right)} \tag{I.52}$$

since $(-1)^n$ for n odd is always -1. Moreover, since the relationship $n = 2 f_s / f_c$ is also valid when Φ is odd, we can further simplify the previous expression as shown next:

$$\left\| \sum_{m=0}^{n-1} (-1)^m \mathrm{e}^{-2j\pi f m\frac{T_s}{2}} \right\|^2 = \frac{\cos^2\left(\dfrac{\pi f}{f_c}\right)}{\cos^2\left(\dfrac{\pi f}{2f_s}\right)} \tag{I.53}$$

If we now put all the partial results of the lines above together, we can express the power spectral density of the modified even constant envelope AltBOC modulation as follows:

$$G_{\text{AltBOC}}^{\Phi_{\text{even}},c}(f)=\frac{4f_c}{\pi^2 f^2}\frac{\sin^2\left(\frac{\pi f}{f_c}\right)}{\cos^2\left(\frac{\pi f}{2f_s}\right)}\left[\cos^2\left(\frac{\pi f}{2f_s}\right)-\cos\left(\frac{\pi f}{2f_s}\right)-2\cos\left(\frac{\pi f}{2f_s}\right)\cos\left(\frac{\pi f}{4f_s}\right)+2\right] \tag{I.54}$$

while for the odd case we will have:

$$G_{\text{AltBOC}}^{\Phi_{\text{odd}},c}(f)=\frac{4f_c}{\pi^2 f^2}\frac{\cos^2\left(\frac{\pi f}{f_c}\right)}{\cos^2\left(\frac{\pi f}{2f_s}\right)}\left[\cos^2\left(\frac{\pi f}{2f_s}\right)-\cos\left(\frac{\pi f}{2f_s}\right)-2\cos\left(\frac{\pi f}{2f_s}\right)\cos\left(\frac{\pi f}{4f_s}\right)+2\right] \tag{I.55}$$

which is the well known expression of the normalized power spectral density of the constant envelope AltBOC modulation when Φ is odd. In the next figure we show the two analyzed versions of the AltBOC modulation, namely the general expression and the constant envelope modified version with a sub-carrier frequency of 15.345 MHz and a code frequency of 10.23 MHz.

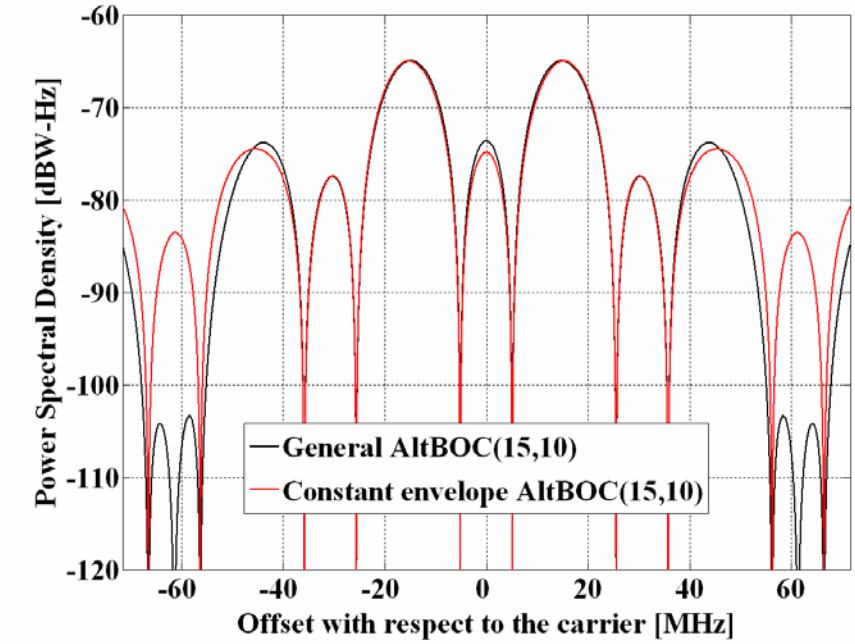

Figure I.4. Power Spectral Density of the general AltBOC(15,10) and the modified constant envelope AltBOC(15,10)

Equally, for an AltBOC(10,10) – thus with Φ even – the difference between the general AltBOC and the constant envelope solution is shown to be minimum:

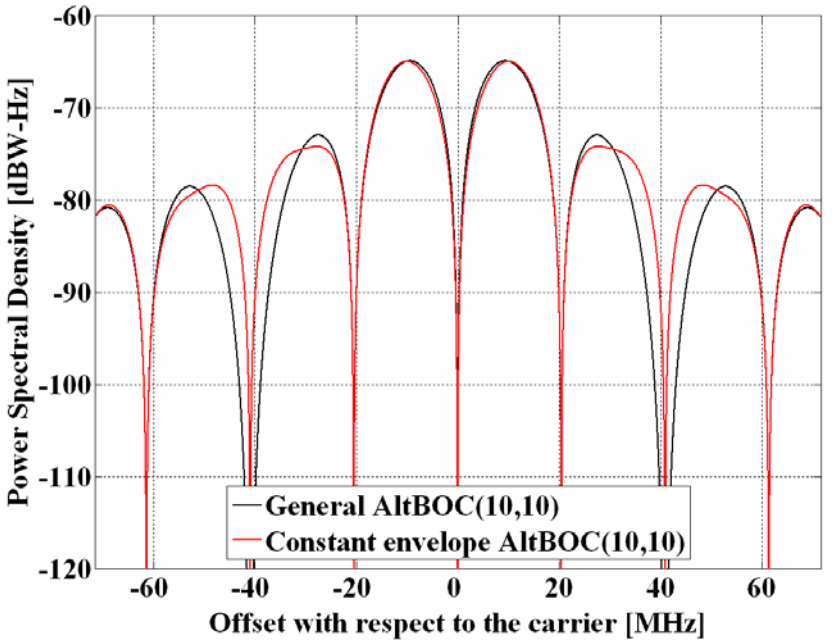

Figure I.5. Power Spectral Density of the general AltBOC(10,10) and the modified constant envelope AltBOC(10,10)

It is interesting to note that the power spectral densities of the general AltBOC modulation and the modified constant envelope AltBOC have similar shapes and only minor differences can be observed in the high order lobes. Indeed, the main and first side lobes are nearly identical being the differences lower than 1 dB. The only differences can be observed in the high frequency components and come from the extra terms that are needed to achieve constant envelope. Nonetheless in real implementations these would be filtered after amplification and thus for most of the bandwidths of interest we can state that there is no qualitative difference between both solutions regarding the spectrum. In terms of implementation, however, it is clear that the constant envelope solution is superior.

J Appendix. PSD of the CBCS modulation

In the next lines the power spectral density of the CBCS modulation will be derived. CBCS is a specific implementation of the MBOC modulation which receives for this particular case the name of CBOC. Thus, all the derivations of this chapter also apply for the CBOC implementation of MBOC that Galileo has selected for the E1 Open Service (OS).

The Composite Binary Coded Symbols modulation, or CBCS for short, is defined as the superposition of a BOC signal with a BCS by means of a modified and optimized Interplex scheme. This last sentence is of great importance because while CBCS specifies the way the signals are multiplexed at payload level, MBOC is more generic and does not say anything about how the time stream should look like.

In the most general case, CBCS($[s], f_c, \rho$) represents the superposition of a BOC(f_c, f_c) with a BCS($[s], f_c$) in such a way that the BCS component has a percentage ρ of power with respect to the total power of the multiplexed signal. Furthermore, the vector $[s]$ indicates the symbols that constitute the subchips of the BCS signal. Next figure depicts schematically the principle:

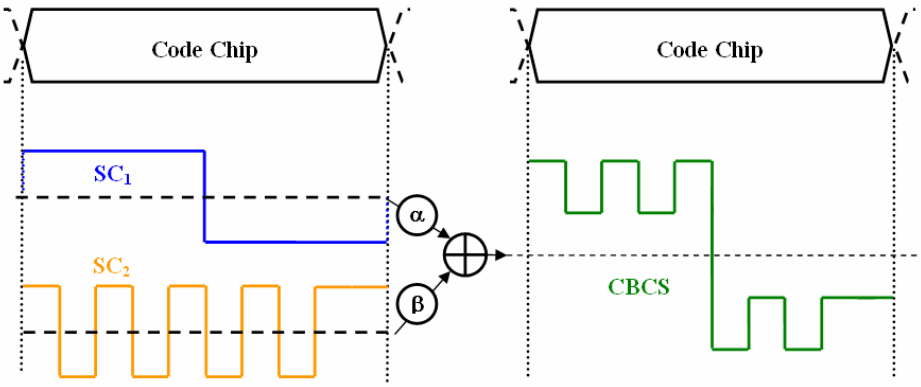

Figure J.1. CBCS chip waveform as a superposition of a BOC signal and a BCS signal

Unlike BPSK, BOC or BCS, the CBCS signal is formed by 4-level sub-carriers. As we have shown in chapter 4.8.4, other multiplex techniques such as the FH-Interplex could have also performed CBCS. However, with important drawbacks. In order to avoid them, a new scheme was proposed in [CNES, 2005]. This has been analyzed in chapter 7.7.9. For facility in the derivations we recall again the mathematical definition of CBCS in the time domain:

$$s(t) = A_1 \left[\begin{array}{c} \frac{c_D(t)}{2}\left[\cos\theta_1 \, s_{\mathrm{BOC}(f_c,f_c)}(t) + \cos\theta_2 \, s_{\mathrm{BCS}([s],f_c)}(t)\right] + \\ + \frac{c_P(t)}{2}\left[\cos\theta_1 \, s_{\mathrm{BOC}(f_c,f_c)}(t) - \cos\theta_2 \, s_{\mathrm{BCS}([s],f_c)}(t)\right] + \\ + j\, s_{\mathrm{PRS}}(t)\left(\frac{\sin\theta_1 + \sin\theta_2}{2}\right) + s_{\mathrm{IM}}(t) \end{array} \right] \tag{J.1}$$

$$s_{\mathrm{IM}}(t) = -j\, c_D(t)\, c_P(t)\, s_{\mathrm{PRS}}(t)\left(\frac{\sin\theta_1 - \sin\theta_2}{2}\right) \tag{J.2}$$

where,

- A_1 is the amplitude of the modulation envelope, sum of the OS data and pilot signals, PRS and the Inter-Modulation product IM,
- θ_1 and θ_2 describe the angular distance between the points of the 8-PSK modulation as depicted in Figure J.2,
- $s_{\mathrm{BOC}(f_c,f_c)}(t)$ represents the BOC(1,1) modulation with a chip rate f_c,
- $s_{\mathrm{BCS}([s],f_c)}(t)$ represents the BCS([s],1) modulation with subchips vector given by [s] and chip rate f_c,
- $s_{\mathrm{PRS}}(t)$ is the PRS modulation $\mathrm{BOC}_{\cos}(15,2.5)$,
- $s_{\mathrm{IM}}(t)$ is the Inter-Modulation product signal, and
- $c_D(t)$ and $c_P(t)$ are the PRN codes for the data and pilot channel of the OS.

The equation above is graphically shown in the figure below. We can recognize that compared with the BOC(1,1) Interplex baseline, two new phase states have appeared to account for the new BCS modulation waveform. Moreover, the quadrature component, namely PRS in the case of Galileo, presents a PSD that is not affected by the waveforms transmitted on the in-phase component.

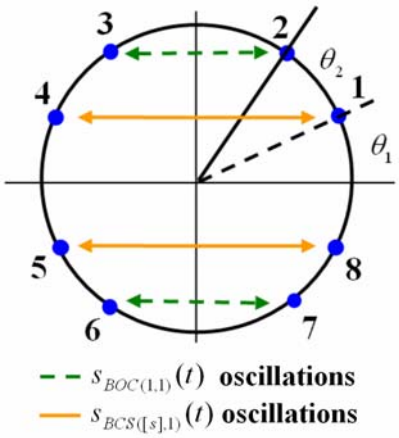

Figure J.2. Oscillation of the BOC and BCS signals in CBCS

It is also of interest to note that thanks to the introduction of the additional BCS, there will always be OS signal being emitted at any time for any combination of code chips. This makes the modulation more efficient and reduces the IM power consequently.

Let us now look at the data and pilot channels of the Open Service in detail. In fact, recalling the CBCS time definition, we can easily separate the data and pilot channels as follows:

$$\begin{aligned} s_D(t) &= A_1 \frac{c_D(t)}{2}\left[\cos\theta_1\, s_{\mathrm{BOC}(f_c,f_c)}(t) + \cos\theta_2\, s_{\mathrm{BCS}([s],f_c)}(t)\right] \\ s_P(t) &= A_1 \frac{c_P(t)}{2}\left[\cos\theta_1\, s_{\mathrm{BOC}(f_c,f_c)}(t) - \cos\theta_2\, s_{\mathrm{BCS}([s],f_c)}(t)\right] \end{aligned} \tag{J.3}$$

As we have shown in the introduction of chapter 4.1.1, the autocorrelation of a signal that is stationary in wide sense adopts the following form:

$$\Re_s(\tau) = E\left[s(t)s^*(t-\tau)\right] = \frac{1}{T_c}\sum_m \Re_c(m)\,\Re_p(\tau - mT_c) \tag{J.4}$$

According to this, if we use the notation of chapter 4, the autocorrelation function of the data channel can be expressed as

$$\Re_D^{\mathrm{OS}}(\tau) = \\ = \frac{A_1^2}{4}\left\{\begin{array}{l} \frac{1}{T_c}\cos^2(\theta_1)\sum_m \Re_{c_D}(m)\Re_{\mathrm{BOC}(f_c,f_c)}(\tau - mT_c) + \frac{1}{T_c}\cos^2(\theta_2)\sum_m \Re_{c_D}(m)\Re_{\mathrm{BCS}([s],f_c)}(\tau - mT_c) + \\ 2\cos(\theta_1)\cos(\theta_2)\sum_k\sum_j E\left[c_{D,k}c_{D,j}\right]E\left[p_{T_c}^{\mathrm{BOC}(f_c,f_c)}(t - kT_c - \theta)\,p_{T_c}^{\mathrm{BCS}([s],f_c)}(t - \tau - jT_c - \theta)\right] \end{array}\right. \tag{J.5}$$

where $p_{T_c}^{\mathrm{BOC}(f_c,f_c)}$ and $p_{T_c}^{\mathrm{BCS}([s],f_c)}$ represent the chip waveforms of BOC(f_c, f_c) and BCS([s], f_c) correspondingly, following the notation of chapter 4.1. This formulation can be further developed if the expectation operator is expressed in integral form as shown next:

$$\Re_D^{\mathrm{OS}}(\tau) = \\ = \frac{A_1^2}{4}\left\{\begin{array}{l} \frac{1}{T_c}\cos^2(\theta_1)\sum_m \Re_{c_D}(m)\Re_{\mathrm{BOC}(f_c,f_c)}(\tau - mT_c) + \frac{1}{T_c}\cos^2(\theta_2)\sum_m \Re_{c_D}(m)\Re_{\mathrm{BCS}([s],f_c)}(\tau - mT_c) + \\ 2\cos(\theta_1)\cos(\theta_2)\sum_m \Re_{c_D}(m)\frac{1}{T_c}\sum_k \int_0^{Tc} p_{T_c}^{\mathrm{BOC}(f_c,f_c)}(t - kT_c - \theta)\,p_{T_c}^{\mathrm{BCS}([s],f_c)}(t - \tau - kT_c + mT_c - \theta)\mathrm{d}t \end{array}\right. \tag{J.6}$$

or equivalently:

$$\Re_D^{\mathrm{OS}}(\tau) = \\ = \frac{A_1^2}{4}\left\{\begin{array}{l} \frac{1}{T_c}\cos^2(\theta_1)\sum_m \Re_{c_D}(m)\Re_{\mathrm{BOC}(f_c,f_c)}(\tau - mT_c) + \frac{1}{T_c}\cos^2(\theta_2)\sum_m \Re_{c_D}(m)\Re_{\mathrm{BCS}([s],f_c)}(\tau - mT_c) + \\ + 2\cos(\theta_1)\cos(\theta_2)\sum_m \frac{1}{T_c}\Re_{c_D}(m)\,\Re_{\mathrm{BOC}(f_c,f_c)/\mathrm{BCS}([s],f_c)}(\tau - mT_c) \end{array}\right. \tag{J.7}$$

If we further assume that the data codes show ideal properties, then $\Re_{c_D}(m) = \delta(m)$ and the autocorrelation of the data channel yields then:

$$\Re_D^{\mathrm{OS}}(\tau) = \frac{A_1^2}{4}\left\{\begin{array}{l} \frac{1}{T_c}\cos^2(\theta_1)\,\Re_{\mathrm{BOC}(f_c,f_c)}(\tau) + \frac{1}{T_c}\cos^2(\theta_2)\,\Re_{\mathrm{BCS}([s],f_c)}(\tau) \\ + \frac{2}{T_c}\cos(\theta_1)\cos(\theta_2)\,\Re_{\mathrm{BOC}(f_c,f_c)/\mathrm{BCS}([s],f_c)}(\tau) \end{array}\right. \tag{J.8}$$

We can repeat now the same steps for the pilot channel and arrive to a similar expression for the pilot autocorrelation:

$$\Re_P^{\mathrm{OS}}(\tau) = \frac{A_1^2}{4}\left\{\begin{array}{l} \frac{1}{T_c}\cos^2(\theta_1)\,\Re_{\mathrm{BOC}(f_c,f_c)}(\tau) + \frac{1}{T_c}\cos^2(\theta_2)\,\Re_{\mathrm{BCS}([s],f_c)}(\tau) \\ - \frac{2}{T_c}\cos(\theta_1)\cos(\theta_2)\,\Re_{\mathrm{BOC}(f_c,f_c)/\mathrm{BCS}([s],f_c)}(\tau) \end{array}\right. \tag{J.9}$$

Comparing the autocorrelation of the pilot OS with that of the data channel, we can recognize that there is only a sign difference in the cross-correlation term, which is in phase for the data channel and in anti-phase for the pilot channel. Now that we have derived the expressions for the data and pilot autocorrelations of the Open Service, the Power Spectral Densities of both channels can be obtained in the following form:

$$G_D^{\mathrm{OS}}(f)=\frac{A_1^2}{4}\begin{cases}\cos^2(\theta_1)f_c\left|S_{\mathrm{BOC}(f_c,f_c)}(f)\right|^2+\cos^2(\theta_2)f_c\left|S_{\mathrm{BCS}([s],f_c)}(f)\right|^2+\\ +2f_c\cos(\theta_1)\cos(\theta_2)\left\{S_{\mathrm{BOC}(f_c,f_c)}(f)S^*_{\mathrm{BCS}([s],f_c)}(f)+S^*_{\mathrm{BOC}(f_c,f_c)}(f)S_{\mathrm{BCS}([s],f_c)}(f)\right\}\end{cases} \tag{J.10}$$

which can be simplified as shown next:

$$G_D^{\mathrm{OS}}(f)=\frac{A_1^2}{4}\begin{cases}\cos^2(\theta_1)f_c\left|S_{\mathrm{BOC}(f_c,f_c)}(f)\right|^2+\cos^2(\theta_2)f_c\left|S_{\mathrm{BCS}([s],f_c)}(f)\right|^2+\\ +4f_c\cos(\theta_1)\cos(\theta_2)\mathrm{Re}\left\{S_{\mathrm{BOC}(f_c,f_c)}(f)S^*_{\mathrm{BCS}([s],f_c)}(f)\right\}\end{cases} \tag{J.11}$$

or equivalently:

$$G_D^{\mathrm{OS}}(f)=\frac{A_1^2}{4}\begin{cases}\cos^2(\theta_1)\,G_{\mathrm{BOC}(f_c,f_c)}(f)+\cos^2(\theta_2)\,G_{\mathrm{BCS}([s],f_c)}(f)+\\ +4f_c\cos(\theta_1)\cos(\theta_2)\,\mathrm{Re}\left\{S_{\mathrm{BOC}(f_c,f_c)}(f)\,S^*_{\mathrm{BCS}([s],f_c)}(f)\right\}\end{cases} \tag{J.12}$$

According to this, the power of the data channel will be

$$P_{\mathrm{OS}_D}=\frac{A_1^2}{4}\left[\cos^2\theta_1+\cos^2\theta_2+2r\cos(\theta_1)\cos(\theta_2)\right] \tag{J.13}$$

where, the cross-correlation between BOC(f_c,f_c) and BCS([s],f_c) is defined as follows:

$$r=\frac{1}{T_c}\int_{T_c}s_{\mathrm{BOC}(f_c,f_c)}(t)\;s_{\mathrm{BCS}([s],f_c)}(t)\mathrm{d}t=\frac{1}{T_c}\int_{-\infty}^{\infty}\left\{\begin{array}{l}S_{\mathrm{BOC}(f_c,f_c)}(f)S^*_{\mathrm{BCS}([s],f_c)}(f)+\\ +S^*_{\mathrm{BOC}(f_c,f_c)}(f)S_{\mathrm{BCS}([s],f_c)}(f)\end{array}\right\}\mathrm{d}f \tag{J.14}$$

If we solve now for the pilot channel, it can be shown that the power spectral density of the pilot OS will be:

$$G_P^{\mathrm{OS}}(f)=\frac{A_1^2}{4}\begin{cases}\cos^2(\theta_1)f_c\left|S_{\mathrm{BOC}(f_c,f_c)}(f)\right|^2+\cos^2(\theta_2)f_c\left|S_{\mathrm{BCS}([s],f_c)}(f)\right|^2+\\ -4f_c\cos(\theta_1)\cos(\theta_2)\,\mathrm{Re}\left\{S_{\mathrm{BOC}(f_c,f_c)}(f)S^*_{\mathrm{BCS}([s],f_c)}(f)\right\}\end{cases} \tag{J.15}$$

or expressed in terms of the power spectral density,

$$G_P^{\mathrm{OS}}(f)=\frac{A_1^2}{4}\begin{cases}\cos^2(\theta_1)\,G_{\mathrm{BOC}(f_c,f_c)}(f)+\cos^2(\theta_2)\,G_{\mathrm{BCS}([s],f_c)}(f)+\\ -4f_c\cos(\theta_1)\cos(\theta_2)\mathrm{Re}\left\{S_{\mathrm{BOC}(f_c,f_c)}(f)\,S^*_{\mathrm{BCS}([s],f_c)}(f)\right\}\end{cases} \tag{J.16}$$

such that

$$P_{\mathrm{OS}_P}=\frac{A_1^2}{4}\left[\cos^2(\theta_1)+\cos^2(\theta_2)-2r\cos(\theta_1)\cos(\theta_2)\right] \tag{J.17}$$

If we sum up now the power spectral densities of the data and pilot channels as given by (J.12) and (J.16), we obtain the general power expression for the power of the composite OS:

$$G_{\mathrm{OS}_D+\mathrm{OS}_P}(f)=\frac{A_1^2}{2}\left[\cos^2(\theta_1)\,G_{\mathrm{BOC}(f_c,f_c)}(f)+\cos^2(\theta_2)\,G_{\mathrm{BCS}([s],f_c)}(f)\right] \tag{J.18}$$

Thus, the total power of the OS signal, with data and pilot together, will be:

$$P_{\mathrm{OS}_D+\mathrm{OS}_P} = \frac{A_1^2}{2}\left[\cos^2(\theta_1)+\cos^2(\theta_2)\right] \tag{J.19}$$

adopting the normalized expression of the OS power spectral density the following form:

$$\overline{G}_{\mathrm{OS}_D+\mathrm{OS}_P}(f) = \frac{\frac{A_1^2}{2}\left[\cos^2(\theta_1)\,G_{\mathrm{BOC}(f_c,f_c)}(f)+\cos^2(\theta_2)\,G_{\mathrm{BCS}([s],f_c)}(f)\right]}{\frac{A_1^2}{2}\left[\cos^2(\theta_1)\int_{-\infty}^{\infty}G_{\mathrm{BOC}(f_c,f_c)}(f)\mathrm{d}f+\cos^2(\theta_2)\int_{-\infty}^{\infty}G_{\mathrm{BCS}([s],f_c)}(f)\mathrm{d}f\right]} \tag{J.20}$$

Since the phase states are sitting on the circle and the power spectral densities of the data and pilot channels are normalized to infinite bandwidth, we can express the normalized power spectral density of the OS signal as follows:

$$\overline{G}_{\mathrm{OS}_D+\mathrm{OS}_P}(f) = \frac{\cos^2(\theta_1)\,G_{\mathrm{BOC}(f_c,f_c)}(f)+\cos^2(\theta_2)\,G_{\mathrm{BCS}([s],f_c)}(f)}{\cos^2(\theta_1)+\cos^2(\theta_2)} \tag{J.21}$$

If we have a close look at the expression above, we can see that we can express the percentage of power that falls on the BCS signal as follows:

$$\rho = \frac{\cos^2(\theta_2)}{\cos^2(\theta_1)+\cos^2(\theta_2)} \tag{J.22}$$

Thus,

$$\overline{G}_{\mathrm{OS}_D+\mathrm{OS}_P}(f) = (1-\rho)G_{\mathrm{BOC}(f_c,f_c)}(f)+\rho\,G_{\mathrm{BCS}([s],f_c)}(f) \tag{J.23}$$

This means, that the total OS power spectral density can be defined as the linear combination of the PSDs of the two waveforms composing the CBCS signal, namely BOC(f_c, f_c) and BCS([s], f_c), weighted by the percentage ρ of power that is put on the BCS component.

If we divide now the expressions of the data and pilot power spectral densities given in (J.12) and (J.16) by the integrated data and pilot power, we obtain the normalized expressions:

$$\overline{G}_D^{\mathrm{OS}}(f) = \frac{\begin{cases}\cos^2(\theta_1)\,G_{\mathrm{BOC}(f_c,f_c)}(f)+\cos^2(\theta_2)\,G_{\mathrm{BCS}([s],f_c)}(f)+\\ +4f_c\,\cos(\theta_1)\cos(\theta_2)\,\mathrm{Re}\left\{S_{\mathrm{BOC}(f_c,f_c)}(f)\,S^*_{\mathrm{BCS}([s],f_c)}(f)\right\}\end{cases}}{\cos^2(\theta_1)+\cos^2(\theta_2)+2r\cos(\theta_1)\cos(\theta_2)} \tag{J.24}$$

where r indicates the correlation between BOC(f_c, f_c) and BCS([s], f_c) for zero offset. Equally, for the pilot channel we would have:

$$\overline{G}_P^{\mathrm{OS}}(f) = \frac{\begin{cases}\cos^2(\theta_1)\,G_{\mathrm{BOC}(f_c,f_c)}(f)+\cos^2(\theta_2)\,G_{\mathrm{BCS}([s],f_c)}(f)+\\ -4f_c\,\cos(\theta_1)\cos(\theta_2)\,\mathrm{Re}\left\{S_{\mathrm{BOC}(f_c,f_c)}(f)\,S^*_{\mathrm{BCS}([s],f_c)}(f)\right\}\end{cases}}{\cos^2(\theta_1)+\cos^2(\theta_2)-2r\cos(\theta_1)\cos(\theta_2)} \tag{J.25}$$

Another expression of interest is the power spectral density of the data and pilot channels with respect to the total OS power. Equally interesting is also to obtain the power of the

BOC(f_c, f_c) and BCS([s], f_c) component with respect to the total OS power. We derive next the corresponding expressions.

Let us study first the power of the data channel with respect to the total OS channel. Indeed, if we divide (J.13) by (J.18), we obtain the next relationship:

$$\frac{P_D^{\mathrm{OS}}}{P_{\mathrm{OS}_D+\mathrm{OS}_P}} = \frac{\int_{-\infty}^{\infty} G_D^{\mathrm{OS}}(f)\,\mathrm{d}f}{\int_{-\infty}^{\infty} G_{\mathrm{OS}_D+\mathrm{OS}_P}(f)\,\mathrm{d}f} = \frac{1}{2}\frac{\cos^2(\theta_1)+\cos^2(\theta_2)+2r\cos(\theta_1)\cos(\theta_2)}{\cos^2(\theta_1)+\cos^2(\theta_2)} \tag{J.26}$$

Equally, the percentage of pilot OS power with respect to the total OS power is:

$$\frac{P_P^{\mathrm{OS}}}{P_{\mathrm{OS}_D+\mathrm{OS}_P}} = \frac{\int_{-\infty}^{\infty} G_P^{\mathrm{OS}}(f)\,\mathrm{d}f}{\int_{-\infty}^{\infty} G_{\mathrm{OS}_D+\mathrm{OS}_P}(f)\,\mathrm{d}f} = \frac{1}{2}\frac{\cos^2(\theta_1)+\cos^2(\theta_2)-2r\cos(\theta_1)\cos(\theta_2)}{\cos^2(\theta_1)+\cos^2(\theta_2)} \tag{J.27}$$

To calculate the total power on the BOC(f_c, f_c) signal, we can use the equation (J.1) and thus,

$$P_{\mathrm{BOC}(f_c,f_c)} = A_1^2\frac{\cos^2(\theta_1)}{2} \tag{J.28}$$

so that the percentage of BOC(f_c, f_c) power with respect to the total OS power will adopt the following form:

$$\frac{P_{\mathrm{BOC}(f_c,f_c)}}{P_{\mathrm{OS}_D+\mathrm{OS}_P}} = 1-\rho = \frac{\cos^2(\theta_1)}{\cos^2(\theta_1)+\cos^2(\theta_2)} \tag{J.29}$$

If we repeat now for the BCS component,

$$P_{\mathrm{BCS}([s],f_c)} = A_1^2\frac{\cos^2(\theta_2)}{2} \tag{J.30}$$

and normalizing (J.30) to the total OS power, we have the percentage ρ of power on the BCS component:

$$\frac{P_{\mathrm{BCS}([s],f_c)}}{P_{\mathrm{OS}_D+\mathrm{OS}_P}} = \rho = \frac{\cos^2(\theta_2)}{\cos^2(\theta_1)+\cos^2(\theta_2)} \tag{J.31}$$

In the same manner, the useful power of the PRS for the quadrature signal can be easily obtained from the signal definition shown at the beginning of the Appendix. In fact:

$$P_{\mathrm{PRS}} = \frac{A_1^2}{4}(\sin\theta_1+\sin\theta_2)^2 \tag{J.32}$$

Equally, for the Inter-Modulation Product we can derive a similar expression:

$$P_{\mathrm{IM}} = \frac{A_1^2}{4}(\sin\theta_2-\sin\theta_1)^2 \tag{J.33}$$

Finally, if we sum up the power of all the desired signals plus the Inter-Modulation term, we find as expected that the CBCS modulation has constant envelope of amplitude A_1:

$$P_{\mathrm{OS}}+P_{\mathrm{PRS}}+P_{\mathrm{IM}} = A_1^2 \tag{J.34}$$

It is interesting to note that while for the BOC(f_c, f_c) Interplex the inter-modulation power only depends on one modulation index, namely m, in the case of CBCS both indexes θ_1 and

θ_2 have to be considered. This means in other words that fixing the IM power is easier with CBCS than it would be if only a BOC(f_c, f_c) were transmitted. The result is thus a more efficient control of the IM power since we have more degrees of freedom to play.

One final but important comment is that Interplex with only BOC(f_c, f_c) can be easily described taking θ_2 equal to π/2.

Once the most important equations describing CBCS have been derived, we study next how to calculate the multiplex parameters when we fix the percentage of power on the BCS component, the power split between data and pilot and the power split between the different signals. Moreover, it is important to note that the expressions derived above were obtained for infinite bandwidth differing thus the results slightly when filtering effects are considered.

According to the [Galileo SIS ICD, 2008] the power split between the OS data and pilot signals shall be 50/50 while the open signals and PRS should have the same power levels. The resulting equations system to solve is then:

$$\begin{cases} \dfrac{\cos^2(\theta_2)}{\cos^2(\theta_1)+\cos^2(\theta_2)} = \rho \\ \dfrac{A_1^2}{2}\left(\cos^2\theta_1+\cos^2\theta_2\right) = P_{\text{OS}} = \dfrac{1}{2} \\ \dfrac{A_1^2}{4}\left(\sin\theta_1+\sin\theta_2\right)^2 = P_{\text{PRS}} = \dfrac{1}{2} \end{cases} \tag{J.35}$$

where the first equation indicates the amount of power that is moved from BOC(f_c, f_c) to the BCS signal and the second and third equations represent the power ratios between the different signals. We can also observe that the equations above do not depend on the specific BCS vector [s] since they only account for power relationships. Nonetheless, as it could be expected, the real BCS vector plays indirectly an outstanding role in assessing if one signal is compatible with the rest of signals in the band or not. In fact, depending on how the specific BCS sequence looks like, the spectral overlapping with the other signals around will be different, determining thus the maximum amount of power ρ that can be put on its BCS part in order not to interfere.

Until now we have analyzed the case when the BCS signal is on both the data and pilot channels as this is the baseline of Galileo for the OS. Nevertheless, for some specific applications, allocating the high frequency components (thus the BCS signal) only on the pilot channel could be of interest. Indeed, the GPS implementation of MBOC, namely TMBOC, goes in this direction.

In order to have all the power of the BCS signal only on the pilot channel and still maintain constant envelope, the expression of the CBCS modulation has to be generalized. Accordingly, (J.1) and (J.2) can be slightly modified as shown next:

$$s(t) = \begin{cases} k_1 d_D(t) c_D(t) s_{\mathrm{BOC}(1,1)}(t) + c_P(t) \left\{ k_2 s_{\mathrm{BOC}(1,1)}(t) - k_3 s_{\mathrm{BCS}([s],1)}(t) \right\} + \\ + j d_{\mathrm{PRS}}(t) c_{\mathrm{PRS}}(t) \left\{ k_4 s_{\mathrm{PRS}}(t) + s_{\mathrm{IM}}(t) \right\} \end{cases} \quad \text{(J.36)}$$

where the constants k_1, k_2, k_3 and k_4 are calculated from

- the power split between data and pilot,
- the relationship of powers between OS and PRS,
- the percentage of power on the BCS signal with respect to the total OS power under the constraint that the phase points are on the unit circle, and
- accounting for the different filter losses of the signals due to bandlimiting.

Mathematically, all these conditions can be expressed as follows

$$\begin{aligned} \frac{k_3^2}{k_1^2 + k_2^2 + k_3^2} &= \rho \\ \frac{k_2^2 + k_3^2}{k_1^2} &= \xi \\ \frac{k_4^2}{k_1^2 + k_2^2 + k_3^2} &= 10^{\beta/10} \end{aligned} \quad \text{(J.37)}$$

where:

- ρ is the percentage of power on the BCS signal,
- ξ indicates the percentage of power that falls onto the pilot channel with respect to the data channel. Thus, if we have a power split of 50/50, $\xi = 1$ and for 75/25, $\xi = 3$,
- and β indicates the power difference between PRS and OS in dB, accounting for the different filter losses of both signals due to satellite bandlimiting.

It should be noted that this calculation ignores the effect of the correlation between the BOC(f_c, f_c) and BCS([s], f_c), which is introduced by virtue of the satellite bandlimiting. Additionally, since all the phase points have to be on the unit circle, we have:

$$\left.\begin{aligned} (k_1 + k_2 + k_3)^2 + (k_4 + \mathrm{IM}_1)^2 &= 1 \\ (k_1 + k_2 - k_3)^2 + (k_4 + \mathrm{IM}_2)^2 &= 1 \\ (k_1 - k_2 + k_3)^2 + (k_4 + \mathrm{IM}_3)^2 &= 1 \\ (k_1 - k_2 - k_3)^2 + (k_4 + \mathrm{IM}_4)^2 &= 1 \\ (-k_1 + k_2 + k_3)^2 + (k_4 + \mathrm{IM}_5)^2 &= 1 \\ (-k_1 + k_2 - k_3)^2 + (k_4 + \mathrm{IM}_6)^2 &= 1 \\ (-k_1 - k_2 + k_3)^2 + (k_4 + \mathrm{IM}_7)^2 &= 1 \\ (-k_1 - k_2 - k_3)^2 + (k_4 + \mathrm{IM}_8)^2 &= 1 \end{aligned}\right\} \Rightarrow \|s(t)\| = 1 \quad \text{(J.38)}$$

since the real component of the signal takes 8 values with equal probability, given as shown in the following table:

Table J.1. Value of the signal *s*(*t*) as a function of the different code inputs

$C_D(t)$	$D_D(t)$	$C_P(t)$	$\mathrm{Re}\{s(t)\}$
+1	+1	+1	$k_1+k_2+k_3$
+1	+1	-1	$k_1+k_2-k_3$
+1	-1	+1	$k_1-k_2+k_3$
+1	-1	-1	$k_1-k_2-k_3$
-1	+1	+1	$-k_1+k_2+k_3$
-1	+1	-1	$-k_1+k_2-k_3$
-1	-1	+1	$-k_1-k_2+k_3$
-1	-1	-1	$-k_1-k_2-k_3$

Additionally, the IM component $\mathrm{IM}=\{\mathrm{IM}_1,\mathrm{IM}_2,...,\mathrm{IM}_8\}$ must take the appropriate value to bring the phase plots to the unit circle. Note that this is true independently of the BCS component is in phase or in anti-phase. Finally, an extra constraint comes from the necessary condition that the Inter-Modulation signal has zero mean:

$$< s_{\mathrm{IM}}(t) >= \frac{1}{8}\sum_{i=1}^{8}\mathrm{IM}_i = 0 \tag{J.39}$$

If we put all the conditions together, we can see that we have totally twelve equations, namely (J.37), (J.38) and (J.39), and twelve unknowns to find, namely IM, k_1, k_2, k_3 and k_4. Unfortunately, while (J.36) covers more cases than (J.1) and (J.2), in general it is not possible to find an explicit expression for the coefficients k_1, k_2, k_3 and k_4.

We show next with an example how the parameters of the CBCS multiplex could be obtained for the hypothetical case that the CBOC implementation of MBOC would allocate the whole BOC(6,1) component on the pilot OS signal. As shown in chapter 4.7, the power ratio between the BCS signal, in this particular case BOC(6,1), and the total OS power is 1/11 at generation. This means that in reality the power after filtering in the satellite will be slightly lower on BOC(6,1). Moreover, let us assume that the PRS power would be 2 dB above the OS power at user level and that the effect of filtering in the satellite is also taken into account. This assumption is different from the baseline when OS and PRS have the same power.

If we solve now for CBOC(6,1,1/11) with all the BOC(6,1) power on the pilot channel, with equal power for pilot and data, with 1/11 of the OS power in the BOC(6,1) before bandlimiting, the composite signal may be defined by

$$s(t)=\begin{cases} 0.3959\,d_D\,c_{\mathrm{OS}}^{D}\,\mathrm{sign}\left(\sin\dfrac{2\pi t}{T_c}\right)+c_{\mathrm{OS}}^{P}\left\{0.3581\,\mathrm{sign}\left(\sin\dfrac{2\pi t}{T_c}\right)-0.1688\,\mathrm{sign}\left(\sin\dfrac{2\pi t}{T_c/6}\right)\right\}+ \\ +\,j\,d_{\mathrm{PRS}}\,c_{\mathrm{PRS}}\left\{0.7915\,\mathrm{sign}\left(\sin\dfrac{2\pi t}{T_{cPRS}/6}\right)+s_{\mathrm{IM}}(t)\right\} \end{cases} \tag{J.40}$$

where the signal $s_{IM}(t)$ is given by:

$$sc_{IM}(t) = \sum_{i=-\infty}^{\infty} a_{|i|_8} \operatorname{rect}(t - iT_c/8) \tag{J.41}$$

adopting $a_{|i|_8}$ the following values:

Table J.2. Values of the Inter-Modulation Signal (IM) to achieve a constant envelope

i	*a*
0	$-4.0614.10^{-1}$
1	$1.9393.10^{-2}$
2	$1.8690.10^{-1}$
3	$1.9985.10^{-1}$
4	$1.9985.10^{-1}$
5	$1.8690.10^{-1}$
6	$1.9393.10^{-2}$
7	$-4.0614.10^{-1}$

We show the Inter-Modulation signal next graphically:

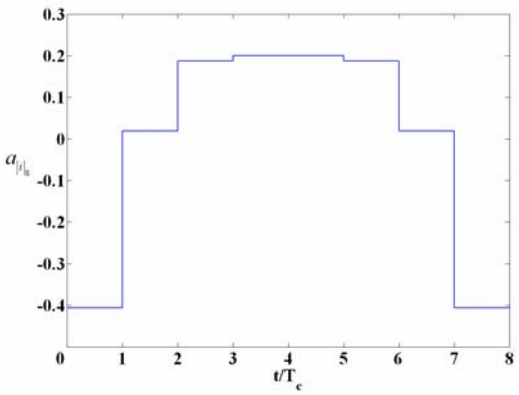

Figure J.3. Inter-Modulation Signal necessary to have a constant envelope when BOC(6,1) is only on the pilot channel

The phase states of the constellation are equally shown in the next figure. As we can see, the main effect is that the number of states has duplicated, what is of course a clear drawback. In addition, it is important to realize that this implementation of CBOC is not compliant with the MBOC spectrum definition since a cross term appears as shown in chapter 4.7.5.4.

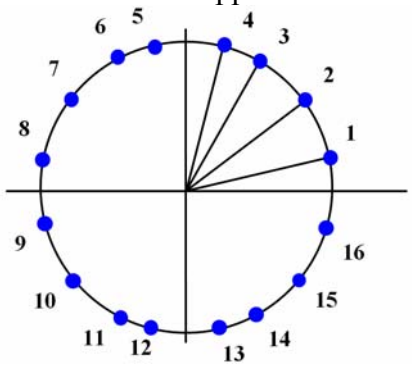

Figure J.4. CBOC 16-PSK modulation that results when all the BOC(6,1) component is placed on the pilot channel

K Appendix. Cramér Rao Lower Bound

The mean-squared error for any estimate of a nonrandom parameter has a lower bound, known in the literature as the Cramér-Rao lower bound or CRLB in short [J.-A. Avila-Rodriguez et al., 2006a]. The Cramér-Rao lower bound defines the ultimate accuracy of any estimation and shows the minimum code pseudorange variance we would have with the best possible receiver implementation. Indeed, the Cramér-Rao lower bound is nothing else than a different way of expressing the Gabor bandwidth which sets the physical limit of a signal for a given bandwidth. This last one is also known in the literature as the root mean square bandwidth.

In our particular case, we are interested in finding the bound of the matrix:

$$E\left[\varepsilon\varepsilon^T\right] = E\left[\left(\hat{\theta}-\theta\right)\left(\hat{\theta}-\theta\right)^T\right] \tag{K.1}$$

being ε the code delay error, θ the real code delay value and $\hat{\theta}$ its estimation. As it can be shown, the Cramér-Rao lower bound is deeply related to the Fisher information matrix F in the following form:

$$E\left[\varepsilon\varepsilon^T\right] \geq b(\theta)b^T(\theta) + \left[I + \nabla_\theta(b)\right]F^{-1}\left[I + \nabla_\theta(b)\right]^T \tag{K.2}$$

where $b(\theta)$ is the bias of the estimate θ and F is the already mentioned Fisher matrix defined by means of the Hessian matrix as follows

$$F = -E\left\{\nabla_\theta \nabla_\theta^T\left[\ln\left[P(\bar{x},\bar{y}/\theta)\right]\right]\right\} \tag{K.3}$$

It must be noted that according to this general definition, the Cramér-Rao lower bound also applies for the case of biased estimates in contrast to the way it is widely used in the general literature where the Cramér-Rao lower bound is understood as the minimum unbiased variance estimate bound.

Looking now at the bound of every parameter in particular, the Cramér-Rao lower bound can be expressed as follows:

$$E\left[\left(\hat{\theta}-\theta\right)^2\right] \geq b_i^2(\theta) + \left\{\left[I + \nabla_\theta(b)\right]F^{-1}\left[I + \nabla_\theta(b)\right]^T\right\}_{ii} \tag{K.4}$$

and for the case the estimator is unbiased, the bound simplifies then to

$$E\left[\left(\hat{\theta}-\theta\right)^2\right] \geq \left[F^{-1}\right]_{ii} \tag{K.5}$$

The most important conclusion that can be drawn from observing the equation above is that for the unbiased case, the estimator is not necessary for the computation of the bound. In fact, we only need the Fisher matrix to compute the CRLB, which only depends on the logarithm of the likelihood function. In other words, only in the case of unbiased estimators the Cramér-

Rao lower bound is independent of the used estimator. Accordingly, using the unbiased Cramér-Rao lower bound when the estimator is biased can lead to wrong conclusions.

Indeed, due to its simplicity, the unbiased Cramér-Rao lower bound is frequently used to assess performance limits. Nevertheless, we must keep in mind that when multipath is present the exact form of the estimator´s bias explicitly enters the computation of the bound. As a consequence, the use of the unbiased Cramér-Rao has to be actually understood as a desperate try to give a lower bound to a problem which is in reality so complicated and nonlinear that computing the bias is nearly impossible.

K.1 Appendix. Single-Path Maximum Likelihood Estimator

The single-path case (ML-1P) occurs when only the direct signal is present, thus no multipath is considered, and can be modelled as follows:

$$z(t) = Ae^{j\phi}m(t-\tau) + n_c(t) = x(t) + jy(t) \tag{K.6}$$

where we have assumed that the signal has been Doppler-compensated and striped of the data. Moreover, A denotes the amplitude, ϕ the phase offset and τ the code delay. For simplicity, we will separate $z(t)$ into its real component $x(t)$ and imaginary component $y(t)$ according to:

$$\begin{aligned} x(t) &= A\cos(\phi)m(t-\tau) + n_x(t) \\ y(t) &= A\sin(\phi)m(t-\tau) + n_y(t) \end{aligned} \tag{K.7}$$

where $n_x(t)$ and $n_y(t)$ are assumed to be independent real-valued zero-mean Gaussian-distributed variables. The real and imaginary signals are sampled on $[0,T]$ and thus we can also express our problem in the discrete domain as follows

$$\begin{aligned} x_k &= A\cos(\phi)m_k(\tau) + n_{x,k} \\ y_k &= A\sin(\phi)m_k(\tau) + n_{y,k} \end{aligned} \tag{K.8}$$

The Maximum Likelihood (ML) estimates of the populational parameters $\theta = (A, \phi, \tau)$ are shown to be obtained by maximizing the probability density function of the observables $\bar{x} = \{x_1, x_2, ..., x_N\}$ and $\bar{y} = \{y_1, y_2, ..., y_N\}$ conditioned to the real values of the parameters of the model:

$$P(\bar{x}, \bar{y} / \theta) = \left(\frac{1}{\sigma\sqrt{2\pi}}\right)^N e^{-\frac{\sum_{k=1}^{N}\left\{[x_k - A\cos(\phi)m_k(\tau)]^2 + [y_k - A\sin(\phi)m_k(\tau)]^2\right\}}{2\sigma^2}} \tag{K.9}$$

where σ^2 is the noise variance of $x(t)$ and $y(t)$. In other words, the ML estimates will maximize the probability to have a set of observables for a given unknown set of multipath parameters.

Before calculating the partial derivatives with respect to the parameters of the model, it is worth it to derive some expressions of interest. We define,

$$\begin{aligned} R_{xm}(\Delta\tau) &= \frac{1}{T}\int_T x(t)m(t-\Delta\tau)dt \\ R_{mm}(\Delta\tau) &= \frac{1}{T}\int_T m(t)m(t-\Delta\tau)dt \end{aligned} \tag{K.10}$$

and we will assume that the integration time is a multiple of the period of the signal.

As we saw above, for the case the estimators are unbiased, the Cramer Rao lower Bound of θ, namely $\hat{\theta}$ can be expressed by means of the Fisher information matrix F. In the case of the ML-1P problem, the Fisher matrix can be simplified and expressed only as a function of the autocorrelation function of $m(t)$ if we take into account the constraints that result from solving the minimization problem. Indeed, the Fisher Hessian matrix simplifies to:

$$F = \frac{N}{\sigma^2} E\left\{ \begin{pmatrix} R_{mm}(0) & 0 & 0 \\ 0 & -\hat{A}\left[\cos\left(\hat{\phi}\right)R''_{xm}(\hat{\tau}) + \sin\left(\hat{\phi}\right)R''_{ym}(\hat{\tau})\right] & 0 \\ 0 & 0 & \hat{A}\left[\cos\left(\hat{\phi}\right)R_{xm}(\hat{\tau}) + \sin\left(\hat{\phi}\right)R_{ym}(\hat{\tau})\right] \end{pmatrix} \right\} \tag{K.11}$$

which can be further simplified if we recall the definition of the model in (K.7), and correlate with the estimated path delay $\hat{\tau}$. According to this, it can be shown that:

$$\begin{aligned} R_{xm}(\hat{\tau}) &= A\cos(\phi)R_{mm}(\hat{\tau}-\tau) \\ R_{ym}(\hat{\tau}) &= A\sin(\phi)R_{mm}(\hat{\tau}-\tau) \end{aligned} \tag{K.12}$$

If we derivate now two times with respect to $\hat{\tau}$, we have:

$$\begin{aligned} R''_{xm}(\hat{\tau}) &= A\cos(\phi)R''_{mm}(\hat{\tau}-\tau) \\ R''_{ym}(\hat{\tau}) &= A\sin(\phi)R''_{mm}(\hat{\tau}-\tau) \end{aligned} \tag{K.13}$$

And substituting now these expressions into the Fisher matrix results in

$$F = \frac{N}{\sigma^2} E\left\{ \begin{pmatrix} R_{mm}(0) & 0 & 0 \\ 0 & -\hat{A}A\left[\cos\left(\hat{\phi}-\phi\right)\right]R''_{xm}(\hat{\tau}-\tau) & 0 \\ 0 & 0 & \hat{A}A\left[\cos\left(\hat{\phi}-\phi\right)\right]R_{xm}(\hat{\tau}-\tau) \end{pmatrix} \right\} \tag{K.14}$$

As it can be shown, the estimates of A, ϕ and τ are unbiased and thus we can express the Fisher matrix of the ML-1P estimator as follows:

$$F = \frac{N}{\sigma^2}\begin{pmatrix} R_{mm}(0) & 0 & 0 \\ 0 & -A^2R''_{xm}(0) & 0 \\ 0 & 0 & A^2R_{xm}(0) \end{pmatrix} = \frac{N}{\sigma^2}\begin{pmatrix} 1 & 0 & 0 \\ 0 & -A^2R''_{xm}(0) & 0 \\ 0 & 0 & A^2 \end{pmatrix} \tag{K.15}$$

where $R_{mm}(0)=1$ if we work with the C/N_0 defined after the filtering. Thus, the Cramér-Rao lower Bound of the estimates can be correspondingly expressed as:

$$CRLB\begin{pmatrix} \hat{A} \\ \hat{\tau} \\ \hat{\phi} \end{pmatrix} = \frac{\sigma^2}{N}\begin{pmatrix} 1 & 0 & 0 \\ 0 & -\dfrac{1}{A^2R''_{xm}(0)} & 0 \\ 0 & 0 & \dfrac{1}{A^2} \end{pmatrix} \tag{K.16}$$

For the particular case of the estimation of the path delay, the Cramer Rao Lower Bound of the error will be therefore

$$CRLB_{\hat{\tau}} = -\frac{1}{E\left\{\frac{\partial^2}{\partial\tau^2}\ln\left[p(\bar{x}/\theta)\right]\right\}} = -\frac{1}{\frac{NA^2R''_{mm}(0)}{\sigma^2}} \tag{K.17}$$

And since $N_0=B_L\sigma^2$ with $B_L=1/2T$ and $2A^2N = 2PN = 2E = C$,

$$CRLB = -\frac{B_L}{\frac{C}{N_0}R''_{mm}(0)} = \frac{B_L}{\frac{C}{N_0}(2\pi)^2\int_{-\infty}^{\infty}f^2S_m(f)df} \tag{K.18}$$

which is the well known expression that we can find in the literature. It is interesting to note that although the phase ϕ was considered in our derivation for completeness, same results would have been obtained for the simplified case with ϕ=0.

The Cramér Rao lower Bound can also be derived if we consider our problem of estimating the amplitude and delay of the direct signal as a fitting exercise where only noise is present. Indeed, recalling again the first equation in (K.7), we have:

$$x(t) = Am(t-\tau) + n_x(t) \tag{K.19}$$

If we define now $f(A,\tau)=Am(t-\tau)$ we can linearize our problem and obtain the estimates and variance using the minimum least squares approach. Indeed both approaches result in the same solution when the noise follows a normal distribution. For simplicity this is the approach we will adopt next for the case that one multipath signal is present (ML-2P).

Once we have calculated the expression of the ML-1P estimator, it is important to note that this estimator will not be optimal when multipath is actually present since the CRLB cannot be used. The alternative would be to use the Minimum Mean-Square Error (MMSE) estimator, optimum in this case, but it presents the problem that its calculation requires an enormous computational power. A solution to this problem is the Multipath Mitigation Technology (MMT) which reduces enormously the computational power needed to solve the 2P-ML problem. We analyze it more in detail in the next chapter.

K.2 Appendix. Two-Path Maximum Likelihood Estimator

For the case that one multipath signal is present, we can express the Doppler-compensated baseband signal model (ML-2P) as follows

$$z(t) = A_1 e^{j\phi_1} m(t-\tau_1) + A_2 e^{j\phi_2} m(t-\tau_2) + n_c(t) = x(t) + jy(t) \tag{K.20}$$

As done in the case of the ML-1P problem above, we separate the real and imaginary components as follows

$$\begin{aligned} x(t) &= A_1 \cos(\phi_1) m(t-\tau_1) + A_2 \cos(\phi_2) m(t-\tau_2) + n_x(t) \\ y(t) &= A_1 \sin(\phi_1) m(t-\tau_1) + A_2 \sin(\phi_2) m(t-\tau_2) + n_y(t) \end{aligned} \tag{K.21}$$

or after sampling, the equivalent discrete problem is shown to be:

$$\begin{aligned} x_k &= A_1 \cos(\phi_1) m_k(\tau_1) + A_2 \cos(\phi_2) m_k(\tau_2) + n_{x,k} \\ y_k &= A_1 \sin(\phi_1) m_k(\tau_1) + A_2 \sin(\phi_2) m_k(\tau_2) + n_{y,k} \end{aligned} \tag{K.22}$$

Now, in order to apply the Least Mean Squares (LMS) approach, we linearize the multipath model equations defined in (K.21) as follows:

$$x(t) \approx A_1 m(t-\tau_1) - \tau_1 A_1 m'(t-\tau_1) + A_2 m(t-\tau_2) - \tau_2 A_2 m'(t-\tau_2) + n_x(t) \tag{K.23}$$

According to this, the discrete matrix problem to solve will be in this case

$$\begin{pmatrix} x_1 \\ x_2 \\ \dots \\ x_N \end{pmatrix} = \begin{pmatrix} m(t_1-\tau_1) & -A_1 m'(t_1-\tau_1) & m(t_1-\tau_2) & -A_2 m'(t_1-\tau_2) \\ m(t_2-\tau_1) & -A_1 m'(t_2-\tau_1) & m(t_2-\tau_2) & -A_2 m'(t_2-\tau_2) \\ \dots & \dots & \dots & \dots \\ m(t_N-\tau_1) & -A_1 m'(t_N-\tau_1) & m(t_N-\tau_2) & -A_2 m'(t_N-\tau_2) \end{pmatrix} \begin{pmatrix} A_1 \\ \tau_1 \\ A_2 \\ \tau_2 \end{pmatrix} + \begin{pmatrix} n_1 \\ n_2 \\ \dots \\ n_N \end{pmatrix} \tag{K.24}$$

what we can express by means of matrices as follows

$$X = M'\beta + N \tag{K.25}$$

Since the variance of the LMS estimator of M is shown to be $\sigma^2_{\hat{M}} = (M'M)^{-1}\sigma^2$, we need to calculate the matrix $M'M$ which, after some math, is shown to simplify to

$$M'M = \begin{pmatrix} 1 & 0 & R_{mm}(\Delta\tau) & A_2 R'_{mm}(\Delta\tau) \\ 0 & -A_1^2 R''_{mm}(0) & -A_1 R'_{mm}(\Delta\tau) & -A_1 A_2 R''_{mm}(\Delta\tau) \\ R_{mm}(\Delta\tau) & -A_1 R'_{mm}(\Delta\tau) & 1 & 0 \\ A_2 R'_{mm}(\Delta\tau) & -A_1 A_2 R''_{mm}(\Delta\tau) & 0 & -A_2^2 R''_{mm}(0) \end{pmatrix} \tag{K.26}$$

where $\Delta\tau = \tau_2 - \tau_1$. As we can see, *M'M* is a function of the multipath delay and thus we will be able to represent the standard deviation (equivalent to the root mean square in this case since all the estimates are unbiased) as a function of the delay of the multipath signal.

Now that we have calculated the matrix *M'M*, the variance of the estimates is shown to be

$$Var\begin{pmatrix} \hat{A}_1 \\ \hat{\tau}_1 \\ \hat{A}_2 \\ \hat{\tau}_2 \end{pmatrix} = \left(M'M\right)^{-1}\sigma^2 \tag{K.27}$$

The result coincides perfectly with that we would have obtained if we would have maximized the probability density function since the noise is Gaussian distributed.

The expression of the inverse matrix of *F* looks a little bit complicated but to study the characteristics of the ML estimates we just have to look at the determinant, since after the inversion this is in the denominator. Thus, evaluating the determinant when $\Delta\tau$ tends to zero we can study the behaviour of the bound. This can be expressed as follows:

$$\|M'M\| = A_1^2 A_2^2 \left\{ R'^4{}_{mm}(\Delta\tau) + 2R'^2{}_{mm}(\Delta\tau)\left[R''_{mm}(0) - R''_{mm}(\Delta\tau)R_{mm}(\Delta\tau)\right] + \left[R^2{}_{mm}(\Delta\tau) - 1\right]\left[R''^2{}_{mm}(\Delta\tau) - R''^2{}_{mm}(0)\right]\right\} \tag{K.28}$$

It is interesting to note that although all the estimates are unbiased, what is a good property in principle, when the separation of the direct and delayed multipath paths $\Delta\tau$ approaches to zero, the determinant of *M'M* makes the variance of the error tend to infinity.

This is a very important characteristic of any unconstraint ML estimate in presence of multipath. In fact, unbiased estimators are preferred in principle but their quality degrades considerably for small path separations since the standard deviation increases when $\Delta\tau$ tends to zero.

K.3 Appendix. Multiple-Path Maximum Likelihood Estimator

Once we have solved the case of one multipath signal present (ML with 2 paths), it is straightforward to generalize the results to any number of multipath signals. In fact, for three paths, one direct signal and two multipath signals, the linearized problem to solve is

$$x(t) \approx \sum_{i=1}^{3} A_i m(t-\tau_i) - \tau_i A_i m'(t-\tau_i) + n_x(t) \tag{K.29}$$

And the variance of the estimates is shown to be:

$$Var\begin{pmatrix} A_1 \\ \tau_1 \\ A_2 \\ \tau_2 \\ A_3 \\ \tau_3 \end{pmatrix} = \frac{1}{N}\begin{pmatrix} 1 & 0 & R_{mm}(\Delta\tau_1) & A_2R'_{mm}(\Delta\tau_1) & R_{mm}(\Delta\tau_2) & A_3R'_{mm}(\Delta\tau_2) \\ 0 & -A_1^2R''_{mm}(0) & -A_1R'_{mm}(\Delta\tau_1) & -A_1A_2R''_{mm}(\Delta\tau_1) & -A_1R'_{mm}(\Delta\tau_2) & -A_1A_3R''_{mm}(\Delta\tau_2) \\ R_{mm}(\Delta\tau_1) & -A_1R'_{mm}(\Delta\tau_1) & 1 & 0 & R_{mm}(\Delta\tau_3) & -A_3R'_{mm}(\Delta\tau_3) \\ A_2R'_{mm}(\Delta\tau_1) & -A_1A_2R''_{mm}(\Delta\tau_1) & 0 & -A_2^2R''_{mm}(0) & -A_2R'_{mm}(\Delta\tau_3) & -A_2A_3R''_{mm}(\Delta\tau_3) \\ R_{mm}(\Delta\tau_2) & -A_1R'_{mm}(\Delta\tau_2) & R_{mm}(\Delta\tau_3) & -A_2R'_{mm}(\Delta\tau_3) & 1 & 0 \\ A_3R'_{mm}(\Delta\tau_2) & -A_1A_3R''_{mm}(\Delta\tau_2) & -A_3R'_{mm}(\Delta\tau_3) & -A_2A_3R''_{mm}(\Delta\tau_3) & 0 & -A_3^2R''_{mm}(0) \end{pmatrix} \tag{K.30}$$

As we did in the case there is only one multipath signal present, we could calculate the determinant of the matrix to be inverted above, in order to study the stability of the variance of the estimates when the multipath delays approach to zero. Although the exact expression does not look very friendly, it can be shown that when $\Delta\tau_1$ and $\Delta\tau_2$ tend to zero, the determinant also approaches to zero and thus the standard deviation also increases to infinity like in the non constraint ML-2P case. Once again, we can see that the use of biased estimators seems to be a better solution to some problems.

L Appendix. Antisymmetric Sequences

MBOC is the result of multiplexing BOC(1,1) and BOC(6,1). In the long process of finding an alternative to BOC(1,1), experts of the STF of the EC realized that some specific BCS sequences seemed to be of special interest for satellite navigation. We have shown in chapter 5 that CBCS presented the problem of having a tracking bias when correlated with a pure BOC(1,1) receiver, what lead to further investigations on alternative BCS sequences with particular symmetry properties. These receive the name of antisymmetric sequences and have been studied in [A.R. Pratt et al., 2006]. In the next lines the most important characteristics are underlined.

Let the binary sequence $S=\{s_i\}$ of length n define a reversed sequence S^* such that:

$$S^* = \{s_{n-1-i}\} \text{ for } i \in 0..(n-1) \tag{L 1}$$

It is important to note that this sequence S can be any generic BCS signal in principle. A sequence is defined to be *symmetric* if $S^* = S$, so that:

$$s_i = s_{n-1-i} \text{ for all } i \in 0..(n-1) \tag{L.2}$$

As we can see, such a definition allows solutions for both n even or odd. Furthermore, a binary sequence is defined as *antisymmetric* if $S^* = -S$, that is:

$$s_i = -s_{n-1-i} \text{ for all } i \in 0..(n-1) \tag{L.3}$$

As we can see, antisymmetric sequences may only be composed with even values of n, since there cannot be a central element, $x_{(n-1)/2}$ which is self inverse.

Another important characteristic of any generic BCS sequence is the balance. As shown in [A.R. Pratt et al., 2006], the balance of a symmetric binary sequence can be determined through a consideration of the sum of the elements. Let $S=\{s_i\}$ be a symmetric binary sequence of length n, then the sum $\Sigma(S)$ of the element values is:

$$\Sigma(S) = \sum_{i=0}^{n-1} s_i = 2\sum_{i=0}^{\frac{n-2}{2}} s_i \text{ for } n \text{ even} \tag{L.4}$$

Moreover, assuming that the sequence is binary and n even, it can also be shown that

$$\Sigma(S) = 2\sum_{i=0}^{\frac{n-2}{2}} s_i = n \mod 4 \tag{L.5}$$

Equally, when n is odd, the sum of the elements of S adopts the following form:

$$\Sigma(S) = s_{\frac{n-1}{2}} + 2\sum_{i=0}^{\frac{n-3}{2}} s_i = n + s_{\frac{n-1}{2}} - 1 \mod 4 \tag{L.6}$$

As we can recognize, all antisymmetric binary sequences with even n are balanced because of their particular construction. Moreover as a consequence of (L.5), the sequence balance, that means $\Sigma(S)=0$, can only be achieved for symmetric binary sequences whose lengths are

multiples of 4. This is a necessary condition for the existence of some zero sum sequences, but not sufficient.

We further define the properties of a product sequence $Z=\{z_i\}$ constructed from 2 binary sequences, X and Y. Z will also have length n and element values $\{+1,-1\}$. In principle, X and Y are restricted to be either symmetric or antisymmetric sequences. Z is derived by forming the inner product from the two seed sequences, X and Y, as follows:

$$z_i = \{x_i . y_i\} \quad \text{for } i \in 0..(n-1) \tag{L.7}$$

The sequence, $Z=\{z_i\}$, may be balanced or unbalanced, as described above, or may be symmetric or antisymmetric. If, for example, the sequences X and Y are both symmetric so will also be Z. If both X and Y are antisymmetric, Z results to be a symmetric sequence. This is shown next:

$$\begin{aligned} x_i &= -x_{n-1-i} \\ y_i &= -y_{n-1-i} \\ z_i &= x_i\, y_i = (-1)^2\; x_{n-1-i}\, y_{n-1-i} = z_{n-1-i} \end{aligned} \tag{L.8}$$

In addition if one of X or Y is antisymmetric, and the other is symmetric, Z will be antisymmetric. In fact, the class of sequences X, Y which can form sequences Z with symmetric properties is wider than the class with seed sequences which are symmetric or antisymmetric.

As shown in [A.R. Pratt et al., 2006], the circular crosscorrelation between two binary sequences, X and Y, of length n, is defined as:

$$R^c_{x,y}(r) = \sum_{i=0}^{n-1} x_i\, y_k \;=\; \sum_{i=0}^{n-1-r} x_i\, y_{i+r} + \sum_{i=n-r}^{n-1} x_i\, y_{i+r-n} \Bigg|_{k=(i+r) \bmod n} \tag{L.9}$$

where $k = (i+r) \bmod n$. This operation corresponds to the formation of another type of derived sequence, $Z=\{z_i\}$, where the family members are determined through circular shifts of the original sequence members. In fact,

$$z^r{}_i = x_i\, y_k \quad \text{where} \quad k = i + r \mod n \tag{L.10}$$

As we can see, the cross-correlation $R^c_{x,y}(r)$ is then the balance, $\Sigma(Z^r)$ of the sequence Z^r.

In the following lines some examples of antisymmetric sequences are given for various lengths n. For length $n=4$, it can be shown that there are two distinct antisymmetric sequences:

$$\begin{aligned} x_1 &= \{+1,+1,-1,-1\} \\ x_2 &= \{+1,-1,+,1-1\} \end{aligned} \tag{L.11}$$

For $n=6$, there are 3 distinct sequences, while for $n=8$ we can find 6. In the same manner, for $n=10$ we have 10 and for $n=12$ there are 20 such sequences. These were tabulated in chapter 4.7.2 with their cross-correlation values at zero offset.

M Appendix. Interference Model

In this Appendix we present the most important expressions that are necessary to assess the degradation that a signal causes on another signal in the shared band. As we have shown in chapter 4.7.8, the methodology is based on the idea of measuring the degradation of a desired signal in terms of the reduction of its effective C/N_0. This figure was also analyzed in Appendix H. This can be caused by either the background noise where all the non GNSS signals are included or by another interfering signal of the same or similar nature. To this group belong all the types of interference from other GNSS signals. We can further distinguish the different GNSS interference sources following this classification:

- I_{Intra}: This type of interference is commonly known as intra-system interference and is due to the signals coming from satellites that belong to the same system as the desired signal.
- I_{Interop}: This type of interference corresponds to the equivalent noise introduced in the receiver by an interfering signal coming from a satellite of a different constellation but with the same signal structure as that of the desired signal.
- I_{Inter}: This type of interference comes from signals with a different signal structure no matter whether the signal belong to the same system or a different one.

If we put now all the GNSS sources of interference together, we have as interfering power:

$$I_{\text{Total}} = I_{\text{Intra}} + I_{\text{Inter}} + I_{\text{Interop}} \tag{M.1}$$

Moreover, we define the equivalent noise power density of each of the interfering signals as:

$$I_X = \frac{\sum_{j=1}^{N_X} C_j \kappa_{js}}{\int_{-\frac{\beta_r}{2}}^{\frac{\beta_r}{2}} G_d\left(f + f_{\text{dop}_s}\right) \mathrm{d}f} \tag{M.2}$$

where

- X defines the type of interference according to the definitions above,
- N_X represents the number of satellites,
- C_j is the received power of satellite j,
- β_r is the receiver bandwidth,
- G_d is the power spectral density of the desired signal s,
- f_{dop_s} is the doppler frequency offset of the desired signal s,
- κ_{js} is the spectral separation coefficient between signal j and the desired signal s. As we saw in chapter 5, this is defined as follows:

$$\kappa_{js} = \int_{-\frac{\beta_r}{2}}^{\frac{\beta_r}{2}} G_j^i\left(f + f_{\text{dop}_j}\right) G_s\left(f + f_{\text{dop}_s}\right) \mathrm{d}f \tag{M.3}$$

where,

- $G_j^i(f)$ is the power spectral density of the interfering signal j
- f_{dop_j} is the doppler frequency offset of the desired signal j.

The GNSS receiver of our model is supposed to stay stationary at the earth's surface so that only the motion of the satellites will be responsible for the Doppler offsets observed at user level. Moreover, we know that while for GPS the absolute Doppler frequency offset does not exceed 4.4 kHz, the range is narrower for Galileo, being the maximum value of 3.3 kHz in the E1/L1 band as shown in Figure M.1 next [S. Wallner et al., 2005]:

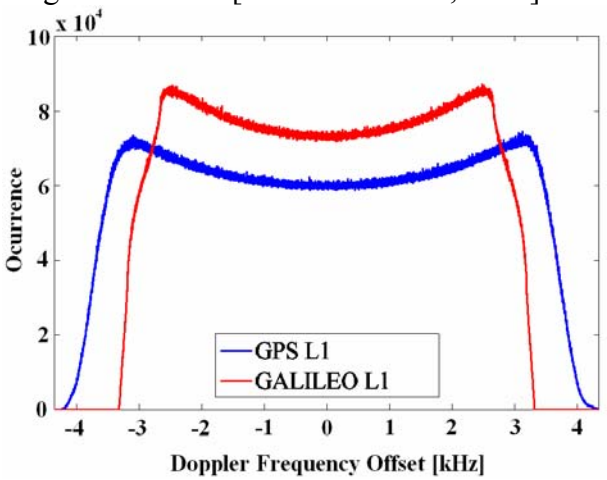

Figure M.1. Histogram of the Doppler Frequency Offsets for GPS and Galileo E1/L1

Once we have defined mathematically the shape of the different sources of interference, we can now compute the degradation suffered by a receiver due to other signals. As we said at the beginning, the interference of one system onto another one is given by the reduction of the effective C/N_0 , which can be expressed as follows:

$$\left(\frac{C}{N_0}\right)_{\text{eff}} = \frac{C}{N_0 + I_{\text{Total}}} \tag{M.4}$$

where N_0 refers to the noise floor. Furthermore, we assume a noise value of -201.5 dBW/Hz for all the purposes. In addition, the degradation of the effective C/N_0 due to intra-system interference can be thus expressed as follows:

$$\Delta\left(\frac{C}{N_0}\right) = \frac{\dfrac{C}{N_0}}{\dfrac{C}{N_0 + I_{\text{Intra}}}} = 1 + \frac{I_{\text{Intra}}}{N_0} \tag{M.5}$$

Equally, for the case of the degradation caused by the inter-system interference we have the following expression:

$$\Delta\left(\frac{C}{N_0}\right) = \frac{\dfrac{C}{N_0 + I_{\text{Intra}}}}{\dfrac{C}{N_0 + I_{\text{Intra}} + I_{\text{Inter}} + I_{\text{Interop}}}} = 1 + \frac{I_{\text{Inter}} + I_{\text{Interop}}}{N_0 + I_{\text{Intra}}} \tag{M.6}$$

Now that we have the necessary mathematical expressions to calculate the degradation suffered by a receiver according to this simplified model, we only need to obtain the power of the desired and interfering signals at each point of the earth. To do that, we have to simulate the satellite positions and movements and account for the attenuations of the signal from the satellite to the receiver. Indeed, once we know the minimum received powers as given in [Galileo SIS ICD, 2008], [GPS ICD 200], [GPS ICD-705, 2005] and [GPS ICD-800, 2006] we obtain the transmission power P_j of each satellite as done by [S. Wallner et al., 2005] and we can derive the power received at user level at every point of the earth according to:

$$C_j = P_j + G_j - A_{\text{dist}} - A_{\text{atm}} - A_{\text{pol}} + G_{\text{user}} \tag{M.7}$$

where

- P_j depicts the transmission power from satellite j,
- G_j is the satellite antenna gain,
- A_{dist} is the attenuation due to the distance between the satellite and the user,
- A_{pol} is the attenuation of the signal due to the mismatch losses in the polarization,
- A_{atm} is the attenuation of the signal due to the atmosphere, and
- G_{user} is the receiver antenna gain.

The satellite antenna gain G_j is a function of the Off-Boresight Angle α as defined next:

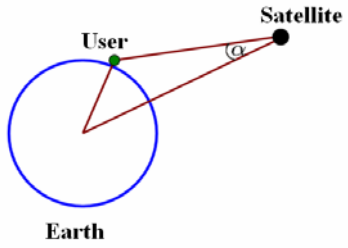

Figure M.2. Definition of Off-Boresight Angle

being the typical satellite antenna gain as shown in the following figure:

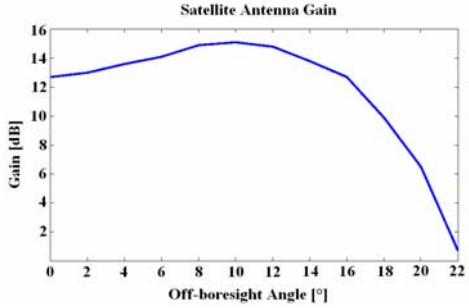

Figure M.3. Assumed Typical Satellite Antenna Gain

Additionally, the signal attenuation due to the free-space losses A_{dist} is given by:

$$A_{\text{dist}} = \left(\frac{c}{4\pi d f_c} \right)^2 \tag{M.8}$$

where,

- c is the speed of light
- d is the distance between the satellite and the user
- and f_c is the carrier frequency

N Appendix. SSC between two QPSK signals

In the next lines the SSC between two QPSK signals is derived. Let us assume for simplicity that the desired QPSK signal adopts the following form [J.-L. Issler et al., 2003]:

$$\sqrt{P_d}\left[d_d(t)c_d^D(t)+jc_d^P(t)\right] \tag{N.1}$$

where,

- $\sqrt{P_d}$ is the amplitude of the desired useful signal,
- $d_d(t)$ is the data modulating the useful PRN data-code in phase,
- $c_c^D(t)$ is the useful data-code, and
- $c_d^P(t)$ is the PRN code of the useful pilot-channel.

Moreover, let us assume the following receiver model as done by [J.-L. Issler et al., 2003]:

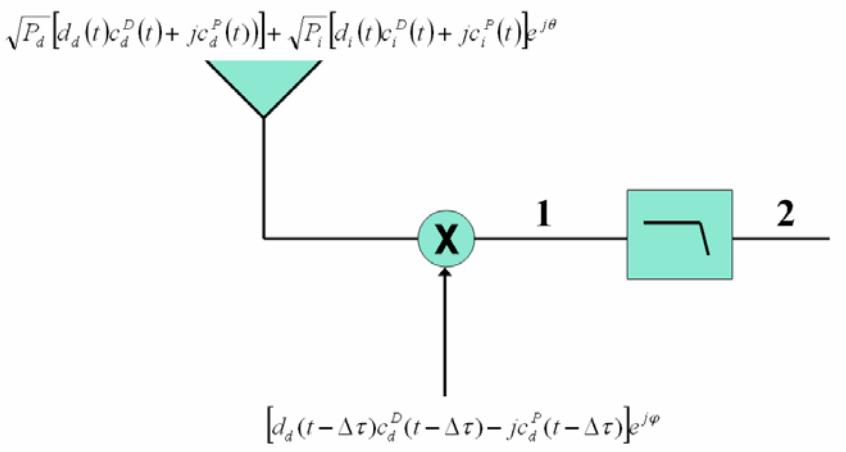

Figure N.1. SSC Receiver Model

And that the interfering received QPSK signal presents the following form:

$$\sqrt{P_i}\left[d_i(t)c_i^D(t)+jc_i^P(t)\right] \tag{N.2}$$

with:

- $\sqrt{P_i}$ is the amplitude of the interfering signal,
- $d_i(t)$ is the data modulating the interfering data-code,
- $c_i^D(t)$ is the interfering data-code,
- $c_i^P(t)$ is the PN code of the interfering pilot-channel.

As we can see, the replica signals generated by the receiver will be:

$$c_d^D(t-\Delta\tau)-jc_d^P(t-\Delta\tau) \tag{N.3}$$

and

$$-c_d^D(t-\Delta\tau)-jc_d^P(t-\Delta\tau) \tag{N.4}$$

where

- $c_d^D(t-\Delta\tau)$ is the PRN code replica of the data-channel,
- and $c_d^P(t-\Delta\tau)$ the PRN code replica of the pilot-channel.

Furthermore, the phase shift between the desired signal and the replica is given by $e^{j\varphi}$ while the phase shift with the interfering signal is $e^{j\theta}$ with $\theta = 2\pi f_d t + \theta_0$, where f_d is the Doppler frequency shift. Equally, if the power ratio between the interfering signal and the desired signal is expressed as follows:

$$\Theta = \sqrt{\frac{P_i}{P_d}} \tag{N.5}$$

the value of the signal $s_1(t)$ at point 1 can thus be expressed as follows:

$$s_1(t) = \sqrt{P_d}\left[\begin{bmatrix} d_d(t)c_d^D(t)d_d(t-\Delta\tau)c_d^D(t-\Delta\tau) + j\,c_d^P(t)d_d(t-\Delta\tau)c_d^D(t-\Delta\tau) \\ -j\,d_d(t)\,c_d^D(t)\,c_d^P(t-\Delta\tau) + c_d^P(t)c_d^P(t-\Delta\tau) \end{bmatrix} e^{j\varphi} \right.$$
$$\left. + \Theta\begin{bmatrix} d_i(t)c_i^D(t)d_d(t-\Delta\tau)c_d^D(t-\Delta\tau) + j\,c_i^P(t)d_d(t-\Delta\tau)c_d^D(t-\Delta\tau) \\ -j\,d_i(t)c_i^D(t)c_d^P(t-\Delta\tau) + c_i^P(t)c_d^P(t-\Delta\tau) \end{bmatrix} e^{j\theta}e^{j\varphi} \right] \tag{N.6}$$

with $e^{j\Omega} = e^{j\theta}e^{j\varphi}$. Moreover, if we integrate (N.6), the signal at the output of the correlator at point 2 will be then:

$$s_2(t) = \sqrt{P_d}\left[\begin{bmatrix} \int_{T_c} c_d^D(t)c_d^D(t-\Delta\tau)\mathrm{d}t + j\,d_d(t-\Delta\tau)\int_{T_c} c_d^P(t)c_d^D(t-\Delta\tau)\mathrm{d}t \\ -j\,d_d(t)\int_{T_c} c_d^D(t)c_d^P(t-\Delta\tau)\mathrm{d}t + \int_{T_c} c_d^P(t)c_d^P(t-\Delta\tau)\mathrm{d}t \end{bmatrix} e^{j\varphi} \right.$$
$$\left. + \Theta\begin{bmatrix} d_i(t)d_d(t-\Delta\tau)\int_{T_c} c_i^D(t)c_d^D(t-\Delta\tau)\mathrm{d}t + \\ +\,j\,d_d(t-\Delta\tau)\int_{T_c} c_i^P(t)c_d^D(t-\Delta\tau)\mathrm{d}t \\ -j\,d_i(t)\int_{T_c} c_i^D(t)c_d^P(t-\Delta\tau)\mathrm{d}t + \int_{T_c} c_i^P(t)c_d^P(t-\Delta\tau)\mathrm{d}t \end{bmatrix} e^{j\theta}\,e^{j\varphi} \right] \tag{N.7}$$

what can be further simplified to:

$$s_2(t) = \sqrt{P_d}\left[\begin{bmatrix} \Re_{c_d^D}(\Delta\tau) + \Re_{c_d^P}(\Delta\tau) \end{bmatrix} e^{j\varphi} \right.$$
$$\left. + \Theta\begin{bmatrix} d_i(t)\,d_d(t)\Re_{c_i^D,c_d^D}(\Delta\tau) + j\,d_d(t)\Re_{c_i^P,c_d^D}(\Delta\tau) \\ -j\,d_i(t)\Re_{c_i^D,c_d^P}(\Delta\tau) + \Re_{c_i^P,c_d^P}(\Delta\tau) \end{bmatrix} e^{j\Omega} \right] \tag{N.8}$$

As we can see, we have assumed that we integrate over the duration of the data bits and thus the bits have no impact on the SSC computation. We can also express equation (N.8) as:

$$s_2(t) = \sqrt{P_d}\,(Y + \Theta Z) \tag{N.9}$$

with:

$$Y = \left[\Re_{c_d^D}(\Delta\tau) + \Re_{c_d^P}(\Delta\tau)\right] e^{j\varphi} \tag{N.10}$$

and

$$Z = \left[d_i(t)\, d_d(t)\, \Re_{c_i^D, c_d^D}(\Delta\tau) + j\, d_d(t)\, \Re_{c_i^P, c_d^D}(\Delta\tau) - j\, d_i(t) \Re_{c_i^D, c_d^P}(\Delta\tau) + \Re_{c_i^P, c_d^P}(\Delta\tau)\right] e^{j\Omega} \tag{N.11}$$

In addition, since the SSC can also be interpreted as the mean power of the cross-correlation function as defined in chapter 5.1.1, and we are interested in the SSC between the interfering signal and the desired signal, we have:

$$\mathrm{SSC}(s_i, s_d) = \lim_{T_c \to \infty} \frac{1}{T_c} \int |N|^2 \mathrm{d}t \tag{N.12}$$

what can be further simplified as follows:

$$\mathrm{SSC}(s_i, s_d) = \lim_{T_c \to \infty} \frac{1}{T_c} \int_{T_c} \left\{ \left[\Re_{c_i^D, c_d^D}(\Delta\tau) + \Re_{c_i^P, c_d^D}(\Delta\tau)\right]^2 + \left[\Re_{c_i^D, c_d^P}(\Delta\tau) - \Re_{c_i^P, c_d^P}(\Delta\tau)\right]^2 \right\} \mathrm{d}t \tag{N.13}$$

or equivalently:

$$\mathrm{SSC}(s_i, s_d) = \begin{cases} \mathrm{SSC}\left(c_i^D, c_d^D\right) + \mathrm{SSC}\left(c_i^P, c_d^P\right) + 2 \lim_{T_c \to \infty} \frac{1}{T_c} \int_{T_c} \Re_{c_i^D, c_d^D}(\Delta\tau) \Re_{c_i^P, c_d^D}(\Delta\tau) \mathrm{d}t \\ + \mathrm{SSC}\left(c_i^D, c_d^P\right) + \mathrm{SSC}\left(c_i^P, c_d^D\right) - 2 \lim_{T_c \to \infty} \frac{1}{T_c} \int_{T_c} \Re_{c_i^D, c_d^P}(\Delta\tau) \Re_{c_i^P, c_d^P}(\Delta\tau) \mathrm{d}t \end{cases} \tag{N.14}$$

where the two integral terms are shown to be much smaller than the others. As a conclusion, we can simplify as follows [J.-L. Issler et al., 2003]:

$$\mathrm{SSC}(s_i, s_d) = \mathrm{SSC}\left(c_i^D, c_d^D\right) + \mathrm{SSC}\left(c_i^P, c_d^P\right) + \mathrm{SSC}\left(c_i^D, c_d^P\right) + \mathrm{SSC}\left(c_i^P, c_d^D\right) \tag{N.15}$$

which is the expression suggested in chapter 5.1.1.

O Appendix. Analytical expressions to compute SSCs

In the next lines we derive analytical expressions to compute the Spectral Separation Coefficients (SSC) between two generic BCS signals using the theory derived in chapters 4 and 5. Later, particular expressions of interest will be obtained.

O.1 Appendix. SSC between two generic BCS signals

As we have seen in chapter 5.1, the Spectral Separation Coefficient (SSC) between two BCS signals can be approximated when the integration time tends to infinity:

$$\mathrm{SSC}_{\mathrm{BCS}\left([\bar{r}],f_c^1\right)-\mathrm{BCS}\left([\bar{s}],f_c^2\right)}=\int_{-\beta_r/2}^{\beta_r/2}G_{\mathrm{BCS}\left(\bar{r},f_c^1\right)}(f)G_{\mathrm{BCS}\left(\bar{s},f_c^2\right)}(f)\mathrm{d}f\equiv SSC_{\mathrm{BCS}_1-\mathrm{BCS}_2} \tag{O.1}$$

where the power spectral density of each MCS signal was derived in (4.23) for the most general case. If we further assume that we work with binary sequences, the expression can be further simplified as follows:

$$G_{\mathrm{BCS}([\bar{s}],f_c^i)}(f)=f_c^i\frac{\sin^2\left(\frac{\pi f}{nf_c^i}\right)}{(\pi f)^2}\left\{n+\sum_{i=1}^{n-1}\sum_{j=i+1}^{n}2s_is_j\cos\left[(j-i)\frac{2\pi f}{nf_c^i}\right]\right\} \tag{O.2}$$

and thus the product of the two power spectral densities will adopt the following form

$$G_{\mathrm{BCS}\left(\bar{r},f_c^1\right)}(f)G_{\mathrm{BCS}\left(\bar{s},f_c^2\right)}=\begin{cases}f_c^1\dfrac{\sin^2\left(\frac{\pi f}{n_1f_c^1}\right)}{(\pi f)^2}\left\{n_1+\sum_{i=1}^{n_1-1}\sum_{j=i+1}^{n_1}2r_ir_j\cos\left[(j-i)\dfrac{2\pi f}{n_1f_c^1}\right]\right\}\times \\ \times f_c^2\dfrac{\sin^2\left(\frac{\pi f}{n_2f_c^2}\right)}{(\pi f)^2}\left\{n_2+\sum_{i'=1}^{n_2-1}\sum_{j'=i'+1}^{n_2}2s_{i'}s_{j'}\cos\left[(j'-i')\dfrac{2\pi f}{n_2f_c^2}\right]\right\}\end{cases} \tag{O.3}$$

Moreover, we can further expand this expression as follows:

$$\begin{aligned}&G_{\mathrm{BCS}\left([\bar{r}],f_c^1\right)}(f)G_{\mathrm{BCS}\left([\bar{s}],f_c^2\right)}\equiv G_{\mathrm{BCS}_1}(f)G_{\mathrm{BCS}_2}(f)= \\ &n_1n_2f_c^1f_c^2\frac{\sin^2\left(\frac{\pi f}{n_1f_c^1}\right)}{(\pi f)^2}\frac{\sin^2\left(\frac{\pi f}{n_2f_c^2}\right)}{(\pi f)^2}+ \\ &+2n_1f_c^1f_c^2\sum_{i'=1}^{n_2-1}\sum_{j'=i'+1}^{n_2}s_{i'}s_{j'}\frac{\sin^2\left(\frac{\pi f}{n_1f_c^1}\right)}{(\pi f)^2}\frac{\sin^2\left(\frac{\pi f}{n_2f_c^2}\right)}{(\pi f)^2}\cos\left[(j'-i')\frac{2\pi f}{n_2f_c^2}\right]+ \\ &+2n_2f_c^1f_c^2\sum_{i=1}^{n_1-1}\sum_{j=i+1}^{n_1}r_ir_j\frac{\sin^2\left(\frac{\pi f}{n_1f_c^1}\right)}{(\pi f)^2}\frac{\sin^2\left(\frac{\pi f}{n_2f_c^2}\right)}{(\pi f)^2}\cos\left[(j-i)\frac{2\pi f}{n_1f_c^1}\right]+ \\ &+4f_c^1f_c^2\sum_{i=1}^{n_1-1}\sum_{j=i+1}^{n_1}\sum_{i'=1}^{n_2-1}\sum_{j'=i'+1}^{n_2}r_ir_js_{i'}s_{j'}\frac{\sin^2\left(\frac{\pi f}{n_1f_c^1}\right)}{(\pi f)^2}\frac{\sin^2\left(\frac{\pi f}{n_2f_c^2}\right)}{(\pi f)^2}\cos\left[(j'-i')\frac{2\pi f}{n_2f_c^2}\right]\cos\left[(j-i)\frac{2\pi f}{n_1f_c^1}\right]\end{aligned} \tag{O.4}$$

After integrating in the receiver bandwidth we can express our SSC as sum of other four terms yielding:

$$\mathrm{SSC}_{\mathrm{BCS}_1-\mathrm{BCS}_2}=\int_{-\beta_r/2}^{\beta_r/2}G_{\mathrm{BCS}_1}(f)G_{\mathrm{BCS}_2}(f)\mathrm{d}f=\mathrm{SSC}_1+\mathrm{SSC}_2+\mathrm{SSC}_3+\mathrm{SSC}_4 \qquad \text{(O.5)}$$

where

$$\mathrm{SSC}_1=n_1n_2f_c^1f_c^2\int_{-\beta_r/2}^{\beta_r/2}\frac{\sin^2\left(\frac{\pi f}{n_1f_c^1}\right)}{(\pi f)^2}\frac{\sin^2\left(\frac{\pi f}{n_2f_c^2}\right)}{(\pi f)^2}\mathrm{d}f \qquad \text{(O.6)}$$

$$\mathrm{SSC}_2=2n_1f_c^1f_c^2\sum_{i'=1}^{n_2-1}\sum_{j'=i'+1}^{n_2}s_{i'}s_{j'}\int_{-\beta_r/2}^{\beta_r/2}\frac{\sin^2\left(\frac{\pi f}{n_1f_c^1}\right)}{(\pi f)^2}\frac{\sin^2\left(\frac{\pi f}{n_2f_c^2}\right)}{(\pi f)^2}\cos\left[(j'-i')\frac{2\pi f}{n_2f_c^2}\right]\mathrm{d}f \qquad \text{(O.7)}$$

$$\mathrm{SSC}_3=2n_2f_c^1f_c^2\sum_{i=1}^{n_1-1}\sum_{j=i+1}^{n_1}r_ir_j\int_{-\beta_r/2}^{\beta_r/2}\frac{\sin^2\left(\frac{\pi f}{n_1f_c^1}\right)}{(\pi f)^2}\frac{\sin^2\left(\frac{\pi f}{n_2f_c^2}\right)}{(\pi f)^2}\cos\left[(j-i)\frac{2\pi f}{n_1f_c^1}\right]\mathrm{d}f \qquad \text{(O.8)}$$

Finally,

$$\mathrm{SSC}_4=$$

$$=4f_c^1f_c^2\sum_{i=1}^{n_1-1}\sum_{j=i+1}^{n_1}\sum_{i'=1}^{n_2-1}\sum_{j'=i'+1}^{n_2}r_ir_js_{i'}s_j\int_{-\beta_r/2}^{\beta_r/2}\frac{\sin^2\left(\frac{\pi f}{n_1f_c^1}\right)}{(\pi f)^2}\frac{\sin^2\left(\frac{\pi f}{n_2f_c^2}\right)}{(\pi f)^2}\cos\left[(j'-i')\frac{2\pi f}{n_2f_c^2}\right]\cos\left[(j-i)\frac{2\pi f}{n_1f_c^1}\right]\mathrm{d}f \qquad \text{(O.9)}$$

Furthermore, it can be shown that an analytical expression can be found for the four integrations above when $\beta_r\to\infty$. In this case, the explicit expressions for the different SSC components adopt the following form:

$$\mathrm{SSC}_1=n_1n_2f_c^1f_c^2\,\Xi\left(f_c^1,n_1,f_c^2,n_2,0,0\right) \qquad \text{(O.10)}$$

$$\mathrm{SSC}_2=2n_1f_c^1f_c^2\sum_{i'=1}^{n_2-1}\sum_{j'=i'+1}^{n_2}s_{i'}s_{j'}\,\Xi\left(f_c^1,n_1,f_c^2,n_2,0,j'-i'\right) \qquad \text{(O.11)}$$

$$\mathrm{SSC}_3=2n_2f_c^1f_c^2\sum_{i=1}^{n_1-1}\sum_{j=i+1}^{n_1}r_ir_j\,\Xi\left(f_c^1,n_1,f_c^2,n_2,j-i,0\right) \qquad \text{(O.12)}$$

$$\mathrm{SSC}_4=4f_c^1f_c^2\sum_{i=1}^{n_1-1}\sum_{j=i+1}^{n_1}\sum_{i'=1}^{n_2-1}\sum_{j'=i'+1}^{n_2}r_ir_js_{i'}s_j\,\Xi\left(f_c^1,n_1,f_c^2,n_2,j-i,j'-i'\right) \qquad \text{(O.13)}$$

where the Ξ function is defined as follows:

$$\Xi\left(f_c^1,n_1,f_c^2,n_2,j'-i',j-i\right)=\int_{-\infty}^{\infty}\frac{\sin^2\left(\frac{\pi f}{n_1f_c^1}\right)}{(\pi f)^2}\frac{\sin^2\left(\frac{\pi f}{n_2f_c^2}\right)}{(\pi f)^2}\cos\left[(j-i)\frac{2\pi f}{n_1f_c^1}\right]\cos\left[(j'-i')\frac{2\pi f}{n_2f_c^2}\right]\mathrm{d}f \qquad \text{(O.14)}$$

which is shown to simplify to the following analytical expression:

$$\Xi\left(f_c^1,n_1,f_c^2,n_2,j-i,j'-i'\right)$$

$$\frac{1}{24f_{c,1}^3f_{c,2}^3n_1^3n_2^3}\left[\begin{array}{l}\left\|f_c^1\left(-1+k_2\right)n_1-f_c^2\left(-1+k_1\right)n_2\right\|^3+\left\|f_c^1\left(1+k_2\right)n_1-f_c^2\left(-1+k_1\right)n_2\right\|^3+\\+\left\|f_c^1\left(-1+k_2\right)n_1+f_c^2\left(-1+k_1\right)n_2\right\|^3-2\left\|f_c^1k_2n_1+f_c^2\left(-1+k_1\right)n_2\right\|^3+\\+\left\|f_c^1\left(1+k_2\right)n_1+f_c^2\left(-1+k_1\right)n_2\right\|^3+4\left\|f_c^1k_2n_1-f_c^2k_1n_2\right\|^3-\\-2\left\|f_c^1\left(1+k_2\right)n_1-f_c^2k_1n_2\right\|^3-2\left\|f_c^1k_2n_1+f_c^2n_2-f_c^2k_1n_2\right\|^3-\\-2\left\|f_c^1\left(-1+k_2\right)n_1+f_c^2k_1n_2\right\|^3-2\left\|f_c^1n_1-f_c^1k_2n_1+f_c^2k_1n_2\right\|^3+\\+4\left\|f_c^1k_2n_1+f_c^2k_1n_2\right\|^3-2\left\|f_c^1\left(1+k_2\right)n_1+f_c^2k_1n_2\right\|^3+\\+\left\|f_c^1\left(-1+k_2\right)n_1-f_c^2\left(1+k_1\right)n_2\right\|^3-2\left\|f_c^1k_2n_1-f_c^2\left(1+k_1\right)n_2\right\|^3+\\+\left\|f_c^1\left(1+k_2\right)n_1-f_c^2\left(1+k_1\right)n_2\right\|^3+\left\|f_c^1\left(-1+k_2\right)n_1+f_c^2\left(1+k_1\right)n_2\right\|^3-\\-2\left\|f_c^1k_2n_1+f_c^2\left(1+k_1\right)n_2\right\|^3+\left\|f_c^1\left(1+k_2\right)n_1+f_c^2\left(1+k_1\right)n_2\right\|^3\end{array}\right] \tag{O.15}$$

Next we show some particularized expressions of the function above since they appear relatively often in the description of the SSC between some of the signals of interest studied in chapter 5.1.1. Moreover, for simplicity and to avoid confusion in the notation, the following change of notation is proposed:

$$\begin{aligned}f_{c,1}&=f_c^1\\f_{c,2}&=f_c^2\end{aligned} \tag{O.16}$$

In fact, it can be shown that

$$\Xi\left(f_{c,1},n_1,f_{c,2},n_2,0,0\right)=\frac{-\left(f_{c,1}n_1+f_{c,2}n_2\right)\left(f_{c,1}^2n_1^2-4f_{c,1}f_{c,2}n_1n_2+f_{c,2}^2n_2^2\right)+\left\|f_{c,1}n_1-f_{c,2}n_2\right\|^3}{6f_{c,1}^3f_{c,2}^3n_1^3n_2^3} \tag{O.17}$$

Equally, the following identity is shown to be also true:

$$\Xi\left(f_c^1,n_1,f_c^2,n_2,j-i,0\right)=\Xi\left(f_{c,1},n_1,f_{c,2},n_2,k_1,0\right)=$$

$$\frac{1}{12\pi^3f_{c,1}^3f_{c,2}^3n_1^3n_2^3}\left[\begin{array}{l}2f_{c,1}^3n_1^3\pi^3\left(2k_1^3-\left(k_1-1\right)^3-\left(k_1+1\right)^3\right)\\+\left(\begin{array}{l}\left\|f_{c,2}\left(1+k_1\right)n_2-f_{c,1}n_1\right\|^3+\left\|f_{c,2}\left(-1+k_1\right)n_2+f_{c,1}n_1\right\|^3+\\+\left\|f_{c,2}\left(1-k_1\right)n_2+f_{c,1}n_1\right\|^3+\left\|f_{c,2}\left(-1+k_1\right)n_2+f_{c,1}n_1\right\|^3+\\-2\left(f_{c,2}n_2k_1+f_{c,1}n_1\right)^3\end{array}\right)\\-2f_{c,1}^3f_{c,2}^3n_1^3n_2^3\left\|\frac{k_1}{f_{c,1}n_1}-\frac{1}{f_{c,2}n_2}\right\|^3\end{array}\right] \tag{O.18}$$

and its symmetric version:

$$\Xi\left(f_c^1, n_1, f_c^2, n_2, 0, j'-i'\right) = \Xi\left(f_{c,1}, n_1, f_{c,2}, n_2, 0, k_2\right) =$$

$$\frac{1}{12 f_{c,1}^3 f_{c,2}^3 n_1^3 n_2^3}\left[\begin{array}{l} 2 f_{c,1}^3 n_1^3\left(2k_2^3-(k_2-1)^3-(k_2+1)^3\right) \\ +\left(\begin{array}{l} \left\|f_{c,1}(1+k_2)n_1 - f_{c,2}\, n_2\right\|^3 + \left\|f_{c,1}(-1+k_2)n_1 + f_{c,2} n_2\right\|^3 + \\ +\left\|f_{c,1}(1-k_2)n_1 + f_{c,2}\, n_2\right\|^3 + \left\|f_{c,1}(1+k_2)n_1 + f_{c,2} n_2\right\|^3 - \\ -2\left(f_{c,1}\, n_1\, k_2 + f_{c,2}\, n_2\right)^3 \end{array}\right) \\ -2 f_{c,1}^3 f_{c,2}^3 n_1^3 n_2^3 \left\|\frac{1}{f_{c,1} n_1} - \frac{k_2}{f_{c,2} n_2}\right\|^3 \end{array}\right] \qquad \text{(O.19)}$$

It is interesting to note the symmetry that (O.18) and (O.19) present, since the one expression can be expressed in terms of the other by just inverting the role of $f_{c,1}$ and n_1 with that of $f_{c,2}$ and n_2. Finally, the general analytical expression for the SSC between two BCS sequences can be expressed as follows:

$$\mathrm{SSC}_{\mathrm{BCS}_1-\mathrm{BCS}_2} = \left\{\begin{array}{l} n_1 n_2 f_c^1 f_c^2\, \Xi\left(f_c^1, n_1, f_c^2, n_2, 0, 0\right) + \\ +2 n_1 f_c^1 f_c^2 \sum_{i'=1}^{n_2-1} \sum_{j'=i'+1}^{n_2} s_{i'} s_{j'}\, \Xi\left(f_c^1, n_1, f_c^2, n_2, 0, j'-i'\right) + \\ +2 n_2 f_c^1 f_c^2 \sum_{i=1}^{n_1-1} \sum_{j=i+1}^{n_1} r_i r_j\, \Xi\left(f_c^1, n_1, f_c^2, n_2, j-i, 0\right) + \\ +4 f_c^1 f_c^2 \sum_{i'=1}^{n_2-1} \sum_{j'=i'+1}^{n_2} \sum_{i=1}^{n_1-1} \sum_{j=i+1}^{n_1} r_i r_j s_{i'} s_{j'}\, \Xi\left(f_c^1, n_1, f_c^2, n_2, j-i, j'-i'\right) \end{array}\right. \qquad \text{(O.20)}$$

O.2 Appendix. Self SSC of a generic BCS signal

As we have seen in chapter 5.2.3, the self SSC of a generic BCS sequence is shown to be:

$$\mathrm{SSC}_{\mathrm{BCS_1-BCS_2}}=\begin{cases} n^2 f_c^2\,\Xi\left(f_c,n,f_c,n,0,0\right)+ \\ +2nf_c^2\sum_{i'=1}^{n-1}\sum_{j'=i'+1}^{n} r_{i'}r_{j'}\,\Xi\left(f_c,n,f_c,n,0,j'-i'\right)+ \\ +2nf_c^2\sum_{i=1}^{n-1}\sum_{j=i+1}^{n} r_i r_j\,\Xi\left(f_c,n,f_c,n,j-i,0\right)+ \\ +4f_c^2\sum_{i'=1}^{n-1}\sum_{j'=i'+1}^{n}\sum_{i=1}^{n-1}\sum_{j=i+1}^{n} r_i r_j s_{i'}s_{j'}\,\Xi\left(f_c,n,f_c,n,j-i,j'-i'\right) \end{cases} \tag{O.21}$$

where the fourth term of the SSC sum can be further expanded as follows:

$$\mathrm{SSC}_4(n)=\sum_{i'=1}^{n-1}\sum_{j'=i'+1}^{n}\sum_{i=1}^{n-1}\sum_{j=i+1}^{n} r_i r_j s_{i'}s_{j'}\,\Xi\left(f_c,n,f_c,n,j-i,j'-i'\right) \tag{O.22}$$

$$\mathrm{SSC}_4(n)=\begin{cases} \left(s_1s_2+s_2s_3+s_3s_4+\ldots\right)\sum_{i=1}^{n-1}\sum_{j=i+1}^{n} r_i r_j\,\Xi\left(f_c,n,f_c,n,j-i,1\right)+ \\ +\left(s_1s_3+s_2s_4+s_3s_5+\ldots\right)\sum_{i=1}^{n-1}\sum_{j=i+1}^{n} r_i r_j\,\Xi\left(f_c,n,f_c,n,j-i,2\right)+ \\ +\left(s_1s_4+s_2s_5+s_3s_6+\ldots\right)\sum_{i=1}^{n-1}\sum_{j=i+1}^{n} r_i r_j\,\Xi\left(f_c,n,f_c,n,j-i,3\right)+\ldots \end{cases} \tag{O.23}$$

or equally:

$$\mathrm{SSC}_4(n)=\begin{cases} \left(s_1s_2+s_2s_3+s_3s_4+\ldots\right)\begin{bmatrix}\left(r_1r_2+r_2r_3+r_3r_4+\ldots\right)\Xi\left(f_c,n,f_c,n,1,1\right)+ \\ \left(r_1r_3+r_2r_4+r_3r_6+\ldots\right)\Xi\left(f_c,n,f_c,n,2,1\right)+ \\ \left(r_1r_4+r_2r_5+r_3r_7+\ldots\right)\Xi\left(f_c,n,f_c,n,3,1\right)+\ldots\end{bmatrix}+ \\ +\left(s_1s_3+s_2s_4+s_3s_5+\ldots\right)\begin{bmatrix}\left(r_1r_2+r_2r_3+r_3r_4+\ldots\right)\Xi\left(f_c,n,f_c,n,1,2\right)+ \\ \left(r_1r_3+r_2r_4+r_3r_6+\ldots\right)\Xi\left(f_c,n,f_c,n,2,2\right)+ \\ \left(r_1r_4+r_2r_5+r_3r_7+\ldots\right)\Xi\left(f_c,n,f_c,n,3,2\right)+\ldots\end{bmatrix}+ \\ +\left(s_1s_4+s_2s_5+s_3s_6+\ldots\right)\begin{bmatrix}\left(r_1r_2+r_2r_3+r_3r_4+\ldots\right)\Xi\left(f_c,n,f_c,n,1,3\right)+ \\ \left(r_1r_3+r_2r_4+r_3r_6+\ldots\right)\Xi\left(f_c,n,f_c,n,2,3\right)+ \\ \left(r_1r_4+r_2r_5+r_3r_7+\ldots\right)\Xi\left(f_c,n,f_c,n,3,3\right)+\ldots\end{bmatrix}+ \\ +\ldots \end{cases} \tag{O.24}$$

This expression can be further simplified using the scalar and shift operator θ. Indeed:

$$\mathrm{SSC}_4(n)=4f_c^2\sum_{l_1=1}^{n-1}\sum_{l_2=1}^{n-1}\left\{\begin{matrix}[r_1,r_2,\ldots r_n]\left[\theta\left([r_1,r_2,\ldots r_n],l_1\right)\right]^T\times \\ \times[s_1,s_2,\ldots s_n]\left[\theta\left([s_1,s_2,\ldots s_n],l_2\right)\right]^T\end{matrix}\right\}\Xi\left(f_c,n,f_c,n,l_1,l_2\right) \tag{O.25}$$

where the operator θ indicates a linear shift of the vector s by l elements to the right according to the following notation:

$$\sum_{i=1}^{n_1-1}\sum_{j=i+1}^{n_1} r_i r_j\,\Xi\left(f_c^1,n_1,f_c^2,n_2,j-i,1\right)=\sum_{l=1}^{n_1-1}[r_1,r_2,...r_{n_1}]\left[\theta\left([r_1,r_2,...r_{n_1}],l\right)\right]^T\Xi\left(f_c^1,n_1,f_c^2,n_2,l,1\right) \tag{O.26}$$

or in its expanded form:

$$\sum_{i=1}^{n_1-1}\sum_{j=i+1}^{n_1} r_i r_j\,\Xi\left(f_c^1,n_1,f_c^2,n_2,j-i,1\right)=\begin{cases}[r_1,r_2,...r_{n_1}][0,r_1,r_2,r_3...r_{n_1-1}]^T s_i s_j\,\Xi\left(f_c^1,n_1,f_c^2,n_2,1,1\right)+\\+[r_1,r_2,...r_{n_1}][0,0,r_1,r_2...r_{n_1-2}]^T s_i s_j\,\Xi\left(f_c^1,n_1,f_c^2,n_2,2,1\right)+\\+[r_1,r_2,...r_{n_1}][0,0,0,r_1...r_{n_1-3}]^T s_i s_j\,\Xi\left(f_c^1,n_1,f_c^2,n_2,3,1\right)+...\\+[r_1,r_2,...r_{n_1}][0,0,0,0...r_1]^T s_i s_j\,\Xi\left(f_c^1,n_1,f_c^2,n_2,n_1-1,1\right)+...\end{cases} \tag{O.27}$$

Summarizing, the different terms of the Self SSC of a BCS signal can also be expressed as:

$$\begin{aligned}\mathrm{SSC}_1(n)&=n^2 f_c^2\,\Xi(f_c,n,f_c,n,0,0)\\ \mathrm{SSC}_2(n)&=2nf_c^2\sum_{l=1}^{n-1}[r_1,r_2,...r_n]\left[\theta\left([r_1,r_2,...r_n],l\right)\right]^T\Xi(f_c,n,f_c,n,0,l)\\ \mathrm{SSC}_3(n)&=2nf_c^2\sum_{l=1}^{n-1}[r_1,r_2,...r_n]\left[\theta\left([r_1,r_2,...r_n],l\right)\right]^T\Xi(f_c,n,f_c,n,l,0)\\ \mathrm{SSC}_4(n)&=4f_c^2\sum_{l_1=1}^{n-1}\sum_{l_2=1}^{n-1}\left\{\begin{matrix}[r_1,r_2,...r_n]\left[\theta\left([r_1,r_2,...r_n],l_1\right)\right]^T\times\\ \times[r_1,r_2,...r_n]\left[\theta\left([r_1,r_2,...r_n],l_2\right)\right]^T\end{matrix}\right\}\Xi(f_c,n,f_c,n,l_1,l_2)\end{aligned} \tag{O.28}$$

Thus, grouping all the contributions of the SSC and since $[r_1,r_2,...r_n]=[s_1,s_2,...s_n]$ we can express the Self SSC of an arbitrary BCS signal as follows:

$$\mathrm{SSC}_{\text{Self BCS}}=\begin{cases}n^2 f_c^2\Xi(f_c,n,f_c,n,0,0)+\\ 4nf_c^2\sum_{l=1}^{n-1}[s_1,s_2,...s_n]\left[\theta\left([s_1,s_2,...s_n],l\right)\right]^T\Xi(f_c,n,f_c,n,l,0)+\\ 4f_c^2\sum_{l_1=1}^{n-1}\sum_{l_2=1}^{n-1}\left\{\begin{matrix}[s_1,s_2,...s_n]\left[\theta\left([s_1,s_2,...s_n],l_1\right)\right]^T\times\\ \times[s_1,s_2,...s_n]\left[\theta\left([s_1,s_2,...s_n],l_2\right)\right]^T\end{matrix}\right\}\Xi(f_c,n,f_c,n,l_1,l_2)\end{cases} \tag{O.29}$$

or equivalently:

$$\mathrm{SSC}_{\text{Self BCS}}=\begin{cases}n^2 f_c^2\Xi(f_c,n,f_c,n,0,0)+\\ 4f_c^2\sum_{l_1=1}^{n-1}\left\{\begin{matrix}n[s_1,s_2,...s_n]\left[\theta\left([s_1,s_2,...s_n],l_1\right)\right]^T\Xi(f_c,n,f_c,n,l_1,0)+\\ \left[\sum_{l_2=1}^{n-1}\left\{\begin{matrix}[s_1,s_2,...s_n]\left[\theta\left([s_1,s_2,...s_n],l_1\right)\right]^T\times\\ \times[s_1,s_2,...s_n]\left[\theta\left([s_1,s_2,...s_n],l_2\right)\right]\end{matrix}\right\}^T\Xi(f_c,n,f_c,n,l_1,l_2)\right]\end{matrix}\right\}\end{cases} \tag{O.30}$$

Moreover, to simplify the notation a little bit more we will do $\bar{s}=[s_1,s_2,...s_n]$ and assuming a particular code frequency, we do the change $\Psi(n,l_1,l_2)=\Xi(f_c,n,f_c,n,l_1,l_2)$. According to this, we can simplify the notation as follows, for a particular chip rate f_c:

$$\mathrm{SSC}_{\text{Self BCS}}=n^2 f_c^2\Psi(n,0,0)+4f_c^2\sum_{l_1=1}^{n-1}\left\{\begin{matrix}n\,\bar{s}\left[\theta\left(\bar{s},l_1\right)\right]^T\Psi(n,l_1,0)+\\ \left[\sum_{l_2=1}^{n-1}\bar{s}\left[\theta\left(\bar{s},l_1\right)\right]\bar{s}\left[\theta\left(\bar{s},l_2\right)\right]^T\Psi(n,l_1,l_2)\right]\end{matrix}\right\} \tag{O.31}$$

O.3 Appendix. SSC between a generic BCS and an arbitrary BOC or BPSK

The general expression for the SSC between a generic BCS signal and a sine or cosine-phased BOC modulation adopts a similar form to the expressions derived in the previous chapters. Indeed, this SSC is a particular case of the general SSC derived in (O.20). Interestingly, the SSC between a generic BCS and an arbitrary BOC signal shares SSC_1 and SSC_3 with the Self SSC of that BCS signal, being only different by the terms SSC_2 and SSC_4.

Indeed, for the case of the sine-phased modulation these are shown to adopt the general:

$$\begin{aligned}
&\mathrm{SSC}_2(n_1) = 2n_1 f_c^1 f_c^2 \sum_{i=1}^{n_2-1} (-1)^i (n_2 - i)\Xi\left(f_c^1, n_1, f_c^2, n_2, 0, i\right) \\
&\mathrm{SSC}_4(n_1) = 4 f_c^1 f_c^2 \sum_{l=1}^{n_1-1} \left\{ [r_1, r_2, \ldots r_{n_1}] \left[\theta\left([r_1, r_2, \ldots r_{n_1}], l\right)\right]^T \sum_{i=1}^{n_2-1} (-1)^i (n_2 - i)\Xi\left(f_c^1, n_1, f_c^2, n_2, l, i\right) \right\}
\end{aligned} \tag{O.32}$$

Grouping together all the terms we have then:

$$\begin{aligned}
&\mathrm{SSC}_{\mathrm{BCS}\left([\bar{r}], f_c^1\right) - \mathrm{BOC}_{\sin}\left(n_2, f_c^2\right)} = \\
&\begin{cases}
n_1 n_2 f_c^1 f_c^2 \,\Xi\left(f_c^1, n_1, f_c^2, n_2, 0, 0\right) + \\
+ 2n_1 f_c^1 f_c^2 \sum_{i=1}^{n_2-1} (-1)^i (n_2 - i)\Xi\left(f_c^1, n_1, f_c^2, n_2, 0, i\right) + \\
+ 2n_2 f_c^1 f_c^2 \sum_{l=1}^{n_1-1} [r_1, r_2, \ldots r_{n_1}] \left[\theta\left([r_1, r_2, \ldots r_{n_1}], l\right)\right]^T \Xi\left(f_c^1, n_1, f_c^2, n_2, l, 0\right) + \\
+ 4 f_c^1 f_c^2 \sum_{l=1}^{n_1-1} \left\{ [r_1, r_2, \ldots r_{n_1}] \left[\theta\left([r_1, r_2, \ldots r_{n_1}], l\right)\right]^T \sum_{i=1}^{n_2-1} (-1)^i (n_2 - i)\Xi\left(f_c^1, n_1, f_c^2, n_2, l, i\right) \right\}
\end{cases}
\end{aligned} \tag{O.33}$$

where the fourth term SSC_4 resembles the expressions that we saw in Appendix B for the derivation of the power spectral density of the sine-phased BOC modulation. Furthermore, it can be shown that the SSC between an arbitrary BCS signal and an arbitrary cosine-phased BOC adopts the following form:

$$\begin{aligned}
&\mathrm{SSC}_{\mathrm{BCS}\left([\bar{r}], f_c^1\right) - \mathrm{BOC}_{\cos}\left(n_2, f_c^2\right)} = \\
&\begin{cases}
n_1 n_2 f_c^1 f_c^2 \,\Xi\left(f_c^1, n_1, f_c^2, n_2, 0, 0\right) + \\
+ 2n_1 f_c^1 f_c^2 \left[\sum_{i=1}^{n_2/2} (-1)^i \,\Xi\left(f_c^1, n_1, f_c^2, n_2, 0, 2i-1\right) + \sum_{i=1}^{n_2/2-1} 2(-1)^i (n_2/2 - i)\Xi\left(f_c^1, n_1, f_c^2, n_2, 0, 2i\right) \right] + \\
+ 2n_2 f_c^1 f_c^2 \sum_{l=1}^{n_1-1} [r_1, r_2, \ldots r_{n_1}] \left[\theta\left([r_1, r_2, \ldots r_{n_1}], l\right)\right]^T \Xi\left(f_c^1, n_1, f_c^2, n_2, l, 0\right) + \\
+ 4 f_c^1 f_c^2 \sum_{l=1}^{n_1-1} \left\{ [r_1, r_2, \ldots r_{n_1}] \left[\theta\left([r_1, r_2, \ldots r_{n_1}], l\right)\right]^T \times \left[\sum_{i=1}^{n_2/2} (-1)^i \,\Xi\left(f_c^1, n_1, f_c^2, n_2, l, 2i-1\right) + \right. \right. \\
\left. \left. + \sum_{i=1}^{n_2/2-1} 2(-1)^i (n_2/2 - i)\Xi\left(f_c^1, n_1, f_c^2, n_2, l, 2i\right) \right] \right\}
\end{cases}
\end{aligned} \tag{O.34}$$

Equally, the SSC between an arbitrary BCS signal with code rate f_c^1 and a BPSK with code rate f_c^2 is shown to be:

$$\mathrm{SSC}_{\mathrm{BCS}\left([\vec{r}],f_c^1\right)-\mathrm{BPSK}(f_c^2)} = \begin{cases} n_1 n_2 f_c^1 f_c^2 \,\Xi\left(f_c^1, n_1, f_c^2, n_2, 0, 0\right) + \\ + 2 n_1 f_c^1 f_c^2 \sum_{i=1}^{n_2-1} (n_2 - i)\Xi\left(f_c^1, n_1, f_c^2, n_2, 0, i\right) + \\ + 2 n_2 f_c^1 f_c^2 \sum_{l=1}^{n_1-1} [r_1, r_2, \ldots r_{n_1}]\left[\theta\left([r_1, r_2, \ldots r_{n_1}], l\right)\right]^T \Xi\left(f_c^1, n_1, f_c^2, n_2, l, 0\right) + \\ + 4 f_c^1 f_c^2 \sum_{l=1}^{n_1-1} \left\{ [r_1, r_2, \ldots r_{n_1}]\left[\theta\left([r_1, r_2, \ldots r_{n_1}], l\right)\right]^T \sum_{i=1}^{n_2-1} (n_2 - i)\Xi\left(f_c^1, n_1, f_c^2, n_2, l, i\right) \right\} \end{cases} \quad \text{(O.35)}$$

O.4 Appendix. SSC between a generic BCS signal and the M-Code

Once we have derived the analytical expression for the SSC between two generic BCS signals in Appendix O.1, we show next some particular expressions. For exemplification the SSC between an arbitrary $\mathrm{BCS}\left(\left[\bar{r}\right], f_c^1\right)$ and the M-Code is presented next. This SSC is shown to be given by:

$$\mathrm{SSC}_{\mathrm{BCS}\left(\left[\bar{r}\right], f_c^1\right)-\mathrm{BOC}(10,5)} = \mathrm{SSC}_{\mathrm{BCS}_1-\mathrm{BOC}(10,5)} = \mathrm{SSC}_1 + \mathrm{SSC}_2 + \mathrm{SSC}_3 + \mathrm{SSC}_4 \tag{O.36}$$

where:

$$\begin{aligned}
\mathrm{SSC}_1 &= n_1 n_2 f_c^1 f_c^2\, \Xi\left(f_c^1, n_1, f_c^2, n_2, 0, 0\right) \\
\mathrm{SSC}_2 &= 2n_1 f_c^1 f_c^2 \sum_{i'=1}^{n_2-1} \sum_{j'=i'+1}^{n_2} s_{i'} s_{j'}\, \Xi\left(f_c^1, n_1, f_c^2, n_2, 0, j'-i'\right) \\
\mathrm{SSC}_3 &= 2n_2 f_c^1 f_c^2 \sum_{i=1}^{n_1-1} \sum_{j=i+1}^{n_1} r_i r_j\, \Xi\left(f_c^1, n_1, f_c^2, n_2, j-i, 0\right) \\
\mathrm{SSC}_4 &= 4 f_c^1 f_c^2 \sum_{i'=1}^{n_2-1} \sum_{j'=i'+1}^{n_2} \sum_{i=1}^{n_1-1} \sum_{j=i+1}^{n_1} r_i r_j s_{i'} s_{j'}\, \Xi\left(f_c^1, n_1, f_c^2, n_2, j-i, j'-i'\right)
\end{aligned} \tag{O.37}$$

As we can recognize, the first sum term is only a variable of n_1 and f_c^1, if we assume that f_c^2 and n_2 are given. In fact, since the second signal is the M-Code BOC(10,5), we can simplify (O.37) and express the total SSC exclusively as a function only of n_1 and f_c^1 as shown next. Let us begin with the first term of the SSC_1:

$$\mathrm{SSC}_1\left(n_1, f_c^1\right) = n_1 n_2 f_c^1 f_c^2\, \Xi\left(f_c^1, n_1, f_c^2, n_2, 0, 0\right)\Big|_{f_c^2=5.115\,\mathrm{MHz}, n_2=4} \tag{O.38}$$

Similarly, if we observe now the second sum term SSC_2, we see that once the chip form of the second signal has been fixed, this term only depends on the variable n_1. In order to accelerate the computation of SSCs we can calculate in advance this term as a function of n_1 given that the second signal is BOC-like, according to the following expression:

$$\mathrm{SSC}_2\left(n_1, f_c^1\right) = 2n_1 f_c^1 f_c^2 \left[-3\Xi\left(f_c^1, n_1, f_c^2, n_2, 0, 1\right) + 2\Xi\left(f_c^1, n_1, f_c^2, n_2, 0, 2\right) - \Xi\left(f_c^1, n_1, f_c^2, n_2, 0, 3\right)\right] \tag{O.39}$$

where we can easily recognize that the coefficients of the terms in brackets, namely -3, +2 and -1, correspond to the values of the generation matrix of BOC(10,5) shown in (5.22)

The third sum term, namely SSC_3, depends on the signal structure of the first signal. Thus, for every $k_1 = j - i$ and every n_1 we will compute the value as a function of k_1 and n_1. We develop now this term to find an expression with which we can calculate everything more easily in a numerical way:

$$\mathrm{SSC}_3\left(n_1, f_c^1\right) = 2n_2 f_c^1 f_c^2 \sum_{i=1}^{n_1-1} \sum_{j=i+1}^{n_1} r_i r_j\, \Xi\left(f_c^1, n_1, f_c^2, n_2, j-i, 0\right) \tag{O.40}$$

Indeed,

$$\mathrm{SSC}_3\left(n_1,f_c^1\right)=2n_2f_c^1f_c^2\left\{\begin{array}{l}[r_1,r_2,...r_{n_1}][0,r_1,r_2,r_3...r_{n_1-1}]^T\Xi\left(f_c^1,n_1,f_c^2,n_2,1,0\right)+\\+[r_1,r_2,...r_{n_1}][0,0,r_1,r_2...r_{n_1-2}]^T\Xi\left(f_c^1,n_1,f_c^2,n_2,2,0\right)+\\+[r_1,r_2,...r_{n_1}][0,0,0,r_1...r_{n_1-3}]^T\Xi\left(f_c^1,n_1,f_c^2,n_2,3,0\right)+...\\+[r_1,r_2,...r_{n_1}][0,0,0,0...r_1]^T\Xi\left(f_c^1,n_1,f_c^2,n_2,n_1-1,0\right)+...\end{array}\right|_{f_c^2=5.115\,\mathrm{MHz},n_2=4}$$

(O.41)

As we can see, we can express the double sum of (O.40) as the single sum of n_1-1 terms, what for the numerical calculations simplifies significantly the problem. As a conclusion, the third term of the SSC is only a function of n_1. Moreover, we can further simplify as follows:

$$\mathrm{SSC}_3\left(n_1,f_c^1\right)=2n_2f_c^1f_c^2\sum_{l=1}^{n_1-1}[r_1,r_2,...r_{n_1}]\left[\theta\left([r_1,r_2,...r_{n_1}],l\right)\right]^T\Xi\left(f_c^1,n_1,f_c^2,n_2,l,0\right)\Big|_{f_c^2=5.115\,\mathrm{MHz},n_2=4}$$

(O.42)

In a similar way, making use of the operator θ, we can now develop the fourth SSC term to have a more compact expression as follows:

$$\mathrm{SSC}_4\left(n_1,f_c^1\right)=4f_c^1f_c^2\sum_{l=1}^{n_1-1}[r_1,r_2,...r_{n_1}]\left[\theta\left([r_1,r_2,...r_{n_1}],l\right)\right]^T\left\{\begin{array}{l}-3\Xi\left(f_c^1,n_1,f_c^2,n_2,l,1\right)+\\+2\Xi\left(f_c^1,n_1,f_c^2,n_2,l,2\right)-\\-\Xi\left(f_c^1,n_1,f_c^2,n_2,l,3\right)\end{array}\right\}\Big|_{f_c^2=5.115\,\mathrm{MHz},n_2=4}$$

(O.43)

or equivalently:

$$\mathrm{SSC}_4\left(n_1,f_c^1\right)=4f_c^1f_c^2\left\{\begin{array}{l}\left(s_1s_2+s_2s_3+s_3s_4\right)\sum_{i=1}^{n_1-1}\sum_{j=i+1}^{n_1}r_ir_j\Xi\left(f_c^1,n_1,f_c^2,n_2,j-i,1\right)+\\+\left(s_1s_3+s_2s_4\right)\sum_{i=1}^{n_1-1}\sum_{j=i+1}^{n_1}r_ir_j\Xi\left(f_c^1,n_1,f_c^2,n_2,j-i,2\right)+\\+s_1s_4\sum_{i=1}^{n_1-1}\sum_{j=i+1}^{n_1}r_ir_j\Xi\left(f_c^1,n_1,f_c^2,n_2,j-i,3\right)\end{array}\right|_{f_c^2=5.115\,\mathrm{MHz},n_2=4}$$

(O.44)

If we recall now all the expressions derived in the preceding lines and group them together, we can see that the SSC between a generic BCS signal and the M-Code will be:

$$\mathrm{SSC}_{\mathrm{BCS}\left([\bar{r}],f_c^1\right)-\mathrm{BOC}(10,5)}=\begin{cases} n_1 f_c^1 f_c^2 \left\{ \begin{array}{l} n_2 \Xi\left(f_c^1,n_1,f_c^2,n_2,0,0\right)+ \\ +2\left[\begin{array}{l} -3\Xi\left(f_c^1,n_1,f_c^2,n_2,0,1\right)+ \\ +2\Xi\left(f_c^1,n_1,f_c^2,n_2,0,2\right)- \\ -\Xi\left(f_c^1,n_1,f_c^2,n_2,0,3\right) \end{array}\right] \end{array} \right\}+ \\ +2 f_c^1 f_c^2 \sum_{l=1}^{n_1-1}[r_1,r_2,...r_{n_1}]\left[\theta\left([r_1,r_2,...r_{n_1}],l\right)\right]^T \left\{ \begin{array}{l} n_2\,\Xi\left(f_c^1,n_1,f_c^2,n_2,l,0\right)+ \\ +2\left[\begin{array}{l} -3\Xi\left(f_c^1,n_1,f_c^2,n_2,l,1\right)+ \\ +2\Xi\left(f_c^1,n_1,f_c^2,n_2,l,2\right)- \\ -\Xi\left(f_c^1,n_1,f_c^2,n_2,l,3\right) \end{array}\right] \end{array} \right\} \end{cases} \tag{O.45}$$

In order to simplify the notation a little bit more, we can do $\Phi(n,l_1,l_2)=\Xi\left(f_c,n,f_c,n,l_1,l_2\right)$ and we can further simplify the expression as follows:

$$\mathrm{SSC}_{\mathrm{BCS}\left([\bar{r}],f_c^1\right)-\mathrm{BOC}(10,5)}\left(n_1,f_c^1\right)=\begin{cases} n_1 f_c^1 f_c^2 \left[\begin{array}{l} n_2\Phi(n_1,0,0)+ \\ 2\left[-3\Phi(n_1,0,1)+2\Phi(n_1,0,2)-\Phi\left(n_1,0,3\right)\right] \end{array}\right]+ \\ 2 f_c^1 f_c^2 \sum_{l=1}^{n_1-1}\bar{r}\left[\theta\left(\bar{r},l\right)\right]^T \left[\begin{array}{l} n_2\Phi(n_1,l,0)+ \\ +2\left\{-3\Phi(n_1,l,1)+2\Phi(n_1,l,2)-\Phi(n_1,l,3)\right\} \end{array}\right] \end{cases} \tag{O.46}$$

O.5 Appendix. Power of a generic BCS signal within a Bandwidth β_r

In this Appendix analytical expressions for the power that falls within a bandwidth β_r are derived. Recalling (4.26), the power spectral density of a generic BCS signal is defined as:

$$G_{\mathrm{BCS}([\bar{s}],f_c)}(f)=f_c\frac{\sin^2\left(\frac{\pi f}{nf_c}\right)}{(\pi f)^2}\left\{n+\sum_{i=1}^{n-1}\sum_{j=i+1}^{n}2s_is_j\cos\left[(j-i)\frac{\omega T_c}{n}\right]\right\}=G_{\text{Subchip pulse}}(f)G_{\text{Mod}}(f) \tag{O.47}$$

and integrating the PSD of a generic BCS in a bandwidth β_r, the total power that comes through the filter can be expressed as follows:

$$P=\int_{-\frac{\beta_r}{2}}^{\frac{\beta_r}{2}}G_{\mathrm{BCS}([\bar{s}],f_c)}(f)\mathrm{d}f=\int_{-\frac{\beta_r}{2}}^{\frac{\beta_r}{2}}f_c\frac{\sin^2\left(\frac{\pi f}{nf_c}\right)}{(\pi f)^2}\left\{n+\sum_{i=1}^{n-1}\sum_{j=i+1}^{n}2s_is_j\cos\left[(j-i)\frac{\omega T_c}{n}\right]\right\}\mathrm{d}f=P_1+P_2 \tag{O.48}$$

or equivalently:

$$P=nf_c\int_{-\frac{\beta_r}{2}}^{\frac{\beta_r}{2}}\frac{\sin^2\left(\frac{\pi f}{nf_c}\right)}{(\pi f)^2}\mathrm{d}f+2f_c\sum_{i=1}^{n-1}\sum_{j=i+1}^{n}s_is_j\int_{-\frac{\beta_r}{2}}^{\frac{\beta_r}{2}}\frac{\sin^2\left(\frac{\pi f}{nf_c}\right)}{(\pi f)^2}\cos\left[(j-i)\frac{\omega T_c}{n}\right]\mathrm{d}f \tag{O.49}$$

where the first integration, namely P_1, is shown to converge to the following expression:

$$P_1=\int_{-\frac{\beta_r}{2}}^{\frac{\beta_r}{2}}\frac{\sin^2\left(\frac{\pi f}{nf_c}\right)}{(\pi f)^2}\mathrm{d}f=\frac{2\left[-1+\cos\left(\frac{\pi\beta_r}{f_cn}\right)\right]}{\beta}+\frac{2\pi\,Si\left(\frac{\pi\beta_r}{f_cn}\right)}{f_cn\pi^2} \tag{O.50}$$

with

$$Si(z)=\int_0^z\frac{\sin(t)}{t}\mathrm{d}t \tag{O.51}$$

Moreover, it can also be shown that in the limit, when the integration bandwidth tends to infinity, (O.50) simplifies to:

$$\lim_{\beta_r\to\infty}P_1=\lim_{\beta_r\to\infty}\int_{-\frac{\beta_r}{2}}^{\frac{\beta_r}{2}}\frac{\sin^2\left(\frac{\pi f}{nf_c}\right)}{(\pi f)^2}\mathrm{d}f=\frac{1}{nf_c} \tag{O.52}$$

In fact,

$$\int_{-\frac{\beta_r}{2}}^{\frac{\beta_r}{2}}\frac{\sin^2\left(\frac{\pi f}{nf_c}\right)}{(\pi f)^2}\mathrm{d}f=\frac{1}{n\pi f_c}\int_{-\frac{nf_c\beta_r}{2\pi}}^{\frac{nf_c\beta_r}{2\pi}}\frac{\sin^2(x)}{x^2}\mathrm{d}x \tag{O.53}$$

where using partial integration, it can be shown that:

$$\int_a^b\frac{\sin^2(x)}{x^2}\mathrm{d}x=-\frac{1}{b}\sin^2(b)+\frac{1}{a}\sin^2(a)+\int_{2a}^{2b}\frac{\sin(x)}{x}\mathrm{d}x \tag{O.54}$$

for two generic integration limits. Moreover, since

$$\int_{-\infty}^{\infty} \frac{\sin^2(x)}{x^2} \mathrm{d}x = 2\int_{0}^{\infty} \frac{\sin^2(x)}{x^2} \mathrm{d}x \tag{O.55}$$

and given the fact that using complex integration we have

$$\int_{0}^{\infty} \frac{\sin(x)}{x} \mathrm{d}x = \frac{\pi}{2} \tag{O.56}$$

the integration limit can be simplified as follows

$$\lim_{\beta_r \to \infty} P_1 = \lim_{\beta_r \to \infty} \int_{-\frac{\beta_r}{2}}^{\frac{\beta_r}{2}} \frac{\sin^2\left(\frac{\pi f}{n f_c}\right)}{(\pi f)^2} \mathrm{d}f = \frac{1}{n\pi f_c} \lim_{\beta_r \to \infty} \int_{-\frac{n f_c \beta_r}{2\pi}}^{\frac{n f_c \beta_r}{2\pi}} \frac{\sin^2(x)}{x^2} \mathrm{d}x = \frac{1}{n f_c} \tag{O.57}$$

since only the integral term of (O.54) is different than zero when $a \to 0$ and $b \to \infty$.

Equally, we can find an explicit expression for the second integration of (O.49):

$$P_2 = \int_{-\frac{\beta_r}{2}}^{\frac{\beta_r}{2}} \frac{\sin^2\left(\frac{\pi f}{n f_c}\right)}{(\pi f)^2} \cos\left[\frac{2\pi k f T_c}{n}\right] \mathrm{d}f \tag{O.58}$$

which can be further simplified as follows:

$$P_2 = \frac{\left[\begin{array}{l} -2 f_c n \cos\left(\frac{\beta_r k \pi}{f_c n}\right) + 2 f_c n \cos\left(\frac{\beta_r \pi}{f_c n}\right)\cos\left(\frac{\beta_r k \pi}{f_c n}\right) + \\ \beta_r (k-1)\pi\, Si\left[\frac{\beta_r \pi (k-1)}{f_c n}\right] - 2\beta_r k \pi\, Si\left[\frac{\beta_r \pi k}{f_c n}\right] + \beta_r (1+k)\pi\, Si\left[\frac{\beta_r \pi (1+k)}{f_c n}\right] \end{array}\right]}{\beta_r f_c n \pi^2} \tag{O.59}$$

where the change $k = j - i$ was made for simplicity in the notation. If we calculate now the limit when the bandwidth of integration tends to infinity, we obtain the simplified expression:

$$\lim_{\beta_r \to \infty} P_2 = \lim_{\beta_r \to \infty} \int_{-\frac{\beta_r}{2}}^{\frac{\beta_r}{2}} \frac{\sin^2\left(\frac{\pi f}{n f_c}\right)}{(\pi f)^2} \cos\left[\frac{2\pi k f T_c}{n}\right] \mathrm{d}f = \frac{\|k-1\| - 2\|k\| + \|k+1\|}{2 n f_c} \tag{O.60}$$

Moreover, since $k \geq 1$ always, it can be shown that the following relationship for P_2 is valid for any k in the limit when β_r tends to infinity:

$$\frac{\|k-1\| - 2\|k\| + \|k+1\|}{2 n f_c} = \frac{k - 1 - 2k + k + 1}{2 n f_c} = 0 \tag{O.61}$$

Finally, combining now (O.50) and (O.59) above, we have the following analytical expressions for the integration of the PSD of a BCS in a finite bandwidth β_r:

$$P = P_1 + P_2 = \int_{-\frac{\beta_r}{2}}^{\frac{\beta_r}{2}} G_{\mathrm{BCS}}(f) \mathrm{d}f \tag{O.62}$$

and thus:

$$P=\left\{\begin{array}{l} nf_c\dfrac{\dfrac{2\left[-1+\cos\left(\dfrac{\pi\beta_r}{f_c n}\right)\right]}{\beta_r}+\dfrac{2\pi\, Si\left(\dfrac{\pi\beta_r}{f_c n}\right)}{f_c n}}{\pi^2}+ \\ +\dfrac{2}{\beta_r n\pi^2}\displaystyle\sum_{i=1}^{n-1}\sum_{j=i+1}^{n}s_i s_j\left[\begin{array}{l} -2f_c n\cos\left(\dfrac{\beta_r k\pi}{f_c n}\right)+2f_c n\cos\left(\dfrac{\beta_r\pi}{f_c n}\right)\cos\left(\dfrac{\beta_r k\pi}{f_c n}\right)+ \\ \beta_r(k-1)\pi\, Si\left[\dfrac{\beta_r\pi(k-1)}{f_c n}\right]-2\beta_r k\pi\, Si\left[\dfrac{\beta_r\pi k}{f_c n}\right]+\beta_r(1+k)\pi\, Si\left[\dfrac{\beta_r\pi(1+k)}{f_c n}\right] \end{array}\right]_{k=j-i} \end{array}\right. \tag{O.63}$$

Combining now (O.52) and (O.60) for the infinite bandwidth case we have:

$$\lim_{\beta_r\to\infty}\int_{-\frac{\beta_r}{2}}^{\frac{\beta_r}{2}}G_{\mathrm{BCS}}(f)\mathrm{d}f=1+\frac{1}{n}\sum_{i=1}^{n-1}\sum_{j=i+1}^{n}s_i s_j\left[\|k-1\|-2\|k\|+\|1+k\|\right]=1 \tag{O.64}$$

As we expected since the definition of the PSD is normalized to infinite bandwidth.

Bibliography

[M. Abramovitz and I.A. Stegun, 1965] M. Abramovitz and I.A. Stegun, *Handbook of Mathematical Functions*, Dover Publications, 1965, New York, USA.

[M. Ananda et al., 1993] M. Ananda, M. Munjal, B. Siegel, R. Sung, K.T. Woo, *Proposed GPS Integrity and Navigation Payload on DSCS*, Proceedings of the IEEE Military Communications Conference, October 1993, Boston, Massachusets, USA.

[F. Antreich and J. A. Nossek, 2007] F. Antreich and Josef A. Nossek, *On Chip Pulse Shape Design for Global Navigation Satellite Systems*, Second CNES Workshop on Galileo Signals and Signal Processing, 24-25 April 2007, ESTEC, Noordwijk, The Netherlands.

[J.-A. Avila-Rodriguez et al., 2005a] J.-A. Avila-Rodriguez, V. Heiries, T. Pany, B. Eissfeller, *Theory on Acquisition Algorithms for Indoor Positioning*, 12th Saint Petersburg International Conference on integrated navigation systems, 23-25 May, 2005, Saint Petersburg, Russia.

[J.-A. Avila-Rodriguez et al., 2004] J.-A. Avila-Rodriguez, G. W. Hein, M. Irsigler and T. Pany, *Combined Galileo/GPS Frequency and Signal Performance Analysis*, Proceedings of the International Technical Meeting of the Institute of Navigation, ION-GNSS 2004, 21-24 September, 2004, Long Beach, California, USA, pp. 632-649.

[J.-A. Avila-Rodriguez et al., 2005b] J.-A. Avila-Rodriguez, G. W. Hein, S. Wallner, T. Schueler, E. Schueler and M. Irsigler, *Revised Combined Galileo/GPS Frequency and Signal Performance Analysis*, Proceedings of the International Technical Meeting of the Institute of Navigation, ION-GNSS 2005, 13-16 September, 2005, Long Beach, California, USA.

[J.-A. Avila-Rodriguez et al., 2005c] J.-A. Avila-Rodriguez, T. Pany, B. Eissfeller, *A theoretical analysis of acquisition algorithms for indoor positioning*, 2nd ESA Workshop on Satellite Navigation User Equipment Technologies NAVITEC 2004, 8-10 December, 2004, Noordwijk, The Netherlands.

[J.-A. Avila-Rodriguez et al., 2006a] J.-A. Avila-Rodriguez, S. Wallner, G.W. Hein, *How to Optimize GNSS Signals and Codes for Indoor Positioning*, Proceedings of the International Technical Meeting of the Institute of Navigation, ION-GNSS 2006, 26-29 September, 2006, Fort Worth Convention Center, Fort Worth, Texas.

[J.-A. Avila-Rodriguez et al., 2006b] J.-A. Avila-Rodriguez, T. Pany, G.W. Hein, *Bounds on Signal Performance Regarding Multipath-Estimating Discriminators*, Proceedings of the International Technical Meeting of the Institute of Navigation, ION-GNSS 2006, 26-29 September, 2006, Fort Worth Convention Center, Fort Worth, Texas, USA.

[J.-A. Avila-Rodriguez et al., 2006c] J.-A. Avila-Rodriguez, S. Wallner, G.W. Hein, E. Rebeyrol, O. Julien, C. Macabiau, L. Ries, A. DeLatour, L. Lestarquit, J.-L. Issler, *CBOC – An Implementation of MBOC*, First CNES Workshop on Galileo Signals and Signal Processing, 12-13 October 2006, IAS (Institut Aero Spatial) Toulouse, France.

[J.-A. Avila-Rodriguez et al., 2006d] J.-A. Avila-Rodriguez, G. W. Hein, S. Wallner, A.R. Pratt, J.I.R. Owen, J.-L Issler, J.W. Betz, C.J. Hegarty, S. Lenahan, J.J. Rushanan, A.L. Kraay, T.A. Stansell, *MBOC: The New Optimized Spreading Modulation Recommended for Galileo E*1 *OS and GPS L*1*C*, ESA Navitec 2006, 11-13 December, 2006, Noordwijk, The Netherlands.

[J.-A. Avila-Rodriguez et al., 2007] J.-A. Avila-Rodriguez, G.W. Hein, S. Wallner, J.-L. Issler, L. Ries, L. Lestarquit, A. de Latour, J. Godet, F. Bastide, A.R. Pratt, J.I.R. Owen, M. Falcone, T. Burger, *The MBOC Modulation: The Final Touch to the Galileo Frequency and Signal Plan*, Proceedings of the International Technical Meeting of the Institute of Navigation, ION-GNSS 2006, 25-28 September, 2006, Fort Worth, Texas, USA.

[J.-A. Avila-Rodriguez et al., 2008] J.-A. Avila-Rodriguez, G.W. Hein, S. Wallner, J.-L. Issler, L. Ries, L. Lestarquit, A. De Latour, J. Godet, F. Bastide, A.R. Pratt, J.I.R. Owen, *The MBOC Modulation: The Final Touch to the Galileo Frequency and Signal Plan*, NAVIGATION: Journal of the Institute of Navigation, Vol. 55, No. 1, pp. 15-28, Spring 2008.

[E. Barankin, 1949] E. Barankin, *Locally Best Unbiased Estimates*, Annals of Mathematical Stastistics vol. 20, pp. 477-501. 1949.

[B.C. Barker et al., 2000] B.C. Barker, J.W. Betz, J.E. Clark, J.T. Correia, J.T. Gillis, S. Lazar, Lt. K. A. Rehborn, J.R. Straton, III, ARINC, *Overview of the GPS M-Code Signal*, Proceedings of the National Technical Meeting of the Institute of Navigation, ION-NTM 2000, 26-28 January 2000, Anaheim, California, USA.

[Beidou, 2006] http://www.globalsecurity.org/space/world/china/beidou.htm J. Pike. Beidou. *Space*. GlobalSecurity.org. Retrieved on 2006-11-09.

[S. Berberich et al., 2001] S. Berberich, P.A. Krauss, A. Botchkovski, *Development of a Flexible Receiver for Galileo Navigation Signal Verification*, Proceedings of the International Technical Meeting of the Institute of Navigation, ION-GNSS 2001, 11-14 September, 2001 - Salt Palace Convention Center, Salt Lake City, Utah, USA.

[J. W. Betz, 1999] J. W. Betz, *The offset carrier modulation for GPS modernization*, in Proceedings of the National Technical Meeting of the Institute of Navigation, ION-NTM 1999, pp. 639–648, January 1999, San Diego, California, USA.

[J.W. Betz, 2000a] J.W. Betz, *Analysis of M-Code Signal Interference with C/A Code Receivers*, Proceedings of the National Technical Meeting of the Institute of Navigation ION-NTM 2000, 26-28 January 2000, Anaheim, California, USA.

[J.W. Betz, 2000b] J.W. Betz, *Effect of Narrowband Interference on GPS Code Tracking Accuracy*, Proceedings of the National Technical Meeting of the Institute of Navigation ION-NTM 2000, 26-28 January 2000, Anaheim, California, USA.

[J.W. Betz and K.R. Kolodziejski, 2000] J.W. Betz and K.R. Kolodziejski 2000, *Extended Theory of Early-Late Code Tracking for a Bandlimited GPS Receiver*, NAVIGATION: Journal of the Institute of Navigation, Vol. 47, No. 3, Fall 2000.

[J.W. Betz, 2001a] J.W. Betz, *Binary Offset Carrier Modulations for Radionavigation*, NAVIGATION: Journal of The Institute of Navigation Vol. 48, No. 4, Winter 2001/02.

[J.W. Betz, 2001b] J. W. Betz, *Effect of Partial-Band Interference on Receiver Estimation of C/N_0: Theory*, Proceedings of the National Technical Meeting of the Institute of Navigation ION-NTM 2001, pp. 16-27, 22-24 January. 2001, Long Beach, California, USA.

[J. W. Betz and D. B. Goldstein, 2002] J. W. Betz and D. B. Goldstein, *Candidate designs for an additional civil signal in GPS spectral bands*, Technical Papers, January 2002, MITRE, Bedford, Massachussets, USA.

[J.W. Betz, 2003] J.W. Betz, *Brief Overview of Binary and Quadraphase Coded Symbols for GNSS*, 2 December 2003, Updated 18 December 2003.

[J.W. Betz et al., 2005] J.W. Betz, J.D. Fite, P.T. Capozza, *Getting to M-Direct Acquisition of the New Military Signal*, GPS World, April 2005, pp. 40-46.

[T. Burger et al., 2002] T. Burger, J. Holthaus, J. Reichel, L. Laux , *Galileo Phase B-2 – Spreading Code Design*, Astrium GmbH, 23 August 2002, GAL2-ASMD-TN-42154-003.

[D.J. Braverman, 1963] D.J. Braverman , *A Discussion of Spread Spectrum Composite Codes*, Aerospace Corporation, Report TDK-269, December 1963

[S. Butman and U. Timor, 1972] S. Butman and U. Timor , *Interplex – An efficient Multichannel PSK/PM Telemetry System*, Proceedings of IEEE Transaction on Communications, Volume 20, No. 3 – June 1972.

[G.L. Cangiani and J.A. Rajan, 2002] G.L. Cangiani and J.A. Rajan, *Programmable Waveform Generator for a Global Positioning System*, Patent : US 6335951 granted 1st January 2002.

[G. L. Cangiani et al., 2002] G. L. Cangiani, R.S. Orr and C.Q. Nguyen, *Methods and Apparatus for Generating a Constant-Envelope Composite Transmission Signal*, Patent number WO/2002/28044, International Application No.: PCT/US2001/30135, Publication date: 4 April 2002

[G.L. Cangiani et al., 2004] G.L. Cangiani, R. Orr, C.Q. Nguyen; Intervote Modulator, European Patent 1334595, granted 22nd December 2004.

[G.L. Cangiani, 2005] G.L. Cangiani, *Methods and Apparatus for Multi-beam Multi-signal Transmission for Actively Phased Array Antenna*, Patent US 6856284, granted 15 February, 2005.

[M.M. Chansarkar and L. Garin, 2000] M.M. Chansarkar and L. Garin, *Acquisition of GPS Signals at Very Low Signal to Noise Ratios*, Proceedings of the National Technical Meeting of the Institute of Navigation, ION-NTM 2000, pp. 731-737, January 26-28, 2000, Anaheim, California, USA.

[CNES, 2005] *Signaux BOC Multiplexage Temporel pseudo-aleatoire - Analyse de nouvelles formes d'onde et modulation pour les signaux Ouverts Galileo* - CNES Technical Note DCT/RF/TT - 2005.139.

[H. Cramér, 1946] H. Cramér. *Mathematical Methods of Statistics*. Princeton, NJ: Princeton University Press.

[H. S. Cobb, 1997] H. S. Cobb, *GPS, Pseudolites, Theory, Desging and Applications*, Ph.D. Thesis, September 1997.

[Compass, 2006a] *China joins EU's satellite network*, Business News, BBC News, 2003-09-19. Retrieved on 2006-11-09.

[Compass, 2006b] P. Marks. *China's satellite navigation plans threaten Galileo*, NewScientist.com. Retrieved on 2006-11-09.

[Compass ITU Filing, 2006] International Telecommunication Union, Annex 3 to Document 8D/274 on the Chinese Satellite Navigation System Compass: 8D-300 CHN Compass 1164-1215 MHz, 8D-301 CHN Compass 1260-1300 MHz, 8D-302 CHN Compass description and 8D-303 CHN Compass 1559-1610 MHz, 16 January 2006.

[P.A. Dafesh et al., 1999a] P.A. Dafesh, S. Lazar, and T. Nguyen, *Coherent Adaptive Sub-carrier Modulation* (*CASM*) *for GPS Modernization*, Proceedings of the National Technical Meeting of the Institute of Navigation, ION-NTM 1999, January 1999, San Diego, California, USA.

[P.A. Dafesh, 1999b] P.A. Dafesh, *Quadrature Product Sub-carrier Modulation* (*QPSM*), IEEE Aerospace Conference Record, March 1999.

[P.A. Dafesh et al., 2000] P.A. Dafesh, L. Cooper, M. Partridge, *Compatibility of the Interplex Modulation Method with C/A and P(Y) code Signals*, Proceedings of the International Technical Meeting of the Institute of Navigation, ION-GNSS 2000, September 2000, Salt Lake City, Utah, USA.

[P.A. Dafesh, 2002] P.A Dafesh, *Coherent Adaptive Sub-carrier Modulation Method*, Patent US 6,430,213, Granted 6 August 2002.

[P.A. Dafesh et al., 2006] P.A. Dafesh, Nguyen, M. Tien, *Quadrature product sub-carrier modulation system*, Patent US 7120198, Granted 10 October 2006.

[R. De Gaudenzi et al., 2000] R. De Gaudenzi, N. Hoult, A Batchelor, G. Burden, M. Quinlan, *Galileo Signal Validation Development*, 2000 John Wiley & Sons, Ltd.

[M. F. Easterling, 1962] M. F. Easterling, *A Skin-Tracking Radar Experiment Involving the COURIER Satellite*, IRE Proceedings of IEEE Transaction Space Electronics and Telemetry, vol. SET-8, pp. 76-64, June 1962.

[T. Fan et al, 2005] T. Fan, V. S. Lin, G. H. Wang, K. P. Maine, P. A. Dafesh and B. Myers, *The RF Compatibility of flexible Navigation Signal Combining Methods*, Proceedings of the National Technical Meeting of the Institute of Navigation, ION-NTM 2005, January 2005, San Diego, California, USA.

[Federal Aviation Administration FAA] Federal Aviation Administration FAA Website http://www.faa.gov/

[W. Feller, 1957] W. Feller, *Introduction to Probability Theory and Its Applications*, John Wiley and Sons, New York, 1957, p. 54.

[GAGAN, 2006a] http://www.indiadaily.com/editorial/10023.asp

[GAGAN, 2006b]
http://www.deccanherald.com/deccanherald/Feb242006/state191112006223.asp

[GAGAN, 2006c]
http://www.skyrocket.de/space/index_frame.htm,
http://www.skyrocket.de/space/doc_sdat/gsat-4.htm

[GAGAN, 2006d] http://www.mycoordinates.org/gagan-july-05-1.php

[Galileo SIS ICD, 2008] Galileo Open Service Signal In *Space Interface Control Document* (OS SIS ICD) Draft 1 01/02/2008, 2008, European Space Agency / Galileo Joint Undertaking http://www.galileoju.com

[Galileo SIS ICD for ICAO, 2005] Galileo JU *The Galileo Signal in Space ICD*, issued to ICAO or 3GPP, Spring 2005

[GATE Testbed] German GALILEO Test and Development Environment GATE http://www.gate-testbed.com

[G. Gibbons, 2007] G. Gibbons, *GLONASS: The Way Ahead*, Inside GNSS – GNSS World, Vol. 2, No. 3, Spring Issue, May 2007, pp. 20-23.

[GLONASS Centre] http://www.GLONASS-center.ru/nagu.txt

[GLONASS Constellation Status]
http://gge.unb.ca/Resources/GLONASSConstellationStatus.txt
http://www.GLONASS-center.ru/constel.html
http://ilrs.gsfc.nasa.gov/satellite_missions/list_of_satellites/GLONASS/
http://russianforces.org/eng/blog/archive/000246.shtml

[GLONASS ICD, 2002] GLONASS SIS ICD 2002. Version 5

[J. Godet, 2001] J. Godet, *Technical Annex to Galileo SRD Signal Plans*, STF annex SRD 2001/2003 Draft 1, July 2003.

[S. A. Gronemeyer and A. L. McBride, 1976] S. A. Gronemeyer and A. L. McBride, MSK and offset QPSK modulation. Proceedings of IEEE Transaction on Communications, v01. COM-24, pp. 809-820, Aug. 1976.

[GPS ICD 200, 2006] IS-GPS-200 Revision D, IRN-200D-001:*NAVSTAR GLOBAL POSITIONING SYSTEM Navstar GPS Space Segment/Navigation User Interface*, dated 7 March 2006.

[GPS ICD-705, 2005] IS-GPS-705, IRN-705-003: Navstar GPS Space Segment/User Segment L5 Interfaces, 22 September 2005.

[GPS ICD-800, 2006] Draft IS-GPS-800 Navstar GPS Space Segment/User Segment L1C Interfaces, 19 April 2006.

[GPS World, 2006]
http://www.gpsworld.com/gpsworld/article/articleDetail.jsp?id=399504&ref=25

[C.J. Hegarty, 2003] C.J. Hegarty, *Alternative Bi-phase GNSS Modulations*, MITRE Memo F82-M04-004, 24 November 2003.

[C.J. Hegarty et al., 2004] C.J. Hegarty, M. Tran and J.W. Betz, *Multipath Performance of the new GNSS Signals*, Proceedings of the National Technical Meeting of the Institute of Navigation, ION-NTM 2004, January 2004, San Diego, California, USA.

[C.J. Hegarty et al., 2005] C.J. Hegarty, J.W. Betz and A. Saidi, *Binary Coded Symbol Modulations for GNSS*, Proceedings of the National Technical Meeting of the Institute of Navigation, ION-NTM 2005, January 2005, San Diego, California, USA.

[G.W. Hein et al., 2001] G. W. Hein, J. Godet, J-L. Issler, J-C. Martin, R. Lucas-Rodriguez and T. Pratt *The Galileo Frequency Structure and Signal Design*, Proceedings of the International Technical Meeting of the Institute of Navigation, ION-GNSS 2001, September 2001, Salt Lake City, Utah, USA.

[G.W. Hein et al., 2002] G.W. Hein, J. Godet, J.-L. Issler, J.-C. Martin, P. Erhard, R. Lucas-Rodriguez and A. R. Pratt, *Status of Galileo Frequency and Signal Design*, Proceedings of the International Technical Meeting of the Institute of Navigation, ION-GNSS 2002, September 2002, Portland, Oregon, USA.

[G.W. Hein et al., 2004] G.W. Hein, M. Irsigler, M., J.-A. Avila-Rodriguez, T. Pany, *Performance of Galileo L1 Signal Candidates*, Proceedings of the European Navigation Conference ENC-GNSS 2004, 16 - 19 May 2004, Rotterdam, The Netherlands

[G.W. Hein et al., 2005] G.W. Hein, J.-A. Avila-Rodriguez, L. Ries, L. Lestarquit, J.-L. Issler, J. Godet, A.R. Pratt, Members of the Galileo Signal Task Force of the European Commission: *A Candidate for the Galileo L1 OS Optimized Signal*, Proceedings of the International Technical Meeting of the Institute of Navigation, ION-GNSS 2005, 13-16 September, 2005, Long Beach, California, USA.

[G.W. Hein and J.-A. Avila-Rodriguez, 2005] G.W. Hein and J.-A. Avila-Rodriguez, *Performance of a Galileo PRS/GPS M-Code Combined Service*, Proceedings of the National Technical Meeting of the Institute of Navigation, ION-NTM 2005, January 24-26, 2005 , San Diego, California, USA.

[G.W. Hein et al., 2006a] G. W. Hein, J.-A. Avila-Rodriguez, S. Wallner, A.R. Pratt, J.I.R. Owen, J.-L Issler, J.W. Betz, C.J. Hegarty, S. Lenahan, J.J. Rushanan, A.L. Kraay, T.A. Stansell, *MBOC: The New Optimized Spreading Modulation Recommended for Galileo L1 OS and GPS L1C*, Proceedings of the International Technical Meeting of the Institute of Navigation, IEEE/ION PLANS 2006, 24-27 April, 2006, Loews Coronado Bay Resort, San Diego, California, USA.

[G.W. Hein et al., 2006b] G. W. Hein, J.-A. Avila-Rodriguez, S. Wallner, A.R. Pratt, J.I.R. Owen, J.-L Issler, J.W. Betz, C.J. Hegarty, S. Lenahan, J.J. Rushanan, A.L. Kraay, T.A. Stansell, *MBOC: The New Optimized Spreading Modulation Recommended for Galileo L1 OS and GPS L1C*, Inside GNSS – Working Papers, Vol.1, No.4, May/June 2006, pp.57-65.

[G.W. Hein et al., 2006c] G.W. Hein, J.-A. Avila-Rodriguez, S. Wallner, *The ~~DaVinci~~ Galileo Code and Others*, Inside GNSS – Working Papers, Inside GNSS, Vol. 1, No. 6, September 2006, pp. 62-73.

[G.W. Hein and J.-A. Avila-Rodriguez, 2006] G.W. Hein, J.-A. Avila-Rodriguez, *Combining Galileo PRS and GPS M-Code*, Inside GNSS – Working Papers, Vol. 1, No. 1, January/February 2006, pp. 48-56.

[G.W. Hein et al., 2007a] G.W. Hein, J.-A. Avila-Rodriguez, S.Wallner, B. Eissfeller, T. Pany and P. Hartl, *Envisioning a Future GNSS System of Systems: Part* 1, Inside GNSS – Working Papers, Vol. 2, No. 1, January/February 2007, pp. 58-67.

[G.W. Hein et al., 2007b] G.W. Hein, J.-A. Avila-Rodriguez, S.Wallner, T. Pany, B. Eissfeller and P. Hartl, *Envisioning a Future GNSS System of Systems: Part* 2, Inside GNSS – Working Papers, Vol. 2, No. 2, March/April 2007, pp. 64-72.

[G.W. Hein et al., 2007c] G.W. Hein, J.-A. Avila-Rodriguez, S.Wallner, T. Pany, M. Irsigler, B. Eissfeller and P. Hartl, *Envisioning a Future GNSS System of Systems: Part* 3, Inside GNSS – Working Papers, Vol. 2, No. 4, May/June 2007.

[V. Heiries et al., 2005] V. Heiries, J.-A. Avila-Rodriguez, G.W. Hein, M. Irsigler, E. Rebeyrol, D. Roviras, *Acquisition Performance Analysis of Alternative Optimized Galileo Signals*, Proceedings of the International Technical Meeting of the Institute of Navigation, ION-GNSS 2005, 13-16 September, 2005, Long Beach, California, USA.

[V. Heiries et al., 2006] V. Heiries, V. Calmettes, L. Ries, D. Roviras, *Solving the Correlation Peak Ambiguity of BOC Signals*, First CNES Workshop on Galileo Signals and Signal Processing, 12-13 October 2006, IAS (Institut Aero Spatial) Toulouse, France.

[J.K. Holmes, 1982] J.K. Holmes, *Coherent Spread Spectrum Systems*, Publisher John Wiley and Sons, Inc. New York, New York, USA.

[J.K. Holmes, 2000] Holmes, J.K., *Code Tracking Loop Performance Including the Effect of Channel Filtering and Gaussian Interference,* Proceedings of the US Institute of Navigation ION-AM 2000, pp. 382-398, 26-28 June, San Diego, California, USA.

[Inside GNSS] www.insidegnss.com

[M. Irsigler et al., 2002] M. Irsigler, G.W. Hein, B. Eissfeller, A. Schmitz-Peiffer, M. Kaiser, A. Hornbostel, P. Hartl, *Aspects of C-Band Satellite Navigation: Signal Propagation and Satellite Signal Tracking*, Proceedings of the European Navigation Conference ENC-GNSS 2002, 27-30 May 2002, Copenhagen, Denmark.

[M. Irsigler et al., 2004] M. Irsigler, G.W. Hein and A. Schmitz-Peiffer, *Use of C-Band frequencies for satellite navigation: benefits and drawbacks*, GPS Solutions, Volume 8, Number 3, 119-139, September 2004, Wiley Periodicals Inc., 2004.

[M. Irsigler et al., 2005] M. Irsigler, J.-A. Avila-Rodriguez, G.W. Hein, *Criteria for GNSS Multipath Performance Assessment*, Proceedings of the 18th International Technical Meeting of the Satellite Division of the Institute of Navigation, ION-GNSS 2005, 13-16 September, 2005, Long Beach, California, USA.

[M. Irsigler, 2008] M. Irsigler, *Multipath Propagation, Mitigation and Monitoring in the Light of Galileo and the Modernized GPS*, PhD Thesis, University FAF Munich, 2008

[J.-L. Issler et al., 2003] J.-L. Issler, L. Ries, L. Lestarquit, O. Nouvel, Q. Jeandel, *Spectral measurements of GNSS Satellite Signals: Need for wide transmitted bands*, Proceedings of the International Technical Meeting of the Satellite Division of the Institute of Navigation, ION-GNSS 2003, September 2003, Portland, Oregon, USA, 2003.

[O. Julien et al., 2004a] Julien, O., C. Macabiau, G. Lachapelle, M.E. Cannon, and C. Mongrédien *A New Unambiguous BOC*(*n,n*) *Signal Tracking Technique,* Proceedings of the European Navigation Conference ENC-GNSS 2004, 16-19 May, 2004, The Netherlands.

[O. Julien et al., 2004b] Julien, O., G. Lachapelle and M.E. Cannon, *A New Multipath and Noise Mitigation Technique using Data/Data-less Navigation Signals*, Proceedings of the International Technical Meeting of the Institute of Navigation, ION-GNSS 2004, pp. 8-19, 24-27 September, 2004, Long Beach, California, USA.

[O. Julien, 2005] Olivier Julien, *Design of Galileo L1F Receiver Tracking Loops*, PhD Thesis, Department of Geomatics Engineering, University of Calgary

http://www.geomatics.ucalgary.ca/links/GradTheses.html

[O. Julien et al., 2006] O. Julien, C. Macabiau, L. Ries, J.-L. Issler, 1 - *Bit processing of Composite BOC* (*CBOC*) *Signals*, First CNES Workshop on Galileo Signals and Signal Processing, 12-13 October 2006, IAS (Institut Aero Spatial) Toulouse, France.

[O. Julien et al., 2007] O. Julien, C. Macabiau, J-L. Issler, L. Ries , *1 Bit Processing of Composite BOC* (*CBOC*) *Signals and Extension to Time-Multiplexed BOC* (*TMBOC*) *Signals*, Proceedings of the National Technical Meeting of the Institute of Navigation, ION-NTM 2007, January 2007, San Diego, California, USA.

[H. Koorapaty, 2004] H. Koorapaty, *Barankin bounds for position estimation using received signal strength measurements*, in Proceedings of the 59th IEEE Vehicular Technology Conference (VTC '04), vol. 5, pp. 2686-2690, Milan, Italy, May 2004.

[G. Lachapelle, 2004] Lachapelle, G., *NAVSTAR GPS: Theory and Applications*, ENGO 625 Lecture Notes, Department of Geomatics Engineering, University of Calgary.

[E.A. Lee and D.B. Messerschmitt, 1994] E.A. Lee and D.B. Messerschmitt, *Digital Communications*, 2nd edition, Norwell, Massachusetts, Kluwer Academic Publishers.

[M. J. Lighthill, 1958] M. J. Lighthill, *Introduction to Fourier Analysis and Generalized Functions*, New York, Cambridge University Press, 1958

[E. D. Kaplan and C. Hegarty, 2006] E. D. Kaplan and C. Hegarty, *Understanding GPS: Principles and Applications-2nd Edition,* Chapter 4.

[D. Klein and B.W. Parkinson, 1984] D. Klein and B.W. Parkinson, *The use of pseudo-satellites for improving GPS performance*, Global Positioning System (red book), Vol III, Institute of Navigation, 135-146.

[LAAS] [http://gps.faa.gov/Programs/LAAS/laas.htm]

[G.D. MacGougan, 2003] G.D. MacGougan, *High Sensitivity GPS Performance Analysis in Degraded Signal Environment*, Master's thesis, Department of Geomatics Engineering, University of Calgary, UCGE Report 20176.

[P.G. Mattos, 2005] P.G. Mattos, *Acquisition of the Galileo OAS L*1 *b/c Signal for the Mass-Market Receiver*, Proceedings of the International Technical Meeting of the Institute of Navigation, ION-GNSS 2005, 13-16 September, 2005, Long Beach, California, USA.

[P.G. Mattos, 2007] P.G. Mattos, *Hardware and Algorithm Implications of Adding Galileo Capability to an SPS GPS Receiver*, Proceedings of the National Technical Meeting of the Institute of Navigation, ION-NTM 2007, January 2007, San Diego, California, USA.

[MBOC Recommendation, 2006]
http://gps.losangeles.af.mil/engineering/icwg/Docs/WGA%20Signed%20Recommendation%20on%20MBOC%20-%2023%20Mar%2006.pdf

[R. McAulay and E. Hofstetter, 1971] R. McAulay and E. Hofstetter, *Barankin Bounds on Parameter Estimation*, IEEE Transactions on Information Theory, vol. IT-17, number 6, pp. 669-676, 1971.

[H. R. Mathwich et al., 1974] H. R. Mathwich, J. F. Balcewicz, and M. Hecht, *The effect of tandem band and amplitude on the Eb/N_0 performance of minimum (frequency) shift keying (MSK)*, Proceedings of IEEE Trans. on Comm., vol. COM-22, pp. 1525-1540, Oct.. 1974.

[T.G. Morley, 1997] T. G. Morley, PhD Thesis, *Augmentation of GPS with Pseudolites in a Marine Environment* May, 1997.

[B. Muth et al., 2007] B. Muth, P. Oonincx, and C. Tiberius, *A Time-Domain Fingerprint for BOC(m,n) Signals*, EURASIP Journal on Advances in Signal Processing, vol. 2007, Article ID 56104, 7 pages, 2007. doi:10.1155/2007/56104

[Optimization Statement, 2006]
http://gps.losangeles.af.mil/engineering/icwg/Docs/EC%20and%20US%20Joint%20Statement%20on%20Galileo%20and%20GPS%20Signal%20Optimization%20-20%2024%20Mar%2006.pdf

[R. S. Orr and B. Veytsman, 2002] R. S. Orr and B. Veytsman., *Methods and Apparatus for Multiplexing Signal Codes via weighted Majority Logic*, Patent number WO/2002/069516, International Application No.: PCT/US2002/005657, Publication date: 6 September 2002

[T. Pany et al., 2002] T. Pany, B. Eissfeller, M. Irsigler and J. Winkel, *Code and Carrier Phase Tracking Performance of a Future Galileo RTK Receiver*, Proceedings of the European Navigation Conference ENC-GNSS 2002, 27-30 May 2002, Copenhagen, Denmark.

[T. Pany, 2003] T. Pany, *Code and Phase Tracking of Generic PRN Signals with Low Sample Rates and a Cramér-Rao Correlator*, NAVIGATION: Journal of The Institute of Navigation, Vol. 51, No. 2, pp. 143-160, 2003.

[T. Pany et al., 2003] T. Pany, B. Eissfeller and J. Winkel, *Tracking of High Bandwidth GPS/Galileo Signals with a Low Sample Rate Software Receiver*, Proceedings of the European Navigation Conference ENC-GNSS 2003, April 2003, Graz, Austria.

[S. Pasupathy, 1979] S. Pasupathy, *Minimal Shift Keying: A Spectrally Efficient Modulation*, IEEE Communications Magazine, 1979

[Philco-Ford Corp., 1968] Philco-Ford Corp., *System Design Analysis*, Space-Ground Subsystem. Ground Station, System Analysis Summary Report, Vol. I, November 15, 1968.

[R. Piriz et al., 2005] R. Piriz, B. Martín-Peiró, M. Romay-Merino, *The Galileo Constellation Design: A Systematic Approach*, Proceedings of the International Technical Meeting of the Institute of Navigation, ION-GNSS 2005, 13-16 September, 2005, California, USA.

[A.R. Pratt and J.I.R. Owen, 2003a] Anthony R. Pratt & John I.R. Owen, *BOC Modulations Waveform*, Proceedings of the International Technical Meeting of the Institute of Navigation, ION-GNSS 2003, 9-12 September 2003, Portland, Oregon, USA.

[A.R. Pratt and J.I.R. Owen, 2003b] A.R. Pratt and J.I.R. Owen, *Performance of GPS Galileo Receivers Using m-PSK BOC Signals,* Proceedings of the International Technical Meeting of the Institute of Navigation, ION-GNSS 2003, 9-12 September 2003, Portland, Oregon, USA.

[A.R. Pratt and J.I.R. Owen, 2005] A.R. Pratt and J.I.R. Owen, *Signal Multiplex Techniques in Satellite Channel Availability - Possible Applications to Galileo*, Proceedings of the International Technical Meeting of the Institute of Navigation, ION-GNSS 2005, 13-16 September 2005, Long Beach, California, USA.

[A.R. Pratt et al., 2006] A.R. Pratt, J.I.R. Owen, G.W. Hein, J.-A. Avila-Rodriguez: *Tracking Complex Modulation Waveforms- How to Avoid Receiver Bias*, Proceedings of the International Technical Meeting of the Institute of Navigation, IEEE/ION PLANS 2006, 24-27 April, 2006, Loews Coronado Bay Resort, San Diego, California, USA.

[A. R. Pratt and J. I. R. Owen, 2007] A. R. Pratt and J. I. R. Owen., *Signals, System, Method and Apparatus*, Patent number WO/2007/148081, International Application No.: PCT/GB2007/002293, Publication date: 27 December 2007

[M. Quinlan et al., 2004] M. Quinlan, G. Burden, S. Rollet, R. De Gaudenzi, S. Harding, *Validation of Novel Navigation Signal Structures for Future GNSS Systems*, 0-7803-841 6-4/04/$20.00 02004 Proceedings of the IEEE.

[QZSS SIS ICD, 2007] Quasi Zenith Satellite System Navigation Service, *Interface Specification for QZSS* (*IS-QZSS*), Japan Aerospace Exploration Agency, January 22, 2007.

[S. H. Raghavan et al., 1997] S. H. Raghavan, J. K. Holmes, S. Lazar, and M. F. Bottjer, *Tricode Hexaphase Modulation for GPS*, Proceedings of the 10th International Technical Meeting of the Institute of Navigation, ION-GNSS 1997, 16-19 September, 1997, Kansas City, Missouri, USA.

[J.A. Rajan and J. Irvine, 2005] J.A. Rajan and J. Irvine, *GPS IIR-M and IIF: Payload Modernization*, Proceedings of the National Technical Meeting of the Institute of Navigation, ION-NTM 2005, 24-26 January 2005, San Diego,California, USA.

[E. Rebeyrol et al., 2005] E. Rebeyrol, C. Macabiau, L. Lestarquit, L. Ries, J-L. Issler, M.L. Boucheret, M. Bousquet , *BOC Power Spectrum Densities*, Proceedings of the National Technical Meeting of the Institute of Navigation, ION-NTM 2005, 24-26 January 2005, Long Beach, California, USA.

[E. Rebeyrol et al., 2006] E. Rebeyrol, C. Macabiau, L. Ries, J.-L. Issler, M. Bousquet, M.-L. Boucheret, *Interplex Modulation for Navigation Systems at the L1 band*, Proceedings of the National Technical Meeting of the Institute of Navigation, ION-NTM 2006, January 2006, San Diego, California, USA.

[Reference Assumptions, 2004] *Reference Assumptions For GPS/Galileo Compatibility Analyses*, Joint United States/European Document, 9 June 2004.

[L. Ries et al., 2002] L. Ries, L. Lestarquit, P. Erhard, F. Legrand, C. Macabiau, Q. Jeandel and C. Bourgat, *Software Simulation Tools for GNSS*2 *BOC Signal Analysis*, Proceedings of the International Technical Meeting of the Institute of Navigation, ION-GNSS 2002, 24-27 September 2002, Oregon Convention Center, Portland, Oregon, USA.

[L. Ries et al., 2003] L. Ries, F. Legrand, L. Lestarquit, W. Vigneau, J.L. Issler , *Tracking and Multipath Performance Assessments of BOC Signals Using a Bit-Level Signal Processing Simulator*, Proceedings of the International Technical Meeting of the Institute of Navigation, ION-GNSS 2003, 9-12 September, 2003, Oregon Convention Center, Portland, Oregon, USA.

[L. Ries and J.-L. Issler 2003] CNES Technical Note DTS/AE/TTL/RN – 2003-48, *Spectral Control with Constant Envelope Modulations Application to Galileo BOC Signals in E*2-*L*1-*E*1.

[L. Ries et al., 2006] L. Ries, J.-L. Issler, L. Lestarquit, J.-A. Avila-Rodriguez and G.W. Hein, *Spread Spectrum Signal*, Patent number WO/2006/075018, International Application No.: PCT/EP2006/050179, Publication date: 20 July 2006

[RTCS/DO 229] RTCA/DO- 229: Minimum Operational Performance Standards (MOPS) for Global Positioning System/Wide Area Augmentation System (GPS/WAAS) Airborne Equipment. Quoting Standards And Recommend Practices (SARPS).

[M. M. Shihabbi et al., 1994] M. M. Shihabbi, T. M. Nguyen and S. M. Hinedi, *A Comparison of Telemetry Signals in the Presence and Absence of a Sub-carrier*, IEEE Transaction on Electromagnetic Compatibility, Vol. 36, No. 1, February, 1994.

[M. Soellner et al., 2003] M. Soellner and P. Erhard, *Comparison of AWGN code tracking accuracy for Alternative-BOC, Complex-LOC and Complex-BOC modulation options in Galileo E5-Band*, Proceedings of the European Navigation Conference ENC-GNSS 2003, April 2003, Graz, Austria.

[F. Soualle and T. Burger, 2002] F. Soualle and T. Burger, *Interference Analysis for the Global Navigation Satellites Systems Galileo and GPS, Astrium* Galileo Phase B2 (post-KPM) document, GAL2-ASMD-TN-42154-002, 15.05.2002.

[F. Soualle et al., 2005] F. Soualle, M. Soellner, S. Wallner, J.-A. Avila-Rodriguez, G.W. Hein, B. Barnes, A.R. Pratt, L. Ries, J. Winkel, C. Lemenager, P. Erhard: *Spreading code selection criteria for the future GNSS Galileo*, Proceedings of the European Navigation Conference GNSS 2005, 19 - 22 July 2005, Munich, Germany.

[F. Soualle et al., 2007] F. Soualle, M. Kaindl, G. Hechenblaikner, M. Middendorf*, Introduction To An Additional Radio Frequency Compatibility Criterion For Code Tracking Performance,* Second CNES Workshop on Galileo Signals and Signal Processing, 24-25 April 2007, ESTEC, Noordwijk, The Netherlands.

[J.J. Spilker, 1977] J.J. Spilker*, Digital Communications by Satellite*, Prentice Hall Inc., Englewood Cliffs, N.J., pp. 600-603, 1977

[J.J. Spilker, 1997a] J.J. Spilker, *GPS Signal Structure and Theoretical Performance* in *Global Positioning System: Theory and Applications Volume I*, Progress in Astronautics and Aeronautics Volume 164, AIAA, pp. 57-120.

[J.J. Spilker, 1997b] J.J. Spilker, *Fundamentals of Signal Tracking Theory* in *Global Positioning System: Theory and Applications Volume I*, Progress in Astronautics and Aeronautics Volume 164, AIAA, pp. 245-328.

[J.J. Spilker, 1997c] J.J. Spilker, *GPS Navigation Data* in *Global Positioning System: Theory and Applications Volume I*, Progress in Astronautics and Aeronautics Volume 164, AIAA, pp. 121-176.

[J.J. Spilker Jr. and R.S. Orr, 1998] J.J. Spilker Jr. and R.S. Orr, *Code Multiplexing Via Majority Logic for GPS Modernization*, ION GPS 1998, 15-18 September 1998, Nashville.

[US-EC Agreement, 2004] http://pnt.gov//public/docs/2004-US-EC-agreement.pdf

[Satellite Tool Kit STK, 2006] Satellite Tool Kit (STK) Educational Bundle Version 8.0.1 by Analytical Graphics, Inc. (AGI), Exton, Pennsylvania, USA, 2006.

[US-EU Joint Document, 2004] *Models And Methodology For GPS/Galileo Radio Frequency Compatibility Analyses*, Joint United States/European Document, 20 June 2004.

[US-Russia Statement, 2006]
http://www.GLONASS-ianc.rsa.ru/i/GLONASS/joint_statement_eng.pdf

[R.C. Tausworthe, 1971] R.C. Tausworthe, *Practical Design of Third-Order Phase-Locked Loops*, Jet Propulsion Lab., California Institute of Technology (internal document) TR 900-450, pp. 19-30, April 1971

[A.J. Van Dierendonck, 1997] A.J. Van Dierendonck, *GPS Receivers* in *Global Positioning System: Theory and Application Volume I*, Progress in Astronautics and Aeronautics Volume 164, AIAA, pp. 329-408.

[J. Von Neumann et al., 1951] J. Von Neumann , A.S. Householder, G.E. Forsythe, and H.H. Germond, *Various techniques used in connection with random digits*, in eds., *Monte Carlo Method*, *National Bureau of Standards Applied Mathematics Series*, 12, Washington, D.C. U.S. Government Printing Office, 1951: pp. 36-38.

[S. Wallner et al., 2005] S. Wallner, G.W. Hein, J.-A. Avila Rodriguez, T. Pany, A. Posfay, *Interference Computations Between GPS and Galileo*, Proceedings of the International Technical Meeting of the Institute of Navigation, ION-GNSS 2005, 13-16 September, 2005, Long Beach, California, USA.

[S. Wallner et al., 2006a] S. Wallner, J.-A. Avila-Rodriguez, G.W. Hein, *Galileo E1 OS and GPS L1C Pseudo Random Codes – Requirements, Generation, Optimization and Comparison*, First CNES Workshop on Galileo Signals and Signal Processing, 12-13 October 2006, IAS (Institut Aero Spatial) Toulouse, France.

[S. Wallner et al., 2006b] S. Wallner, J.-A. Avila-Rodriguez, G.W. Hein, *Interference Computations between Several GNSS Systems*, ESA Navitec 2006, December 11-13, 2006, Noordwijk, The Netherlands.

[S. Wallner 2007] S. Wallner, *Private Conversation*, March 2007, Munich, Germany.

[G.H. Wang et al., 2004] G.H. Wang, V.S. Lin, T. Fan, K.P. Maine, P.A. Dafesh , *Study of Signal Combining Methodologies for GPS III's Flexible Navigation Payload*, Proceedings of the International Technical Meeting of the Institute of Navigation, ION-GNSS 2004, 21-24 September, 2004, Long Beach, California, USA.

[P. Ward, 1994] P. Ward, *Dual Use of Military Anti-Jam GPS Receiver Design Techniques for Commercial Aviation RF Interference Integrity Monitoring*, Proceedings of the US Institute of Navigation ION-AM 1994.

[P. Ward, 1996] P. Ward, *Satellite Signal Acquisition and Tracking* in *Understanding GPS: Principles and Applications*, Artech House Inc.

[P. Ward, 2004] P. Ward, *A Design Technique to Remove the Correlation Ambiguity in Binary Offset Carrier* (*BOC*) *Spread Spectrum Signals* (*Revised Version*), Proceedings of the National Technical Meeting of the Institute of Navigation, ION-NTM 2004, 26-28 January, 2004, pp. 886- 896, San Diego, California, USA.

[R. Watson, 2005] R. Watson, *High-Sensitivity GPS L1 Signal Analysis for Indoor Channel Modeling*, Master's thesis, Department of Geomatics Engineering, University of Calgary, UCGE Report 20216.

[L.R.Weill, 2003] L. R. Weill, *Multipath mitigation—how good can it get with new signals?*" *GPS World*, vol. 16, no. 6, pp. 106–113, 2003.

[J. Winkel, 2002] J. Winkel, *Modeling and Simulating Generic GNSS Signal Structures and Receiver in a Multipath Environment*, Ph.D. Thesis, University FAF Munich, Neubiberg, Germany.

[J. Winkel, 2006] J. Winkel, *Spreading Codes for a Satellite Navigation System*, Patent number WO/2006/063613, International Application No.: PCT/EP2004/014488, Publication date: 22 June 2006

[R. Zandbergen et al., 2004] R. Zandbergen, S. Dinwiddy, J. Hahn, E. Brewer, D. Blonski, *Galileo Orbit Selection*, Proceedings of the National Technical Meeting of the Institute of Navigation, ION-NTM 2004, 21-24 September, 2004, Long Beach, California, USA.